Secrets of Snakes Page 1159

6 December 2013 | $10

Science

Single-Cell Biology

AAAS

SPECIAL SECTION

Single-Cell Biology

page 1159

CONTENTS continued >>

ON THE WEB THIS WEEK

>> *Science* Podcast
Listen to stories on noisy gene expression, results from drilling at the Tohoku-Oki fault, the benefits of snake venom, and more.

>> Find More Online
Check out *Science* Express, our podcast, videos, daily news, our research journals, and *Science* Careers at **www.sciencemag.org**.

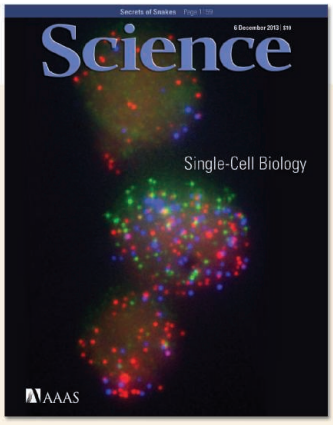

COVER

Variation among three individual mouse embryonic fibroblasts in a micrograph in which individual messenger RNA transcripts from three genes fluoresce with different colored markers (cell diameter: ~12.5 micrometers). Such techniques that allow measurements in single cells provide new insights into biological control mechanisms and are the subject of a special section starting on page 1187.

Image: Dina Faddah and Rudolf Jaenisch, Whitehead Institute for Biomedical Research

DEPARTMENTS

Published by AAAS

SCIENCE PRIZE ESSAY

RESEARCH ARTICLES

REPORTS

page 1171

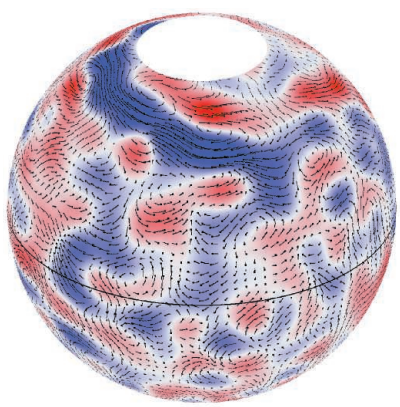

page 1217

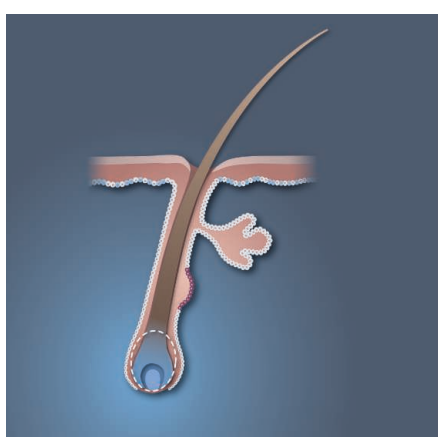

pages 1183 & 1226

CREDIT: (MIDDLE) DAVID HATHAWAY/NASA

SCIENCE (ISSN 0036-8075) is published weekly on Friday, except the last week in December, by the American Association for the Advancement of Science, 1200 New York Avenue, NW, Washington, DC 20005. Periodicals Mail postage (publication No. 484460) paid at Washington, DC, and additional mailing offices. Domestic individual membership and subscription (51 issues): $149 ($74 allocated to subscription). Domestic institutional subscription (51 issues): $990; Foreign postage extra: Mexico, Caribbean (surface mail) $55; other countries (air assist delivery) $85. First class, airmail, student, and emeritus rates on request. Canadian rates with GST available upon request, GST #1254 88122. Publications Mail Agreement Number 1069624. **Printed in the U.S.A.**

Change of address: Allow 4 weeks, giving old and new addresses and 8-digit account number. **Postmaster:** Send change of address to AAAS, P.O. Box 96178, Washington, DC 20090–6178. **Single-copy sales:** $10.00 current issue, $15.00 back issue prepaid includes surface postage; bulk rates on request. **Authorization to photocopy** material for internal or personal use under circumstances not falling within the fair use provisions of the Copyright Act is granted by AAAS to libraries and other users registered with the Copyright Clearance Center (CCC) Transactional Reporting Service, provided that $30.00 per article is paid directly to CCC, 222 Rosewood Drive, Danvers, MA 01923. The identification code for *Science* is 0036-8075. *Science* is indexed in the *Reader's Guide to Periodical Literature* and in several specialized indexes.

EDITED BY STELLA HURTLEY

Deep Drilling for Earthquake Clues

The 2011 M_w 9.0 Tohoku-Oki earthquake and tsunami were remarkable in many regards, including the rupturing of shallow trench sediments with huge associated slip (see the Perspective by **Wang and Kinoshita**). The Japan Trench Fast Drilling Project rapid response drilling expedition sought to sample and monitor the fault zone directly through a series of boreholes. **Chester *et al.*** (p. 1208) describe the structure and composition of the thin fault zone, which is predominately comprised of weak clay-rich sediments. Using these same fault-zone materials, **Ujiie *et al.*** (p. 1211) performed high-velocity frictional experiments to determine the physical controls on the large slip that occurred during the earthquake. Finally, **Fulton *et al.*** (p. 1214) measured in situ temperature anomalies across the fault zone for 9 months, establishing a baseline for frictional resistance and stress during and following the earthquake.

Oscillation Stabilizes the Progenitor State

Transcription factors regulate fate choice between different neural lineages, but the same transcription factors are also expressed in neural progenitor cells. **Imayoshi *et al.*** (p. 1203, published online 31 October) analyzed the details of expression of several transcription factors in mouse neural cells. In neural progenitor cells, several different transcription factors were expressed in an oscillatory manner, whereas differentiated neurons stably expressed a single lineage-specific factor.

Giant Solar Cells

Convection motions within the Sun transport heat from its interior to its surface. The hot regions are seen as granular (~1000 kilometers across) and supergranular (~30,000 kilometers across) cells in the Sun. Using data from the Helioseismic Magnetic Imager on the Solar Dynamics Observatory, **Hathaway *et al.*** (p. 1217) found evidence for even larger cells that have long been predicted by theory but not unambiguously detected. The flows associated with these giant cells transport angular momentum toward the equator and are important for maintaining the Sun's equatorial rotation.

Good Foundations, Poor Access

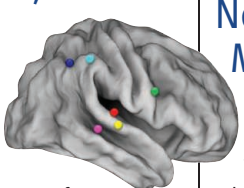

Dyslexia makes reading and spelling difficult. **Boets *et al.*** (p. 1251) analyzed whether for adult readers with dyslexia the internal references for word sounds are poorly constructed or whether accessing those references is abnormally difficult. Brain imaging during phonetic discrimination tasks suggested that the internal dictionary for word sounds was correct, but accessing the dictionary was more difficult than normal.

Dissecting Chromosome Segregation

During cell division, the centromere regions of chromosomes assemble multiprotein organelles called kinetochores that form attachments to spindle microtubules. Working in *Caenorhabditis elegans*, **Cheerambathur *et al.*** (p. 1239, published online 14 November) describe a mechanism controlling the formation of kinetochore-spindle microtubule attachments that is essential for accurate chromosome segregation. The findings suggest the existence of crosstalk between the two major protein complexes involved in forming spindle microtubule attachments: the kinetochore dynein module, which initially captures spindle microtubules, and the Ndc80 complex, which ultimately forms the dynamic end-coupled attachments that segregate chromosomes.

Nonlinear Optics Made Easier

Nonlinear optical materials can change their optical properties in the presence of light. The nonlinearity results from the constructive addition of interacting photons, but the amount of nonlinear light produced is crucially dependent on meeting strict phase-matching conditions of the interacting photon fields. **Suchowski *et al.*** (p. 1223; see the Perspective **Kauranen**) now show that metamaterials can be designed with optical properties that relax the phase-matching requirements. At a specific wavelength where the metamaterial exhibits zero refractive index, the photons are found to interact nonlinearly with the phasematching done automatically.

Toward a New Physics

The search for physics beyond the Standard Model is carried out at accelerator facilities such as the Large Hadron Collider but also on a smaller scale in atomic and molecular physics experiments. One of the signatures of this "new physics" would be a nonvanishing electric dipole moment of the electron, but experiments designed to look for it need to distinguish between the signal and many potential artifacts. **Loh *et al.*** (p. 1220) introduce a method based on the spectroscopy of polarized molecular ions that avoids some of the sources of systematic error.

Epithelial Stem Cells

Much remains to be known about how epithelial stem cells are generated and maintained. **Lim *et al.*** (p. 1226; see the Perspective by **Frede and Jones**) describe a mechanism of stem cell maintenance where epidermal stem cells generate their own self-renewing Wnt signals rather than being controlled by adjacent "niche" signals. These stem cells also express secreted Wnt inhibitors that become localized to more differentiated progeny cells. These autocrine Wnt signals and paracrine long-range Wnt inhibitors may balance stem cell self-renewal and differentiation.

Hedgehog View to a Kill

Hedgehog (Hh) signaling is best known for its role in development and is a key signaling component of primary cilia. Hh signaling plays a role in T cell development, but whether Hh signaling plays a role in the function of mature effector T cells is unclear. **De la Roche *et al.*** (p. 1247; see the Perspective by **Le Borgne and Shaw**) now show that T cell receptor signaling triggers Hh signaling. When Hh signaling is disrupted, centrosome polarization to the immunological synapse is reduced, and cytotoxic T cell–mediated killing is impaired.

CREDITS (TOP TO BOTTOM): JAMSTEC/IODP; BOETS *ET AL.*

Published by AAAS

Additional summaries

Light Turns the Array

The organization of cortical microtubule arrays in higher plant cells is essential for organizing cell and tissue morphogenesis, but it is not clear how specific architectures are acquired and reconfigured in response to environmental cues. **Lindeboom *et al.*** (p. 1202, published online 7 November; see the Perspective by **Roll-Mecak**) used live-cell imaging and genetic studies to show that the microtubule-severing protein, katanin, plays a crucial role in reorienting cortical arrays from transverse to longitudinal in *Arabidopsis* seedlings in response to blue light perception. Katanin localized to microtubule intersections where, stimulated by blue light receptors, it preferentially catalyzed the severing of the newer microtubule. The microtubule "plus" end created by severing were observed to grow preferentially, effectively building a new population of microtubules orthogonal to the initial array. The net effect of this process steers the growing seedling toward light.

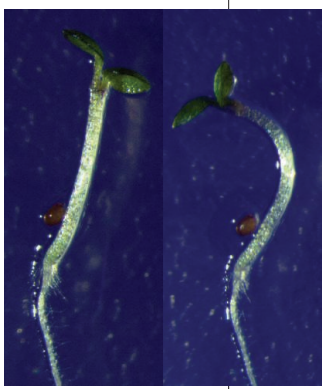

CREDIT: LINDEBOOM *ET AL.*

Avian Affinity for H7N9

Structural analyses of the binding of avian origin H7N9 influenza viruses have revealed how the receptor-binding characteristics differentiate between birds and mammals, and studies involving the use of whole viruses have suggested that the virus is acquiring human-type receptor specificity. In contrast, **Xu *et al.*** (p. 1230) show that the H7 hemagglutinin strongly retains its specificity for avian-type receptors by using cocrystal structures with receptor analogs and glycan binding analysis with recombinant hemagglutinin against a library of receptor analogs. Thus, current human H7N9 viruses appear to remain poorly adapted to human receptors, and additional mutations will be required to achieve specificity for human-type receptors equivalent to those of human pandemic viruses.

Dual-Duty Active Site

O-linked N-acetylglucosamine transferase (OGT) catalyzes the addition of N-acetylglucosamine (GlcNac) to serine or threonine residues, influencing the localization and function of proteins. Because its activity is sensitive to the nutrient uridine diphosphate (UDP)–GlcNac, OGT has been proposed to regulate cellular responses to nutrient status. Recently, OGT in the presence of UDP-GlcNac was shown to cleave host cell factor–1 (HCF-1), a transcriptional coregulator of human cell-cycle progression. This cleavage is required for HCF-1 maturation. Through a combination of structural, biochemical, and mutagenesis studies, **Lazarus *et al.*** (p. 1235) show that both cleavage and glycosylation of HCF-1 occur in the OGT active site. Cleavage occurs between cysteine and glutamine and converts the glutamine into a serine which can then be glycosylated.

Command and Control

Innate lymphoid cells are vital for the development of gut-associated lymphoid tissues, maintenance of the epithelial barrier, and protection against intestinal microbes; their dysfunction can promote immune pathology. Immunoglobulin A (IgA) production is important for maintenance of the gut epithelial barrier and the composition of the gut microbiota. Through the generation of knockout mouse models, **Kruglov *et al.*** (p. 1243) were able to distinguish how soluble and membrane-bound lymphotoxins expressed by innate lymphoid cells in the gut specifically regulate IgA production and thereby control gut microbiota composition.

Not Too Much, Not Too Little

The microRNA miR128 is expressed in brain neurons of the mouse. **Lek Tan *et al.*** (p. 1254) now find that miR128 is crucial to stable brain function. Mice deficient in miR128 developed hyperactivity and were susceptible to fatal seizures, whereas overexpression of miR128 correlated with reduced motor activity and reduced susceptibility to proconvulsive drugs. Experiments using ex vivo–isolated adult brain tissues suggested that miR-128 controlled motor activity by governing the signaling network that determines the intrinsic excitability and signal responsiveness of neurons.

Marcia McNutt is Editor-in-Chief of *Science*.

What Awaits the New NSF Director

IN THE COMING DAYS, THE UNITED STATES SENATE WILL CONSIDER THE CONFIRMATION OF DR. France Córdova as director of the U.S. National Science Foundation (NSF). If confirmed, Dr. Córdova will be the latest in a line of distinguished scientists to lead the nearly $7 billion agency, the most important source of funding for basic research outside of the biomedical sciences. Rather than turning over with the election of a new president, the NSF director is appointed to a 6-year term. During the roughly 2000 days that Córdova will have at the helm, she will need to deal with many forces that threaten the nation's ability to innovate. One major impediment is the continuing threat of mandatory budget cuts from sequestration, whose impact this year included fewer grants awarded and delays to many research projects.

NSF also faces a renewed push from Congress to micromanage its activities: Proposed legislation would alter the agency's time-honored peer-review process by requiring that funded proposals meet one or more congressionally defined national goals. Congress has already required the agency to use "extra criteria" in evaluating proposals for support from its social science programs. I urge the new director to speak up strongly against these new threats and return the agency to its independence.

The bleak fiscal environment presents particular challenges for fields that rely on large and costly facilities. In the recent past, a scientific community could expect to build a major new facility (e.g., a research ship, aircraft, or observatory) with funds from the Major Research Equipment and Facilities Construction (MREFC) account, and by the time it was built, growth in the program budget would be sufficient to support its operations. In the future, that won't be the case. Programs that are fortunate enough to receive an MREFC award will have to plan their operational phase quite differently. One possibility is for the community to identify facilities that they are willing to sunset just as a new facility comes online, and shift the funds accordingly. Another approach is to identify a partner to assume long-term operations of the assets. For example, Incorporated Research Institutions for Seismology (IRIS), one of the implementing organizations for the EarthScope project, encouraged the adoption of USArray seismic stations by other federal and state agencies and educational institutions at the end of the stations' deployment. The transitions have allowed important research and monitoring to continue rather than waste the nation's investment.

Another management imperative is to provide appropriate incentives to work across program lines because the majority of NSF funding flows through its disciplinary directorates. In the past, budget growth has provided NSF directors and associate directors with matching funds to spur exciting opportunities in interdisciplinary, multidisciplinary, and transdisciplinary research. An important aspect of promoting innovation has also been enabling U.S. participation in international collaborations as part of sustaining the nation's position as a global leader in science. For NSF to tackle the most important problems, no matter where they might be found, it is important that flexible funds be found each year to enable new discoveries that can only emerge in the absence of a "silo" system. I urge the new director to argue strongly for sufficient increases in the NSF budget to jump-start innovation and allow the United States to be a full partner at the forefront of international research partnerships.

The United States is no longer in a period when major new capacity can be added without shutting down something else. The new NSF director will likely face difficult choices with unpopular solutions. The scientific community is very fortunate that someone of the caliber, experience, and credentials of Dr. Córdova has agreed to be nominated for this important position. Congress should confirm her quickly and give her the resources needed to be successful so that she can begin shepherding an agency whose actions are defining for the country's future well-being.

– Marcia McNutt

10.1126/science.1248875

Published by AAAS

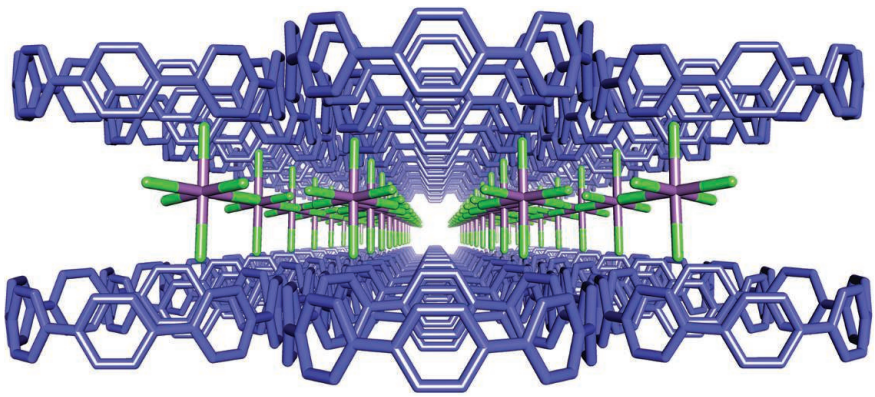

CHEMISTRY

Radical Ring

Charge transport in conjugated π-bonded carbon frameworks is central to the operation of organic photovoltaic systems. Multiple studies have therefore probed the role of charge delocalization in facilitating this process. Kayahara *et al.* examined a simple model system, [8]cycloparaphenylene, in which eight phenyl rings are bound to one another at the para positions to form a loop. Applying one equivalent of nitrosyl hexafluoroantimonate as an oxidant stripped one electron from the compound, whereas five equivalents cleanly stripped two. Spectroscopic analyses by electron spin resonance (for the radical monocation) and nuclear magnetic resonance (for the dication) were consistent with complete spin and charge delocalization throughout the loop. Both salts were also relatively stable under a nitrogen atmosphere. The dication was characterized by x-ray crystallography and manifested a belt geometry, with a coplanar arrangement of all the constituent phenyl rings normal to the loop plane. — JSY

Angew. Chem. Int. Ed. **52**, 10.1002/anie.201306881 (2013).

CANCER

Resistance, Gene by Gene

About half of melanoma patients harbor an identical tumor-specific mutation in the *BRAF* gene, which encodes a protein kinase that helps drive cell growth. One of the most exciting recent advances in clinical cancer research was the discovery that this subgroup of patients respond—sometimes dramatically—to a new class of drugs targeting the MAPK pathway through which BRAF signals. Unfortunately, in most patients the melanoma recurs within a year because the tumor cells develop drug resistance. Understanding the mechanisms by which resistance arises is essential for optimizing the clinical benefits of these drugs.

Johannessen *et al*. used a highly systematic approach to identify candidate genes and signaling networks that contribute to resistance. After exploiting a technology that allowed them to activate each of nearly 16,000 genes individually in human melanoma cell lines containing mutant *BRAF*, the authors then treated the panel of cells with the drugs and monitored which cells showed altered drug sensitivity. Among the unexpected "hits" revealed by this assay were a cyclic AMP signaling network and a group of transcription factors important in melanocyte development, each suggesting potential new strategies for overcoming resistance. — PAK

Nature 10.1038/nature12688 (2013).

CELL BIOLOGY

Playing Kissy with the Relatives

Our understanding of how bacteria actually respond to their natural environment is sparse. Individual cells of several groups of bacteria co-

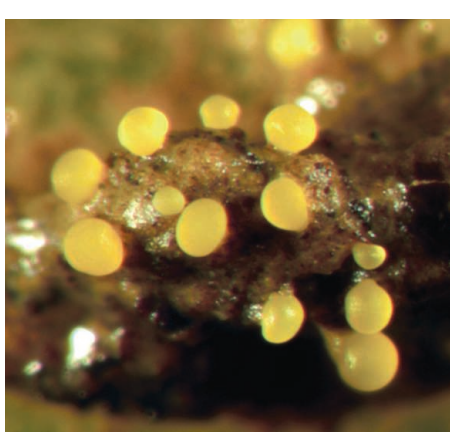

operate to form multicellular fruiting bodies, but how do they select with whom to cooperate and avoid freeloaders or predators? Pathak *et al.* have discovered that when they cooperate, cells of the social bacterium *Myxococcus xanthus* exchange large quantities of membrane material. First, however, these cells want to know with whom they are getting intimate. It turns out that a polymorphic surface receptor, TraA, encodes a spectrum of receptors that can spot degree of relatedness via degree of affinity for the cognate Tra pair on other cells encountered. If close relatives are rare in the environment, this mechanism allows a less-related cell in the neighborhood to be selected as a stopgap that will cooperate enough to allow some form of multicellular reproductive structure to be built. — CA

PLOS Genet. **9**, 10.1371/journal.pgen.1003891 (2013).

MOLECULAR BIOLOGY

Bridging the Genome

Alternative splicing is one means by which the genome is able to generate functional diversity through the differential expression of transcripts, but the regulation and process of how transcripts become alternatively spliced are not well understood. Lovci *et al.* examined the Rbfox family of RNA-binding proteins with cross-linking immunoprecipitation and sequencing (CLIP-seq) and demonstrated that binding sites are conserved within mammalian genomes and that Rbfox clusters tended to be within distal introns (more than 500 nucleotides away from annotated exons). These clusters were determined to be associated with alternatively spliced exons, with downstream clusters correlating with inclusion of an exon and upstream clusters correlating with the exclusion of the exon. Mutation of Rbfox binding sites in vitro demonstrated that these proteins function in alternative splicing and that conserved RNAs with specific secondary structures bridge the exons that are alternatively spliced. On the basis of these results, the authors propose that a distal binding site of Rbfox proteins is brought into the vicinity of the exon via an RNA bridge. — LMZ

Nat. Struct. Mol. Biol. 10.1038/nsmb.2699 (2013).

ARCHAEOLOGY

King Solomon's Silver

Isotope analysis of archaeological materials can play critical roles in both dating of the artifacts and identification of their origin. Thompson and Skaggs use the lead isotope ratios in silver from

Continued on page 1149

CREDITS (TOP TO BOTTOM): EIICHI KAYAHARA; MICHIEL VOS/WIKIMEDIA COMMONS

Continued from page 1147

silver hoards to investigate trade patterns during a Mediterranean "Dark Age" between 1200 and 800 BCE precipitated by the collapse of palace-based economies in the Near East. Lead isotope analysis of 48 precoinage silver artifacts from what was southern Phoenicia [the region between the Yarkon River and Akko (Acre) in present-day Israel] and dated from 1200 to 800 BCE shows that they have isotope ratios similar to those of galena (the mineral form of lead sulfide) and other lead ores from southern and

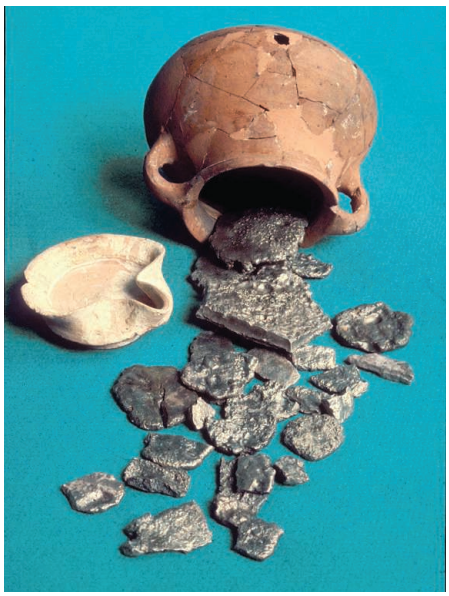

CREDIT: WWW.BIBLELANDPICTURES.COM/ALAMY

southwestern Sardinia, and the Iberian Peninsula. These analyses tentatively identify regions in the western Mediterranean as contributing mineral resources to Phoenician precolonial silver trade and production. The results correlate with ancient documentary sources indicating Phoenician precolonial silver trade with Sardinia and Spain and suggest that the Phoenician precolonial expansion into the west may have involved the acquisition of silver. Thompson and Skaggs further support suggestions that the legendary Tarshish region, a possible source of King Solomon's silver, may have been a refinery town, possibly Nora, on Sardinia. — GR

Internet Archaeol. **35**, 10.11141/ia.35.6 (2013).

CHEMISTRY

Pressuring CO_2 to React

One sustainable approach for converting CO_2 from large-scale industrial production processes into chemicals and fuels is by reacting it with hydrogen generated from solar or wind energy. The catalytic hydrogenation of CO_2 into methanol offers a potential route for conversion, but most commercial catalysts, which use copper and zinc oxide supported on alumina and operate at pressures of 50 to 100 atm, have low single-pass conversions and require product separation and reactant recycling. Bansode and Urakawa, noting that high pressures thermodynamically favor the methanol product, studied this reaction on such catalysts at higher pressures. They could boost single-pass conversions to >95% at 355 atm and 260°C and at high H_2 partial pressures (H_2/CO_2 ratios > 10:1). These conditions should suppress formation of CO as a final product, but the increasing conversion for methanol as temperature was increased to 260°C suggests that the reaction proceeds initially through reduction to CO. This reaction is endothermic and competes with exothermic methanol synthesis. They also show that addition of a solid acid catalyst, H-ZSM-5, as a physical mixture led to the single-pass production of dimethyl ether with selectivities of >80%; when this catalyst was added in a second series reactor, light alkanes or propylene could be produced as well. — PDS

J. Catal. **309**, 66 (2014).

CLIMATE SCIENCE

Forward into the Past

It has been well established that high concentrations of atmospheric CO_2 caused by anthropogenic emissions will persist for thousands of years after those emissions cease and that the consequences for climate will last even longer than that. Suggestions have been made that CO_2 could be removed from the atmosphere artificially in order to speed global climate recovery, but what can be expected from such a capture scheme? MacDougall uses a climate model of intermediate complexity, employing scenarios of CO_2 removal that move from the more idealized schemes used in past studies toward more realistic ones, in order to continue refining our understanding of what would be the effects of such an undertaking. He finds that by assuming a moderate value of climate sensitivity and that CO_2 is removed from the atmosphere as fast as it was added once emissions cease, surface air temperatures like those of preindustrial times can be approached by the year 3000 CE in all but the most extreme emission scenarios. Other components of the climate system, such as mass of the polar ice sheets, and sea level, will take longer to recover, however. So, even if we dial back atmospheric CO_2 concentrations by massive geoengineering, we will be living with the effects of fossil fuel burning for many hundreds of years, at the least. — HJS

Geophys. Res. Lett. **40**, 5480 (2013).

Published by AAAS

AROUND THE WORLD

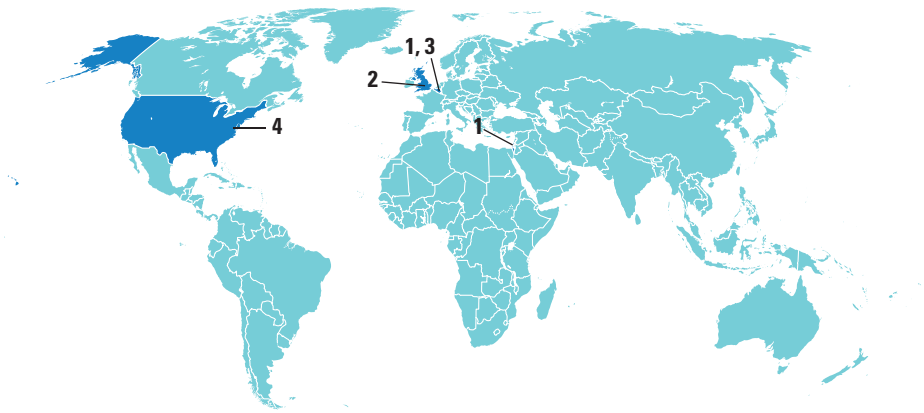

Tel Aviv, Israel and Brussels **1**

Israel to Join Horizon 2020

Thanks to a late-night deal reached last week, Israeli scientists will be able to take part in the European Union's Horizon 2020 funding program. The country's government had threatened not to participate in the 7-year, €70 billion program because of E.U. guidelines, slated to take effect in January, that prohibit funds from going to Israeli

Dealmakers. Israeli Prime Minister Benjamin Netanyahu with Catherine Ashton earlier this year.

organizations or activities in the territories occupied after June 1967, which include the West Bank, the Golan Heights, Gaza, and East Jerusalem.

The 26 November agreement leaves those guidelines in place, but allows Israel to append a statement saying that it does not accept them. "Israel recorded its position of principle against the guidelines while accepting to participate in the E.U. program run by E.U. rules," says Maja Kocijancic, spokesperson for E.U. foreign commissioner Catherine Ashton.

The guidelines will have little impact on most funding decisions: Only three projects funded under Horizon 2020's predecessor, the Seventh Framework Programme, would be ineligible under the new guidelines. **http://scim.ag/2020deal**

London **2**

Dubious Dance Paper Finally Withdrawn

After years of wrangling, a controversial study on symmetry and dance has been retracted. The 2005 *Nature* paper reported that Jamaican men and women with more symmetric bodies were better dancers—a finding that would support the theory that dance evolved as a sexually selected courtship ritual. The 27 November retraction notice gives no reason.

Biologist Robert Trivers of Rutgers University in New Brunswick, New Jersey, one of the authors, says he recognized problems with the data after publication, and accuses co-author William Brown of preselecting dancers and changing the values on some measures of symmetry. An April investigation at Rutgers found several types of fraud, including biased selection of subjects, but Brown denied these accusations.

"It took them 8 years after publication of the paper, and 5 after we submitted a retraction, and 4½ years after we published *proof* of fraud (later borne out by Rutgers' investigation) for them finally to 'retract' a paper now cited 136 times," Trivers writes in an e-mail, adding that journals have no incentive to reveal fraud. **http://scim.ag/_symm**

Brussels **3**

GM Maize Study Retracted

The journal *Food and Chemical Toxicology* has retracted a much-criticized paper that links a strain of genetically modified

Tossed out. Research suggesting that GM maize poses health risks has been dubbed "inconclusive."

(GM) maize with diseases in rats. Elsevier, the journal's publisher, said in a 28 November statement that "the results presented (while not incorrect) are inconclusive, and therefore do not reach the threshold of publication for *Food and Chemical Toxicology*."

In the 2-year study, rats who received various doses of Monsanto's herbicide-resistant NK603 maize suffered from more tumors, organ damage, and premature deaths than control animals. Many scientists dismissed the paper as flawed when it was published in September 2012. Explaining the retraction, the journal's editor-in-chief, Wallace Hayes, cited the low number of animals in each study group and the high natural incidence of tumors in the strain of rat used.

At a press conference in Belgium, the paper's author, biologist Gilles-Eric Séralini of the University of Caen, countered that his experiment was modeled after Monsanto's own NK603 toxicity study. He called the decision an attempt by the GM crop industry to muzzle scientists who question the safety of its products. **http://scim.ag/_maize**

Silver Spring, Maryland **4**

FDA Reins in 23andMe

DNA testing company 23andMe is facing pressure from the U.S. Food and Drug Administration (FDA) over its $99 Personal Genome Service. In a 22 November warning letter, the agency demanded that 23andMe stop selling the service without FDA authorization and charged that potential inaccuracies in the DNA tests could prompt buyers to make misinformed medical decisions.

Company CEO Anne Wojcicki defended the accuracy of the tests in a 27 November

Science LIVE

Join us on Thursday, 12 December, at 3 p.m. EST for a live chat with experts on **the evolution of deadly infectious diseases since the Middle Ages. http://scim.ag/science-live**

CREDITS (LEFT TO RIGHT): EUROPEAN UNION/EUROPEAN EXTERNAL ACTION SERVICE; JEREMY KEITH/WIKIMEDIA COMMONS

Published by AAAS

THEY SAID IT

"We never promised it would survive. We did promise it would be exciting and an extraordinary scientific event. We delivered on that."

—Astronomer Karl Battams of the Naval Research Laboratory in Washington, D.C., on comet ISON's disintegration.

letter to customers, but added, "we recognize that the FDA needs to be convinced of the quality of our data as well." 23andMe submitted documentation to FDA for some of the test's uses in 2012, but FDA says it failed to provide requested information.

The crackdown on direct-to-consumer genomics has been "a long time coming," says Jennifer Wagner, an attorney and researcher at the University of Pennsylvania's Center for the Integration of Genetic Healthcare Technologies. While many question FDA's authority to regulate in this area, she says other companies will watch how 23andMe is "navigating this uncertain world."
http://scim.ag/_23andMe

NEWSMAKERS

EPA Hires Science Integrity Officer

Unlike many federal agencies, the U.S. Environmental Protection Agency (EPA) created a full-time position to implement its scientific integrity policy. Now, it has picked a longtime advocate to do the job.

Francesca Grifo, who led the scientific integrity program at the Union of Concerned Scientists (UCS), will oversee the four main goals of EPA's policy: a culture of scientific integrity; public communication; rigorous peer review; and professional development. One task for Grifo, who started on 25 November, will be educating staff members about the policy and its protections to help them deal with political pressure. If problems come to light, Grifo will work with the inspector general to investigate.


Grifo

UCS has ranked EPA's policy, finalized about a year and a half ago, as one of the stronger ones in the U.S. government. Jeff Ruch of Public Employees for Environmental Responsibility in Washington, D.C., says he is hopeful for progress under Grifo's leadership. "She is coming from an organization that is probably responsible for the adoption of scientific integrity policies," he says. **http://scim.ag/_Grifo**

FINDINGS

Asian Teens Remain on Top in Test of Student Knowledge

Shanghai students have widened their lead in the latest global comparison of the educational skills of 15-year-olds. Asian city-states dominate the rankings, released on 3 December, while U.S. students continue to lag behind their counterparts in the industrial world.

The Programme for International Student Assessment measures how well students can apply what they've learned in reading, mathematics, and science to practical problems. The 2012 results are similar to 2009 and earlier versions. Of 65 participants, which included both countries and smaller entities such as states and provinces, Shanghai once again leads the way in all three subjects, while Singapore and Hong Kong hold down the next two spots in math and science. Korea and Japan are the only large nations in the top 10. (China does not participate as a country.)

The United States ranks 26th in math and 21st in science out of the 34 countries in the Organisation for Economic Co-operation and Development (OECD), which conducts the assessment. In addition to compiling head-to-head rankings, OECD collects data on educational policies and practices around the world.
http://scim.ag/_12PISA

Random Sample

High School Team Tackles Lunar Mystery

When the Lunar Reconnaissance Orbiter relayed images in 2011 of oddly striped boulders on the moon—some of them a dozen or more meters across—three students at Kickapoo High School in Springfield, Missouri, in search of a class science project decided to investigate. They joined a 2-semester research program through the Center for Lunar Science and Exploration in Houston, Texas. With mentor Georgiana Kramer, a planetary scientist there, the team has now netted a scientific paper.

The Kickapoo Lunar Research Team spent several months trying to explain the stripes. Researchers had already floated several possibilities. Kramer suspected that the light-colored layers were probably regolith, material blasted from impact craters elsewhere on the moon. But the students found that such debris accumulates much too slowly to account for the banding.

Through their calculations, they arrived at a new explanation: The striping formed as molten material cooled deep within the moon's crust. "I was surprised at the answer they came up with," Kramer says. But the team has support for the theory: Some banded rocks on Earth form by a similar process, says team member Abby Delawder. "These banded rocks are nothing like any other rocks found on the moon's surface," she notes. "It's clear they were blasted upward by an impact." Unlike the average high school project, this one appeared among graduate student posters at NASA's annual Lunar Science Institute Forum in Mountain View, California, in 2012 and will be published in a forthcoming issue of the journal *Icarus*.

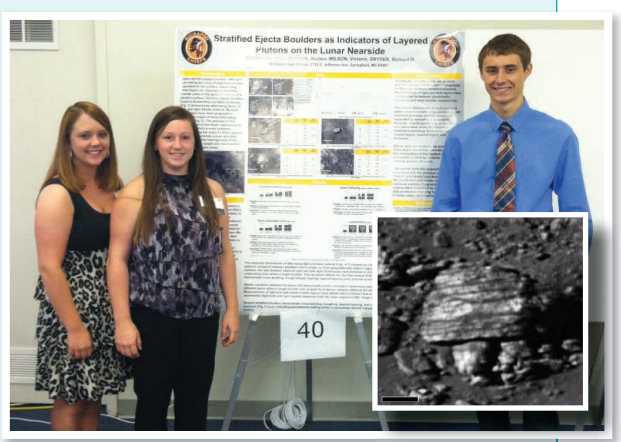

Students (*left to right*) Abby Delawder, Victoria Wilson, and Austen Beason studied striped moon boulders (*inset*). Scale bar represents 10 meters.

CREDITS (LEFT TO RIGHT): PR NEWSWIRE; UNION OF CONCERNED SCIENTISTS; ANDREW SHANER/LPI; COURTESY OF PETER SCHULTZ

Published by AAAS

Property or person? A series of lawsuits could free U.S. chimpanzees from captivity.

ANIMAL RIGHTS

Lawsuits Seek 'Personhood' For Chimpanzees

Chimpanzees are getting their day in court. An animal rights group known as the Nonhuman Rights Project (NhRP) filed lawsuits in three New York counties this week in an attempt to get judges to declare that the great apes are legal persons and free them from captivity. The litigation, on behalf of two research chimps at Stony Brook University and two chimps on private property, is the first salvo in a coordinated campaign to secure "legal personhood" for a variety of animals across the United States.

If NhRP is successful in New York, it could be a significant step toward upending millennia of law defining animals as property and could set off a "chain reaction" that could bleed over to other jurisdictions, says Richard Cupp, a law professor at Pepperdine University in Malibu, California, and a proponent of focusing on animal welfare rather than animal rights. "But if they lose it could be a significant step backward for the movement. They're playing with fire."

The effort began nearly 30 years ago in the mind of a Boston attorney named Steven Wise. An early member of the Animal Legal Defense Fund (ALDF), a then-small group of lawyers dedicated to obtaining rights for pets, livestock, and other creatures in U.S. courts, Wise began thinking about what it would take to turn animals into legal persons. "But in 1985, the law, the science, and the court of public opinion wasn't ready," he says, so he began writing a series of law review articles—then books—on the topic. Wise, who holds a bachelor's degree in chemistry, relied heavily on animal cognition research, arguing that creatures like chimpanzees and dolphins were so self-aware that keeping them in captivity was tantamount to slavery. "It's a terrible torture we inflict on them, and it has to stop," he says. "And all of human law says the way things stop is when courts and legislatures recognize that the being imprisoned is a legal person. Otherwise, they ignore them."

In 2007, Wise founded NhRP, an association of about 60 lawyers, scientists, and policy experts who began to formulate a strategy to gain legal personhood for animals. He felt he now had public sentiment on his side. Support for animal research was declining, lawmakers were imposing tough new restrictions on factory farms, and ALDF had blossomed into a national organization with chapters at most U.S. law schools. "Animal rights had entered the mainstream," he says. "I felt that judges were willing to hear my arguments."

They hadn't in the past. In 1993, Wise attempted to sue on behalf of a dolphin that had been transferred to a Navy facility, but the judge ruled that, as nonpersons, animals don't have the legal "standing" to sue. (More recently, a federal judge dismissed a 2011 lawsuit by People for the Ethical Treatment of Animals when it tried to argue that SeaWorld had violated the 13th Amendment of the U.S. Constitution by keeping orcas as "slaves.")

NhRP is taking an entirely different tack. The strategy is based on the 1772 case of James Somerset, a black slave who escaped from his owner in England. He was captured and imprisoned on a ship bound for the slave markets of Jamaica. Abolitionists petitioned Lord Mansfield, chief justice of the Court of King's Bench, to issue a common law writ of habeas corpus, which allows a person being held captive to have a say in court. Mansfield granted the writ, tacitly acknowledging that Somerset was a "person," and freed him. The case helped spark the eventual abolition of slavery in England.

Wise, who wrote a book on the Somerset case, calls it a "metaphor and a blueprint" for NhRP. "It was a transubstantiation," he says. "It turned a legal thing into a legal person."

In its new litigation, the group is applying two crucial aspects of the case. First, it is trying to modify the common law rather than appealing to written statutes or the Constitution. "Common law changes as

society changes," Wise says. "Judges can rely on their own morals." And second, the group will petition for a writ of habeas corpus, which gets around the legal-standing roadblock by allowing someone else to argue on the captive's behalf.

NhRP spent 5 years honing its strategy. The group also had to find sympathetic jurisdictions—courts that had, for example, been early proponents of civil rights and animal welfare. "We were looking for judges who might aspire to be as great as Lord Mansfield," Wise says.

The upshot: lawsuits filed in three New York trial courts on behalf of four resident chimpanzees. "We scoured the entire state for captive chimps," Wise says, "and these were the only ones we could find." One, named Tommy, lives in Gloversville in a "used trailer lot … isolated in a cage in a dark shed," according to an NhRP press release. Another, Kiko, resides in a cage on private property in Niagara Falls, the group says. The final two, Hercules and Leo, are research chimps at Stony Brook University. Wise says 11 scientists have filed affidavits in the cases; most of them, including Jane Goodall, have worked with nonhuman primates. NhRP is seeking only one legal right at this point: the right to bodily liberty. If the group wins any of the cases, it will ask that the animals be transferred to a chimpanzee sanctuary in Florida. Any loss, Wise says, will immediately be appealed.

Anatomist Susan Larson, who studies the Stony Brook chimpanzees to shed light on the origin of bipedalism in humans, says she is "very shocked and upset" by the lawsuit. She says the chimps, which are on loan from the New Iberia Research Center in Louisiana, live in an indoor enclosure composed of three rooms—"about the size of an average bedroom"—plus another room where they can climb, hang, and jump from ladders and tree trunks. "Everything I do with these animals I've done on myself," she says. "I understand that animal rights activists don't want these animals mistreated, but they're hampering our ability to study them before they become extinct."

Regardless of what happens, the cases won't set legal precedent unless they are heard by a higher state court, says Cupp, the legal expert. If Wise's group wins in one of these higher courts, the decision could confer personhood to all captive chimps in the state. A loss could set the opposite precedent, he notes, potentially dooming the movement nationwide.

Frankie Trull, the president of the National Association for Biomedical Research in Washington, D.C., says her organization is ready to fight back if it looks like personhood is advancing in the courts. Chimpanzees are important models for behavioral research, as well as for developing vaccines against viruses like hepatitis C, she says. "Assigning rights to animals akin to what humans have would be chaotic for the research community," she says. "First it's chimps; what's next?"

> ***"Assigning rights to animals akin to what humans have would be chaotic for the research community. First it's chimps; what's next?"***
>
> **—FRANKIE TRULL, NATIONAL ASSOCIATION FOR BIOMEDICAL RESEARCH**

Wise has an answer for that. His group is already preparing litigation for other states and other animals. "Gorillas, orangutans, elephants, whales, dolphins—any animal that has these sorts of cognitive capabilities, we would be comfortable bringing suit on behalf of," he says. Some would be research animals; others would be creatures that simply live in confined spaces, like zoos and aquariums. "No matter how these first cases turn out … we're going to file as many lawsuits as we can over the next 10 or 20 years."

That worries researchers like Heidi Harley, a comparative psychologist at the New College of Florida in Sarasota who has studied dolphin communication at aquariums and theme parks for 30 years. "I don't think there's anyone who works with these animals who doesn't think about their welfare on a regular basis," she says. "But there's still so much we don't know about them. I don't think we know enough to know what's best for them." Marine mammal scientist Louis Herman, who ran a dolphin lab in Hawaii for 34 years, is concerned that the personhood movement will draw resources away from initiatives to save animals in the wild. "Cetacean kills, elephant kills, gorilla kills is where continued and even great effort and protection is needed," he writes in an e-mail. "We should not be diverted from that goal."

Chimp research may be on its way out even without NhRP. In June, the National Institutes of Health (NIH) announced plans to retire all but 50 of its 360 research chimpanzees and phase out much of the chimp research it supports; any projects that continue, such as behavioral studies, will have to meet stricter welfare guidelines (*Science*, 5 July, p. 17). The U.S. Fish and Wildlife Service, meanwhile, has recommended that captive chimps be listed as endangered, which would limit any research that isn't in their best interest. "Soon, the type of work I do will no longer be possible," Larson says.

Stephen Ross wonders if there's a compromise. Ross, the director of the Lester E. Fisher Center for the Study and Conservation of Apes at the Lincoln Park Zoo in Chicago, Illinois, has studied chimp behavior and cognition for more than 20 years. He helped design the zoo's expansive ape habitat—replete with a bamboo forest, termite mounds, and dozens of trees—and played a role in crafting NIH's new chimp policy. "I think these animals should have some rights. They should have the right to be comfortable and live in an engaging environment," he says. "But you don't need personhood to do that." Instead, Ross advocates ending private ownership of chimps, which is hard to police, as well as invasive research. All other chimpanzees, whether located at zoos or universities, should live in large enclosures, with access to the outside, and in groups of at least seven individuals.

"I think we share a common philosophy," Ross says of NhRP. "We want to make things better for chimps. We just disagree on how to get there."

–DAVID GRIMM

Slippery slope. Legal personhood for chimpanzees could affect other animals like dolphins.

CREDIT: LAWRENCE MIGDALE/GETTY IMAGES/PHOTO RESEARCHERS

Published by AAAS

HUMAN EVOLUTION

Elusive Denisovans Sighted in Oldest Human DNA

For 4 years, paleogeneticist Svante Pääbo has been chasing a ghost species of ancient human. Known only by its DNA and three scrappy fossils from Denisova Cave in Siberia, this extinct lineage has left genetic traces in living Southeast Asians, so Pääbo expected to find its DNA in bones from across Asia. He had come up empty. Now, his team at the Max Planck Institute for Evolutionary Anthropology in Leipzig, Germany, has finally found part of the broken Denisovan trail—not in some mysterious Asian fossil, but in a proto-Neandertal from Spain.

In a technical feat, the team sequenced the oldest human DNA yet, an almost complete mitochondrial genome from a sliver of thighbone 300,000 to 400,000 years old. The bone, with its Denisovan signature, came from Sima de los Huesos, or "Pit of the Bones," in Spain's Atapuerca Mountains. "I would have guessed we'd find Denisova DNA somewhere in China, but not in Western Europe," Pääbo says. Paleogeneticist Matthias Meyer, who actually did the sequencing, agrees: "Nobody believed it. Even I was skeptical at first."

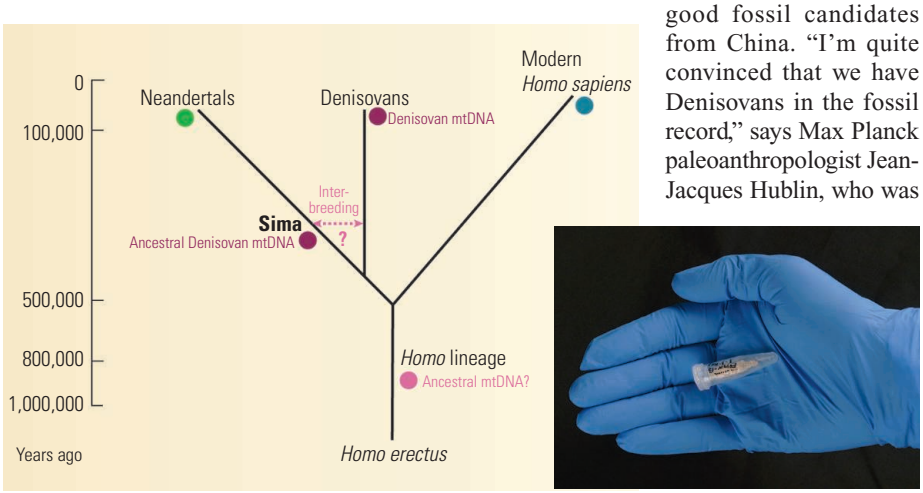

Lines of descent. A Spanish fossil (*right*) yielded mitochondrial DNA ancestral to that found in Denisovans from Siberia (purple dots). Two scenarios (pink) show how this DNA may have been inherited—by interbreeding, or from an archaic ancestor. Later, this mtDNA was lost in Neandertals and *Homo sapiens*, which have two distinct mtDNA lineages (green and blue dots).

The DNA is three or four times older than the previous record-holder, which researchers retrieved in 2006 from a 100,000-year-old Neandertal. The achievement promises "further advances in disentangling the relationships of the various human groups known from the last 600,000 years," says paleoanthropologist Chris Stringer of the Natural History Museum in London, who was not a member of the team. But for now, the unexpected discovery, reported in *Nature* this week, complicates rather than clarifies the picture of how modern humans, Neandertals, and Denisovans evolved in the past half million years. "It is all much more complex than we thought," says co-author Juan-Luis Arsuaga, a paleontologist at the Complutense University of Madrid.

Paleoanthropologists caught their first glimpse of the Denisovans in 2010, when Pääbo's group sequenced an mtDNA genome from a girl's pinky finger from Denisova Cave. Later, the nuclear genome showed the Denisovans were more closely related to Neandertals than to modern humans (*Science*, 28 January 2011, p. 392). Denisovan DNA shows up in some Southeast Asians, suggesting that ancient Denisovans mixed with our ancestors in Asia.

But the Asian hunt has proved unsuccessful so far. Poor DNA preservation thwarted the team's efforts on several good fossil candidates from China. "I'm quite convinced that we have Denisovans in the fossil record," says Max Planck paleoanthropologist Jean-Jacques Hublin, who was not a co-author. "What is frustrating is not being able to merge the fossil evidence and the genetic evidence."

The deep pit at Sima de los Huesos holds plentiful fossils, including more than 6000 bones from at least 28 individuals. The excavation team, led by Arsuaga, classifies the bones as *Homo heidelbergensis*, a species that lived about 600,000 to 250,000 years ago in Europe, Africa, and Asia and gave rise to Neandertals and perhaps also to *Homo sapiens*. Pääbo's group hoped to compare DNA from the Sima bones to those of their Neandertal descendants, who appeared in Europe about 130,000 years ago.

To extract and analyze such old DNA, Meyer and his colleagues developed a new method to sequence single strands of DNA as short as 35 to 45 base pairs in length (*Science*, 31 August 2012, p. 1028). They eliminated modern contaminating DNA by analyzing only DNA segments with uracil, a base usually found in RNA and a signature of older, degraded DNA.

Instead of a proto-Neandertal genome, however, the painstaking work yielded one that looked more like ancestral Denisovan mtDNA. Borrowing a mutation rate calculated for modern humans, the team estimated that the fossil was about 400,000 years old, matching the age from other fossil dating methods.

What was Denisovan DNA doing in a proto-Neandertal 7500 kilometers from Siberia? The authors propose several scenarios. Perhaps the pre-Neandertal Sima people interbred with very early Denisovans and so picked up their mtDNA. Or perhaps the "Denisovan" mtDNA is really the signature of an even more ancient hominin lineage, for example *Homo erectus*. Both the Sima people and the later Denisovans might have inherited this archaic mtDNA from their common ancestor (see diagram). Later Neandertals and modern humans might also have inherited the archaic mtDNA, but lost it over time. (Most mtDNA lineages eventually go extinct even if the species that carried them persists.)

The paper leaves some researchers frustrated. The authors "arrive at no conclusion," grumbles paleoneurologist Emiliano Bruner of the Spanish National Research Center for Human Evolution in Burgos. "This is not a great advance, leaving all hypotheses still on."

But the first glimpse of genetic material from a new period is almost always unsatisfying, Stringer notes. Researchers can "put the bigger picture together" only when multiple samples can be compared. More DNA from Sima—especially the much more informative DNA from the cell nucleus—would help. "I think we will get nuclear DNA," Pääbo says. For now, says paleoanthropologist Ian Tattersall of the American Museum of Natural History in New York City: "All I can say is, this gets mysteriouser and mysteriouser."

–ANN GIBBONS

With reporting by Michael Balter.

CREDITS (LEFT TO RIGHT): AP PHOTO/RIA-NOVOSTI/MIKHAIL KLIMENTYEV/PRESIDENTIAL PRESS SERVICE; NATALIYA SADOVSKAYA/WIKIMEDIA COMMONS; ASTAKHOV DMITRY ITAR-TASS PHOTOS/NEWSCOM

RUSSIA

A Painful Cure for Ailing Academy

Perched on a gentle rise above the Moskva River in Moscow's Sparrow Hills district, the Russian Academy of Sciences's (RAS's) new presidium complex, twin towers crowned with ornate sculptures known affectionately as the "golden brain," is the seat of power of Russia's scientific elite. These days, however, the view from Sparrow Hills is bleak. In recent weeks, the academy has faced a forced merger, the appointment of a new overlord with no background in science, and now, a painful downsizing.

This week, pink slips were due to go out to about 2000 of the 2500 scientists in the administrations of RAS and the two sister academies with which it is merging, according to an RAS source who requested anonymity. RAS's 483 institutes have begun assessing which of the academy's roughly 55,000 researchers will keep their jobs—though formal firings may not happen until the end of 2014. "Word of mouth is that at least 30% of staff will be laid off. Inefficient institutes will be closed or merged with others," says biochemist Yegor Vassetzky, a Russian expat at the Institut Gustave Roussy in Paris who has been in contact with colleagues back home. "People are completely panicked." Even RAS's iconic presidium complex may be at risk.

Almost everyone agrees that RAS is in dire need of reform. Founded by Peter the Great in 1724, the academy grew especially powerful during the Soviet era. After the Soviet Union collapsed in 1991, critics argued that concentrating research in RAS-run institutes harmed university education and research. They called for RAS to shrink and evolve into an entity resembling the U.S. National Academy of Sciences, an honorific body that does not manage research. RAS's leadership successfully resisted change for 2 decades—until President Vladimir Putin this year took decisive steps that were "meted out like a punishment," says Roald Sagdeev, a plasma physicist at the University of Maryland, College Park, and former director of RAS's Space Research Institute.

Putin has said that the reforms will restore luster to an ailing scientific establishment. Others claim to see the machinations of individuals in Putin's inner circle bent on harming the academy or stripping it of its estimated $10 billion in real estate holdings. In June, Putin's administration unveiled legislation ordering the merger of the three academies and the creation of a new Federal Agency for Scientific Organizations (FASO) that from 1 January will oversee the combined academies and their assets.

Many prominent scientists inveighed against the bill, arguing that its measures would erode rather than improve Russian science, and Russia's parliament delayed a final vote until September (*Science*, 5 July, p. 18). Putin invited feedback on the legislation and asked recently elected RAS President Vladimir Fortov, an accomplished plasma physicist, if he would wear two hats: as director of the merged academies and as head of FASO. After the law's enactment in September with minor revisions sparked more protests, Putin issued a 1-year moratorium on any firings or sale of RAS property holdings that would result in "irreplaceable losses."

In a surprise move, Putin did not follow through on what Sagdeev calls a "rhetorical" offer to appoint Fortov as FASO head. Putin instead in October brought in Mikhail Kotyukov, a 36-year-old specialist in finance and credit from the Siberian city of Krasnoyarsk who had risen quickly in the bureaucratic ranks to become deputy finance minister. In a 22 November interview with *Poisk*, a Russian science weekly, Kotyukov declared that his task is to "build a more modern economic model for Russian science," while leaving research to the scientists. "I've heard nothing bad about him," Sagdeev says, "but I don't think he'll serve any positive role."

Fortov, who will remain RAS president, has pledged to cooperate with Kotyukov. "From the beginning, Fortov has played the role of the good boy, trying to find a reasonable compromise to save the academy," Sagdeev says. That strategy failed, he says: "Putin simply cheated him." Neither Fortov nor Kotyukov could be reached for comment.

The contours of the amalgamated academy are still in flux. Sources say that many of the medical academy's 32 institutes will be transferred to the health ministry; likewise, the agricultural academy's 255 institutes may be shorn off and given to the ag ministry.

But the merged academy's flat budget in 2014 of $2.9 billion is forcing institutes to start making hard choices about whom to support. In such a dismal environment, Sagdeev predicts, "an exodus of young scientists from Russia is unavoidable." Others contend the opposite will happen. Alexei Khokhlov, a polymer physicist and vice-rector of Moscow State University, says that a "clever winnowing" of the bloated academy "may give better opportunities for more able researchers, young researchers, and those overseas who want to come home." At least some of the crème of Russian science may thrive during the shakeup, as Putin has mandated big pay increases for influential scientists.

But for RAS's embattled leadership, the news just gets worse. Russia's state property office now says that RAS never asserted ownership rights to its complex in Sparrow Hills, the newspaper *Kommersant* reported on 29 November. FASO is reportedly sizing up the property for its new digs.

–RICHARD STONE

With reporting by Daniel Clery.

Published by AAAS

NEUROSCIENCE

Faulty Brain Connections in Dyslexia?

A scientific fight is brewing around the cause of dyslexia, a learning disability that hinders reading and other language skills. On page 1251, a Belgian research team argues that the core of the disorder lies not in faulty mental representations of words, as has been argued for decades, but in the brain's ability to access that information.

"This is the most conclusive study on this issue I've seen in the last 5 years," says Franck Ramus, a cognitive scientist at the École Normale Supérieure in Paris. "If the results hold, they modify significantly our understanding of dyslexia." That could mean that certain auditory training programs for dyslexia are unlikely to help, he adds.

So far, dyslexia hasn't been associated with deficits in vision, hearing, or general intelligence. Instead, the disability, found in roughly 10% of the population, seems to be the result of a subtle yet significant snarl in the brain's ability to process information about words.

Anyone acquiring a new language must first learn all of the small units of sound it contains, called phonemes. Next, they must learn to group all the different ways a given phoneme can be spoken—in high or low tones, for example, or with an accent—while distinguishing between closely related sounds, such as "d" and "b."

For the past 40 years, researchers have thought that people with dyslexia don't develop precise "phonetic representations" and thus can't recognize fine distinctions in language, says Bart Boets, a developmental psychologist at the Catholic University of Leuven in Belgium, who led the new study. The distorted representations, like smudged words in a dictionary, might not be evident in everyday speech, but they could make learning to read and spell quite difficult, especially for words that don't follow obvious spelling or pronunciation rules, such as "bough" and "cough."

Some researchers believe, however, that people with dyslexia have intact phonetic representations, but can't easily access them because of impaired brain connections. The new study "is about testing these two hypotheses against each other," Ramus says.

The hypotheses have been very difficult to disentangle because behavioral tasks that test phonological skills "always tap both the representation and the access to this representation simultaneously," Boets says. He and his colleagues used functional magnetic resonance imaging (fMRI) to take 3D snapshots of all the brain's activity as study participants—23 severely dyslexic adults and 22 controls—listened to different speech sounds. This "really gives you a sense of a neural fingerprint of phonetic representations," Boets says.

Each participant listened to series of four nonsense words, followed by related words in which a consonant, vowel, or both had been switched: "ba-ba-ba-ba-da-da-da-da," for example. The participants were asked to identify what had changed, a task that Boets theorized requires robust mental representations of the different phonemes. The research team found that the accuracy of the dyslexic group's answers and the crispness of their neural responses were equal to or even better than those of the normally reading group. "Their [phonetic] representations turned out to be perfectly intact!" Boets says.

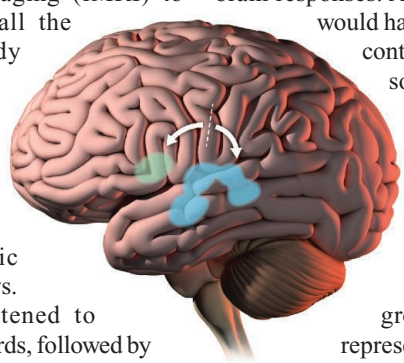

Failure to communicate. Therapies for dyslexia (*left*) may need rethinking if it is caused by faulty communication (*below*) among brain regions such as Broca's area (green) and the auditory cortex (blue).

The dyslexic subjects were about 50% slower to make their responses, however. When the team analyzed overall brain activity, they found that the dyslexics had less coordination between 13 brain regions that process basic phonemes and a region called Broca's area, responsible for higher level language processing. Further analysis showed that the weaker the coordination between those two brain regions, the slower the participants' responses. To Boets, the conclusion that dyslexia reflects poor access to information about phonemes, rather than poor information itself, is "almost inescapable."

Neuroscientist Michael Merzenich at the University of California, San Francisco, is skeptical. He is not convinced that the isolated "hot spots" of brain activity measured in the study actually represent different phonemes. Moreover, decades of "very extensive and compelling" evidence show that people with dyslexia do, indeed, process phonetic representations with lower fidelity than normal, he adds. "You can't just ignore this literature," Merzenich says.

Iris Berent, a linguist at Northeastern University in Boston, adds that the phonemic differences that the Belgian team used to test their subjects were large, making them a "very coarse" probe of brain responses. A more sensitive measure would have been to test the subtler contrasts between ambiguous sounds with which people with dyslexia actually struggle, she says.

Boets counters that the experiment realistically recreates that ambiguity. Ramus agrees that if the dyslexic group had degraded neural representations of these sounds, "you should be able to see it in the fMRI data." Boets is already pondering ways of improving the brain connections that he believes are at fault in dyslexia. "It's not inconceivable to design interventions that specifically target these connections, such as noninvasive electrical stimulation" to restore communication between brain regions, he says.

–EMILY UNDERWOOD

Published by AAAS

SECRETS OF SNAKES

Exotic, elusive, and dangerous, snakes have fascinated humankind for millennia. They can be hard to find, yet their 3000 species have conquered almost every corner of the planet. They play key roles in religion and mythology—and even now snakebites kill an estimated 100,000 people annually.

These days, molecular biologists, too, are falling under the spell of snakes, pursuing the secrets of their bizarre anatomy and powerful venoms. To mark the publication of the first two snake genomes, *Science* reporters take a close look at the work of scientists who were bitten—in some cases literally—by snakes.

CREDIT: HENRIK SORENSEN/GETTY IMAGES

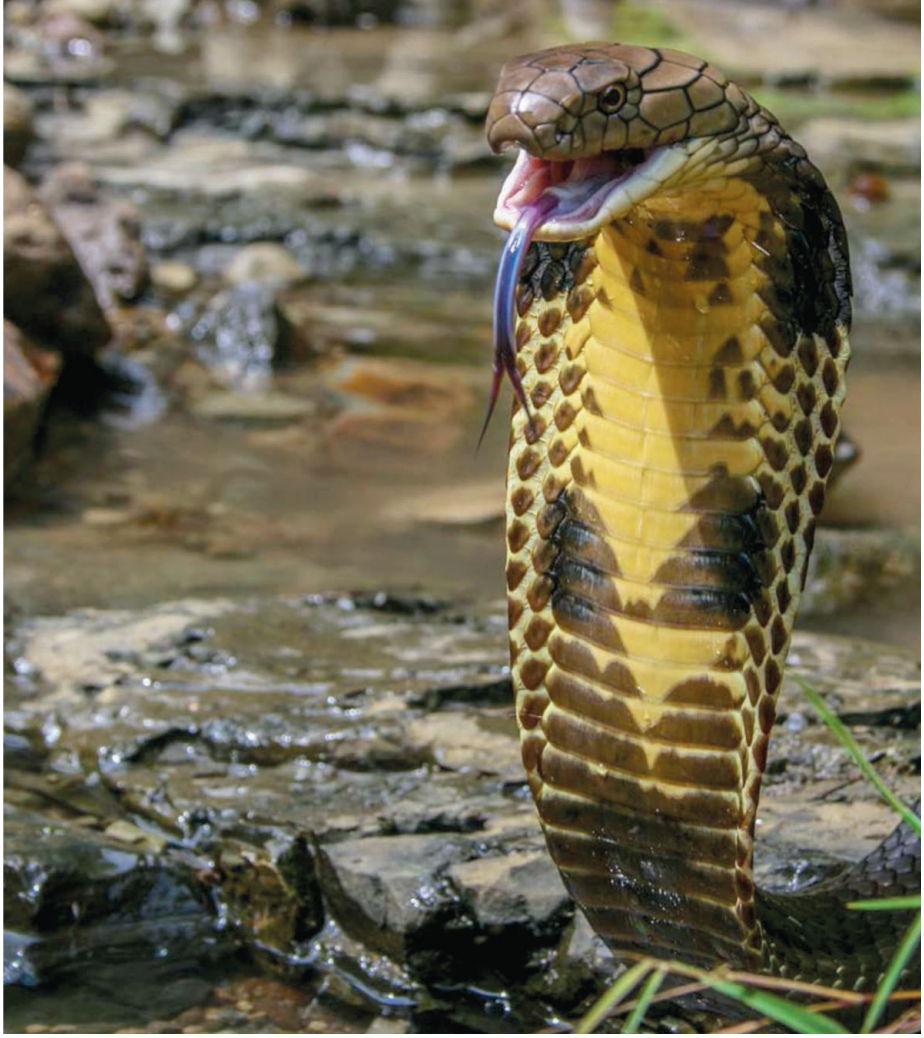

Speed kings. The king cobra (*left*) and the Burmese python (*previous page*) have evolved rapidly.

Genes for Extremes

The first two snake genomes, published this week, reflect the amazing evolutionary tales of a prey-crushing python and a venomous cobra

Harry Greene has long been crazy about snakes—but less so about molecular biology. A veteran herpetologist at Cornell University, Greene has tracked down bushmasters, rattlers, and other snakes in 30 countries; once, in a Brazilian swamp, he brushed up against a green anaconda as long as a mid-size car (*Science*, 26 March 2010, p. 1577). But like many of his fellow snake researchers, he long eschewed molecular biology. "I'm so over that," Greene now says.

He's not the only one. Researchers have recently started delving deep into the molecular biology of venom, where some hope to find clues to important new drugs (see story on p. 1162). And in papers published online this week by the *Proceedings of the National Academy of Sciences*, two teams describe the genomes of the Burmese python and the king cobra—the first snake genomes ever published.

The two studies reveal the molecular basis for snake features that Greene and other researchers have long marveled about. The Burmese python eats three to five times a year, strangling prey 1.5 times its size. ("Imagine if I could eat a 270-pound cheeseburger, with no hands and no implements, and that made up a third of my annual energy budget," Greene says.) The king cobra, the largest venomous snake in the world at 4 meters long, has developed a fearsome venom consisting of 73 peptides and proteins that swiftly immobilize and kill its prey, mostly other snakes. Together, the papers represent "the opposite ends of the extreme evolution that has occurred in snakes," says Bryan Grieg Fry, an evolutionary biologist at the University of Queensland in Brisbane, Australia.

Greene says he was thrilled by what the genome studies turned up. "It's almost like expedition research, except it's in a genome and not in a tropical forest," he says. "I think these papers are going to lead the way for all kinds of work by younger researchers." The new genome analyses, along with studies of when and where the newly revealed genes are active, show that snakes as a group have evolved very quickly, changing the function of existing genes and coming up with additional ones to gain new abilities.

"A lot of people think of snakes as these simple tubes, but life is hard as a tube," says David Pollock, an evolutionary biologist at the University of Colorado School of Medicine in Aurora. "The bottom line is that snakes have done a lot of really impressive things in adapting at all levels": physiological, morphological—and molecular.

Forking path

Snakes have slithered their way through oceans and across all the continents save Antarctica; their 3000 species have infiltrated nearly every conceivable habitat from termite mounds to rainforest canopies. But they got their start in a specialized niche where legs were a handicap. A few researchers think snakes first evolved while living in water, but most now contend that they originated from lizards that went underground (*Science,* 8 November, p. 683). There, they acquired not just the serpentine body type, but also an economical metabolism able to deal with low oxygen levels. Eyes weren't needed, so they degenerated. When snakes surfaced again, lacking limbs for capturing prey, some species evolved venom instead. And they developed visual systems quite different from those of their lizard relatives.

Pythons belong to a group that branched off early from these resurfaced snakes. They switched their diet from insects to larger animals and instead of biting their prey to death, started to constrict their powerful bodies around their meals to strangle them. (Pythons don't have venom.) Cobras took a different evolutionary path, developing outer teeth that move independently from their inner teeth. That way, their fangs could specialize for injecting venom while the inner teeth could help swallow prey.

The plan to sequence the python genome came from evolutionary biologist Todd Castoe of the University of Texas, Arlington. As a postdoctoral fellow working with Pollock, Castoe had studied a variety of vertebrate mitochondrial genomes. Comparisons had shown that these small genomes, found in cellular organelles, had evolved faster in snakes than in other groups. Castoe wanted to know if this was true for snakes' nuclear genomes as well.

CREDIT: FREEK VONK

Published by AAAS

They decided that the Burmese python, which lives in Southeast Asia and recently invaded the Florida Everglades, was an appealing target because of its astonishing metabolic patterns, documented extensively by evolutionary physiologist Stephen Secor of the University of Alabama, Tuscaloosa. Pythons can go without food for months at a time; when they do finally eat, organs like the kidney, liver, and gut can double in size in less than 3 days, while the snake's metabolism revs up to 40 times its usual rate. Getting to the molecular basis of this massive organ growth, Castoe hoped, might also yield some clues to how to treat cancer or heart disease.

As part of the study, the scientists checked the activity of genes in the heart, kidney, small intestine, and liver before a meal and again 1 and 4 days after eating. "The magnitude of the gene expression response really floored us," Castoe recalls. Half the python's genes changed their activity significantly within 48 hours. With the study in hand, "people are going to have a ton of new targets for looking at the genomics" of how snakes adapt physiologically, predicts Harvard University evolutionary biologist Scott Edwards.

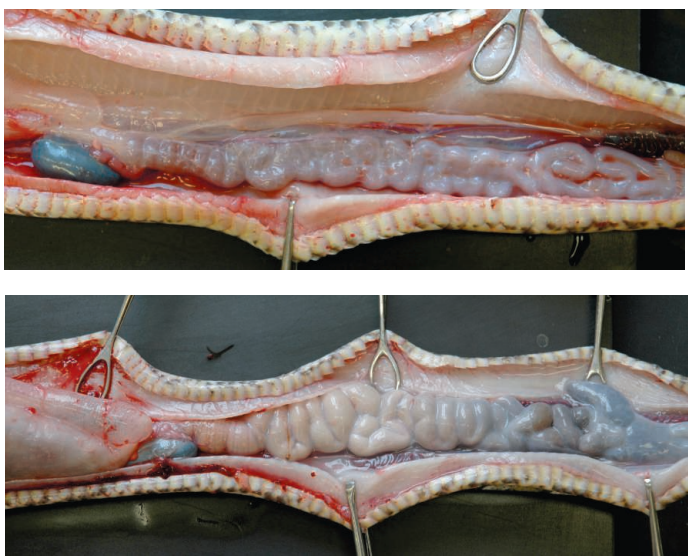

Gut reaction. The Burmese python's small intestine shrinks (*top*) in response to fasting but expands greatly within days of a meal (*bottom*). So do its liver and kidneys.

Toxic mix

The python's ballooning organs represent one evolutionary extreme; the venom of the king cobra is another. The cobra, which occurs in India, China, and Southeast Asia, competes with the African black mamba and Australia's inland taipan for the title of the most dangerous snake on Earth. The initiative to sequence it came from Freek Vonk of the Naturalis Biodiversity Center in Leiden, the Netherlands, who picked the king cobra in part because it happens to be his favorite species (see story on p. 1164).

Vonk teamed up with Nicholas Casewell, an evolutionary biologist at Bangor University in the United Kingdom, and a large group of scientists at 15 other institutes. They not only sequenced the genome, but also measured gene activity in the venom gland and in the so-called accessory gland, a poorly understood gland through which the venom passes before it leaves the cobra's mouth.

Vonk and his colleagues discovered that the two glands have very different gene activity patterns. The accessory gland doesn't produce toxins but makes many different lectins, a group of proteins that bind carbohydrates. In some other snake venoms, toxic lectins are part of the mix, but in the cobra, lectins are never released into the venom. The accessory gland's role may be to activate the venom somehow, but "we really don't know" what lectins do exactly, Casewell says.

The venom gland itself relies on 20 gene families for its toxins. Examining the genes, the team discovered a few toxins known from other snakes but never before seen in cobras, such as nerve growth factor and an enzyme called phospholipase B; they also identified proteins unknown in any other snake venom, such as insulin-like growth factor. Its gene was active only in the venom gland, the researchers report—but they have no idea what role the growth factor might play in venom.

The scientists found that the genes for each toxin family were also used in other parts of the body in the snake's evolutionary past, and some are used even today. "These dangerous proteins are co-opted from elsewhere in the body and [are] turned into weapons and diversified," says Frank Burbrink, an evolutionary biologist at the City University of New York. Genes involved in blood clotting, for example, may have been turned on in the venom gland through some regulatory quirk, and now they help bring down the prey's cardiovascular system.

In some cases, the gene was modified and ceased to perform its original role; more often it was duplicated, setting the new copy free to evolve toxicity. Duplication "gives you more material for selection to work on," says developmental biologist Michael Richardson of Leiden University, the last author on the paper. Often, a gene was copied more than once, allowing each copy to mutate in different ways, yielding an ever more sophisticated mix.

That gives the snake an advantage in an evolutionary arms race. The cobra's prey evolve constantly as well, developing ways to resist the toxins. For snakes, this genetic competition can be deadly, because ineffective venom can enable potential prey to turn on the snake and kill it. By analyzing how genes in the venom families had changed over time compared to matching genes in the python, other snakes, and the green anole lizard—the only lizard species sequenced so far—the researchers showed that venom genes were under intense positive selection. "It's a great demonstration of natural selection at work on the genome," Vonk says. Jimmy McGuire, an evolutionary biologist at the University of California, Berkeley, calls the paper "a stunning piece of work, just amazing."

Castoe and his colleagues also documented broader evidence of rapid evolution in snake genomes. They compared the 7442 genes found as single copies in both the cobra and the python with the same genes in all other land vertebrates sequenced so far. The bottom line: Snake genomes have changed a lot—and they have changed very fast to meet the demands of their unusual lifestyles. In snakes, about 10 times more genes are under positive selection than in other vertebrates, Castoe says, meaning that mutations in those genes were likely advantageous.

The comparison enabled the researchers to pinpoint where in the evolutionary history of snakes these changes occurred: 516 of them in the common ancestor of cobras and pythons, most of them having to do with snakelike qualities such as left-right asymmetry in their organs and shifts in metabolism; 174 changes in the cobra lineage; and 82 in the python lineage. The scientists have only just begun to milk their data. They hope to sequence more snake genomes as well; Castoe is already planning to decipher the genome of a blind snake, which looks and lives much the way the first snakes likely did. Another 10 snake genomes are likely to come out within the next couple of years, Casewell says.

Greene says he can't wait. "Natural history has all of the questions," he explains, "but molecular biology has the key to the answers."

–ELIZABETH PENNISI

CREDITS (TOP TO BOTTOM): IAN MCDONNELL/ISTOCKPHOTO; STEPHEN M. SECOR (2)

Published by AAAS

Precious poison. A scientist collects venom from a Malayan pit viper.

From Toxins To Treatments

Researchers are hoping to find lifesaving drugs in the deadly venoms from snakes and other animals

SÃO PAULO, BRAZIL—If Kathleen Grego ever needs a reminder of the power of a snake's venom, she only has to look at her left thumb. A few years ago, the head of the herpetology department at the Instituto Butantan here was bitten by a jararacussu, a venomous pit viper. One of the snake's fangs sliced straight through her fingernail and discharged its deadly venom into her flesh. Grego was taken to the hospital down the road and immediately received antivenom, but her fingernail still bears a vertical scar and the top of her thumb looks like it has caved in on one side, where the toxins digested muscle and other tissue.

Grego could have lost a lot more than a bit of flesh. The peptides and proteins in jararacussu venom can latch on to molecules that regulate blood pressure and coagulation, causing a crash of the cardiovascular system and death. Other snakes produce toxins that wreak havoc in the cellular machinery of the nervous system, paralyzing the victim. Nature has had millions of years to perfect this molecular sabotage and turn snakes into accomplished killers.

But more and more researchers are studying venom's powers to heal rather than harm. Interfering in key pathways in the body is exactly what drugs are supposed to do, and hidden in the complex mixtures produced by snakes' venom glands are strings of amino acids that can dull pain, lower blood pressure, and more. Peptides yet to be found might prevent heart attacks or even treat cancer. "People have started realizing that there are a lot of very unique proteins with tremendous specificity in the venom of snakes," says Kini Manjunatha, a researcher at the National University of Singapore (NUS). "I am confident there will be more drugs from snakes."

The field has leaped ahead in recent years by combining two new technologies that help scientists quickly identify unknown peptides in venom: mass spectrometry and next-generation sequencing. And it's not just snakes that researchers are interested in. The number of venomous animals is estimated to be more than 170,000; even if the average venom contained just 250 peptides, a very conservative estimate, that's "a huge natural library" of more than 40 million compounds worth exploring, says Pierre Escoubas, a French researcher who started VenomeTech, a company that aims to produce drugs from venom.

Milking snakes

Precedents for the work go back to the 1960s, when Brazilian researchers studying the effects of venom from a lancehead viper found that it contained a range of peptides called BPFs that dramatically lowered blood pressure. Chemists at Bristol-Myers Squibb developed a small molecule, captopril, that mimics one of these peptides; it was the first of the so-called ACE inhibitors, which went on to earn billions of dollars and are used to this day.

In 1998, the U.S. Food and Drug Administration approved a blood thinner named eptifibatide, modeled on a rattlesnake peptide that binds to blood platelets and prevents them from aggregating in clots. A year later, a similar drug called tirofiban, inspired by a protein from vipers, hit the market. Several other drugs based on snake venom, including powerful painkillers, are now being tested in clinical trials.

The path to any such drug starts in a place like the Instituto Butantan, which breeds snakes and milks them for their venom. In one of the lab's rooms, three black plastic bins are set up on the floor in a neat row. Each of the bins contains several liters of CO_2, in which a snake is slowly falling into a daze. Grego's colleague Sávio Sant'Anna opens one of the containers; with a metal hook on a long wooden stick, he fishes out the snake, a gray viper with dark brown markings, and carries it over to a metal table.

With a swift movement, Sant'Anna grabs

CREDIT: VOLKER STEGER/SCIENCE PHOTO LIBRARY

Published by AAAS

the snake's head, forcing its mouth wide open. Then he pushes back the protective skin covering each of the snakes' fangs with a pair of tweezers and forces the teeth through a sheet of cellophane covering a glass flask. Gently massaging the venom glands helps milk the deadly venom, a few drops of which collect at the bottom of the flask.

Sometimes, researchers already know what to look for in their harvest—but it can be hard to find. Yara Cury, another researcher at the institute, had read early 20th century reports that the venom of the South American rattlesnake (*Crotalus durissus terrificus*) had an analgesic effect, and in the 1990s, she confirmed that it reduced pain in animal studies. But identifying and purifying the peptide responsible, now called crotalphine and in development by a Brazilian pharmaceutical company, took years. "Venoms can contain several hundreds or thousands of peptides," says Glenn King, who researches venom at the University of Queensland in Brisbane, Australia. "Looking at them one by one would take you a lifetime."

To identify the individual compounds, scientists now use mass spectrometry, breaking proteins into smaller fragments and then sorting them by weight. The fragments form "ladders" differing by one amino acid each; by determining the mass difference between adjacent fragments, researchers can, in theory, identify the amino acids and infer the peptide's sequence. "But current technology only allows you to do that for the smallest toxins, about 15 to 20 amino acids long," Escoubas says. Peptides don't break after every single amino acid, and snake toxins that are 40, 50, or even 60 amino acids long leave scientists with a plethora of possible solutions.

Sequencing technology can help scientists solve this puzzle by giving them a genetic template of the snake's toxic peptides. "You milk the hell out of the animal," King says. "Then you give it 3 days." During that time, the animal starts producing new venom by activating genes encoding the various venom peptides. Researchers sequence messenger RNA from the venom gland, fishing out any typical toxin patterns. With that list of sequences, they can go back to the mass spectrometry data and interpret it.

That's quite a revolution, Escoubas says. "Before, we were taking some venom from an animal and painfully doing some biochemistry on some peptides," he says. "Now we go to the coding language of the venom."

Online
sciencemag.org
Podcast interview with author Kai Kupferschmidt (http://scim.ag/pod_6163).

Blessing in disguise. Scientists recently reported that the venom of the Chinese red-headed centipede contains a powerful painkiller.

A wider net

So far, snake toxins have been the most popular study objects, partly because snakes produce larger amounts of venom than most other animals do. But the venom of spiders, scorpions, cone snails, or centipedes is just as interesting—or even more so. "There are only 1500 species of venomous snakes, but 50,000 species of venomous spiders," Escoubas says. Spiders also have more toxins per venom, probably because they prey on insects, a hugely diverse group of animals that requires an equally diverse arsenal. Species other than snakes have already yielded drugs. Ziconotide, a peptide in cone snail venom, was approved in 2004 to treat chronic pain; exenatide, isolated from the saliva of a venomous lizard called the Gila monster, has become a blockbuster drug for type 2 diabetes.

It's time to explore the toxic treasure trove more systematically, Escoubas says. He leads a partnership that received €6 million in E.U. funding in 2011 for VENOMICS, a 4-year project aiming to produce a library of venom peptides that can be screened for their therapeutic potential. The group plans to look at some 200 different venomous creatures, which should result in about 50,000 peptides, Escoubas says—a massive step up from the 3000 to 4000 venom peptides described in the past 50 years. (Of those 50,000, the group aims to produce 10,000 in the lab.) So far, they have analyzed venom from 70 animals, including snakes, spiders, and a centipede, collected in places like Tahiti and French Guiana.

Pain therapy is a particularly promising area, venom experts say. In 2006, researchers discovered that a mutation in Nav1.7, a protein channel that lets sodium flow into human cells, makes people insensitive to all types of pain. The finding excited pharmacologists about the prospect of treating pain by disrupting that channel, but finding small molecules that block Nav1.7 without affecting eight similar channels in humans has proven all but impossible.

Venomous animals, however, seem very adept at doing exactly that. In September, King and colleagues from China reported in the *Proceedings of the National Academy of Sciences* that a string of 46 amino acids from the venom of the Chinese red-headed centipede specifically blocked Nav1.7 and acted as a strong painkiller in rodents. The molecule is "absolutely deadly to insects," King says, but in humans it could lead to a powerful pain therapy.

Winding road

Identifying a promising compound in venom is often only the beginning of a long, winding road. Used as drugs, peptides have the advantage that they can be more selective than small molecules, leading to fewer side effects, says Björn Hock, a peptide engineer at Merck, but they have several drawbacks: They're expensive to make, they sometimes elicit immune reactions, and, perhaps the biggest stumbling block, they usually need to be injected because they are broken down in the stomach when taken orally. That's why most future drugs based on snake venoms will, like captopril, be small molecules that mimic the function of the original peptide, predicts Johannes Eble, who researches the effect of snake venom on cell adhesion molecules at Frankfurt University Hospital in Germany.

But Escoubas is convinced that peptides' problems can be addressed. Peptide chemistry has greatly improved, making synthesis cheaper, and the injection pens developed for insulin show that drugs don't have to be a pill or a capsule to be successful.

Published by AAAS

Exenatide is a case in point, King says: "Who would have thought that a 37-residue peptide drug with bad stability would become a billion-dollar drug?"

Moreover, some venom peptides may be stable enough to be taken orally. Many have multiple disulfide bonds, bridges between the sulfur atoms in the amino acid cysteine, that make the peptide stable enough to resist degradation by the enzymes in gastrointestinal juices, King says. A toxin derived from cone snails that's under investigation to treat neuropathic pain was recently shown to work when taken orally.

NUS's Manjunatha, meanwhile, has discovered an analgesic peptide developed from king cobra venom that he says is 20 to 200 times more potent than morphine—and active orally. Placed under the tongue, the 11 amino acid peptide is absorbed by the mucosal membrane, he says.

Manjunatha, who has patents on dozens of other snake peptides, was born and brought up in a small village in India surrounded by forests. "A lot of people lost their limbs or died" from snakebites, he says. When he started out as a researcher, he wanted to understand what makes toxins so dangerous: "Why are human proteins helpful and snake venom proteins so harmful?" Now, Manjunatha says he realizes an even more interesting question is which of those lethal snake peptides can help humankind most. **–KAI KUPFERSCHMIDT**

CREDIT: NATURALIS BIODIVERSITY CENTER

The Freek Show

Snake scientist Freek Vonk can't choose between research and starring in wildlife documentaries. And so far, he doesn't have to

LEIDEN, THE NETHERLANDS—On an October afternoon, a throng of children is waiting expectantly at the entrance of the Naturalis Biodiversity Center, a museum and research center just outside the city center. At 2 p.m. sharp, a green Land Rover pulls up, a door swings open, and a tall, blond young man jumps out. He's wearing jungle boots, khaki shorts, and a denim shirt—as if he were on safari in Africa instead of in an academic town. A platinum blonde-haired woman emerges from the passenger seat, and soon the couple is mobbed by kids screaming for autographs.

The man is Dutch biologist and snake scientist Freek Vonk, and he has just arrived at his workplace, along with his girlfriend, talk show host Eva Jinek. He's in safari gear because he is opening a new exhibition at the center. *Freek's Favorites* showcases 45 animal species that fascinate Vonk; Naturalis has invited kids and their parents to come celebrate.

At 30, Vonk has already built a respectable career studying snakes—animals he has been obsessed with for half his life. He has a couple of *Nature* papers to his name, and he is the first author on a study of the king cobra genome, published this week in the *Proceedings of the National Academy of Sciences* (*PNAS*) (see story on p. 1160). But here in the Netherlands, Vonk is known primarily as a TV celebrity. His wildlife shows air every day, and Naturalis has made Vonk its public face.

Just how Vonk—whose first name is pronounced "Frake"—manages to combine research and showmanship is baffling to some. He credits his attention deficit hyperactivity disorder, which made it hard to get through high school but now prevents him from ever doing nothing. "It's always go, go, go. It's nonstop with Freek," confirms Nicholas Casewell of Bangor University in the United Kingdom, a co-author of the new paper. In 2014, Vonk plans to further study the evolution of cobra venom, but he will also be filming abroad for 4 months.

Vonk's shows are about animals, ecology, evolution—but they're also adventures, presented with an un-Dutch touch of machismo. He wrestles with crocodiles, yanks snakes from their hiding places, and bares his torso for a bath in the Amazon after a day in the jungle. Many say he seems to be emulating one of his childhood heroes, Steve Irwin, an Australian conservationist known for his exciting wildlife documentaries. (Irwin died in 2006 after a stingray pierced his chest.)

It's a style not everybody likes. "You don't have to jump on crocodiles or show what a daredevil you are," says experimental

Published by AAAS

zoologist Johan van Leeuwen of Wageningen University in the Netherlands. Vonk is "a very good biologist," Van Leeuwen adds, "but if he's trying to become like Irwin, he's on the wrong path."

But Vonk says his "hands-on approach" shows nature's exciting side and can promote conservation and raise interest in living things. During the opening ceremony at Naturalis, he puts a living snake around a boy's neck but also urges his young audience to consider a career in biology. The kids are impressed. "Freek loves animals. He isn't afraid of anything," a young fan says. "And he was bitten by a shark!"

Bitten by a passion

Two weeks later, on the terrace of a trendy cafe in Amsterdam, Vonk sets down his Heineken to show three impressive scars on his right hand. His crew was filming blacktip sharks off the South African coast earlier this year when one of the animals mistook his moving hand for a fish, he says. "Fortunately I resisted the impulse to pull back. He let go pretty quickly."

Over dinner, Vonk explains how his two disparate careers got started when, at age 15, he was enthralled by a snake belonging to a friend's brother. "They're so different than any other animal," he says, "that long limbless body, that little tongue that's always moving back and forth. … There's this cloud of mysticism surrounding them."

"If the snake is in, I'm out," his mother declared when he told his parents he wanted a snake, too. She soon gave up her opposition, however, figuring it would be best to let her son follow his passions. After high school, Vonk studied biology at Leiden University—mostly as a way to learn more about snakes. For his bachelor's degree, he wanted to do a research project at the lab of developmental and evolutionary biologist Michael Richardson. "I told him that we don't really do reptiles," Richardson recalls, "but that we'd be happy to make some room in a corner of the lab."

Vonk started comparing histological sections from the venom glands of various lizards, as part of a broader study on venom evolution in lizards and snakes by Bryan Fry of the University of Melbourne. Their paper, with Vonk as fourth author, was published by *Nature* in 2006. His master's work, also in Richardson's lab, led to another *Nature* paper, with Vonk as the first author, on the evolution of fangs. A striking picture of a Lataste's viper landed it on the cover.

Both papers triggered a wave of local media attention, and journalists discovered that the enthusiastic young researcher had charisma and a knack for storytelling. A

Cover boy. Vonk posed with one of his own pythons for an interview in a Dutch newspaper.

popular prime-time talk show contracted him to bring an animal—usually a scary one—into the studio on a regular basis and talk about it. The formula made some biologists wince but proved hugely popular. In 2009, Vonk was approached by a TV producer who wanted to take him to Africa to produce a series aimed at kids. *Freek in the Wild*, as the show is now called, became a huge success. This month, he will start filming a new prime-time series targeting adults, *Freek in Australia*.

With the fame came a stream of interview requests. The fact that Jinek, his girlfriend, is a well-known TV personality has added to Vonk's appeal. "Now the gossip press is after me as well," he says.

Mr. Science

Four weeks after its tumultuous opening, *Freek's Favorites* has sent visits to Naturalis soaring, says its director, Edwin van Huis. Van Huis hired Vonk last year, weeks after he finished his Ph.D., offering him a half-time job. Vonk also has a starring role in a new crowd-funding campaign to buy a *Tyrannosaurus rex* skeleton dug up by Dutch researchers in Montana this year. If Naturalis can raise the €5 million to €7 million it needs to buy the fossil, it will be the first *T. rex* on permanent display in Europe.

Van Huis says he hired Vonk primarily because he's a good scientist, "but we also like the way he can reach people with his enthusiasm. Freek represents what Naturalis is all about." Vonk's high-octane style may seem to clash with the museum's almost 200-year tradition, but Van Huis says he hopes it will attract a broader and younger audience. "I'm an old fart myself, I grew up with David Attenborough," says Van Huis, referring to the iconic British documentary maker. "But young people don't like that style anymore."

Managers at Dutch reptile shelters raised another worry about Vonk's work in a newspaper story 2 weeks ago: They said his shows may entice people to get reptiles they don't know how to take care of, which then get dropped at their facilities. Vonk, stung by the story, says he has always conveyed the opposite message: "Don't take a snake lightheartedly. It's not for everyone."

Vonk wants to combine his two careers as long as he can: "If I don't have to choose, why would I?" In the long run, he's hoping for an international audience. Talks with Discovery and National Geographic a few years ago didn't pan out; one problem is that his English isn't good enough. He hopes to improve it by living in the United States for a year. "I need to start thinking in American," he says.

Risky business

Vonk won't show off the collection of snakes he still keeps in his apartment in The Hague. "I don't want to talk about snakes in captivity," he says, and he's worried about being seen as a hobbyist. He's moving out soon and is now giving away most of his animals. He'll keep his king cobras, however, the species he loves best and whose genome is analyzed in this week's *PNAS* paper. "I figured we might as well choose an icon to sequence": the largest venomous snake and an endangered species. "They're very intelligent," he adds. "When they're looking at you, you can see that they're thinking, anticipating."

They're also very dangerous. A friend of Vonk's, British snake breeder Luke Yeomans, died in 2011 after being bitten by a king cobra in his snake sanctuary. Yeomans's widow donated six of his cobras to Vonk—although not the one that killed his friend.

The tragedy drove home the risks of his own work, Vonk says. He has had his share of mishaps, including two bites by venomous snakes. There was that shark, of course, and a few other close encounters. The one that most impressed him was with a Cape cobra, one of Africa's most dangerous snakes. Lying on the ground, a small camera mounted on his head, Vonk was taunting the snake to film how it responded, when suddenly it lunged at him, so close to his face that he could feel a breeze as its fangs raked the air. "If it had bitten me, I would have had a real problem," he says.

He now asks his producer to say "Cape cobra" whenever he's taking too much risk just to get a good shot. "It means: Watch out, Freek," he says. "You're going too far."

–MARTIN ENSERINK

CREDITS (TOP TO BOTTOM): GLOBALP/ISTOCKPHOTO; COURTESY OF *VOLKSKRANT*/CORNELIE TOLLENS

Published by AAAS

Island of The Snakes

The invasive brown tree snake has devastated Guam's ecosystems. Can it be eradicated?

As the leader of a specialized team of snake hunters based on Guam, biologist James Stanford was used to getting calls at odd hours. Early in the morning on 20 March 2005, his cellphone rang. On the line was a worried official with the Division of Fish & Wildlife on Saipan, one of the Northern Mariana Islands, some 200 kilometers away. He urgently needed Stanford's help.

The previous night, just after 1 a.m., a flight attendant had glimpsed a meter-long snake slithering off the runway at Saipan International Airport. The plane had come from Guam. Alarmed, her supervisor immediately called a government hotline set up to protect Saipan's native wildlife from invasive predators. Guam is a stronghold of the invader that its island neighbors fear most: the brown tree snake.

Since arriving on Guam, a U.S. territory in the western Pacific, in the 1940s, brown tree snakes (*Boiga irregularis*) have extirpated native birds, bats, and lizards and disrupted entire ecosystems. Although harmless to adult humans, they have slipped into houses and tried to swallow infants' arms, sickening them with mild venom. By crawling onto power lines, the snakes have caused up to 200 blackouts a year, electrocuting themselves in the process.

To prevent the spread of brown tree snakes, the U.S. Department of Agriculture (USDA) inspects all cargo leaving Guam and kills snakes in the forests surrounding ports and runways. The U.S. Geological Survey (USGS) runs a rapid response team, headed by Stanford until earlier this year, to help investigate sightings on other islands.

The report from Saipan sounded credible, so Stanford didn't hesitate. He grabbed the packed suitcase he always kept at home, and after picking up some search equipment and a trained Labrador retriever, he and three other biologists with USGS caught the next flight to Saipan. Their mission: Find any snakes and kill them.

That's not easy. Even when brown tree snakes are abundant, as on Guam, it is hard to know how many there are. But years of research on Guam have provided unique and valuable insights into tracking snake populations, says J. D. Willson, an ecologist at the University of Arkansas, Fayetteville.

Monitoring the snakes will be crucial to the next challenge: beating them back. Researchers are now testing new tools. In September, USDA started dropping poisoned bait from helicopters into fenced-off forests. This approach, some say, finally raises the possibility of eradicating the brown tree snake from Guam.

Invade and conquer

In the summer of 1944, the U.S. military was amassing forces in the Pacific to advance the battle against Japanese troops. Materiel from the Admiralty Islands of Papua New Guinea was transported to large Navy and Air Force bases on Guam. The brown tree snake, native to Papua New Guinea, came along for the ride.

Away from its usual predators—thought to include large monitor

Looking up. Research has improved the ability to find tree snakes.

CREDIT: BJORN LARDNER

Published by AAAS

lizards and feral pigs—and in a climate that allows year-round reproduction, the snake went wild. The native fauna was clueless, because the only endemic snake on the island was a blind, harmless species. By the 1970s, many bird populations began to collapse. Without birds to eat spiders, forests grew thick with webs. When USGS biologist Gordon Rodda first visited Guam's forests in 1987, "it was like being parachuted onto another planet," he recalls.

At first, most scientists blamed disease, such as avian malaria, which afflicted Hawaii. It took years of research by ecologist Julie Savidge of Colorado State University, Fort Collins, to reveal the true culprit. "I had a terrible time convincing people that tree snakes were responsible," she says. One reason was that the snakes seemed to be rare. "The number of snakes you see has little to do with the number of snakes that are there," Willson says.

When they followed up on Savidge's work in the 1980s, Rodda and other federal biologists were astounded to discover the density of brown tree snakes. Tropical forests typically contain one or two snakes per hectare; on Guam, biologists could trap 55 brown tree snakes per hectare. Having polished off native species, the snake had found other sources of food, including rats and other introduced wildlife. It is also an extraordinary generalist that has been caught scavenging soiled diapers and used tampons.

Authorities on other Pacific islands began to fear what could happen if the snakes spread. USDA's Animal and Plant Health Inspection Service started an interdiction program on Guam in 1993 and fenced off loading areas at ports and airports. Ever since, inspectors have patrolled nightly with spotlights. Every piece of cargo leaving the island is searched by teams of Jack Russell terriers, agile and energetic snake hunters. And each week, traps baited with caged, live mice are placed on the fences and in nearby forests. Some of the traps have poisoned bait: dead mice stuffed with 80 milligrams of acetaminophen, a widely used pain reliever that kills a snake in about 24 hours. Since 1993, the combined efforts have caught more than 150,000 brown tree snakes. Those that are trapped, rather than poisoned, are euthanized.

The government and university researchers who have developed these control measures have also investigated the snake's biology and improved their survey methods. A unique experimental facility has helped tremendously. In 2004, USGS enclosed a 5-hectare site with a snake-proof fence. Rodda and his colleagues then captured all 122 snakes inside and implanted each one with a transponder tag. As a backup, they also marked each animal by clipping a unique pattern of scales, a classic method in herpetology.

Defense line. Fences, traps, and constant vigilance are needed to prevent tree snakes from sneaking off the island of Guam.

The setup has allowed the team to test traps and other control tools on a real-world population. One important conclusion is that the traps rarely collect small snakes. As it turns out, young snakes don't like the mice used as bait; they prefer geckos. Unfortunately, baiting traps with geckos would be too expensive, so catching young snakes by hand is the only way to get them.

Thanks to the testing ground, scientists have honed their ability to catch snakes. During searches, teams of experts and volunteers fan out, armed with hooked staffs to pull snakes from branches. They spend hours aiming their headlights into the trees, looking for the sheen of snakeskin.

Over the years, the team has identified some two dozen factors that can help or hinder the search. For example, a moonless night increases the odds of success by 20%, as does a calm night without fluttering leaves. Even the type of headlamp makes a difference. Snake hunting still takes twice as much time per snake caught as using traps, but it has become more effective. As a result, even though Stanford's team didn't find the reported snake on Saipan after 2 weeks of nightly searching, they could be confident that the island didn't harbor a population.

Attack from above

Now, a new phase in the battle has begun. USDA wants to scale up the use of poison bait, so its officers are strapping dead rodents to pieces of cardboard attached to biodegradable streamers. When tossed from a helicopter, the mice get snagged in the tree canopy, available to tree snakes but not to animals on the ground. This could be an easier way to kill snakes in remote or rugged terrain.

Initial tests were promising. Dozens of mice were dropped on a 6-hectare site last year, some of them with tiny radio transmitters implanted. All 30 snakes that ate bait with transmitters died, the researchers reported last fall. (A toad and monitor lizard had also eaten one toxic mouse each, but did not appear to be the worse for it.) In September, USDA expanded the tests to two 55-hectare fenced sites on Andersen Air Force Base. Helicopters will drop bait there every few weeks for 16 months. Researchers will compare the snake populations to those at a nearby reference site.

The ultimate aim is to eradicate the brown tree snake from the island. "We are nowhere near that goal," says Daniel Vice, USDA's supervisory wildlife biologist in Barrigada, Guam. Among the hurdles are the island's considerable size—it's two-thirds the size of New York City—and the biology of the snake. Females often hide out for months after mating and can store sperm for years, producing new offspring even if the males have been extirpated. Visual searches alone can't confirm success; for the 5-hectare USGS plot, for example, it would take 42 searches, each requiring 36 person-hours, to be 95% certain that the last snake had been found.

But Robert Reed of USGS in Fort Collins isn't discouraged. He expects that aerial poisoning will sharply reduce the snake population across the landscape. Even without full eradication, that might allow restoration of native birds, some of which persist in zoos. "I think it will become possible at some point," says Daniel Simberloff, an invasive species biologist at the University of Tennessee, Knoxville. And as snakes' numbers dwindle, other islands need to worry a little less about suffering Guam's misfortune.

–ERIK STOKSTAD

CREDITS (TOP TO BOTTOM): AMWU/ISTOCKPHOTO; USDA/FLICKR

Published by AAAS

LETTERS

edited by Jennifer Sills

Science Communication: Narratively Speaking

IN THE NEWS STORY BY J. COHEN "GREAT PRESENTERS: LIGHTING UP THE AUDITORIUM" (SPECIAL section on Communication in Science, 4 October, p. 78), Bonnie Bassler includes in her rules of presentation, "Tell stories." As a scientist turned filmmaker who specializes in making content meaningful and memorable, I could not agree more. But how? The power of storytelling rests in the specifics, so to answer this question, let me tell you a story.

In the fall of 2013, I was recruited to give a makeover to the plenary panel discussion for the 2013 meeting of the Coastal and Estuarine Research Federation (CERF). The organizer told me that she wanted me to do my "story thing."

Within two days, the other two presenters and I were embroiled in an e-mail battle—neither of them wanted to change their standard presentations. So I quit. But then they reconsidered, kindly assuring me that they had given enough successful presentations in their careers and could afford one debacle.

By shifting from e-mail to telephone meetings, we immediately found common ground, which grew into friendship. Acting as a stage director, I asked them—the actors—to present their material to me, and I then began shaping the new structure and focus.

We changed the title from "Responding to Sea Level Rise" to "Sea Level Rise: New, Certain, and Everywhere." We then set about crafting three "stories" around these keywords by rearranging the content to create better narrative structure. We took material that began as a list of facts (in the style of And, And, And), and we molded it into stories using the universal narrative template: And, But, Therefore (ABT) (*1*). Once the "But" and "Therefore" are added [a technique lifted from "South Park" co-creator Trey Parker (*1*)], the format takes a shape that conveys tension and resolution—the crucial elements of a great story. For example, we streamlined the facts supporting new sea level rise into the premise: "Sea level was relatively stable for 8000 years AND coastal communities were built on the assumption of stability, BUT over the past 150 years the level has been rising. THEREFORE, a new approach to coastline management is needed." To further engage our audience, we asked scientists in advance to contribute thoughts and photographs in ABT style through the CERF Web site (*2*), and we incorporated their submissions into the presentation. A month later, our plenary panel packed the 1000-seat ballroom at CERF and received rave reviews (watch the video at http://vimeopro.com/cerfvideo/cerf2013).

My fellow presenters and I learned a lot from this. First, it is possible for an old dog to teach old dogs new tricks. Second, you get back what you invest; we had four lengthy conference calls and two rehearsals before the event. None of us had ever devoted this much effort to a presentation. Third, everyone can and should incorporate narrative structure to their science communication endeavors.

Scientists must overcome the problem of "storyphobia." Recent research shows that narrative structure enhances brain activity (*3*). We have created a world that is awash in information, the meaning of which could be lost if we don't work to process it through narrative structure. It is essential for today's world of rapid communication and must become second nature to scientists to ensure effective communication.

RANDY OLSON

Prairie Starfish Productions, Raleigh Studios, Hollywood, CA 90038, USA, and Wrigley Institute of Environmental Studies, University of Southern California, Los Angeles, CA 90089, USA. E-mail: info@randyolsonproductions.com

References

1. Randy Olson Great Challenges Day at TEDMED 2013 (www.youtube.com/watch?v=ERB7ITvabA4).
2. CERF 2013, Sea Level Rise—New, Certain, and Everywhere (www.sgmeet.com/cerf2013/responding_to_sea_level.asp).
3. U. Hasson *et al.*, *Projections* **2**, 1 (2008).

Science Communication: Power of Community

J. BOHANNON'S NEWS STORY "WHO'S afraid of peer review?" (special section on Communication in Science, 4 October, p. 60) incriminates many open-access (OA) journals. Our journal, *PLOS ONE*, was not implicated. It rejected the fraudulent paper promptly and for the right reasons, as Bohannon acknowledges. Still, the "study" was disappointing: It was not controlled, which would have required seeking to entrap a matched set of closed-access journals, yet it claims that a source of the problem is open access. It then concludes that profitability for OA journals is driven by volume, without acknowledging that the same is true for closed-access journals. The issues raised by Bohannon's exercise are not about open-

Letters to the Editor

Letters (~300 words) discuss material published in *Science* in the past 3 months or matters of general interest. Letters are not acknowledged upon receipt. Whether published in full or in part, Letters are subject to editing for clarity and space. Letters submitted, published, or posted elsewhere, in print or online, will be disqualified. To submit a Letter, go to www.submit2science.org.

CREDIT: AAAS

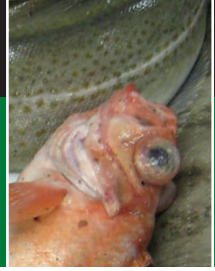

Fisheries-induced evolution
1176

SciLifeLab Prize
1185

access journals; they are about science and technical publishing and the peer-review processes used throughout the industry.

In the short term, all scientific publishers have a responsibility to reinforce and strengthen prepublication review. We must improve the efficiency of peer review and continue to perform checks that uncover conflicts of interest, identify financial disclosures, confirm author affiliations, and ensure compliance with international standards of animal and human testing.

Even with these tools, peer review will never be flawless. As *Science* Editor-in-Chief Marcia McNutt points out, it is "time-honored" and the "gold standard" ("Improving scientific communication," Editorial, 4 October, p. 13), but that doesn't mean our methods of evaluation can't and shouldn't be improved. This is the real challenge. And this is why the Public Library of Science (PLOS) is working to transform scientific communication by developing better measures of scientific quality both before publication (currently traditional peer review) and after publication (currently the dreaded impact factor).

To this end, PLOS is developing article-level metrics that enable the scientific community itself to confer on a research contribution its credibility, relevance, and importance, independent of the journal in which it is published. Peer review at its best is a continual process of critique and assessment.

ELIZABETH MARINCOLA
Chief Executive Officer, The Public Library of Science, San Francisco, CA 94111, USA. E-mail: emarincola@plos.org

Science Communication: Quality at Stake

THE FERMENT IN THE SCIENTIFIC PUBLISHING world was nicely illuminated in J. Bohannon's News story "Who's afraid of peer review?" (special section on Communication in Science, 4 October, p. 60). Bohannon revealed how the open-access (OA) movement may have had the unintended consequence of undermining quality peer review. The proliferation of certain OA journals that publish as many papers as possible to maximize their revenue has led to the publication of much mediocre science; it has also led to increased competition for the best papers, weakening established journals published by scientific societies, which insist on rigorous peer review. The traditional subscription-based model for financing scientific journals had the advantage of incentivizing quality: Why would a subscriber want to pay for a journal that publishes junk science?

We fully support open access. The public should have access to the science that its tax dollars fund. But it is equally important to assure quality control and to develop a new financial model that does not place the full OA page charge burden on authors.

LESLIE M. LOEW[1]*† AND DA-NENG WANG[2]‡
[1]Center for Cell Analysis and Modeling, University of Connecticut Health Center, Farmington, CT 06030, USA. [2]Skirball Institute of Biomolecular Medicine, New York University School of Medicine, New York, NY 10016, USA.
*Corresponding author. E-mail: les@volt.uchc.edu
†Editor in Chief, *Biophysical Journal*
‡Chair, Biophysical Society Publications Committee

Science Communication: Flawed Citation Indexing

WE USED A STRATEGY SIMILAR TO THE ONE used by J. Bohannon ("Who's afraid of peer review?," News, special section on Communication in Science, 4 October, p. 60) to uncover the dangers encountered in open-access bibliometric tools offered by Google Scholar. We uploaded fake documents authored by a nonexisting researcher to the Web to test the capacity of Google Scholar Citations and Metrics to detect false documents and citations. As a result of these documents, the number of citations received by our research group was boosted, affecting the Google Scholar profile of 47 researchers and 52 journals (*1*). The main problem is that these tools rely on automatic indexing, retrieving any document uploaded to an academic Web domain. The controlled environment in which scientific knowledge is reasonably well controlled by peer review and journal selection processes has shifted toward an open environment in which we rely on our trust in each individual researcher's conscience.

The pressure felt by editors and authors to perform well according to bibliometric indicators fueled by national evaluation agencies has already led some editors to artificially boost the citations received by their journals (*2*). Although fraud cannot be fully avoided by any control system, citation indexes in general, and those developed by Google in particular, should be transparent, exposing those who indulge in malpractice.

EMILIO DELGADO LÓPEZ-CÓZAR,[1,2] NICOLÁS ROBINSON-GARCÍA,[1]* DANIEL TORRES-SALINAS[2,3]
[1]Evaluación de la Ciencia y de la Comunicación Científica (EC3), Departamento de Información y Documentación, Universidad de Granada, 18071, Spain. [2]EC3Metrics, Granada, 18002, Spain. [3]EC3, Centro de Investigación Médica Aplicada, Universidad de Navarra, Pamplona, 31008, Spain.
*Corresponding author. E-mail: elrobin@ugr.es

References

1. E. Delgado López-Cózar, N. Robinson-García, D. Torres-Salinas, *J. Am. Soc. Inform. Sci. Technol.* (http://arxiv.org/ftp/arxiv/papers/1212/1212.0638.pdf).
2. R. van Noorden, J. Tollefson, *Nature* **500**, 510 (2013).

Science Communication: Self-Publishing's Benefits

THE NEWS STORY "THE SEER OF SCIENCE PUBLISHING" (T. Rabesandratana, special section on Communication in Science, 4 October, p. 66) draws attention to *F1000Research*, a

TECHNICAL COMMENT ABSTRACTS

Comment on "Poverty Impedes Cognitive Function"

Jelte M. Wicherts and Annemarie Zand Scholten

Mani *et al*. (Research Articles, 30 August, p. 976) presented laboratory experiments that aimed to show that poverty-related worries impede cognitive functioning. A reanalysis without dichotomization of income fails to corroborate their findings and highlights spurious interactions between income and experimental manipulation due to ceiling effects caused by short and easy tests. This suggests that effects of financial worries are not limited to the poor.

Full text at http://dx.doi.org/10.1126/science.1246680

Response to Comment on "Poverty Impedes Cognitive Function"

Anandi Mani, Sendhil Mullainathan, Eldar Shafir, Jiaying Zhao

Wicherts and Scholten criticized our study on statistical and psychometric grounds. We show that (i) using a continuous income variable, the interaction between income, and experimental manipulation remains reliable across our experiments; (ii) our results in the cognitive control task do not appear driven by ceiling effects; and (iii) our observed post-harvest improvement is robust to the presence of learning.

Full text at http://dx.doi.org/10.1126/science.1246799

Comment on "Poverty Impedes Cognitive Function"

Jelte M. Wicherts[1]* and Annemarie Zand Scholten[2]

Mani *et al*. (Research Articles, 30 August, p. 976) presented laboratory experiments that aimed to show that poverty-related worries impede cognitive functioning. A reanalysis without dichotomization of income fails to corroborate their findings and highlights spurious interactions between income and experimental manipulation due to ceiling effects caused by short and easy tests. This suggests that effects of financial worries are not limited to the poor.

Mani *et al*. (*1*) recently presented four laboratory experiments and a field study that aimed to show that poverty impedes cognitive functioning. We criticize their results on statistical and psychometric grounds.

Mani *et al*. ran three randomized experiments in which U.S. adults were assigned to read one of two sets of financial scenarios that differed in their activation of financial concerns. Although participants' income varied from $7560 to $160,000, Mani *et al*. used a median split to analyze income data. This procedure has been criticized strongly for being associated with lower power, loss of information on individual differences, and its inability to pinpoint nonlinear relations (*2*). Of the two measures of cognitive functioning in Mani *et al*.'s studies, only the Raven's scores are fairly symmetrically distributed. We therefore submitted these data to linear regressions involving family income (mean-centered to facilitate interpretation) and an interaction between income and the type of scenario. Results are given in Table 1. In none of the three core experiments (1, 3, and 4) was the interaction significant when analyzed without unnecessary dichotomization of income. We also analyzed data from study 2, which aimed to show that the effect of poverty-related worries could be distinguished from a form of test anxiety and would not occur in similar, but nonfinancial, scenarios. We note that the second experiment is appreciably smaller ($N = 39$ people) than the other three experiments ($N > 95$ people) and so is associated with lower statistical power. Of importance are the regression weights; those from study 2 are not appreciably different than those in the core studies.

The second measure of cognitive functioning employed by Mani *et al*., cognitive control, showed nonnormal distributions that render them unsuitable for linear analyses (see Fig. 1). The measure was developed specifically to assess cognitive control among children and showed clear ceiling effects, as it did in earlier work involving adults (*3*). Because higher-income adults outperform lower-income adults, the easiness of the control test is particularly problematic in the higher-income range; more than half of the participants in the above-median income group acquired a perfect or near-perfect score (11 or 12 correct out of 12 items). In fact, the negative skew was so extreme that satisfactory normalization of the scores using a Box-Cox transformation was impossible. However, if the transformed, platykurtotic scores are subjected to a linear regression, the interaction is no longer significant in two of the three core experiments. Had the test been able to discriminate between higher levels of cognitive control, the difference between financial scenarios might have been established for the rich participants also. Hence, the core interaction that was meant to indicate that the poverty-related scenario only affected the poor may be an artifact of the cognitive control test's being too easy (*4*, *5*). Latent variable modeling could be used to deal with such issues (*6*–*8*).

We note that a highly relevant potential confound in the field study presented by Mani *et al*. is the possibility of retesting effects. The lack of any retesting effect in Mani *et al*.'s field study involving Indian farmers is clearly at odds with one of the more robust findings in the literature on cognitive testing (*9*). Retesting effects on the Raven's tests are particularly profound among test-takers with little education (*10*).

Mani *et al*. go beyond the data by concluding that "The poor…are less capable not because of inherent traits, but because the very context of poverty…impedes cognitive capacity." We note that the correlation between income and IQ also appears in longitudinal studies in which IQ was measured years before incomes (*11*). Further research is needed to fully grasp whether poverty indeed affects cognitive performance, as proposed by Mani *et al*., or whether the effect found in their experiments is a test artifact.

The stronger cognitive impediment experienced by the poor could merely be the result of an inappropriate statistical test and an overly easy cognitive control measure. The latter could obscure an equally "threatening" effect in the rich, simply because they were unable to obtain higher scores when not threatened. With such methodological issues remaining to be addressed, the authors' proposal of far-reaching policy changes, such as timing HIV educational campaigns to harvest cycles, seems premature.

Table 1. Linear regressions of Raven's accuracy on mean-centered income and scenario and the interaction between income and scenario. Income is mean-centered to improve interpretability and avoid multicollinearity. Conditional and unconditional bootstrapping corroborated these results. *B* indicates unstandardized regression weight, with standard error (SE).

Experiment	Predictor	*B*	SE	*t*	*P*
1	Intercept	0.414	0.026	15.98	<0.001
	Hard scenario	−0.042	0.037	−1.13	0.260
	Family income (centered)	0.001	0.001	1.18	0.242
	Scenario X family income	0.002	0.001	1.75	0.084
2	Intercept	0.411	0.036	11.40	<0.001
	Hard scenario	−0.032	0.050	−0.63	0.535
	Family income (centered)	0.000	0.002	−0.05	0.964
	Scenario X family income	0.002	0.002	1.04	0.308
3	Intercept	0.416	0.033	12.68	<0.001
	Hard scenario	−0.098	0.046	−2.16	0.033
	Family income (centered)	0.001	0.001	1.26	0.209
	Scenario X family income	0.002	0.001	0.99	0.323
4	Intercept	0.449	0.031	14.54	<0.001
	Hard scenario	−0.085	0.045	−1.91	0.060
	Family income (centered)	0.001	0.001	1.26	0.211
	Scenario X family income	0.002	0.001	1.40	0.164

References

1. A. Mani, S. Mullainathan, E. Shafir, J. Zhao, *Science* **341**, 976–980 (2013).
2. R. C. MacCallum, S. Zhang, K. J. Preacher, D. D. Rucker, *Psychol. Methods* **7**, 19–40 (2002).

[1]Jelte Wicherts, Department of Methodology and Statistics, Tilburg University, P.O. Box 90153, 5000 LE, Tilburg, Netherlands. [2]Department of Child Development and Educational Sciences, University of Amsterdam, Amsterdam, Netherlands.

*Corresponding author. E-mail: j.m.wicherts@uvt.nl

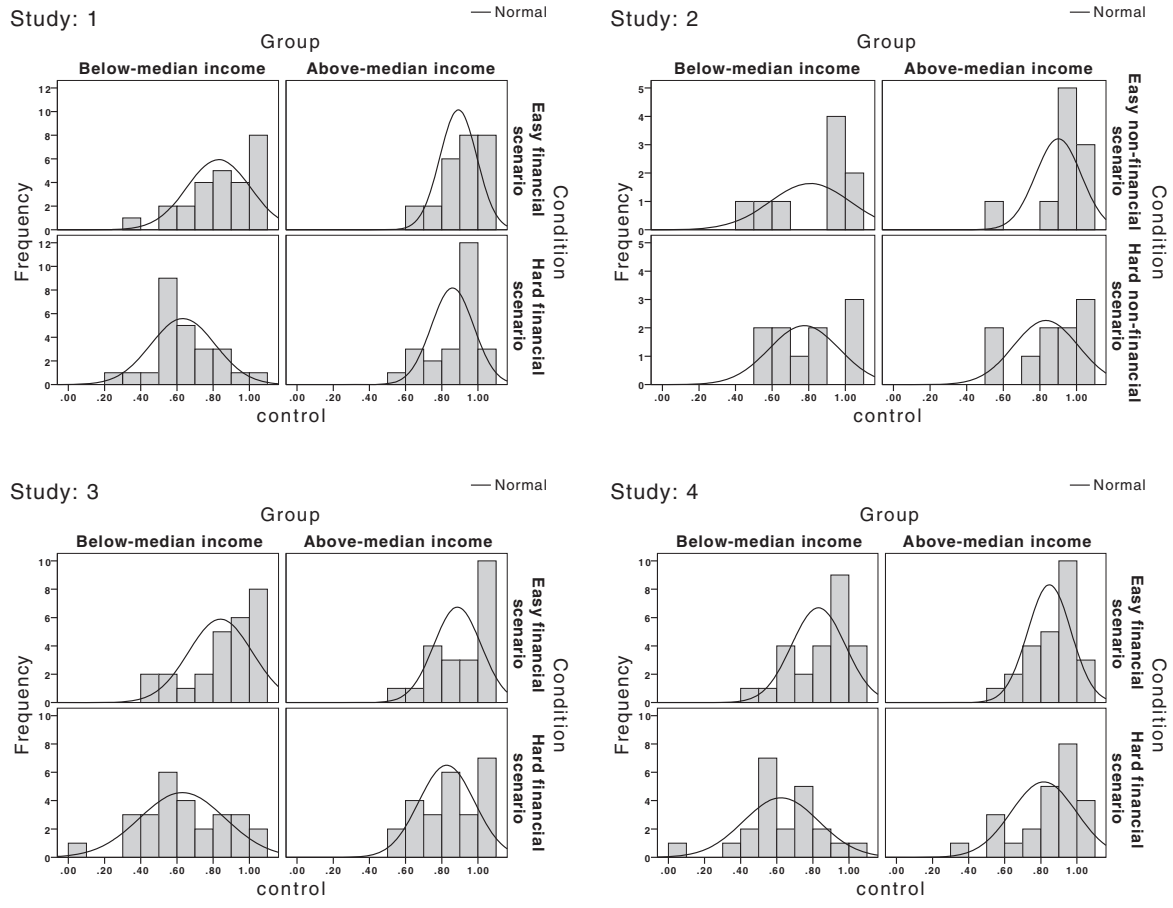

Fig. 1. Histograms of scores on the Cognitive Control test scores for easy and hard scenarios and the above- and below-median income groups in studies 1 to 4 from Mani *et al*.

3. M. C. Davidson, D. Amso, L. C. Anderson, A. Diamond, *Neuropsychologia* **44**, 2037–2078 (2006).
4. S. Kang, N. Waller, *Appl. Psychol. Meas.* **29**, 87–105 (2005).
5. S. Embretson, *Appl. Psychol. Meas.* **20**, 201–212 (1996).
6. J. M. Wicherts, C. V. Dolan, D. J. Hessen, *J. Pers. Soc. Psychol.* **89**, 696–716 (2005).
7. J. M. Wicherts, W. Johnson, *Proc. Biol. Sci.* **276**, 2675–2683 (2009).
8. J. M. Wicherts, A. Zand Scholten, *Intelligence* **38**, 169–178 (2010).
9. J. P. Hausknecht, J. A. Halpert, N. T. Di Paolo, M. O. Moriarty Gerrard, *J. Appl. Psychol.* **92**, 373–385 (2007).
10. J. M. Wicherts, C. V. Dolan, J. S. Carlson, H. L. J. van der Maas, *Learn. Individ. Differ.* **20**, 135–151 (2010).
11. T. Strenze, *Intelligence* **35**, 401–426 (2007).

1 October 2013; accepted 29 October 2013
10.1126/science.1246680

journal offering immediate publication with post-publication peer review and revision.

The idea of post-publication review is not new. Fifteen years ago I launched naturalSCIENCE (http://naturalscience.com), which offered free online publication of original research with post-publication comment. However, scientists were reluctant to contribute and publicly comment. If thinking has changed, I see little necessity for publishers or publication fees. All that is required is a science-friendly blog platform that handles scientific notation and math, edits tables, and forces standardized formatting of references. Volunteered peer reviews could be handled with standard blog comment machinery; reviewers could be required to establish their bona fides by making their identities and scientific resumés publicly available. If revised, earlier drafts could remain available for the benefit of those interested in following the development of the paper.

However, most scientists currently still depend for advancement on publishing in high-impact journals that, whatever one may think of citations analysis, undoubtedly attract the majority of the better papers and do a great deal more than most low-impact journals to add value through reviewing, fact checking, copyediting, graphics editing, table editing, and rewriting.

If it emerges at all, science self-publishing seems unlikely to have great impact on top journals but will divert content from the proliferating multitude of low-impact journals. Such a development could have many benefits, such as a reduction in cost of science communication; a leak-proof channel for the immediate announcement of breakthrough results; a convenient means for the dissemination of negative results; the opportunity for novice scientists to receive a wider range of advice and criticism than they could expect from the perfunctory review process used by marginal commercial journals; and a means for reviewers to receive recognition for ideas or information disclosed in the course of a review.

ALFRED N. BURDETT
Heron Publishing, Victoria, BC V8R 6A1, Canada. E-mail: alfredburdett@gmail.com

theBUZZ

Open Access and Peer Review

For his 4 October News story "Who's afraid of peer review?" (special section on Communication in Science, p. 60), J. Bohannon investigated whether open-access journals would accept his flawed submission. His results elicited more than 200 comments, available at http://comments.sciencemag.org/content/10.1126/science.342.6154.60.

A selection of your thoughts:

…A correlation analysis between impact factor and rejection rate would have provided other important answers. **—Eugenio Santoro**

It's a shame the author did not extend the scope of his research by sending his spoof paper also to traditional, subscription-based journals! **—Gabor Cocumelo**

I am the editor of a social science journal, and this problem is not about open access or traditional publishing. It is about too many papers, overworked academics who do peer review as a courtesy, and the "publish or perish" mentality of the academic appointment system…. The entire system of academic publishing is broken. Open Access is an attempt by many to build a new system. It is unfortunate that it has been diverted from its course by those who do not share its values. **—Peta Wellstead**

…Calling the predators "open-access publishers" is a disservice, as it obscures the issue; it would be like calling pyramid scheme operators "savings & loan banks" or snake oil salespeople "physicians."… **—Xing Chen**

Bohannon does not challenge open access, and he did not criticize all open-access publishing. Determining the degree of similar problems in paper journals would require a similar study. This was not Bohannon's task. We have all seen stupidity among reviewers and authors at paper journals. What we do not see in subscription journals is the cash incentive to publish utter rubbish. **—Ken Friedman**

…Research publications have been made criteria for promotion in Indian medical institutions, paving the way for emergence of thousands of spurious journals that publish your paper for a said charge on the next day without any peer review or copyediting…. **—Venkataramana Kandi**

Why is AAAS attempting to smear OA publications? Operating a sting to discredit an OA publication is not science, not journalism, and not entertainment. The authors and the editors of *Science* should feel embarrassed…. **—Ed Hinchey**

…What I find most intriguing is that there is apparently no central publishing ethics board or council to do the job Mr. Bohannon's investigation clearly reveals is necessary…. **—Philip Badiz**

…I have been confronted myself, repeatedly, with such untrustworthy magazines inviting an open-access paper, after I had published an article in a respectable subscription journal…. **—Peter Prudon**

…It is ironic that journals that charge submission fees are excluded from this test, as this model (or membership fees) is perhaps the better model to prevent vanity publishing (as the publisher is not incentivized to accept as many articles as possible). **—Gunther Eysenbach**

…It is getting easier to parse what is important to one's research needs, and it is becoming less important where "good ideas that work" are published. **—Kevin Henderson**

…Isn't our job to read every paper with scrutiny, regardless of where it is published?... **—Alen Piljic**

…The core issue is one of oversight and the impact this may have on the dissemination of accurate information to the scientific community…. Overlooked data in one paper get passed on like a faulty gene, and each time it gets passed on, the number of people influenced by it increases…. **—Chell Price**

Published by AAAS

EXHIBITION

Placing Climate Change

Deborah Dixon

The charitable organization Cape Farewell fosters collaborations among artists, scientists, and communicators that engage the public in the issue of anthropogenic climate change. Its current Sea Change program, launched in 2010, focuses on Scotland's western and northern isles. The program aims to produce creative responses to climate change and to involve local initiatives, concerns, and knowledge in the process. To do so, it has initiated partnerships with a range of community groups, cultural producers, research teams, and education sites across Scotland. The exhibition Sea Change now at the Royal Botanic Garden Edinburgh—combining films, glass, textiles, prints, and multimedia works—offers an opportunity to reflect on this complex engagement of people and place and to consider how climate change science can be undertaken, and communicated, in conjunction with an interpretive, rigorous artistic practice.

Sea Change (Tionndadh na Mara)

Elinor Gallant and Ruth Little, curators
Royal Botanic Garden Edinburgh. Through 26 January 2014. www.rbge.org.uk/whats-on/event-details/3091

The ground floor of the John Hope Gateway houses educational displays on plant diversity and the entangled ecologies of plant species. Sea Change uses simple partitions to carve out a long, narrow passage on one side of the ground floor that takes visitors past a series of image-based works before opening out into a busy, oval-shaped space that also holds sculptures. These include Anne Bevan and Ian Butler's *Ghost* (2012), a three-dimensional acrylic resin print that replicates and enlarges otherwise invisible foraminifera. Small enclosed areas lodging video installations punctuate the oval. One of the films shown, David Harradine/Fevered Sleep's *It's the Skin You're Living In* (2012), relocates the figure of the polar bear, that iconic image of climate change, from the High Arctic to the everyday space of the kitchen.

Also showing on the ground floor of the Gateway building is Andy Crabb and Peter Cutts's short film *Sea Changes*, which documents the project's summer 2013 expedition to the Orkney and Shetland islands. Photographs by Jennifer Wilcox displayed on the floor above provide another perspective on that voyage. Together, the film and photograph series provide glimpses of how scientists and artists began to share disciplinary practices (principally around data collection) as well as of the fragility of the northern isles' ecologies.

Near the entrance, Sea Change marks the site of the exhibition itself with pressed herbarium specimens of bog species collected during historical botanical expeditions to the Scottish Hebrides. These are placed alongside works from seven artists produced for the Sexy Peat/Tìr mo Rùin project, an ongoing Highland Print Studio–Cape Farewell partnership on the culture and ecology of the Isle of Lewis blanket bog. Alex Boyd's *Stacaiseal (Stacashal)* (2013), for example, is in part a response to the earlier documentation of the Scottish coastline by landscape photographer Thomas Joshua Cooper, who selected "peripheral" locations on a map, tracked them down, and photographed them using an antique field camera. Boyd's four-part series, by contrast, looks north, east, south, and west from the heart of the island, firmly placing it at the center of tectonic and climatic processes. A similar elemental focus can be found in Shona Illingworth's *Topologies of Air, Blueprint Series 1* (2013). Her images evoke a sense of the turbulence of north Atlantic weather systems and their uncanny power to frustrate various marine and aeronautical feats of engineering that promise some measure of control over the wind-blown landscape. *Topologies of Air* sits well alongside *Bird Score* (2013), which is part of Hanna Tuulikki's larger *Guth an Eòin/Voice of the Bird* project. This five-movement composition for nine female voices, woven together from fragments of Gaelic bird-themed songs, evokes the sounds, movements, and interactions of several species of waders, wildfowl, and seabirds found in the Hebrides. *Bird Score* shapes lyrics into various bird shapes that swoop, float, and flock across a white background.

The creative responses on show capture something of the scope of what has been reductively referred to as "climate change." A wealth of observable and measurable shifts in weather patterns, bird migrations, plant ranges, fishing stocks, soil erosion rates, and so on combine to aid our understanding of the interconnections among climate, ocean, landforms, botany, and biology as well as the myriad of human activities that have led to claims of an Anthropocene. In this vein, the works usefully highlight the range of scientific expertises—from ornithology to marine biology—that seek to make climate change knowable. They also, however, capture some-

CREDIT: ALEX BOYD/COURTESY HIGHLAND PRINT STUDIO/CAPE FAREWELL

Alex Boyd's *Stacashal—Summit Cairn (view East)*, from the Sexy Peat/Tìr mo Rùin series.

The reviewer is at the School of Geographical and Earth Sciences, University of Glasgow, East Quadrangle, University Avenue, Glasgow G12 8QQ, Scotland, UK. E-mail: deborah.dixon@glasgow.ac.uk

Published by AAAS

thing of the intangible experience of living with climate change. Though Scotland's islands that form the exhibition's focus are important in part because they are "climate change hotspots," they are also, as several of the artworks intimate, harbingers of a world to come. In bringing home the impact of climate change on place, the Sea Change exhibition makes a persuasive case for climate change as a complex, ever-present problem that admits of no single, overarching solution but which can, nevertheless, be addressed in the everyday actions of local communities.

10.1126/science.1247393

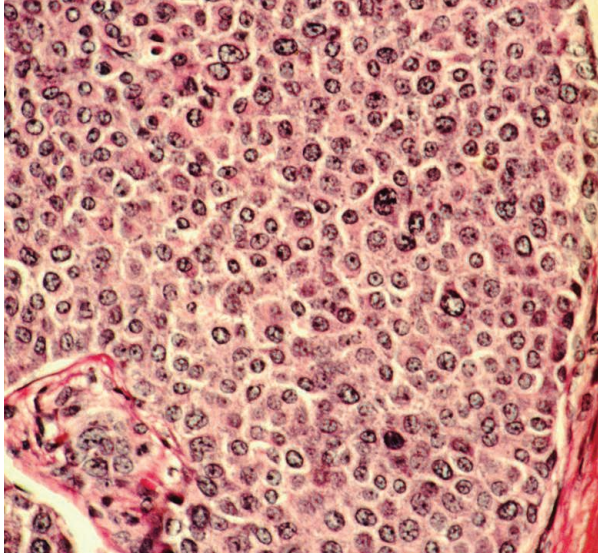

Photomicrograph of breast tissue with cancer cells.

MEDICINE

Up Close and Personal with Cancer

Mary L. Disis

A cancer diagnosis can be emotionally devastating, and people respond to the bad news in many different ways. Some people become mentally debilitated by the information and have difficulty making decisions about treatment. Others seem to take a cancer diagnosis in stride and overtly show no changes in the activities of their daily lives. Commonly, when scientists are diagnosed with a particular cancer, their response is to learn everything possible about the disease in an effort to feel some sort of control over the situation. George Johnson's *The Cancer Chronicles* recounts his attempt to harness the vast amount of information concerning the origins and pathways of cancer growth in an effort to understand what is happening to loved ones affected by cancer. The task is overwhelming. As the author notes at the book's start, "I imagined the expanse [of information] before me as a boundless rain forest whose breadth and diversity could never be captured within a single book or even a single mind." But Johnson, an award-winning science writer with the *New York Times*, is no scientific neophyte. His labor has produced a fascinating compilation of selected discoveries in cancer research that helped shape his deeper understanding of the disease process.

The Cancer Chronicles
Unlocking Medicine's Deepest Mystery

by George Johnson
Alfred A. Knopf, New York, 2013. 299 pp. $27.95, C$32. ISBN 9780307595140. Bodley Head, London. £18.99. ISBN 9781847921666.

The Cancer Chronicles comprises two distinct narratives. The first, reflecting the impetus for the book, recounts the personal story of how cancer has affected the lives of the author's family. Both his wife and, later, his brother were diagnosed with advanced-stage cancers, which carry grim prognoses. Johnson takes the reader step by step through diagnosis, treatment, and disease outcomes. His account highlights how difficult and chaotic the process of receiving an accurate cancer diagnosis and initiating therapy can be. As Johnson's wife and brother progress through treatment—and, in one case, relapse—his search for information follows the unfolding development of the cancers.

The second, interwoven, chronicle tells the story of cancer cells themselves. Johnson details the documentation of cancer in dinosaurs, prehistoric humans, Greek and Roman civilizations, and bodies from medieval times. He follows his epidemiologic review of ancient cases with a well-annotated progression through key discoveries that have shaped our understanding and treatment of cancer. Johnson discusses complex issues in cancer etiology, cancer biology, and even cancer politics. The examples and discoveries he presents have specific meaning for what is happening in the lives of his family members as they confront their illnesses. In addition, the studies considered address important questions the author has posed: "[H]ow much [about cancer] is timeless and inevitable … and how much has been brought on by pollution, industrial chemicals, and other devices of man?" "Why do some cancers metastasize?" These and other queries broached by Johnson illuminate issues that are crucial for anyone who has been touched by cancer.

The book succeeds on many levels. Johnson alternates between the two chronicles from chapter to chapter. The device of using his personal experience to select the breakthroughs or topics he discusses works well. He tells his personal story with an emotional distance that allows a smooth transition from technically oriented material to the family thread and back again. The author has deftly organized and presented vast amounts of scientific information so that they support the personal chronicle; every example seems to fit. In addition, the book is artfully written. Throughout it, Johnson's use of metaphor provides novel descriptions that are interesting to any reader, whether seasoned in the science of cancer or a novice. For example, when describing the process of metastasis, he writes, "cancer cells wandering the corridors of the circulatory system are looking for … a molecular 'zip code' identifying the organ where they are likely to thrive." An extended description of the blight of Russian thistle destroying the beauty of Johnson's garden in New Mexico is literal as well as metaphorical, describing what damage cancer was inflicting on his wife's body and, potentially, their relationship. Lastly, the book succeeds because Johnson's writing conveys his passion about the science. His presentations of pivotal discoveries are rich not only with scientific detail but also with insights into the personalities of the researchers and the importance of their findings in the context of their particular time periods.

Despite the author's goal of putting together some pieces of the puzzle, by the end of *The Cancer Chronicles*, one has far more questions than answers. Attending a conference to learn about the most recent research, Johnson observes that there are "[s]o many little subcultures even in the cancer world." The reader gets a sense of the current difficulty in sorting through and making sense of the recent explosion of data in cancer biology. Johnson deftly states, "the curse of this age of microspecialization and the proliferation of ''omics' is to separate the ridiculome from the relevantome." We are left questioning whether the beast of cancer can ever be tamed.

10.1126/science.1246818

The reviewer is at the Division of Oncology, Department of Medicine, University of Washington, 850 Republican Street, Box 358050, Seattle, WA 98195, USA. E-mail: ndisis@uw.edu

TECHNOLOGY

Advanced Manufacturing Policies and Paradigms for Innovation

U.S. innovation is heavy on early-stage R&D; it requires additional focus on manufacturing stages.

William B. Bonvillian*

Manufacturing in the United States is usually not pictured as part of the innovation process. This is a fragmented, disconnected view; innovation demands to be looked at as a system, from early-stage research through production. In contrast, Germany has a culture of engineering and Japan of artisanship and quality that embrace histories of production innovation and manufacturing success. Both nations have higher-wage and higher-cost manufacturing sectors than the United States, yet they have run major trade surpluses in manufactured goods, whereas the United States has run large deficits (*1*, *2*).

Can the United States reinvigorate its manufacturing sector? Government and industry are exploring "advanced manufacturing" (AM): innovative manufacturing technologies and related processes that can grow productivity, speed product development, and customize products to offset higher wages and costs [pp. 155–161 (*3*)]. The White House has formed the Advanced Manufacturing Partnership (AMP) with industry and universities to work on production innovation and policy (*4*), federal R&D agencies are developing AM agendas (*5*), numerous reports have been produced [e.g., p. 6 in (*3*)], and legislation is being developed in Congress (*6*). The U.S. case could offer lessons for other developed nations that give priority to their service economies; strengthened U.S. production models could benefit many nations. Other developed nations with high-cost manufacturing are exploring AM as well, led by Germany and the United Kingdom, and China has a comparable "Strategic Emerging Industries" plan to secure production leadership (*7*–*9*).

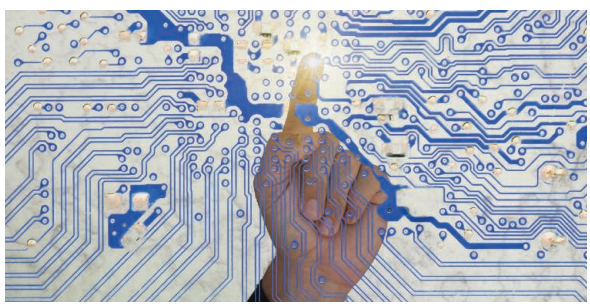

CREDIT: BUENA VISTA IMAGES/GETTYIMAGES

Production in the U.S. Innovation System

Much innovation occurs in the production stage. Moving from prototype to product can take years. It requires solving engineering design problems, overcoming production and component cost problems, building production processes, creating an efficient production system, developing and applying new production and product business models, educating a workforce, building a supply chain, financing scale up, actually scaling up production to fit evolving market conditions, and reducing all these steps to a routine. The initial innovation is often thoroughly reworked. These are highly creative elements needed at the outset of production at scale, requiring much science and engineering at nearly every point. The research-to-prototype stages begin the innovation process, but the pre- and outset-of-production stages are also vital. These stages are critical for incremental technology advance, as well as for breakthrough and radical technology innovation.

Despite manufacturing strength in the 19th and early 20th centuries, U.S. innovation since World War II and the Cold War has become front-end loaded, largely focused on early-stage research and development (R&D). If an innovation system must also encompass the back end—the prototype, demonstration, test-bed, and initial production phases—the United States has a gap (*10*). China, which has passed the United States in manufacturing net output, is focused on the back end of innovation, particularly production, as it works to build its front-end R&D system. Although many have assumed China achieved production leadership through lower wages and costs, recent work suggests it is able to rapidly scale up production volume through advanced processes that are integrated across regional firms and tied to system efficiencies and cost savings [pp. 121–154 in (*3*); (*11*, *12*)].

One part of the U.S. innovation system—the defense sector—has worked at both the front and back ends, undertaking R&D; prototyping; demonstration; test beds; and, through product procurement, often initial market creation. This system (*13*) jumpstarted key innovation waves of the 20th century: aviation, electronics, space, computing, and the Internet (*14*). With the decline in defense procurement and R&D support in the post–Cold War era, this innovation role has become less central (*15*).

Decline in U.S. production capability is increasingly apparent (*16*–*19*). Manufacturing employment fell by 31% between 2000 and 2010. Some have argued that this is due to productivity gains, but recent data do not bear this out. Output fell in this period in 16 of the 19 manufacturing sectors per government data measures, and output appears overstated in the remaining sectors. Because output is a key factor in productivity, manufacturing productivity appears substantially lower than we have been assuming; therefore, there are other structural causes of the deep manufacturing job losses. This is reflected in investment data: Manufacturing fixed-capital plant investment declined in 15 of 19 measured industrial sectors in this decade. Recent data suggest that an uptick in U.S. production employment is part of the slow economic recovery, but the numbers are modest, not close to overtaking the size of the decline (*20*). Yet manufacturing remains crucial: Industrial firms are at the core of the innovation talent system, employing 64% of scientists and engineers and performing 70% of private sector R&D (*21*).

Innovate (T)Here and Produce (T)Here?

Since World War II, the U.S. economy has been organized around world leadership in technology. It developed a comparative advantage over other nations in innovation and, as a result, led nearly all the significant innovation waves of the 20th century. The operating assumption was that the United States would innovate and translate those innovations into products. By innovating here and producing here, it would realize the full range of economic gains from innovation at all the stages, from research and development through production at scale,

*Director, Washington Office, Massachusetts Institute of Technology, Washington, DC 20002, USA. E-mail: bonvill@mit.edu

Published by AAAS

and the follow-on life cycle of the product. It worked—the United States became the world's richest economy.

The United States since 1940 has been playing out economic growth theory—that the predominant factor in economic growth is technological and related innovation (*22*)—and demonstrating that it works, with its model increasingly emulated abroad. But in recent years, with the advent of a global economy, the innovate-here-and-produce-here model is breaking down. In some industrial sectors, firms can now sever R&D and design from production. Codable information technology (IT)–based specifications for goods that tie to software-controlled production equipment have enabled "distributed" manufacturing (*23*). Now the innovate-here-and-produce-there model appears to work well for many IT and commodity products.

However, there appear to be many sectors where the distributed model does not work and that still require a close connection between research, design, and production, e.g., capital goods, aerospace products, energy equipment, and complex pharmaceuticals. Here, the production infrastructure provides constant feedback to the R&D and/or design phases. Product innovation is most efficient when tied to a close understanding of and linkage to manufacturing processes. However, if R&D/design and production are tightly linked, these innovation stages may have to follow production offshore. Produce-here-and-innovate-there may be even more disruptive than innovate-here-and-produce-there. This brings the foundations of U.S. innovation-based economic success into question. If federal R&D investments, for example, no longer translate as well into U.S. economic growth, innovation support may erode.

Paradigms for Manufacturing Innovation

If technological and related innovation is the core factor in economic growth, this points toward an innovation-oriented strategy in production. Although industry has been discussing macro factors in manufacturing recovery—tax, trade, currency valuation, and regulation—there are structural factors in the manufacturing innovation system that require focus. If production turns out to be important to the health of the overall innovation system because the two are interdependent, we have a systems problem not simply a macro policy problem. What could be undertaken?

Historically, manufacturing leadership has depended on leading new technology "paradigms" and combining these with new process and business models to support them. This was the road map for Britain's leadership of the industrial revolution built around the steam engine and textile machinery (*24*), for America's leadership in the 19th century through interchangeable machine-made parts and mass production capability (*25*), and for Japan's consumer electronics and auto leadership in the 1970s–80s through quality production (*26*). The United States will not be interested in competing with low-cost, low-wage, increasingly innovative emerging nations by slashing its wage base, so it must improve its productivity and efficiency to be cost-competitive. There appear to be new manufacturing "paradigms" at hand, discussed below, that could play roles in transforming production (*27*). The willingness of numerous industries to compete for and share the costs of federal investments in AM areas indicates that these are well past the speculative stage.

CREDIT: FLOTO & WARNER/GETTYIMAGES

"*Network-centric" production*. Embed IT advances throughout manufacturing value chains, including a mix of advanced IT, radio-frequency identification tags, and sensors, so that each element in the production process becomes "smart," to optimize efficiencies from resource through production through product life cycle. Use new decision-making tools from "big data" analytics, with advanced robotics, supercomputing, and advanced simulation and modeling. The cost and complexity of software, a major component in complex products, is an inhibitor in efficient production. Integrating software development at the outset with design, as well as new systems for hardware and software integration, appears to be key.

Advanced materials. Create a "materials genome," using supercomputing to design all possible materials with designer features, then fit new materials precisely to product needs for strength, flexibility, weight, and production cost. Evolve new biomaterials from synthetic biology. Explore biofabrication and "lightweight everything."

Nanomanufacturing. Fabricate at the nano scale. Embed nano-features into products to raise efficiency and performance.

Mass customization. Produce one or small lots at the cost of mass production—for example, through three-dimensional printing and additive manufacturing, where products can be fabricated in highly complex forms through printing from powders as opposed to traditional machine-tool processes.

Distribution efficiency. Driving even 10% out of the cost of product distribution can shift decisions on whether to produce in the United States or abroad. Further IT advances that yield distribution efficiencies, including in the supply chain, could yield this.

Energy efficiency. Excess energy is "waste," a nonrecoverable production cost. U.S. manufacturing has long been overly energy-intensive. Energy-efficiency technologies and processes, such as through power electronics, could significantly drive down production costs.

Filling the Gaps

If the United States needs new production paradigms, there are gaps that must be filled in the innovation system to realize them. First, U.S. R&D remains strong, but lacks an R&D effort organized around AM challenges (*28*). Most of the potential paradigms need R&D input, but both R&D and implementation also require corresponding technology strategies developed by industry, government, and university experts, to fill a second gap. These strategies would identify the AM technology opportunities, the R&D to get there, the collaborative process required, and design the test bed for implementation, as a prelude to more in-depth ongoing technology road-mapping processes. In addition to manufacturing R&D tied to a collaborative technology strategy, "manufacturing institutes," recommended by the AMP report, could fill

Published by AAAS

a third gap (*27*). One institute, an industry-university consortium around additive manufacturing (*29*), has now started. Other institutes, with costs shared between federal agencies, states, and industry, are proposed for digital manufacturing, lightweight materials, and power electronics.

Why institutes? The majority of the U.S. manufacturing sector consists of small and midsize firms that are risk-averse and thinly capitalized; thus, they are not in a position to perform research or adopt new technologies and processes unless the costs and efficiency gains are fully demonstrated and understood. Although larger firms once assisted their supply chains in this role, playing a vertical integration function, in an era of intense global competition, they have often cut back to their core competencies. Therefore, they are less able to assist suppliers and have their own competitive problems adapting. As Massachusetts Institute of Technology's (MIT's) Suzanne Berger puts it, manufacturing firms are "increasingly home alone" [pp. 15–20 in (*3*), (*30*)]. Taking a page from Germany's Fraunhofer system [pp. 121–140 in (*3*)], institutes could act as test beds, providing a range of industries and firms, small and large, with an opportunity to collaborate on, test, and prove prototypes for advanced production technologies and processes.

A fourth gap is talent. How will technical workers and engineers be trained to work with advanced technologies and develop processes and routines so as to introduce them into production systems? The institutes could help in this role, and the Department of Labor recently made awards for a $400 million program that requires community colleges to create online workforce education in AM. A new credentialing system between community colleges and industry organizations for manufacturing skills and development of an AM engineering curriculum could help. Without a workforce fluent with AM, it simply cannot be introduced.

Economy-wide macro policies in trade, tax, and currency valuation will be needed, too. But a focus on the structural problems in the gap-ridden manufacturing innovation system is critical. These initial steps—advanced manufacturing R&D, a strategy for new manufacturing paradigms, collaborative institutes, and training talent—speak to this structural question. The AMP report proposes addressing a number of these gaps (*17*, *27*).

Production is the central way an economy scales growth. Services are largely face-to-face and tend to scale gradually, but production can scale rapidly and enable geometric economic expansion. Firms will also increasingly offer high-value goods tied to services to provide customers with solutions; the tradable good can scale, making the accompanying service tradeable and scaleable as well [pp. 111–114 in (*3*)]. This means the success of services-dominant economies like the United States increasingly will be linked to success in manufacturing (*31*). Production is the major enabler of "increasing returns" in an economy (*32*), a foundational societal wealth creator [pp. 248–270 and 317–319 in (*24*)]. Unless the United States treats production as a critical element that must be better connected into its innovation system, it risks erosion of that system.

References and Notes

1. U.S. Bureau of Economic Analysis, U.S. International Trade in Goods and Services (1992–2012); www.bea.gov/international/index.htm#trade.
2. Organization for Economic Cooperation and Development, Goods Trade Balance, Trade: Key Tables from OECD, Table 3, 8 January 2013; www.oecd-ilibrary.org/trade/goods-trade-balance_20743920-table2.
3. S. Berger and MIT Task Force on Production in the Innovation Economy, *Making in America* (MIT Press, Cambridge, MA, 2013).
4. About the Advanced Manufacturing Partnership 2.0; www.manufacturing.gov/amp.html.
5. For example, www1.eere.energy.gov/manufacturing/; www.darpa.mil/Our_Work/TTO/Programs/Adaptive_Vehicle_Make__%28AVM%29.aspx; and www.manufacturing.gov/agency_partners.html.
6. S. 1468, H.R. 2996, 1st. Sess. (2013).
7. Industry 4.0 Working Group, National Academy of Science and Engineering, "Securing the future of German manufacturing: Recommendations for implementing the strategic initiative Industry 4.0" (Sponsored by the Federal Ministry of Education and Research, Bonn, Germany, April 2013).
8. Technology Strategy Board (UK), *High Value Manufacturing: Key Technology Area, 2008–11* (TSB, Swindon, UK, 2008); http://webarchive.nationalarchives.gov.uk/20130221185318/www.innovateuk.org/_assets/pdf/corporate-publications/tsb_highvaluemanu.pdf.
9. S. Shipp *et al.*, "Emerging trends in advanced manufacturing" (Paper P-4603, Institute for Defense Analysis, Alexandria, VA, 2012), pp. 68–72; https://www.ida.org/upload/stpi/pdfs/p-4603_final2a.pdf.
10. W. Bonvillian, *Sci. Publ. Policy*; 10.1093/scipol/sct059 (2013).
11. J. Nahm, E. S. Steinfeld *World Dev.* **54**, 288 (2014).
12. D. Breznitz, M. Murphree, *Run of the Red Queen* (Yale Univ. Press, New Haven, CT, 2011).
13. W. Bonvillian, R. Van Atta, ARPA-E and DARPA: Applying the DARPA model to energy innovation. *J. Technol. Transf.* **36**, 469 (2011).
14. V. W. Ruttan, *Is War Necessary for Economic Growth?: Military Procurement and Technology Development* (Oxford Univ. Press, New York, 2006).
15. V. W. Ruttan, *Issues Sci. Technol. Online* (Winter 2006); www.issues.org/22.2/ruttan.html.
16. Sources for data in this paragraph are (*17*), (*18*); pp. 25–64 in (*3*); and (*19*), and sources cited therein.
17. W. Bonvillian, *Innovations* **7**, 97 (2012).
18. Information Technology and Innovation Foundation, *Worse Than the Great Depression* (ITIF, Washington, DC, 2012); http://www2.itif.org/2012-american-manufacturing-decline.pdf.
19. S. Helper, T. Krueger, H. Wial, *Why Does Manufacturing Matter? Which Manufacturing Matters? A Policy Framework* (Brookings Institution, Washington, DC, 2012).
20. Bureau of Labor Statistics, Databases, tables and calculations, manufacturing-all employees (2013); http://data.bls.gov/timeseries/CES3000000001?data_tool=XGtable.
21. G. Tassey, Rationales and mechanisms for revitalizing U.S. manufacturing R&D strategies. *J. Technol. Transf.* **35**, 283 (2010).
22. R. M. Solow, *Growth Theory, an Exposition* (Oxford Univ. Press, New York, ed. 2, 2000).
23. S. Berger, *How We Compete: What Companies Around the World Are Doing to Make It in Today's Global Economy* (Doubleday Currency, New York, 2005), pp. 251–277.
24. W. Rosen, *The Most Powerful Idea in the World, A Story of Steam, Industry, and Invention* (Random House, New York, 2010).
25. C. R. Morris, *The Dawn of Innovation: The First American Industrial Revolution* (Public Affairs, New York, 2012).
26. J. Womack, D. Jones, D. Roos, *The Machine That Changed the World* (Free Press, New York, 1990).
27. President's Council of Advisors on Science and Technology, "Advanced manufacturing partnership, report to the President on capturing domestic competitive advantage in advanced manufacturing" (PCAST, Executive Office, Washington, DC, 2012).
28. D. Breznitz, P. Cowhey, "America's two systems of innovation: Recommendations for policy changes to support innovation, production and job creation" (Connect Innovation Institute, San Diego, CA, 2012), pp. 16–19.
29. National Additive Manufacturing Innovation Institute, http://namii.org.
30. MIT Taskforce on innovation and Production, "Preview of the MIT production in the innovation economy report" (MIT Press, Cambridge, MA, 2013), p. 27; http://web.mit.edu/press/images/documents/pie-report.pdf.
31. OECD, "Science, technology and industry scoreboard 2013" (OECD, Paris, 2013), p. 47.
32. B. Arthur, *Increasing Returns and Path Dependence in the Economy* (Univ. of Michigan Press, Ann Arbor, 1994).

10.1126/science.1242210

EVOLUTION

How Fisheries Affect Evolution

Commercial fishing alters the genetic traits of fish stocks.

Andrea Belgrano[1,2] and Charles W. Fowler[3]

The extensive exploitation of marine resources by modern fisheries (see the figure) has wide-ranging effects on marine ecosystems. Across the world's oceans, size-selective harvesting by commercial fisheries has been a key driving force behind changes in phenotypic traits such as body size and age at maturation (*1*–*3*). These changes have altered the trophic structure of the affected ecosystems, disturbed predator-prey relationships, and modified trophic cascade dynamics (*3*, *4*). Phenotypic changes can involve both ecological and evolutionary reactions to the effect of fishing, and there has been much debate about the relative roles of these reactions. This is important because genetic changes could result in long-term reductions in catches. Recent work has provided evidence for fisheries-induced evolutionary changes, with important implications for the sustainability of fisheries.

Although there is evidence for phenotypic changes in fisheries around the world, the underlying causes are difficult to determine in complex marine ecosystems. To tease apart ecological and genetic contributions, Wijk *et al*. exposed populations of male and female guppies (*Poecilia reticulata*) to different harvesting conditions over three generations (*1*). Only adult male body size was selected for, because females continue to grow after maturation. The authors provide evidence of changes at individual genetic loci in the male guppies; some of these loci have previously been associated with body size. The work thus provides direct evidence that size selection by fisheries can induce evolutionary changes.

Exploration of the economic effect of fisheries-induced evolution has added to our understanding of how fisheries may cause genetic change. Eikeset *et al*. have used a bioeconomic model for the Northeast Arctic cod stock (*5*) to show that evolutionary effects tend to be strongest when a stock is harvested using a strategy of intermediate size-selective harvesting. The authors compared two models. In the first, evolution was allowed to occur in response to fishing. In the second, no evolutionary changes could occur. The comparison showed that fisheries-induced evolution involving the intermediate selectivity results in faster growth and earlier maturation—results that are consistent with those of other research on fisheries-induced evolution.

Multispecies catch. Recent research has shown that size-selective commercial fishing causes genetic changes in fish, with wide-ranging implications for sustainable fishing.

PHOTO CREDIT: J. A. D. FISHER/MEMORIAL UNIVERSITY OF NEWFOUNDLAND

Fisheries-induced evolution may also affect macroecological patterns of functional traits. Such patterns include relationships between body size, abundance, and latitudinal distribution of different species (*6*, *7*). A recent analysis involving 326 species of northwest Atlantic fish showed a clear disruption of normal relationships between body size and latitude as a consequence of fishing that is often size selective (*6*).

The effects of commercial fishing are not the only example of human-induced trait changes among wild populations; such changes have also been seen in terrestrial and freshwater systems (*3*). Anthropogenic evolutionary changes such as fisheries-induced evolution are of particular concern because they affect the dynamics of whole populations, communities, and ecosystems. The resulting changes are often detrimental to the health of the ecosystems; recovery involves evolutionary time scales, and there may be enduring loss of ecosystem services.

The refinement of existing bioeconomic models (*5*) would benefit from the growing body of new information on genetically based variations in body size, including the work reported in (*1*). Such refined models could be used to support the implementation of ecosystem-based fishery management that aims to conserve ecosystem structure and function and to provide global sustainability (*8*). Body size is a useful trait to help guide management and conservation because it is involved in many macroecological patterns that account for the numerous interactions among species within complex food webs (*3*, *4*) and within webs of ecoevolutionary interactions (*3*). Size selectivity has been included in fisheries management in the hope that it would reduce the effects of commercial fishing on ecosystems and increase yields, but there is increasing evidence that it does not maximize production or reduce effects (*8*). One alternative proposal for fisheries management is "balanced harvesting" (*8*), which promotes a distribution of harvest mortality

[1]Swedish University of Agricultural Sciences, Department of Aquatic Resources, Institute of Marine Research, Turistgatan 5, SE-453 30 Lysekil, Sweden. [2]Swedish Institute for the Marine Environment (SIME), Box 260, SE-405 30 Göteborg, Sweden. [3]Biology Department, Seattle University, 901 12th Avenue, Post Office Box 222000, Seattle, WA 98122–1090, USA. E-mail: andrea.belgrano@slu.se; fowlerc@seattleu.edu

Published by AAAS

across species, stocks, and sizes in proportion to natural productivity in an attempt to avoid selectivity and conserve species-level traits (such as body size and age at maturation), as well as ecosystem-level traits (such as population variation). Although such suggestions have yet to be field-tested, the balanced harvesting proposal emphasizes the ecosystem complexities that must be taken into account to achieve sustainable harvesting (*2*, *8*).

There is an urgent need to define what is sustainable in terms of selectivity, both within and among species (*2*), across the full range of body size to address the evolutionary effects of commercial harvesting (*9*, *10*). Scientists are just beginning to appreciate that fisheries affect evolution through effects extending well beyond individual species to communities and ecosystems (*3*, *6*). Further research regarding the wide-ranging effects of fisheries-induced evolution is needed to elucidate the complex web of evolutionary and coevolutionary interactions involved. Such research will help commercial fisheries to ensure not only the survival and sustainable use of individual fish species but of the ecosystems that these species—and commercial fisheries—depend on (*11*, *12*).

References

1. S. J. van Wijk *et al.*, *Front. Ecol. Environ* **11**, 181 (2013).
2. S. Zhou *et al.*, *Proc. Natl. Acad. Sci. U.S.A.* **107**, 9485 (2010).
3. E. P. Palkovacs *et al.*, *Evol. Appl.* **5**, 183 (2012).
4. N. L. Shackell *et al.*, *Proc. Biol. Sci.* **277**, 1353 (2010).
5. A. M. Eikeset *et al.*, *Proc. Natl. Acad. Sci. U.S.A.* **110**, 12259 (2013).
6. J. A. D. Fisher *et al.*, *Ecology* **91**, 2499 (2010).
7. R. Trebilco *et al.*, *Trends Ecol. Evol.* **28**, 423 (2013).
8. S. M. Garcia *et al.*, *Science* **335**, 1045 (2012).
9. M. Yamamichi *et al.*, *Am. Nat.* **178**, 287 (2011).
10. K. H. Andersen, K. Brander, *Proc. Natl. Acad. Sci. U.S.A.* **106**, 11657 (2009).
11. S. Naeem *et al.*, *Science* **336**, 1401 (2012).
12. T. A. Branch *et al.*, *Trends Ecol. Evol.* **28**, 409 (2013).

10.1126/science.1245490

IMMUNOLOGY

Do T Cells Have a Cilium?

The T cell immunological synapse may function as a surrogate cilium.

Marie Le Borgne[1,2] and Andrey S. Shaw[1,2]

It is claimed that all mammalian cells express a single cilia. Although the origin of this idea is unclear, it hasn't stopped immunologists from looking for cilia on hematopoietic cells. But is this a fruitless search? On page 1247 of this issue, de la Roche *et al*. (*1*) suggest that a cilia equivalent does exist in T lymphocytes, perhaps masquerading as a structure associated with T cell activation.

Cilia are microtubule structures extending from the cell surface that enable motility (flagella) and signal transduction (primary cilia). At the base of a cilium is the basal body, composed of the two centrioles. When not attached to the plasma membrane, the two centrioles constitute the microtubule-organizing center (MTOC) or centrosome, a structure that nucleates microtubules. Formation and maintenance of cilia require a specialized transport process called intraflagellar transport, which involves cilia-specific motors (dyneins and kinesins) and specific adaptors (intraflagellar transport proteins) that facilitate the movement of material from the base to the tip of the cilia and back again (*2*).

Cilia have not previously been observed in lymphocytes, so evidence for their presence in these cells is indirect and functionally based. During cytolytic cell killing, the MTOC in T cells becomes juxtaposed with the plasma membrane (*3*), similar to the positioning of centrioles during mitosis and like the basal body at the base of a cilium (*2*). With the MTOC apposed to the membrane, motors that are directed toward the MTOC (dyneins) are sufficient to transport secretory vesicles to the membrane. T lymphocytes also appear to express intraflagellar transport proteins, which are important in the recycling of T cell receptors during T cell activation (*4*).

Primary cilia function mainly as a sensory organ. Important signal transduction receptors are transported to the tip of the cilium where they initiate signaling pathways. An important ciliary signaling pathway is controlled by the secreted protein Hedgehog (Hh). Hh plays critical roles during embryogenesis and adult tissue homeostasis. Disruptions of Hh signal transduction lead to congenital abnormalities such as polydactyly, skeletal abnormalities, and holoprosencephaly, whereas persistent Hh signaling is associated with various cancers (*5*). Because Hh signaling in mammalian cells requires primary cilia, de la Roche *et al*.

[1]Department of Pathology and Immunology, Washington University School of Medicine, 660 South Euclid, Saint Louis, MO 63110, USA. [2]Howard Hughes Medical Institute, Washington University School of Medicine, 660 South Euclid, Saint Louis, MO 63110, USA. E-mail: ashaw@wustl.edu

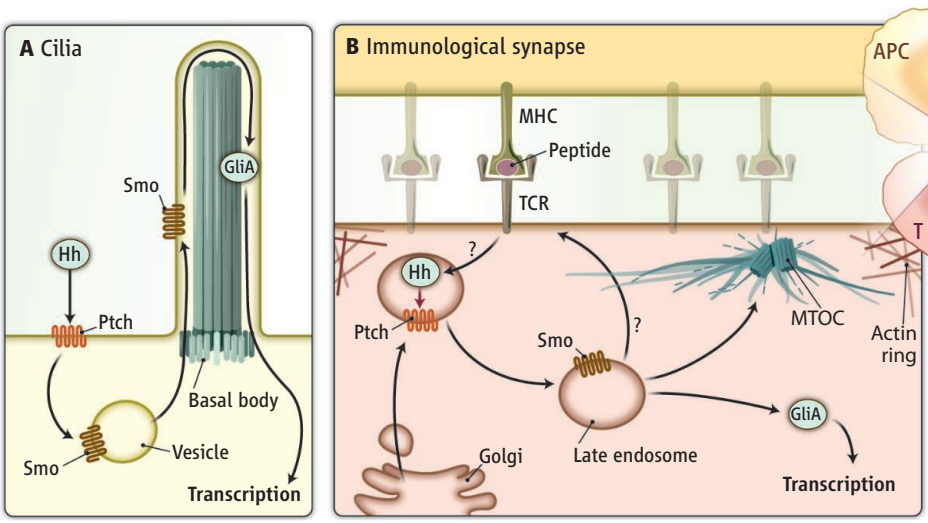

Comparison of Hh signaling in the cilium and in the synapse. (**A**) Conventional Hh signaling pathway is initiated by extracellular Hh binding to Ptch. This releases Smo, which migrates to the cilium where it induces Gli activation (GliA). GliA requires Gli trafficking to the tip of the cilia and back. (**B**) In T cells, T cell receptor (TCR) engagement stimulates Hh activation of Ptch in vesicles of the secretory pathway. This leads to the translocation of vesicles containing Smo to the plasma membrane, activation of Gli, and MTOC recruitment to the immune synapse. APC, antigen-presenting cell; MHC, major histocompatibility complex.

CREDIT: V. ALTOUNIAN/SCIENCE

investigated whether T lymphocytes use the Hh signaling pathway.

Hh signaling involves the ligand, Hh; its cell surface receptor, Patched (Ptch); and another transmembrane protein, Smoothened (Smo). In the absence of Hh, Ptch functions as an inhibitor of Smo. Hh binding to Ptch releases Smo, allowing it to be transported to the tip of the cilium. This activates the Gli family of transcription factors to control genes involved in proliferation, development, and pattern formation (*5*); activates the RAC guanosine triphosphatase to modify actin important for cell migration and dendritic spine formation (*6*, *7*); and induces a metabolic switch to glycolysis (*8*).

De la Roche *et al*. show that mouse naïve T cells express all components of the Hh signaling pathway and that Gli expression increased over the course of several days in response to T cell receptor activation. Gli1 induces its own expression (*2*), so an increase in Gli1 is indicative of Hh signaling. Hh appears to stimulate Ptch in the same cell, as both ligand and receptor are found together in secretory vesicles. Ptch signaling only occurs in the vesicle as cells did not respond to exogenous Hh. Imaging showed that these vesicles are distinct from the late endosomes that contained internalized Smo. This indicates that Hh binds to its cognate receptor within the same T cell. Moreover, activation of the T cell receptor (and presumably Hh signaling) increased Hh production and induced the translocation of Smo to the immunological synapse. The absence of Smo or treatment of T cells with inhibitors of the Hh signaling pathway attenuated the ability of cytotoxic T cells to kill target cells in vitro.

De la Roche *et al*. propose that the T cell immunological synapse functions as a surrogate cilium. The immunological synapse is a specialized organization of proteins at the contact surface between a T cell and an antigen-presenting cell. It is composed of an outer ring that is rich in actin and adhesion proteins (integrins), and a central region that is free of actin, where secretion occurs. Because the MTOC makes contacts with the membrane in this central area, the authors suggest that the center of the synapse functions as the lymphocyte equivalent of a cilium. Actin clearance from the synapse and MTOC polarization toward the synapse were impaired in T cells lacking Smo. Rac-mediated actin remodeling is also controlled by Hh (*6*, *7*), and de la Roche *et al*. found that Rac expression increased in a Smo-dependent manner. The observation that Smo relocates to the immunological synapse following T cell receptor activation with antigen-presenting cells is consistent with the role of the synapse as a cilium surrogate.

Several aspects of the pathway described by de la Roche *et al*. are distinct from the canonical Hh signaling pathway, suggesting that further clarification is needed (see the figure). Hh is usually secreted and functions in a concentration gradient, but the pathway described by the authors occurs within a single cell and is therefore not dependent on a gradient. Because Smo and Ptch are localized in distinct vesicles, how Ptch regulates Smo and whether translocation of Smo to the membrane requires intraflagellar transport proteins is unclear. T cell receptor signaling increased their expression but did not enhance colocalization of Ptch and Hh in secretory vesicles, so why activation of the Hh pathway is not constitutive is not clear. Because cytotoxic T cells use secretory lysosomes to kill their targets, T cell receptor signaling could initiate trafficking changes that allow Hh signaling to direct secretory lysosomes containing Smo to the plasma membrane. How Smo relocation leads to Gli activation, and if it is important for MTOC polarization toward the immunological synapse, remains to be determined.

Do these data support the idea that the immunological synapse is a frustrated cilium? Hh signaling functions in *Drosophila melanogaster* without cilia, so Hh signaling does not necessarily require cilia (*5*). And while the ability of the MTOC to interact with the plasma membrane during secretion is reminiscent of the basal body below the cilia, basal bodies are anchored to the plasma membrane by a specialized complex of proteins. The MTOC of the cytotoxic T cell appears to have a much more dynamic interaction with the plasma membrane, interacting only transiently with it (*3*). If the function of primary cilia, however, is mainly to sequester signaling components, this may be achieved in T cells through a specialized vesicular trafficking system. In this context, the Hh pathway may control such traffick to the membrane through MTOC translocation.

References

1. M. de la Roche *et al*., *Science* **342**, 1247 (2013).
2. S. C. Goetz, K. V. Anderson, *Nat. Rev. Genet.* **11**, 331 (2010).
3. J. C. Stinchcombe *et al*., *Nature* **443**, 462 (2006).
4. F. Finetti *et al*., *Nat. Cell Biol.* **11**, 1332 (2009).
5. J. Briscoe, P. P. Thérond, *Nat. Rev. Mol. Cell Biol.* **14**, 418 (2013).
6. N. Sasaki *et al*., *Mol. Cell. Neurosci.* **45**, 335 (2010).
7. A. H. Polizio *et al*., *J. Biol. Chem.* **286**, 19589 (2011).
8. R. Teperino *et al*., *Cell* **151**, 414 (2012).

10.1126/science.1248078

GEOPHYSICS

Dangers of Being Thin and Weak

Kelin Wang[1] and Masataka Kinoshita[2]

Ocean drilling data show that the large trench-breaching rupture of the 2011 Tohoku–Oki earthquake occurred along a thin and weak fault zone.

Why did the plate boundary fault at the Japan Trench slip tens of meters to generate a devastating tsunami in the Tohoku–Oki earthquake on 11 March 2011? Does the large slip in the shallow part of the fault represent a common process in subduction zones, or does it reflect site-specific geological conditions? Using the scientific drilling vessel *Chikyu* and working at the limit of drilling technology, researchers of the Japan Trench Fast Drilling Project (JFAST) have retrieved rock samples and made measurements in the culprit fault zone to seek answers. Their findings are reported in three papers in this issue. Based on different types of observations, Chester *et al*. on page 1208 (*1*), Fulton *et al*. on page 1214 (*2*), and Ujiie *et al*. on page 1211 (*3*) show that an important reason for the large slip is that the shallow fault zone is thin and weak.

The Tohoku rupture started at a depth of about 20 to 30 km and rapidly propagated in all directions along the plate boundary fault (referred to as the megathrust) to grow into a magnitude 9 earthquake (see the figure). According to various observations, the maximum slip exceeded 50 m near or at the trench. The large shallow slip caused the sloping sea floor above the megathrust to leap eastward, and the sudden disturbance to the seawater resulted in a huge tsunami.

Faults slip at a wide variety of rates. Earthquake rupture, or seismic slip, is fault slip at the highest rate. Traditionally, the shallowest portion of a subduction mega-

[1]Pacific Geoscience Centre, Geological Survey of Canada, Natural Resources Canada, Sidney, British Columbia, Canada V8L 4B2. [2]Kochi Institute for Core Sample Research, JAMSTEC, Nankoku, Kochi, 783-8502 Japan. E-mail: kelin.wang@nrcan-rncan.gc.ca

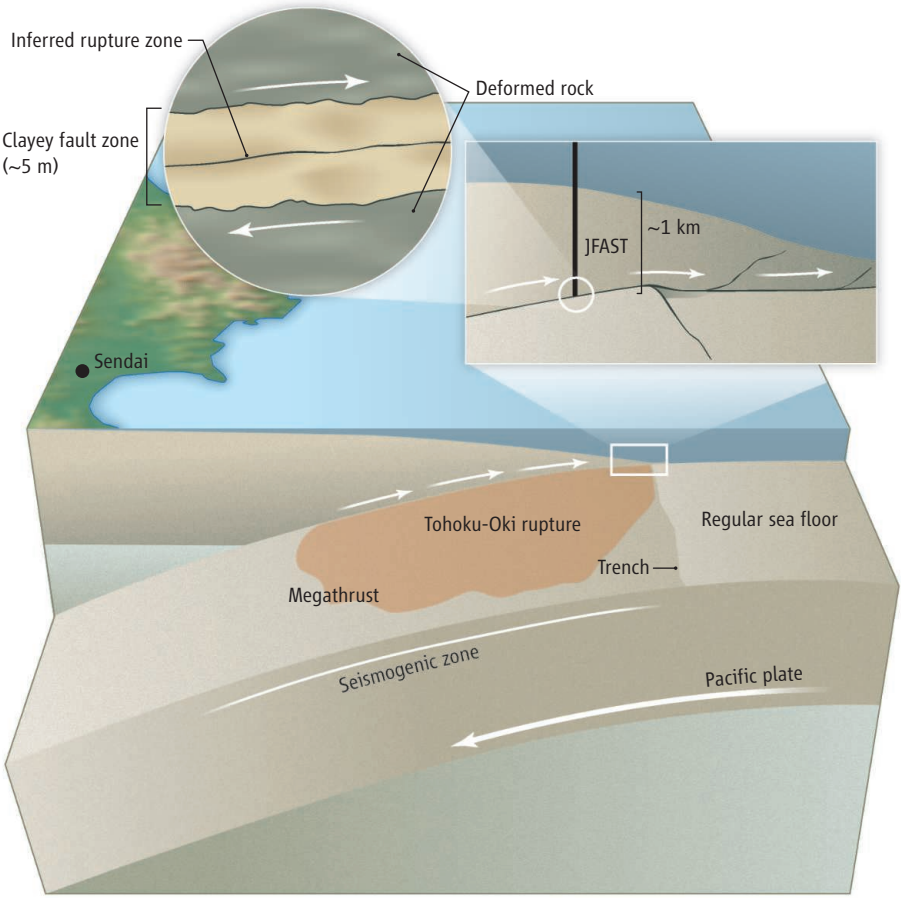

Probing into a giant rupture. The Tohoku-Oki earthquake involved the largest (~50 m or more) recorded fault slip in a single earthquake. To understand the geological mechanisms that led to the earthquake, JFAST drilled to the megathrust under a water depth of ~7 km. Chester *et al*. show that the fault zone is thinner (~5 m) than observed in other subduction zones and consists of weak clay. Ujiie *et al*. find that the fault zone material becomes even weaker at seismic slip rates. Fulton *et al*. report borehole temperature anomalies that indicate very low frictional stress. These results suggest that the trench-breaching large slip was facilitated by a thin and weak fault zone at shallow depths.

thrust is expected to resist earthquake rupture because its frictional strength increases with slip rate (rate strengthening) (*4*). Seismic slip is expected to initiate in a deeper zone (see the figure), where the frictional strength falls with slip rate (rate weakening), and to become smaller as it propagates toward the trench (see the figure). This model is supported by observations in some subduction zones, such as Sumatra (*5*), and is similar to what is seen for many continental earthquakes, in which surface rupture is often smaller than slip at depth. The large shallow slip in the Tohoku-Oki earthquake thus came as a surprise.

There are different hypotheses regarding the shallow megathrust at the Japan Trench. In one view, the rate-weakening seismogenic zone extends all the way to the trench. In another, the shallow megathrust is rate-strengthening but unable to resist a large slip propagating from the deeper part of the fault (*4*, *6*). In a third view, it is rate-strengthening when slipping slowly but becomes very weak if the slip accelerates to seismic rates (~1 m/s) (*7*). Such high-rate weakening has been observed in recent laboratory rock friction experiments regardless of rock type, and various mechanisms have been proposed to explain it (*8*). Somewhat similar to the third view but without involving high-rate slip is the idea of conditional stability, according to which some rate-strengthening faults can become rate-weakening in response to a small sudden increase in slip rate. The JFAST findings bring us closer to determining which of these views is correct.

By analyzing core samples and in situ geophysical measurements made in the boreholes, Chester *et al*. found the fault zone to be less than 5 m thick—thinner than in other modern or ancient (but now exhumed) subduction zones (*9*). The extraordinary localization of shear is caused by a layer of weak clay along which the fault develops. The actual slip zone of the Tohoku-Oki earthquake within this clayey fault (see the figure) is expected to be only millimeters to centimeters thick (*10*). JFAST was able to retrieve core samples from only about 60% of the clayey fault and probably missed the Tohoku slip zone. However, by exposing the available samples to friction experiments, Ujiie *et al*. show that this weak clay becomes even weaker if put in a 0.8-mm-thin zone that is driven to slip at seismic rates, especially if pore fluid is not allowed to diffuse away during the slip. With temperature monitoring in a nearby hole, Fulton *et al*. found that the amount of frictional heat generated by the huge Tohoku rupture was extremely small, putting the weakness of the shallow megathrust during the earthquake beyond doubt. Lin *et al*. (*11*) previously presented a stress analysis based on JFAST borehole observations that is also consistent with a very weak megathrust.

The weakness of plate boundary faults has long been recognized. An earlier suggestion of extremely low strength of the Japan Trench megathrust (*12*) has been dramatically verified by a reversal of upper-plate stress from compression to tension as a result of the Tohoku-Oki earthquake (*13*, *14*). The JFAST results not only identify the geological reason why the shallow megathrust is so weak, but also show that it may have become even weaker during the magnitude 9 earthquake. Seismic rupture occurs along extremely thin slip zones (*10*). The weak clay layer that makes the fault zone very thin provides a structural condition to host seismic rupture. The third view about the Japan Trench shallow megathrust discussed above—low-rate strengthening but high-rate weakening—can explain why the huge shallow slip did not happen everywhere along the trench during the Tohoku-Oki earthquake and not every time the seismogenic zone ruptured in the past.

JFAST's achievements are remarkable given the technological challenges of drilling at water depths of ~7 km. Yet even with *Chikyu*, the only existing scientific drilling vessel capable of drilling at such water depths, drilling efforts can only reach the shallowest part of the immense rupture zone (see the figure) and so far only in one location. Although very large slip occurred at the trench in the Tohoku-Oki earthquake, it is unclear whether the peak value of the slip was at the trench or some distance landward of it, and why there were no aftershocks in the most seaward 45 km of the upper plate (*15*). Further research is required to determine how fault behavior varies with depth as well as laterally along the trench.

CREDIT: ADAPTED BY P. HUEY/*SCIENCE*

Published by AAAS

Concerning plate boundary geodynamics and tsunami hazard, an important question is whether Tohoku-type large shallow slip occurs commonly. The results of Chester *et al*. suggest that the shallow megathrust at the Japan Trench has special traits not seen in many other subduction zones. Ujiie *et al*. show that, because of lower clay contents, the fault zone material in the Nankai Trough in southwest Japan is not as weak as that in the Japan Trench.

The JFAST data show how direct borehole sampling and monitoring can help to elucidate the slip behavior of the shallow megathrust. Results from other ongoing and future megathrust drilling projects, such as those at Nankai and off Costa Rica, will enable comparisons between different subduction zones. However, while studying the shallow part of the fault, scientists must keep in mind that subduction earthquakes may generate devastating tsunamis even without huge shallow slip as in Tohoku, such as in Sumatra in 2004 and Chile in 2010.

References and Notes

1. M. F. Chester *et al*., *Science* **342**, 1208 (2013).
2. P. M. Fulton *et al*., *Science* **342**, 1214 (2013).
3. K. Ujiie *et al*., *Science* **342**, 1211 (2013).
4. Y. Hu, K. Wang, *J. Geophys. Res.* **113**, B12411 (2008).
5. Y.-J. Hsu *et al*., *Science* **312**, 1921 (2006).
6. J. E. Kozdon, E. M. Dunham, *Bull. Seismol. Soc. Am.* **103** (2B), 1275 (2013).
7. H. Noda, N. Lapusta, *Nature* **493**, 518 (2013).
8. G. Di Toro *et al*., *Nature* **471**, 494 (2011).
9. C. D. Rowe *et al. Geology* **41**, 991 (2013).
10. Z. K. Shipton, J. P. Evans, R. E. Abercrombie, E. E. Brodsky, in *Earthquakes: Radiated Energy and the Physics of Faulting,* Geophysical Monograph Series 170, R. Abercrombie, Ed. (American Geophysical Union, Washington, DC, 2006), pp. 217–222.
11. W. Lin *et al.*, *Science* **339**, 687 (2013).
12. K. Wang, K. Suyehiro, *Geophys. Res. Lett.* **26**, 2307 (1999).
13. A. Hasegawa *et al*., *Earth Planet. Sci. Lett.* **355-356**, 231 (2012).
14. Unlike fault strength, stress drop along the megathrust during an earthquake can be estimated from seismic and geodetic measurements. The stress drop during the Tohoku-Oki earthquake is measured at only a few megapascals. A stress reversal in the upper plate would not happen if this value were only a small fraction of megathrust strength.
15. K. Obana *et al*., *Earth Planet. Sci. Lett.* **382**, 111 (2013).

10.1126/science.1246518

BOTANY

Shining Light at Microtubule Crossroads

Severing at microtubule crossovers reorients the plant microtubule network and redirects plant growth in response to light.

Antonina Roll-Mecak

The microtubule cytoskeleton, the network of cable-like tubulin polymers found throughout the cytoplasm in all eukaryotic cells, is central to cell division and differentiation throughout biology. Nowhere is this more true than in the plant kingdom. Here, microtubule organization patterns the deposition of cellulose, the prime constituent of cell walls, thus controlling the ability of plants to grow in the direction of light, or phototropism. The research article by Lindeboom *et al*. on page 1202 of this issue (*1*), together with several recently published studies (*2*, *3*), provides fundamental insights into the mechanism used by plants to switch the orientation of their cortical microtubule array, and therefore the morphology and function of the cells that harbor them, in response to light.

During cell elongation, cortical microtubules, those on the inner face of the plasma membrane, in the *Arabidopsis* hypocotyl (the stem of a germinating seedling) are arranged in parallel arrays with a predominant orientation almost perpendicular to the axis of expansion of the stem (see the figure, panel B, left). In response to light, microtubules undergo a rapid 90° reorientation, so they are now parallel to the stem, thereby changing the cellulose deposition pattern that controls cellular elongation. In an imaging tour de force, Lindeboom *et al*. now show that this reorientation of the microtubule array proceeds through two phases. The first phase involves γ-tubulin–dependent nucleation of new microtubules at angles ~40° from the existing transverse microtubules, thus generating crossovers. The second involves microtubule number amplification through severing at these microtubule crossovers (see the figure, panel B, center). Microtubule crossovers were previously shown to be hotspots for severing in cortical arrays (*4*). The new microtubule end generated by severing grows at a shallow angle, maintaining the overall orientation of the longitudinal "seed" microtubule, and thereby serves not only to amplify the number of microtubules but also to maintain the general orientation of the seed. This bifurcation of the microtubule by severing and regrowth is reminiscent of a railroad turntable where the subunits of the incoming train are separated from each other and then allowed to progress at different angles (see the figure).

The key player in this process is the microtubule-severing enzyme katanin, an AAA adenosine triphosphatase (ATPase) that is thought, by analogy with its family member spastin, to sever the microtubule through extraction of tubulin subunits from the microtubule lattice (*5*, *6*). Lindeboom *et al*. show that green fluorescent protein–labeled katanin is recruited to microtubule crossovers and that this recruitment precedes the formation of new microtubule plus ends (the growing ends of microtubules). A katanin null mutant shows no creation of new microtubule plus ends, as well as impaired reorientation of the array upon exposure to light. Because some of the new ends created by severing the microtubules do not depolymerize but are stable and able to regrow, severing has an overall constructive rather than destructive role and contributes to the net growth of the microtubule array.

One implication of this crossover-activated severing mechanism is that as the array gradually reorients and the population of longitudinal microtubules increases, the frequency of severing decreases (because there are fewer crossovers), thus dampening new microtubule generation and stabilizing the array in its new orientation. Interestingly, a complementary study by Zhang *et al*. (*2*), which makes similar observations, proposes that the dominant outcome of severing in the transverse hypocotyl microtubule array is depolymerization, with severing ultimately serving to eliminate unaligned, discordant cortical microtubules. Future studies will likely address the relative contributions of these two outcomes to overall array reorientation.

How does katanin distinguish crossover sites from bundled or single microtubules? A central question in cell biology concerns

Cell Biology and Biophysics Unit, Porter Neuroscience Research Center, National Institutes of Health, 35 Convent Drive, MSC 3700, Bethesda, MD 20892, USA. E-mail: antonina@mail.nih.gov

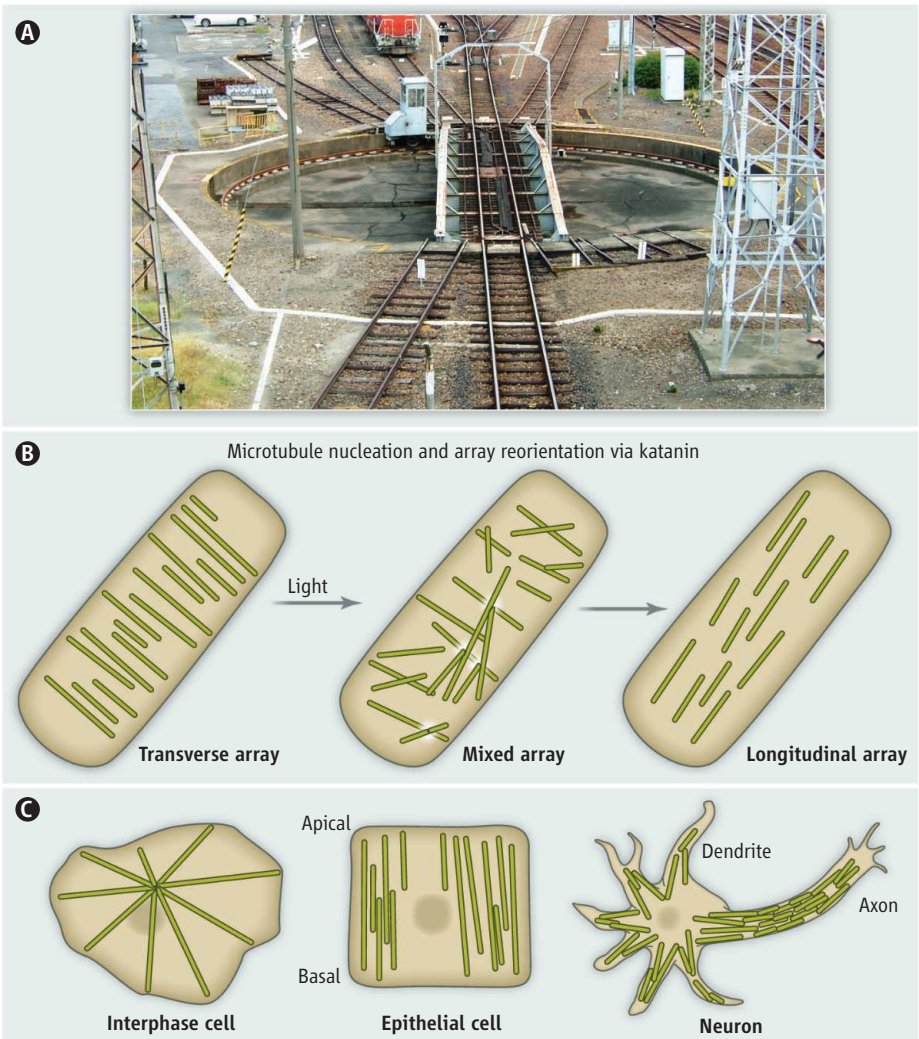

Making and remodeling microtubule arrays. (**A**) Severing dependent microtubule growth is analogous to a railroad turntable that splits two tracks. (**B**) Microtubule amplification and array reorientation are driven by katanin severing in the stem of a growing plant. (**C**) Microtubules are arranged in diverse patterns best adapted to cell type and organism: interphase cell, radial; epithelial cell, parallel; neuron, tiled.

the means by which nanometer-scale proteins sense and respond to cellular architecture at the micrometer scale. In vitro, katanin severs microtubules at any point along their length (*7*); however, experiments with dynamic microtubules or complex microtubule geometries more closely resembling those in cells have not been performed, and the fate of the new microtubule end generated by a microtubule-severing enzyme in vitro is still not known (does it catastrophically depolymerize, or is it able to regrow?). Katanin consists of a catalytic subunit (p60), which hydrolyzes ATP to locally disassemble the microtubule, and a regulatory subunit (p80) that enhances severing activity and targets the enzyme to specific subcellular locations (*6*). Katanin assembles into a hexamer with multiple microtubule-binding domains that could be maximally engaged only when two microtubules cross each other (*5*, *6*). It is also possible that the regulatory subunit, of which *Arabidopsis* encodes four, senses microtubule crossovers. Future studies will address whether p60 targeting to crossovers is impaired in p80 mutants.

Additional factors could also sense the microtubule crossover and regulate katanin function. A recent study in *Arabidopsis* pavement and petiole cells revealed that severing frequency at microtubule crossovers inversely correlates with the presence of the microtubule-associated protein SPIRAL2, which itself induces microtubule crossovers (*3*). The phenotypes of katanin and spiral2 mutants are diametrically opposed. The katanin mutant displays complex crossovers formed by multiple microtubules, whereas the spiral2 mutant has very few. How SPIRAL2 itself senses crossovers is not clear, but it might be transported along the microtubule to crossover sites (*3*). Last, katanin activity is sensitive to tubulin posttranslational modifications that could chemically mark microtubule crossover sites for severing action (*8*). Future in vitro studies with microtubule arrays of diverse geometries and in the presence of various microtubule-associated proteins will be essential in understanding the feedback between array architecture and katanin function.

A severing-dependent mechanism for microtubule amplification and array reorientation has been postulated to be important not only in the morphogenesis of noncentrosomal plant cortical arrays (*9*), but also in mitotic and meiotic spindles, epithelial cells, and neurons (*10*–*13*); however, it has not been directly observed in vivo until now, partly because the high microtubule density in these systems had impeded direct observation of severing. Centrosomes act as microtubule-organizing centers in animals; however, they pattern microtubules in an isotropic or radial array. Most cells in our body do not have radial microtubule arrays; many cells lack centrosomes altogether (*12*). Furthermore, the majority of microtubules in neurons or epithelial cells are disconnected from the centrosome (see the figure, panel C). Microtubule number amplification by severing is an attractive mechanism for generating the microtubule mass needed to fill long neuronal processes and offers the possibility of fast reorientation of the microtubule array in response to local stimuli. Thus, the mechanistic insights from the studies by Lindeboom *et al*. and Zhang *et al*. are likely to be relevant in other systems and firmly establish microtubule severing by katanin as a driving force in the making and remodeling of noncentrosomal ordered microtubule arrays.

References and Notes

1. J. J. Lindeboom *et al*., *Science* **342**, 1245533 (2013); 10.1126/science.1245533.
2. Q. Zhang *et al*., *Curr. Biol.* **23**, 2191 (2013).
3. R. Wightman, G. Chomicki, M. Kumar, P. Carr, S. R. Turner, *Curr. Biol.* **23**, 1902 (2013).
4. R. Wightman, S. R. Turner, *Plant J.* **52**, 742 (2007).
5. A. Roll-Mecak, R. D. Vale, *Nature* **451**, 363 (2008).
6. A. Roll-Mecak, F. J. McNally, *Curr. Opin. Cell Biol.* **22**, 96 (2010).
7. F. J. McNally, R. D. Vale, *Cell* **75**, 419 (1993).
8. C. P. Garnham, A. Roll-Mecak, *Cytoskeleton* **69**, 442 (2012).
9. G. O. Wasteneys, *J. Cell Sci.* **115**, 1345 (2002).
10. M. Srayko *et al*. *Curr. Biol.* **16**, 1944 (2006).
11. A. Roll-Mecak, R. D. Vale, *J. Cell Biol.* **175**, 849 (2006).
12. F. Bartolini, G. G. Gundersen, *J. Cell Sci.* **119**, 4155 (2006).
13. F. J. Ahmad *et al*., *J. Cell Biol.* **145**, 305 (1999).

Acknowledgments: Supported by the intramural program of the National Institute of Neurological Disorders and Stroke.

10.1126/science.1248235

PHYSICS

Freeing Nonlinear Optics from Phase Matching

Optical metamaterials that have a refractive index of zero can boost the efficiency of nonlinear optical processes.

Martti Kauranen

The advent of lasers quickly led to the demonstration of nonlinear optical effects. One of the simplest examples of a nonlinear effect is doubling the input frequency of light with a nonlinear crystal. The output intensity of the frequency-doubled light then grows nonlinearly with the intensity of the laser beam. To maximize macroscopic nonlinear signals, the wavelets emitted by the elementary nonlinear sources need to add up in phase. On page 1223 of this issue, Suchowski *et al.* (*1*) report an interesting approach to phase matching with metamaterials—artificial nanostructures with unusual optical properties created by tailoring their structural features (*2*). The authors avoided the phase-matching problem by relying on a metamaterial that has a refractive index for the interacting wavelengths near zero (keeping in mind that the refractive index of the vacuum is not zero but unity). Furthermore, they achieve equal nonlinear emission in two opposite directions simultaneously, whereas conventional phase-matching techniques maximize the nonlinear signal in only one direction.

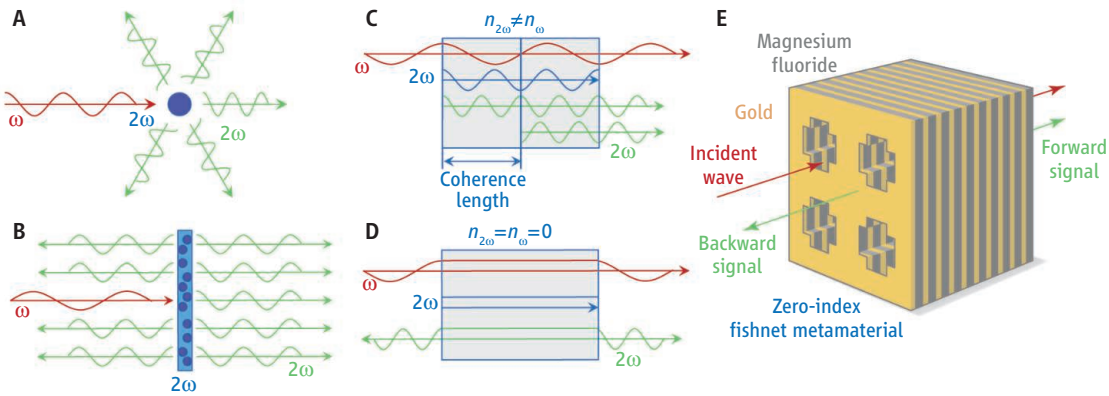

Phase matching for second harmonic (SH) generation. The spatial oscillations of the fundamental wave and SH source polarization are shown by red and blue lines, respectively; green lines indicate SH wavelets. (**A**) An elementary SH source emits in all directions. (**B**) A thin film emits symmetrically in the forward and backward directions. (**C**) For thick samples, the phase relation between the SH wavelets is lost after a coherence length, because the source and wavelets oscillate at different rates. (**D**) In a material with refractive index *n* of zero for both wavelengths, the oscillations do not occur and all SH wavelets add up in phase in the forward and backward directions. (**E**) The fishnet structure of Suchowski *et al.*, with zero refractive index, demonstrates equal nonlinear generation in the forward and backward directions for four-wave mixing.

Phase matching is challenging because the wave oscillations in propagation are determined by the refractive index of the material, and the refractive index depends on wavelength. To better understand the phase-matching problem, a closer look at frequency doubling, or second harmonic (SH) generation, is helpful. A wave at the fundamental frequency ω incident on a nonlinear material (such as lithium niobate) gives rise to an oscillating source polarization at the SH frequency 2ω. When the source is a single atom or molecule (see the figure, panel A), SH emission occurs in all directions. For thin-film sources (see the figure, panel B), the SH wavelets add up in phase only in the forward and backward directions, which represents transverse phase matching (perpendicular to the direction of propagation).

For thicker samples (see the figure, panel C), the wave oscillations in propagation become important, and their rate is proportional to the refractive index. The source oscillations follow the fundamental field but occur twice as rapidly. In general, however, the refractive index for the SH wavelets is different because of the higher frequency. The wavelets from different locations then lose their phase relation after a distance known as coherence length. The coherence length for forward SH generation is typically on the order of 10 μm, but is only about 100 nm in the backward process, making it much weaker.

Perfect phase matching in the forward direction occurs when the refractive indices for the two wavelengths are equal. This condition can be achieved in birefringent crystals for different polarizations of the interacting waves. Quasi–phase matching (*3*) relies on micro- or nanostructuring the material so that it reverses the sign of its nonlinearity after every coherence length, thereby restoring the phase relation between the wavelets. This approach is possible for either the forward or the backward process, but not for both at the same time. Finally, if the refractive index can be reduced to zero, the oscillations cease in the material, and all of the wavelets add up in phase in all directions (see the figure, panel D). This case is the one demonstrated by Suchowski *et al.* in a metamaterial.

Metamaterials first received attention because they can possess a negative refractive index (*4*), which allows imaging with resolution below the diffraction limit (*5*). Metamaterials usually consist of metal-dielectric composites, whose plasmonic resonances (collective oscillations of electrons) can enhance optical effects, including nonlinear ones (*6*). Nonlinear experiments on metamaterials in the optical regime have mainly been limited to thin, surface-type samples (*7*–*9*), where phase matching is not a constraint. However, negative-index bulk materials and their phase-matching properties have been studied in the microwave regime (*10*).

Suchowski *et al.* extend these concepts to a new regime where the refractive index is near zero. They used a "fishnet" metamaterial (*11*, *12*), which consists of alternat-

Department of Physics, Tampere University of Technology, P.O. Box 692, FI-33101 Tampere, Finland. E-mail: martti.kauranen@tut.fi

Published by AAAS

ing layers of metal and dielectric perforated with holes (see the figure, panel E). The experiment was performed using four-wave mixing (FWM) instead of the simpler SH generation. The main reason for this is that the structure has a near-zero index only over a narrow wavelength range around 1330 nm. Whereas SH generation involves two very different input and output wavelengths, FWM occurs between nearby wavelengths. Typically, interaction among three beams of nearby frequencies gives a fourth (signal) beam also at a nearby frequency, which is useful for creating multiple frequencies for fiber-optic communications.

Suchowski *et al*. used a laser producing ultrashort-duration (femtosecond) pulses. Because such pulses consist of several frequency components, the FWM process occurs between different frequency components of each pulse, allowing pulse timing and beam alignment difficulties to be avoided. The signal can be detected at a nearby frequency, and all the interacting frequencies are now in the range where the metamaterial has a near-zero index. The forward and backward FWM signals are indeed equally strong, even though the sample cannot be considered thin.

The fishnet metamaterial is highly anisotropic with different properties in the sample plane and along its normal. In the present experiment, the sample has near-zero index only for light propagating along the sample normal, whereas light propagating in the sample plane experiences a very different index (*13*). This anisotropy benefits the experiment because transverse phase matching is enforced in the sample plane, thereby maintaining high directionality of the forward and backward signals. In contrast, an isotropic metamaterial with zero index would emit in all directions, which is undesirable for signal collection.

The present metamaterial has a period of 80 nm in the direction of propagation. The results could potentially arise from a type of quasi–phase matching, but the authors exclude this possibility by estimating that the coherence length for backward FWM is about 460 nm, much longer than the period. They also show (in supplementary material) that essentially identical results are obtained from treating the structure as an effective metamaterial and from accounting for each layer of the structure separately.

It is relatively easy to phase-match FWM between nearby wavelengths in almost any material, albeit only in one direction. Furthermore, the FWM efficiency reported by of Suchowski *et al*. remains low (10^{-5}). Nevertheless, their work demonstrates a completely new principle for overcoming the phase-matching problem. In addition, the possibility of generating equal nonlinear signals in two opposite directions could find use in new types of nonlinear oscillators (*14*). From a more general viewpoint, the report shows that metamaterials can control nonlinear processes in unprecedented ways, opening the path toward nonlinear structures with unconventional emission properties.

References

1. H. Suchowski *et al*., *Science* **342**, 1223 (2013).
2. C. M. Soukoulis, M. Wegener, *Nat. Photonics* **5**, 523 (2011).
3. M. M. Fejer, G. A. Magel, D. H. Jundt, R. L. Byer, *IEEE J. Quantum Electron.* **28**, 2631 (1992).
4. V. G. Veselago, *Sov. Phys. Usp.* **10**, 509 (1968).
5. J. B. Pendry, *Phys. Rev. Lett.* **85**, 3966 (2000).
6. M. Kauranen, A. V. Zayats, *Nat. Photonics* **6**, 737 (2012).
7. M. W. Klein, C. Enkrich, M. Wegener, S. Linden, *Science* **313**, 502 (2006).
8. E. Kim, F. Wang, W. Wu, Z. Yu, Y. Shen, *Phys. Rev. B* **78**, 113102 (2008).
9. H. Husu *et al*., *Nano Lett.* **12**, 673 (2012).
10. A. Rose, D. Huang, D. R. Smith, *Phys. Rev. Lett.* **107**, 063902 (2011).
11. S. Zhang *et al*., *Phys. Rev. Lett.* **95**, 137404 (2005).
12. J. Valentine *et al*., *Nature* **455**, 376 (2008).
13. C. Rockstuhl, C. Menzel, T. Paul, T. Pertsch, F. Lederer, *Phys. Rev. B* **78**, 155102 (2008).
14. C. Canalias, V. Pasiskevicius, *Nat. Photonics* **1**, 459 (2007).

10.1126/science.1247622

DEVELOPMENT

Permission to Proliferate

Epidermal stem cells produce the signals that control tissue homeostasis.

Julia Frede and Philip H. Jones

Maintaining proliferating adult tissues involves a critical balance. Exactly the right number of cells must be produced to replace those lost from the tissue; otherwise, tissue failure or tumor formation will ensue. In mammalian epidermis, differentiated cells are shed from the tissue surface and replaced by dividing stem cells in the basal layer (see the figure) (*1*). On average, each cell division generates one daughter that goes on to divide and produce more such cells, while the other cell differentiates and migrates to the surface of the epidermis (*2*). Cell production must be adjusted in response to surface abrasion or injury, implying that proliferation is regulated by signals from nearby cells. One candidate for this role is the secreted protein Wnt, as mutations that disrupt its downstream cellular signaling pathway result in hairless, thin epidermis (*3*, *4*). Two studies—by Lim *et al*. (*5*) on page 1226 of this issue and by Choi *et al*. (*6*)—elucidate how Wnt functions in the epidermis. They show that Wnt and Wnt inhibitors balance the renewal and differentiation of epidermal stem cells and are both secreted by the stem cells themselves. This suggests autocrine regulation as distinct from the prevailing idea that stem cells are regulated by signals from other cell types in a "niche."

To identify cells receiving Wnt signals, Lim *et al*. and Choi *et al*. generated transgenic mouse strains that allowed them to track cells that express the Wnt target gene *Axin2*. Both studies found Axin2-expressing cells in the proliferative basal layer of the epidermis. Lim *et al*. used a genetic technique to label Axin2-expressing cells in the hind-paw skin of the mouse, which lacks hair follicles that may feed cells into the epidermis under conditions of stress or injury (*7*). The label is transmitted to daughter cells, producing clones (*8*). Using statistical analysis of the clone size distribution, Lim *et al*. found that Axin2-expressing cells constitute a self-maintaining population of functionally equivalent cells. Each cell in the basal layer divides to generate two dividing daughters, two differentiating daughters, or one cell of each type. Although the outcome of individual divisions is unpredictable, the odds are balanced, so homeostasis is achieved across the Axin2-expressing population. Similar balanced outcomes of division leading to "population self-renewal" occur in tail and ear epidermis and the esophageal epithelium (*2*, *9*–*11*).

A question that arises from these observations is how an injury to the paw can be healed. To achieve this, an excess of proliferating cells must be produced. In tail epidermis, this is accomplished by "reserve" cells,

MRC Cancer Unit, University of Cambridge, Hutchison–MRC Research Centre, Box 197, Cambridge Biomedical Campus, Cambridge CB2 0XZ, UK. E-mail phj20@mrc-cu.cam.ac.uk

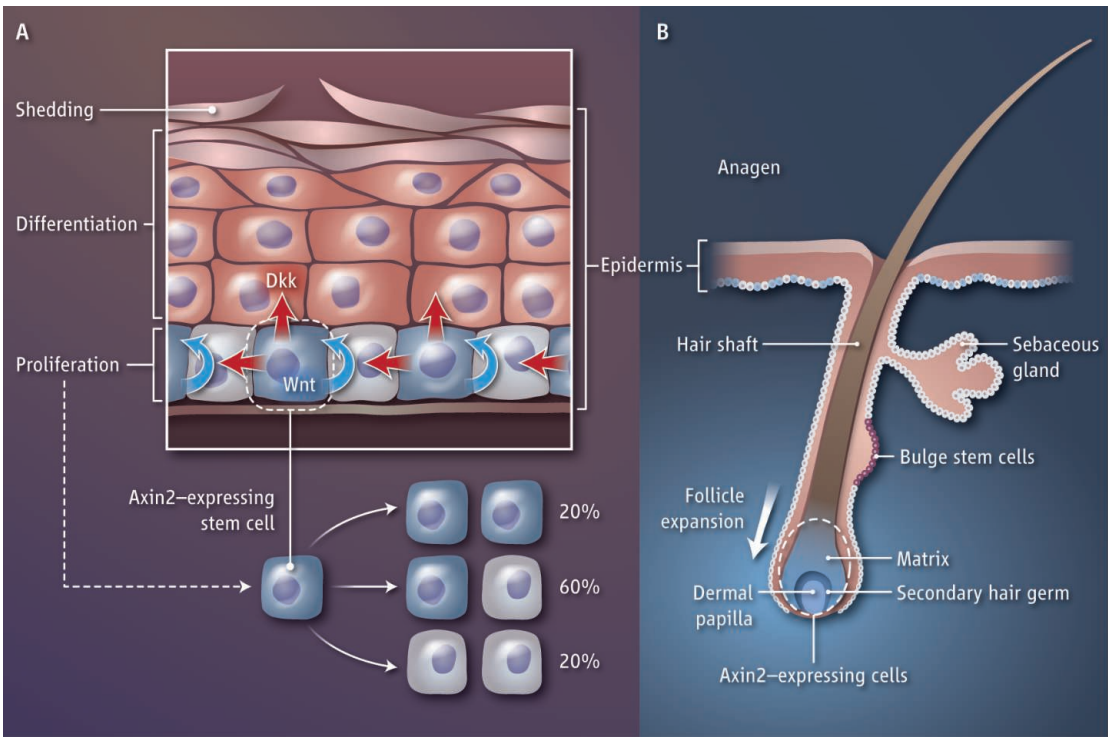

Stem cell signals. (**A**) Axin2-expressing stem cells (blue) in the basal layer of the mouse epidermis divide, producing stem and differentiating (gray) daughters with the probabilities shown (%). The daughter cells produce both Wnt (blue arrow) and Dkk (red arrow). Wnt promotes proliferation. Dkk accumulates in the suprabasal layer (red), blocks Wnt signaling, and promotes differentiation. (**B**) In the growth phase of the hair cycle, the lower part of the follicle expands (anagen). Axin2 expression (and Wnt signaling) is observed in proliferating cells in the dermal papilla, secondary hair germ, matrix, and hair shaft progenitors, but is absent from the bulge stem cells. Deletion of *β-catenin* or overexpression of *Dkk1* arrests proliferation.

which are slow-cycling under normal conditions but mobilized upon injury (*10*). However, Lim *et al*. could not detect a reserve population in the paw, and after injury, Axin2-expressing progeny make a proportionate contribution to wound repair. This suggests that cells expressing Axin2 in the vicinity of a wound may transiently switch from balanced cell production to generating an excess of proliferating cells, enabling them to heal a wound themselves, behavior also evident in esophageal epithelium (*11*). The Axin2-expressing cells may reasonably be called "stem cells" as they both maintain and repair the tissue and are not underpinned by "reserve" cells. These observations add to a growing body of evidence for behavioral plasticity in injured epithelia, with proliferating cells changing fate and differentiated cells reentering the cell division cycle to repair injured tissues (*12*–*14*).

This demonstrates that Wnt signaling is active in epidermal stem cells, but does it regulate their behavior? In the canonical Wnt signaling pathway, the protein β-catenin accumulates in the cytoplasm in response to Wnt-initiated signaling and eventually translocates to the nucleus where it controls gene expression. Lim *et al*. and Choi *et al*. show that deleting the β-*catenin* gene in Axin2-expressing cells results in their differentiation; overexpressing the gene encoding dickkopf (*Dkk*), an inhibitor of Wnt signaling, in basal cells produces a thinned epidermis with fewer proliferating cells. Lim *et al*. show that basal cells that express Axin2 express several *Wnt* family members and the *Dkk1* and *Dkk3* genes, arguing that Wnt may act in an autocrine manner on stem cells. They also show that Dkk protein accumulates in the suprabasal layers, suggesting that differential diffusion of both molecules restricts Wnt activation to the basal layer of the epidermis. Wnt signaling is needed for stem cell self-renewal and the relative amounts of stem cell–derived Wnt and Dkk may regulate stem cell fate.

What about the hair follicles? These are sustained by multiple populations of stem cells, both in the upper follicle, which is continuous with the epidermis, and in the bulge and lower follicle, which undergoes cycles of expansion (anagen), regression (catagen), and quiescence (telogen) (*1*). Choi *et al*. demonstrate that Axin2 expression is very low in resting follicles, but high in the intensely proliferative cells of the expanding lower follicle during anagen. Inducible deletion of *β-catenin* or expression of *Dkk1* in resting follicles prevented the onset of anagen and, if carried out during anagen, halted proliferation and triggered premature follicle regression. This indicates that Wnt signaling is essential to initiate and sustain follicle expansion. Choi *et al*. also noted that the slow-cycling stem cells of the hair follicle bulge do not express Axin2 and therefore are unaffected by loss of Wnt signaling. The authors also observed that long-term induction of Dkk1expression produced bald mice, in which the follicle and bulge stem cells persisted. When Dkk1 expression ceased, follicular proliferation and differentiation were reactivated, indicating that Dkk1 drives follicles into a state of "suspended animation." Thus, Wnt signaling is required for proliferation, but not survival, of hair follicle and bulge stem cells.

The results of Lim *et al*. and Choi *et al*. suggest that the balance of autocrine Wnt and Dkk signaling in maintains epidermal and hair follicle stem cells in a proliferative state. How cells might escape the autocrine loop of Wnt signaling and commence the differentiation process remains unclear. Perhaps small fluctuations in Wnt pathway activity explain the apparently stochastic onset of stem cell differentiation. Whether Wnt contributes to the injury response of stem cells also remains to be elucidated.

References

1. G. Solanas, S. A. Benitah, *Nat. Rev. Mol. Cell Biol.* **14**, 737 (2013).
2. E. Clayton *et al*., *Nature* **446**, 185 (2007).
3. J. J. Barrott, G. M. Cash, A. P. Smith, J. R. Barrow, L. C. Murtaugh, *Proc. Natl. Acad. Sci. U.S.A.* **108**, 12752 (2011).
4. H. Clevers, R. Nusse, *Cell* **149**, 1192 (2012).
5. X. Lim *et al*., *Science* **342**, 1226 (2013).
6. Y. S. Choi *et al*., *Cell Stem Cell* 10.1016/j.stem.2013.10.003 (2013).
7. V. Levy, C. Lindon, Y. Zheng, B. D. Harfe, B. A. Morgan, *FASEB J.* **21**, 1358 (2007).
8. M. P. Alcolea, P. H. Jones, *Nat. Rev. Cancer* **13**, 161 (2013).
9. D. P. Doupé, A. M. Klein, B. D. Simons, P. H. Jones, *Dev. Cell* **18**, 317 (2010).
10. G. Mascré *et al*., *Nature* **489**, 257 (2012).
11. D. P. Doupé *et al*., *Science* **337**, 1091 (2012).
12. D. P. Doupé, P. H. Jones, *Bioessays* **35**, 443 (2013).
13. S. J. Buczacki *et al*., *Nature* **495**, 65 (2013).
14. P. R. Tata *et al*., *Nature* **503**, 218 (2013).

10.1126/science.1248274

CREDIT: H. MACDONALD/*SCIENCE*

SCIENCE & SCILIFELAB PRIZE

From Persistence to Cross-Species Emergence of a Viral Zoonosis

Interdisciplinary research on zoonotic pathogens illuminates ecology and evolution, while guiding disease prevention and control.

Daniel G. Streicker

Emerging infectious diseases threaten all forms of life on Earth. Many pathogens of great historical and contemporary significance have originated from other species, triggering pandemics, disrupting agriculture, and challenging efforts to conserve endangered wildlife. Despite decades of research on species-jumping pathogens, the most central questions in the field remain major stumbling blocks for societies that seek to mitigate their impacts. These questions include which pathogens are most likely to emerge, which hosts are most likely to share pathogens, and what will be the long-term fate of newly emerged pathogens? Part of the challenge is that emergence, by nature, transcends scientific disciplines, occurring as the product of human behavior, environmental change, population, cellular and molecular biology, and evolution. Solutions therefore demand innovative pairing of theory and fundamental science with applied research and evidence-based policy-making.

Science and SciLifeLab are pleased to present the grand prize–winning essay on the topic of Environmental Life Science by Daniel G. Streicker, the 2013 winner of the *Science* & SciLifeLab Prize for Young Scientists.

My doctoral research used viral infections of bats to answer fundamental questions about pathogen emergence and to help guide control of a major zoonosis in the developing world. Working on bats was partly pragmatic—natural populations can easily be sampled in large numbers, and existing surveillance systems for reportable diseases, such as rabies, provide rich data sets. This choice was also driven by the fact that bats are a major source of highly pathogenic viruses, including severe acute respiratory syndrome (SARS), Nipah, Hendra, and Ebola viruses, which often emerge in the context of anthropogenic change with devastating outcomes for humans and animals (*1*). From an ecological and evolutionary perspective, the high species diversity of bats also presents a unique and fascinating system to test hypotheses on cross-species emergence in complex host communities.

Working with bat tissue samples from public health laboratories across the United States, I first constructed a data set of hundreds of rabies virus sequences from more than 20 bat species. Using ecological and molecular sequence data from both bats and viruses, I developed a novel population genetic framework to quantify transmission rates between species. This analysis (*2*) showed that, counter to the popular notion that rapid evolution in RNA viruses should make ecological overlap the best predictor of which host species share viruses, the genetic similarity of hosts constituted the strongest barrier to both initial infection and viral establishment in new species. The strong phylogenetic constraints on cross-species transmission move us closer to predicting the species origins of viral emergence.

Despite recurrent cross-species transmission in many natural systems, sustained pathogen transmission in newly infected species is rare. This outcome, although fortunate for agricultural, veterinary, and public health interests, represents an obstacle to identifying the mechanistic underpinnings of emergence, because many independent introduction events must be tracked to deduce the predictors of successful emergence. Dozens of historical host shifts among American bat species make rabies an ideal system to explore the epidemiological and evolutionary repeatability of viral emergence. Genomic and demographic inference showed that rabies followed distinct evolutionary pathways to become established in different host species. Further, viruses for which greater adaptive evolutionary changes occurred took longer to establish endemic transmission in new hosts. This work (*3*), addressed the outstanding question of how much evolution happens during host shifts, which may help anticipate the speed and likelihood of viral establishment in new host species. A related study explored the interactions between host ecology and viral evolution by quantifying the rate of molecular evolution across 21 bat-associated rabies viruses. The tempo of viral evolution was surprisingly variable and profoundly dependent on host ecology. Viruses in temperate bats evolved more slowly (by a factor of up to 22) than those in tropical and subtropical species, a likely consequence of seasonal interruption of transmission during hibernation. These results (*4*) imply that bat rabies risk for humans and domestic animals in the tropics will be less predictable than in the temperate zone and demonstrated how host biology can shape the speed of viral evolution.

These studies highlight the power of integrated ecological and evolutionary analyses to reveal general patterns in the frequency, origins, and dynamical outcomes of cross-species transmission. However, they offer no easy solutions for policy-makers seeking to prevent disease. Efforts to control wildlife zoonoses often rely on interventions such as culling; a method perceived to offer the possibility of

Bats as a model and a source of emerging viruses. Cross-cutting research across ecology, phylogenetics, mathematical modeling, and public health on species such as the common vampire bat can illuminate basic principles of disease biology and provide crucial tools to mitigate the impacts of emerging viruses on health, agriculture, and conservation.

Institute of Biodiversity, Animal Health, and Comparative Medicine, University of Glasgow, Glasgow, G12 8QQ, Scotland, UK. E-mail: daniel.streicker@glasgow.ac.uk

Published by AAAS

pathogen elimination, thereby providing a cost-efficient alternative to mass vaccination of humans or domestic animals. Yet, interventions in reservoirs are notoriously challenging and controversial because of limited understanding of pathogen persistence in complex wildlife systems (*5*, *6*). The only bat that is culled to manage zoonotic disease is the common vampire bat *Desmodus rotundus*, found throughout the neotropics (see the photo). Despite control campaigns since the 1960s, lethal human rabies outbreaks transmitted by this species are common, and annual livestock deaths number in the thousands (*7*). In 2007, I launched a collaborative research program aimed at reducing this burden through enhanced understanding of rabies ecology in vampire bats. Findings from this project question the core assumptions underlying culling bats for disease control. By monitoring more than 1000 bats across a network of colonies in Peru for nearly 4 years, I showed that rabies exposure in vampire bats was unrelated to colony size. This work (*8*) further showed that culled colonies had either equivalent or higher rates of viral exposure compared with those that were not. Exploration of these data with mechanistic mathematical models suggested that high rates of bat dispersal drive viral persistence and may inherently limit the efficacy of culling, especially if culling increases bat dispersal (*9*). These results challenge the conventional wisdom that fewer bats equals less disease and provide a view toward more effective rabies control in Latin America through spatially synchronized interventions.

My thesis work at the interface between ecology, evolution, and anthopogenic change underscores emerging diseases as one of the most fascinating, challenging, and important topics in the environmental life sciences. Together, these studies provide salient examples of how transdisciplinary collaboration can illuminate fundamental concepts in disease biology, while advocating a science-guided path to anticipate and prevent future disease emergence.

References

1. C. H. Calisher *et al.*, *Clin. Microbiol. Rev.* **19**, 531 (2006).
2. D. G. Streicker *et al.*, *Science* **329**, 676 (2010).
3. D. G. Streicker *et al.*, *Proc. Natl. Acad. Sci. U.S.A.* **109**, 19715 (2012).
4. D. G. Streicker *et al.*, *PLOS Pathog.* **8**, e1002720 (2012).
5. J. O. Lloyd-Smith *et al.*, *Trends Ecol. Evol.* **20**, 511 (2005).
6. D. G. Streicker *et al.*, *Ecol. Lett.* **16**, 975 (2013).
7. World Health Organization, *World Health Organ. Tech. Rep. Ser.* **2013**, 1 (2013).
8. D. G. Streicker *et al.*, *Proc. Biol. Sci.* **279**, 3384 (2012).
9. J. Blackwood *et al.*, *Proc. Natl. Acad. Sci. U.S.A.* 10.1073/pnas.1308817110 (2013).

10.1126Science.1247566

2013 Grand Prize Winner

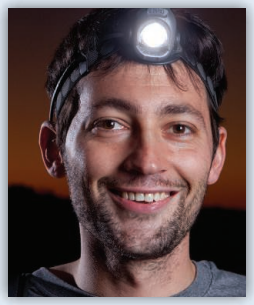

The author of the grand prize–winning essay in the category of Environmental Life Science, **Daniel G. Streicker**, is a Sir Henry Dale Research Fellow at the Institute of Biodiversity, Animal Health and Comparative Medicine at the University of Glasgow. His research applies longitudinal field studies, phylogenetics, and epidemiological modeling to understand the process by which infectious diseases emerge and establish in new host species. He received his Ph.D. from the Odum School of Ecology at the University of Georgia in 2011 and worked previously as an Emerging Infectious Diseases Fellow at the U.S. Centers for Disease Control and Prevention. He received the 2013 Robert C. Anderson Award for Best Dissertation in Life Science from the University of Georgia and has received funding from the National Science Foundation, the Wellcome Trust, the Royal Society, the American Philosophical Society, and National Geographic.

2013 First Runner-Up

Gabriel D. Victora for his essay in the category of Molecular and Cellular Biology, "Stop, Go, and Evolve," is the first runner-up. Dr. Victora is a Whitehead Fellow at the Whitehead Institute for Biomedical Research in Cambridge, Massachusetts, where he heads the Laboratory of Lymphocyte Dynamics. He received his Ph.D. from New York University School of Medicine for work done jointly at this institution and at the Rockefeller University. His work combines mouse genetics with intravital microscopy to study the development of high-affinity antibodies in the germinal center. He is a recipient of the 2011 Weintraub Award for Graduate Research, the 2012 March of Dimes Foundation Basil O'Connor Scholar Award, and the 2012 National Institutes of Health director's Early Independence Award. http://scim.ag/SciLifeLab_Victora

2013 Finalists

Weizhe Hong for his essay in the category of Developmental Biology, "Assembly of a Neural Circuit," is a finalist. Dr. Hong is a Helen Hay Whitney Fellow at California Institute of Technology, working on neural mechanisms underlying social and emotional behaviors in David Anderson's laboratory. Dr. Hong received a B.Sc. degree in biological sciences at Tsinghua University and a Ph.D. degree from Stanford University, where he worked in Liqun Luo's laboratory and studied the cellular and molecular mechanisms of wiring specificity in olfactory system development. Dr. Hong received the Genetics Society of America's Larry Sandler Memorial Award for the best Ph.D. dissertation on *Drosophila*-related research and presented the Larry Katz Memorial Lecture at the Cold Spring Harbor Conference for the best Ph.D. dissertation on neural circuit research. http://scim.ag/SciLifeLab_Hong

Dominic Schmidt for his essay in the category of Genomics/Proteomics/Systems Biology, "Dynamics and Evolution of Vertebrate Transcriptional Regulator Binding," is a finalist. Dr. Schmidt is a Strategy Consultant at L.E.K. Consulting in London where he works as a strategic adviser to the biopharma and life sciences industry. He received his Ph.D. in Oncology from the University of Cambridge where he combined experimental and computational approaches across multiple species to study how gene-regulation and genomes are evolving. Before getting his Ph.D., he received his German diploma degree in biochemistry at the Max Planck Institute for Molecular Genetics and the Free University of Berlin. http://scim.ag/SciLifeLab_Schmidt

For the full text of all winning essays and further information, see the *Science* site at http://scim.ag/SciLifeLab.

CREDITS: (TOP TO BOTTOM) NANCY EVELYN, KATHLEEN DOOHER, YE EMILY WU, MARK WOOD

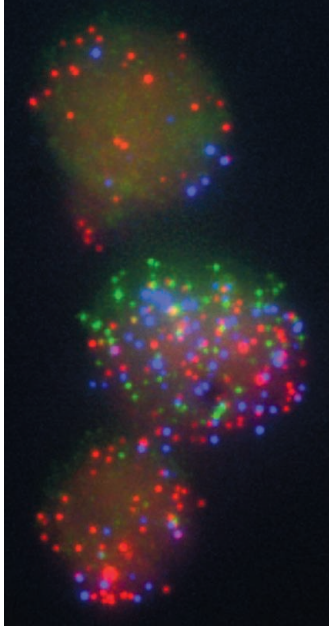

INTRODUCTION

Cells Go Solo

THE SCIENTIFIC LITERATURE CONTAINS AN ENORMOUS BODY OF WORK IN WHICH large numbers of cells have been broken open and homogenized to prepare samples for biochemical characterization and, certainly, much has been learned from such studies. But more recently, it has become possible to monitor events in single cells, thus allowing investigators to test whether existing "averaged" readings of the state of many cells from traditional large-scale assays accurately represent the behavior of the individual cells being studied. Such single-cell measurements are providing a wealth of information—sometimes unanticipated and often previously obscured—about how cells respond to perturbations or signals. In this special issue, three Reviews provide examples of fundamental insights into cellular regulation that are revealed when it is possible to measure enzymatic activity, transcriptional responses, or the metabolic state in individual cells.

An obvious advantage of single-cell measurements is the ability to measure variations or "noise" in the responses of the individual cells to similar or identical conditions. In many instances, it is possible to monitor the time course of cellular responses. Gene transcription can be particularly noisy, with bursts of RNA synthesis occurring in some cells but not others of the same population. Thus, fundamental questions arise about the nature of these systems. Perhaps variation in response is advantageous in conserving resources or in assuring that some cells survive in a changing environment. Or it may be that biophysical constraints of small numbers of molecules and the characteristics of the enzymes at work dictate such variability as unavoidable. Sanchez and Golding review recent work in model systems, from bacteria to animal cells, that attempts to resolve whether the kinetics of transcription are encoded in the architecture of promoter sequences in DNA—and might therefore vary throughout the genome—or are determined by physical or biophysical properties that would impose more global constraints throughout the cell.

Levine *et al.* explore another previously hidden phenomenon. Continuous measurements of protein activation show that many undergo asynchronous pulsatile responses, which are obscured in average measurements from a population of cells. They discuss how cellular circuits are wired to produce such responses and what the advantages of such control systems might be.

Zenobi highlights methodological advances, particularly in mass spectrometry, that are enabling quantitation of the abundance of molecular components of single cells. Challenges abound for the goal of making simultaneous measurements to characterize the rapidly changing metabolic state of individual cells. But the promise of new insights across a broad range of disciplines is sustaining a steady effort to tap into the large store of new knowledge lying hidden within the confines of single cells.

– L. BRYAN RAY

Single-Cell Biology

CONTENTS

Reviews

See also more cell biology in this issue: Research Articles on pages 1202 and 1203 and Podcast

Science

Published by AAAS

REVIEW

Genetic Determinants and Cellular Constraints in Noisy Gene Expression

Alvaro Sanchez[1]* and Ido Golding[2,3,4]*

In individual cells, transcription is a random process obeying single-molecule kinetics. Often, it occurs in a bursty, intermittent manner. The frequency and size of these bursts affect the magnitude of temporal fluctuations in messenger RNA and protein content within a cell, creating variation or "noise" in gene expression. It is still unclear to what degree transcriptional kinetics are specific to each gene and determined by its promoter sequence. Alternative scenarios have been proposed, in which the kinetics of transcription are governed by cellular constraints and follow universal rules across the genome. Evidence from genome-wide noise studies and from systematic perturbations of promoter sequences suggest that both scenarios—namely gene-specific versus genome-wide regulation of transcription kinetics—may be present to different degrees in bacteria, yeast, and animal cells.

The advent of rapid, inexpensive DNA sequencing methods allows scientists to map not only the protein-coding genes in the genomes of many organisms, but also the regulatory sequences present in those genomes. A key challenge for biologists in the next few decades is understanding how these regulatory sequences control the expression of every gene in the cell and how they collectively determine the topology and dynamics of gene regulatory networks.

The regulation of gene expression traditionally has been studied in experiments that measured the average gene expression level in populations containing millions of cells. These studies relate the average rate of gene expression for a gene to its regulatory DNA sequence (the promoter architecture) (*1*). This approach has a major shortcoming, however, because averaging over populations masks differences in gene expression that may occur between individual cells (*2*). These differences may in turn have consequences for the whole multicellular community or organism, which makes it important to understand gene expression in single cells.

Within a single cell, gene expression is inherently stochastic, or random (*2*). Protein-coding genes are typically present in only one or two copies per cell. Whether a gene is transcribed at any given moment depends on the arrival, by diffusion, of multiple regulatory proteins to their designated binding sites, as well as the occurrence of multiple biochemical steps required for initiation of transcription (*3*). These biochemical reactions are all essentially single-molecule events and thus stochastic, resulting in substantial randomness in the production of mRNA. Broadly, two stochastic kinetic modes of transcription have been observed in individual cells: "Poissonian," in which mRNAs are synthesized in random, uncorrelated events, with a probability that is uniform over time (*4*, *5*); and "bursty," in which mRNA is produced in episodes of high transcriptional activity (bursts) followed by long periods of inactivity (Fig. 1 and Box 1) (*5*–*8*). The kinetic features of mRNA production are in turn propagated to the proteins translated from them. The end result is temporal fluctuations, and corresponding cell-to-cell variability, in mRNA and protein numbers. This cell-to-cell variability is referred to as gene expression noise (Box 2) (*2*).

Bursty transcription typically leads to higher noise than does Poissonian transcription. In particular, the burst size controls the magnitude of the noise, and it is approximately proportional to the Fano factor (the ratio between the variance and the mean of the distribution of mRNA or protein numbers per cell). Thus, genes with large burst sizes are characterized by broader distributions of protein and mRNA, larger Fano factor, and higher noise as compared with those of genes with small burst sizes.

The inherent randomness associated with gene expression raises an important question: Are the stochastic kinetics of transcription—and therefore the resulting variability in mRNA and protein levels—encoded by the promoter regulatory sequence, just as the mean expression level of a gene appears to be? Two alternative answers have been put forward. One view is that the stochastic kinetics of gene activity are genetically determined by the promoter architecture and governed by the binding and unbinding of various regulatory elements such as histones and transcription factors to their corresponding binding sites (*9*–*15*). In this view, it is the process of gene regulation, as it acts on each promoter individually, that causes bursting in some genes but not in others.

An alternative view is that transcription kinetics are dominated by genome-wide constraints that lead to general—as opposed to gene-specific—modulation of transcriptional kinetics (*16*–*19*). These constraints may reflect any number of physiological or biophysical mechanisms. Proposed mechanisms include cell-cycle–dependent regulation of promoter activity (*20*) as well as inherent features of the transcription process, such as the cooperative recruitment of RNA polymerases (*21*). Notwithstanding the specific details, this view implies that gene-specific transcriptional regulation acts on top of these gene-nonspecific constraints and has only a secondary effect on the observed kinetic features, such as transcription bursts.

In the first view described above, transcriptional kinetics (in particular, bursting) are gene-specific and free from global constraints. One consequence of this is that at both very low and very high rates of transcription promoter activity is expected to be regular in time and well-described by Poisson statistics (Fig. 1, top). At intermediate rates of transcription, when genes are neither expressed at full capacity nor very infrequently, different genes may vary greatly in their temporal kinetics and exhibit either regular (Poissonian) or bursty behavior, depending on the particular mechanisms of transcriptional regulation for each gene (Fig. 1, top).

In contrast, global constraints on transcriptional kinetics that affect all genes (Fig. 1, bottom) result in a more limited space of possible kinetic behaviors. For instance, one such constraint that has been recently reported (*16*–*18*) is the presence of inherent and global bursting kinetics even in fully active gene loci. Thus, highly expressed genes are not Poissonian but instead characterized by large burst sizes (Fig. 1, bottom) (*16*, *17*) and therefore large cell-to-cell variability in mRNA and protein expression. Because this constraint operates globally, all genes in the cell follow a characteristic trend between the burst size and the mean amount of expression (Fig. 1, bottom).

The two views described above represent two limiting cases; it is possible that single-cell transcriptional kinetics are affected, to varying degrees, by both gene-specific (promoter architecture) and genome-wide processes. This Review critically examines both views and the evidence supporting each of them. An organism for which there is strong evidence for a genetic origin of transcriptional noise is the yeast *Saccharomyces cerevisiae.* In the prokaryote *Escherichia coli*, as well as other eukaryotic systems, the picture is less definitive than in yeast, but some evidence exists pointing to the presence of global constraints.

Transcriptional Kinetics in Yeast are Gene-Specific

The relation between noise and the mean expression level has been examined in several studies that measured gene expression at the single-cell

[1]The Rowland Institute at Harvard, Harvard University, Cambridge, MA 02142, USA. [2]Verna and Marrs McLean Department of Biochemistry and Molecular Biology, Baylor College of Medicine, Houston, TX 77030, USA. [3]Center for Theoretical Biological Physics, Rice University, Houston, TX 77005, USA. [4]Center for the Physics of Living Cells, University of Illinois at Urbana-Champaign, Urbana, IL 61801, USA.

*Corresponding author. E-mail: sanchez@rowland.harvard.edu (A.S.); golding@bcm.edu (I.G.)

level for a complete yeast genomic library (*22*) or a large set of promoters (*14*, *23*, *24*). As noted above, it is possible to estimate the burst size from the degree of cell-to-cell variability in protein concentration (supplementary materials). The results of all of these experiments are consistent in that they find no obvious trend between the mean expression level from a promoter and the estimated burst size (Fig. 2A). The only global constraint observed in the noise measurements is the one corresponding to the limiting case of Poissonian transcription, followed by Poissonian translation of mRNA into protein (*2*).

These global noise experiments also reveal relationships between noise measured for a given promoter and the known properties of that promoter. The majority of low-noise promoters have a characteristic architecture [depleted proximal nucleosome (DPN)] that is defined by a nucleosome-free region immediately downstream of the initiation site. In contrast, the majority of high-noise promoters have a second type of architecture [occupied proximal nucleosome (OPN)], characterized by the lack of a nucleosome-free region. They are also enriched for strong TATA boxes (*25*, *26*).

The model emerging from these findings is that promoter switching between inactive (promoter occluded by nucleosome) and active (nucleosome free, preinitiation complex formed) states may result in bursty transcription, in turn leading to the higher noise observed in nucleosome-covered promoters. Within this picture, the strong TATA box would ensure that the promoter is expressed strongly when active, increasing the burst size (*11*).

This model is further supported by single-mRNA counting experiments in fixed cells (Fig. 3A and Box 1) (*27*, *28*). These studies examined the mRNA distributions for 12 different constitutive promoters that have low nucleosome density and were characterized as "low noise" in genomic studies. All of these promoters exhibited close-to-Poissonian mRNA copy-number distributions and sub-Poissonian (with lower variance than a Poissonian distribution of the same mean) nascent RNA copy number distributions, which is consistent with the absence of bursts. In contrast, promoters that are not constitutive, but regulated by nucleosomes and transcription factors, exhibited broader mRNA distributions consistent with bursty transcription (Fig. 3A). These single-cell mRNA counting experiments substantiated the notion that the observed differences in protein noise between promoters [as in the studies above (*22*–*24*)] reflect the fluctuations of the mRNA species (which in turn are driven by transcriptional kinetics). The mRNA-counting studies specifically predicted that in the low-noise, nucleosome-depleted promoters, transcription events should occur regularly in time, in a simple Poissonian manner. This prediction was confirmed in experiments in which the kinetics of transcription were followed in real-time by using temporal correlation analysis of fluorescently labeled mRNA molecules in live yeast cells (*4*). Both the constitutive promoter *MDN1* and the cell-cycle–activated promoter *POL1* were transcribed in random, uncorrelated events with a single rate of initiation that varied during the cell cycle (*4*)

The evidence above indicates that the kinetic mechanism of transcription for a yeast promoter is mainly encoded by the DNA sequence of the promoter. To substantiate this picture, investigators deliberately altered yeast promoter architecture and examined the resulting change in gene expression noise. The systematic alterations included the presence or absence of a TATA box and its strength (*12*, *24*); the number (*15*, *29*), location (*15*), and nucleosomal coverage (*30*) of transcription-factor binding sites; the presence of nucleosome-disfavoring sequences (*13*); and the mode of action of a transcription factor [whether it was acting as an activator or as a repressor (*14*)]. All of these architectural elements were found to strongly affect the relationship between the mean amount of expression and the burst size, in a way that is consistent with the expectation from simple models of transcriptional kinetics (Fig. 3) (*10*).

The evidence indicates that the stochastic transcriptional kinetics for a given gene in yeast is mainly determined by its promoter architecture, and no strong global constraints have been observed. Promoter switching introduced by transcription factors and nucleosomes stochastically associating and dissociating leads to a bursty transcription and correspondingly higher degree of noise than that observed in constitutive promoters (*11*). Additional promoter features such as the strength (*12*, *13*) and copy number (*15*, *29*) of transcription-factor binding sites, their location within the promoter (*15*), and the specific mechanism of gene regulation by the transcription factors bound to them (*14*) all affect noise in gene expression.

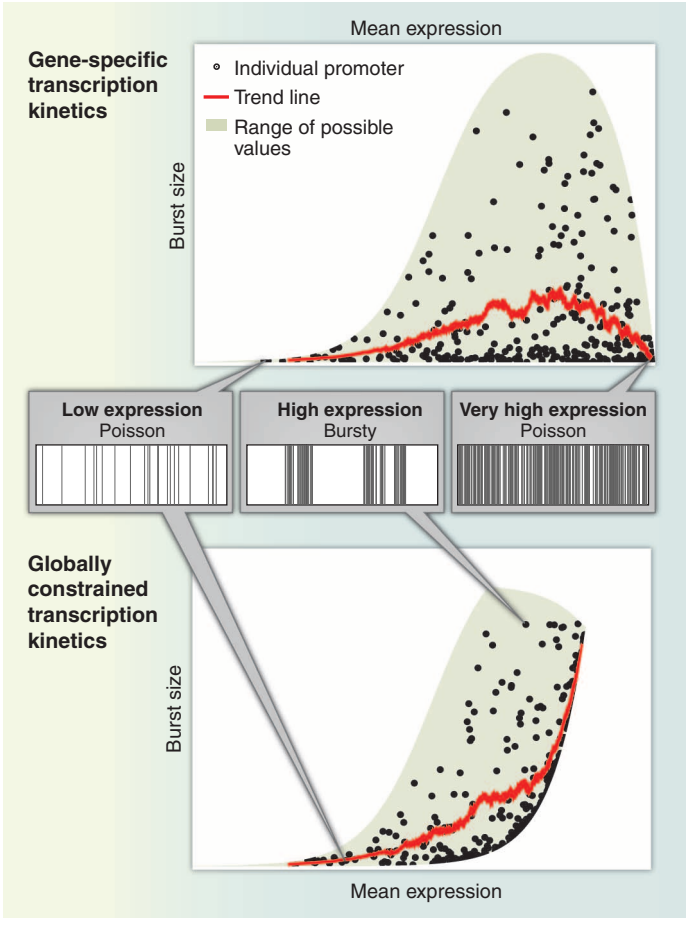

Fig. 1. Gene-specific versus global determinants of transcription kinetics. Two alternative scenarios are presented, representing different ways in which stochastic promoter activity may be governed. (**Top**) In the first scenario, the rates of promoter activation and inactivation are controlled exclusively by gene-specific mechanisms. (**Bottom**) In the second scenario, gene-specific regulation occurs in the presence of a global constraint on the kinetics. We illustrate the consequences of the two scenarios using simple mathematical "toy models" of promoter kinetics (supplementary materials). For each model, we calculate both the mean expression level and the size of transcription bursts for a large set of promoters and plot these two variables against each other. In the plot, black markers denote 300 randomly chosen individual promoters, the red curve represents the smoothed behavior of 10^4 promoters, and the shaded region is a guide-to-the-eye that depicts the full range of possible burst sizes for a given mean expression (supplementary materials).

Evidence for Global Noise Constraints in *E. coli*

A small number of studies have directly examined transcriptional kinetics in *E. coli*. Live-cell mRNA labeling (Box 1) has been used to visualize the synthesis of individual mRNA molecules in real time from a synthetic *E. coli* promoter (*6*, *17*). Analysis of how adding an inducer of gene expression affected the bursting parameters revealed that the burst frequency was modulated at low concentration of inducer, whereas

the burst size was modulated at high concentration of inducer (Fig. 2B, iii) (*17*). Transcription was bursty even for fully induced conditions (*6*). The $P_{lac/ara}$ promoter investigated in this study is a derivative of the *lac* promoter (P_{lac}), whose mechanism of regulation by *lac* repressor is thought to be well understood (*1*). However, simple theoretical models, based on these well-characterized mechanisms of gene regulation, failed to explain the observed effect of inducer on the bursting parameters (*9*). The transcriptional kinetics of the wild-type *lac* promoter have also been investigated as reflected in protein synthesis (*31*). These studies also indicate an increase in transcriptional burst size at high inducer concentration (*31*).

A predicted consequence of the observed modulation of the bursting parameters described above is that the Fano factor of the mRNA distribution should increase as the mean increases. This was observed for the *lac* promoter in the presence of various concentrations of inducer (*17*). Six other promoters were also studied under diverse conditions. Unexpectedly, it was found that all of them yielded values of the Fano factor that were very similar to those observed for the *lac* promoter (Fig. 2B, i) (*17*). The authors interpreted this finding as indicating that the promoters investigated all modulate their bursting parameters in a similar fashion: modulation of the burst frequency when expression is low and of the burst size when expression is higher.

An examination of the protein copy-number distribution for a genomic library in *E. coli* (*32*) found that the Fano factor did indeed increase with the mean level of gene expression, in a pattern very reminiscent of the RNA data described above (Fig. 2B, i and ii) (*17*) and consistent with the earlier protein distributions measured for P_{lac} (*31*). The authors offered an alternative interpretation for the observed relationship between the Fano factor and the mean protein concentration: that the increase in the Fano factor does not result from transcription bursts of increased size, but rather reflects the dominance of extrinsic noise (that caused by cell-to-cell differences in gene expression parameters) at high rates of expression. In support of this hypothesis, measurements of extrinsic noise coincided with the noise baseline observed at high rates of expression (*32*).

The difficulty to discriminate between alternative models on the basis of the relationship between the noise and the mean amount of expression underscores the potential pitfalls associated with overinterpreting static copy-number distributions. In addition to extrinsic noise, other effects may be confounded with stochasticity in transcription and translation. For instance, the statistics of protein and mRNA partitioning during cell division may in some cases lead to noise-mean scaling that is indistinguishable from that of stochastic transcription and translation (*33*). Effects due to the cell cycle may also be mistakenly attributed to stochastic transcription (*20*).

To achieve a mechanistic understanding of how promoter architecture affects transcriptional kinetics and noise in *E. coli*, the path previously taken in yeast will have to be emulated by measuring gene expression noise in promoters whose architecture is systematically perturbed (*12*–*15*, *29*). Such noise studies need to be accompanied by direct measurements of transcription kinetics in live cells.

Mammalian Cells and Other Eukaryotes

The studies reviewed above support the idea that constitutive genes in budding yeast are expressed in a Poissonian, nonbursty manner. However, it would be wrong to assume that this result is typical of all eukaryotic cells. Transcriptional kinetics of multiple genes in *Dictyostelium discoideum* (another single-celled eukaryotic organism), including housekeeping genes, were found to be bursty (*7*). Beyond protozoans, bursting kinetics seem to be the rule, rather than the exception, in many different types of animal cells, including cultured mammalian cells (*5*, *8*, *16*, *34*), fly embryos (*18*, *35*, *36*), and in the mouse (*37*).

Real-time transcriptional kinetics of both natural and synthetic promoters inserted into mouse fibroblasts (*34*) revealed transcriptional bursting from these promoters, and a refractory period after the bursts. Synthetic promoters engineered to differ in the number of binding sites for a

Box 1. Methods for probing gene expression at the single-cell level. (**A**) Transcription can be followed in real time in live cells by labeling nascent mRNA with fluorescently tagged RNA-binding proteins that are strongly expressed in the cell (*4*–*6*). (Transcriptional kinetics in *E. coli*, L. -h. So and I. Golding; adapted with permission from *Physical Biology of the Cell*, R. Phillips, J. Kondev, and J. Theriot; Garland Science.) (**B**) Distributions of the numbers of mRNA molecules per cell can be measured with single-mRNA counting techniques, such as single-molecule fluorescent in situ hybridization (smFISH) applied to fixed cells (*8*, *27*, *35*). [mRNA distribution from animal cells (*8*)]. These mRNA distributions carry the signature of the transcriptional kinetics.

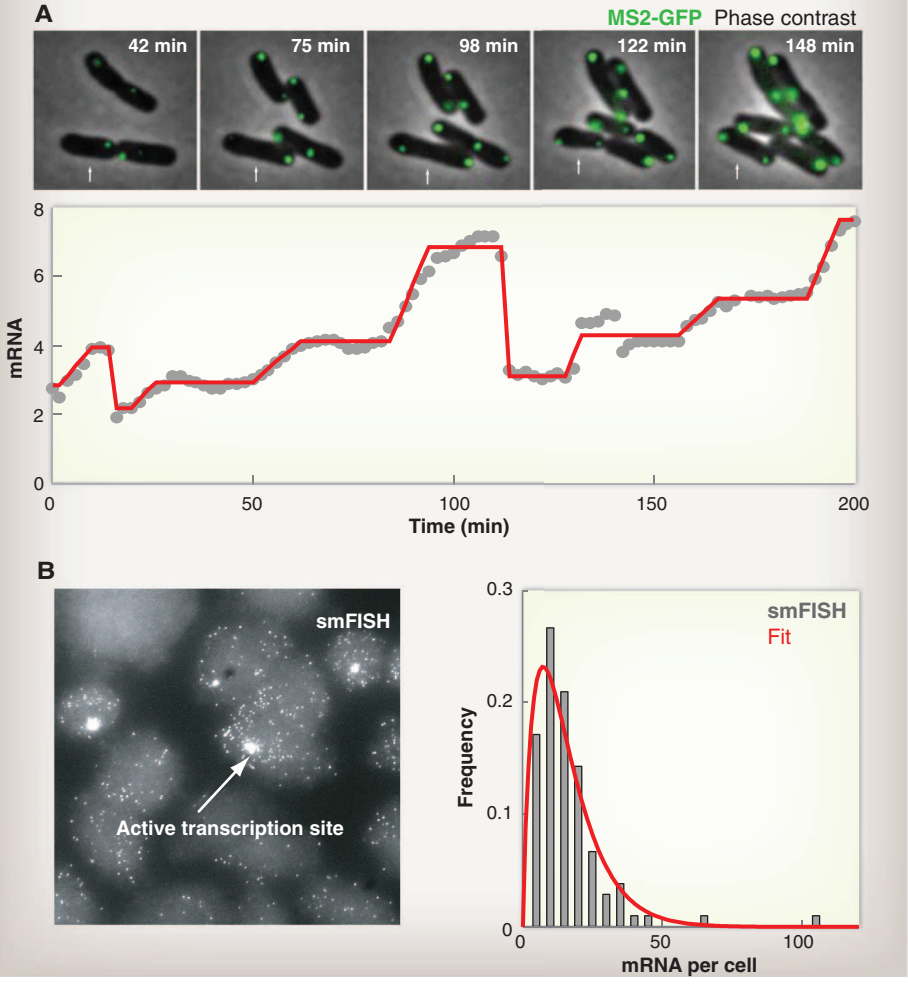

transcriptional activator or their binding strength showed that both of those architectural features can affect the burst size. This might be interpreted as evidence that promoter architecture can allow decoupling the mean amount of expression from the noise. However, when the bursting parameters were measured for these different promoters as a function of their mean level of expression, a single trend line was followed closely by all of the promoters regardless of their regulatory sequence (Fig. 2C, i).

The existence of a nontrivial trend line between the noise and the mean amount of protein in the cell was also observed in a study that analyzed single-cell gene expression from a weak viral promoter randomly inserted at over 8000 genomic loci in a line of human T lymphocytes (*16*). Evidence of bursting was found across the whole set of loci in which the lentiviral reporter was able to integrate. Similar to the modulation of bursting discussed

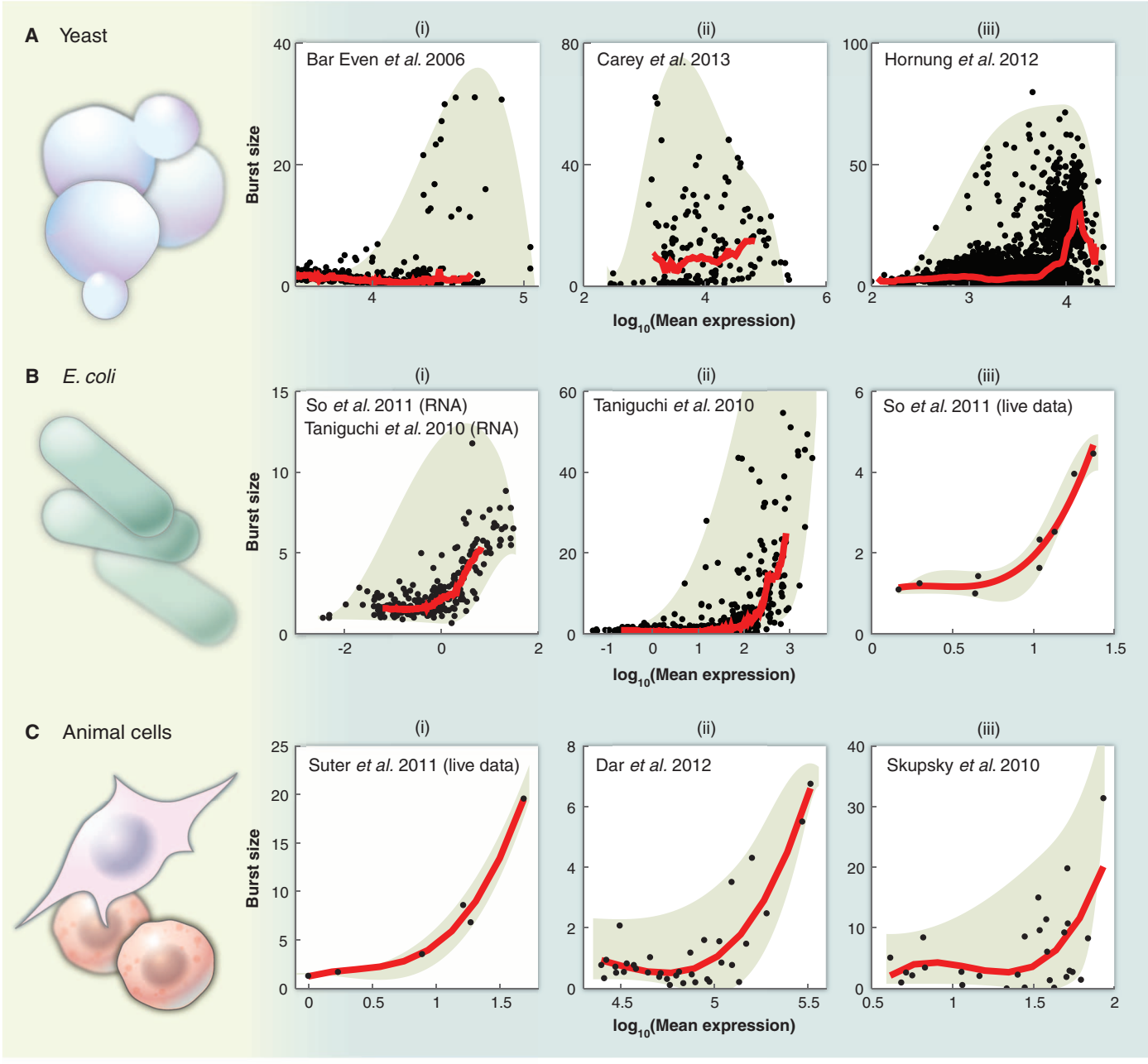

Fig. 2. Evidence for genome-wide constraints on promoter kinetics in bacteria and mammalian cells, but not yeast. (**A**) Data from three studies in yeast (*14*, *23*, *24*) show no obvious correlation between the mean expression level of a gene and the transcription burst size. In particular, both low-expression and high-expression genes can exhibit nonbursty behavior, which is consistent with a scenario of gene-specific regulation. In contrast, (**B**) two studies in *E. coli* (*17*, *32*) and (**C**) three in mammalian cells (*16*, *34*, *38*) show that higher expression is accompanied by increased burstiness, which is consistent with the presence of a global cellular constraint on promoter kinetics. Excluding live-cell measurements [(B), iii and (C), i], the burst sizes were estimated by using the Fano factor of the corresponding distribution [protein measurements, excluding (B), i], after correcting for the level of extrinsic noise. Black circles designate the individual measurements. Red curves are calculated trend lines. The shaded area highlights the full range of burst sizes covered by each data set. More details are available in the supplementary materials.

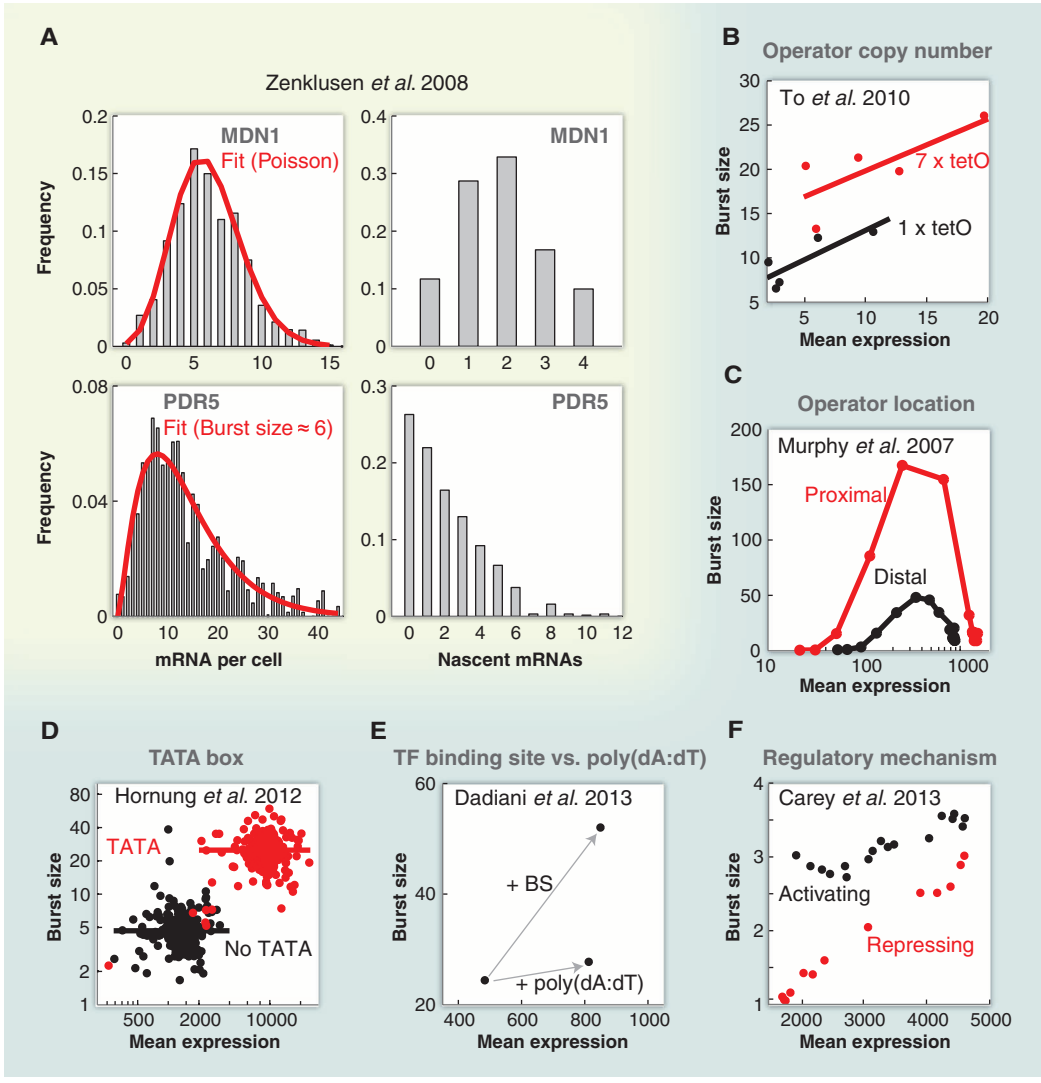

Fig. 3. Bursting kinetics in yeast are promoter-dependent and not subject to strong constraints. (**A**) Both Poissonian and bursty kinetics are found in endogenous yeast promoters. Copy-number statistics of mature (left) and nascent (right) mRNA are consistent with Poissonian promoter activity for MDN1 (top) while indicating bursty activity of PDR5 (bottom) [adapted by permission from Macmillan Publishers: Nature Structural & Molecular Biology (*27*) copyright 2008]. (**B** to **E**) Manipulating promoter architecture leads to a different relation between the mean expression and the burst size, so that two promoters with the same mean expression level can exhibit different burst sizes. The burst size is plotted as a function of the mean amount of expression for various perturbations of promoter architecture—specifically, (B) changing of the number of operator sites from one to seven (*29*); (C) changing of the position of the operator site from a location proximal to the first transcribed nucleotide, to a more distant location (*15*); (D) the presence (red dots) or absence (black dots) of a TATA box (*24*), including spontaneous mutations that delete it (red dots that overlap with the promoters lacking the TATA box); or (E) promoters engineered to yield the same mean level of expression by either adding a nucleosome disfavoring poly dA:dT sequence or by increasing the strength of a transcription factor binding site (+BS) (*13*). (**F**) The same transcription factor acting as a repressor (red dots) or as an activator (black dots) of a promoter leads to different burst sizes for the same mean level of expression (*14*). More details are available in the supplementary materials.

Box 2. Glossary.

Fano factor: The ratio between the variance (standard deviation squared) and the mean of a measured quantity. The Fano factor ofmRNA number per cell can serve as an estimate for the size of transcription bursts.

Gene expression noise: Variability in the level of gene expression between genetically identical cells, due in part to random fluctuations in the production of mRNA and protein.

Poisson process: The simplest random process, in which events occur with a constant probability over time.

Promoter: A region of DNA that controls transcription from a gene. An important element of eukaryotic promoters is the TATA box, which strongly affects the strength of the promoter.

Transcription bursts: The production of multiple mRNAs within a short time, followed by a period of promoter inactivity.

above for *E. coli* (*17*), the data were consistent with modulation of burst frequency at low expression, and of burst size at high expression (Fig. 2C, ii). A similar study of HIV promoters integrated at random locations in the genome of T cells also showed a trend-line between the burst size and the mean expression level (Fig. 2C, iii) (*38*).

Cellular Constraints That Impose Bursting?

The widespread observation of transcriptional bursting from bacteria to animal cells has prompted the idea that bursting may be a beneficial trait, possibly allowing an optimal allocation of resources or better processing of information from the environment (*17*). Bursting might also be an unavoidable kinetic feature of transcription, reflecting biophysical constraints that apply to most genes within a given organism (*19*, *21*, *39*).

But are transcription bursts really unavoidable? A good test case is the behavior of promoters acting at full capacity. In the absence of any constraints, such promoters are expected to exhibit Poissonian, nonbursty kinetics (Fig. 1). In *E. coli*, ribosomal promoters are transcribed at an average rate that is very close to the upper boundary imposed by RNA polymerase elongation (*40*). This suggests that they can be expressed continuously and without large bursts at full capacity. On the other hand, the hypothesis that biophysical or cellular constraints impose

bursting even in highly expressed promoters is consistent with the finding that fully induced mRNA-coding promoters display strong bursting (*6*) and highly non-Poissonian mRNA distributions (*17*). More experiments in which the architecture of a promoter is systematically varied are needed for elucidating the mechanisms governing transcription kinetics in bacteria—in particular, whether bursting is governed by universal or gene-specific constraints.

As for animal cells, bursting is prevalent in endogenous promoters (*5*, *8*, *18*, *34*–*36*), but a few counter examples also exist. A highly expressed viral promoter inserted in mammalian cells was found to be expressed continuously in a burst-free manner (*5*). RNA counting in *Drosophila* embryos also suggests that highly expressed genes can act close to full transcriptional capacity and exhibit nearly Poissonian statistics (*36*) [a counterexample is available at (*18*)]. These counterexamples appear to indicate that bursting is not an unavoidable by-product of transcription in all animal cells. Only a limited number of promoters, many of which are synthetic, have been studied in animal cells. Moreover, most experiments have been done in vitro with cell lines. In their natural context, animal cells are arranged in a complex multicellular environment, which may affect gene expression. Experimental advances that make it possible to count individual mRNA molecules in fixed animals or embryos (*18*, *35*–*37*) offer a promising avenue to better understand transcriptional kinetics in multicellular environments.

Reference and Notes

1. L. Bintu *et al.*, *Curr. Opin. Genet. Dev.* **15**, 125–135 (2005).
2. A. Raj, A. van Oudenaarden, *Cell* **135**, 216–226 (2008).
3. A. Coulon, C. C. Chow, R. H. Singer, D. R. Larson, *Nat. Rev. Genet.* **14**, 572–584 (2013).
4. D. R. Larson, D. Zenklusen, B. Wu, J. A. Chao, R. H. Singer, *Science* **332**, 475–478 (2011).
5. S. Yunger, L. Rosenfeld, Y. Garini, Y. Shav-Tal, *Nat. Methods* **7**, 631–633 (2010).
6. I. Golding, J. Paulsson, S. M. Zawilski, E. C. Cox, *Cell* **123**, 1025–1036 (2005).
7. T. Muramoto *et al.*, *Proc. Natl. Acad. Sci. U.S.A.* **109**, 7350–7355 (2012).
8. A. Raj, C. S. Peskin, D. Tranchina, D. Y. Vargas, S. Tyagi, *PLOS Biol.* **4**, e309 (2006).
9. A. Sanchez, H. G. Garcia, D. Jones, R. Phillips, J. Kondev, *PLOS Comput. Biol.* **7**, e1001100 (2011).
10. A. Sanchez, S. Choubey, J. Kondev, *Annu. Rev. Biophys.* **42**, 469–491 (2013).
11. J. M. Raser, E. K. O'Shea, *Science* **304**, 1811–1814 (2004).
12. W. J. Blake *et al.*, *Mol. Cell* **24**, 853–865 (2006).
13. M. Dadiani *et al.*, *Genome Res.* **23**, 966–976 (2013).
14. L. B. Carey, D. van Dijk, P. M. A. Sloot, J. A. Kaandorp, E. Segal, *PLOS Biol.* **11**, e1001528 (2013).
15. K. F. Murphy, R. M. Adams, X. Wang, G. Balázsi, J. J. Collins, *Nucleic Acids Res.* **38**, 2712–2726 (2010).
16. R. D. Dar *et al.*, *Proc. Natl. Acad. Sci. U.S.A.* **109**, 17454–17459 (2012).
17. L.-H. So *et al.*, *Nat. Genet.* **43**, 554–560 (2011).
18. S. C. Little *et al.*, *Cell* **154**, 789–800 (2013).
19. H. Salman *et al.*, *Phys. Rev. Lett.* **108**, 238105 (2012).
20. C. J. Zopf *et al.*, *PLOS Comput. Biol.* **9**, e1003161 (2013).
21. P. Guptasarma, *Bioessays* **18**, 325–332 (1996).
22. J. R. S. Newman *et al.*, *Nature* **441**, 840–846 (2006).
23. A. Bar-Even *et al.*, *Nat. Genet.* **38**, 636–643 (2006).
24. G. Hornung *et al.*, *Genome Res.* **22**, 2409–2417 (2012).
25. I. Tirosh, N. Barkai, *Genome Res.* **18**, 1084–1091 (2008).
26. Y. Field *et al.*, *PLOS Comput. Biol.* **4**, e1000216 (2008).
27. D. Zenklusen, D. R. Larson, R. H. Singer, *Nat. Struct. Mol. Biol.* **15**, 1263–1271 (2008).
28. S. J. Gandhi *et al.*, *Nat. Struct. Mol. Biol.* **18**, 27–34 (2011).
29. T.-L. To, N. Maheshri, *Science* **327**, 1142–1145 (2010).
30. L. Bai *et al.*, *Dev. Cell* **18**, 544–555 (2010).
31. P. J. Choi *et al.*, *Science* **322**, 442–446 (2008).
32. Y. Taniguchi *et al.*, *Science* **329**, 533–538 (2010).
33. D. Huh, J. Paulsson, *Nat. Genet.* **43**, 95–100 (2011).
34. D. M. Suter *et al.*, *Science* **332**, 472–474 (2011).
35. A. Paré *et al.*, *Curr. Biol.* **19**, 2037–2042 (2009).
36. A. N. Boettiger, M. Levine, *Cell Rep.* **3**, 8–15 (2013).
37. S. Itzkovitz *et al.*, *Nat. Cell Biol.* **14**, 106–114 (2012).
38. R. Skupsky, J. C. Burnett, J. E. Foley, D. V. Schaffer, A. P. Arkin, *PLOS Comput. Biol.* **6**, e1000952 (2010).
39. H. Bremer, M. Ehrenberg, *Biochim. Biophys. Acta* **1262**, 15–36 (1995).
40. S. Liang *et al.*, *J. Mol. Biol.* **292**, 19–37 (1999).

Acknowledgments: We apologize to our colleagues whose work could not be cited because of space limitations. We thank the following for sharing data and insights with us: A. Bar-Even, N. Barkai, A. Boettiger, M. Dadiani, A. Depace, T. Gregor, J. Kondev, D. Larson, R. Philips, A. Raj, E. Segal, and D. Zenklusen. I.G. thanks his laboratory members for help preparing the manuscript. Work in the Sanchez lab is supported by a Junior Fellowship from the Rowland Institute at Harvard. Work in the Golding lab is supported by the U.S. National Institutes of Health grant R01 GM082837, U.S. National Science Foundation grants 082265 (Physics Frontiers Center: Center for the Physics of Living Cells) and PHY-1147498 (CAREER), and Welch Foundation grant Q-1759. The authors declare no conflicts of interest.

Supplementary Materials

www.sciencemag.org/content/342/6163/1188/suppl/DC1
Supplementary Text
Table S1

10.1126/science.1242975

REVIEW

Functional Roles of Pulsing in Genetic Circuits

Joe H. Levine,* Yihan Lin,* Michael B. Elowitz†

A fundamental problem in biology is to understand how genetic circuits implement core cellular functions. Time-lapse microscopy techniques are beginning to provide a direct view of circuit dynamics in individual living cells. Unexpectedly, we are discovering that key transcription and regulatory factors pulse on and off repeatedly, and often stochastically, even when cells are maintained in constant conditions. This type of spontaneous dynamic behavior is pervasive, appearing in diverse cell types from microbes to mammalian cells. Here, we review recent work showing how pulsing is generated and controlled by underlying regulatory circuits and how it provides critical capabilities to cells in stress response, signaling, and development. A major theme is the ability of pulsing to enable time-based regulation analogous to strategies used in engineered systems. Thus, pulsatile dynamics is emerging as a central, and still largely unexplored, layer of temporal organization in the cell.

How inherently dynamic are individual living cells? Conventionally, we assume that in a constant external condition, the cell maintains a correspondingly constant internal state. In this view, the concentrations and activities of key cellular regulatory molecules, such as the transcription factors that control gene expression, generally remain steady over time or fluctuate stochastically around fixed mean values. Processes whose intrinsic dynamics are essential for their function, such as the cell cycle and circadian clock, or neural action potentials, are considered the exception rather than the rule. Recently, however, single-cell experiments have begun to reveal a very different picture of cellular regulation. In this view, many genetic circuits actively and spontaneously generate dynamic pulses in the activity of key regulators, and these pulses temporally organize critical cellular functions. Increasingly, it appears that even in constant conditions, cells behave like the proverbial duck, maintaining a calm appearance above the surface, while paddling furiously below.

Recent insights into the temporal organization of cellular regulatory activities have emerged from quantitative time-lapse microscopy and fluorescent reporter genes, which together allow researchers to accurately track the dynamic behavior of specific proteins over time in individual living cells. A recurring theme from these studies is that many regulatory factors undergo continual,

[1]Howard Hughes Medical Institute, Division of Biology and Biological Engineering, California Institute of Technology, Pasadena, CA, USA.

*These authors contributed equally to this work.
†Corresponding author: E-mail: melowitz@caltech.edu

repetitive pulses of activation. Each of these pulses involves the coherent activation and deactivation of the regulator, through changes in its concentration, modification state, or localization, on time scales ranging from minutes to hours (Fig. 1) (*1*–*6*). Pulsing is generated by genetic circuits that activate and deactivate key regulators and modulate pulse characteristics, such as frequencies and amplitudes. Pulsing is thus distinct from transcriptional bursting, which results from the stochastic nature of gene expression (*7*). Here, we use the term "pulsing" to denote a broad spectrum of repetitive phenomena that range from irregular and stochastic to more uniform and periodic dynamics.

Pulsing has previously gone undetected even in well-studied systems. Because pulses are typically unsynchronized between cells, they have been difficult to detect with traditional techniques that average over large cell populations. Pulsatile dynamics can produce "long-tailed" distributions in static measurements based on flow cytometry and microscopy snapshots. However, time-lapse movies that track molecular activities over time in individual living cells are required to definitively reveal pulses (Fig. 1A).

The discovery of pulsing in core regulatory systems provokes several fundamental questions: How widespread is pulsatile regulation? What cellular functions does it enable? And, what genetic circuit mechanisms does the cell use to generate and regulate pulsing? In this review, we first survey the growing list of pulsatile phenomena in diverse cellular systems. We next explain how pulsing facilitates specific cellular functions that could be more difficult to achieve with static regulation. In particular, we highlight the regulatory flexibility that comes from independently controlling the timing and amplitudes of pulses. We then discuss the circuit mechanisms that enable cells to generate and control pulsatile dynamics. Finally, we suggest additional ways, not yet discovered, in which pulsatile regulation could potentially enhance cellular capabilities. Owing to space limitations, we will focus primarily on more recently discovered pulsatile systems, rather than other beautiful and well-studied examples such as the cell cycle, circadian rhythm, calcium dynamics, and multicellular phenomena based on coordinated pulsing (*8*).

Pulsatile Regulatory Dynamics Pervade the Cell

Pulsing has been observed in many types of proteins, from alternative bacterial sigma factors to mammalian tumor suppressors like p53, and has been shown to function in diverse processes, from stress response to signaling to differentiation (Fig. 1B). To appreciate the pervasiveness of pulsing, consider the soil bacterium, *Bacillus subtilis*, for which many stress responses have been analyzed with time-lapse movies. In this species, pulsing occurs in at least three systems: genetic competence, which allows cells to take up DNA (*9*); sporulation initiation, which controls transformation of cells into dormant spores (*10*); and the general stress response pathway (*1*). Similarly, in yeast, pulsing has been observed in two distinct stress response pathways, mediated by the transcription factors Msn2/4 and Crz1 (*2*, *11*).

Mammalian cells exhibit many pulsatile factors. The stress response pathways mediated by p53, which controls the DNA damage response (*3*, *12*, *13*), and nuclear factor κB (NF-κB), which is involved in immune responses (*5*, *14*, *15*), both

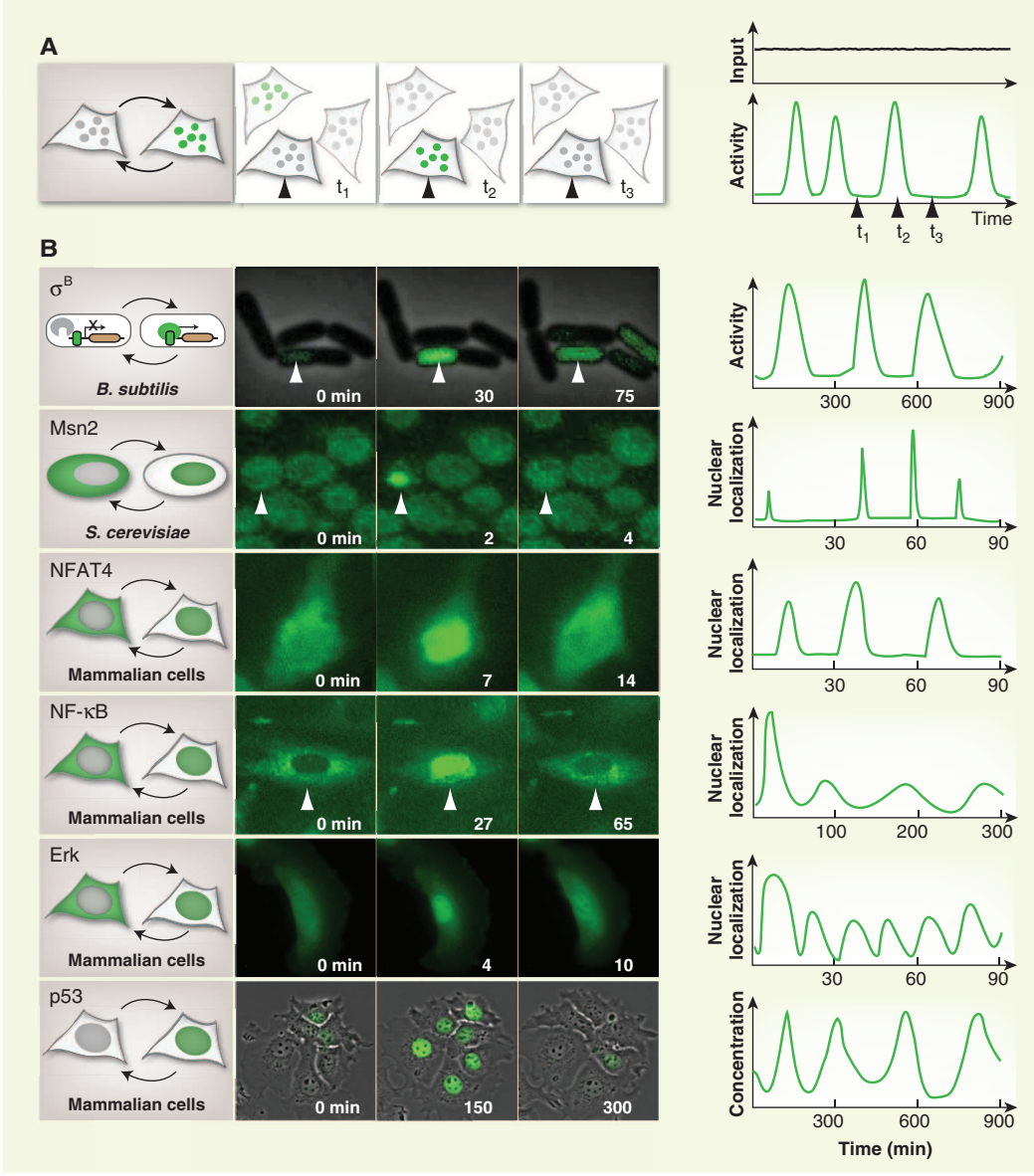

Fig. 1. Pulsing is ubiquitous in cellular regulation. (**A**) Pulsatile dynamics involve the transient, simultaneous activation of many molecules of a given type (circles), even under constant environmental conditions. Cells pulse asynchronously, making pulsing difficult to detect with static snapshots and necessitating tracking of cell lineages over time (right, schematic). (**B**) Pulsing occurs in a diverse array of pathways, molecular types, organisms, and time scales (*1*–*6*). For each example, a schematic of the type of regulation is shown at left, a typical filmstrip is shown at center, and a qualitative schematic plot of typical dynamics is shown at right.

pulse. Similarly, signaling pathways such as extracellular signal–regulated kinase (ERK) mitogen-activated protein kinase (MAPK), which responds to growth factors and regulates cell proliferation (*6*, *16*–*18*), nuclear factor of activated T cells 4 (NFAT4) (*4*), and transforming growth factor β (TGF-β) (*19*) have all been shown to pulse in response to activation by extracellular signals. Finally, the developmental transcription factor Hes1 also pulses in multiple cell types (*20*–*22*). The prevalence of pulsatility across these pathways raises the likely but generally unexplored possibility that multiple pulsatile systems coexist, and interact, in individual cells.

Functions of Pulsatile Cellular Dynamics

The power of pulsatile regulation arises from the ability to independently regulate pulse amplitudes, frequencies, and durations (Fig. 2A). By controlling these features in different ways, individual systems implement diverse functions, some of which may be challenging to achieve through less dynamic regulation.

Frequency Modulation Enables Coordination

Several pulsatile systems are controlled through frequency-modulated (FM) pulsing (*1*, *11*, *17*). In yeast, the transcription factor Crz1, which mediates the calcium response, is activated in a series of stereotyped pulses, even when cells are maintained in constant conditions (*11*). During each pulse, Crz1 molecules simultaneously localize to the nucleus, where they can activate target genes, remain there for ~2 min, and then return to the cytoplasm. Extracellular calcium concentration modulates the frequency, but not the amplitude or duration, of these pulses. In a similar way, the ERK kinase can also be activated in FM pulses (*17*). Even under constant environmental conditions and ligand concentrations, ERK activates in a series of pulses of ~30-min duration, whose frequency is modulated by extracellular levels of the epidermal growth factor (EGF) (*17*). Finally, in *B. subtilis*, the σ^B alternative sigma factor, which mediates the general stress response, is also activated in a series of stochastic pulses lasting about 1 hour each (*1*). Energy stresses that reduce cellular adenosine 5′-triphosphate concentrations modulate the frequency of these pulses.

What functional capabilities could FM pulsing provide for cells? One possibility is that it allows the cell to control the fraction of time that a regulator is active, rather than controlling the concentration of active regulator (Fig. 2B). Such time-based regulation is analogous to "bang bang" control, a well-known design principle in engineering, which similarly involves modulating the

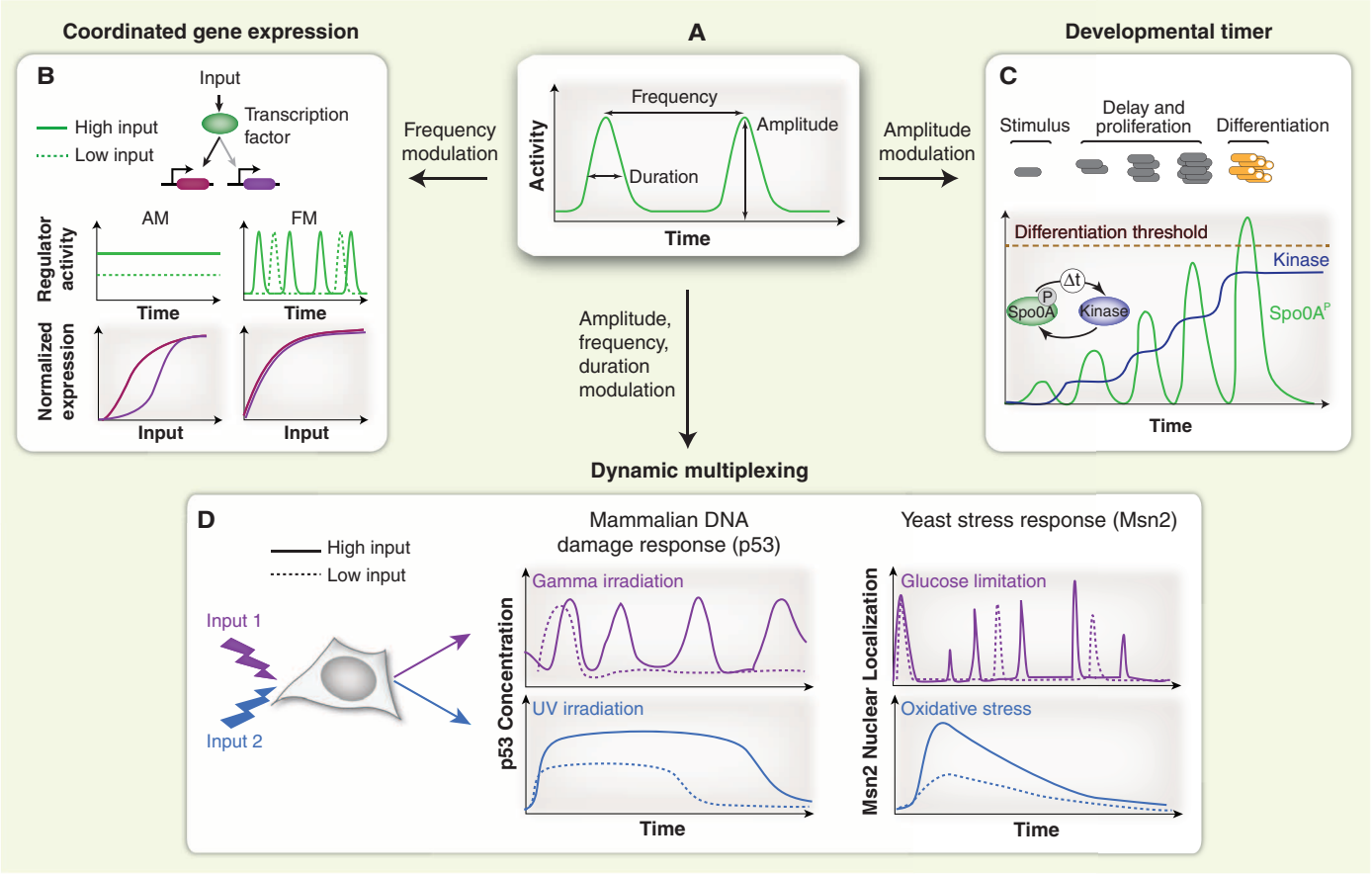

Fig. 2. Pulsing enables diverse cellular functions. (**A**) Cells modulate pulse characteristics, including amplitude, frequency, and duration, to implement diverse regulatory functions. (**B**) A transcription factor (green) may activate different target promoters at different thresholds or with different affinities (light and dark arrows). Concentration-based regulation (amplitude modulation, AM) would therefore lead to different, nonproportional, response profiles (bottom left). In contrast, frequency-modulated (FM) pulsing, by effectively controlling the fraction of time that all target genes are expressed, leads to expression of targets in fixed proportions (bottom right), indicated by overlap of expression curves (each is normalized to its own maximum) (*11*). (**C**) Pulsed regulation functions in a developmental timer. *B. subtilis* respond to sudden nutrient limitation by proliferating for multiple cell cycles before sporulating (schematic). A model of the underlying circuit (inset) is based on a positive-feedback loop (arrows) with a hypothesized time delay (Δ*t*). This circuit can generate progressive growth in pulses of phosphorylation of the sporulation master regulator Spo0A (green trace), via steplike growth in the kinase concentration (blue trace). The timer terminates when a threshold level of Spo0A is reached (dashed line) (*10*). (**D**) Examples in which dynamic multiplexing enables a single pathway to transmit multiple signals (*2*, *13*). In each case, distinct types and levels of inputs generate distinct dynamic activation patterns for the indicated regulatory protein.

fraction of time that a system is on. Transcription factors activate multiple target genes, but may do so with varying strength, affinity, and degrees of nonlinearity. As a result, increasing the concentration of a transcription factor by a given amount will affect different target promoters to different extents. By contrast, in FM regulation, a given percentage change in transcription factor pulse frequency causes the same percentage change in the fraction of time that the transcription factor activates each of its targets. Expression levels of target genes are then proportional to pulse frequency, and also proportional to one another, as indicated schematically in Fig. 2B (bottom right). This coordination function was demonstrated experimentally for Crz1, which activates many targets in yeast (*11*). Coordination could be a useful function of pulsing in other systems and contexts as well, whenever diverse targets need to be regulated in fixed ratios.

Amplitude Modulation and Phasing Facilitates a Developmental Timer

Developmental timers enable cells to defer their response to signals for multiple cell cycles. In such systems cells detect a signal, proliferate for a defined amount of time or number of cell cycles, and then differentiate. A classic example is oligodendrocyte differentiation, where progenitors divide up to eight times before differentiating (*23*). Recently, pulsing was discovered in a developmental timer in *B. subtilis*, which, under some conditions, responds to sudden nutrient limitation by transforming into a dormant spore after five cell cycles have been completed (*10*) (Fig. 2C). During this period, the master transcription factor that controls sporulation, Spo0A, is phosphorylated (activated) once per cell cycle in a sequence of pulses with progressively growing amplitudes until it reaches a level high enough to initiate sporulation (*24*). Each pulse of Spo0A phosphorylation activates expression of a cognate kinase, which in turn increases the amplitude of subsequent Spo0A phosphorylation pulses (Fig. 2C). Thus, the system is based on a pulsed positive-feedback loop.

What role does pulsing play in this timer? Creating a multi–cell-cycle deferral time with continuous (nonpulsatile) genetic circuits is challenging in proliferating cells, as dilution of cellular components during cell growth forces most protein concentrations to relax to their steady-state values over a time scale of about one cell cycle or faster. Positive-feedback loops can help to solve this problem, by compensating for dilution with increased protein production. However, mathematical modeling suggests that continuous positive feedback is extremely sensitive to parameters, continually compounding small errors, making it infeasible for a timer operating in individual cells. By contrast, a pulsed positive-feedback loop can help overcome this problem. By effectively breaking up the positive-feedback loop in time, so that Spo0A phosphorylation and kinase accumulation occur in distinct temporal intervals, pulsing makes the timer circuit less sensitive to changes in circuit parameters. It thereby provides a more robust mechanism

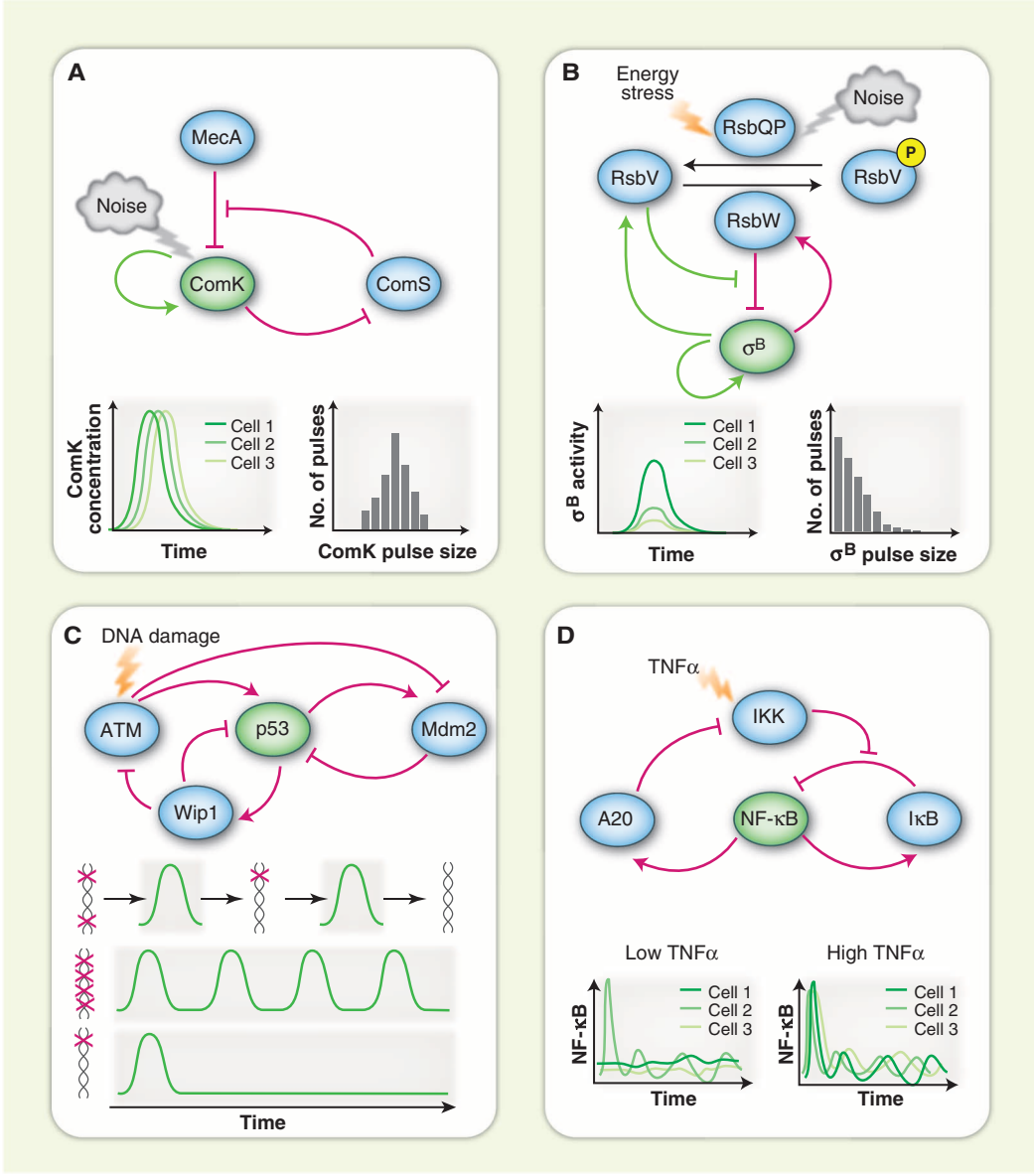

Fig. 3. Circuit mechanisms of pulse generation and modulation. (**A**) The *B. subtilis* competence circuit generates stereotyped pulses of ComK activation (*9*). Green and red arrows represent positive and negative feedbacks, respectively. Pulses are stereotyped, as indicated by three identical traces (bottom left) and unimodal pulse size distribution (bottom right). (**B**) The *B. subtilis* general stress response (σ^B) circuit combines transcriptional feedback and an ultrasensitive phosphoswitch, and produces a nonstereotyped distribution of pulse amplitudes (bottom right) (*1*). (**C** and **D**) Mammalian cell pulse-generation mechanisms use multiple negative feedbacks. (C) In the p53 circuit, double-stranded DNA damage activates p53 pulses through ATM kinase. Pulses may lead to subsequent DNA repair (*12*). (D) NF-κB pulse mechanism. This circuit displays digital activation behavior, with the fraction of cells that pulse depending on the level of stimulus (*5*).

for implementing a cell-autonomous developmental timer (*10*).

Dynamic Signal Processing Expands Signaling Pathway Capabilities

Signal transduction pathways face the challenge of internally representing, or encoding, the identity, amplitude, and timing of many different external signals. Cells address this challenge, at least in part, by dynamic multiplexing, which encodes information about the stimulus in the dynamics of a regulator. Dynamic multiplexing systems typically encode stimulus information in the frequency, amplitude, and duration of pulses of pathway activation (*1*, *2*, *5*, *13*, *25*, *26*) (Fig. 2D), and also in the presence or absence of pulses themselves.

One of the best-studied examples is the tumor suppressor p53 (*3*, *12*, *13*). Both γ-irradiation and ultraviolet (UV) irradiation activate p53, but cause distinct cellular responses: cell cycle arrest (and survival) and apoptosis, respectively (*3*). The two responses are related to the different dynamics of p53 activation: γ-irradiation produces a series of p53 activity pulses, whose number is controlled by the radiation dosage, whereas UV irradiation generates a sustained nonpulsatile response, whose amplitude and duration depend on dose (Fig. 2D) (*13*). If p53 dynamics are controlled directly through chemical manipulation, converting pulsatile dynamics into sustained dynamics is sufficient to switch the cell fate (*3*). Evidently, the cell uses p53 dynamics to encode distinct input signals and decodes these dynamics to determine cell fates.

In the immune system, NF-κB displays repeated pulses of nuclear localization in response to constant amounts of its input, tumor necrosis factor alpha (TNFα) (*5*, *14*, *15*). Cells encode TNFα concentration in the probability of activating NF-κB in a cell, and the number of pulses once activated (*5*). Pulse characteristics in turn control the differential expression of genes of various immune response stages (*5*, *15*). Thus, NF-κB uses dynamic multiplexing to represent the amplitude of its input.

Complex dynamic multiplexing is not specific to multicellular organisms. In yeast, the general stress response pathway, mediated by the Msn2/4 transcription factors, encodes stimulus information using diverse nuclear localization dynamics (*2*). Glucose limitation generates repeated stochastic Msn2 localization pulses, several minutes each, at a frequency modulated by glucose concentration. In contrast, oxidative stress induced by H_2O_2 generates a single, adaptive Msn2 localization pulse whose amplitude is modulated by H_2O_2 concentration. These dynamics may allow the cell to activate target genes in a stress type and intensity-dependent manner. The decoding of Msn2 dynamics appears to depend on the interaction kinetics between Msn2 and its target promoters (*2*, *27*).

Even bacteria can multiplex. In *B. subtilis*, the alternative sigma factor σ^B is activated post-translationally both by energy stresses mentioned above (*1*), and also by environmental stresses such as salt and ethanol (*26*). Unlike the FM pulsing observed in response to energy stresses, the response to environmental stresses depends on the rate at which the stress increases. That is, a sudden increase in stress generates much more σ^B activity than a gradual ramp to the same stress level (*26*). This allows a rapidly increasing stress to induce not only its specific targets, but also, through σ^B, many other stress targets as well, effectively anticipating potential future stresses (*26*). Rate-encoding schemes like this may similarly be observed in other general stress pathways where rate of change of stress can be experimentally manipulated (*28*). Thus, the type of stress (energy versus environmental), the magnitude of stress, and the rate of change of environmental stress are all dynamically encoded in this pathway.

Together these examples demonstrate that pulsatile responses, by modulating pulse amplitude, frequency, and duration, dynamically encode information in many pathways [see also (*25*)].

Pulsatile Gene Expression Implements Bet-Hedging

Fast pulses may occur many times in a cell cycle, but some systems show slower pulses, with durations of one cell cycle or longer. Here, pulses could generate something resembling a transient alternative cell state. Single-cell studies have revealed that individual microbial cells use such slow pulsing to produce a repertoire of transient phenotypic states, even when grown in constant conditions (*9*, *29*). In many cases, slow pulses are initiated in a probabilistic manner, effectively

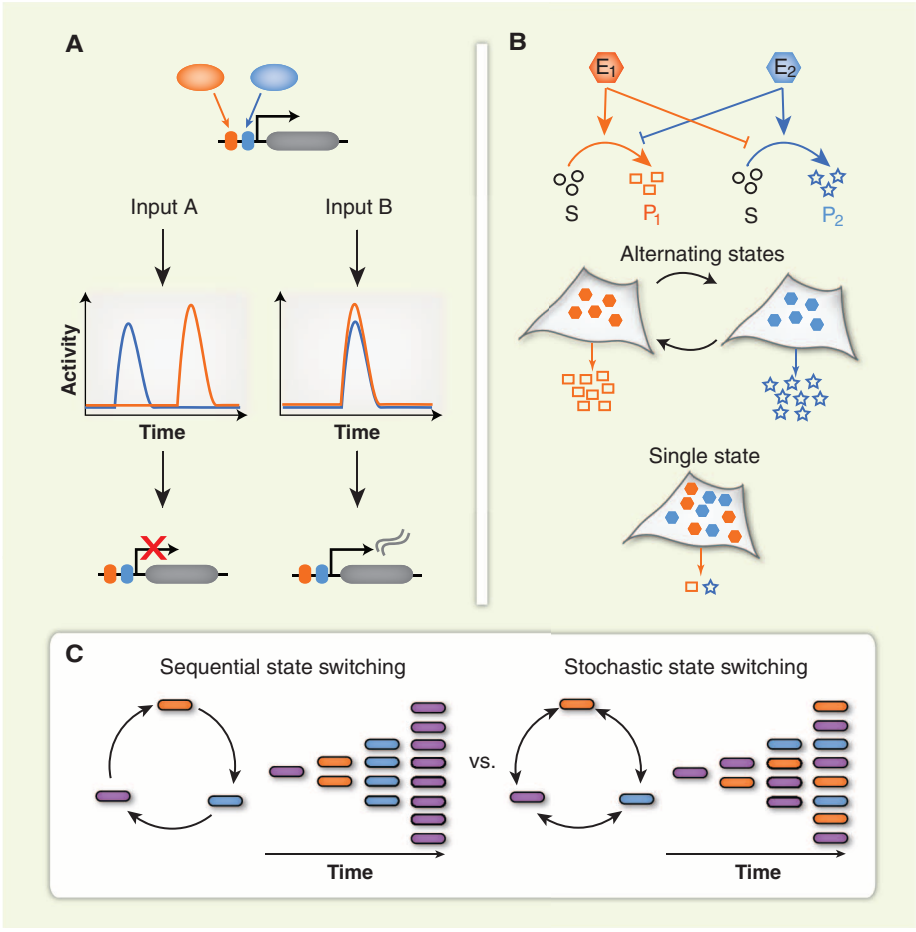

Fig. 4. Other potential regulatory functions of pulsing. (**A**) Regulation could occur through modulation of the relative pulse dynamics of two factors that co-regulate a common target. Inputs could modulate the relative level of synchronization of the regulator pulses. Here, we assume a target promoter activated only when both factors are present simultaneously. (**B**) Pulsing may reduce conflicts between incompatible pathways by temporally alternating between states in which only one or the other pathway is active (middle), rather than by simultaneously expressing conflicting programs (bottom). (**C**) Stochastic pulsing systems enable random switching between cellular states. In contrast to sequential switching, stochastic state switching allows cells to diversify cellular states on the time scale of about one cell cycle when the pulse duration is similar to the cell cycle time.

implementing a bet-hedging strategy whereby cells randomize their individual states to adapt to uncertain future environmental changes (*29*, *31*, *32*). A classic example of microbial bet-hedging is antibiotic persistence, where individual bacterial cells stochastically switch between an antibiotic-sensitive state of rapid growth, and an antibiotic-resistant state with no or slow growth (*29*). Even a small fraction of persister cells can ensure the survival of a microbial population in response to antibiotic treatment, with important biomedical consequences (*33*).

Several systems are known to implement slow pulsing as a bet-hedging strategy. For example, in *B. subtilis*, at any given time, a fraction of the population enters a state of genetic competence for ~10 hours and then returns to vegetative growth (*9*). In the competent state, cells can take up extracellular DNA and recombine it with their own genome, a gamble that adaptive genetic material may be available in the environment. These transient competence events are controlled by an excitable genetic circuit (see below), which generates stereotyped pulses of the master competence regulator ComK, affecting many aspects of cell state.

Mycobacterium smegmatis uses a stochastic pulsing strategy that affects persistence in response to isoniazid (INH) (*34*), an antibiotic that requires activation by bacterial catalase-peroxidase KatG. The normal role of KatG is to catabolize and inactivate toxic reactive oxygen species. However, when INH is present, KatG appears to play a second, opposite, role, promoting killing of cells by activating INH (*34*). By analyzing individual cells in time-lapse movies, the authors observed that cells express *katG* in low-frequency stochastic pulses (*34*). These pulses effectively increase cell-to-cell variability in KatG concentration and may be advantageous to population survival, by assuring that at least some cells survive in both the presence and absence of INH. The role of pulsing has also been computationally investigated in the *mar* antibiotic resistance regulon of *Escherichia coli* (*35*). Here, a mixture of positive and negative feedback allows *marA* expression to stochastically pulse in low-stress conditions, allowing the population to bet hedge against sudden antibiotic appearance while retaining the ability to fully induce MarA in response to antibiotic stress. These examples suggest generally that dynamic, pulsatile gene regulation may be involved in other bacterial persistence contexts.

The Role of Pulsing in Cellular Differentiation

A fundamental question in development is how transcription factors control cell fate decisions. In some cases, the role of an individual transcription factor can be complex, promoting multiple, seemingly conflicting, cellular behaviors. Recent single-cell studies indicate that some of these transcription factors activate in a pulsatile fashion and suggest that this pulsatility may function to balance their conflicting activities (*20*). For example, during neural development, to ensure an adequate population of neurons, neural progenitors divide multiple times before differentiating into postmitotic neurons. This maintains their developmental potential while proliferating. Developmental regulators, including Hes1, play a critical role in this process. High concentrations of Hes1 maintain the progenitor state by repressing proneural genes. But they also block proliferation. In contrast, low amounts of Hes1 allow proliferation but permit differentiation away from the progenitor state. How do neural progenitors use Hes1 to juggle the conflicting tasks of maintaining the progenitor state, while allowing proliferation?

A potential resolution of this apparent paradox is provided by the observation that Hes1 expression oscillates in neural progenitors with a period of 2 to 3 hours (*20*). Hes1 oscillations might dynamically balance periods in which cell division is possible (low Hes1) with other periods in which the progenitor state is maintained (high Hes1), effectively causing the cells to alternate between two behaviors, rather than choosing one or the other. Hes1 also functions in an intercellular feedback loop mediated by Notch-Delta signaling, which may play a role in these oscillations (*20*).

Recently, optogenetic approaches have begun to enable forward experimental tests of the role of pulsing in fate determination by allowing direct manipulation of transcription factor dynamics. For example, optogenetic control of the transcription factor Ascl1, a Hes1 target that also oscillates in neural progenitors, revealed that the dynamics of Ascl1 can influence cell fate (*22*). More specifically, oscillatory Ascl1 expression maintained the neural progenitor state, while sustained high expression promoted neural differentiation (*22*). These observations are now provoking further questions about how developmental regulator dynamics control cell fate decisions in this and other systems.

The Mechanisms Behind Pulsatile Cellular Dynamics

How do gene circuits generate pulses and modulate their characteristics? Mechanisms for pulsing and oscillation have begun to be elucidated in a few cases, revealing both shared features and qualitative differences across systems.

In *B. subtilis,* transient differentiation into the competent state involves pulses of the master transcriptional regulator ComK. ComK directly activates its own transcription, and indirectly turns itself off, through a slower negative-feedback loop (*9*, *30*). This circuit is excitable, meaning that any fluctuations (noise) that enable ComK to cross a threshold and begin to turn itself on trigger stereotyped pulses of ComK activation, with a relatively uniform duration (*9*) (Fig. 3A). The excitability of this circuit enables the system to independently tune the frequency and duration of these pulses (*9*).

Excitability might seem like an ideal property for any pulse-generating system. However, although the *B. subtilis* σ^B system also pulses, it does so with a different, nonexcitable circuit architecture (*1*). This system converts levels of energy stress into the frequency of pulses. In the absence of stress, σ^B is sequestered in an inactive form by its cognate anti-sigma factor RsbW. It can be released from this complex by the anti-anti-sigma factor RsbV. RsbV is normally phosphorylated, and thereby inactivated, by RsbW, but it can be dephosphorylated, and activated, by the phosphatase RsbQP, an energy stress sensor.

σ^B pulses are generated in two stages: First, the RsbV phosphoswitch responds ultrasensitively to RsbQP activity, causing RsbV to be suddenly dephosphorylated in response to a threshold-crossing fluctuation in RsbQP activity. Dephosphorylation, in turn, activates σ^B, initiating a pulse. Tuning basal RsbQP expression can modulate pulse frequency by changing the likelihood of RsbQP fluctuations tripping the phosphoswitch. Second, active σ^B transcriptionally activates its own operon, amplifying the pulse, but also upregulating RsbW, which, because of its kinase activity, eventually shuts the phosphoswitch back off, terminating the pulse (Fig. 3B). Through these two stages, the system effectively implements a simple "DC to AC" pulse frequency encoder. In contrast to the excitable dynamics of the competence circuit, which generate stereotyped pulses, the σ^B system generates a long-tailed distribution of pulse sizes at any stress level (Fig. 3, A and B). It remains unclear why nonexcitable dynamics are present in the σ^B system.

In mammalian cells, the p53 pulse generator has been studied extensively through experiments and mathematical modeling. Its mechanism appears to be based on repeated activation of an upstream stress sensor (*12*, *13*). The kinase ataxia telangiectasia mutated (ATM) repeatedly initiates pulses by phosphorylating p53 in response to γ-irradiation and subsequent DNA double-strand breaks. These pulses are transmitted directly, through modification of p53 protein, and indirectly (through the kinase Chk2) to activate p53, initiating a pulse. The pulse terminates because p53 transcriptionally activates its negative regulator Mdm2, which targets p53 for degradation. p53 also resets itself in another way, by negatively regulating ATM through the phosphatase Wip1. Thus, the recurrent activation of the upstream sensor, together with multiple negative-feedback loops, appears to enable repeated p53 pulses as long as DNA damage persists (*12*, *13*) (Fig. 3C).

Control of NF-κB nuclear localization provides another example of pulse generation. In resting cells, NF-κB is found in the cytoplasm as an inactive complex with its inhibitor IκB (inhibitor of κB). In response to a constant amount of TNFα, NF-κB exhibits repeated nuclear localization pulses (*5*, *14*, *15*). These pulses occur in a "digital" fashion, in that they are all-or-none

at the level of individual cells (*5*). In this case, pulses are generated by a circuit containing multiple negative-feedback loops (Fig. 3D). One negative-feedback loop, which engages at a faster time scale, involves the transcriptional activation of IκB by NF-κB, which in turn antagonizes NF-κB. The second feedback loop, which is engaged over longer time scales, involves transcriptional activation of the A20 protein, which blocks activation of kinase IKK that in turn activates NF-κB (*36*). The way in which these two feedback loops work together to generate the dynamic responses of NF-κB observed in individual cells, and where the stochastic variability arises, are not fully understood.

Several features appear common to many pulsatile circuits. First, negative feedback loops occur in all examples. A delayed negative-feedback may be essential for both allowing pulses to build up and also ensuring that they ultimately terminate. In general, this is facilitated by separation of time scales, whereby negative feedback can be slow compared to processes that initiate or amplify pulses. However, positive feedback loops have been identified in bacterial, but not mammalian, circuits. This may reflect incomplete knowledge, or qualitatively different pulse-generation mechanisms, as positive-feedback loops in oscillators can have a strong impact on circuit behavior (*37*). Second, noise helps generate pulses. For both bacterial circuits, pulsing was reduced or eliminated when cells were placed in a filamentous state with reduced noise (*1*, *9*). Moreover, the bacterial competence circuit displayed more variability in pulse durations than a rewired variant, suggesting that variable durations may play an adaptive role (*30*). The mammalian circuits are also variable, most notably in the example of digital activation in NF-κB. Finally, some dynamics, such as those of ERK activation and NF-κB activity at high input levels, become increasingly periodic. Indeed, theoretical models have demonstrated that circuits with mixed feedback loops can exhibit a variety of dynamical behaviors including multistability, oscillations, and pulsing, depending on parameter regimes (*38*), so this feature may not be sufficient to guarantee pulsatility. It will be interesting to understand experimentally how these circuits transition between stochastic pulsing and oscillatory behaviors.

Potential Functions for Pulsing

Pulsing offers a flexible mode of regulation that can be adapted to many cellular contexts. More pulsatile systems and corresponding functions likely remain to be discovered. Here we discuss some potential additional functions that pulsatile systems might provide in the cell.

Pulsing Could Enable Time-Based Combinatorial Regulation

So far, most pulse systems have been analyzed in isolation. But gene regulation is frequently combinatorial, and pulsing transcription factors likely co-regulate targets with other regulators. For example, the NFAT signaling pathway responds to changes in the intracellular concentration of calcium by nuclear localization of NFAT1 and NFAT4 transcription factors (*4*). NFAT4 localizes to the nucleus in rapid, repeated stochastic bursts on a time scale of minutes. In contrast, NFAT1 localizes to the nucleus in a slower and nonpulsatile fashion. Thus, NFAT4 can be activated by brief calcium pulses, whereas NFAT1 filters them out. The combination of both isoforms could enable more advanced signal-processing functions. For example, a promoter activated by both isoforms could respond faithfully to rapid activation, via NFAT4, while filtering out brief drops in calcium, via NFAT1.

Can multiple pulsing signaling pathways interact with each other? The relative timing of pulses between two different transcription factors could affect cellular regulation. In neurobiology, the relative timing of action potentials at pre- and postsynaptic neurons controls the strengthening or weakening of synaptic connections through spike timing–dependent plasticity (STDP) (*39*). Analogously, inputs might modulate the time interval between pulses of two transcription factors that cooperatively regulate a common target gene, such that transcription occurs only when both bind the promoter at the same time. In this hypothetical scheme, in one condition, unsynchronized pulses of the two factors might produce relatively little temporal overlap between the two pulses, and therefore generate low target transcription (Fig. 4A, left). By contrast, in another condition, pulsing might synchronize between two factors, enabling them to more productively activate target expression (Fig. 4A, right).

Pulsing Could Help Cells Share Limited Resources

Pulsing and oscillation could also help manage conflicting or incompatible physiological processes, enabling cells to alternate between conflicting regulatory programs by separating them in time (Fig. 4B). A classic example occurs in some cyanobacteria, which temporally alternate between incompatible nitrogen fixing and respiration phases (*40*). The yeast metabolic cycle provides another example of this strategy. In chemostat cultures, yeast cells undergo respiratory cycles of 4 to 5 hours, switching between reductive and oxidative phases (*41*). This temporal compartmentalization separates energy-intensive processes such as protein translation from oxidative damage–sensitive processes such as DNA replication, and may also occur in unsynchronized single cells (*42*).

Pulsing Can Randomize Sequences of Cellular States

In previous examples, cells switch among cellular states in a well-defined order, just as the eukaryotic cell cycle steps sequentially through distinct phases. By contrast, stochastic pulsing systems could permit a nondeterministic sequence of states (Fig. 4C). This may be advantageous in the context of bet-hedging, by allowing cells to dynamically control the distribution of states within a cell population.

Summary and Outlook

Our traditional view of cellular regulation as a largely steady-state process is ceding ground to a more dynamic picture. Evidently, cells are controlled by regulatory factors that show repetitive, pulsatile, and often stochastic dynamics even under constant conditions. Time-based control provides many capabilities in electrical circuits, so perhaps it is not surprising that cells have evolved related dynamics, despite their very different physical substrates and functional constraints. Understanding both the similarities and differences in the use of temporal dynamics represents an exciting challenge. Despite the fascinating discoveries of the last few years, several fundamental questions about dynamic cellular regulation remain to be answered.

A first challenge will be to develop reporters that can be tracked over time in single living cells and are sensitive to diverse molecular activities. Such reporters could enable the discovery of otherwise hidden dynamics. For example, the new membrane potential sensor PROPS (proteorhodopsin optical proton sensor) quickly led to the discovery of rapid, repeated pulsatile membrane voltage dynamics in bacteria (*43*).

A second critical challenge is determining the biological functions provided by different pulsing systems. In most cases, we lack a clear understanding of the functional capabilities pulsing dynamics provide and why they have been selected over other alternatives. One possible solution is to control a regulator's dynamics directly—for example, via pharmacological or optogenetic techniques—allowing a comparison between functional outcomes of time-based and concentration-based regulation. These techniques are already beginning to reveal different roles for pulsing and static regulation in the p53 stress response pathway, ERK MAPK regulation of cell proliferation, the neural developmental regulator Ascl1, and the yeast stress response regulator Msn2 (*3*, *18*, *22*, *27*).

Third, from the standpoint of synthetic biology, the pervasiveness of pulsing raises the question of what forms of information processing and control are best suited to the cellular milieu (*44*). Most synthetic biology efforts have been based on continuous circuit design paradigms such as layered feed-forward logic circuits (*45*). Incorporating pulsatile dynamics into engineered circuits may more effectively address or exploit specific features of the cellular environment, such as noise, protein turnover, and shared regulatory resources (*46*). The relatively small number of

components necessary for several pulse systems (*1*, *47*) suggests that it may be feasible to integrate pulsatility into synthetic circuits and potentially take advantage of regulatory schemes previously unexplored by traditional engineering disciplines.

The behavior of genetic circuits, and their response to pharmacological perturbations, critically depends not just on their connectivity but also on their dynamics. A deeper understanding of the prevalence, functions, and mechanisms of these dynamics in cells will open up new ways of analyzing and controlling cells and help to inform our understanding of the basic design principles of genetic circuits.

References and Notes

1. J. C. Locke, J. W. Young, M. Fontes, M. J. Hernández Jiménez, M. B. Elowitz, *Science* **334**, 366–369 (2011).
2. N. Hao, E. K. O'Shea, *Nat. Struct. Mol. Biol.* **19**, 31–39 (2011).
3. J. E. Purvis *et al*., *Science* **336**, 1440–1444 (2012).
4. N. Yissachar *et al*., *Mol. Cell* **49**, 322–330 (2013).
5. S. Tay *et al*., *Nature* **466**, 267–271 (2010).
6. H. Shankaran *et al*., *Mol. Syst. Biol.* **5**, 332 (2009).
7. A. Raj, A. van Oudenaarden, *Cell* **135**, 216–226 (2008).
8. A. Goldbeter, *Biochemical Oscillations and Cellular Rhythms: The Molecular Bases of Periodic and Chaotic Behaviour* (Cambridge Univ. Press, Cambridge, 1997).
9. G. M. Süel, R. P. Kulkarni, J. Dworkin, J. Garcia-Ojalvo, M. B. Elowitz, *Science* **315**, 1716–1719 (2007).
10. J. H. Levine, M. E. Fontes, J. Dworkin, M. B. Elowitz, *PLOS Biol.* **10**, e1001252 (2012).
11. L. Cai, C. K. Dalal, M. B. Elowitz, *Nature* **455**, 485–490 (2008).
12. E. Batchelor, C. S. Mock, I. Bhan, A. Loewer, G. Lahav, *Mol. Cell* **30**, 277–289 (2008).
13. E. Batchelor, A. Loewer, C. Mock, G. Lahav, *Mol. Syst. Biol.* **7**, 488 (2011).
14. D. E. Nelson *et al*., *Science* **306**, 704–708 (2004).
15. L. Ashall *et al*., *Science* **324**, 242–246 (2009).
16. C. Cohen-Saidon, A. A. Cohen, A. Sigal, Y. Liron, U. Alon, *Mol. Cell* **36**, 885–893 (2009).
17. J. G. Albeck, G. B. Mills, J. S. Brugge, *Mol. Cell* **49**, 249–261 (2013).
18. K. Aoki *et al*., *Mol. Cell* **52**, 529–540 (2013).
19. A. Warmflash *et al*., *Proc. Natl. Acad. Sci. U.S.A.* **109**, E1947–E1956 (2012).
20. H. Shimojo, T. Ohtsuka, R. Kageyama, *Neuron* **58**, 52–64 (2008).
21. T. Kobayashi *et al*., *Genes Dev.* **23**, 1870–1875 (2009).
22. I. Imayoshi *et al*., *Science* 10.1126/science.1242366 (2013).
23. S. Temple, M. C. Raff, *Cell* **44**, 773–779 (1986).
24. M. Vishnoi *et al*., *Mol. Microbiol.* **90**, 181–194 (2013).
25. J. E. Purvis, G. Lahav, *Cell* **152**, 945–956 (2013).
26. J. W. Young, J. C. Locke, M. B. Elowitz, *Proc. Natl. Acad. Sci. U.S.A.* **110**, 4140–4145 (2013).
27. A. S. Hansen, E. K. O'Shea, *Mol. Syst. Biol.* **9**, 704 (2013).
28. D. Muzzey, C. A. Gómez-Uribe, J. T. Mettetal, A. van Oudenaarden, *Cell* **138**, 160–171 (2009).
29. N. Q. Balaban, J. Merrin, R. Chait, L. Kowalik, S. Leibler, *Science* **305**, 1622–1625 (2004).
30. T. Çağatay, M. Turcotte, M. B. Elowitz, J. Garcia-Ojalvo G. M. Süel, *Cell* **139**, 512–522 (2009).
31. M. Acar, J. T. Mettetal, A. van Oudenaarden, *Nat. Genet.* **40**, 471–475 (2008).
32. D. M. Wolf, V. V. Vazirani, A. P. Arkin, *J. Theor. Biol.* **234**, 227–253 (2005).
33. K. Lewis, *Nat. Rev. Microbiol.* **5**, 48–56 (2007).
34. Y. Wakamoto *et al*., *Science* **339**, 91–95 (2013).
35. J. Garcia-Bernardo, M. J. Dunlop, *PLOS Comput. Biol.* **9**, e1003229 (2013).
36. S. L. Werner *et al*., *Genes Dev.* **22**, 2093–2101 (2008).
37. T. Y.-C. Tsai *et al*., *Science* **321**, 126–129 (2008).
38. P. Rué, J. Garcia-Ojalvo, *Annu. Rev. Biophys.* **42**, 605–627 (2013).
39. G. Q. Bi, M. M. Poo, *J. Neurosci.* **18**, 10464–10472 (1998).
40. I. Berman-Frank *et al*., *Science* **294**, 1534–1537 (2001).
41. B. P. Tu, A. Kudlicki, M. Rowicka, S. L. McKnight, *Science* **310**, 1152–1158 (2005).
42. S. J. Silverman *et al*., *Proc. Natl. Acad. Sci. U.S.A.* **107**, 6946–6951 (2010).
43. J. M. Kralj, D. R. Hochbaum, A. D. Douglass, A. E. Cohen, *Science* **333**, 345–348 (2011).
44. N. Nandagopal, M. B. Elowitz, *Science* **333**, 1244–1248 (2011).
45. T. S. Moon, C. Lou, A. Tamsir, B. C. Stanton, C. A. Voigt, *Nature* **491**, 249–253 (2012).
46. A. Eldar, M. B. Elowitz, *Nature* **467**, 167–173 (2010).
47. J. Stricker *et al*., *Nature* **456**, 516–519 (2008).

Acknowledgments: We thank M. Dunlop, J. Dworkin, N. Friedman, J. Garcia-Ojalvo, R. Kishony, G. Lahav, J. McKinney, R. Murray, R. Phillips, G. Suel, S. Tay, N. Wingreen, and members of the Elowitz lab including M. Budde, F. Ding, P. Li, J. Markson, and A. Rosenthal for critical comments and feedback. This work was supported by NIH grants R01 GM079771-06, R01 GM086793A, and P50GM068763; Defense Advanced Research Projects Agency Biochronicity program grant D12AP00025; and the Packard Foundation.

10.1126/science.1239999

REVIEW SUMMARY

Single-Cell Metabolomics: Analytical and Biological Perspectives

R. Zenobi

READ THE FULL ARTICLE ONLINE
http://dx.doi.org/10.1126/science.1243259

Cite this article as R. Zenobi, *Science* **342**, 1243259 (2013).
DOI: 10.1126/science.1243259

Background: In recent years, there has been a surge in the development and application of single-cell genomics, transcriptomics, proteomics, and metabolomics. The metabolome is defined as the full complement of small-molecule metabolites found in a specific cell, organ, or organism. The most interesting potential application of single-cell metabolomics may be in the area of cancer—for example, identification of circulating cancer cells that lead to metastasis. Other fields where single-cell metabolomics is expected to have an impact are systems biology, stem cell research, aging, and the development of drug resistance; more generally, it could be used to discover cells' chemical strategies for coping with chemical or environmental stress. Relative to other single-cell "-omics" measurements, metabolomics provides a more immediate and dynamic picture of the functionality (i.e., of the phenotype) of a cell, but is arguably also the most difficult to measure. This is because the metabolome can dynamically react to the environment on a very short time scale (seconds or less), because of the large structural diversity and huge dynamic range of metabolites, because it is not possible to amplify metabolites, and because tagging them with fluorescent labels would distort their normal function.

Advances: Although deep biological insight based on single-cell metabolomics has not yet been obtained, important steps have been taken toward this goal. Advances in mass spectrometry (MS), MS imaging, capillary electrophoresis, optical spectroscopy, and in the development of fluorescence biosensors now allow the simultaneous determination of hundreds of metabolites in a single cell, with sensitivities in the attomole range. Modern array formats, in particular microfluidic platforms, contribute to our ability to perform such measurements rapidly and with high throughput. Several recent studies show how novel biological insight can be extracted from single-cell metabolomics. Substantial differences in the metabolomes of different snail neurons—for example, in B1 and B2 type neurons—have been found, immediately after isolating them and after overnight culturing. Glycosphingolipids could be labeled with a fluorescent tag, and in lysates of neurons incubated with such conjugates, all metabolic products derived from them were fluorescent and could be identified. Phosphorylation of 3′-deoxy-3′-fluorothymidine in lymphoma cells and solid tumors could be followed after treatment with cancer drugs. The biological effect of treating yeast cells by 2-deoxy-D-glucose (2DG) on the metabolome could be followed. The fact that single-cell measurements exhibited a much larger spread in metabolite concentrations than population measurements was exploited to determine many metabolite-metabolite correlations, which were altered in 2DG-treated yeast cells relative to controls.

Outlook: The metabolome is an excellent indicator of phenotypic heterogeneity and has been recognized as a key factor in rare-cell survival when populations are subjected to major chemical or environmental challenges. Metabolomics at the single-cell level, however, is only just coming of age. Improvements leading to more complete coverage of the metabolome, better and faster identification of metabolites, and nondestructive measurement are anticipated.

ARTICLE OUTLINE

BACKGROUND READING

P. Nemes, A. M. Knolhoff, S. S. Rubakhin, J. V. Sweedler, Single-cell metabolomics: Changes in the metabolome of freshly isolated and cultured neurons. *ACS Chem. Neurosci*. **3**, 782 (2012).

D. C. Essaka *et al*., Metabolic cytometry: Capillary electrophoresis with two-color fluorescence detection for the simultaneous study of two glycosphingolipid metabolic pathways in single primary neurons. *Anal. Chem*. **84**, 2799 (2012).

P. J. O'Brien *et al*., Monitoring metabolic responses to chemotherapy in single cells and tumors using nanostructure-initiator mass spectrometry (NIMS) imaging. *Cancer Metab*. **1**, 4 (2013).

A. J. Ibáñez *et al*., Mass spectrometry-based metabolomics of single yeast cells. *Proc. Natl. Acad. Sci. U.S.A*. **110**, 8790 (2013).

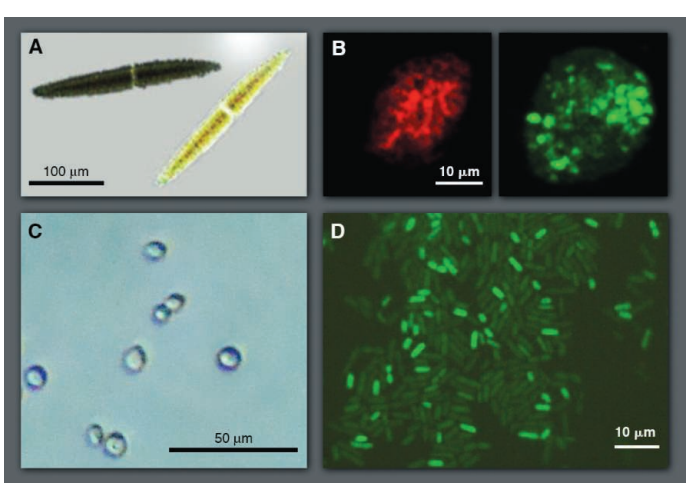

Single-cell analysis uses a wide variety of imaging and chemical analysis methods to study vastly different cell types and sizes. (**A**) *Closterium acerosum* (algal cells, ~300 μm × 40 μm; optical micrograph). (**B**) *Euglena gracilis* (algal cells, diameter ~20 μm); Raman image of β-carotene distribution (left) and fluorescence emission from proplastids (right). (**C**) Baker's yeast (diameter ~5 μm); optical micrograph. (**D**) *Escherichia coli* (diameter ~0.75 μm, length 1 to 3 μm); fluorescence micrograph (image courtesy of M. Heinemann, University of Groningen).

Department of Chemistry and Applied Biosciences, ETH Zürich, CH-8093 Zürich, Switzerland.
E-mail: zenobi@org.chem.ethz.ch

REVIEW

Single-Cell Metabolomics: Analytical and Biological Perspectives

R. Zenobi

There is currently much interest in broad molecular profiling of single cells; a cell's metabolome—its full complement of small-molecule metabolites—is a direct indicator of phenotypic diversity of single cells and a nearly immediate readout of how cells react to environmental influences. However, the metabolome is very difficult to measure at the single-cell level because of rapid metabolic dynamics, the structural diversity of the molecules, and the inability to amplify or tag small-molecule metabolites. Measurement techniques including mass spectrometry, capillary electrophoresis, and, to a lesser extent, optical spectroscopy and fluorescence detection have led to impressive advances in single-cell metabolomics. Even though none of these methodologies can currently measure the metabolome of a single cell completely, rapidly, and nondestructively, progress has been sufficient such that the field is witnessing a shift from feasibility studies to investigations that yield new biological insight. Particularly interesting fields of application are cancer biology, stem cell research, and monitoring of xenobiotics and drugs in tissue sections at the single-cell level.

Every person is different, and this individual phenotype is based on genetic, epigenetic, developmental, and environmental differences. What about cells in a clonal or isogenic culture, whose members are all derived from a single common ancestor? Even in this case there are differences in phenotype, attributable to environmental influences (including the cell cycle), the age of an original cell, and other factors that affect the phenotype of individual cells in the culture. Imagine a hypothetical situation in which all cells in a clonal population are perfectly synchronized and grown in exactly the same conditions. Even then, different phenotypes will develop in the population after some time, frequently as a result of stochastic biological processes (Fig. 1A). "Stochastic" in a biological context refers to irregularities or "noise" in the rates at which biochemical reactions run. This is quite pronounced for processes that involve very few or single molecules—for example, DNA transcription and protein expression (*1*). To assess how different the resulting phenotypes are, single-cell measurements are necessary; population measurements yield only average values (Fig. 1B). Stratification in tissues may also warrant single-cell measurements. For example, neurons are a cell type in which individual differences are required for function. Excitation of an individual neuron in a mammal can initiate the movement of a whisker, change learning, and thus affect the entire organism's behavior. Even in a complex ensemble of sensory neurons, individual neurons have different receptor fields and are therefore distinct.

In recent years, there has been a surge in the development and application of single-cell molecular profiling [for reviews with a focus on metabolomics, see (*2*–*8*)]. The metabolome can be defined as the full complement of small-molecule metabolites (with molecular weights of less than ~2 kD) found in a specific cell, organ, or organism (*9*). For the present purposes, the metabolome (Fig. 1C) includes endogenous as well as exogenous small molecules [e.g., pyruvate, lactate, sugars, adenosine monophosphate (AMP), adenosine diphosphate (ADP), adenosine triphosphate (ATP), etc.], drugs and their metabolites (often referred to as xenobiotics), and lipids, as well as peptides that are not degradation products of proteins (e.g., neuropeptides that are important in cellular signaling). Nucleic acids with short sequences may qualify in terms of their molecular weight, but they are considered part of the cellular transcriptome rather than the metabolome. Salts are not considered metabolites.

The genotype of a cell describes its "potential" whereas the phenotype describes its function, but the link between the two is often obscure (*10*). Relative to single-cell genomics, transcriptomics, or proteomics, metabolomics provides the most immediate and dynamic picture of the functionality (i.e., the phenotype) of a cell, but is arguably also the most difficult to measure: Whereas the genome is more or less static, and the transcriptome and proteome change on a time scale of minutes to hours (*11*), the metabolome reacts to environmental influences on a time scale of seconds or even milliseconds (*12*). This fast dynamics is one of the major challenges for single-cell metabolomics. It requires protocols that quench the metabolism of cells to be studied, because they experience sample preparation itself as an environmental stress and will react to it (*13*). Other challenges include the large structural diversity of the compounds that encompass the metabolome (Fig. 1C), the large dynamic range (from a few molecules per cell to 10^{10} molecules for major metabolites in larger cells), our inability to amplify metabolites (as is commonly done with DNA), and the need to refrain from fluorescent labeling: Very few metabolites are autofluorescent, and attaching a label would in most cases prevent a metabolite from performing its biological function.

Detecting and understanding cancer cells is among the most interesting potential applications of single-cell metabolomics (*14*, *15*). The detection of cancerous cells that display abnormally high metabolic rates among many others with normal metabolism, including circulating cancer cells that lead to metastasis, would be one such application. In the framework of cancer therapy, one might identify cells in a tissue that develop resistance to a drug treatment, or, more generally, discover the chemical strategies of how some cells successfully cope with chemical or environmental stress, whereas others die (*16*). Other potential uses of single-cell metabolomics (relative to other "-omics" methodologies) are to obtain input and output data for mathematical models of cellular metabolism (*17*), to learn more about aging (*18*, *19*), and to predict the developmental fate of stem cells.

Have single-cell metabolomic data already yielded deep biological insight? I would argue that this is not yet the case. One reason is that stochasticity cannot generally be followed by studying metabolites; there are only indirect and often small effects on the metabolome from stochastic biochemical processes. Moreover, important metabolites appear in numerous nodes of the metabolic network in cells; that is, either multiple correlations between major metabolites are needed to obtain any insight, or, alternatively, precise measurements on rare and low-concentration metabolites with highly specialized roles need to be performed, which is difficult. However, a few studies discussed below (*20*–*23*) have already enhanced our knowledge about biological systems.

This review focuses on the rapidly developing analytical methodology, but also discusses what can be learned about a biological system if metabolomic data are collected at the single-cell level rather than from population averages (Fig. 1B), on how the variations in the metabolome among many single cells can give new information about the causes and consequences of cell variability, and on whether these variations are adaptive, an epigenetic phenomenon, or a basic property of biochemistry.

General Considerations for Single-Cell Metabolomics

Unless the sample is a cell suspension, the first step of sampling (*2*, *6*) is to isolate appropriate cells from an organism, which is sometimes done manually, under microscopic observation. Once cells are isolated, some approaches sample an

Department of Chemistry and Applied Biosciences, ETH Zürich, CH-8093 Zürich, Switzerland. E-mail: zenobi@org.chem.ethz.ch

individual cell directly; others involve cell culture, for example, in a microfluidic device. A major issue, as explained above, is a suitable sample preparation that does not upset the metabolism of the cells to be investigated. One way to cope with this problem is to keep the cells in a native environment as long as possible. A number of highly successful microfluidic chips that gently trap cells have been presented in the literature (*24*–*27*). Key functions of these microfluidic platforms are to isolate cells, culture them under well-controlled conditions, inject highly defined amounts of chemicals into the growth medium, and selectively release cells for analysis, which may involve an on-chip lysis step (*28*). Another option is to shock-freeze cells before subjecting them to measurement (*23*) to quench the metabolism.

Another issue is the required sensitivity. Cell sizes vary widely. Typical mammalian cells have diameters around 10 μm (volume = 1 pl); the giant neurons of the sea slug *Aplysia californica*, which have frequently been used in early single-cell studies because they can be manipulated manually under a microscope, can reach 500 μm. On the other end of the size spectrum are model organisms such as yeast (diameter ≈ 5 μm) and bacteria with diameters on the order of 1 μm (volume = 1 fl). Assuming a metabolite concentration of 1 mM, the absolute amounts that need to be detected in these tiny volumes are thus in the range of 1 amol to 1 fmol, which is challenging, even for major metabolites. Interestingly, the concentration sensitivity is less of an issue: The presence of a single molecule inside a 6-fl bacterial cell translates into a concentration of 0.28 nM; that is, it will generally not be necessary to measure concentrations lower than nanomolar.

Furthermore, cells are usually grown in medium rich with molecules that are similar or even identical to metabolites. Thus, it is critical to differentiate between the metabolites in the surrounding medium (footprinting) and the metabolites within the cell (fingerprinting).

Finally, high-throughput formats for sampling cells are clearly necessary; an isolated measurement on one single cell may be less meaningful in a biological context (although if a single cell could be precisely and continuously analyzed in its morphological and molecular aspects, biological insight could be obtained from that single cell). To generate statistically significant data, hundreds or thousands of measurements are generally necessary, which presents another challenge. A number of strategies that enable high-throughput interrogation of many single cells have been developed. Classical high-throughput formats are flow cytometry and modifications thereof, such as fluorescence-activated cell sorting (FACS; Fig. 2A). Flow cytometry measurements are, however, generally not at all linked to metabolites and may be used to separate a cell culture into two or several subpopulations that are subsequently analyzed. Special formats of cytometric measurements have thus been developed—for example, a mass spectrometric readout following flow cytometric sample delivery (*29*). Other high-throughput formats include microarray printing of controlled numbers of cells (*30*) and many different lab-on-a-chip devices (*31*). One such platform developed by Di Carlo and Lee that allows gentle trapping is shown in Fig. 2B (*24*). Many U-shaped hydrodynamic trapping structures allow both arrayed culture of individual adherent cells and simultaneous control of fluid perfusion with uniform environments for individual cells. Cell loading can be achieved in less than 30 s.

High-density chips are also becoming available to allow measurements by mass spectrometry (MS). As described below, MS is one of the most successful methods for single-cell metabolomics—which, however, means that high-throughput preparation of single-cell samples becomes the bottleneck. One possible solution involves MAMS (microarray for mass spectrometry) chips (*32*), as shown in Fig. 2C. A very attractive feature of MAMS chips is that the hydrophilic wells surrounded by an "omniphobic" polysilazane coating on the surface allow automated isolation of small volumes containing single cells from cell suspensions, by simply dragging the liquid over the surface of the chip. Current versions of such MAMS chips allow 10,000 to 50,000 wells to be filled and subsequently analyzed; the number of cells per well is given by a Poisson distribution.

Preparing Single-Cell Samples for Analysis

Microfluidics

Although microfluidics is not an analysis method per se, microfluidic devices are extremely useful in presenting single-cell samples for readout by optical spectroscopy, mass spectrometry, or other means. The job of the microfluidic device is to transport, immobilize, culture, infuse with reagents, hold for observation, and retrieve single cells in a high-throughput fashion. Formats include patch-clamp array (*33*), dynamic single-cell culture array (*24*), and integrated microfluidic array plate (iMAP) (*34*), in all cases using microscale soft

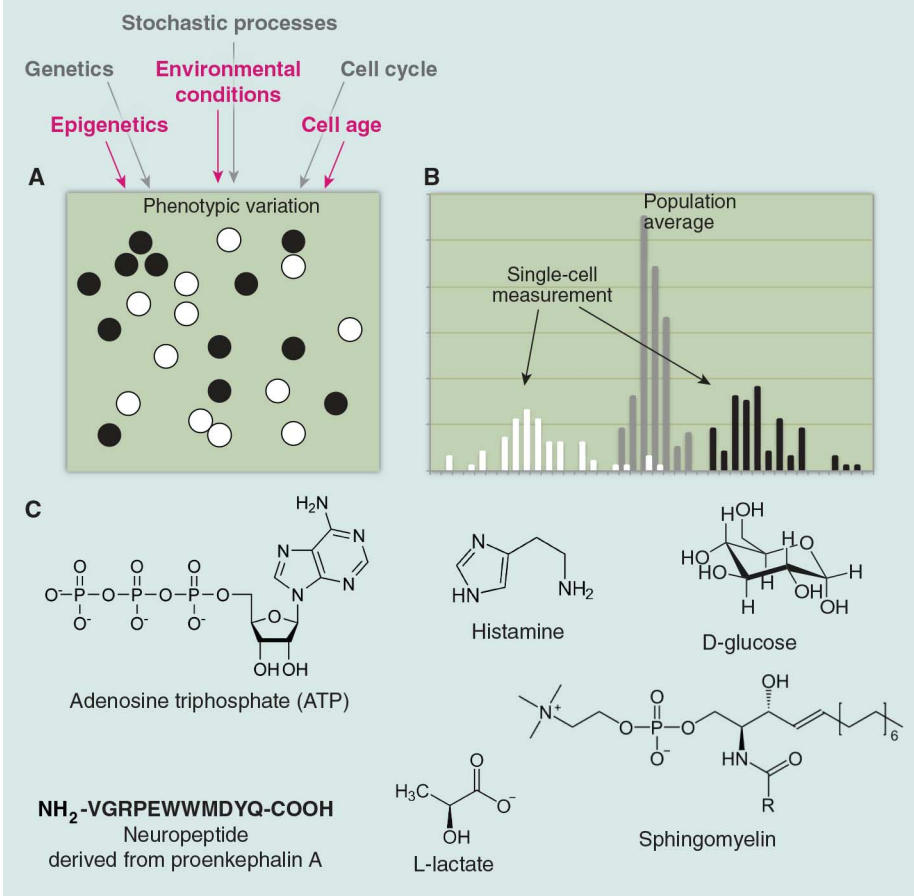

Fig. 1. Development of different phenotypes in cell cultures. (**A**) Reasons for phenotypic variations can range from genetic differences to stochastic processes. (**B**) Hypothetical histogram of a population average (gray bars) and a single-cell measurement (white and black bars) of the same parameter (e.g., a metabolite concentration) revealing bistability only in the case of the single-cell determination. (**C**) Some examples of metabolites, illustrating the large structural diversity of compounds covered by metabolomics.

lithography with polydimethylsiloxane (PDMS) as the material. The dynamic single-cell culture array (Fig. 2B) allows an arrayed culture of many individual adherent cells (~100 in a field of view of ~1 mm^2). Trapping is passive and self-terminating in the sense that once a site is filled with a cell, the altered hydrodynamic flow around the filled site prevents other cells from entering it. This device has not been used for chemical measurements so far, but it appears to provide a very gentle growth environment, as shown for the high rate (95%) of survival of HeLa cells after 24 hours of perfusion culture on the array. The iMAP array is based on gravity-driven flow and sedimentation to capture the cells, with close to 100% capture rate. It features open access for fluid exchange; gene expression, protein immunoassay, and cytotoxicity data can be accessed in parallel.

Another strategy is the dynamic microfluidic array based on fluidic resistance (*25*). The flow channel has a meander-like shape with some additional small "bays" (hydrodynamic traps) where cells get trapped passively. To selectively release beads or cells from such a bay, a microbubble is generated by laser heating of an Al pattern near an individual trap. The authors wrote that the heating is of no concern for the integrity of the beads that were investigated (the Al structure reaches temperatures of >130°C), but one would probably have to worry about the transient temperature jump as an environmental influence to which a cell's metabolome would react. Although this device has so far been developed and operated only with beads rather than with cells, 100 objects could be trapped and individually addressed. For single-cell analyses, such a microfluidic device would be operated with medium as the circulating liquid and be used to deliver individually addressable cells to a subsequent analysis (e.g., by mass spectrometry).

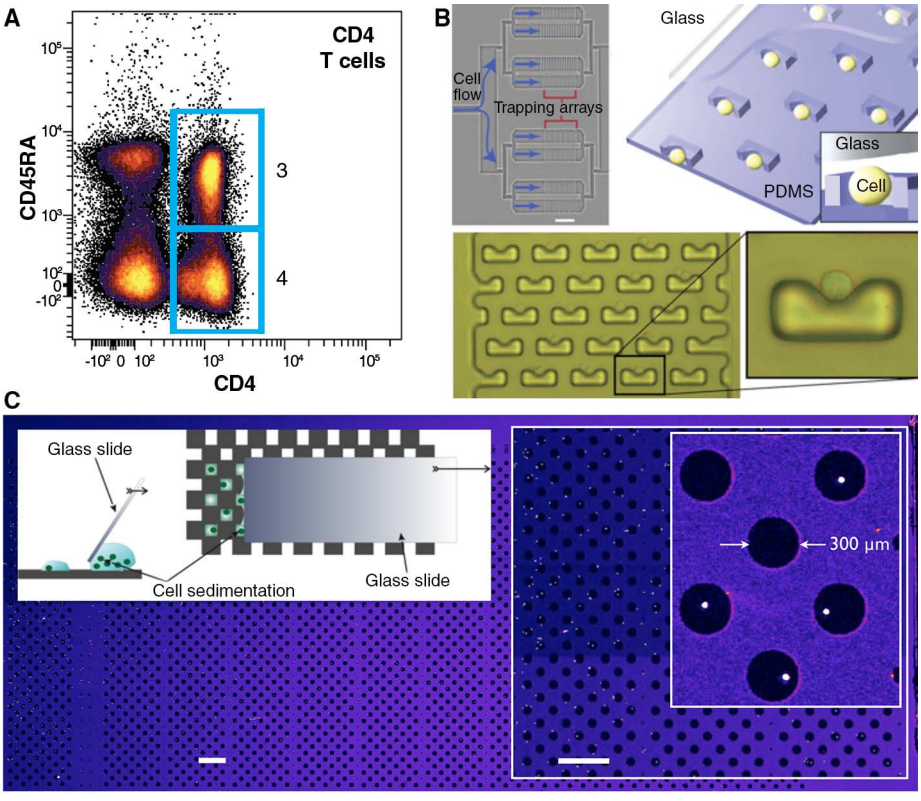

Fig. 2. High-throughput methods for preparing single cell for chemical analysis. (**A**) Flow cytometry of human bone marrow cells, using fluorescent antibodies that bind to cell surface antigens (here, CD45RA versus CD4). Each dot in the plot originates from a single cell. [Reproduced from (*92*)] (**B**) Microfluidic single-cell trapping array. Upper left: Increasingly higher magnifications depict the cell-trapping device as a whole (scale bar, 500 μm; cells and media flow enter from the left). Lower left: High-resolution bright-field micrograph of the trapping array with trapped cells. Lower right: Magnification showing the details of one trapped cell. Trapping is a gentle process, and no cell deformation is observed for routinely applied pressures. Upper right: Diagram of the device and mechanism of trapping (not drawn to scale). [Reproduced, with permission, from (*24*)] (**C**) Microarray for mass spectrometry (MAMS) chip. Scale bars, 1440 μm; diameter of individual wells, 300 μm. On a MAMS array the size of a 1″ x 3″ microscope slide, 2860 wells can be placed. *Chlamydomonas reinhardtii* algal cells; chlorophyll fluorescence readout measured with a LS 400 scanner (Tecan, Männedorf/Switzerland). [Image courtesy of Jasmin Krismer, ETH Zürich, and Jens Sobek, Functional Genomics Center, Zürich]

Microchamber arrays can be used not only for single-cell isolation but also for the analysis of intracellular biomolecules. This design is based on PDMS valves that encapsulate single cells in circular reservoirs with volumes of ~625 pl. These microchambers can be opened and closed rapidly and reversibly; such a design allows incubation, washing, labeling, and lysis steps to be done with single cells (*35*). The lysate remains contained in the small volume of the microchamber; although dilution still occurs, it is controlled and limited such that various target analytes can be directly studied, cell by cell. This format has been used for analyzing the cofactors NADH (reduced nicotinamide adenine dinucleotide) and its phosphate NADPH, and for quantitative assays of a number of intracellular biomolecules, including compounds such as cyclic AMP (cAMP) in human embryonic kidney (HEK) T-Rex cells, production of which is stimulated by the hormone lutropin (*36*). Attomole amounts of cAMP (between 250 and 1000 amol, increasing with the level of stimulation by lutropin) were detected. Because a competitive enzyme-linked immunosorbent assay (ELISA) was used for detection, this format provides the equivalent of a single-cell immunoassay.

There are many other microfluidic formats for single-cell trapping, culturing, and handover to analysis [for further information, see (*31*, *37*–*39*)], although in many cases these are not specially designed for obtaining chemical information on metabolites. Some formats allow very interesting microscopic observations to be conducted—for example, the observation of aging processes of budding yeast cells throughout their life span (*19*), which revealed remarkable age-associated changes in phenotypes and substantial heterogeneity in cell aging and apoptosis. This is, however, not a metabolomics study, and the same is true for most other microfluidic platforms: In connection with metabolomics, their usefulness is to observe and classify individual cells, stimulate them inside the microfluidic device, and deliver them in a rapid but controlled fashion to a subsequent analysis step that identifies the metabolites.

Nanoscale Devices

Nanoscale devices can be used to manipulate single cells or deliver chemicals into cells in a controlled fashion. A nanowire waveguide-based approach allows single-cell optical endoscopy (*40*), a hollow atomic force microscopy (AFM) probe can be inserted through the cell wall and used to deliver liquids into the cytoplasm (*41*), and a nanochannel has been used to deliver precise amounts of biomolecules into living cells (i.e., a kind of precision transfection technique) (*42*). Nanoscale devices are also being developed to analyze cells, as summarized in (*43*)—for example, optically through near-field methods, through AFM, or electrochemically by scanning conductance microscopy. Although much of the relevant literature cites the potential and especially the need

for high-throughput operation, most of these nanoscale approaches are at present slow, serial, and difficult to control.

Analytical Methodologies for Identifying Metabolites in Single Cells

Mass Spectrometry

Mass spectrometry (MS) is rapidly becoming one of the most widely used methods for ultrasensitive and simultaneous detection of many metabolites at the single-cell level. Label-free, highly sensitive, and information-rich, MS has contributed since the early days to this field. MS can be used as a detector for flow cytometry (*29*), with a capability of infusing hundreds of cells in a few minutes. Histamine (0.75 ± 0.33 fmol) and serotonin (0.11 ± 0.06 fmol) have been detected in rat peritoneal mast cells, however, without any obvious correlation of the amounts of the two amines in each cell. Giant neurons of *A. californica* (*20*, *44*) provide the ease of handling very large cells. Principal components analysis of large data sets with more than 300 distinct cell-related signals revealed significant differences in the metabolomes of various *Aplysia* neurons—for example, in B1 and B2 type neurons—immediately after isolating them and after overnight culturing. It was also possible to determine absolute concentrations of several metabolites in the isolated neurons. For example, intracellular glutamic acid concentration was 11 mM in one type of neuron and 4 mM in others. This particular strategy involved both capillary electrophoresis (CE) and MS, which affords a quite powerful way to identify and detect metabolites (*44*).

Among the modern ionization methods, matrix-assisted laser desorption/ionization (MALDI) has sufficient sensitivity for single-cell analyses. However, the presence of intense matrix signals in the ≤500-dalton range is of great concern for metabolomics. A number of strategies have thus been developed to circumvent this problem. Matrix-free ionization methods based on nanophotonic effects are available—for example, using desorption-ionization from porous silicon (DIOS) or silicon nanopost arrays (NAPAs), which in the hands of some laboratories feature a sensitivity in the subfemtomole or even sub-attomole range (*45*, *46*). NAPA-MS revealed metabolic differences in stressed and control yeast cell populations (*47*). The sensitivity was enough to determine metabolites in samples consisting of 1 to 80 cells in a semi-quantitative manner, and more than 100 peaks could be assigned to various metabolites, representing ~9% of the ~1200 known yeast metabolites. Following oxidative stress, up-regulation of glutathione, cysteinylglycine, glutamylcysteine, and urate (among others) was observed, whereas compounds related to folate biosynthesis, such as amino-4-deoxychorismate or dihydroneopterin phosphate, were down-regulated, indicating that the cells redirected resources from growth to fighting stress.

Another strategy is to use MALDI matrices that generate only few well-defined signals. An excellent compound is 9-aminoacridine (9-AA), which has the added benefit of promoting formation of negative ions (*48*). This is useful for detection of metabolites in their deprotonated form, such as small organic acids or phosphorylated compounds. Single-cell detection sensitivity for metabolites in yeast has been shown using 9-AA (*49*), and the same matrix has been used in subsequent single-cell studies (*4*, *50*, *51*). Negative ion mode MALDI and 9-AA allowed detection of 26 different metabolites in single yeast cells (*23*). Hundreds of cells were measured in this study with a MAMS chip, and the effect of a chemical perturbation by 2-deoxy-D-glucose (2DG) on the metabolome was measured (Fig. 3A). The fact that single-cell measurements exhibited a much larger spread in metabolite concentrations relative to population measurements was exploited to determine many metabolite-metabolite correlations, which were altered in the case of 2DG-treated yeast cells versus controls.

Alternatively, electrospray ionization (ESI)–based methods can be used. A method called laser ablation electrospray ionization (LAESI; Fig. 3B) was developed for in situ mass spectrometric analysis of individual cells at atmospheric pressure (*52*). Single-cell probing was achieved by delivering mid-infrared (IR) laser pulses (that are absorbed by the water in the sample) through the etched tip of a GeO_2-based glass fiber, and the laser ablation products were post-ionized in a pure solvent ESI plume. Metabolic analysis was achieved from single cells and small cell populations of *Allium cepa* and *Narcissus pseudonarcissus* bulb epidermis, as well as single eggs of *Lytechinus pictus*. Among the 332 peaks detected for *A. cepa*, 35 were assigned to metabolites with the help of accurate mass and MS-MS measurements. Differences in the metabolite profile of adjacent cells with different pigmentation could be discerned for *N. pseudonarcissus*; *A. cepa* showed metabolic differences as a function of cell age. The cells of these plant species, however, were rather large, on the order of 70 × 400 μm. A completely different ESI-based approach dubbed live single-cell video mass spectrometry (*53*, *54*) involves inserting an electrospray needle into a cell under video microscopic observation, removing some of the cytoplasm, and then directly electrospraying the liquid via the same needle into an ambient inlet mass spectrometer (Fig. 3C). This method is even able to distinguish between cytoplasm-specific and granule-specific signals, showing, for example, differences in the subcellular metabolite distribution of a rat leukemia mast cell line (RBL 2H3) model. Around 1000 peaks belonging to metabolites were distinguished in plant tissue (from *Pelargonium zonale*, geranium), and a combination of high-resolution MS, tandem mass spectrometry, and database searches yielded tentative assignments for more than 20 signals (*55*). This method, however, can hardly be called high-throughput. Sampling the contents of the cells is still best done manually and is difficult, and mass spectrometric analysis is performed off-line, in a second step. At best, a few cells can be analyzed per hour.

Mass Spectrometry Imaging

Mass spectrometry imaging (MSI) is dealt with separately here because of the completely different manner in which samples are prepared and subjected to analysis (*56*). Both MALDI and secondary ion mass spectrometry (SIMS) imaging are used. On research-grade MALDI-MS instruments, MSI can now be done with a spatial resolution of <1 μm (*57*, *58*), at ambient pressures, and with very high mass accuracy and mass resolution (*59*). This corresponds to subcellular resolution for many kinds of cells. For the sake of generating enough signal per spot, the spatial resolution is often chosen to be somewhat lower, in the range of 5 to 30 μm, which is also the spatial resolution achieved by commercial MALDI instruments with imaging capabilities (*60*). MSI is capable of detecting and identifying a broad range of metabolites and is often applied to tissue sections, where a cell-by-cell distinction is feasible. One of the premier applications of MALDI-MSI is the visualization of drugs and their metabolites in tissue section or even whole animal thin sections. Although single-cell resolution is in principle available, it is often not used in such studies, for the sake of increasing the speed of data acquisition, or because it is simply not required. For example, in tuberculosis-infected rabbit lung tissue sections, the distribution of the second-line tuberculosis drug moxifloxacin was imaged at several time points after dosing (*61*). The drug was observed to accumulate in granulomatous lesions in amounts higher than those in the surrounding lung tissue, with an inhomogeneous distribution within the granulomas; very low amounts were observed in the caseum relative to the cellular granuloma regions.

Nanostructure-initiator mass spectrometry (NIMS) imaging has been used to follow the reaction of individual cancerous cells and cancer xenografts to chemotherapy (*22*). Phosphorylation of 3′-deoxy-3′-fluorothymidine (FLT, a thymidine analog) to FLT monophosphate (FLT-MP) was followed in lymphoma cells and solid tumors after treatment of the specimens with rapamycin or FLT. Although FLT is readily transported out of cells, FLT-MP is not, and its accumulation serves as an indirect indicator of drug-induced metabolic changes of treated cells. Complementary liquid chromatography–tandem MS (LC-MS/MS) measurements on extracts of many cells were also conducted, with consistent results.

Secondary ion mass spectrometric imaging is capable of generating chemical maps of complex surfaces, such as tissue sections or cell cultures, with subcellular resolution [down to <100 nm (*62*–*64*)]. In SIMS, a compromise often must be

found between very high spatial resolution and the ability to detect intact molecular species: SIMS with highly focused primary ion beams capable of sub–100 nm resolution generally operates in the "dynamic SIMS" mode (i.e., a high primary ion dose is necessary to generate enough signal). This, however, turns out to be detrimental to the integrity of larger organic molecules. There have been reports of studies that combine MALDI imaging with SIMS, the latter providing the higher spatial resolution if required (*65*). Both allow label-free and simultaneous determination of the identity and distribution of xenobiotics and their metabolites as well as endogenous substances in tissue. This is an interesting extension to whole-body

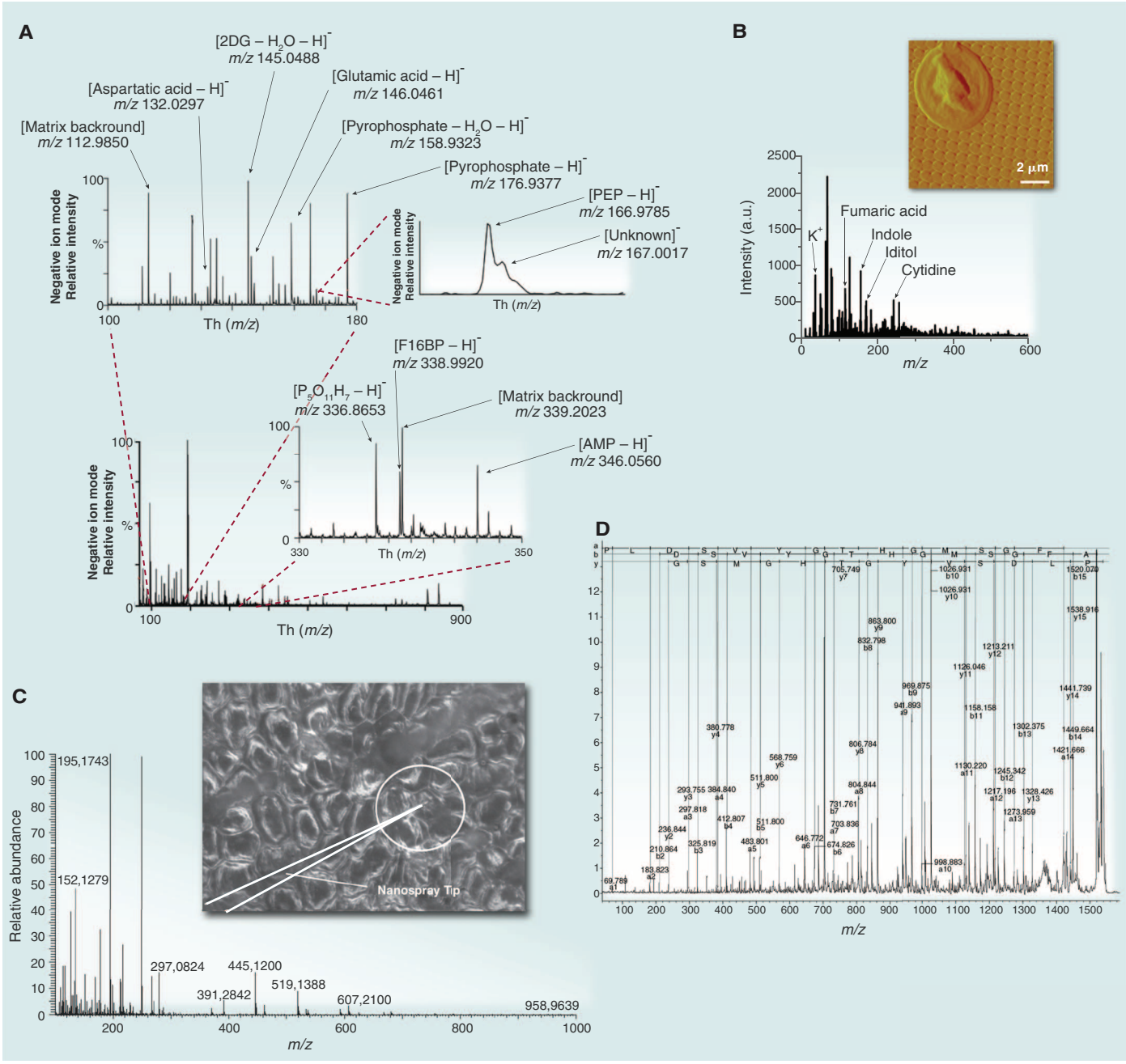

Fig. 3. Analyses of metabolites at the single-cell level by mass spectrometry, showing the capability of this method. (A) Full-scan negative-ion mode MALDI mass spectrum of a single YSBN.6 (*S. cerevisiae*) cell (*m/z* = 70 to 900) treated with 2DG; the measurement took place 1 min after the spike of 2DG into the growth medium occurred. Inset shows two spectra: (i) *m/z* = 100 to 180; (ii) *m/z* = 330 to 350. [Reproduced, with permission, from (*23*)] **(B)** LDI mass spectrum of a single yeast cell from a NAPA in the mass range of metabolites. Four of the ~24 putatively assigned metabolites are labeled. Inset: AFM image of a single yeast cell deposited on a NAPA substrate before LDI-MS analysis. [Reproduced, with permission, from (*46*)] **(C)** Example of full spectrum (*m/z* range 100 to 1000) and photograph of *Pelargonium zonale* single-cell contents extraction by the nanoelectrospray tip from a leaf cell. [Reproduced, with permission, from (*55*)] **(D)** MALDI time-of-flight (MALDI-TOF) imaging detects strong neuropeptide signals in MS and MS/MS modes from cell culture samples of cultured pedal neurons. The automatically generated MS/MS peak assignment for *m/z* 1540 yields the sequence that corresponds to the known amino acid sequence for *Aplysia* pedal peptide, PLDSVYGTHGMSGFA. [Reproduced, with permission, from (*60*)]

microautoradiography, eliminating the need for radiochemistry and providing molecule-specific information.

Mass spectrometric analyses have in common that among all the analytical methods presented, they yield the most detailed information about the compounds that are detected. A good strategy is to use accurate mass measurement (*59*), which often restricts the possible elemental compositions of a signal to only a handful or ideally, to a unique sum formula (see Box 1). Sometimes tandem MS (MS/MS) can even be performed on signals from a single cell (*55*), although normally this is not possible because of an insufficient signal-to-noise ratio. Alternatively, MS/MS analysis can be done on the same, accurately measured mass-to-charge ratio (*m/z*) signal from a larger sample, assuming that the same compound appears in the single-cell data. MS/MS may not always give the information sought. For example, differently phosphorylated carbohydrates exhibit very similar MS/MS spectra and therefore may be indistinguishable by mass spectrometry. Finally, an increasing number of databases list metabolites for various species (Box 1). Looking up putative metabolites in a database definitely has its merits, in particular for automated data interpretation, although it helps little in the quest to identify new metabolites.

Fluorescence-Based Detection, Fluorescence Biosensors, and FRET Biosensors

Fluorescence microscopy is in principle an excellent, sensitive, nondestructive, and widely available method to image single cells, and in combination with fluorescent tags, it can also provide chemical specificity. With modern image processing, it is straightforward to get information in a high-throughput fashion. However, very few metabolites are autofluorescent; examples include the detection of carotenoids in red yeast (*66*), the distinction of tumor cells in a tissue through autofluorescence spectroscopy and decay kinetics (*67*), or the localization of chlorophyll pigments related to the photosynthetic reaction center II and internal antennae of photosystem II in algal cells (*68*). Attaching fluorescent labels to low–molecular weight metabolites turns out to be too invasive: The fluorescent tag itself will disturb the biochemical function of the metabolite. Thus, methods that provide indirect fluorescent readout as a function of the presence or concentration of a metabolite are required. "Smart" designs of fluorescent proteins (FPs) can be exploited in various ways for use as biosensors (*69*): by activating the fluorescence by small-molecule ligand binding to the FP, by inducing a conformational change of the FP in the presence of a metabolite, by oligomerization-dependent fluorescence of more than one FP moiety, or through Förster resonance energy transfer (FRET) of two different FPs, activated by binding of a metabolite. Often such formats are referred to as "nanosensor probes."

Numerous fluorescence-based methods exist to detect AMP, ADP, or ATP—for example, an assay in which a dipicolylamine ligand, a naphthalimide chromophore, and a Zn(II) center form a fluorescent complex in the presence of ATP (*70*). High Stokes shift (>70 nm), high fluorescence quantum yield, good selectivity against other organic and inorganic phosphates, and a sensitivity down to 1 μM ATP were some of the key characteristics. One problem with fluorescence detection is that a fluorescence signal is readily perturbed by changes in the environment (e.g., by changes in pH, temperature, or solvent polarity). Ratiometric measurements that involve simultaneous determination of two fluorescent signals at different wavelengths can circumvent these problems and yield greater precision for quantitative determinations. Binding-induced modulation of FRET is a possible embodiment of a ratiometric measurement. Such a FRET biosensor has been useful for detecting nucleoside polyphosphates (*71*). It showed good sensitivity (<<1 μM for ATP) and excellent linearity; the authors were able to follow the energy charge of cells in a human cancer (HeLa) cell line after treatment with 20 mM 2-deoxyglucose and 1 mM KCN. A problem, however, was the limited selectivity: Binding of a range of nucleoside polyphosphates to the FRET sensor molecules was reported.

There are a number of difficulties that render fluorescence microscopy less suitable for true metabolomics: Genetically encoded nanosensor probes exist for only a handful of specific small molecules (*72*), and it is relatively complex to express the biochemical machinery for indirect fluorescence detection. Often tedious optimization is required, the specificity and optical contrast are sometimes not satisfactory, and the genetic modification may affect the native physiology of such cells. Also, the number of different fluorescent reporter tags that can be simultaneously imaged is limited (to around 10). In fact, the literature does not seem to include any report of simultaneous detection of multiple target metabolites; however, dozens to hundreds would be required for true metabolomics. On the other hand, fluorescence is extremely useful for ultrasensitive detection, down to the level of a single molecule. This has been shown for proteins in individual cells that were handled through microfluidics (*1*, *73*)

Box 1. Identification of metabolite signals from mass spectrometry data and database searches.

Nominal mass: 180 daltons → 141 different possible elemental compositions that include C, H, N, O, S, Cl, Br, and I; very large number of isomers. Includes the elemental composition $C_6H_{12}O_6$. Some elemental compositions are not chemically sensible, for example, HO_9Cl, $C_{12}HCl$, or C_{15}.

Accurate mass: 180.06339 → 2 possible elemental compositions with less than 1 ppm deviation, $C_5H_6N_7O$ (chemically unlikely) and $C_6H_{12}O_6$ (a carbohydrate). 32 different isomers (fructose, galactose, gulose, sorbose, inositols, etc., including stereoisomers: D and L forms).

MS/MS information: Glucose (D-glucose and L-glucose indistinguishable by tandem MS)

Selection of Databases on Metabolites and Mass Spectrometry

Human Metabolome Database (www.hmdb.ca): a freely available electronic database containing detailed information about small-molecule metabolites found in the human body.

Pubchem (http://pubchem.ncbi.nlm.nih.gov): provides information on the biological activities of small molecules.

Metabolights (www.ebi.ac.uk/metabolights): a database for metabolomics experiments and derived information. The database is cross-species, is cross-technique, and covers metabolite structures and their reference spectra.

Kegg (www.genome.jp/kegg): a database resource for understanding high-level functions and utilities of the biological system, such as the cell, the organism, and the ecosystem, from molecular-level information.

Metlin (http://metlin.scripps.edu): a repository of metabolite information and tandem mass spectrometry data, for use in metabolomics experiments.

Yeastnet (www.comp-sys-bio.org/yeastnet): a portal to the consensus yeast metabolic network as reconstructed from the genome sequence and literature.

The Yeast Metabolome Database (www.ymdb.ca): a manually curated database of small-molecule metabolites found in or produced by *Saccharomyces cerevisiae*. It covers metabolites described in textbooks, scientific journals, metabolic reconstructions, and other databases.

ChemBioFinder (http://chembiofinder.cambridgesoft.com): an online chemistry and biology reference database with almost 2 million compounds indexed and linked to other Web sites.

Chemspider (www.chemspider.com): free chemical structure database providing fast text and structure search access to more than 28 million structures from hundreds of data sources.

Massbank (www.massbank.jp): public repository of mass spectral data, useful for the chemical identification and structure elucidation of chemical compounds detected by mass spectrometry.

and was a key method to detect stochasticity in expression of small–copy number proteins in single cells. It is also very powerful for ultrasensitive detection after CE separation of the chemical contents of cells (*21*, *74*, *75*).

Vibrational Spectroscopy

In some cases, vibrational spectroscopy can be used to distinguish certain metabolites in single cells (*76*). As opposed to detection through fluorescent tags, vibrational spectroscopy is label-free and thus amenable to spectroscopically active compounds (e.g., pigments) as long as they are present in sufficiently high concentration. An example is the localization of β-carotene by its 1150 and 1515 cm^{-1} Raman bands with subcellular resolution (~550 nm per pixel) in *Euglena gracilis* algal cells (*68*). Complementary single-cell MS data were also recorded in this case. A colocalization of β-carotene and the plastids containing internal antennae of photosystem II was shown. Synchrotron-based IR spectroscopy, with multiple low-emittance beams and a large focal plane array detector, was used to achieve a pixel size of 540 nm in the mid-IR, about two orders of magnitude smaller than is possible with conventional thermal or synchrotron IR sources (*77*). Detailed spectroscopic information was available, for example, from images of the CH_3 stretching (2950 cm^{-1}) and the amide I (1654 cm^{-1}) modes, with single-cell resolution, on thin sections of cancerous prostate tissue with chronic inflammation. Corneal epithelial cells have been isolated from biopsies of live tissues by FACS; these were divided into putative stem cells (SCs), transit-amplifying (TA) cells, and terminally differentiated (TD) cells (*78*). DNA regions of the spectra (1080 and 1225 cm^{-1}) and some protein regions (1443 cm^{-1}) primarily distinguished SCs from TA cells and TD cells, whereas amide regions and lipids (1550, 1650, and 1740 cm^{-1}) could be used to distinguish TA cells and TD cells. A stimulated Raman scattering microscopy technique (*79*) allows visualization of various biomolecules (e.g., lipids) by their saturated C-H vibrations at 2845 cm^{-1}, proteins by their amide I band at 1655 cm^{-1}, or nucleic acids by their 785 and 1090 cm^{-1} bands. Pixel sizes on the order of 200 nm are possible with this technique; that is, subcellular spatial resolution is possible. The notable feature of vibrational spectroscopy is that absolutely no staining or labeling of the cells is required. On the other hand, the spectra are not really specific for metabolites, but instead reveal all compounds that are highly concentrated and spectroscopically active. This often leads to spectral congestion of IR and Raman spectra, which renders them less suitable as tools for metabolomics.

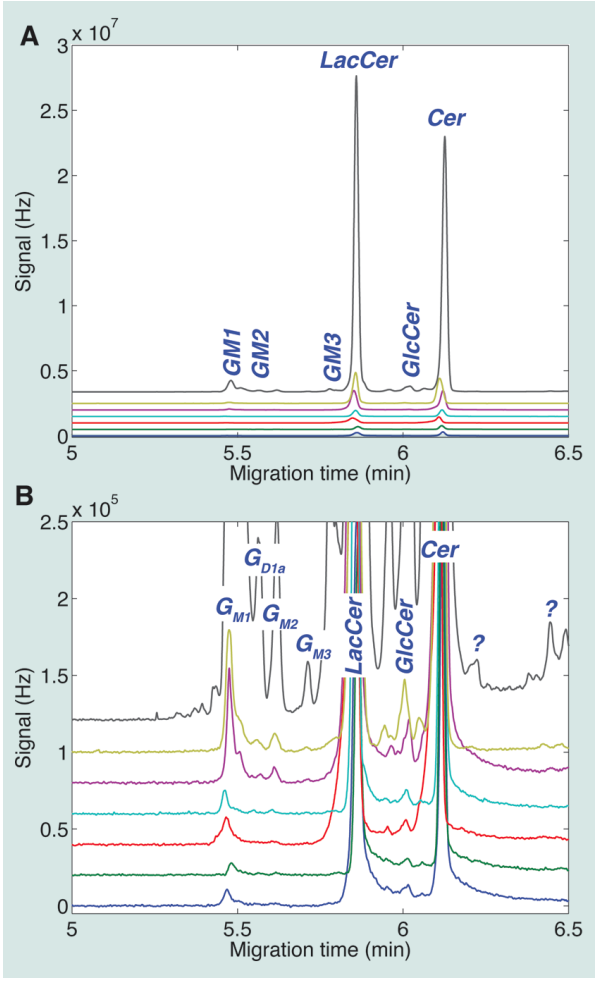

Fig. 4. Separation-based detection of metabolites in neuronal cells. (**A** and **B**) Separation by capillary electrophoresis and fluorescence detection of metabolic products from the glycosphingolipid LacCer labeled with BODIPY dye, shown at full scale (A) and expanded scale (B). Unknown components are marked with "?". Vastly different levels of metabolites are found for different cells. [Reproduced, with permission, from (*21*)]

Separation-Based Chemical Analyses

Capillary electrophoresis and capillary LC have been used without exception for single-cell studies involving separation on a column, for the obvious reason that they can handle very small volumes. It is possible to detect metabolites, including amino acids and neurotransmitters, in quantities of tens of femtomoles in large snail neurons after capillary separation and voltammetric as well as fluorescence detection (*80*), and even sub-attomole detection limits for serotonin with amperometry have been reported (*81*). This approach is currently most successfully used for single-cell proteomics (*82*, *83*), although some applications to metabolites have appeared in the literature (*84*–*86*). In particular, quantitative studies have been reported on glycosphingolipids in single neurons with one- (*74*), two- (*21*), and three-color (*75*) fluorescence detection (Fig. 4). The general strategy is to label one or more glycolipids [for example, mammalian ganglioside GM1 and lactosylceramide in (*21*)] with fluorophores, incubate cells with these conjugates, and follow glycolipid catabolism and anabolism by the appearance of fluorescent products. These were identified by aspirating single cells into a capillary, lysing them inside it, and separating the metabolic products by CE. Identification was possible by comparison with standard compounds, taking into account the slightly different migration times of the labeled glycosphingolipids. About a dozen metabolites were identified, and individual cells showed vastly different uptake of the labeled glycosphingolipids. A dynamic range of six orders of magnitude and a separation power of ~10^6 theoretical plates were reached. For glycosphingolipids labeled with boron dipyrromethane (BODIPY) fluorophores, extreme sensitivities of 34 ± 1 to 67 ± 7 molecules could be achieved, depending on the exact nature of the label. Obviously, the greater the number of distinct fluorophores that are introduced, the more metabolic pathways that can be followed simultaneously. The limitations, however, are the same as simultaneous detection by a number of different fluorescence channels, as well as the disturbance of the metabolism itself by the presence of the rather bulky fluorophores.

Combining CE separation with MS detection is also a very powerful technique (*20*, *44*, *48*). For example, a sheathless CE-ESI-MS interface allowed detection of close to 20 metabolites in extracts of *E. coli* with sensitivities ranging

from 20 nM (~0.8 fmol) for ADP-ribose to 2.5 μM for α-ketoglutarate (*48*). Qualitative and quantitative metabolomic investigation has also been reported for single neurons by CE-ESI-MS (*20*, *44*, *87*).

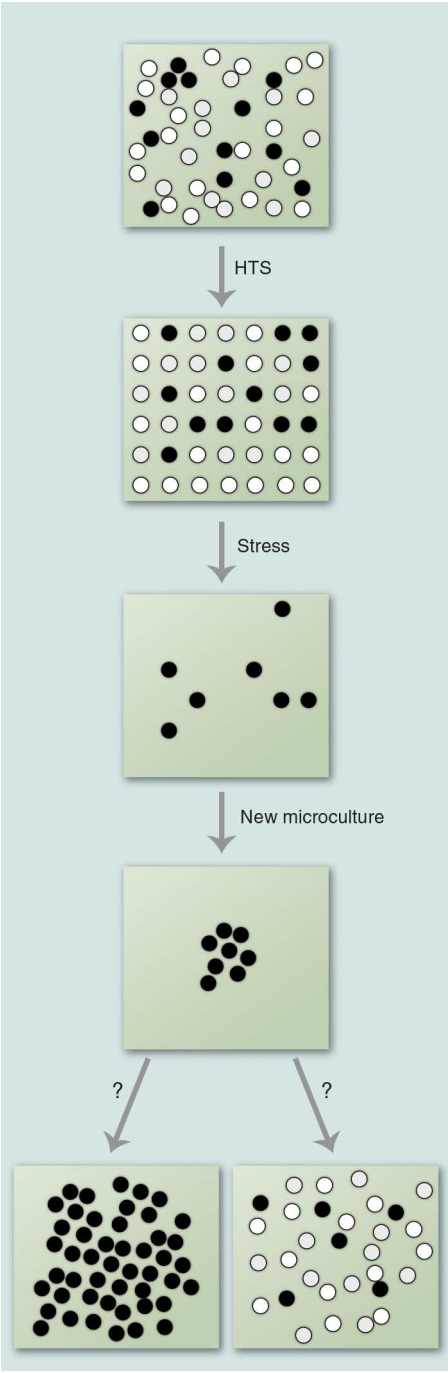

Fig. 5. Schematic representation of high-throughput screening of many individual cells exhibiting three different phenotypes (white, gray, black). After applying stress (e.g., nutrient restriction or drug treatment), only the black cells survive. A new microculture from these survivor cells may develop either into a population with a uniform phenotype (all black offspring cells) or—more likely—into a population with diverse phenotypes.

Discussion and Outlook

The chemical signature of phenotypic heterogeneity in cellular populations is a property that can only be assessed by single-cell measurements. It appears to be an evolvable trait, with the metabolome being the most immediate indicator of how individual members of a cell culture react to a stimulus or to environmental stress. Biological insight can already be obtained by precise analysis of cell conditions (outside and inside, e.g., by optical microscopy) and comparing these data with metabolomics data. The underlying cause of phenotypic heterogeneity, however, is hardly metabolic, but rather genetic, epigenetic, or based on stochastic processes. It is now well established that phenotypic heterogeneity enhances rare-cell survival (*88*, *89*); in other words, "extreme" phenotypes may rescue an entire population that suffered a major chemical or environmental challenge (such as a dose of medication). Metabolomics is expected to be a good way of identifying such cells, although genomic and proteomic data, ideally from the same cell, should also contribute. However, to extract the genome, the proteome, and the metabolome from one and the same cell currently poses great experimental difficulties; to date, there are no experimental protocols that allow this to be accomplished. An approximation may be to grow a microculture from a single or a few cells that have survived a certain perturbation, and perform metabolomics along with genomics, transcriptomics, and proteomics on aliquots of this microculture. The question is then whether heterogeneity will develop in this microculture, too, and how rapidly. This question can be answered using high-throughput, single-cell analyses (Fig. 5).

MS and separations are clearly the most successful single-cell metabolomics methods, both in terms of coverage of the metabolome and speed. Hundreds of metabolite signals have been discerned, although usually from fairly large cells such as snail neurons or plant cells. The identification from smaller cells (yeast, bacteria) is much more difficult. Identification is relatively tedious: Comparisons of elution time of metabolite and standard compound in electrophoretic measurements, and of signals obtained from large numbers of cells (including comparison to standards in MS/MS), are required. Unfortunately, both MS and CE are destructive; fluorescence and spectroscopic methods that detect metabolites nondestructively only cover single or very few metabolites. Moreover, with the exception of some high-resolution imaging methods, current single-cell analyses cannot distinguish molecular locations of compounds in subcellular compartments such as the membrane, cytoplasm, or nucleus. This leads to averaging over a single cell and in that sense presents a limitation of current methodology.

There are a number of further requirements for single-cell metabolomics to become truly useful for systems biology and medical diagnosis: (i) More extensive coverage of the metabolome. Even for model organisms such as yeast [the size of the yeast metabolome is 1168 compounds (*90*, *91*); in the yeast metabolome database, www.ymdb.ca, 2027 small molecules are listed], the coverage of the best methods currently available is <10% of the full metabolome. (ii) Faster identification of metabolites from single-cell data, and in general measurements with high throughput. The recently introduced mass cytometry method (*92*), in which antibodies marked with unusual elements (lanthanum, cerium, erbium, ytterbium, etc.) are used to encode particular antigens of cells, could be extended to metabolites if suitable antibodies or aptamers can be found. (iii) Protocols for discovery of new or unknown metabolites. (iv) Nondestructive metabolite measurements. A possible strategy for this last challenge would be a two-step approach, where a metabolomic method with a large chemical scope is first used to pinpoint key compounds that indicate, for example, a disease state, followed by development and implementation of nondestructive fluorescence nanosensors that specifically target these key compounds.

References and Notes

1. L. Cai, N. Friedman, X. S. Xie, Stochastic protein expression in individual cells at the single molecule level. *Nature* **440**, 358–362 (2006). doi: 10.1038/nature04599; pmid: 16541077
2. L. M. Borland, S. Kottegoda, K. S. Phillips, N. L. Allbritton, Chemical analysis of single cells. *Annu. Rev. Anal. Chem* **1**, 191–227 (2008). doi: 10.1146/annurev.anchem.1.031207.113100; pmid: 20636079
3. M. Heinemann, R. Zenobi, Single cell metabolomics. *Curr. Opin. Biotechnol.* **22**, 26–31 (2011). doi: 10.1016/j.copbio.2010.09.008; pmid: 20934866
4. A. Amantonico, P. L. Urban, R. Zenobi, Analytical techniques for single-cell metabolomics: State of the art and trends. *Anal. Bioanal. Chem.* **398**, 2493–2504 (2010). doi: 10.1007/s00216-010-3850-1; pmid: 20544183
5. A. Svatoš, Single-cell metabolomics comes of age: New developments in mass spectrometry profiling and imaging. *Anal. Chem.* **83**, 5037–5044 (2011). doi: 10.1021/ac2003592; pmid: 21630635
6. R. Trouillon, M. K. Passarelli, J. Wang, M. E. Kurczy, A. G. Ewing, Chemical analysis of single cells. *Anal. Chem.* **85**, 522–542 (2013). doi: 10.1021/ac303290s; pmid: 23151043
7. S. S. Rubakhin, E. V. Romanova, P. Nemes, J. V. Sweedler, Profiling metabolites and peptides in single cells. *Nat. Methods* **8** (suppl.), S20–S29 (2011). doi: 10.1038/nmeth.1549; pmid: 21451513
8. A. Oikawa, K. Saito, Metabolite analyses of single cells. *Plant J.* **70**, 30–38 (2012). doi: 10.1111/j.1365-313X.2012.04967.x; pmid: 22449041
9. J. B. German, B. D. Hammock, S. M. Watkins, Metabolomics: Building on a century of biochemistry to guide human health. *Metabolomics* **1**, 3–9 (2005). doi: 10.1007/s11306-005-1102-8; pmid: 16680201
10. S. Sauer *et al.*, Miniaturization in functional genomics and proteomics. *Nat. Rev. Genet.* **6**, 465–476 (2005). doi: 10.1038/nrg1618; pmid: 15931170
11. M. Acar, J. T. Mettetal, A. van Oudenaarden, Stochastic switching as a survival strategy in fluctuating environments. *Nat. Genet.* **40**, 471–475 (2008). doi: 10.1038/ng.110; pmid: 18362885

12. K. E. Weibel, J.-R. Mor, A. Fiechter, Rapid sampling of yeast cells and automated assays of adenylate, citrate, pyruvate and glucose-6-phosphate pools. *Anal. Biochem.* **58**, 208–216 (1974). doi: 10.1016/0003-2697(74)90459-X; pmid: 4363436
13. C. A. Sellick, R. Hansen, G. M. Stephens, R. Goodacre, A. J. Dickson, Metabolite extraction from suspension-cultured mammalian cells for global metabolite profiling. *Nat. Protoc.* **6**, 1241–1249 (2011). doi: 10.1038/nprot.2011.366; pmid: 21799492
14. S. Yamamura *et al.*, Single-cell microarray for analyzing cellular response. *Anal. Chem.* **77**, 8050–8056 (2005). doi: 10.1021/ac0515632; pmid: 16351155
15. Y. Tokimitsu *et al.*, Single lymphocyte analysis with a microwell array chip. *Cytometry A* **71**, 1003–1010 (2007). doi: 10.1002/cyto.a.20478; pmid: 17972305
16. A. L. Bishop, F. A. Rab, E. R. Sumner, S. V. Avery, Phenotypic heterogeneity can enhance rare-cell survival in 'stress-sensitive' yeast populations. *Mol. Microbiol.* **63**, 507–520 (2007). doi: 10.1111/j.1365-2958.2006.05504.x; pmid: 17176259
17. S. J. Jol, A. Kümmel, M. Terzer, J. Stelling, M. Heinemann, System-level insights into yeast metabolism by thermodynamic analysis of elementary flux modes. *PLOS Comput. Biol.* **8**, e1002415 (2012). doi: 10.1371/journal.pcbi.1002415; pmid: 22416224
18. F. Wang *et al.*, Robust measurement of telomere length in single cells. *Proc. Natl. Acad. Sci. U.S.A.* **110**, E1906–E1912 (2013). doi: 10.1073/pnas.1113505109; pmid: 22421136
19. S. S. Lee, I. Avalos Vizcarra, D. H. Huberts, L. P. Lee, M. Heinemann, Whole lifespan microscopic observation of budding yeast aging through a microfluidic dissection platform. *Proc. Natl. Acad. Sci. U.S.A.* **109**, 4916–4920 (2012). doi: 10.1073/pnas.1113505109; pmid: 22421136
20. P. Nemes, A. M. Knolhoff, S. S. Rubakhin, J. V. Sweedler, Single-cell metabolomics: Changes in the metabolome of freshly isolated and cultured neurons. *ACS Chem. Neurosci.* **3**, 782–792 (2012). doi: 10.1021/cn300100u; pmid: 23077722
21. D. C. Essaka *et al.*, Metabolic cytometry: Capillary electrophoresis with two-color fluorescence detection for the simultaneous study of two glycosphingolipid metabolic pathways in single primary neurons. *Anal. Chem.* **84**, 2799–2804 (2012). doi: 10.1021/ac2031892; pmid: 22400492
22. P. J. O'Brien *et al.*, Monitoring metabolic responses to chemotherapy in single cells and tumors using nanostructure-initiator mass spectrometry (NIMS) imaging. *Cancer Metab.* **1**, 4 (2013). doi: 10.1186/2049-3002-1-4
23. A. J. Ibáñez *et al.*, Mass spectrometry-based metabolomics of single yeast cells. *Proc. Natl. Acad. Sci. U.S.A.* **110**, 8790–8794 (2013). doi: 10.1073/pnas.1209302110; pmid: 23671112
24. D. Di Carlo, L. Y. Wu, L. P. Lee, Dynamic single cell culture array. *Lab Chip* **6**, 1445–1449 (2006). doi: 10.1039/b605937f; pmid: 17066168
25. W. H. Tan, S. Takeuchi, A trap-and-release integrated microfluidic system for dynamic microarray applications. *Proc. Natl. Acad. Sci. U.S.A.* **104**, 1146–1151 (2007). doi: 10.1073/pnas.0606625104; pmid: 17227861
26. C. H. J. Schmitz, A. C. Rowat, S. Köster, D. A. Weitz, Dropspots: A picoliter array in a microfluidic device. *Lab Chip* **9**, 44–49 (2009). doi: 10.1039/b809670h; pmid: 19209334
27. Z. Zhu, O. Frey, D. S. Ottoz, F. Rudolf, A. Hierlemann, Microfluidic single-cell cultivation chip with controllable immobilization and selective release of yeast cells. *Lab Chip* **12**, 906–915 (2012). doi: 10.1039/c2lc20911j; pmid: 22193373
28. G. B. Salieb-Beugelaar, G. Simone, A. Arora, A. Philippi, A. Manz, Latest developments in microfluidic cell biology and analysis systems. *Anal. Chem.* **82**, 4848–4864 (2010). doi: 10.1021/ac1009707; pmid: 20462184
29. E. N. Fung, E. S. Yeung, Direct analysis of single rat peritoneal mast cells with laser vaporization/ionization mass spectrometry. *Anal. Chem.* **70**, 3206–3212 (1998). doi: 10.1021/ac980290q; pmid: 11013722
30. S. R. Ellis *et al.*, Direct lipid profiling of single cells from inkjet printed microarrays. *Anal. Chem.* **84**, 9679–9683 (2012). doi: 10.1021/ac302634u; pmid: 23116365
31. A. Schmid, H. Kortmann, P. S. Dittrich, L. M. Blank, Chemical and biological single cell analysis. *Curr. Opin. Biotechnol.* **21**, 12–20 (2010). doi: 10.1016/j.copbio.2010.01.007; pmid: 20167469
32. P. L. Urban *et al.*, High-density micro-arrays for mass spectrometry. *Lab Chip* **10**, 3206–3209 (2010). doi: 10.1039/c0lc00211a; pmid: 20938499
33. A. Y. Lau, P. J. Hung, A. R. Wu, L. P. Lee, Open-access microfluidic patch-clamp array with raised lateral cell trapping sites. *Lab Chip* **6**, 1510–1515 (2006). doi: 10.1039/b608439g; pmid: 17203154
34. I. K. Dimov *et al.*, Integrated microfluidic array plate (iMAP) for cellular and molecular analysis. *Lab Chip* **11**, 2701–2710 (2011). doi: 10.1039/c1lc20105k; pmid: 21709914
35. K. Eyer, P. Kuhn, C. Hanke, P. S. Dittrich, A microchamber array for single cell isolation and analysis of intracellular biomolecules. *Lab Chip* **12**, 765–772 (2012). doi: 10.1039/c2lc20876h; pmid: 22183159
36. K. Eyer, S. Stratz, P. Kuhn, S. K. Küster, P. S. Dittrich, Implementing enzyme-linked immunosorbent assays on a microfluidic chip to quantify intracellular molecules in single cells. *Anal. Chem.* **85**, 3280–3287 (2013). doi: 10.1021/ac303628j; pmid: 23388050
37. M.-H. Wu, S.-B. Huang, G.-B. Lee, Microfluidic cell culture systems for drug research. *Lab Chip* **10**, 939–956 (2010). doi: 10.1039/b921695b; pmid: 20358102
38. D. Gao *et al.*, Recent developments in microfluidic devices for *in vitro* cell culture for cell-biology research. *Trends Analyt. Chem.* **35**, 150–164 (2012). doi: 10.1016/j.trac.2012.02.008
39. F. S. O. Fritzsch, C. Dusny, O. Frick, A. Schmid, Single-cell analysis in biotechnology, systems biology, and biocatalysis. *Annu. Rev. Chem. Biomol. Eng.* **3**, 129–155 (2012). doi: 10.1146/annurev-chembioeng-062011-081056; pmid: 22468600
40. R. Yan *et al.*, Nanowire-based single-cell endoscopy. *Nat. Nanotechnol.* **7**, 191–196 (2011). doi: 10.1038/nnano.2011.226; pmid: 22179570
41. A. Meister *et al.*, FluidFM: Combining atomic force microscopy and nanofluidics in a universal liquid delivery system for single cell applications and beyond. *Nano Lett.* **9**, 2501–2507 (2009). doi: 10.1021/nl901384x; pmid: 19453133
42. P. E. Boukany *et al.*, Nanochannel electroporation delivers precise amounts of biomolecules into living cells. *Nat. Nanotechnol.* **6**, 747–754 (2011). doi: 10.1038/nnano.2011.164; pmid: 22002097
43. X. T. Zheng, C. M. Li, Single cell analysis at the nanoscale. *Chem. Soc. Rev.* **41**, 2061–2071 (2012). doi: 10.1039/c1cs15265c; pmid: 22134665
44. P. Nemes, A. M. Knolhoff, S. S. Rubakhin, J. V. Sweedler, Metabolic differentiation of neuronal phenotypes by single-cell capillary electrophoresis-electrospray ionization-mass spectrometry. *Anal. Chem.* **83**, 6810–6817 (2011). doi: 10.1021/ac2015855; pmid: 21809850
45. J. Wei, J. M. Buriak, G. Siuzdak, Desorption-ionization mass spectrometry on porous silicon. *Nature* **399**, 243–246 (1999). doi: 10.1038/20400; pmid: 10353246
46. B. N. Walker, J. A. Stolee, A. Vertes, Nanophotonic ionization for ultratrace and single-cell analysis by mass spectrometry. *Anal. Chem.* **84**, 7756–7762 (2012). doi: 10.1021/ac301238k; pmid: 22881122
47. B. N. Walker, C. Antonakos, S. T. Retterer, A. Vertes, Metabolic differences in microbial cell populations revealed by nanophotonic ionization. *Angew. Chem.* **125**, 3738–3741 (2013). doi: 10.1002/ange.201207348
48. J. L. Edwards, R. T. Kennedy, Metabolomic analysis of eukaryotic tissue and prokaryotes using negative mode MALDI time-of-flight mass spectrometry. *Anal. Chem.* **77**, 2201–2209 (2005). doi: 10.1021/ac048323r; pmid: 15801754
49. A. Amantonico, J. Y. Oh, J. Sobek, M. Heinemann, R. Zenobi, Mass spectrometric method for analyzing metabolites in yeast with single cell sensitivity. *Angew. Chem.* **120**, 5462–5465 (2008). doi: 10.1002/ange.200705923
50. P. L. Urban *et al.*, Carbon-13 labelling strategy for studying the ATP metabolism in individual yeast cells by micro-arrays for mass spectrometry. *Mol. Biosyst.* **7**, 2837–2840 (2011). doi: 10.1039/c1mb05248a; pmid: 21850345
51. S. R. Fagerer *et al.*, Analysis of single algal cells by combining mass spectrometry with Raman and fluorescence mapping. *Analyst* **138**, 6732–6736 (2013). doi: 10.1039/C3AN01135F; pmid: 23841224
52. B. Shrestha, A. Vertes, In situ metabolic profiling of single cells by laser ablation electrospray ionization mass spectrometry. *Anal. Chem.* **81**, 8265–8271 (2009). doi: 10.1021/ac901525g; pmid: 19824712
53. N. Tsuyama, H. Mizuno, E. Tokunaga, T. Masujima, Live single-cell molecular analysis by video-mass spectrometry. *Anal. Sci.* **24**, 559–561 (2008). doi: 10.2116/analsci.24.559; pmid: 18469458
54. H. Mizuno, N. Tsuyama, T. Harada, T. Masujima, Live single-cell video-mass spectrometry for cellular and subcellular molecular detection and cell classification. *J. Mass Spectrom.* **43**, 1692–1700 (2008). doi: 10.1002/jms.1460; pmid: 18615771
55. M. Lorenzo Tejedor, H. Mizuno, N. Tsuyama, T. Harada, T. Masujima, In situ molecular analysis of plant tissues by live single-cell mass spectrometry. *Anal. Chem.* **84**, 5221–5228 (2012). doi: 10.1021/ac202447t; pmid: 22243623
56. B. Prideaux, M. Stoeckli, Mass spectrometry imaging for drug distribution studies. *J. Proteomics* **75**, 4999–5013 (2012). doi: 10.1016/j.jprot.2012.07.028; pmid: 22842290
57. M. Koestler *et al.*, A high-resolution scanning microprobe matrix-assisted laser desorption/ionization ion source for imaging analysis on an ion trap/Fourier transform ion cyclotron resonance mass spectrometer. *Rapid Commun. Mass Spectrom.* **22**, 3275–3285 (2008). doi: 10.1002/rcm.3733; pmid: 18819119
58. A. Zavalin *et al.*, Direct imaging of single cells and tissue at sub-cellular spatial resolution using transmission geometry MALDI MS. *J. Mass Spectrom.* **47**, 1473–1481 (2012). doi: 10.1002/jms.3108; pmid: 23147824
59. A. Römpp *et al.*, Histology by mass spectrometry: Label-free tissue characterization obtained from high-accuracy bioanalytical imaging. *Angew. Chem. Int. Ed.* **49**, 3834–3838 (2010). doi: 10.1002/anie.200905559; pmid: 20397170
60. T. A. Zimmerman, S. S. Rubakhin, J. V. Sweedler, MALDI mass spectrometry imaging of neuronal cell cultures. *J. Am. Soc. Mass Spectrom.* **22**, 828–836 (2011). doi: 10.1007/s13361-011-0111-2; pmid: 21472517
61. B. Prideaux *et al.*, High-sensitivity MALDI-MRM-MS imaging of moxifloxacin distribution in tuberculosis-infected rabbit lungs and granulomatous lesions. *Anal. Chem.* **83**, 2112–2118 (2011). doi: 10.1021/ac1029049; pmid: 21332183
62. R. Casting, G. Slodzian, Microanalyse par émission ionique secondaire. *J. Microsc.* **1**, 395 (1962).
63. M. L. Heien, P. D. Piehowski, N. Winograd, A. G. Ewing, Lipid detection, identification, and imaging single cells with SIMS. *Methods Mol. Biol.* **656**, 85–97 (2010). doi: 10.1007/978-1-60761-746-4_4; pmid: 20680585
64. S. Chandra, Quantitative imaging of chemical composition in single cells by secondary ion mass spectrometry: Cisplatin affects calcium stores in renal epithelial cells. *Methods Mol. Biol.* **656**, 113–130 (2010). doi: 10.1007/978-1-60761-746-4_6; pmid: 20680587
65. E. G. Solon, A. Schweitzer, M. Stoeckli, B. Prideaux, Autoradiography, MALDI-MS, and SIMS-MS imaging in pharmaceutical discovery and development. *AAPS J.* **12**, 11–26 (2010). doi: 10.1208/s12248-009-9158-4; pmid: 19921438

66. G.-H. An, O.-S. Suh, H.-C. Kwon, K. Kim, E. A. Johnson, Quantification of carotenoids in cells of *Phaffia rhodozyma* by autofluorescence. *Biotechnol. Lett.* **22**, 1031–1034 (2000). doi: 10.1023/A:1005614010003
67. P. Weber, M. Wagner, P. Kioschis, W. Kessler, H. Schneckenburger, Tumor cell differentiation by label-free fluorescence microscopy. *J. Biomed. Opt.* **17**, 101508 (2012). doi: 10.1117/1.JBO.17.10.101508; pmid: 23223984
68. P. L. Urban, T. Schmid, A. Amantonico, R. Zenobi, Multidimensional analysis of single algal cells by integrating microspectroscopy with mass spectrometry. *Anal. Chem.* **83**, 1843–1849 (2011). doi: 10.1021/ac102702m; pmid: 21299196
69. P. Dedecker, F. C. De Schryver, J. Hofkens, Fluorescent proteins: Shine on, you crazy diamond. *J. Am. Chem. Soc.* **135**, 2387–2402 (2013). doi: 10.1021/ja309768d; pmid: 23317378
70. A. J. Moro, P. J. Cywinski, S. Körsten, G. J. Mohr, An ATP fluorescent chemosensor based on a Zn(II)-complexed dipicolylamine receptor coupled with a naphthalimide chromophore. *Chem. Commun.* **46**, 1085–1087 (2010). doi: 10.1039/b919661g; pmid: 20126721
71. Y. Kurishita, T. Kohira, A. Ojida, I. Hamachi, Rational design of FRET-based ratiometric chemosensors for in vitro and in cell fluorescence analyses of nucleoside polyphosphates. *J. Am. Chem. Soc.* **132**, 13290–13299 (2010). doi: 10.1021/ja103615z; pmid: 20812684
72. L. F. Barros *et al.*, Small is fast: Astrocytic glucose and lactate metabolism at cellular resolution. *Front. Cell. Neurosci.* **7**, 27 (2013). doi: 10.3389/fncel.2013.00027; pmid: 23526722
73. B. Huang *et al.*, Counting low–copy number proteins in a single cell. *Science* **315**, 81–84 (2007). doi: 10.1126/science.1133992; pmid: 17204646
74. D. C. Essaka *et al.*, Single cell ganglioside catabolism in primary cerebellar neurons and glia. *Neurochem. Res.* **37**, 1308–1314 (2012). doi: 10.1007/s11064-012-0733-1; pmid: 22407243
75. R. B. Keithley *et al.*, Capillary electrophoresis with three-color fluorescence detection for the analysis of glycosphingolipid metabolism. *Analyst* **138**, 164–170 (2013). doi: 10.1039/c2an36286d; pmid: 23154386
76. W. E. Huang, M. Li, R. M. Jarvis, R. Goodacre, S. A. Banwart, Shining light on the microbial world: The application of Raman microspectroscopy. *Adv. Appl. Microbiol.* **70**, 153–186 (2010). doi: 10.1016/S0065-2164(10)70005-8; pmid: 20359457
77. M. J. Nasse *et al.*, High-resolution Fourier-transform infrared chemical imaging with multiple synchrotron beams. *Nat. Methods* **8**, 413–416 (2011). doi: 10.1038/nmeth.1585; pmid: 21423192
78. S. W. Fogarty *et al.*, Sub-cellular spectrochemical imaging of isolated human corneal cells employing synchrotron radiation-based Fourier-transform infrared microspectroscopy. *Analyst* **138**, 240–248 (2013). doi: 10.1039/c2an36197c; pmid: 23152953
79. X. Zhang *et al.*, Label-free live-cell imaging of nucleic acids using stimulated Raman scattering microscopy. *ChemPhysChem* **13**, 1054–1059 (2012). doi: 10.1002/cphc.201100890; pmid: 22368112
80. R. T. Kennedy, M. D. Oates, B. R. Cooper, B. Nickerson, J. W. Jorgenson, Microcolumn separations and the analysis of single cells. *Science* **246**, 57–63 (1989). doi: 10.1126/science.2675314; pmid: 2675314
81. R. A. Wallingford, A. G. Ewing, Separation of serotonin from catechols by capillary zone electrophoresis with electrochemical detection. *Anal. Chem.* **61**, 98–100 (1989). doi: 10.1021/ac00177a004; pmid: 2923274
82. D. Cohen *et al.*, Chemical cytometry: Fluorescence-based single-cell analysis. *Annu. Rev. Anal. Chem.* **1**, 165 (2008). doi: 10.1146/annurev.anchem.1.031207.113104
83. S. Hu *et al.*, Capillary sieving electrophoresis/micellar electrokinetic capillary chromatography for two-dimensional protein fingerprinting of single mammalian cells. *Anal. Chem.* **76**, 4044–4049 (2004). doi: 10.1021/ac0498314; pmid: 15253641
84. S. N. Krylov *et al.*, Correlating cell cycle with metabolism in single cells: Combination of image and metabolic cytometry. *Cytometry A* **37**, 14–20 (1999). doi: 10.1002/(SICI)1097-0320(19990901)37:1<14::AID-CYTO2>3.0.CO;2-J; pmid: 10451502
85. S. N. Krylov, E. A. Arriaga, N. W. C. Chan, N. J. Dovichi, M. M. Palcic, Metabolic cytometry: Monitoring oligosaccharide biosynthesis in single cells by capillary electrophoresis. *Anal. Biochem.* **283**, 133–135 (2000). doi: 10.1002/elps.201200488; pmid: 23161493
86. K. Klepárník, Recent advances in the combination of capillary electrophoresis with mass spectrometry: From element to single-cell analysis. *Electrophoresis* **34**, 70–85 (2013). doi: 10.1002/elps.201200488; pmid: 23161493
87. P. Nemes, S. S. Rubakhin, J. T. Aerts, J. V. Sweedler, Qualitative and quantitative metabolomic investigation of single neurons by capillary electrophoresis electrospray ionization mass spectrometry. *Nat. Protoc.* **8**, 783–799 (2013). doi: 10.1038/nprot.2013.035; pmid: 23538882
88. A. L. Bishop, F. A. Rab, E. R. Sumner, S. V. Avery, Phenotypic heterogeneity can enhance rare-cell survival in 'stress-sensitive' yeast populations. *Mol. Microbiol.* **63**, 507–520 (2007). doi: 10.1111/j.1365-2958.2006.05504.x; pmid: 17176259
89. M. E. Lidstrom, M. C. Konopka, The role of physiological heterogeneity in microbial population behavior. *Nat. Chem. Biol.* **6**, 705–712 (2010). doi: 10.1038/nchembio.436; pmid: 20852608
90. J. Förster, I. Famili, P. Fu, B. Ø. Palsson, J. Nielsen, Genome-scale reconstruction of the *Saccharomyces cerevisiae* metabolic network. *Genome Res.* **13**, 244–253 (2003). doi: 10.1101/gr.234503; pmid: 12566402
91. M. J. Herrgård *et al.*, A consensus yeast metabolic network reconstruction obtained from a community approach to systems biology. *Nat. Biotechnol.* **26**, 1155–1160 (2008). doi: 10.1038/nbt1492; pmid: 18846089
92. S. C. Bendall *et al.*, Single-cell mass cytometry of differential immune and drug responses across a human hematopoietic continuum. *Science* **332**, 687–696 (2011). doi: 10.1126/science.1198704; pmid: 21551058

Acknowledgments: I thank A. Ibáñez and M. Zenobi-Wong for critical reading of this manuscript and for helpful suggestions, and J. Krismer and J. Sobek for making data available for Fig. 2. I am also indebted to a number of talented individuals: A. Amantonico, S. Fagerer, M. Heinemann, A. Ibáñez, J. Krismer, M. Pabst, R. Steinhoff, and P. L. Urban have all contributed substantially to the success of the single-cell metabolomics project in the author's laboratory over the past few years. Supported by the Swiss National Science Foundation, ETH Zürich, and the European Union.

10.1126/science.1243259

A Mechanism for Reorientation of Cortical Microtubule Arrays Driven by Microtubule Severing

Jelmer J. Lindeboom, Masayoshi Nakamura, Anneke Hibbel, Kostya Shundyak, Ryan Gutierrez, Tijs Ketelaar, Anne Mie C. Emons, Bela M. Mulder, Viktor Kirik, David W. Ehrhardt*

READ THE FULL ARTICLE ONLINE
http://dx.doi.org/10.1126/science.1245533

Cite this article as J. J. Lindeboom *et al.*, *Science* **342**, 1245533 (2013).
DOI: 10.1126/science.1245533

Introduction: Organization of the cortical cytoskeleton guides the growth and morphogenesis of organisms, from bacteria to higher plants, that depend on cell walls. By positioning wall-building enzymes, the cytoskeleton acts as an interior scaffold to direct construction of the cell's exterior. In plants, environmental and hormonal signals that modulate cell growth cause reorganization of cortical microtubule arrays. These arrays do not appear to be remodeled by moving individual microtubules, but rather by rules that govern how microtubules are assembled or disassembled. In this Research Article, we investigate the mechanism by which blue light, an important signal from the environment, causes a rapid 90° reorientation of cortical arrays in growing cells of the plant axis.

Methods: We used spinning-disk confocal microscopy to image the reorganization of cortical microtubule arrays in real time and visualize functional proteins tagged with fluorescent proteins. We developed image-analysis methods to measure changes in array organization and behaviors of individual microtubules during array reorientation. To test hypotheses about signaling and reorganizational mechanisms, we analyzed mutants in light-perception pathways and in activity of the microtubule-severing protein katanin. Finally, we conducted photomorphogenesis assays in plant seedlings to place our findings in a physiological context.

Results: We discovered a mechanism, based on microtubule severing by the protein katanin, that reorients cortical microtubule arrays in response to perception of blue light. Specifically, we observed that katanin localized to microtubule crossovers, where it was required to preferentially catalyze the severing of the newer microtubule, an activity that was stimulated by the function of phototropin blue light receptors. New plus ends created by severing were stabilized and immediately grew at a high frequency, resulting in the effective creation of new microtubules. Most microtubules generated during reorientation were created by this mechanism, producing ~83% of new longitudinal microtubules. Cortical arrays failed to reorient in a mutant lacking the katanin protein. Microtubules produced by severing at crossovers can make new crossovers and, thus, opportunities for further rounds of severing and initiation, constituting a molecular amplifier that rapidly builds a new population of microtubules orthogonal to the initial array. Further experiments put this mechanism in a physiological context by revealing that katanin function is required for directional blue light to stimulate bending of the plant axis toward the light source.

Discussion: Cortical microtubule arrays in higher plants are being recognized as systems with self-organizing properties arising from rules governing the outcomes of microtubule interactions. In this Research Article, we present evidence that one outcome of microtubule interaction, katanin-mediated severing at crossover sites, is regulated by light perception and acts to reorient the array. Severing is thought to help build microtubule arrays in neurons and meiocytes, but it has been difficult to test this idea directly because of imaging limitations. With live imaging of plant cell cortical arrays, we have been able to investigate the cellular function of severing at the level of individual molecular events, revealing how generation of microtubules by severing is used to construct a new array.

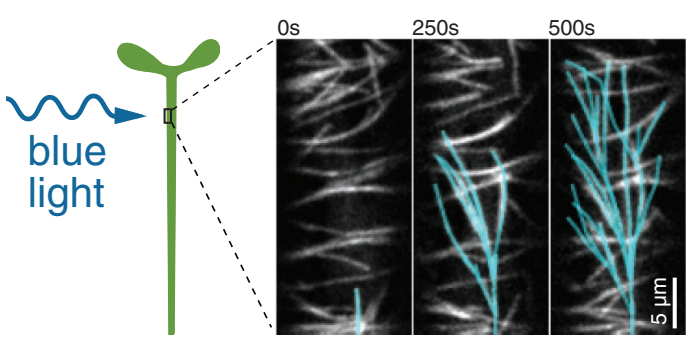

Blue light perception stimulates generation of a cascade of newly oriented microtubules by katanin severing. A confocal microscopy time series of the cortical microtubule array (white, preexisting; blue, newly assembled) in an *Arabidopsis* epidermal cell is shown. Perception of blue light by phototropin receptors has stimulated severing at microtubule intersections. Growth of the new ends creates new and co-oriented microtubules. Together, the organization of the preexisting array and the statistical behavior of severing favor the growth of longitudinal microtubules, driving array reorientation.

FIGURES IN THE FULL ARTICLE

SUPPLEMENTARY MATERIALS

Figs. S1 to S8
Movies S1 to S13

RELATED ITEMS IN *SCIENCE*

A. Roll-Mecak, Shining light at microtubule crossroads. *Science* **342**, 1180–1181 (2013).
DOI: 10.1126/science.1248235

The list of author affiliations is available in the full article online.
*Corresponding author. E-mail: ehrhardt@stanford.edu

A Mechanism for Reorientation of Cortical Microtubule Arrays Driven by Microtubule Severing

Jelmer J. Lindeboom,[1,2] Masayoshi Nakamura,[1] Anneke Hibbel,[2,3] Kostya Shundyak,[4] Ryan Gutierrez,[1,5] Tijs Ketelaar,[2] Anne Mie C. Emons,[2] Bela M. Mulder,[2,4] Viktor Kirik,[1,6] David W. Ehrhardt[1,5]*

Environmental and hormonal signals cause reorganization of microtubule arrays in higher plants, but the mechanisms driving these transitions have remained elusive. The organization of these arrays is required to direct morphogenesis. We discovered that microtubule severing by the protein katanin plays a crucial and unexpected role in the reorientation of cortical arrays, as triggered by blue light. Imaging and genetic experiments revealed that phototropin photoreceptors stimulate katanin-mediated severing specifically at microtubule intersections, leading to the generation of new microtubules at these locations. We show how this activity serves as the basis for a mechanism that amplifies microtubules orthogonal to the initial array, thereby driving array reorientation. Our observations show how severing is used constructively to build a new microtubule array.

Cytoskeletal arrays based on tubulin are ancient and found across all cellular life. These arrays are organized into specific configurations that are necessary for diverse essential processes such as chromosome segregation, intracellular transport, cell motility, and generation of cell shape. To support these diverse functions, microtubule arrays are remodeled into new arrangements over the course of the cell cycle and in response to environmental and developmental information. In many cases, centralized bodies such as centrosomes act to organize microtubule arrays by tethering and positioning nucleation complexes, setting up their functional architecture. Though centrosomal arrays have been well studied, comparatively little is understood about how microtubule arrays are organized and dynamically reorganized without the aid of centrosomes, despite the fact that acentrosomal arrays are common across diverse phyla and are featured in most differentiated animal cells (*1*).

Lacking centrosomes altogether, higher plants create highly ordered microtubule arrays at the cell cortex. By organizing cell wall biogenesis and growth (*2*–*4*), these arrays direct cell and tissue morphogenesis and, thus, support essential functions such as photosynthesis, nutrient acquisition, and reproduction. The architectures of cortical microtubule arrays are dynamic and responsive to a range of signals (*5*), including light (*6*). In rapidly elongating cells of the embryonic shoot axis (a tissue known as the hypocotyl), cortical arrays are organized transversely to the axis of cell and tissue growth (Fig. 1A). Blue light stimulation, a potent signal to hypocotyl growth, causes these transverse arrays to undergo a 90° reorientation (*7*–*9*) within minutes (Fig. 1B), redirecting cellulose deposition to build and organize the cell wall (*3*). The molecular and cellular mechanisms driving reorientation of these acentrosomal arrays are not known. We investigated this question employing quantitative live-cell imaging and genetic tests, revealing a mechanism for reorientation that features the microtubule-severing protein katanin in creating microtubules to build a new array.

New Microtubules Primarily Initiate at Microtubule Crossovers During Reorientation

In the absence of a central organizer, the question of where and how new microtubules arise is critical for understanding how arrays are built and remodeled. To address this question, we imaged microtubule dynamics in elongating hypocotyl cells as they were stimulated by blue light delivered by the imaging energy itself. The location and orientation of all observable microtubule initiations in the imaged area of each cell were measured over the course of reorientation (Fig. 1B). To aid in the detection of new growing ends, we performed a walking image subtraction on the microtubule signal and selected the positive difference, a manipulation that results in clearly discerned "comets" (see materials and methods and movie S1). By revealing growing ends together with the labeled microtubule lattice, microtubule initiations could be distinguished from rescue events. During reorientation, we observed two distinct modes for the initiation of new microtubule growth, both of which were associated with existing microtubules. First, we observed events marked by a labeled γ-tubulin complex protein (GCP2-3×GFP; GCP2, γ-tubulin complex protein 2; GFP, green fluorescent protein) at the site of initiation, indicating the presence and likely participation of a γ-tubulin nucleation complex (Fig. 2A and movie S2) (*10*). Second, we observed frequent initiation events in which GCP2-3×GFP was not detected (Fig. 2, B and C, and movie S3). Almost all (98%) of these events arose from locations where one microtubule crossed over another. By

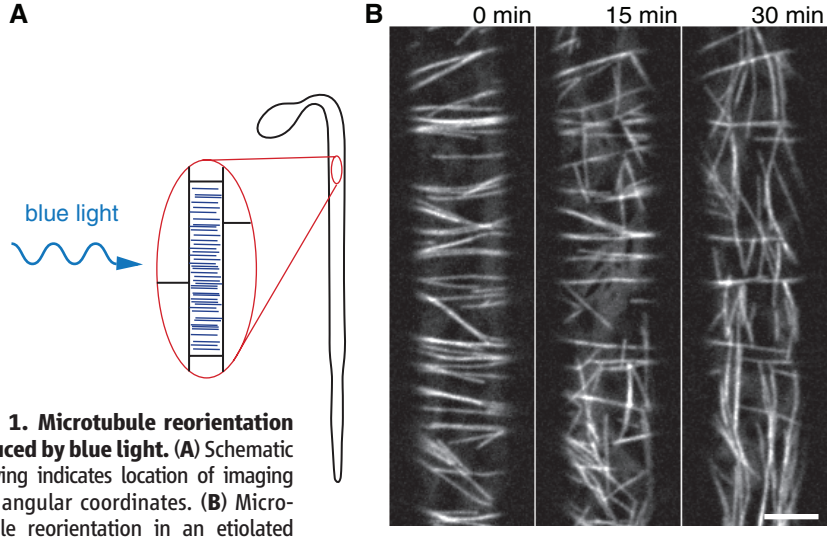

Fig. 1. Microtubule reorientation induced by blue light. (**A**) Schematic drawing indicates location of imaging and angular coordinates. (**B**) Microtubule reorientation in an etiolated hypocotyl cell expressing mCherry-TUA5 and GCP2-3×GFP (only mCherry-TUA5 signal is shown). Scale bar, 5 μm. See also movie S1.

[1]Department of Plant Biology, Carnegie Institution for Science, Stanford, CA 94305, USA. [2]Laboratory of Cell Biology, Wageningen University, 6708 PB Wageningen, Netherlands. [3]Max Planck Institute of Molecular Cell Biology and Genetics, Dresden, Germany. [4]Fundamenteel Onderzoek der Materie (FOM) Institute for Atomic and Molecular Physics (AMOLF), 1098 XG Amsterdam, Netherlands. [5]Department of Biology, Stanford University, Stanford, CA 94305, USA. [6]School of Biological Sciences, Illinois State University, Normal, IL 61790, USA.

*Corresponding author. E-mail: ehrhardt@stanford.edu

contrast, nearly all (97%) microtubules marked by GCP2-3×GFP arose at locations other than crossovers (Fig. 2D; $P < 0.00001$, Fisher's exact test). The initiations at crossovers were not rare, but in fact constituted the majority of all detected initiations (62%, 133 out of 212 initiations, seven plants). Thus, we discovered evidence for an atypical initiation mechanism acting at microtubule crossovers, which dominated during the course of array reorientation.

Katanin Localizes to Crossovers and Is Required to Initiate New Microtubules

We hypothesized that the atypical initiations at crossovers might be the result of severing followed by instantaneous growth of the newly created plus end. In experiments in which microtubules are severed in vitro, the newly created plus ends transition immediately to depolymerization (*11*, *12*). Similar depolymerization had been observed to originate from microtubule crossovers in plant cell cortical arrays, implicating crossovers as sites of severing (*13*). We reasoned that if a population of plus ends produced by severing at crossovers immediately resumed growth, these would appear as new growing ends emerging from crossovers (fig. S1). If true, then disruption of the responsible severing protein would eliminate both formation of depolymerizing plus ends and atypical initiations at crossovers. A prime candidate for the severing protein was katanin (KTN1), which had been shown to sever microtubules in vitro (*14*). We assayed events at microtubule crossovers in *ktn1-2*, a mutant for the single gene in *Arabidopsis* encoding the catalytic katanin P60 subunit (*10*, *15*). Whereas in wild-type (WT) plants, either creation of a new depolymerizing plus end (fig. S3A) or initiation of a new growing end (Fig. 2, B and F) was observed at 47% of the crossovers formed during the observation interval (522 out of 1115 crossovers), both outcomes were abolished in the mutant (0 out of 1304 crossovers) (Fig. 2E). Newly created minus ends were typically observed to be stable or to show slow loss (fig. S3A). Evidence for rapid depolymerization from new minus ends was not observed in this data set. We conclude that katanin is necessary for microtubule severing at crossovers and is required to generate the atypical initiations we observed at these locations, which are most simply explained as the immediate growth of plus ends created by severing (fig. S1).

As a further test for whether katanin acts directly to sever microtubules at crossovers, we asked if the katanin protein itself is recruited to these locations at the time of apparent severing. We expressed a GFP-KTN1 fusion protein in the *ktn1-2* mutant, which complemented the *ktn1-2* mutant phenotype (fig. S2), and showed distinct localization to microtubule crossovers, as visualized with coexpressed mCherry-TUA5 (*4*) (68% of crossovers at any time, 610 out of 891 crossovers in five plants). Recruitment of GFP-KTN1 to crossovers preceded 100% of events in which either discontinuities or new growing ends were observed ($N = 402$ events in five plants), and recruitment was lost after a short time lag (Fig. 2, F and G, fig. S3, and movies S4 to S6). The frequency with which evidence of severing was observed was not significantly dependent on the crossover angle (fig. S4).

When a crossover is made, a preexisting microtubule is crossed by a new microtubule. We found that the frequency of severing was not evenly distributed but occurred 1.7 times more often at the new microtubule (330 at the new microtubule versus 192 at the old; $P < 0.0001$, binomial test). Together, these data indicate that KTN1 is recruited to microtubule crossovers, where it preferentially catalyzes severing of the newer microtubule, often resulting in a new growing plus end.

New Microtubules Initiated by Severing Account for Most New Longitudinal Microtubules

Mathematical modeling of microtubule severing has shown that if severing leads only to depolymerizating new plus ends, such as observed in vitro, it does not increase the number of microtubules (*16*). Therefore, the observation of plus-end growth immediately after severing in vivo is noteworthy, because only those events have the

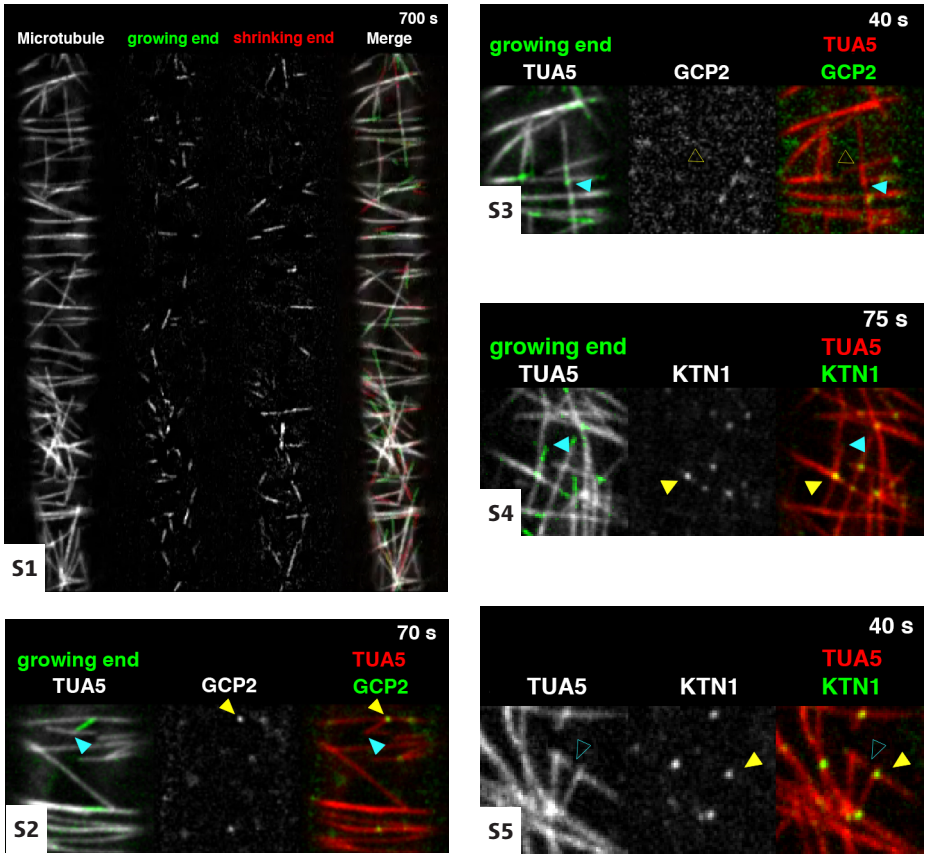

Movie S1. Cortical microtubule array reorientation from transverse to longitudinal in a dark-grown hypocotyl cell expressing mCherry-TUA5. Image processing using a time-phased walking subtraction was used to detect growing and shrinking ends, displayed here as green and red comets, respectively (see materials and methods). Highlighting growth and shrinkage in this way is a useful aid for detecting and measuring microtubule initiation events without expression of end-labeling proteins.

Movie S2. A new microtubule is generated from a GCP2-3×GFP particle. The blue and yellow arrowheads indicate the new growing microtubule end and the GCP2 signal, respectively (see Fig. 2A).

Movie S3. Generation of a new microtubule at a microtubule crossover without a GCP2-3×GFP particle. The solid blue and open yellow arrowheads indicate the new growing end and the microtubule crossover without the GCP2 particle, respectively (see Fig. 2B).

Movie S4. Microtubule severing at a crossover marked by a GFP-KTN1 signal, resulting in a new growing end. The blue and yellow arrowheads indicate the growing new end and the GFP-KTN1 particle, respectively (see Fig. 2F).

Movie S5. Microtubule severing at a GFP-KTN1 signal, resulting in a depolymerizing new microtubule plus end. The open blue and solid yellow arrowheads indicate the depolymerizing new microtubule plus end and the GFP-KTN1 particle, respectively (see fig. S3A).

potential to make a positive contribution to building a new array, as they effectively act as nucleations. To investigate how both nucleation events associated with γ-tubulin complexes and katanin-dependent initiations may contribute to the evolution of organization after blue light stimulation, we measured the angles of all new growing ends with respect to both the existing microtubules they were associated with and to cellular coordinates (Fig. 3, A to G). We further scored new growing ends for their association with GCP2-3×GFP. Consistent with previous observations (*10*, *17*), most new growing ends marked by GCP2-3×GFP (those from γ-tubulin complexes) arose in a narrow range of angles centered around 40° to the mother microtubule, with a minority arising in parallel to the mother microtubule (Fig. 3A). These nucleations had a bias to diagonal angles with respect to the cell elongation axis (Fig. 3E), consistent with most mother microtubules lying in transverse orientation. These initiations were initially high in number but fell rapidly after light stimulation (Fig. 3C). By contrast, new growing ends without GCP2-3×GFP (those arising from crossovers, see Fig. 2B) were generated at high angles (most >63°) with respect to one of the partner microtubules (Fig. 3B) and orientated in the same direction as the other partner, consistent with severing that results in a growing new plus end. These initiations peaked ~13 min after light stimulation (Fig. 3D) and were biased strongly to longitudinal orientations relative to cellular coordinates (Fig. 3F). Initiation of growing new ends at crossovers accounted for 83% of all observed longitudinal initiations (71 out of 84 initiations in seven plants) during reorientation (Fig. 3H). Thus, severing by katanin at crossovers appears to be a central engine of cortical array reorientation, quantitatively accounting for the great majority of new longitudinal microtubules.

Generation of New Microtubules by Katanin Has the Properties of an Amplifier

We observed that initiations from crossovers were often not isolated events, but occurred as a series of linked events whereby a single longitudinal microtubule gives rise to a large number of longitudinal microtubules, producing a bifurcating pattern (Fig. 3I and movie S7). When the initial longitudinal microtubule is severed, both the original and the newly generated plus ends typically continue to grow in a longitudinal orientation, creating new crossovers and further opportunities for severing. As the probability of severing is higher for the newer microtubule, this process constitutes a sequential amplifying mechanism to rapidly generate many longitudinal microtubules from a single longitudinal seed.

Katanin Function Is Required for Array Reorientation

To establish whether katanin function is required for microtubule array reorientation, we measured the ability of cortical arrays in the seedling axis to reorient in response to blue light stimulus (see materials and methods). We found that the *ktn1-1* mutant (*18*) was defective in stimulated reorientation (Fig. 4A and movie S8). Transverse order decreased slightly over time (materials and methods and Fig. 4, B and C), but estimates of reorientation speeds were extremely slow ($P < 0.001$, Mann-Whitney U test; Fig. 4D), and none of the 14 measured cells were able to reorient within the 1-hour observation period, as opposed to 100% of the wild type. These results indicated that katanin function is necessary for rapid cortical array reorientation in response to blue light stimulus.

Blue Light Signals Array Reorientation Through Phototropins

Although blue light was employed as a stimulus, it was not known which photoreceptors the light might act through, nor if the activity of those receptors was linked to cortical severing and microtubule initiation at crossovers. We measured array reorientation in mutants for the two major classes of blue light photoreceptors in *Arabidopsis*, cryptochrome (*cry1 cry2*) (*19*) and phototropin (*phot1 phot2*) (*20*). We observed a small but significant reduction in array reorientation speed in the *cry1 cry2* mutant ($P < 0.05$, Mann-Whitney U test) and a dramatic reduction in the *phot1 phot2* mutant ($P < 0.001$, Mann-Whitney U test) (Fig. 5, A to C; fig. S5; and movie S10). Thus, we conclude that cortical array reorientation is influenced by cryptochrome signaling but is primarily under the control of the phototropin receptors. The *phot2* allele in the double-mutant line is not a null (*21*), so complete loss of phototropin activity would reasonably be expected to be even more deficient in reorientation response.

PHOT1 and PHOT2 Regulate Microtubule Severing

Whereas most new microtubules were initiated from microtubule crossovers in WT cells (57%), the reverse was true in *phot1 phot2* mutants, in which only a minority initiated from crossovers

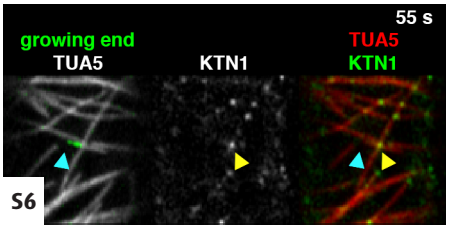

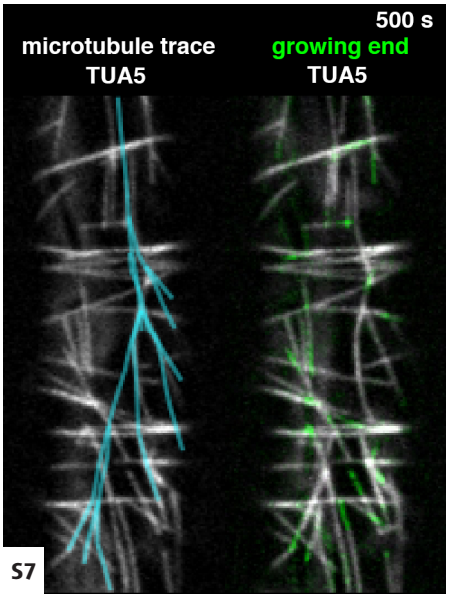

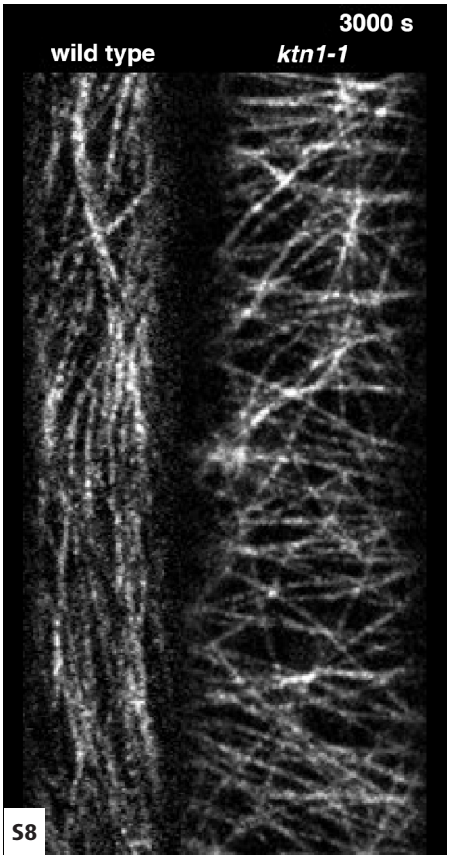

Movie S6. Three new growing microtubules (blue arrowheads) originate from a single crossover location. In each case, GFP-KTN1 (yellow arrowheads) localizes to the crossover in the moments leading up to the initiation (see fig. S3B).

Movie S7. Amplification of the number of longitudinal microtubules by microtubule severing. The blue overlay shows the paths of all microtubules that formed by microtubule severing from one single original microtubule (see Fig. 3I).

Movie S8. Time-lapsed imaging of cortical microtubule arrays in WT and *ktn1-1* mutant seedlings expressing GFP-TUB6. Array reorientation in the *ktn1-1* mutant is severely inhibited (see quantitation in Fig. 4A).

(30%), a significant shift ($P < 0.00001$, Fisher's exact test; fig. S6D). To address the mechanisms responsible, we asked if the likelihood of initiating a new microtubule at a crossover was up-regulated by phototropin signaling. In *phot1 phot2* cells, severing was detected at 36% of crossovers formed during reorientation (220 of 616), whereas in the wild type the frequency was 1.3 times higher at 47% (522 of 1115) (Fig. 5D), a highly significant difference ($P < 0.00001$, Fisher's exact test). By contrast, we did not observe a significant difference in the proportion of microtubule-severing events that resulted in a new growing plus end ($P > 0.05$, Fisher's exact test, two-tailed), showing no evidence that PHOT1 PHOT2 influences stabilization of the new plus ends. There was also no evidence of a significant difference between WT and mutant cells for the frequency of severing at the preexisting versus new microtubule (63 versus 69% respectively, $P > 0.05$, Fisher's exact test). Taken together, these data indicate that blue light signaling through PHOT1 PHOT2 significantly increases the rate of producing new microtubules at crossovers by increasing the likelihood of severing by katanin at these sites. We cannot, however, determine from these data if the increase in severing rate stimulated by blue light is sufficient to trigger reorientation.

We note that because the severing mechanism acts as a sequential amplifier, a modest increase in severing likelihood at each amplification step can have a relatively large effect on the total gain and, thus, the rate of reorientation. This idea is supported by the observation that the number of growing microtubules created at crossovers in the wild type is 2.8 times higher during reorientation than in the *phot1 phot2* double mutant, an increase much greater than the 1.3-fold change in severing likelihood per crossover.

The PHOT1 PHOT2 Pathway Influences Microtubule Nucleation

Initiations from sites other than crossovers, 97% of which are associated with detectable γ-tubulin complexes (Fig. 2D), decreased sharply during the course of reorientation (Fig. 3C). In the *phot1 phot2* mutant, the initial frequency of these initiations was higher than in the wild type, and this

Movie S9. Automated analysis of microtubule reorientation. The left panel shows the reorientation movie of a WT cell. The right panels show the output of the ImageJ plugin LOCO, which uses a configurable rotating filter to measure the local orientation of linear structures in the neighborhood of each pixel (see materials and methods). Different colors indicate the local preferential orientations for pixels above a threshold level. The contour plot on the upper right shows the evolution of the fraction pixels of each angle over time, as calculated from LOCO output. The graph on the lower left shows the evolution of the transverse and longitudinal order parameters calculated from these data.

Movie S10. Cortical microtubule array reorientation from transverse to longitudinal in dark-grown *Arabidopsis* hypocotyl cells expressing YFP-TUA5. Reorientation in the *phot1 phot2* mutant is delayed relative to in the wild type (see quantitation in fig. S5).

Movie S11. Two subsequent microtubule nucleations marked by a GCP2-3×GFP–labeled complex generating a longitudinal microtubule from a transversely oriented microtubule (see fig. S7A).

Movie S12. Example of a diagonally oriented microtubule bending toward longitudinal orientation after making multiple crossovers (see fig. S7B).

Movie S13. Amplification of the number of longitudinal microtubules by microtubule severing. The blue overlay shows the paths of all microtubules that formed by microtubule severing from one single original microtubule (see fig. S7C).

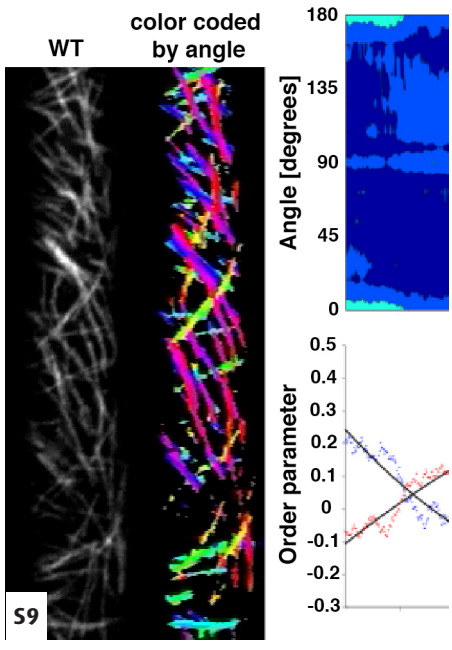

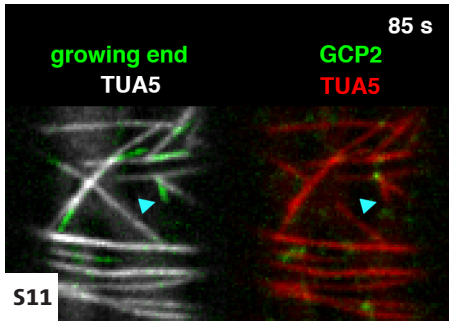

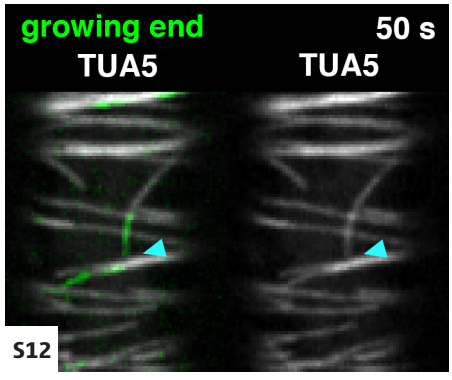

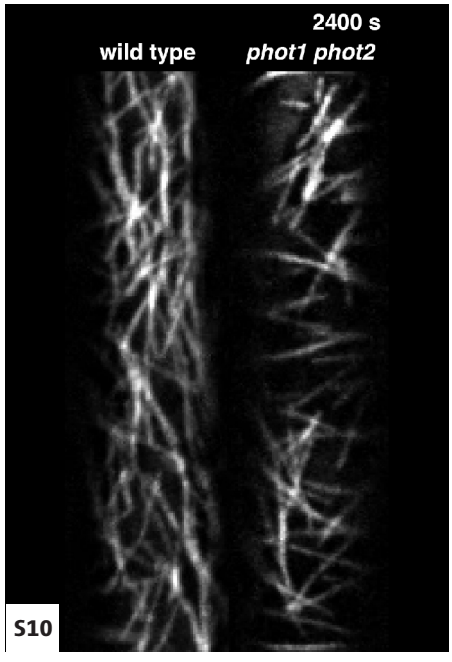

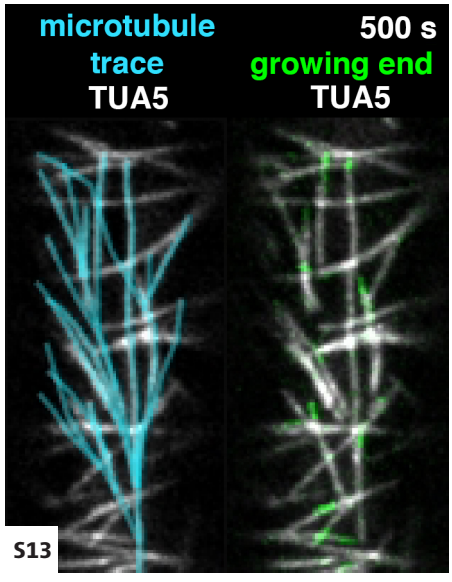

rate decreased less rapidly, yielding a net increase per unit area of 1.5-fold (fig. S6A). We infer from these results that the likelihood of nucleation from γ-tubulin complexes is reduced by a consequence of PHOT1 PHOT2 function, perhaps indirectly, which, together with promotion of katanin severing at crossovers, contributes to the observed switch in prevalence between initiation by nucleation from γ-tubulin complexes or from severing at crossovers in the *phot1 phot2* mutant. The proportion of microtubules initiated in parallel to the mother microtubule was significantly higher in the *phot1 phot2* mutant ($P < 0.01$, Fisher's exact test, two-tailed; fig. S6, B and C). Thus, PHOT1 PHOT2 may also regulate the ratio of branching to parallel nucleation from γ-tubulin complexes, as has been observed for TONNEAU2 (*22*).

Seeding and Orientating the Amplification of New Microtubules by Severing

The severing mechanism identified here requires a population of longitudinal microtubules to begin with to "seed" the amplification of new microtubules. Branching nucleation starting from transverse microtubules creates mostly diagonal microtubules (Fig. 3E), but a subsequent branching event can create a longitudinal microtubule (fig. S7A and movie S11). The observed PHOT1 PHOT2–dependent preference for branching over parallel nucleation may enhance longitudinal seeding by increasing the likelihood of sequential branching. In addition, diagonal microtubules were also observed to acquire a longitudinal orientation by adopting a curved trajectory of growth (fig. S7B and movie S12). The frequency of creating crossovers and generating new growing ends by severing is highest when the distance between crossovers is shortest, a parameter that is minimized when discordant microtubules grow at right angles to the existing ordered array. Thus, we propose that the existing transverse array acts as an oriented template for the preferential amplification of longitudinally oriented seeds generated by branching nucleation or curved polymer growth (Fig. 6, fig. S7C, and movie S13).

Stability of Reorientation

In principle, reorientation by severing could be reversible. Once sufficient longitudinal order is created, transverse microtubules might be amplified, causing the array to switch back. The substantial drop observed in microtubule nucleation (Fig. 3C) may help suppress such a reversal. Likewise, initiation by severing at crossovers

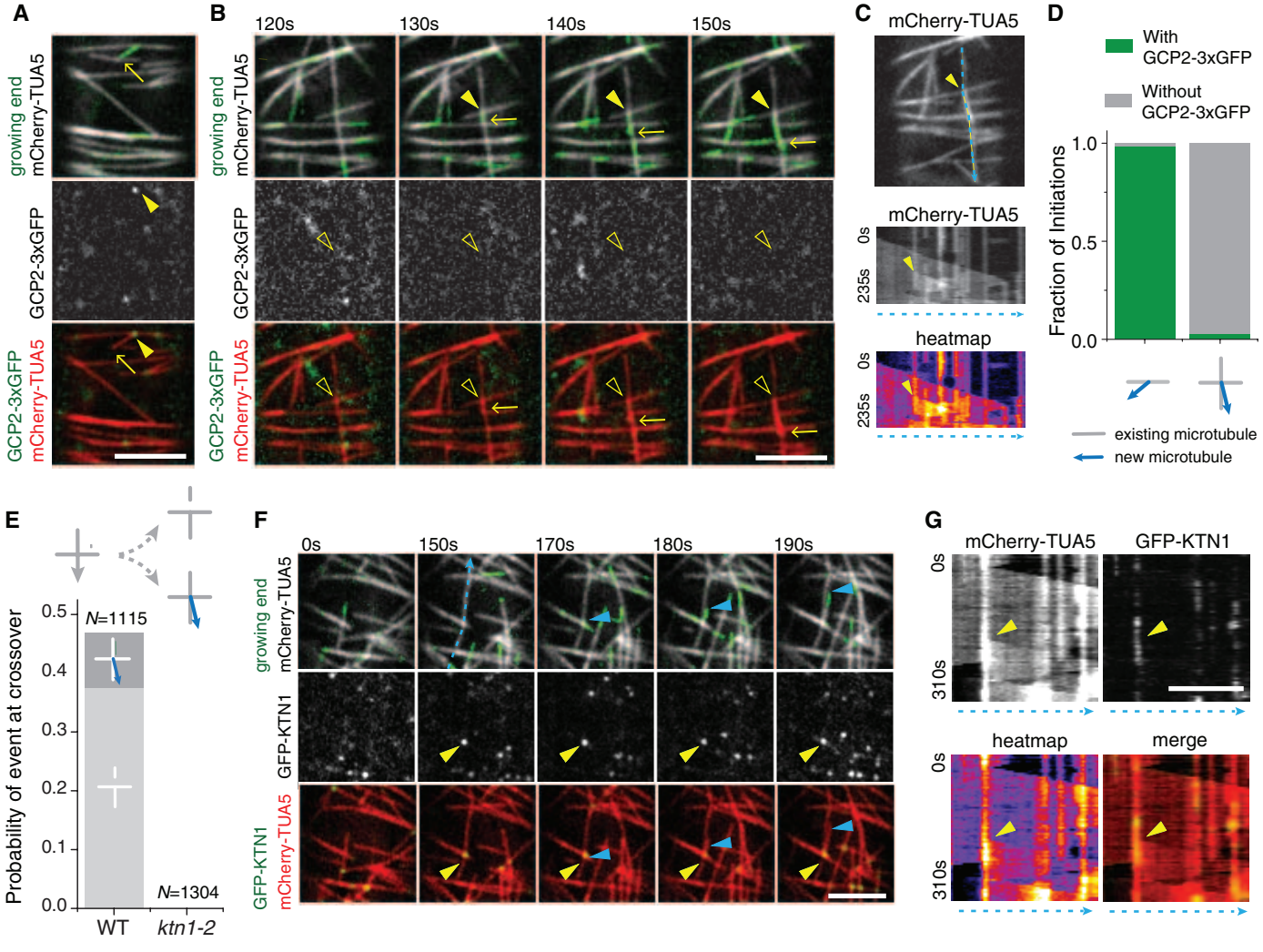

Fig. 2. Generation of new microtubules during light-induced microtubule reorientation. (**A**) Example of a new microtubule (arrows) being generated from a GCP2-3×GFP–labeled complex (solid arrowheads). See also movie S2. (**B**) New microtubule growth (arrows) initiated at a microtubule crossover without GCP2-3×GFP signal (open arrowheads). See also movie S3. (**C**) Kymograph of the initiation shown in (B). Dashed blue line in top panel shows location of the kymograph line. Arrowheads show the position of microtubule initiation. (**D**) Fraction of new microtubules marked by a GCP2-3×GFP–labeled complex, classified by localization at microtubule crossovers or not at crossovers (N = 345 events in seven plants). (**E**) Relative frequencies of observed microtubule-severing events at crossovers in WT (N = 1115 events in five cells) and *ktn1-2* mutant plants (N = 1304 in five cells). (**F**) Localization of GFP-KTN1 (yellow arrowheads) at an initiation event (blue arrowheads) from a crossover. See also movie S4. (**G**) Kymographs of microtubule initiation from a crossover from the dashed blue line in (F). Scale bars, 5 μm.

also falls to low levels as reorientation nears completion and the number of crossovers (and, thus, opportunities for severing) drops. The basis for the reduction in nucleation rate remains to be identified. It also remains to be determined if the existing transverse array is actively disassembled after blue light signaling, or if it is simply passively turned over, as generation of transverse microtubules during reorientation is low. Finally, whereas microtubule initiation by severing appears to account for most new longitudinal microtubules, our observations do not exclude contributions to reorientation from other mechanisms.

Phototropism Requires Katanin Function

Blue light signaling through PHOT1 and PHOT2 has been shown to be involved in both phototro-

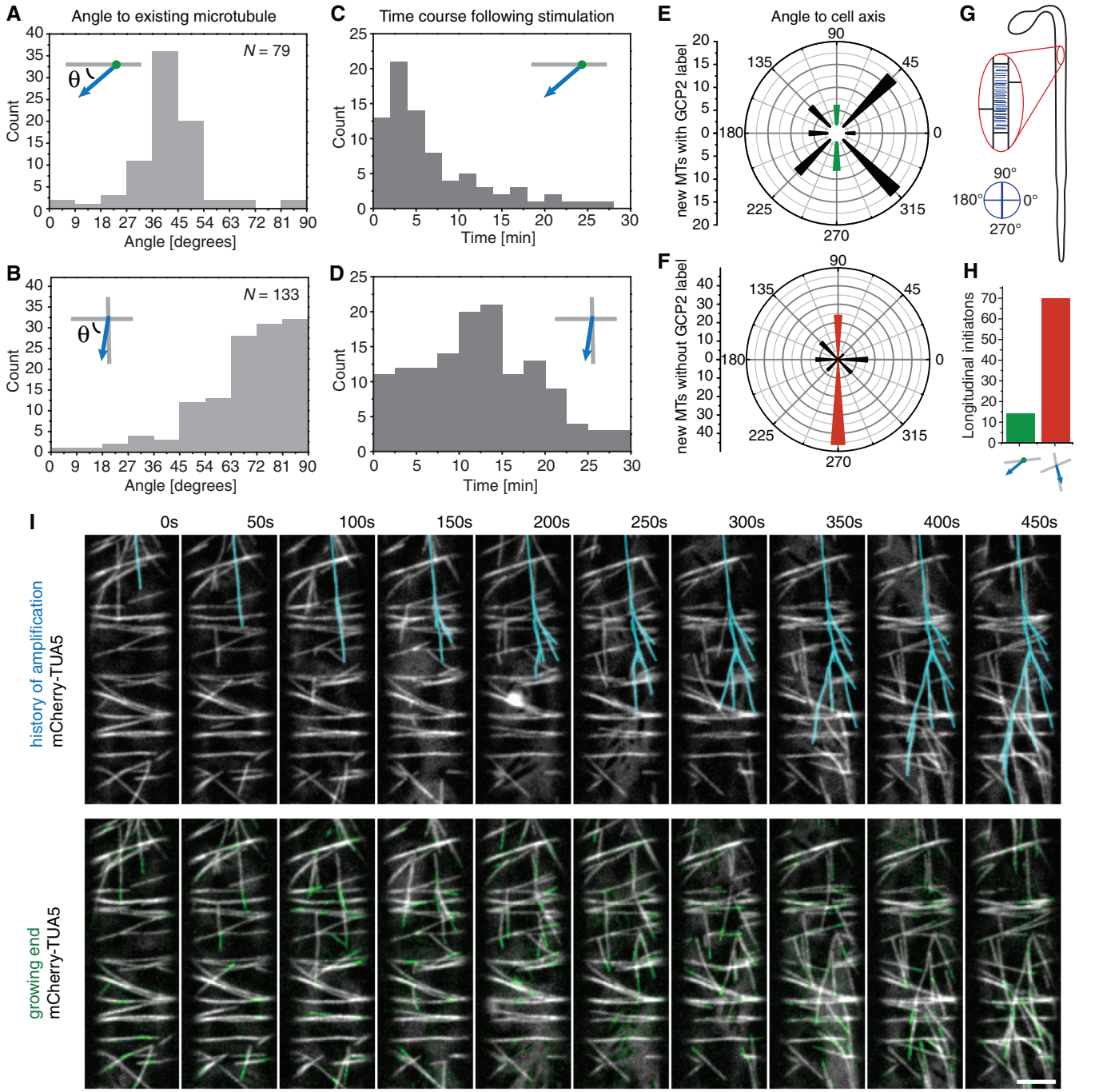

Fig. 3. Microtubule generation during the reorientation process. (**A** and **B**) Histograms of angles between an existing microtubule and a new microtubule, (A) associated with a GCP2-3×GFP label and (B) associated with crossovers (scored as not associated with GCP2-3×GCP, see text and Fig. 2B). (**C** and **D**) Histograms of microtubule initiations over time after blue light stimulation, (C) associated with a GCP2-3×GFP label and (D) associated with crossovers. (**E** and **F**) Polar histograms of new microtubule orientations to the cell axis, where the elongation axis is at 90°, (E) associated with a GCP2-3×GFP label and (F) associated with crossovers. (**G**) Schematic drawing of a dark-grown seedling. The angle reference indicates how the reported angles map onto the cell and plant axis. (**H**) Bar graph comparing the number of microtubule initiations longitudinal to the cell axis originating from a GCP2-3×GFP label to associated with crossovers (seven plants on 3319 μm^2). Of the 212 new microtubules analyzed, 79 were marked by a GCP2-3×GFP–labeled complex and 133 were not. (**I**) Microtubule-severing–dependent amplification of longitudinal microtubules. The blue overlay shows the paths of all microtubules formed by microtubule severing originating from one single microtubule. Scale bar, 5 μm. See also movie S7.

pism and growth inhibition of the hypocotyl axis (*23*, *24*). Our observation that the *ktn1-1* mutant is defective in cortical array reorientation presented us with a genetic test to ask whether microtubule reorientation was required for either response. When we measured growth suppression, we found that the *phot1 phot2* mutant failed to show significant reduction in hypocotyl growth speed after the blue light was turned on, but the *ktn1-1* mutant showed an immediate reduction in growth speed, with similar kinetics as in WT plants (fig. S8, A and B). These data indicate that katanin-dependent microtubule reorientation is not required for growth inhibition mediated by phototropin signaling, providing genetic confirmation of an earlier correlative study in peas, where growth inhibition was observed to occur significantly more rapidly than cortical microtubule array reorientation (*7*). Thus, although cellulose synthase trajectories are reoriented in concert with cortical microtubules (*3*), our results, together with those of Laskowski (*7*), indicate that such reorientation of the direction of cellulose deposition may not be sufficient to explain rapid growth inhibition.

To determine if phototropism is dependent on katanin activity, we employed a photocurvature assay described by Christie *et al*. (*25*) (Fig. 7, A and B). The *ktn1-1* mutant showed significantly less 8-hour light-stimulated bending (17.2° ± 1.9°, N = 14 plants) than the wild type (44.8° ± 3.7°, N = 14 plants) (Fig. 7C; $P < 0.001$, Student's t test). The growth in length of the hypocotyls of *ktn1-1* mutant plants during the hypocotyl-bending assay (0.56 ± 0.03 mm) was not significantly different from that of the wild type (0.47 ± 0.03 mm) (Fig. 7D; $P > 0.05$, Student's t test), indicating that the reduced phototropism was not the result of a defect in elongation in the *ktn1-1* mutant. The reduction of photocurvature in the *ktn1-1* mutant indicates that katanin activity is required to generate normal photocurvature. Microtubule reorientation on the illuminated side of sunflower hypocotyls and maize coleoptiles was observed previously and was thought to contribute to differential expansion and photo curvature (*9*). Under conditions that stimulate photo curvature in *Arabidopsis*, we also found that cortical arrays reoriented on the illuminated side of the axis in a PHOT1 PHOT2–dependent fashion (fig. S8C). Given these observations and the demonstrated linkage between microtubule orientation and regulation of directional cell expansion under many conditions (*5*), our genetic results are consistent with the possibility that phototropin-stimulated microtubule reorientation on the illuminated side of the axis is an important contributor to phototropism of the hypocotyl axis.

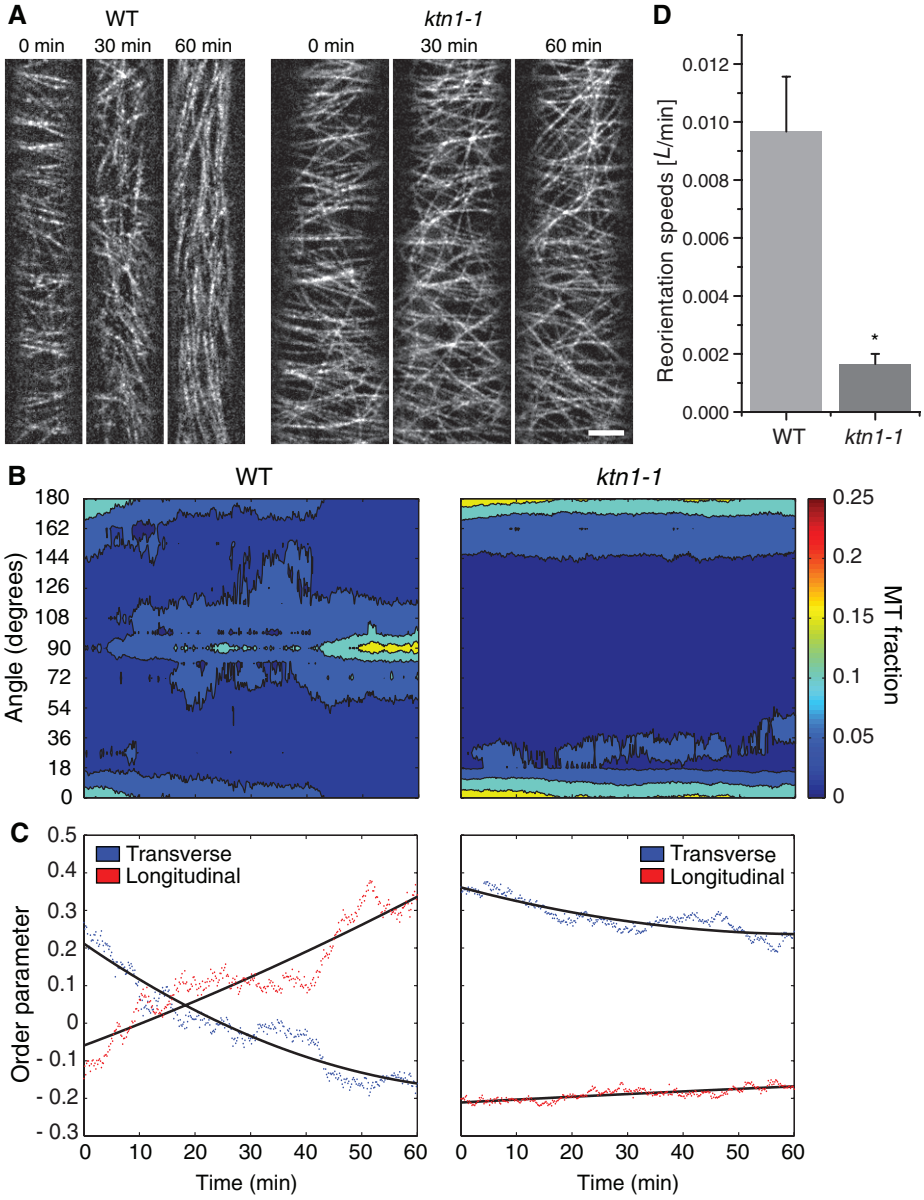

Fig. 4. Katanin activity is required for microtubule reorientation. (**A**) Microtubule reorientation in WT (Ws) and *ktn1-1* mutant etiolated hypocotyl cells. Scale bar, 5 μm. See also movie S8. (**B**) Distributions of microtubule (MT) angles over time (see materials and methods). Time is indicated in (C). (**C**) Transverse (*T*) and longitudinal (*L*) order parameters over time with a quadratic fit (black line) for the cells in (A). (**D**) Mean reorientation speed (*L*/min) comparing the wild type (13 cells) and *ktn1-1* (14 cells). Error bars denote SEM. The asterisk indicates a significant difference in a Mann-Whitney *U* test ($P < 0.001$).

Discussion

The mechanism revealed here for microtubule array reorganization stands in interesting contrast to current models. Live-cell imaging and modeling studies have indicated that cortical microtubule arrays in higher plants have self-ordering properties (*26*–*32*). Differential regulation of microtubule stability tied to location in the cell has been proposed to act on self-ordering of the array as a whole to produce specific array patterns, an idea supported by studies of microtubule stabilization at specific cell edges by CLASP (*33*) and destabilization in defined plasma membrane domains by MIDD1 (*34*). By contrast, katanin-dependent amplification does not rely on localized regulation of stability, but depends on the preexisting microtubule organization. The new order created does not depend on global self-ordering but arises from the accumulation of independent amplification events. Remodeling of cortical arrays in response to application of plant hormones has also been described recently in hypocotyl cells (*35*, *36*). The mechanism has not been identified, but the progressive nature of new ordering (*36*) indicates that the pathway is distinct from that caused by blue light signaling.

Cortical arrays in plant cells feature distributed γ-tubulin nucleation complexes that are recruited in a distributed fashion, primarily to existing microtubules (*10*, *17*). Our observations in this study reveal a second means of generating new microtubules in these acentrosomal arrays, based on microtubule severing by katanin. Like nucleation

from γ-tubulin complexes, the location and geometry of microtubule generation by this alternative mechanism is tied to the distribution of existing microtubules. This mechanism was not only important in its prevalence but was also a target of signaling and actually dominated during our observations of cortical array reorientation. It will be interesting to assess the contribution of this mode of microtubule generation in the maintenance and transitions of other arrays in higher plants.

Katanin function is important for diverse cellular and developmental processes across a broad range of biological diversity, including neuronal development, spindle assembly and function, mitosis, cell migration, turnover of cilia and flagella, cell morphogenesis, and cell wall biogenesis (*37*–*41*). However, the specific role or roles of microtubule severing in supporting those processes are typically not well understood, often due to challenges in performing dynamic studies because of the high density of the arrays under study (*42*). In some cases, severing appears to play a relatively straightforward role in separating microtubules from their nucleation centers (*10*, *43*, *44*), facilitating microtubule turnover. Observations in the meiotic spindles of *Caenorhabditis elegans* have led to the proposal that katanin-mediated severing may also be used to build new organization in acentrosomal arrays by making new microtubules (*42*, *45*, *46*), a possibility that has

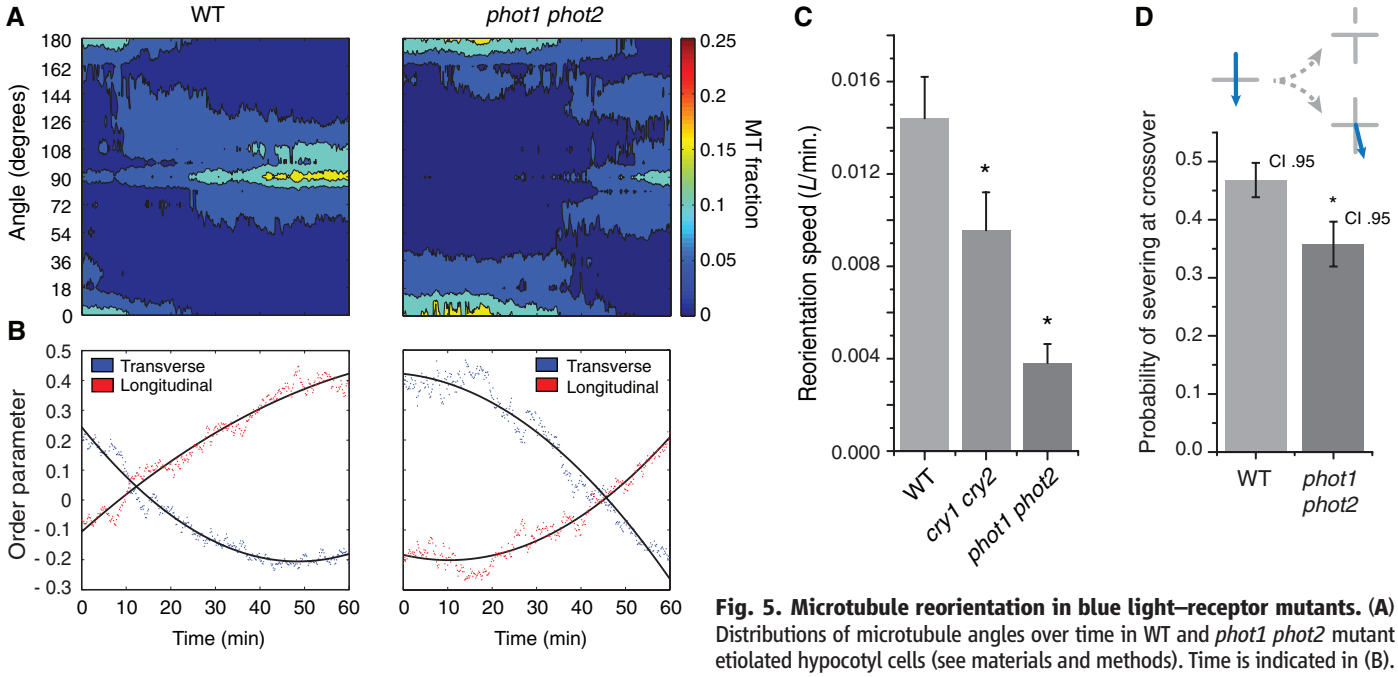

Fig. 5. Microtubule reorientation in blue light–receptor mutants. (**A**) Distributions of microtubule angles over time in WT and *phot1 phot2* mutant etiolated hypocotyl cells (see materials and methods). Time is indicated in (B). (**B**) Transverse (*T*) and longitudinal (*L*) order parameters over time with a quadratic fit (black line) for the cells in (fig. S5). (**C**) Mean reorientation speed (*L*/min) comparing the wild type (18 cells), *cry1 cry2* (13 cells), and *phot1 phot2* (10 cells). Asterisks indicate a significant difference in a Mann-Whitney *U* test ($P < 0.001$). Error bars denote SEM. (**D**) Probability of microtubule crossovers resulting in severing in WT and *phot1 phot2* mutant cells differs significantly ($P < 0.00001$, Fisher's exact test, two-tailed), indicated by an asterisk ($N = 1115$ on 656 μm^2 in wild type in five plants and $N = 616$ on 648 μm^2 in *phot1 phot2* in five plants). Error bars indicate 95% confidence interval (CI).

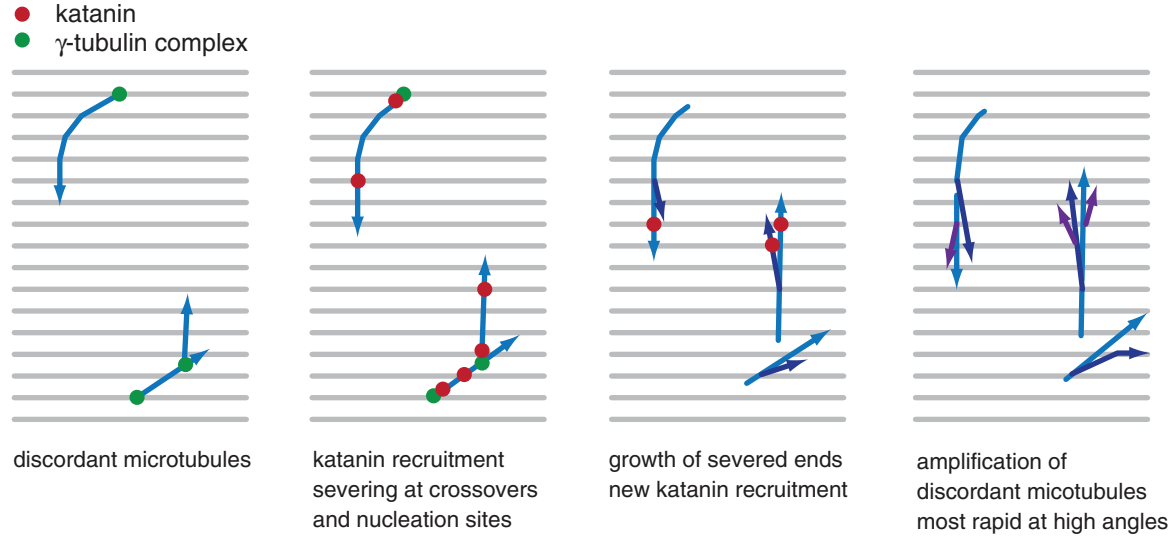

Fig. 6. Schematic representation of katanin-dependent amplification of longitudinal microtubules during cortical array reorientation.

also been suggested in neuronal arrays (*42*). The low-density two-dimensional geometry and optical accessibility of plant cortical arrays have allowed us to test this proposal by visualizing katanin recruitment, individual severing events, and their outcomes. These experiments have revealed a previously undiscovered and unexpected mechanism for selectively amplifying a subpopulation of microtubules based on severing at microtubule intersections. Our studies further highlight plant cortical arrays as useful systems for investigating the roles of widely conserved functions, such as severing and nucleation, in the dynamic reorganization of acentrosomal microtubule arrays.

Materials and Methods

Plant Material

All live-cell imaging experiments were performed in 3-day-old dark-grown etiolated hypocotyls of *A. thaliana*. Three constructs were used for imaging of cortical microtubules: 35S:YFP-TUA5 (YFP, yellow fluorescent protein) (*25*), 35S:GFP-TUB6 (*47*), and 35S:mCherry-TUA5 (*4*). The wild type and the *cry1-104 cry2-1* (*19*) and *phot1-5 phot2-1* double-mutant lines (*48*) expressing the YFP-TUA5 marker were in the Columbia (Col0) ecotype. The wild type and the *ktn1-1* mutant expressing the GFP-TUB6 marker were in the Wassilewskija Ws ecotype (*47*). WT *Arabidopsis* plants expressing YFP-TUA5 and mCherry-TUA5 were in the Col-0 ecotype. γ-tubulin complexes were visualized by expression of GCP2-3×GFP from native upstream sequences (*10*).

The GFP-KTN1 construct was generated from the katanin p60 subunit (At1g80350) genomic region including a 1005–base pair region 5′-upstream from the initiation ATG codon and a 1039–base pair region 3′-downstream from the stop codon. A sequence encoding smRS-GFP (*49*) inserted at *SmaI* and *NaeI* sites, which were introduced before the initiation ATG codon of KAT1 by polymerase chain reaction. The insert was excised by NotI and was introduced into the binary vector pBIN19. The resulting binary vector was used to transform *ktn1-2* mutant plants (Col0 ecotype) (*10*, *15*). mCherry-TUA5 expressing plants were then crossed to the *GFP-KTN1*/*ktn1-2* lines, and progeny expressing both reporters were analyzed.

Plant Growth

Seeds were surface-sterilized, stratified for 3 days at 4°C, and sown on 1% agar containing Hoagland's no. 2 basal salts at pH 5.7 for all experiments except the photocurvature assays, for which we used 0.5× Murashige and Skoog media (*50*) with 1% (w/v) sucrose and 1% (w/v) agar at pH 5.6. After 1 hour of light exposure on a bench top, plates were incubated in a near-vertical position at 22°C and wrapped in foil for 60 to 72 hours.

Specimen Mounting for Confocal Microscopy

Seedlings were mounted under red safelight conditions (Paterson PTP760U Safelight) to prevent de-etiolation. Seedlings were gently placed on a cover slip in sterile water and affixed under a 1-mm-thick 1% agarose pad.

Microscopes

In experiments where microtubule reorientation and/or GCP2-3×GFP were imaged, we used a spinning-disk confocal microscope equipped with a CSU-X1 spinning-disk head (Yokogawa) on a Nikon Eclipse Ti body with Perfect Focus system (Nikon) (*4*, *51*). In experiments where mCherry-TUA5 and GFP-KTN1 were imaged, we used a CSU-X1 spinning-disk confocal head mounted on a Leica DMI6000B microscope with Adaptive Focus Control (Leica) and a 100× Plan Apo 1.4 N.A. oil immersion objective. GFP was excited at 488 nm and mCherry at 561 nm using a multichannel dichroic filter (Di01-T405/488/568/647, Semrock) and an FF01525/50 or an FF01605/64 bandpass emission filter (Semrock) for GFP and mCherry, respectively. Images were acquired with an Evolve electron-multiplying (EM) charge-coupled device camera (Photometrics) at an EM gain of 300, controlled by Slidebook software (Intelligent Imaging Innovations).

Confocal Imaging

To ensure that the imaging and light conditions were the same for every experiment, we measured the laser power of the 491-nm laser (and 561 nm for the mCherry excitation) at the optical-fiber output that goes in the spinning-disk head and set it to 8.2 mW, which corresponded to 1.05 mW at the back focal plane of the objective. Images used for measuring the reorientation speeds of cells were acquired with a 300-ms exposure time every 10 s over 60 min and every 5 s over 30 min for the movies used for analyzing microtubule initiations and severing. The mCherry-TUA5 GCP2-3×GFP plants were imaged with every 5-s interval over 30 min with a power of ~1.05 mW at the back focal plane of the objective and 500-ms exposure time for both the 491- and 561-nm lasers at the optical fiber. In experiments where mCherry-TUA5 and GFP-KTN1 were imaged, we used 800-ms exposure every 5 s over 30 min with ~5 mW at the end of optical fiber. For measurements of initiations and severing, rectangular sample regions were defined in each image series, and detectible events of interest (initiations, crossover formation, and shortening of new plus ends) were exhaustively assayed throughout the duration of the time series.

Image Analysis for Microtubule Orientations

To quantify microtubule orientation and order, we developed an automated image-analysis tool in the form of an ImageJ plugin, LOCO (local orientation). LOCO identifies the orientation of high-contrast linear objects in images, such as fluorescently labeled microtubule arrays, assigning each pixel above a threshold level with a value for the local orientation of the signal, as defined by a configurable rotating kernel. The plugin allows the user to define the kernel dimension, the

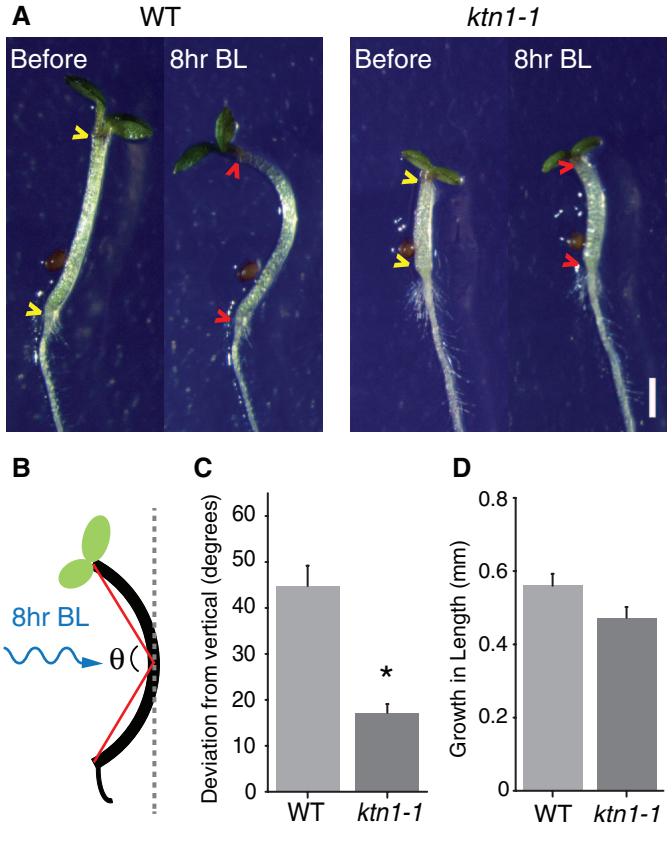

Fig. 7. Microtubule reorientation and the phototropic response. (**A**) Seedlings of the wild type (Ws) and *ktn1-1* before and after photocurvature assay. BL, blue light. Scale bar, 1 mm. (**B**) Pictogram of the measurement of photocurvature (θ). (**C**) Mean angle of curvature in the wild type and *ktn1-1*. Error bars indicate SEM (N = 14 for both wild type and *ktn1-1*). The asterisk represents a significant difference between the wild type and *ktn1-1* ($P < 0.001$, Student's t test, two-tailed). (**D**) Mean hypocotyl growth of the wild type and the *ktn1-1* mutant during the photocurvature assay [growth as calculated by subtracting the measured hypocotyl length between yellow carets from the measured hypocotyl length between red carets in (A)]. Error bars indicate SEM. N = 50 for the wild type and 43 for *ktn1-1*.

angular interval, and the threshold value. In our analysis, we chose a width of 3 pixels, a length of 21 pixels, an interval of 9° (corresponding to 20 angles over a 180° rotation interval), and a threshold value determined by the default ImageJ threshold (*52*). The chosen pixel width of 3 was comparable to the width of the typical microtubule signal and the length of 21 made the orientation filter sensitive to orientation of the signal with no observable border effects. Images were padded with a border of zero-value pixels at a width equivalent to $(k - 1)/2$, where k is the kernel length. At each pixel of the image, the kernel was rotated every 9° over the 180° range, and pixel intensities were summed over the kernel. Intensities were calculated using bilinear interpolation. The angle that resulted in the highest integrated kernel intensity was returned as the preferential angle value for that pixel. As visual output, the plugin produces an image of pixel angle values above the threshold level (movie S9). These data sets were processed further in MATLAB (MathWorks) to create heat maps of angular distributions over time and calculate order parameters. The LOCO plugin is available at http://carnegiedpb.s3.amazonaws.com/loco.zip.

Microtubule Reorientation Analysis

The image analysis produced the calculated local orientation about all pixels above the threshold value over 20 bins. To determine the moment in time when the longitudinal microtubule order becomes dominant over the transverse order, we defined two filter functions: T for transverse order and L for longitudinal order (*51*). With 90° defining the transverse axis, these values were calculated as follows: For T, the fraction of angular values in a transverse bin 45° wide centered at 90° was given a weighting of 1, the fraction at all other orientations given a weighting of –1/3, and these products summed. The weightings were chosen so that an isotropic distribution of angles yields a value $T = 0$, and a distribution contained entirely within the transverse bin yields a value $T = 1$. Likewise, L was constructed using a longitudinal bin 45° wide centered at 0°. We fitted the values of T and L over time using a quadratic polynomial. We wanted to focus on the buildup of the longitudinal order, so we used the average increase in longitudinal order over time as the measure for the speed of reorientation. Because L levels off as longitudinal order is obtained, we calculated this value from the start of acquisition until L reached 0, an interval over which L increased approximately linearly. In cases where L did not reach zero, we divided the total increase in L by the total observation time. So in short, we defined the reorientation speed as $L_T = 0/T_L = 0$. Movies that did not show clear transverse order at the start ($T_0 < 0.1$, ~10% of the plants) were excluded, as they did not provide information on reorientation dynamics. These calculations and procedures were incorporated into a MATLAB script to enable rapid processing of large data sets and limit observer bias.

Microtubule Initiation Analysis

As a visual aid for detecting new microtubules, we performed a time-phased image subtraction with a phase shift of three frames on the mCherry-TUA5 signal and selected the positive and negative difference using MATLAB. The positive difference corresponds to polymer gain, and the negative difference corresponds to polymer loss. This manipulation results in comets reminiscent of fluorescent labeling of plus-end binding proteins (+TIPs). We made the comets from the positive-difference image green and added them to the grayscale microtubule images. We found that a difference of three frames (or 15 s) was optimal for the visibility of the growing microtubule ends. The negative-difference images were processed in the same way as red comets, as shown by the overlay in movie S1. Like growing ends labeled with +TIPs, the comets produced by time-phased subtraction are easily discerned and quantified, but this method has a couple of distinct advantages over +TIP labeling. First, when using +TIP labeling, it can be challenging to distinguish new microtubule initiations from rescue events. Second, the organization of the microtubule array needs to be inferred by tracking the trajectories of the labeled plus ends. However, because losses at both plus and minus ends are not seen, the actual distribution of microtubule lattices cannot be known at any given time by plus-end tracking alone. The time-phased subtraction technique addresses both of these challenges because the lattice signal and loss events are also imaged. Further, the time-phased subtraction technique avoids unwanted perturbation of microtubule dynamics and behaviors caused by overexpression of a +TIP protein.

For all new microtubules, we scored the position, time, whether it originated from a preexisting microtubule, the angle of the preexisting microtubule, the angle of the new microtubule relative to the existing microtubule, the angle of the new microtubule relative to the cell axis (as indicated in Fig. 1B), whether the new microtubule originated from a microtubule crossover, and whether GCP2-3×GFP was present in the GFP channel (in the double labeled line). When a new microtubule initiated from a crossover, the orientation was always within a narrow range of one of the microtubules before the severing event occurred. We therefore calculated the angle between the newly created plus end and the microtubule, with the microtubule with the highest angle to that.

For the crossover analysis, we marked the position and moment of crossover creation, the moment of crossover disappearance, and whether a GFP-KTN1 signal was present (in the double labeled lines). When a crossover disappeared, we asked whether severing of the new microtubule had taken place and whether that microtubule started off in a growing or shrinking state. We asked the same questions for the preexisting microtubule at the crossover.

Hypocotyl Elongation and Photo Curvature

To measure hypocotyl elongation, 3-day-old dark-grown seedlings germinated on vertically oriented plates were imaged with a red safelight for illumination (Paterson PTP760U Safelight) and imaged with a Nikon D80 camera with a macro lens at 1-s exposure time, with a 5-min time interval. After 1 hour, we turned on a blue light (10 μmol m^{-2} s^{-1}) with a diode array (EagleLight) parallel to the plate. We made kymographs along the elongation axis of the hypocotyls to measure the growth speeds before and after blue light induction.

Photo curvature was analyzed according to methods described in (*25*). Plant seedlings were germinated in the light for 3 days and illuminated from the side by monochromatic 2–μmol m^{-2} s^{-1} blue light (EagleLight) for 8 hours after 2 days dark acclimation.

References and Notes

1. F. Bartolini, G. G. Gundersen, Generation of noncentrosomal microtubule arrays. *J. Cell Sci.* **119**, 4155–4163 (2006). doi: 10.1242/jcs.03227; pmid: 17038542
2. T. I. Baskin, On the alignment of cellulose microfibrils by cortical microtubules: A review and a model. *Protoplasma* **215**, 150–171 (2001). doi: 10.1007/BF01280311; pmid: 11732054
3. A. R. Paredez, C. R. Somerville, D. W. Ehrhardt, Visualization of cellulose synthase demonstrates functional association with microtubules. *Science* **312**, 1491–1495 (2006). doi: 10.1126/science.1126551; pmid: 16627697
4. R. Gutierrez, J. J. Lindeboom, A. R. Paredez, A. M. C. Emons, D. W. Ehrhardt, *Arabidopsis* cortical microtubules position cellulose synthase delivery to the plasma membrane and interact with cellulose synthase trafficking compartments. *Nat. Cell Biol.* **11**, 797–806 (2009). doi: 10.1038/ncb1886; pmid: 19525940
5. H. Shibaoka, Plant hormone-induced changes in the orientation of cortical microtubules: Alterations in the cross-linking between microtubules and the plasma membrane. *Annu. Rev. Plant Physiol. Plant Mol. Biol.* **45**, 527–544 (1994). doi: 10.1146/annurev.pp.45.060194.002523
6. K. Zandomeni, P. Schopfer, Reorientation of microtubules at the outer epidermal wall of maize coleoptiles by phytochrome, blue-light photoreceptor, and auxin. *Protoplasma* **173**, 103–112 (1993). doi: 10.1007/BF01378999
7. M. J. Laskowski, Microtubule orientation in pea stem cells: A change in orientation follows the initiation of growth rate decline. *Planta* **181**, 44–52 (1990). doi: 10.1007/BF00202323
8. K. Ueda, T. Matsuyama, Rearrangement of cortical microtubules from transverse to oblique or longitudinal in living cells of transgenic *Arabidopsis thaliana*. *Protoplasma* **213**, 28–38 (2000). doi: 10.1007/BF01280502
9. P. Nick, R. Bergfeld, E. Schafer, P. Schopfer, Unilateral reorientation of microtubules at the outer epidermal wall during photo- and gravitropic curvature of maize coleoptiles and sunflower hypocotyls. *Planta* **181**, 162–168 (1990). doi: 10.1007/BF02411533; pmid: 11541053
10. M. Nakamura, D. W. Ehrhardt, T. Hashimoto, Microtubule and katanin-dependent dynamics of microtubule nucleation complexes in the acentrosomal *Arabidopsis* cortical array. *Nat. Cell Biol.* **12**, 1064–1070 (2010). doi: 10.1038/ncb2110; pmid: 20935636
11. R. A. Walker, S. Inoué, E. D. Salmon, Asymmetric behavior of severed microtubule ends after ultraviolet-microbeam irradiation of individual microtubules in vitro. *J. Cell Biol.* **108**, 931–937 (1989). doi: 10.1083/jcb.108.3.931; pmid: 2921286
12. P. T. Tran, R. A. Walker, E. D. Salmon, A metastable intermediate state of microtubule dynamic instability that

differs significantly between plus and minus ends. *J. Cell Biol.* **138**, 105–117 (1997). doi: 10.1083/jcb.138.1.105; pmid: 9214385
13. R. Wightman, S. R. Turner, The roles of the cytoskeleton during cellulose deposition at the secondary cell wall. *Plant J.* **54**, 794–805 (2008). doi: 10.1111/j.1365-313X.2008.03444.x; pmid: 18266917
14. V. Stoppin-Mellet, J. Gaillard, M. Vantard, Functional evidence for in vitro microtubule severing by the plant katanin homologue. *Biochem. J.* **365**, 337–342 (2002). pmid: 12020351
15. D. Lin *et al*., Rho GTPase signaling activates microtubule severing to promote microtubule ordering in *Arabidopsis*. *Curr. Biol.* **23**, 290–297 (2013). doi: 10.1016/j.cub.2013.01.022; pmid: 23394835
16. S. H. Tindemans, B. M. Mulder, Microtubule length distributions in the presence of protein-induced severing. *Phys. Rev. E* **81**, 031910 (2010). doi: 10.1103/PhysRevE.81.031910; pmid: 20365773
17. T. Murata *et al*., Microtubule-dependent microtubule nucleation based on recruitment of γ-tubulin in higher plants. *Nat. Cell Biol.* **7**, 961–968 (2005). doi: 10.1038/ncb1306; pmid: 16138083
18. M. Nakamura, T. Hashimoto, A mutation in the *Arabidopsis* γ-tubulin-containing complex causes helical growth and abnormal microtubule branching. *J. Cell Sci.* **122**, 2208–2217 (2009). doi: 10.1242/jcs.044131; pmid: 19509058
19. J. Mao, Y.-C. Zhang, Y. Sang, Q.-H. Li, H.-Q. Yang, A role for *Arabidopsis* cryptochromes and COP1 in the regulation of stomatal opening. *Proc. Natl. Acad. Sci. U.S.A.* **102**, 12270–12275 (2005). doi: 10.1073/pnas.0501011102; pmid: 16093319
20. J. M. Christie, Phototropin blue-light receptors. *Annu. Rev. Plant Biol.* **58**, 21–45 (2007). doi: 10.1146/annurev.arplant.58.032806.103951; pmid: 17067285
21. H.-Y. Cho *et al*., Physiological roles of the light, oxygen, or voltage domains of phototropin 1 and phototropin 2 in *Arabidopsis*. *Plant Physiol.* **143**, 517–529 (2007). doi: 10.1104/pp.106.089839; pmid: 17085510
22. A. Kirik, D. W. Ehrhardt, V. Kirik, *TONNEAU2/FASS* regulates the geometry of microtubule nucleation and cortical array organization in interphase *Arabidopsis* cells. *Plant Cell* **24**, 1158–1170 (2012). doi: 10.1105/tpc.111.094367; pmid: 22395485
23. S. Gallagher, T. W. Short, P. M. Ray, L. H. Pratt, W. R. Briggs, Light-mediated changes in two proteins found associated with plasma membrane fractions from pea stem sections. *Proc. Natl. Acad. Sci. U.S.A.* **85**, 8003–8007 (1988). doi: 10.1073/pnas.85.21.8003; pmid: 16593988
24. E. Huala *et al*., *Arabidopsis* NPH1: A protein kinase with a putative redox-sensing domain. *Science* **278**, 2120–2123 (1997). doi: 10.1126/science.278.5346.2120; pmid: 9405347
25. J. M. Christie *et al*., phot1 inhibition of ABCB19 primes lateral auxin fluxes in the shoot apex required for phototropism. *PLOS Biol.* **9**, e1001076 (2011). doi: 10.1371/journal.pbio.1001076; pmid: 21666806
26. S. L. Shaw, R. Kamyar, D. W. Ehrhardt, Sustained microtubule treadmilling in *Arabidopsis* cortical arrays. *Science* **300**, 1715–1718 (2003). doi: 10.1126/science.1083529; pmid: 12714675
27. R. Dixit, R. Cyr, Encounters between dynamic cortical microtubules promote ordering of the cortical array through angle-dependent modifications of microtubule behavior. *Plant Cell* **16**, 3274–3284 (2004). doi: 10.1105/tpc.104.026930; pmid: 15539470
28. J. F. Allard, J. C. Ambrose, G. O. Wasteneys, E. N. Cytrynbaum, A mechanochemical model explains interactions between cortical microtubules in plants. *Biophys. J.* **99**, 1082–1090 (2010). doi: 10.1016/j.bpj.2010.05.037; pmid: 20712991
29. E. C. Eren, R. Dixit, N. Gautam, A three-dimensional computer simulation model reveals the mechanisms for self-organization of plant cortical microtubules into oblique arrays. *Mol. Biol. Cell* **21**, 2674–2684 (2010). doi: 10.1091/mbc.E10-02-0136; pmid: 20519434
30. R. J. Hawkins, S. H. Tindemans, B. M. Mulder, Model for the orientational ordering of the plant microtubule cortical array. *Phys. Rev. E* **82**, 011911 (2010). doi: 10.1103/PhysRevE.82.011911; pmid: 20866652
31. S. H. Tindemans, R. J. Hawkins, B. M. Mulder, Survival of the aligned: Ordering of the plant cortical microtubule array. *Phys. Rev. Lett.* **104**, 058103 (2010). doi: 10.1103/PhysRevLett.104.058103; pmid: 20366797
32. X.-Q. Shi, Y.-Q. Ma, Understanding phase behavior of plant cell cortex microtubule organization. *Proc. Natl. Acad. Sci. U.S.A.* **107**, 11709–11714 (2010). doi: 10.1073/pnas.1007138107; pmid: 20547876
33. C. Ambrose, J. F. Allard, E. N. Cytrynbaum, G. O. Wasteneys, A CLASP-modulated cell edge barrier mechanism drives cell-wide cortical microtubule organization in *Arabidopsis*. *Nat. Commun.* **2**, 430 (2011). doi: 10.1038/ncomms1444; pmid: 21847104
34. Y. Oda, H. Fukuda, Initiation of cell wall pattern by a Rho- and microtubule-driven symmetry breaking. *Science* **337**, 1333–1336 (2012). doi: 10.1126/science.1222597; pmid: 22984069
35. A. Sambade, A. Pratap, H. Buschmann, R. J. Morris, C. Lloyd, The influence of light on microtubule dynamics and alignment in the *Arabidopsis* hypocotyl. *Plant Cell* **24**, 192–201 (2012). doi: 10.1105/tpc.111.093849; pmid: 22294618
36. L. Vineyard, A. Elliott, S. Dhingra, J. R. Lucas, S. L. Shaw, Progressive transverse microtubule array organization in hormone-induced *Arabidopsis* hypocotyl cells. *Plant Cell* **25**, 662–676 (2013). doi: 10.1105/tpc.112.107326; pmid: 23444330
37. D. J. Sharp, J. L. Ross, Microtubule-severing enzymes at the cutting edge. *J. Cell Sci.* **125**, 2561–2569 (2012). doi: 10.1242/jcs.101139; pmid: 22595526
38. A. Roll-Mecak, F. J. McNally, Microtubule-severing enzymes. *Curr. Opin. Cell Biol.* **22**, 96–103 (2010). doi: 10.1016/j.ceb.2009.11.001; pmid: 19963362
39. O. Hamant, Integrative cell biology: Katanin at the crossroads. *Curr. Biol.* **23**, R206–R208 (2013). doi: 10.1016/j.cub.2013.01.031; pmid: 23473565
40. D. H. Burk, R. Zhong, Z.-H. Ye, The katanin microtubule severing protein in plants. *J. Integr. Plant Biol.* **49**, 1174–1182 (2007). doi: 10.1111/j.1672-9072.2007.00544.x
41. M. Uyttewaal *et al*., Mechanical stress acts via katanin to amplify differences in growth rate between adjacent cells in *Arabidopsis*. *Cell* **149**, 439–451 (2012). doi: 10.1016/j.cell.2012.02.048; pmid: 22500806
42. A. Roll-Mecak, R. D. Vale, Making more microtubules by severing: A common theme of noncentrosomal microtubule arrays? *J. Cell Biol.* **175**, 849–851 (2006). doi: 10.1083/jcb.200611149; pmid: 17178905
43. M. Casanova *et al*., Microtubule-severing proteins are involved in flagellar length control and mitosis in trypanosomatids. *Mol. Microbiol.* **71**, 1353–1370 (2009). doi: 10.1111/j.1365-2958.2009.06594.x; pmid: 19183280
44. M. Q. Rasi, J. D. K. Parker, J. L. Feldman, W. F. Marshall, L. M. Quarmby, Katanin knockdown supports a role for microtubule severing in release of basal bodies before mitosis in *Chlamydomonas*. *Mol. Biol. Cell* **20**, 379–388 (2009). doi: 10.1091/mbc.E07-10-1007; pmid: 19005222
45. K. McNally, A. Audhya, K. Oegema, F. J. McNally, Katanin controls mitotic and meiotic spindle length. *J. Cell Biol.* **175**, 881–891 (2006). doi: 10.1083/jcb.200608117; pmid: 17178907
46. M. Srayko, E. T. O'toole, A. A. Hyman, T. Müller-eichert, Katanin disrupts the microtubule lattice and increases polymer number in *C. elegans* meiosis. *Curr. Biol.* **16**, 1944–1949 (2006). doi: 10.1016/j.cub.2006.08.029; pmid: 17027492
47. M. Nakamura, K. Naoi, T. Shoji, T. Hashimoto, Low concentrations of propyzamide and oryzalin alter microtubule dynamics in *Arabidopsis* epidermal cells. *Plant Cell Physiol.* **45**, 1330–1334 (2004). doi: 10.1093/pcp/pch300; pmid: 15509858
48. T. Kinoshita *et al*., Phot1 and phot2 mediate blue light regulation of stomatal opening. *Nature* **414**, 656–660 (2001). doi: 10.1038/414656a; pmid: 11740564
49. S. J. Davis, R. D. Vierstra, Soluble, highly fluorescent variants of green fluorescent protein (GFP) for use in higher plants. *Plant Mol. Biol.* **36**, 521–528 (1998). doi: 10.1023/A:1005991617182; pmid: 9484447
50. T. Murashige, F. Skoog, A revised medium for rapid growth and bio assays with tobacco tissue cultures. *Physiol. Plant.* **15**, 473–497 (1962). doi: 10.1111/j.1399-3054.1962.tb08052.x
51. J. J. Lindeboom *et al*., Cortical microtubule arrays are initiated from a nonrandom prepattern driven by atypical microtubule initiation. *Plant Physiol.* **161**, 1189–1201 (2013). doi: 10.1104/pp.112.204057; pmid: 23300168
52. W. S. Rasband, ImageJ: Image processing and analysis in Java. Astrophysics Source Code Library ascl:1206.013 (2012).

Acknowledgments: D.W.E., J.J.L., M.N., and V.K. designed experimental strategy. J.J.L., M.N., A.H., and V.K. carried out experiments. J.J.L., M.N., A.H., and D.W.E. analyzed data. K.S., R.G., J.J.L., B.M.M., and D.W.E. designed and created image-analysis tools. D.W.E., J.J.L., and M.N. wrote the manuscript. B.M.M., A.H., R.G., V.K., T.K., and A.M.C.E. edited the manuscript. We thank W. Briggs, A. Murphy, R. Hangarter, E. Spalding, T. Hashimoto, M. Janson, and S. Shaw for advice and discussions. This work was supported by NSF award 1158372 (D.W.E.); the Carnegie Institution for Science (D.W.E.); the research program of the Stichting voor Fundamenteel Onderzoek der Materie (FOM), which is financially supported by the Nederlandse Organisatie voor Wetenschappelijk Onderzoek (NWO) (B.M.M.); the European Union NEST program CASPIC award 28974 (J.J.L. and K.S.); TOYOBO BIOFOUNDATION (M.N.); and the Human Frontier Science Program (M.N.).

Supplementary Materials

www.sciencemag.org/content/342/6163/1245533/suppl/DC1
Figs. S1 to S8
Movies S1 to S13

4 September 2013; accepted 29 October 2013
Published online 7 November 2013;
10.1126/science.1245533

Oscillatory Control of Factors Determining Multipotency and Fate in Mouse Neural Progenitors

Itaru Imayoshi,[1,2,3,4]*† Akihiro Isomura,[1,5]† Yukiko Harima,[1,5] Kyogo Kawaguchi,[6] Hiroshi Kori,[5,7] Hitoshi Miyachi,[1] Takahiro Fujiwara,[3] Fumiyoshi Ishidate,[3] Ryoichiro Kageyama[1,3,5]*

The basic helix-loop-helix transcription factors Ascl1/Mash1, Hes1, and Olig2 regulate fate choice of neurons, astrocytes, and oligodendrocytes, respectively. These same factors are coexpressed by neural progenitor cells. Here, we found by time-lapse imaging that these factors are expressed in an oscillatory manner by mouse neural progenitor cells. In each differentiation lineage, one of the factors becomes dominant. We used optogenetics to control expression of Ascl1 and found that, although sustained Ascl1 expression promotes neuronal fate determination, oscillatory Ascl1 expression maintains proliferating neural progenitor cells. Thus, the multipotent state correlates with oscillatory expression of several fate-determination factors, whereas the differentiated state correlates with sustained expression of a single factor.

Analyses of populations of mouse hematopoietic progenitors suggest that general fluctuations in the transcriptome affect lineage choice (*1*). On the other hand, analyses of individual cells do not show an effect of transcriptome fluctuation on lineage choice (*2*). Fate choice could be a gradual process based on transcriptome-wide fluctuations or discrete processes through different subpopulation states. To address these issues, we studied the expression patterns of fate determination factors in individual mouse cells in the multipotent state and during fate choice processes.

In the developing murine nervous system, neural progenitor cells (NPCs) proliferate (reproducing themselves) and also differentiate into three cell types, neurons, oligodendrocytes, and astrocytes (thus demonstrating multipotency). Transcription factors that regulate the proliferation of NPCs and the differentiation of each cell type include basic helix-loop-helix (bHLH) transcription factors (*3*, *4*). For example, proneural bHLH genes such as *Ascl1* (also known as *Mash1*) and *Neurogenin2* (*Ngn2*) promote neuronal fate determination and suppress astrocytic gene expression (*5*–*7*). The bHLH gene *Olig2* regulates oligodendrocyte specification, whereas the bHLH genes *Hes1* and *Hes5* maintain NPCs by repressing proneural gene expression (*8*–*12*). In addition, *Ascl1* and *Olig2* regulate oligodendrocyte and motor neuron development, respectively (*8*–*10*, *13*–*18*). One model suggests that *Hes* genes, expressed by NPCs, repress expression of other bHLH genes; down-regulation of *Hes*

[1]Institute for Virus Research, Kyoto University, Shogoin-Kawahara, Sakyo-ku, Kyoto 606-8507, Japan. [2]The Hakubi Center, Kyoto University, Kyoto 606-8302, Japan. [3]World Premier International Research Initiative–Institute for Integrated Cell-Material Sciences (WPI-iCeMS), Kyoto University, Kyoto 606-8501, Japan. [4]Japan Science and Technology Agency, Precursory Research for Embryonic Science and Technology (PRESTO), 4-1-8 Honcho, Kawaguchi, Saitama 332-0012, Japan. [5]Japan Science and Technology Agency, Core Research for Evolutional Science and Technology (CREST), 4-1-8 Honcho, Kawaguchi, Saitama 332-0012, Japan. [6]Department of Physics, Graduate School of Science, The University of Tokyo, Tokyo 113-0033, Japan. [7]Department of Information Sciences, Ochanomizu University, Tokyo 112-8610, Japan.

*Corresponding author. E-mail: rkageyam@virus.kyoto-u.ac.jp (R.K.); iimayosh@virus.kyoto-u.ac.jp (I.I.)
†These authors contributed equally to this work.

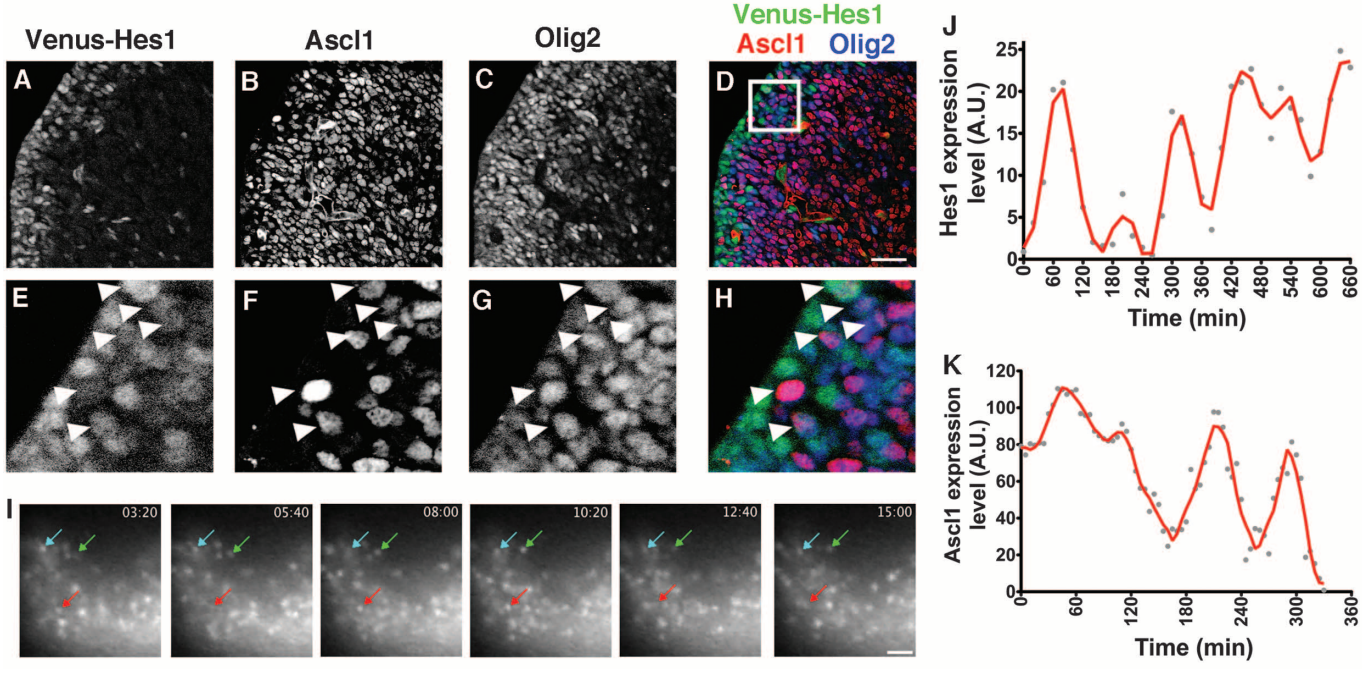

Fig. 1. Variable expression levels of bHLH factors in NPCs of the ventral telencephalon. (**A** to **H**) The expression of Hes1, Ascl1, and Olig2 in the ventral telencephalon at perinatal stages was examined by immunohistochemistry. The boxed region in (D) is enlarged in (E) to (H). Many cells were positive for all three bHLH factors (Hes1, Ascl1, and Olig2; arrowheads), whereas others were mostly positive for two of them. (**I** to **K**) Bioluminescence imaging and quantification of Luc2-Hes1 [(I) and (J)] and Luc2-Ascl1 (K) expression in slice cultures of the ventral telencephalon of reporter mice. Scale bars indicate 50 μm for (A) to (D) and (I). A.U., arbitrary units.

genes allows up-regulation of proneural genes or *Olig2* and subsequent differentiation into neurons or oligodendrocytes (*4*). However, *Ascl1* is expressed by dividing NPCs and postmitotic neurons, and *Ascl1* up-regulates the expression of genes involved in cell cycle progression of NPCs as well as in cell cycle exit and neuronal differentiation (*19*, *20*). Furthermore, *Hes1* promotes the maintenance of NPCs and astrocyte differentiation (*11*, *12*, *21*, *22*). *Olig2* is also involved in NPC proliferation (*23*). Thus, these bHLH genes exert contradictory functions.

Hes1 expression oscillates with a period of about 2 to 3 hours in many cell types, including NPCs (*24*, *25*). *Ngn2* expression also oscillates in NPCs, probably because it is periodically repressed by Hes1 oscillation. In differentiating neurons, which lack Hes1 expression, *Ngn2* expression is steady (*25*). Thus, the pattern of bHLH gene expression differs between NPCs and neurons, although our previous time-lapse imaging study only monitored messenger RNA (mRNA) production (*25*). Because transcription and translation can be dissociated (*26*), we studied protein expression at the single-cell level. We found that Hes1, Ascl1, and Olig2 protein expression oscillates in NPCs.

Variable Levels of bHLH Transcription Factor Expression in NPCs

Ascl1, Hes1, and Olig2 are expressed by NPCs in the ventral telencephalon, which generate neurons, astrocytes, and oligodendrocytes during perinatal stages of mouse development (*14*–*18*, *27*, *28*). The expression levels of these transcription factors were variable from cell to cell (Fig. 1, A to H). Many cells were positive for all three bHLH factors (Hes1, Ascl1, and Olig2), whereas others expressed only two (Fig. 1, E to H). By contrast, differentiating neurons, oligodendrocytes, and astrocytes expressed only one of them at later stages (i.e., Ascl1, Olig2, and Hes1, respectively) (*18*, *22*, *29*). To examine the expression of these bHLH factors, we generated transgenic mice carrying reporters in which fluorescent (Venus or mCherry) or firefly luciferase (Luc2) complementary DNA (cDNA) was inserted in frame into the 5′ region of each bHLH gene in bacterial artificial chromosome (BAC) clones so that a bHLH factor fused with either Venus, mCherry, or Luc2 was expressed (table S1 and fig. S1, A to F). We also generated knock-in mice in which Venus was inserted in frame into the 5′ region of the *Hes1* gene for Hes1 imaging (table S1 and fig. S2A), those in which Venus or luciferase (Eluc) was inserted in frame into the 5′ region of the *Hes5* gene for Hes5 imaging (table S1 and fig. S2, B and C), and Sox2 reporter mice expressing a Luc2-Sox2 fusion protein (table S1 and fig. S1G). The reporter expression in these mice was similar to endogenous expression (fig. S3). Reporter expression also correlated well with endogenous protein expression in NPCs (fig. S4). The brain structures and the NPC competency of these reporter mice, including homozygous Venus-Hes1 fusion knock-in mice, were apparently normal (fig. S5).

We used time-lapse imaging of brain slices from the ventral telencephalon of reporter mice and found that Hes1 and Ascl1 expression oscillate in NPCs (Fig. 1, I to K, and movie S1).

Oscillatory Expression of bHLH Factors in NPCs

We next prepared NPCs from the ventral telencephalon of perinatal reporter mice. We used

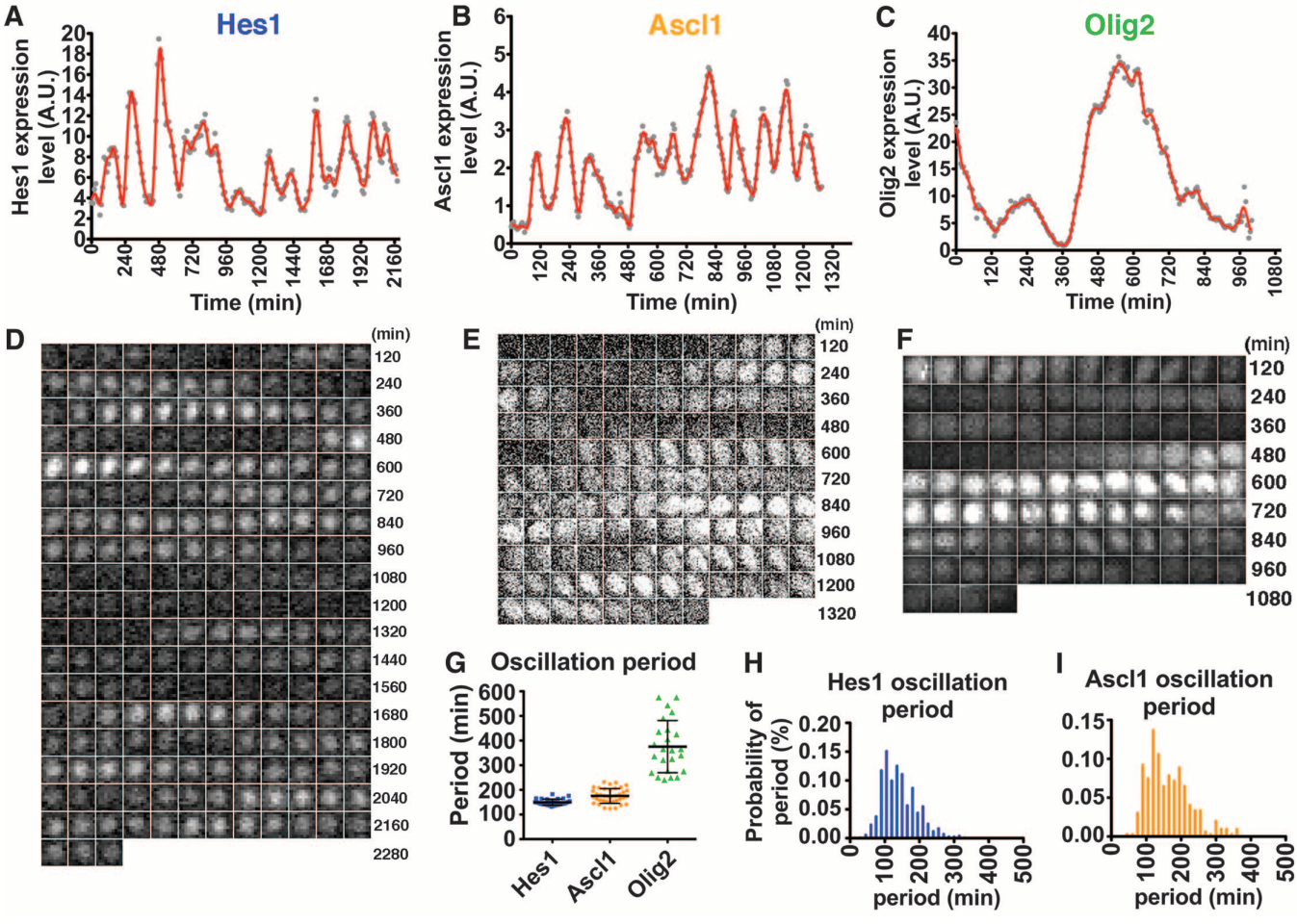

Fig. 2. Oscillatory expression of bHLH factors in self-renewing NPCs derived from the ventral telencephalon. (**A** to **F**) Bioluminescence images and quantification of Luc2-Hes1 [(A) and (D)], Luc2-Ascl1 [(B) and (E)], and Luc2-Olig2 [(C) and (F)] reporter expression. (**G** to **I**) The distribution of the oscillation periods of Hes1, Ascl1, and Olig2 derived from bioluminescence measurements (n > 25 NPCs for each factor). Error bars in (G) indicate SD.

acutely dissociated NPCs and those (designated NS cells) maintained in vitro for at least 10 generations in the presence of epidermal growth factor (EGF) and basic fibroblast growth factor (bFGF) (*30*, *31*). Both cell types exhibited similar expression oscillations in the progenitor state and during cell fate choice. These NPCs expressed Ascl1, Olig2, and Hes1 at variable levels (fig. S6) and generated γ-aminobutyric acid–releasing (GABAergic) neurons, oligodendrocytes, and astrocytes (fig. S7) (*14*). Their competency to generate neurons and oligodendrocytes was significantly reduced in the absence of Ascl1 and Olig2, respectively (fig. S7, G, H″, I, and K). These NPCs also showed a reduced ability to generate astrocytes in the absence of Hes1 (fig. S7, F′ and J). Compared with the bHLH factors, the NPC-specific factor Sox2 (*32*) was expressed at a relatively constant level (fig. S6, A, E, and J).

We used time-lapse imaging to analyze expression patterns of bHLH factors. Hes1 protein expression oscillated in NPCs [average period of 149.9 ± 12.3 min (SD)] (Fig. 2, A, D, G, and H′; fig. S8; and movie S2). Hes5 expression in NPCs oscillated in phase with Hes1 expression (figs. S9 and S10). Ascl1 expression oscillated in NPCs (average period of 175.4 ± 29.5 min) (Fig. 2, B, E, G, and I; fig. S11; and movie S3). The Ascl1 protein level was up-regulated during S and G_2 in some cells (~30%; fig. S11, C and D); after cell division, both daughter cells showed equal amounts of Ascl1, and expression oscillations resumed in cells that remained undifferentiated (fig. S11D). Olig2 protein expression also oscillated but more slowly (average period of 375.5 ± 105.8 min) than Hes1 and Ascl1 protein oscillations (Fig. 2, C, F, and G; fig. S12; and movie S4). The average expression levels of these factors are different between G_1 and S, G_2, and M (fig. S13), although their expression oscillated throughout the cell cycle. By contrast, two other factors characteristic of NPCs were expressed steadily: Sox2 and Nestin (figs. S13C and S14 and movie S5).

Hes1 and Ascl1 expression are inversely correlated (fig. S15, A and D) (*33*); Hes1 represses Ascl1 expression by binding to the *Ascl1* promoter (*34*). Oscillating Hes1 would periodically repress Ascl1 expression, thereby driving oscillations in Ascl1 expression. Indeed, oscillatory Ascl1 expression was lost in the absence of Hes1 (fig. S11, E and F). Expression of Olig2, on the other hand, changes independently of Ascl1 and Hes1 (fig. S15, B, C, E, and F).

We next examined whether the oscillations in bHLH factor expression levels create a bias in differentiation competency. We separated NPCs of the fluorescent reporter mice into Hes1-high, Hes1-low, Ascl1-high, Ascl1-low, Olig2-high, and Olig2-low fractions (fig. S16, A to C). All cell fractions kept in NS media returned to original diverse levels of Hes1, Ascl1, and Olig2 expression within 2 days, suggesting that diverse levels represent different phases of expression oscillation (fig. S16, D to L). All cells generated neurospheres at similar efficiencies (fig. S16, M to R).

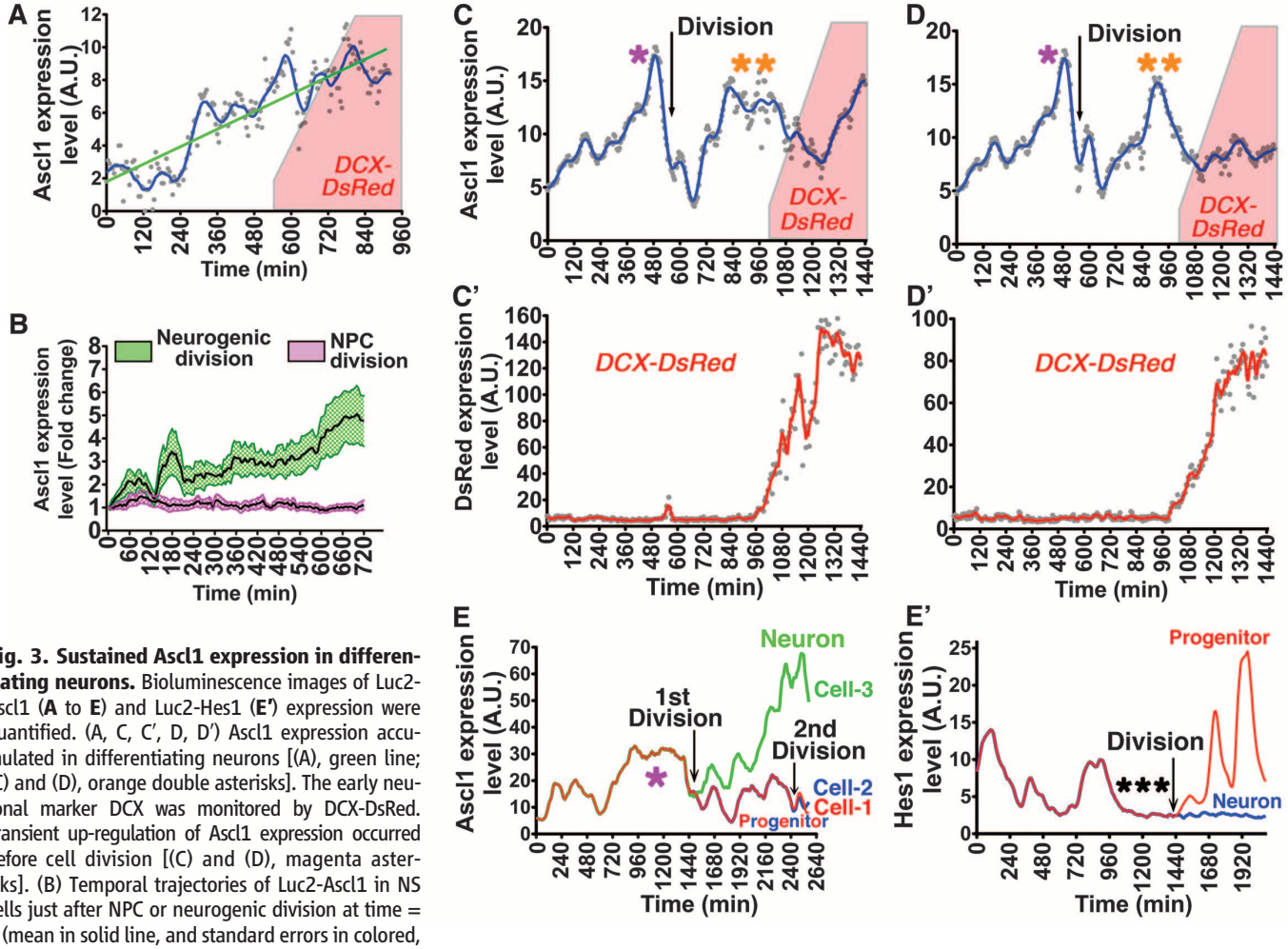

Fig. 3. Sustained Ascl1 expression in differentiating neurons. Bioluminescence images of Luc2-Ascl1 (**A** to **E**) and Luc2-Hes1 (**E′**) expression were quantified. (A, C, C′, D, D′) Ascl1 expression accumulated in differentiating neurons [(A), green line; (C) and (D), orange double asterisks]. The early neuronal marker DCX was monitored by DCX-DsRed. Transient up-regulation of Ascl1 expression occurred before cell division [(C) and (D), magenta asterisks]. (B) Temporal trajectories of Luc2-Ascl1 in NS cells just after NPC or neurogenic division at time = 0 (mean in solid line, and standard errors in colored, $n > 19$ for each division). Division-mode effect, $P = 0.0022$; interaction between division mode and time, $P < 0.0001$, repeated measures analysis of variance (ANOVA). (E) This acutely dissociated NPC underwent asymmetric cell division. Ascl1 was equally distributed in both daughter cells after the first cell division. Ascl1 expression accumulated in a daughter neuron (green) but resumed oscillating in a daughter NPC (red), which underwent the second division. (E′) Hes1 expression was repressed before asymmetric cell division (asterisks). The suppression of Hes1 expression was maintained in a daughter neuron (blue line), whereas Hes1 oscillation resumed in a daughter NPC (red line).

After sorting, each cell population was cultured in a differentiation medium. Hes1-high and Hes1-low cells preferentially differentiated into astrocytes and neurons, respectively (fig. S17, A and B). Ascl1-high (and Olig2-low), and Olig2-high (and Ascl1-low) cells preferentially differentiated into neurons and oligodendrocytes, respectively (fig. S17, A and C to G). These results suggest that the different expression levels of the bHLH factors bias the fate choice of NPCs. However, such transient high expression is neither required nor sufficient for cell fate determination: NPCs with high expression of any of Ascl1, Olig2, and Hes1 were all able to differentiate into any of the three cell types (fig. S17).

Sustained Expression of bHLH Factors During Cell Fate Choice

We next examined how the expression of these bHLH factors changes during cell fate choice. During neuronal differentiation, Ascl1 protein accumulated after cell division (Fig. 3, A to D), in contrast to oscillatory expression in NPCs, and 6 to 8 hours later the early neuronal marker doublecortin (DCX) was expressed (Fig. 3, A and C to D′). Ascl1 expression continued to be up-regulated in many cells (76.7%, Fig. 3, A to C) but not in others (23.3%, Fig. 3D) after DCX expression was initiated, raising the possibility that the minimum requirement for neuronal differentiation is accumulation of Ascl1 over 6 to 8 hours during G1.

In acute dissociation culture from the ventral telencephalon, many NPCs underwent asymmetric cell division, in which one daughter cell remained undifferentiated while the other differentiated into a neuron. In these NPCs, Ascl1 expression was up-regulated (at least twofold compared with the average) before cell division and seemed to be equally distributed in both daughter cells (Fig. 3E). In the daughter neuron, Ascl1 expression accumulated after cell division, whereas it resumed oscillating in the daughter NPC (Fig. 3E). Before neurogenic cell division (one or both daughter cells underwent neuronal differentiation), Ascl1 expression was transiently up-regulated (at least twofold compared with the average) in many cases: ~90% of their mother cells exhibited such transient up-regulation of Ascl1 before cell division (fig. S18B). However, ~30% of mother cells did so when they produced two daughter NPCs (figs. S11, C and D, and S18B). Thus, the transient up-regulation of Ascl1 before cell division is not decisive but merely lends a bias toward neuronal fate choice.

In those NPCs whose daughter cells underwent neuronal differentiation, Hes1 expression was repressed before cell division (Fig. 3E′ and fig. S18, A, E, and F) but not when both cells remained NPCs (fig. S18, A, C, and D). The suppression of Hes1 expression was maintained in daughter neurons (Fig. 3E′ and fig. S18, E and F), whereas Hes1 oscillation resumed in daughter NPCs (Fig. 3E′). Thus, it is likely that transient down-regulation of Hes1 expression and the concomitant up-regulation of Ascl1 before cell division directs NPCs toward neuronal fate choice and that sustained expression of Ascl1 after cell division irreversibly determines neuronal fate. Down-regulation of Hes1 could be caused by fluctuations of the expression levels of Notch intracellular domain (NICD), an active form of Notch signaling (*35*) (fig. S19). Indeed, when stable NICD expression was induced from the Rosa26 locus in NPCs, both Hes1 and Hes5 expression oscillated sustainably, and there was no down-regulation of these factors (figs. S20 and S21). By contrast, in the presence of a γ-secretase inhibitor, which inhibits Notch signaling activity, Ascl1 and Olig2 expression was up-regulated to stable expression (fig. S22).

During astrocyte differentiation, Hes1 protein expression still oscillated but at high average and trough levels (Fig. 4, A and B, and fig. S23, B and C). Twelve to 24 hours later, expression of the astrocyte marker glial fibrillary acidic protein (GFAP) began (fig. S23A). Ascl1 and Olig2 expression became undetectable within 10 hours during astrocyte differentiation (fig. S23, D to G). During oligodendrocyte differentiation, Olig2 protein expression oscillated but at high trough levels (Fig. 4, C and D, and fig. S24, A, C, and E). A few days after induction of oligodendrocyte differentiation, Olig2 expression was down-regulated, and expression of the mature oligodendrocyte marker 2',3′-cyclic-nucleotide-3′-phosphodiesterase (CNPase) (fig. S25) was up-regulated (Fig. 4E and fig. S24, B, D, and G). During this period, Ascl1 and Hes1 expression were down-regulated (fig. S24, H to J). Thus, bHLH fate determination factors are coexpressed in an oscillatory manner in NPCs, but, as the cell fate choice becomes established, one factor accumulates and the other two are lost. Although oscillatory expression of multiple fate determination factors underlies the multipotent state of NPCs, this oscillatory pattern gives way to stable and dominant expression of one factor during cellular differentiation.

Light-Induced Control of Expression Pattern

To demonstrate the functional importance of oscillatory or sustained expression patterns, we adopted the optogenetic gene expression system by using the *Neurospora crassa* photoreceptor Vivid that was fused with Gal4 DNA binding domain and p65 activation domain (GAVPO) (*36*). The codon usage was optimized for mammalian cells to increase expression efficiency, and the target mRNA was destabilized by introducing the 3′ untranslated region of mouse *Ascl1* mRNA (fig. S26A). With this system, we can induce gene expression comparable to endogenous

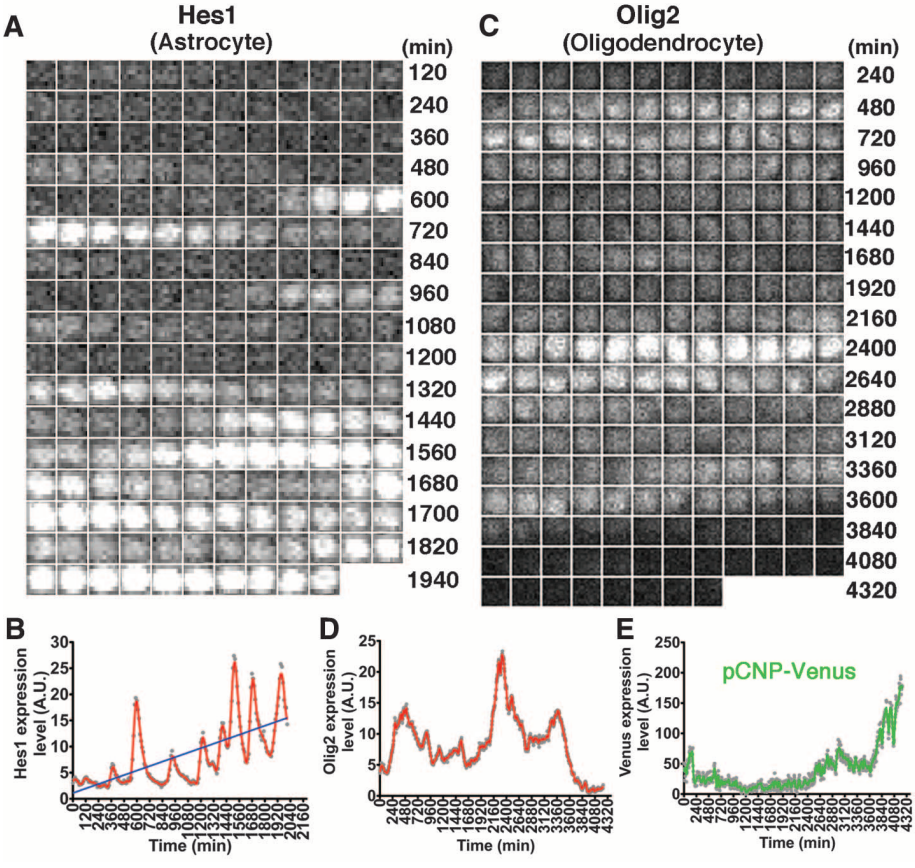

Fig. 4. Expression dynamics of bHLH factors during gliogenesis. (**A** and **B**) Bioluminescence imaging (A) and quantification (B) of Luc2-Hes1 expression during astrocyte differentiation. Astrocyte specification was induced at time = 0 by leukemia inhibitory factor and bone morphogenetic protein 4. (**C** to **E**) Bioluminescence imaging (C) and quantification (D) of Luc2-Olig2 expression and quantification of pCNP-Venus (E) in a single cell during oligodendrocyte differentiation, which was induced by T3 at time = 0.

levels (fig. S26, D to G). Repeated exposure of blue light with 3-hour intervals generated oscillatory expression with a 3-hour period, whereas repeated exposure with 30-min intervals generated sustained expression at both cell-population (Fig. 5A) and single-cell levels (Fig. 5, B and C, and movie S6).

Because *Ascl1* is known to promote the cell cycle progression of NPCs and their cell cycle exit and neuronal differentiation (*20*), we asked whether these contradictory functions of Ascl1 are regulated by different expression patterns. We introduced the Ascl1-inducible system into *Ascl1*-null NS cells, which produce no neurons (fig. S7) and proliferate more slowly than wild-type NS cells (*20*). *Ascl1*-null NS cells have a low proportion [4 to 5%; phosphohistone H3$^+$ (PH3$^+$)] of dividing cells (Fig. 5E), whereas wild-type NS cells have 14 to 15% PH3$^+$ dividing cells (fig. S29C). However, light-induced oscillatory expression of Ascl1 increased the proportion of dividing cells in the *Ascl1*-null NS cell population to ~10% PH3$^+$ (Fig. 5, E to G), suggesting that Ascl1 oscillation enhanced NPC proliferation. These NS cells did not differentiate into neurons (βIII-tubulin$^+$) even after 3 days (Fig. 5D). The period of this oscillation is important, because a 6-hour period did not affect NPC proliferation (fig. S27). By contrast, light-induced sustained expression of Ascl1 enhanced neuronal differentiation (βIII-tubulin$^+$) of *Ascl1*-null NS cells (Fig. 5, H to K). A higher level of sustained Ascl1 expression increased the efficiency of neuronal differentiation (compare Fig. 5H versus fig. S28E). Oscillatory Ascl1 expression did not induce neuronal differentiation even at a higher amplitude (fig. S28, A to C) but increased the number of proliferating NPCs (fig. S28D). By contrast, sustained Ascl1 expression at similar levels increased neuronal differentiation (fig. S28E). These results indicate that distinct expression patterns, but not the levels, of Ascl1 are important for a choice between proliferation and differentiation.

We used the Ascl1-inducible system in wild-type NS cells, where endogenous Ascl1 expression oscillates (fig. S29). Oscillatory light stimulation with 3-hour intervals did not affect the neurogenesis or proliferation of these cells (figs. S29, A to I, and S30, A to D). By contrast, sustained Ascl1 expression for 72 hours increased neuronal formation even in the presence of bFGF and EGF, a condition that inhibits neurogenesis (figs. S29, J to Q, and S30E). At least 6 to 8 hours of sustained Ascl1 expression was required for generation of neurons (Fig. 5, L to P), agreeing with the above notion about the minimal requirement for neuronal differentiation. This requirement for elapsed time suggests that only NS cells that are caught at G1 could be redirected by light-induced expression of Ascl1 into neuronal development. The Ascl1-inducible system was also introduced into the dorsal telencephalon, which normally expresses very low levels of Ascl1. The oscillatory expression of Ascl1 did not induce neuronal differentiation but did maintain Nestin$^+$ NPCs in the ventricular zone, whereas the sustained expression of Ascl1 increased the number of βIII-tubulin$^+$ neurons that migrated out of the ventricular zone (fig. S31). Thus, manipulation of Ascl1 gene expression can impose a choice favoring proliferation or differentiation according to whether the Ascl1 expression is oscillatory or sustained.

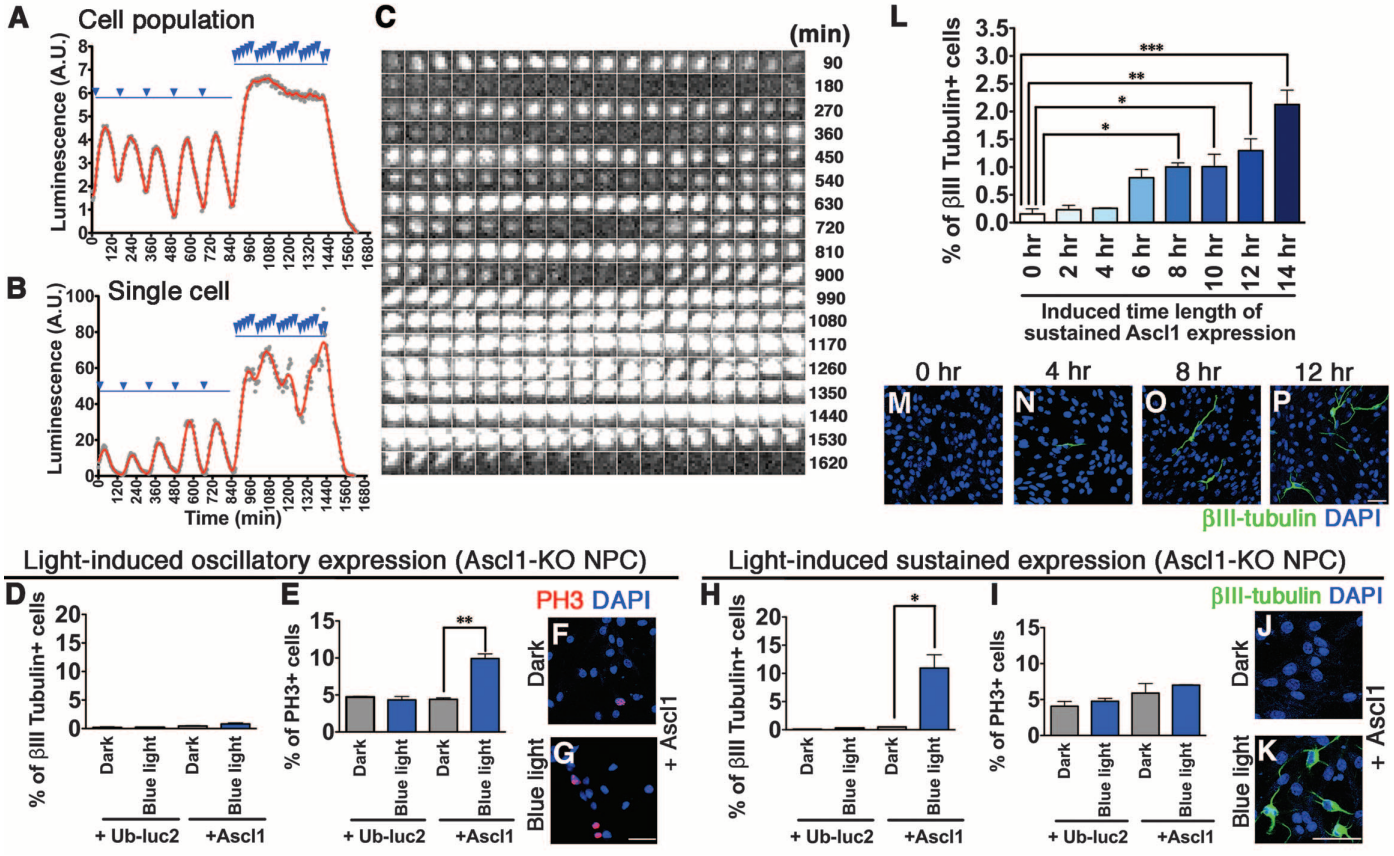

Fig. 5. Light-induced oscillatory or sustained expression of Ascl1 in NPCs. (**A** to **C**) Time-lapse imaging (C) and quantification [(A) and (B)] of gene expression at cell-population (A) and single-cell levels [(B) and (C)] induced by blue light. (**D** to **K**) According to the schedule of light exposure (fig. S26B; light intensity of 1.11 μmol/m^2 per s), oscillatory [(D) to (G)] and sustained [(H) to (K)] Ascl1 expression was induced in *Ascl1*-null NPCs, which were cultured in the presence of bFGF and EGF, a condition that inhibits neurogenesis. Oscillatory Ascl1 expression induced nearly no βIII-tubulin$^+$ neuron formation (D) but significantly increased the proportion of dividing cells (PH3$^+$) compared with the control [ubiquitin (Ub)–luc2] [(E) to (G)]. Sustained Ascl1 expression significantly increased βIII-tubulin$^+$ neuron formation compared with the control (Ub-luc2) (H, J, K). DAPI, 4′,6-diamidino-2-phenylindole. *P < 0.05, **P < 0.01; two-tailed Student's t test. Error bars indicate SE. (**L** to **P**) According to the schedule of light exposure (fig. S26C), sustained Ascl1 expression was induced in NPCs for indicated time lengths, and neuronal formation was examined. *P < 0.05, **P < 0.01, ***P < 0.001, one-way ANOVA followed by Tukey post hoc test. Scale bars, 12.5 μm for (F), (G), (J), and (K) and 12.5 μm for (M) to (P).

Discussion

Our data suggest that multipotency is a state of multiple oscillating neurogenic and gliogenic determination factors and that cell fate choice is a process of sustained expression of a single factor. This switching may be induced by the fluctuations of Notch signaling (supplementary text). The detailed mechanism by which the oscillatory and sustained Ascl1 expression differentially regulates downstream gene expression remains to be determined. A recent report indicates that the proneural factor Ngn2 is differentially phosphorylated between NPCs and neurons and controls the expression of its target genes differently depending on its phosphorylation status (*37*). We speculate that oscillatory and sustained expression of proneural factors could be involved in the different posttranscriptional modulation that is responsible for target gene selectivity. We also demonstrated that the light-switchable gene expression system offers an efficient way to control the proliferation and differentiation of stem cells by changing the light-exposure pattern rather than using different growth factors or chemicals, showing its applicability to the regeneration technology.

References and Notes

1. H. H. Chang, M. Hemberg, M. Barahona, D. E. Ingber, S. Huang, *Nature* **453**, 544–547 (2008).
2. C. Pina *et al.*, *Nat. Cell Biol.* **14**, 287–294 (2012).
3. N. Bertrand, D. S. Castro, F. Guillemot, *Nat. Rev. Neurosci.* **3**, 517–530 (2002).
4. S. E. Ross, M. E. Greenberg, C. D. Stiles, *Neuron* **39**, 13–25 (2003).
5. K. Tomita, K. Moriyoshi, S. Nakanishi, F. Guillemot, R. Kageyama, *EMBO J.* **19**, 5460–5472 (2000).
6. Y. Sun *et al.*, *Cell* **104**, 365–376 (2001).
7. M. Nieto, C. Schuurmans, O. Britz, F. Guillemot, *Neuron* **29**, 401–413 (2001).
8. Q. R. Lu *et al.*, *Cell* **109**, 75–86 (2002).
9. Q. Zhou, D. J. Anderson, *Cell* **109**, 61–73 (2002).
10. H. Takebayashi *et al.*, *Curr. Biol.* **12**, 1157–1163 (2002).
11. T. Ohtsuka *et al.*, *EMBO J.* **18**, 2196–2207 (1999).
12. Y. Nakamura *et al.*, *J. Neurosci.* **20**, 283–293 (2000).
13. R. Mizuguchi *et al.*, *Neuron* **31**, 757–771 (2001).
14. C. M. Parras *et al.*, *EMBO J.* **23**, 4495–4505 (2004).
15. S. Gokhan *et al.*, *J. Neurosci.* **25**, 8311–8321 (2005).
16. C. M. Parras *et al.*, *J. Neurosci.* **27**, 4233–4242 (2007).
17. E. J. Kim, J. Battiste, Y. Nakagawa, J. E. Johnson, *Mol. Cell. Neurosci.* **38**, 595–606 (2008).
18. M. A. Petryniak, G. B. Potter, D. H. Rowitch, J. L. Rubenstein, *Neuron* **55**, 417–433 (2007).
19. E. Pastrana, L.-C. Cheng, F. Doetsch, *Proc. Natl. Acad. Sci. U.S.A.* **106**, 6387–6392 (2009).
20. D. S. Castro *et al.*, *Genes Dev.* **25**, 930–945 (2011).
21. T. Ohtsuka, M. Sakamoto, F. Guillemot, R. Kageyama, *J. Biol. Chem.* **276**, 30467–30474 (2001).
22. Y. Wu, Y. Liu, E. M. Levine, M. S. Rao, *Dev. Dyn.* **226**, 675–689 (2003).
23. K. L. Ligon *et al.*, *Neuron* **53**, 503–517 (2007).
24. H. Hirata *et al.*, *Science* **298**, 840–843 (2002).
25. H. Shimojo, T. Ohtsuka, R. Kageyama, *Neuron* **58**, 52–64 (2008).
26. R. Lu *et al.*, *Nature* **462**, 358–362 (2009).
27. S. W. Levison, J. E. Goldman, *J. Neurosci. Res.* **48**, 83–94 (1997).
28. C. A. G. Marshall, J. E. Goldman, *J. Neurosci.* **22**, 9821–9830 (2002).
29. S. Fukuda, T. Kondo, H. Takebayashi, T. Taga, *Cell Death Differ.* **11**, 196–202 (2004).
30. L. Conti *et al.*, *PLOS Biol.* **3**, e283 (2005).
31. S. M. Pollard, L. Conti, Y. Sun, D. Goffredo, A. Smith, *Cereb. Cortex* **16** (suppl. 1), i112–i120 (2006).
32. L. H. Pevny, S. K. Nicolis, *Int. J. Biochem. Cell Biol.* **42**, 421–424 (2010).
33. J. H. Baek, J. Hatakeyama, S. Sakamoto, T. Ohtsuka, R. Kageyama, *Development* **133**, 2467–2476 (2006).
34. H. Chen *et al.*, *Proc. Natl. Acad. Sci. U.S.A.* **94**, 5355–5360 (1997).
35. E. H. Schroeter, J. A. Kisslinger, R. Kopan, *Nature* **393**, 382–386 (1998).
36. X. Wang, X. Chen, Y. Yang, *Nat. Methods* **9**, 266–269 (2012).
37. C. Hindley *et al.*, *Development* **139**, 1718–1723 (2012).

Acknowledgments: We are grateful to F. Guillemot, J. Johnson, H. Takebayashi, K. Ikenaka, D. Melton, A. Miyawaki, A. Sakaue-Sawano, Q. Lu, and Y. Yang for reagents and S. Kitano, M. Sakamoto, H. Shimojo, and Center for Meso-Bio Single-Molecule Imaging (CeMI), WPI-iCeMS, Kyoto University for technical help. This work was supported by Core Research for Evolutional Science and Technology (R.K. and H.K.), Grant-in-Aid for Scientific Research on Innovative Areas (Ministry of Education, Culture, Sports, Science, and Technology 22123002) (R.K.), Scientific Research (A) [Japan Society for Promotion of Science (JSPS) 24240049] (R.K.) and Young Scientists (A) (JSPS 24680035) (I.I.), and Takeda Foundation (R.K.). I.I. and R.K. designed the project and wrote the manuscript. A.I. developed the light-induced gene expression system. I.I., A.I., Y.H., and H.M. performed experiments, and T.F. and F.I. conducted fluorescent imaging analyses. K.K. and H.K. performed computer simulation. A national (Japanese) patent application, "Optogenetic control of proliferation and differentiation of stem cells" (2013-193582), has been filed by Kyoto University.

Supplementary Materials

www.sciencemag.org/content/342/6163/1203/suppl/DC1
Materials and Methods
Supplementary Text
Figs. S1 to S31
Table S1
References (*38*–*55*)
Movies S1 to S6

25 June 2013; accepted 24 September 2013
Published online 31 October 2013;
10.1126/science.1242366

REPORTS

Structure and Composition of the Plate-Boundary Slip Zone for the 2011 Tohoku-Oki Earthquake

Frederick M. Chester,[1]* Christie Rowe,[2] Kohtaro Ujiie,[3] James Kirkpatrick,[4] Christine Regalla,[5] Francesca Remitti,[6] J. Casey Moore,[7] Virginia Toy,[8] Monica Wolfson-Schwehr,[9] Santanu Bose,[10] Jun Kameda,[11]† James J. Mori,[12] Emily E. Brodsky,[7] Nobuhisa Eguchi,[13] Sean Toczko,[13] Expedition 343 and 343T Scientists‡

The mechanics of great subduction earthquakes are influenced by the frictional properties, structure, and composition of the plate-boundary fault. We present observations of the structure and composition of the shallow source fault of the 2011 Tohoku-Oki earthquake and tsunami from boreholes drilled by the Integrated Ocean Drilling Program Expedition 343 and 343T. Logging-while-drilling and core-sample observations show a single major plate-boundary fault accommodated the large slip of the Tohoku-Oki earthquake rupture, as well as nearly all the cumulative interplate motion at the drill site. The localization of deformation onto a limited thickness (less than 5 meters) of pelagic clay is the defining characteristic of the shallow earthquake fault, suggesting that the pelagic clay may be a regionally important control on tsunamigenic earthquakes.

For the 11 March 2011 moment magnitude (M_w) = 9.0 Tohoku-Oki earthquake, pronounced coseismic weakening of the plate-boundary fault may explain the nearly total stress drop, the associated change from a thrust to normal faulting stress state in the wedge (*1*–*3*), and the large slip that breached the trench (*4*–*6*). Friction and other properties of faults relevant to slip behavior depend on the composition (e.g., clay content) and structure (e.g., orientation, thickness, and rock fabric) of the active slip zones.

[1]Center for Tectonophysics, Department of Geology and Geophysics, Texas A&M University, College Station, TX 77843, USA. [2]Earth and Planetary Sciences Department, McGill University, Montreal, Canada. [3]Graduate School of Life and Environmental Sciences, University of Tsukuba, Tsukuba, Japan; Institute for Research on Earth Evolution, Japan Agency for Marine-Earth Science and Technology, Yokosuka, Japan. [4]Department of Geosciences, Colorado State University, Fort Collins, CO 80523, USA. [5]Department of Geosciences, Pennsylvania State University, University Park, PA 16802, USA. [6]Dipartimento di Scienze della Terra, Università di Modena e Reggio Emilia largo, Modena, Italy. [7]Department of Earth and Planetary Sciences, University of California Santa Cruz, Santa Cruz, CA 95064, USA. [8]Department of Geology, University of Otago, Dunedin, New Zealand. [9]Center for Coastal and Ocean Mapping/Joint Hydrographic Center, University of New Hampshire, Durham, NH 03824, USA. [10]Department of Geology, University of Calcutta, Kolkata, India. [11]Department of Earth and Planetary Science, The University of Tokyo, Tokyo, Japan. [12]Earthquake Hazards Division, Disaster Prevention Research Institute, Kyoto University, Kyoto, Japan. [13]Center for Deep Earth Exploration, Japan Agency for Marine-Earth Science and Technology, Yokohama, Japan.

*Corresponding author. E-mail: chesterf@tamu.edu
†Present address: Earth and Planetary System Science, Department of Natural History Sciences, Hokkaido University, N10 W8, Sapporo 060-0810, Japan.
‡Expedition 343 and 343 T Scientists authors and affiliations are listed in Supplementary Materials.

The Japan Trench Fast Drilling Project (JFAST), Integrated Ocean Drilling Program (IODP) Expedition 343 and 343T (1 April to 24 May and 5 to 19 July 2012) was designed to locate and directly sample the shallow, active slip zone of the M_w = 9.0 Tohoku-Oki earthquake (*7*). The JFAST drill site (C0019) is seaward of the 2011 Tohoku-Oki earthquake hypocenter and just landward of the Japan Trench, about 200 km offshore of Sendai city (Fig. 1). In this area, the earthquake exhibited relatively low speed of rupture propagation with long-period radiation akin to tsunami earthquakes (*8*, *9*), with exceptionally large slip at the trench (*4*, *10*). A predrilling multichannel seismic survey of the drill site (*11*) showed that the frontal prism of the upper plate lacks coherent reflectors. In the subducting plate below the prism and seaward to the outer rise, the basaltic crust and overlying sediments are offset by normal faults with several hundred meters throw (*11*, *12*). The drill site sits atop a horst (Fig. 1B).

The drilling vessel *Chikyu* drilled three closely spaced holes to >844 meters below the seafloor (mbsf) to reach the strong seismic reflectors thought to mark the top of the basalt of the subducting plate (Fig. 1B), thus crossing the plate boundary. We deployed logging-while-drilling tools, including natural gamma ray and multiple resistivity sensors, to record data for the entire depth of the first hole; core samples were recovered from key intervals of the second hole, and a temperature-sensing observatory was installed in the third hole (*7*). The integration of geophysical data with analyses of core samples allowed identification of the top of the geologic plate boundary at ~820 mbsf, which coincides with the seismic reflector interpreted as the plate boundary fault (*7*, *11*, *12*) that extends seaward past the horst and into the trench graben (Fig. 1C). Analysis of the temperature data recovered from the third borehole indicates the Tohoku-Oki earthquake rupture occurred at essentially the same depth as the plate-boundary fault identified in the logging and coring boreholes [fig. S1 (*13*)]. On the basis of a palinspastic reconstruction of our structural interpretation (fig. S2), we estimate that the cumulative displacement across the plate-boundary fault at the drill site is ~3.2 km.

The top of the plate-boundary fault zone is identified by changes in lithology, sediment age, log signature, and orientations of bedding determined from resistivity image logs (*7*). From 275 to ~820 mbsf, bedding is dipping ~30° to 70° with strikes normal to the plate convergence direction. Core samples from 690 to ~820 mbsf contain Pliocene to Pleistocene radiolaria. Below ~820 mbsf, the bedding uniformly dips <10° and displays high gamma ray signatures to ~835 mbsf (Fig. 2). Radiolarian microfossils in core samples confirm that the shallowly dipping, high gamma-ray strata are Late Miocene mudstones and Cretaceous pelagic clay. The transition to high resistivity and low gamma ray at ~835 mbsf represents the transition from pelagic clay to Cretaceous chert. The subhorizontal strata (below ~820 mbsf) are lithologically similar to the basal sediments documented on the outer rise of the Pacific Plate about 260 km to the northeast at site 436 of the Japan Trench transect, Leg 56, Deep Sea Drilling Project

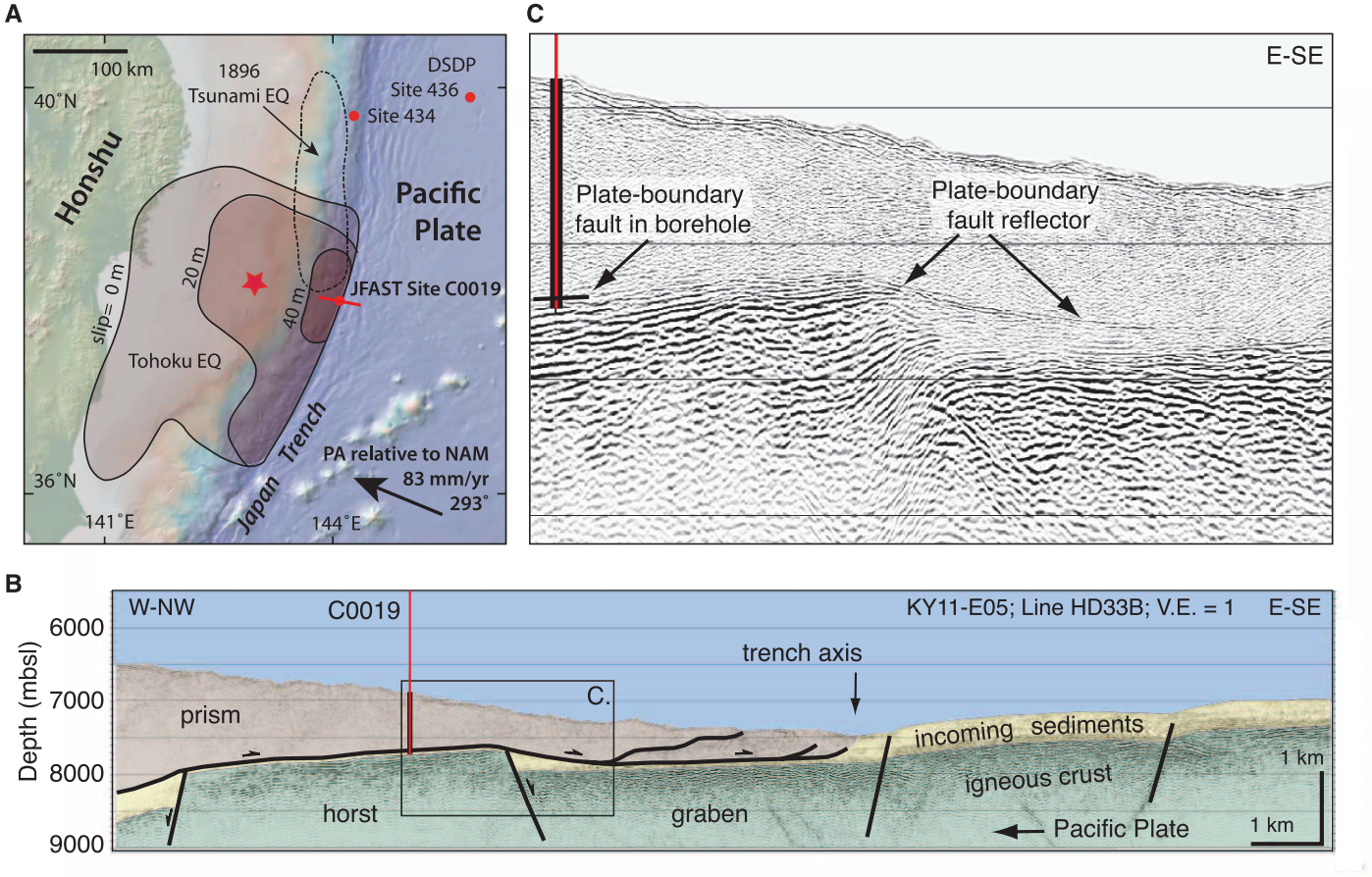

Fig. 1. Location and structural setting of the JFAST drill site. (**A**) Red dots indicate ocean drilling sites, and the red star is the epicenter of the Tohoku-Oki earthquake (EQ). Contours show the coseismic slip inferred from various data sets, and the dashed line shows the approximate rupture area of the 1896 Meiji-Sanriku tsunami earthquake (*6*, *8*, *9*, *23*). The direction of motion of the Pacific Plate (PA) relative to Honshu [North American Plate, NAM (*28*)] is shown. The red line shows the approximate orientation of the in-line seismic profile HD33B (*29*). DSDP indicates Deep Sea Drilling Project. (**B**) A portion of the in-line seismic profile (HD33B) showing the location of the boreholes, frontal prism and trench, the normal-faulted basal pelagic sediments and oceanic basalt, and the interpreted location of the plate-boundary fault and associated faults in the sediments. mbsl, meters below sea level; V.E., vertical exaggeration. (**C**) Seismic data show the presence of a faint but continuous reflector, interpreted as the plate-boundary fault [see also (*11*)] identified in the drill hole, that continues eastward above the top of the basement of the horst and cuts down into the sediment fill of the graben of the trench.

(*14*) (Fig. 1). We therefore identified the top of the plate-boundary fault at the contact between the inclined bedding of the deformed prism and the flat-lying basal sediments of the subducting plate at ~820 mbsf (Fig. 2).

The plate-boundary fault zone consists of a layer of brown clay with a unique scaly fabric not seen in any other portion of the core (Fig. 2). About 1 m of the scaly clay unit was recovered in core 17R (343_C0019E-17R-1) from the depth 821.5 to 822.65 mbsf. The contacts between the scaly clay and the bounding sediments were not recovered in cores, but, on the basis of adding the lengths of 17R and neighboring unrecovered sections, the total thickness of the scaly clay layer is less than 4.86 m (Fig. 2).

Log signature, lithology, chemical differences, and the tectonic fabric distinguish the scaly clay of core 17R as unique relative to all other sediments penetrated by the borehole (fig. S3). A greater concentration of K, Al, and Mn in the scaly clay layer relative to other core samples (fig. S3) and a comparison of the scaly clay to the basal reference section at site 436 suggest that the scaly clay is a Paleogene pelagic clay tectonically emplaced to its current position by slip within the fault zone. An increase in number of small shear bands [dark seams and bands (*7*)] and an increase in bulk density toward the scaly clay layer demarcate a ≤10-m-thick zone of fault-related deformation (Fig. 2); resistivity across the fault zone remains fairly constant, suggesting a lack of open fractures (Fig. 2 and fig. S3).

The scaly fabric defines a spaced, anastomosing foliation, dipping 0° to 30° that bounds variably shaped and sized lenses of clay (Fig. 2), similar to scaly fabrics in core recovered from other subduction thrusts (*15*). The scaly surfaces are lustrous and commonly striated, indicating distributed shear across the network of localized surfaces. The spacing of the surfaces is centimeter scale at the base of core 17R but decreases to millimeter scale near the top of the core, reflecting an increase in the magnitude of shear strain toward the upper tectonic contact. The scaly clay is bicolored (reddish-brown and dark brown to black), and the juxtaposition of the two colors of clay highlights a prominent, sharp contact in the upper, highly sheared section (Fig. 2). The contact is slightly wavy at the cm scale with amplitude less than 1 mm and truncates without deflection the foliations that are not parallel across the contact. We infer that this contact records seismic slip, although not necessarily that of the Tohoku-Oki earthquake, because the contact has characteristics similar to surfaces of large, localized slip and to surfaces of seismic rupture in other faults (*16*, *17*). Other surfaces of large, localized slip may lie within or at the boundaries of the scaly-clay layer at depth intervals that were not recovered during

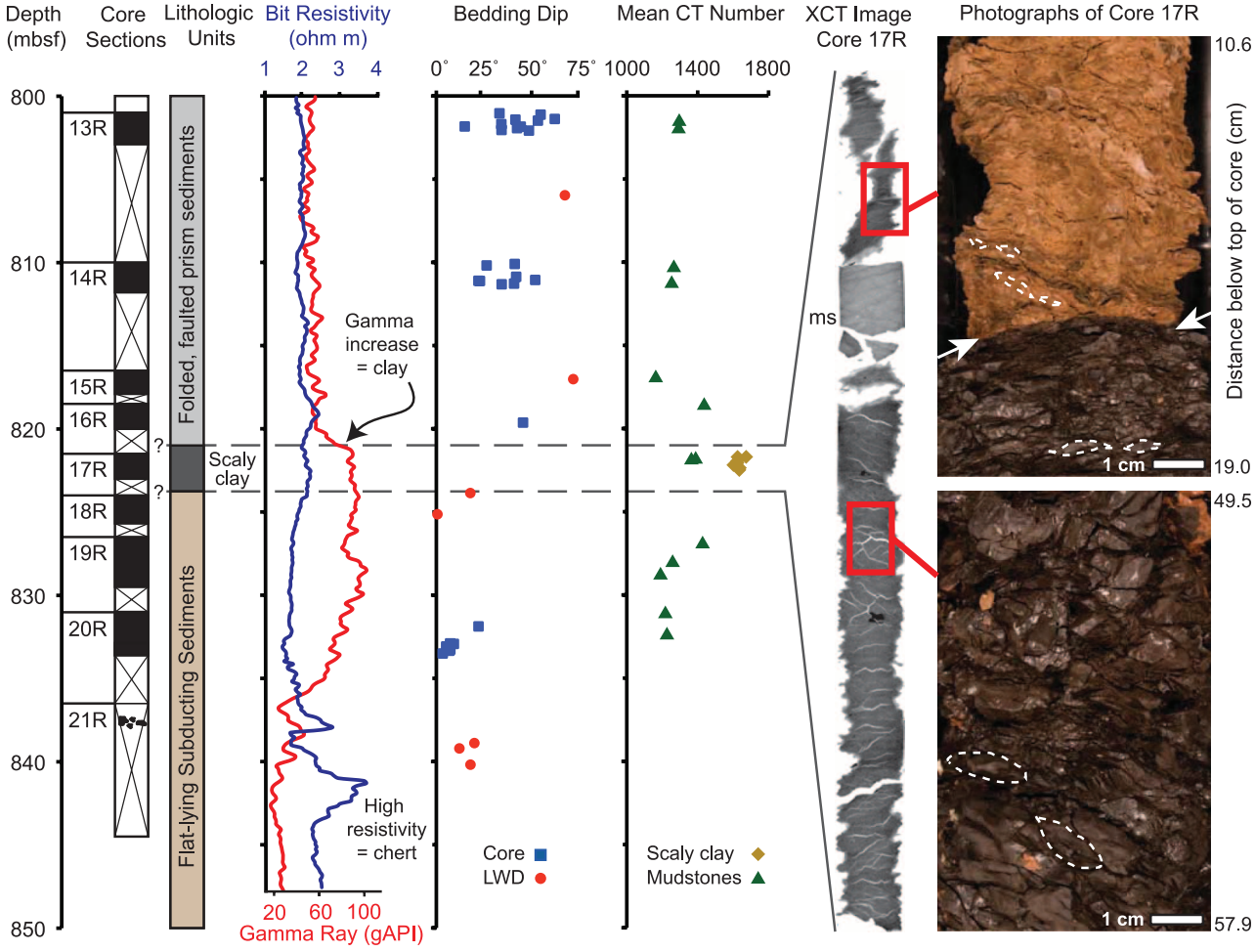

Fig. 2. Logs, core data, and images of the sampled plate-boundary fault zone. Sections of core recovery (black) and no recovery (white) for each cored interval (numbered) shown on left. Other data shown versus depth from the lower prism through the subducting sediments include lithologic units, resistivity (blue curve) and gamma ray (red curve; gAPI, American Petroleum Institute gamma ray units), bedding dip as determined from resistivity images (red circles; LWD, logging while drilling) and measured in core (blue squares), and mean computed tomography (CT) number (a proxy for density) in hanging wall and footwall mudstones (green triangles) and in the scaly clay (yellow diamonds) (*29*). The elevated CT number for the clay relative to that for the deformed mudstones likely reflects both consolidation and chemistry. X-ray CT image and core photos show scaly clay fabric. A few phacoids are outlined to demonstrate fabric scale and orientation (parallel to phacoid long axis). The sharp slip surface between red-brown and dark brown scaly clays with different fabric orientations is indicated with white arrows. Note that curvature of the surface of the core causes some planar features to appear curved.

coring and also would be candidate horizons of the Tohoku-Oki rupture.

The fault zone at the drill site is thinner with more penetrative scaly fabric and with less extensive deformation in adjacent sediments than fault zones observed in previous ocean-drilling and onland studies (*18*, *19*). Accommodation of kilometers of shear displacement in the <5-m-thick scaly clay demonstrates marked long-term slip localization and that the clay layer has been weak relative to the bounding mudstones over the duration of fault activity (*16*, *20*). Indeed, the layer must be weaker than the surrounding sediments during periods of both seismic slip and interseismic creep. This finding is corroborated by direct laboratory measures of sliding friction for samples of the scaly clay at high shear rates (*21*) and of similar clay-rich materials at low shear rates (*22*).

Large slip during most historical earthquakes in the northwest Pacific did not extend close to the trench, but, when it has, there have been devastating consequences from unusually large tsunamis [the 1896 Meiji-Sanriku and 2011 Tohoku-Oki earthquakes (*23*, *24*)]. Similar to the shallow slip zone of the 2011 Tohoku-Oki earthquake, some other subduction zones show evidence that the lithostratigraphy of the incoming plate influences the location and the architecture of the plate-boundary fault [e.g., Barbados (*25*) and Sumatra (*26*)]. The pelagic sediments below the plate-boundary fault at the JFAST drill site are similar to those over much of the northwestern Pacific Plate (*27*). Because the site shares a history and stratigraphy with the rest of the northern Japan Trench, it is possible that the structure and relative mechanical properties observed here may be representative of the subduction thrusts throughout the region.

References and Notes

1. A. Hasegawa, K. Yoshida, T. Okada, *Earth Planets Space* **63**, 703–707 (2011).
2. A. Kato, S. Sakai, K. Obara, *Earth Planets Space* **63**, 745–748 (2011).
3. W. Lin *et al.*, *Science* **339**, 687–690 (2013).
4. T. Fujiwara *et al.*, *Science* **334**, 1240 (2011).
5. Y. Ito *et al.*, *Geophys. Res. Lett.* **38**, L00G05 (2011).
6. Y. Fujii, K. Satake, S. Sakai, M. Shinohara, T. Kanazawa, *Earth Planets Space* **63**, 815–820 (2011).
7. F. M. Chester, J. J. Mori, N. Eguchi, S. Toczko, Expedition 343/343T Scientists, *Proc. IODP*, **343/343T** (2013); available online at http://publications.iodp.org/proceedings/343_343T/343title.htm.
8. C. J. Ammon, T. Lay, H. Kanamori, M. Cleveland, *Earth Planets Space* **63**, 693–696 (2011).
9. K. D. Koper, A. R. Hutko, T. Lay, C. J. Ammon, H. Kanamori, *Earth Planets Space* **63**, 599–602 (2011).
10. S. Kodaira *et al.*, *Nat. Geosci.* **5**, 646–650 (2012).
11. Y. Nakamura, S. Kodaira, S. Miura, C. Regalla, N. Takahashi, *Geophys. Res. Lett.* **40**, 1713–1718 (2013).
12. T. Tsuru *et al.*, *J. Geophys. Res. Solid Earth* **107**, 2357 (2002).
13. P. M. Fulton *et al.*, *Science* **342**, 1214–1217 (2013).
14. Shipboard Scientific Party, *Init. Rep. DSDP* **56 and 57** (Part 1), 399–446 (1980); available online at www.deepseadrilling.org/56_57/volume/dsdp56_57pt1_07.pdf.
15. P. Vannucchi, A. Maltman, G. Bettelli, B. Clennell, *J. Struct. Geol.* **25**, 673–688 (2003).
16. F. M. Chester, J. S. Chester, *Tectonophysics* **295**, 199–221 (1998).
17. A. M. Lin, Z. K. Ren, Y. Kumahara, *J. Struct. Geol.* **32**, 781–791 (2010).
18. C. D. Rowe, J. C. Moore, F. Remitti, IODP Expedition 343/343T Scientists, *Geology* **41**, 991–994 (2013).
19. H. M. Savage, E. E. Brodsky, *J. Geophys. Res.* **116**, B03405 (2011).
20. R. H. Sibson, *Bull. Seismol. Soc. Am.* **93**, 1169–1178 (2003).
21. K. Ujiie *et al.*, *Science* **342**, 1211–1214 (2013).
22. D. A. Lockner, C. Morrow, D. Moore, S. Hickman, *Nature* **472**, 82–85 (2011).
23. Y. Tanioka, K. Satake, *Geophys. Res. Lett.* **23**, 1549–1552 (1996).
24. T. Lay *et al.*, *J. Geophys. Res. Solid Earth* **117**, B04311 (2012).
25. G. Wallace, J. C. Moore, C. G. DiLeonardo, *Geol. Soc. Am. Bull.* **115**, 288–297 (2003).
26. S. M. Dean *et al.*, *Science* **329**, 207–210 (2010).
27. D. R. Horn, B. M. Horn, M. N. Delach, *Geol. Soc. Am.* **126**, 1–22 (1970).
28. C. DeMets, R. G. Gordon, D. F. Argus, *Geophys. J. Int.* **181**, 1–80 (2010).
29. Materials and methods are available as supplementary materials on *Science* Online.

Acknowledgments: This research used samples and data provided by the IODP (www.iodp.org/access-data-and-samples). We thank all drilling and logging operation staff on board the D/V *Chikyu* during expedition 343 and 343T. Part of this work was supported by the U.S. Science Support Program of IODP, and participation by E.B. was funded in part by the Gordon and Betty Moore Foundation. F.M.C., C. Rowe, K.U., C. Regalla, J. Kirkpatrick, F.R., J.C.M., and E.E.B. prepared figures and wrote the manuscript; C. Regalla, J. Kirkpatrick, F.R., V.T., M.W.-S., S.B., and J. Kameda provided structural and lithologic descriptions of core samples; J.J.M., E.E.B., S. Kodaira, F.M.C., P. Fulton, N.E., and S.T. organized and managed the expedition; all expedition scientists contributed to the paper by providing shipboard measurements and scientific discussions.

Supplementary Materials

www.sciencemag.org/content/342/6163/1208/suppl/DC1
Materials and Methods
Supplementary Text
Figs. S1 to S3
References

24 July 2013; accepted 30 October 2013
10.1126/science.1243719

Low Coseismic Shear Stress on the Tohoku-Oki Megathrust Determined from Laboratory Experiments

Kohtaro Ujiie,[1,2]* Hanae Tanaka,[1] Tsubasa Saito,[1] Akito Tsutsumi,[3] James J. Mori,[4] Jun Kameda,[5] Emily E. Brodsky,[6] Frederick M. Chester,[7] Nobuhisa Eguchi,[8] Sean Toczko,[8] Expedition 343 and 343T Scientists†

Large coseismic slip was thought to be unlikely to occur on the shallow portions of plate-boundary thrusts, but the 11 March 2011 Tohoku-Oki earthquake [moment magnitude (M_w) = 9.0] produced huge displacements of ~50 meters near the Japan Trench with a resultant devastating tsunami. To investigate the mechanisms of the very large fault movements, we conducted high-velocity (1.3 meters per second) friction experiments on samples retrieved from the plate-boundary thrust associated with the earthquake. The results show a small stress drop with very low peak and steady-state shear stress. The very low shear stress can be attributed to the abundance of weak clay (smectite) and thermal pressurization effects, which can facilitate fault slip. This behavior provides an explanation for the huge shallow slip that occurred during the earthquake.

Megathrust earthquakes commonly occur in subduction zones at depths where there is strong locking between the plates and long-term strain accumulation (*1*, *2*). In general, unconsolidated, soft sediments in the shallow region of the plate-boundary thrust (décollement) were thought to slip aseismically and have low levels of locking (*3*). The widely accepted view was that rupture during large earthquakes was unlikely to produce large slip on the shallow décollement (*1*–*3*). However, the coseismic fault slip extended all the way to the trench axis during the 11 March 2011 Tohoku-Oki earthquake [moment magnitude (M_w) = 9.0] with very large slip (~50 m), resulting in the huge tsunami that devastated much of the east coast of northern Honshu, Japan (*4*–*8*).

The Integrated Ocean Drilling Program (IODP) Expedition 343 and 343T, Japan Trench Fast Drilling Project (JFAST), provided an invaluable opportunity to investigate the plate-boundary décollement near the Japan Trench (*9*). JFAST successfully drilled the décollement at ~820 m

[1]Graduate School of Life and Environmental Sciences, University of Tsukuba, Tsukuba, Japan. [2]Institute for Research on Earth Evolution, Japan Agency for Marine-Earth Science and Technology, Yokosuka, Japan. [3]Graduate School of Science, Kyoto University, Kyoto, Japan. [4]Disaster Prevention Research Institute, Kyoto University, Kyoto, Japan. [5]Department of Natural History Sciences, Hokkaido University, Sapporo, Japan. [6]Department of Earth and Planetary Sciences, University of California Santa Cruz, Santa Cruz, CA 95060, USA. [7]Center for Tectonophysics, Department of Geology and Geophysics, Texas A&M University, College Station, TX 77843–3115, USA. [8]Center for Deep Earth Exploration, Japan Agency for Marine-Earth Science and Technology, Yokohama, Japan.

*Corresponding author. E-mail: kujiie@geol.tsukuba.ac.jp
†Expedition 343 and 343T Scientists authors and affiliations are listed in the supplementary materials.

below the sea floor (mbsf) in water depths of ~6900 m at site C0019, located at the toe of the frontal prism in the area of large shallow slip during the 2011 earthquake. The décollement mostly consists of highly sheared clays that are marked by polished and striated surfaces wrapping around more intact lenses. The sheared clays are red-brown and dark brown to black in color and are similar to pelagic clays deposited on the incoming Pacific Plate (*10*, *11*). Summing the unrecovered intervals with the actual core recovery of highly deformed material constrains the total thickness of the décollement interval to be less than 4.86 m. The total thickness of the décollement-related damage zone is ≤10 m, including both overlying frontal prism material and underlying subducted sediments. The drilling results at site C0019 clarified that plate-boundary faulting in this region is highly localized in pelagic clay (*10*).

To determine frictional properties that control the earthquake slip, we used a rotary shear apparatus capable of high velocity and large slip to conduct laboratory tests on the décollement material taken from site C0019 (*12*). The recovered décollement material may not include the principal slip surface of the Tohoku-Oki earthquake, but it is the host material of the earthquake slip zone, and therefore studying its frictional behavior at high slip rates helps us understand the obersved large coseismic slip. Experimental parameters were set at an equivalent slip rate of 1.3 m s^{-1}, normal stresses of ~2.0 MPa, and displacements of ~15 to 60 m, which are comparable to the conditions of fault slip during the earthquake. We also simulated permeable and impermeable conditions during high-velocity shearing because permeability is an important factor in controlling frictional behavior. The actual fault conditions during the earthquake could be partially drained and thus lie between these two end-member cases.

The measurements of shear stress at a normal stress of 2.0 MPa showed an initial peak during slip of less than 1-m displacement, then quickly dropped to steady-state values of ~0.4 and ~0.2 MPa for the permeable and impermeable cases, respectively (Fig. 1, A and B). Compared with the permeable tests, the impermeable tests show lower values of shear stress (Fig. 1C) (*12*). For the same amount of displacement, the calculated temperature in the gouge is always smaller for the impermeable tests compared with the permeable tests, likely because thermal expansion of pore fluids raises the local fluid pressure in the sheared gouge and thus decreases the effective normal stress. The axial displacement data indicate that the section of rock specimen-gouge compacted and then dilated for both the permeable and impermeable tests. There is more compaction in the permeable tests relative to the impermeable tests, consistent with an easier escape of water from the gouge to the specimen (permeable Berea sandstone). The initial compaction during impermeable tests may be due to the development of foliated zones in the gouge (Fig. 2C). For permeable tests, the dilation occurs in association with the thermal expansion of quartz grains in the sandstone that is noteworthy at temperatures of 500° to 573°C (*13*). For the impermeable tests, thermal expansion of quartz grains is unlikely to occur because of the smaller temperature rise in the gouge and a smaller fraction of quartz in the specimen (Indian gabbro); therefore, the dilation is attributed to thermal expansion of pore fluid in the gouge material itself. These experimental results indicate that for impermeable conditions, the gouge material of the shallow décollement can be weakened due to effective thermal pressurization (*14*–*16*).

For permeable tests, there is a dependence of shear stress on normal stress (Fig. 1C). For the impermeable tests, the shear stress at the peak and steady state is weakly dependent and independent of normal stress, respectively. We extrapolate the relations between the steady-state shear stress and normal stress under permeable and impermeable cases (equations in Fig. 1C) to the effective normal stress at a depth of 820 mbsf on the décollement at site C0019 (7 MPa) (*17*). This yields values of shear stress for the in situ condition under permeable and impermeable cases of 1.32 and 0.22 MPa, respectively, which correspond to values for the in situ apparent coefficient of friction under permeable and impermeable conditions of 0.19 and 0.03, respectively. JFAST installed temperature sensors across the fault zone to estimate the frictional heat associated with the huge shallow slip during the 2011 Tohoku-Oki earthquake. The slip-averaged shear stress and

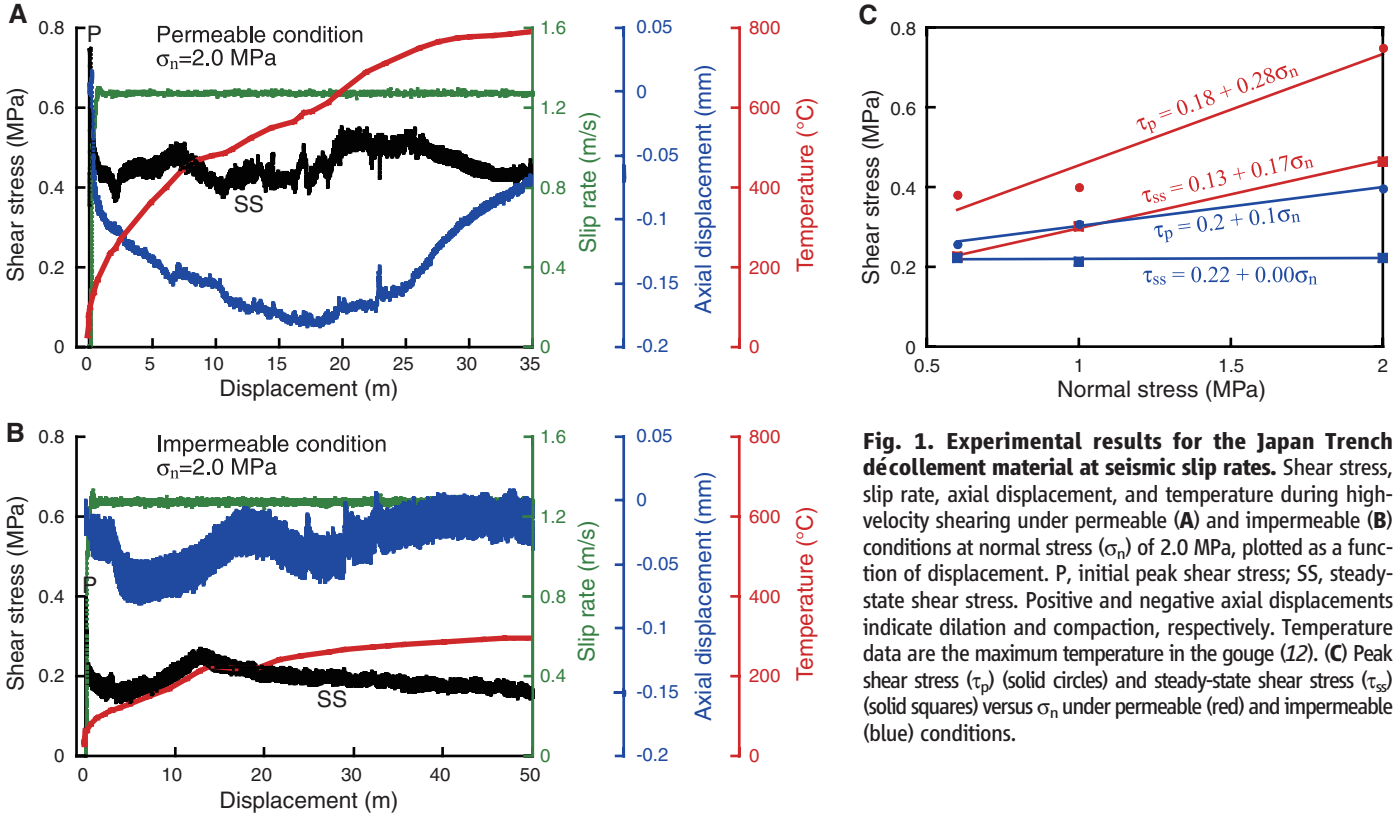

Fig. 1. Experimental results for the Japan Trench décollement material at seismic slip rates. Shear stress, slip rate, axial displacement, and temperature during high-velocity shearing under permeable (**A**) and impermeable (**B**) conditions at normal stress (σ_n) of 2.0 MPa, plotted as a function of displacement. P, initial peak shear stress; SS, steady-state shear stress. Positive and negative axial displacements indicate dilation and compaction, respectively. Temperature data are the maximum temperature in the gouge (*12*). (**C**) Peak shear stress (τ_p) (solid circles) and steady-state shear stress (τ_{ss}) (solid squares) versus σ_n under permeable (red) and impermeable (blue) conditions.

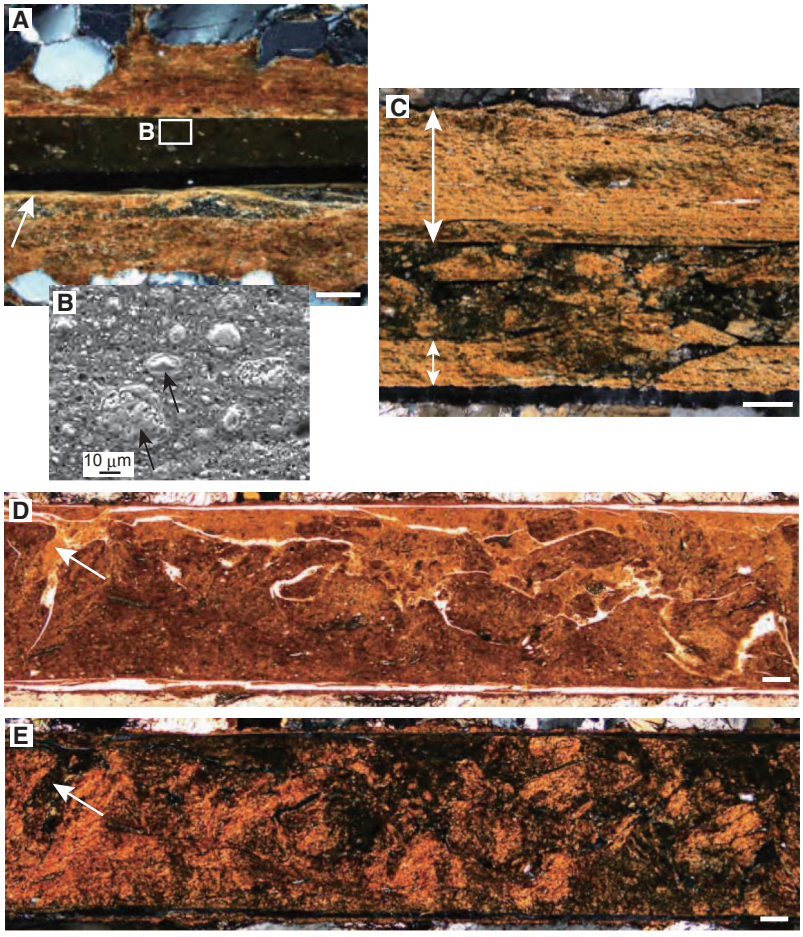

Fig. 2. Microstructures of experimental samples. (**A**) Microstructures after testing under permeable conditions under cross-polarized light. The white arrow indicates the zone of foliated clay. (**B**) Scanning electron microscope back-scattered image showing random orientation of clay-clast aggregates (black arrows) in the matrix. Location of the image is shown in (A). (**C** to **E**) Microstructures after tests under impermeable conditions. (C) Two foliated zones (double white arrows) are apparent in the gouge under cross-polarized light. A portion of the lower foliated zone is just incorporated into the matrix (the middle-lower part of the photograph). (D) Injection structures (white arrow) and fragmentation of clays, suggesting the mobilization of the gouge material due to fluidization, under plane-polarized light. (E) Same as in (D) under cross-polarized light. All microstructural features in this figure are absent in the gouge before high-velocity shearing. White scale bars, 0.1 mm.

the apparent coefficient of friction estimated from the temperature anomaly at the plate-boundary thrust are 0.54 MPa and 0.08, respectively (*17*). Comparisons of these values show that the frictional level estimated from the fault-zone temperature measurements is intermediate between the permeable and impermeable laboratory results on the fault gouge, but closer to the impermeable condition. It is likely that the Tohoku earthquake faulting occurred under only weakly drained or impermeable conditions.

After the experiments, we examined microstructures of the gouge. Thin sections cut tangential to the outer rims of the specimen assembly (2.5 mm from the cylinder boundary and 33 mm from the upper and lower boundaries of the rock specimen) show clay foliations parallel to gouge boundaries and random orientation of fragments in the matrix (Fig. 2). The thickness of the gouge layer before high-velocity shearing is 0.8 mm. Following the permeable experiments, some fragments in the gouge matrix are defined by quartz or feldspar grains surrounded by a cortex of concentric clays (Fig. 2B). These spherical aggregates resemble clay-clast aggregates, which are seen after dry (room humidity) frictional experiments on clay-rich gouges (*18*–*20*). The clay-clast aggregates may form as the water escapes from the gouge during permeable experiments. Following the impermeable experiments, the foliated zones in the gouge are incorporated into the extremely fine-grained matrix in some places (Fig. 2C). In other places, injection of extremely fined-grained material and mixing of materials of different colors without shear surfaces are observed (Fig. 2, D and E). These deformation features and temporal relation of microstructures show that the slip along the foliated zone was followed by fluidization (a phenomenon by which gouge materials in suspension move with a mean free path like that of gas molecules, which is favored by low effective normal stress). The microstructures of the fluidized gouge and the independence of steady-state shear stress on normal stress under the impermeable condition are compelling indications

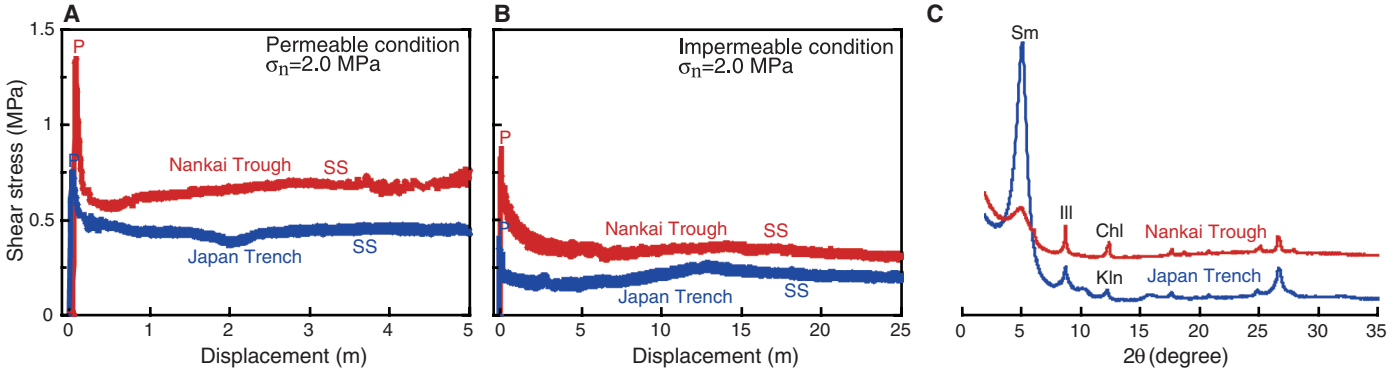

Fig. 3. Comparison of experimental results for décollement materials of the Japan Trench and the Nankai Trough. Shear stress measured during high-velocity shearing under permeable (**A**) and impermeable (**B**) conditions at σ_n of 2.0 MPa, plotted as a function of displacement. P, initial peak shear stress; SS, steady-state shear stress. (**C**) X-ray diffraction patterns for the décollement materials from the Japan Trench and the Nankai Trough, obtained for the <2-μm fractions in the ethylene-glycoled state. Sm, smectite; Ill, illite; Chl, chlorite; Kln, kaolinite.

of thermal pressurization of pore fluid and that the gouge behaved like a fluid during high-velocity shearing.

Our experiments show that the Japan Trench décollement material behaves in a manner that promotes further large displacement once high-velocity slip initiates, predominately due to very low shear stress. To understand if this is similar to the behavior of material from other subduction zones, we also performed high-velocity friction experiments on décollement materials for the Nankai Trough (*12*). Like materials from the Japan Trench, the Nankai Trough materials also exhibit lower shear stress in the experiments under impermeable conditions than in those under permeable conditions, consistent with the idea that low-permeability conditions better contain pore fluid so that thermal pressurization occurs more effectively (Fig. 3, A and B). However, when we compare the data obtained under the same experimental conditions for the two different regions, the décollement material from the Japan Trench has overall lower shear stress from peak to steady-state conditions than the material from the Nankai Trough.

The clay content and clay mineralogy of the fault-zone material differs between the Japan Trench and the Nankai Trough (Fig. 3C) (*12*). The décollement of the Nankai Trough developed in the hemipelagic mudstone (*21*), whereas that of the Japan Trench is localized in pelagic clays (*10*). The total clay content in the Nankai décollement is estimated to be 65% (*21*), compared with 85% for the Japan Trench décollement. The smectite content in the Nankai Trough and Japan Trench décollements is 31 and 78% of the total mineralogy, respectively (*12*). Smectite is known as one of the lowest-friction minerals (*22*, *23*). The abundance of smectite means that large slip on the shallow plate-boundary thrust of the Japan Trench can occur more easily than for the Nankai Trough.

Our results indicate that large slip resulted from coseismic weakening of the fault due to the abundance of smectite and thermal pressurization. Seismic slip could be promoted even in unstrained portions at shallow depths, as the slip propagates through the smectite-rich fault material under fluid-saturated, impermeable conditions. Similar pelagic clay is widely distributed on the ocean floor, and plate-boundary décollements have developed in these smectite-rich sediment layers at several subduction zones (*24*, *25*). Such regions also have the potential for very large coseismic displacements on shallow faults, which could generate very large tsunamis similar to the 2011 Tohoku-Oki earthquake.

References and Notes

1. S. L. Bilek, T. Lay, *Geophys. Res. Lett.* **29**, 18-1–18-4 (2002).
2. J. C. Moore, D. Saffer, *Geology* **29**, 183–186 (2001).
3. K. Wang, Y. Hu, *J. Geophys. Res.* **111**, B06410 (2006).
4. S. Ide, A. Baltay, G. C. Beroza, *Science* **332**, 1426–1429 (2011).
5. Y. Ito *et al.*, *Geophys. Res. Lett.* **38**, L00G05 (2011).
6. T. Fujiwara *et al.*, *Science* **334**, 1240 (2011).
7. S. Kodaira *et al.*, *Nat. Geosci.* **5**, 646–650 (2012).
8. Y. Fujii, K. Satake, S. Sakai, M. Shinohara, T. Kanazawa, *Earth Planets Space* **63**, 815–820 (2011).
9. J. Mori, F. M. Chester, N. Eguchi, S. Toczko, *IODP Sci. Prosp.* 343 10.2204/iodp.sp.343.2012 (2012).
10. F. M. Chester *et al.*, *Science* **342**, 1208–1211 (2013).
11. Shipboard Scientific Party, Site 436: Japan Trench outer rise, Leg 56. Vol. 56, 57 (Pt. 1) (1980).
12. Material and methods are available as supplementary materials on *Science* Online.
13. B. J. Skinner, *Geol. Soc. Am.* **97**, 75–96 (1966).
14. R. H. Sibson, *Nature* **243**, 66–68 (1973).
15. C. W. Mase, L. Smith, *J. Geophys. Res.* **92**, 6249–6272 (1987).
16. J. R. Rice, *J. Geophys. Res.* **111**, B05311 (2006).
17. P. M. Fulton *et al.*, *Science* **342**, 1214–1217 (2013).
18. S. Boutareaud *et al.*, *Geophys. Res. Lett.* **35**, L05302 (2008).
19. K. Ujiie, A. Tsutsumi, *Geophys. Res. Lett.* **37**, L24310 (2010).
20. F. Ferri *et al.*, *J. Geophys. Res.* **116**, B09208 (2011).
21. M. Kinoshita *et al.*, in *Proceedings of the Integrated Ocean Drilling Program* (IODP, Tokyo, 2009), vol. 314/315/316; 10.2204/iodp.proc.314315316.133.2009.
22. J. D. Byerlee, *Pure Appl. Geophys.* **116**, 615–626 (1978).
23. M. J. Ikari, D. M. Saffer, C. Marone, *J. Geophys. Res.* **114**, B05409 (2009).
24. A. Maltman, P. Labaume, B. Housen, *Proc. Ocean Drill. Program Sci. Rep.* **156**, 279–292 (1997).
25. H. Tobin, P. Vannucchi, M. Meschede, *Geology* **29**, 907–910 (2001).

Acknowledgments: For this research, we used samples and data provided by the IODP (www.iodp.org/access-data-and-samples). We thank all drilling and logging operation staff on board the *D/V Chikyu* during Expedition 343 and 343T. We acknowledge two anonymous reviewers for their thoughtful reviews. Part of this work was supported by the U.S. Science Support Program of IODP. K.U. was supported by grant 21107005 (Ministry of Education, Culture, Sports, Science and Technology of Japan). E.E.B was supported by the Gordon and Betty Moore Foundation.

Supplementary Materials

www.sciencemag.org/content/342/6163/1211/suppl/DC1
Materials and Methods
Supplementary Text
Figs. S1 to S5
Tables S1 and S2
References (*26*–*30*)

19 July 2013; accepted 30 October 2013
10.1126/science.1243485

Low Coseismic Friction on the Tohoku-Oki Fault Determined from Temperature Measurements

P. M. Fulton,[1]* E. E. Brodsky,[1] Y. Kano,[2] J. Mori,[2] F. Chester,[3] T. Ishikawa,[4] R. N. Harris,[5] W. Lin,[4] N. Eguchi,[6] S. Toczko,[6] Expedition 343, 343T, and KR13-08 Scientists†

The frictional resistance on a fault during slip controls earthquake dynamics. Friction dissipates heat during an earthquake; therefore, the fault temperature after an earthquake provides insight into the level of friction. The Japan Trench Fast Drilling Project (Integrated Ocean Drilling Program Expedition 343 and 343T) installed a borehole temperature observatory 16 months after the March 2011 moment magnitude 9.0 Tohoku-Oki earthquake across the fault where slip was ~50 meters near the trench. After 9 months of operation, the complete sensor string was recovered. A 0.31°C temperature anomaly at the plate boundary fault corresponds to 27 megajoules per square meter of dissipated energy during the earthquake. The resulting apparent friction coefficient of 0.08 is considerably smaller than static values for most rocks.

Earthquake rupture propagation and slip are moderated by the dynamic shear resistance on the fault. Any complete model of earthquake growth therefore requires quantification of shear stress, which is difficult to measure. Historically, the shear stress during an earthquake was thought to nearly equal that controlled by static friction, but recent laboratory experiments and field observations have brought this assumption into question (*1*, *2*). Direct measurement of the magnitude of earthquake stress is challenging because seismological measurements only record stress changes.

Rapid-response drilling provides a solution (*3*). Because the frictional stress during slip results in dissipated heat, subsurface temperature measurements soon after a major earthquake can record the temperature increase over the fault and its decay. If the slip on the fault is known, the thermal observations allow one to infer the frictional shear stress (*4*, *5*). On 15 July 2012, as part of the Japan Trench Fast Drilling Project (JFAST) [Integrated Ocean Drilling Program (IODP) Expedition 343 and 343T], we installed a sub–sea-floor temperature observatory in the

[1]Department of Earth and Planetary Sciences, University of California, Santa Cruz, CA, USA. [2]Disaster Prevention Research Institute, Kyoto University, Kyoto, Japan. [3]Center for Tectonophysics, Department of Geology and Geophysics, Texas A&M University, College Station, TX, USA. [4]Kochi Institute for Core Sample Research, Japan Agency for Marine-Earth Science and Technology, Kochi, Japan. [5]Oregon State University, Corvallis, OR, USA. [6]Center for Deep Earth Exploration, Japan Agency for Marine-Earth Science and Technology, Yokohama, Japan.

*Corresponding author. E-mail: pfulton@ucsc.edu
†Expedition 343, 343T, and KR13-08 Scientists authors and affiliations are listed in the supplementary materials.

Japan Trench through the plate boundary fault zone (Hole C0019D) (Fig. 1), which was identified through logging and coring in two adjacent boreholes ~30 m away along strike (Holes C0019B and C0019E, respectively) (supplementary text) (*6*). The deep-sea drilling vessel *Chikyu* developed procedures to allow drilling and installation of the observatory at the requisite 6900-m water depth, making it the deepest open-ocean borehole observatory. The observatory consisted of a string of 55 temperature-sensing data loggers with ~0.001°C accuracy that extended beneath the sea floor in a fully cased 4.5-inch-inner-diameter borehole (Fig. 1). Ten of the instruments also recorded pressure at <1 kPa accuracy to provide control on sensor depths.

On 26 April 2013, the Japan Agency for Marine-Earth Science and Technology deep-sea research vessel (R/V) *Kairei* recovered the observatory sensor string with the remotely operated vehicle *Kaiko7000II*. All 55 sensors and the sinker bar were recovered from a maximum depth of 820.6 m below sea floor (mbsf). The water depth of the observatory is ~8 m deeper than the adjacent coring and logging holes, and thus the fault depth relative to the sea floor is expected to be shallower than observed in logging and coring. The successful recovery implies that there was negligible afterslip or distributed deformation in the borehole 16 to 25 months after the mainshock.

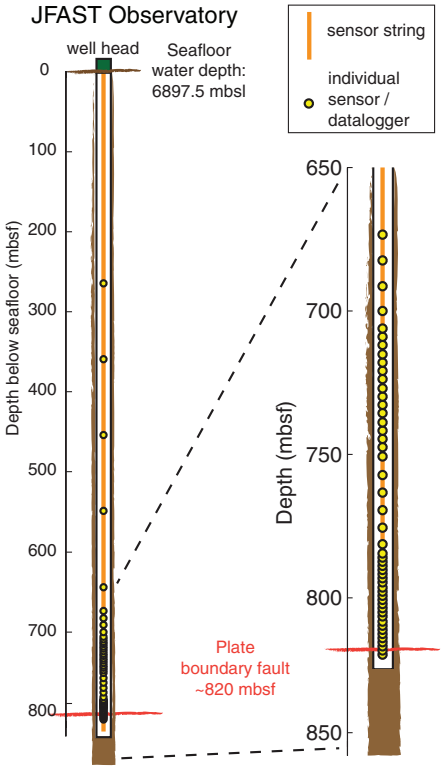

Fig. 1. Observatory configuration. The observatory sensor string of 55 temperature-sensing data loggers attached to a rope was installed within 4.5-inch steel casing that is open at the sea floor and has a check-valve at the bottom preventing inflow of fluid.

The temperature data reveal a background geothermal gradient of 26.29° ± 0.13°C km^{-1} within the region of 650 to 750 mbsf, resulting in a vertical heat flow value of 30.50 ± 2.52 mW m^{-2} when combined with thermal conductivity of 1.16 ± 0.09 W m^{-1} $°C^{-1}$ over this interval (supplementary methods). The temperature from 812 m to the bottom at 820 m is elevated by as much as 0.31°C relative to this background gradient (Fig. 2). This is the largest temperature anomaly within the data set and centered on 819 mbsf at the stratigraphic level estimated for the décollement fault zone (*6*, *7*).

We interpret the temperature anomaly as the frictional heat from the 2011 Tohoku-Oki earthquake. This signal is larger than previous rapid-response measurements of frictional heat across a fault after an earthquake (*4*, *5*) and is temporally resolved so that its transient nature is distinguished. The temperature data record the combination of the background geotherm, the decaying signature of frictional heating during the 2011 Tohoku-Oki earthquake, and transient effects caused by drilling the borehole and hydrologic processes. Low temperatures relative to the background geotherm early in the experiment (Fig. 2) reflect the effects of water circulation during drilling and equilibration of the observatory upon installation. Because this drilling disturbance acts as a line source compared to the plane or slab source from frictional heating on the fault, its characteristic diffusion time is much shorter, allowing measurement of the frictional heat during the 9-month observatory experiment (*8*, *9*) (supplementary text).

To connect the temperature data to the stress on the fault during slip, we modeled the combined effects of the drilling disturbance and frictional heating on the evolution of the temperature field over time and find the energy during the earthquake dissipated as heat that maximizes the normalized cross-correlation between simulations and data (supplementary text and Fig. 3). Parameter values are constrained by independent drilling and material properties data (supplementary text and table S1).

From an inversion exploring a wide range of depths, the preferred location of the frictional boundary is 821.3 mbsf, which is 7718.8 m below mean sea level [7717.8 to 7719.6 mbsl, 90% confidence interval (CI); supplementary text and table S2]. The inversion places the fault below the deepest data logger because the width of the predicted temperature anomaly requires extension to depth for the homogeneous thermal properties used here. However, the peak of the temperature anomaly appears to be above the deepest temperature sensor in the data of Fig. 2, and the width of the anomaly may be governed by a thermal property structure not included in our model. If we constrain the inversion to require the fault to lie near the peak in temperature above the deepest sensor, the preferred location is 819.8 mbsf (7717.3 mbsl). In either case, the inferred depth of the fault in the observatory hole from the frictional heat is above the hard chert as inferred from the rate of penetration during drilling. The fault inferred from the temperature data is at the same stratigraphic level as the plate boundary fault found in the neighboring coring and logging holes (*6*, *7*).

The depth-constrained inversion results in an overlapping range of 27 MJ m^{-2} (19 to 51 MJ m^{-2}, 90% CI) of dissipated frictional heat energy during the earthquake along the plate boundary (Fig. 3). The unconstrained inversion of the temperature observations indicates 31 MJ m^{-2} (20 to 69 MJ m^{-2}, 90% CI) (figs. S4 to S6). In both cases, the dissipated energy in this region of highest slip along the trench (*10*) is comparable to the spatially averaged radiated energy from the earthquake of 6 to 17 MJ m^{-2} (*11*, *12*) (supplementary text).

Alternative interpretations for a positive temperature anomaly around a fault include the effects of locally reduced thermal conductivity or advection of heat by fluid flow up a permeable fault zone. The magnitude and scale of the observed anomaly, however, are unlikely to be the result of thermal-conductivity differences; the high thermal gradient within the ~20 m zone would require a thermal conductivity of 0.73 W m^{-1} $°C^{-1}$, in contrast to values of 1.14 ± 0.07 W m^{-1} $°C^{-1}$ measured on core samples from comparable intervals in hole C0019E. Rather than a large decrease at the fault zone, measurements throughout the hanging wall and footwall intervals covered by the sensors reveal relatively uniform values before a sharp increase to 1.40 ± 0.19 W m^{-1} $°C^{-1}$ within chert beneath the sensor string at >829 mbsf (fig. S2). Assuming similar composition, a value of 0.73 W m^{-1} $°C^{-1}$ would require a bulk porosity of ~80 to 86%. Even if the fault zone is dominated by fractures, such large porosities over tens of meters are unlikely and not supported by logging data or cores recovered from adjacent boreholes.

Fluid flow up a fault conduit may also result in a positive temperature anomaly, as is observed at 784 mbsf (Fig. 2). Generalized models of the effects of fluid flow on a frictional heat signal after an earthquake have shown that large flow velocities resulting from a combination of high permeabilities (>10^{-14} m^2) and driving overpressures are required (*9*). High permeability around 784 mbsf is indicated by resistivity logs and prolonged drilling anomaly decay time (*13*) (fig. S9). Zones of high permeability, most susceptible to the transient drilling disturbance, are also inferred around 765, 800, and 810 mbsf.

None of these indications of high permeability are present at the depth of the inferred slip zone of ~820 mbsf, and additional pore fluid chemistry data confirm that little fluid flow occurs along the plate boundary (supplementary text and fig. S9). The sudden cooling of the anomaly at 784 mbsf after a large local earthquake on 7 December 2012, and the corresponding heating of a high-permeability zone at 763 mbsf, are consistent with the upward propagation of

a fluid pulse driven by either direct stresses or permeability-altering effects of the December 2012 earthquake that changed the preferred flow path for fluids (*14*, *15*). This interpretation is consistent with borehole images in the interval that show steeply dipping structures conducive to vertical migration of fluids (*13*). Spatially correlated temperature variations within these permeable zones during times of suspected advective fluid flow are suggestive of episodic fluctuations in flow velocity. Such large variations are not observed within the décollement. At 784 mbsf, the standard deviation of roughly daily-to-weekly variability is 100% greater than within the décollement before the December earthquake, and at 763 mbsf it is 60% greater after the earthquake (supplementary text).

The time after the earthquake in which the temperature observations were made is many times as large as the characteristic diffusion time across the slip zone for reasonable estimates of

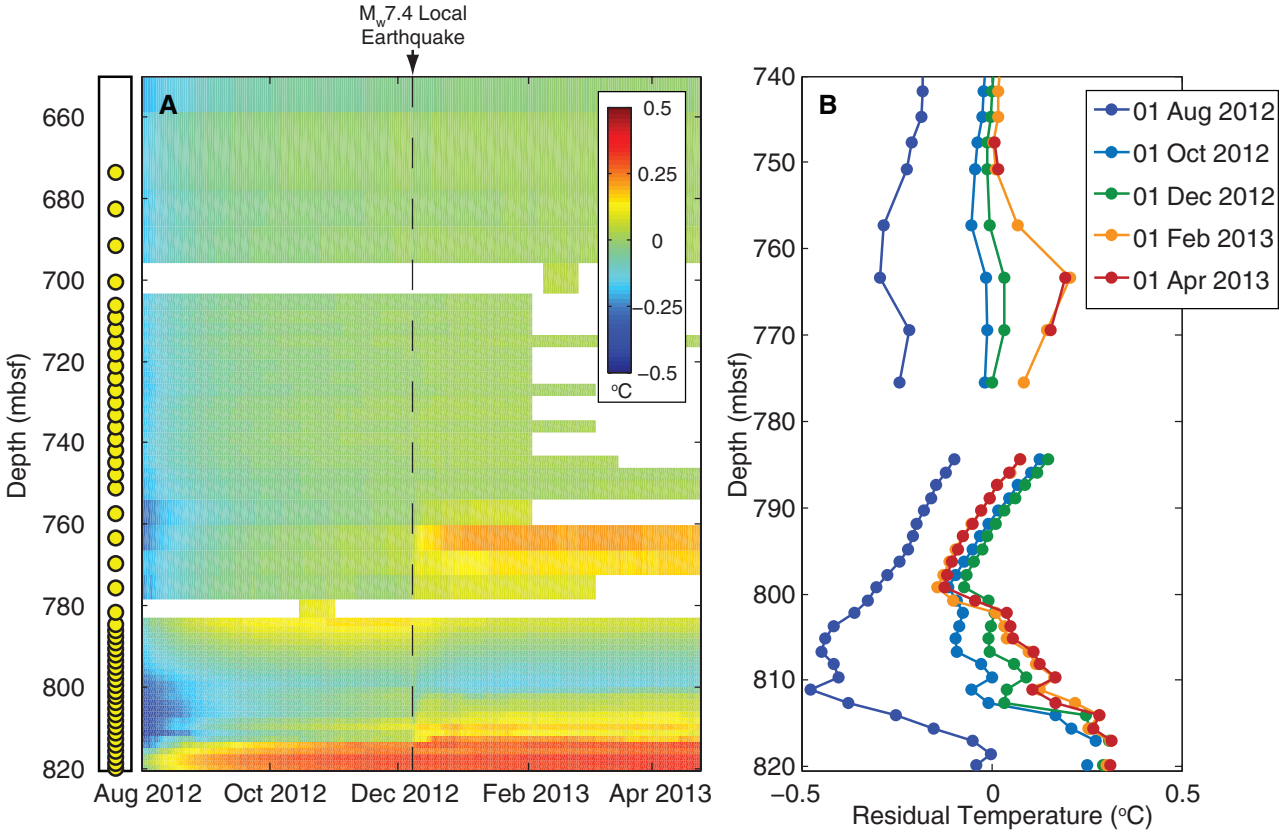

Fig. 2. Sub–sea-floor residual temperature field. (**A**) Time-space map of data >650 mbsf. Yellow dots show sensor positions, and each row represents the corresponding sensor's data. Each column is the daily average temperature after an average background geotherm is removed (supplementary text). A local moment magnitude (M_w) = 7.4 earthquake occurred 17:18:30 Japan Standard Time on 7 December 2012 (dashed line). The second deepest sensor (818.51 mbsf) failed on 22 September 2012; subsequent data in that row are interpolated from sensors 1.5 m above and below. Periods of no data collection are otherwise shown by white. Sensors at 700 and 781 mbsf were programmed to only record for ~2.5-week periods at 1-Hz sampling rate. Data including five broadly spaced shallower depths are included in fig. S1. (**B**) Depth profiles of residual temperature (i.e., with background geotherm removed) from five dates through the experiment separated by 2-month intervals. The times correspond to the vertical tick marks in Fig. 2A. The *y* axis is expanded compared to that in (A) showing data from >740 mbsf. Relatively cool temperatures in August reflect the effects of drilling disturbance.

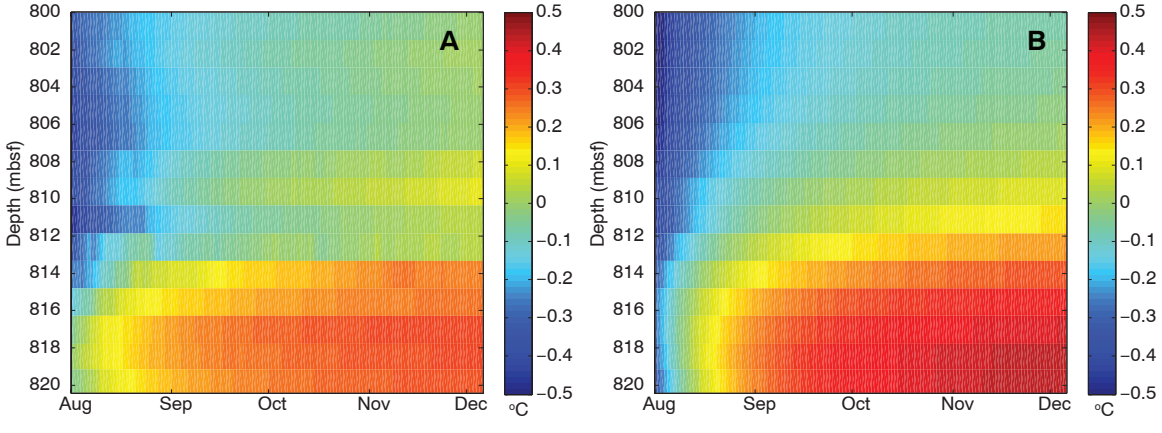

Fig. 3. Time-space map of residual temperature near inferred slip zones. (**A**) A magnified view of Fig. 2A showing the residual temperature anomaly near the plate boundary from 1 August to 6 December 2012. (**B**) Simulated residual temperature from model inversions in which fault depth is constrained. Similar results from an inversion in which fault depth is unconstrained are shown in fig. S4.

slip zone thickness. Therefore, the measurable temperature anomaly from frictional heating is independent of the slip zone thickness and slip duration and does not directly constrain these parameters (supplementary text). However, by assuming a slip duration ≥50 s and slip zone thickness ≥1 mm, we estimate the maximum peak temperature within the slip zone at this location to be <1250°C (supplementary methods) (fig. S7).

The geotherm itself also provides a constraint on the long-term integrated energy dissipated on the fault zone (*16*, *17*). The conductive vertical heat flux of 30.50 ± 2.52 mW m^{-2} measured here is consistent with subduction thermal models with very little or no long-term displacement-averaged dissipated energy in the form of heat along the plate boundary (*17*).

The dissipated energy is the earthquake parameter best constrained by the temperature data; however, laboratory experiments and theoretical models are often based on the coefficient of friction. For a total of 50 m of slip on the fault (*10*), our best estimate of 27 MJ m^{-2} of local dissipated energy during the earthquake implies an average shear stress of 0.54 MPa. To compare our results to other studies, we assume an effective normal stress of 7 MPa based on the fault's depth, hydrostatic pore pressure, and measured rock densities, to infer the equivalent coseismic coefficient of friction (supplementary text). The resultant apparent coefficient of friction is 0.08. The result is "apparent" because the effective normal stress is inferred from estimates of pore pressure and fault dip (supplementary text). The very low values of shear stress and apparent coefficient of friction, which represent displacement averages during the earthquake, are consistent with values determined from high-velocity (1.3 m s^{-1}) friction experiments on the Japan Trench plate boundary fault material (*18*).

An average shear stress during slip of 0.54 MPa and apparent coefficient of friction of 0.08, as constrained by a measured frictional heat anomaly ~1.5 years after the Tohoku-Oki earthquake, suggest that either friction on the fault is remarkably low throughout the seismic cycle or that there was near total stress release at the JFAST location (*19*, *20*). This very low shear resistance during slip may help explain the large slip at shallow depths that contributed to the large devastating tsunami.

References and Notes

1. J. Byerlee, *Pure Appl. Geophys.* **116**, 615–626 (1978).
2. G. Di Toro *et al.*, *Nature* **471**, 494–498 (2011).
3. E. E. Brodsky, K.-F. Ma, J. Mori, D. M. Saffer, *Sci. Drill.* 10.2204/iodp.sd.8.11.2009 (2009).
4. Y. Kano *et al.*, *Geophys. Res. Lett.* **33**, L14306 (2006).
5. H. Tanaka *et al.*, *Geophys. Res. Lett.* **33**, L16316 (2006).
6. F. M. Chester *et al.*, *Science* **342**, 1208–1211 (2013).
7. The depth interval from which a 1.15-m core of scaly-clay, identified as the fault zone in (*6*), extends from 7709.5 to 7714.3 mbsl in the coring hole 30 m away. In the logging hole, the fault is interpreted at 7709.5 to 7711.5 mbsl, 15 to 17 m above a decrease in rate of penetration associated with entering a hard chert layer at 7726.5 mbsl. A similar decrease in rate of penetration in the observatory hole is observed at 7727.5 mbsl. All depth correlations between holes contain an estimated several meters of uncertainty due to fluctuations of the ship's absolute elevation, flexure of the 7 km of drill stand, borehole deviation, layer-thickness variations, and fault dip.
8. E. Bullard, *Geophys. J. Int.* **5**, 127–130 (1947).
9. P. M. Fulton, R. N. Harris, D. M. Saffer, E. E. Brodsky, *J. Geophys. Res.* **115**, B09402 (2010).
10. T. Fujiwara *et al.*, *Science* **334**, 1240–1240 (2011).
11. T. Lay, H. Kanamori, *Phys. Today* **64**, 33–39 (2011).
12. S. Ide, A. Baltay, G. C. Beroza, *Science* **332**, 1426–1429 (2011).
13. F. M. Chester, J. J. Mori, S. Toczko, N. Eguchi, the Expedition 343/343T Scientists, Japan Trench Fast Drilling Project (JFAST). *IODP Proceedings* 343/343T (2013).
14. C.-Y. Wang, M. Manga, *Earthquakes and Water*, vol. 114, Lecture Notes in Earth Sciences (Springer, Berlin, 2010).
15. J. E. Elkhoury, E. E. Brodsky, D. C. Agnew, *Nature* **441**, 1135–1138 (2006).
16. K. Wang, T. Mulder, G. C. Rogers, R. D. Hyndman, *J. Geophys. Res.* **100**, 12907–12918 (1995).
17. G. Kimura *et al.*, *Earth Planet. Sci. Lett.* **339-340**, 32–45 (2012).
18. K. Ujiie *et al.*, *Science* **342**, 1211–1214 (2013).
19. K. Wang, K. Suyehiro, *Geophys. Res. Lett.* **26**, 2307–2310 (1999).
20. W. Lin *et al.*, *Science* **339**, 687–690 (2013).

Acknowledgments: We thank all drilling and operations staff on board the deep-sea drilling vessel *Chikyu* during IODP Expedition 343 and 343T and R/V *Kairei* during KR12-16, KR13-04, and KR13-08, operated by Japan Agency for Marine-Earth Science and Technology. The data are provided by IODP via CDEX (www.iodp.org/access-data-and-samples). The data analysis is funded by the Gordon and Betty Moore Foundation through grant GBMF3289 to E.E.B.

Supplementary Materials

www.sciencemag.org/content/342/6163/1214/suppl/DC1
Materials and Methods
Supplementary Text
Figs. S1 to S9
Tables S1 and S2
References (*21*–*26*)

23 July 2013; accepted 30 October 2013
10.1126/science.1243641

Giant Convection Cells Found on the Sun

David H. Hathaway,[1]* Lisa Upton,[2,3] Owen Colegrove[4]

Heat is transported through the outermost 30% of the Sun's interior by overturning convective motions. These motions are evident at the Sun's surface in the form of two characteristic cellular structures: granules and supergranules (~1000 and ~30,000 kilometers across, respectively). The existence of much larger cells has been suggested by both theory and observation for more than 45 years. We found evidence for giant cellular flows that persist for months by tracking the motions of supergranules. As expected from the effects of the Sun's rotation, the flows in these cells are clockwise around high pressure in the north and counterclockwise in the south and transport angular momentum toward the equator, maintaining the Sun's rapid equatorial rotation.

The Sun, like most stars, has an outer convection zone in which heat generated by nuclear reactions in its core is transported to its surface by overturning convective motions. These motions were evident in early telescopic observations of the Sun as granules, which are bright grain-like structures with typical diameters of ~1000 km, lifetimes of ~10 min, and flow velocities of ~3000 m s^{-1}. Much larger structures—supergranules—were evident from their flow velocities, as seen in the Doppler shift of atomic spectral lines formed in the Sun's surface layers (*1*, *2*). Supergranules have diameters of ~30,000 km, lifetimes of ~24 hours, and flow velocities of ~500 m s^{-1}. Both granules and supergranules cover the entire solar surface but are substantially modified by the intense magnetic fields in and around sunspots.

The existence of even larger convection cells—giant cells—was proposed shortly after supergranules were detected (*3*). These cells are expected to span the 200,000-km-deep solar convection zone, to have diameters of ~200,000 km and lifetimes of ~1 month, and to be heavily influenced by the Sun's 27-day rotation. Hydrodynamical models of convective motions in the Sun's rotating convection zone (*4*–*6*) suggest that these cells should be elongated north-to-south near the equator and be sheared off at higher latitudes by the Sun's differential rotation (the equatorial regions rotate once in ~25 days, whereas the polar regions rotate once in ~35 days). These "banana" cells should transport angular momentum toward the Sun's equator—a critically important process for maintaining the differential rotation.

The observational evidence for the existence of giant cells has been only suggestive. Magnetic structures of a similar size and shape have been

[1]NASA Marshall Space Flight Center, Huntsville, AL 35812, USA. [2]Department of Physics and Astronomy, Vanderbilt University, Nashville, TN 37235, USA. [3]Department of Space Science, University of Alabama in Huntsville, Huntsville, AL 35899, USA. [4]Department of Physics and Astronomy, University of Rochester, Rochester, NY 14627, USA.

*Corresponding author. E-mail: david.hathaway@nasa.gov

observed (*7*), but these structures are fully explained (*8*) by the transport of magnetic elements away from active region sunspots by well-characterized flows: differential rotation, supergranules, and the poleward meridional circulation. The best evidence for the existence of giant cells are observations indicating that large-scale-velocity features do exist in the spectrum of motions and are moving with the Sun's rotation (*9*–*11*).

We measured the motions of the supergranules themselves, with the expectation that the supergranules will be carried from the centers to the boundaries of the giant cells by these larger, long-lived flows. We obtained images of the line-of-sight Doppler shifts of a spectral line formed by traces of iron in the Sun's lower atmosphere with the Helioseismic and Magnetic Imager (HMI) on the NASA Solar Dynamics Observatory (SDO) every 45 s (*12*). These 4096- by 4096-pixel images were averaged over 12 min, blurred over 11-by-11 pixels, and resampled at 512- by 512-pixel resolution for our measurements. The line-of-sight motion of the HMI instrument relative to the Sun was removed, as was the Doppler signal owing to the Sun's solid-body rotation and imaging artifacts produced in the instrument itself. The data were then mapped to heliographic longitude and latitude. Two large-scale Doppler velocity signals (an east-west gradient owing to the Sun's differential rotation relative to the solid-body rotation and a disk-center-to-limb variation owing to the correlation between radial up-flow and brightness in the granules) were then measured and removed from the data so as to fully isolate the supergranule flow structures (Fig. 1).

We generated these images of supergranules hourly starting in May 2010. We determined the motions of the supergranules by means of local cross-correlation tracking (*13*) using image pairs separated by 8, 16, and 24 hours. We cross-correlated the signal in 21- by 21-pixel blocks in the earlier image with similar blocks in the later image in order to find the displacement that gives the highest correlation. We set a lower limit to acceptable correlations. This had the effect of eliminating the most uncertain measurements—primarily from disk center, where the Doppler signal due to these horizontal flows is weak. We determined the displacements to within a fraction of a pixel using a parabolic fit to the correlations about the peak. These displacements yield velocities in longitude and latitude for the group of supergranules covered by the pixel block at each location. This process produces hourly 256- by 256-pixel images of the flow velocities of the supergranules. We averaged these flow velocity images over each 27-day solar rotation using the longitude of the central meridian to position them relative to the other hourly velocity images. This typically gave an average over ~300 hours at each location. These supergranule flow velocity maps are dominated by the axisymmetric flows: differential rotation and meridional flow. Removing these longitudinally averaged velocities reveals the giant cells as large-scale and long-lived velocity structures in the supergranule flow velocity maps (Fig. 2 and figs. S1 and S2).

The most striking features are those seen at higher latitudes. The longitudinal velocity maps show velocity structures that are swept back in longitude at higher latitudes in each hemisphere. These features persist and drift in longitude by ~180° over the three 27-day rotation intervals, indicating lifetimes of at least 3 months and a rotation period of ~32 days at those latitudes. The structures at lower latitudes are less well defined and shorter lived. However, although less pronounced, the low-latitude structures seen in the latitudinal velocity maps do appear to be aligned north-to-south. A low-latitude north-south alignment has also been noted in the structure of the supergranulation pattern itself (*14*).

We found virtually the same cellular patterns for all three time lags (fig. S3) but with weaker flow velocities from the shorter time lags. The

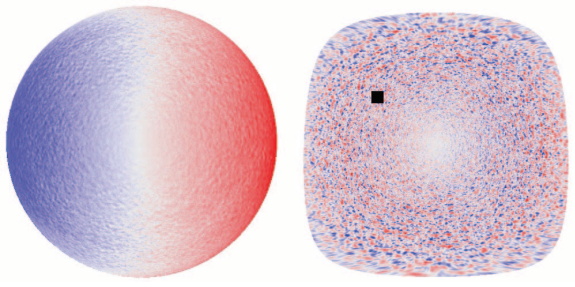

Fig. 1. Doppler velocity images. (**Left**) A 12-min average Doppler velocity image from the HMI instrument, with red representing red-shifted pixels and blue representing blue-shifted pixels (with a velocity range of ±3000 m s^{-1}). (**Right**) The same data mapped to heliographic longitude and latitude, with the instrumental signals and global flows removed in order to isolate the pattern of supergranule cells (with a velocity range of ±600 m s^{-1}). The black square shows the size of the block of pixels used in the local correlation tracking procedure.

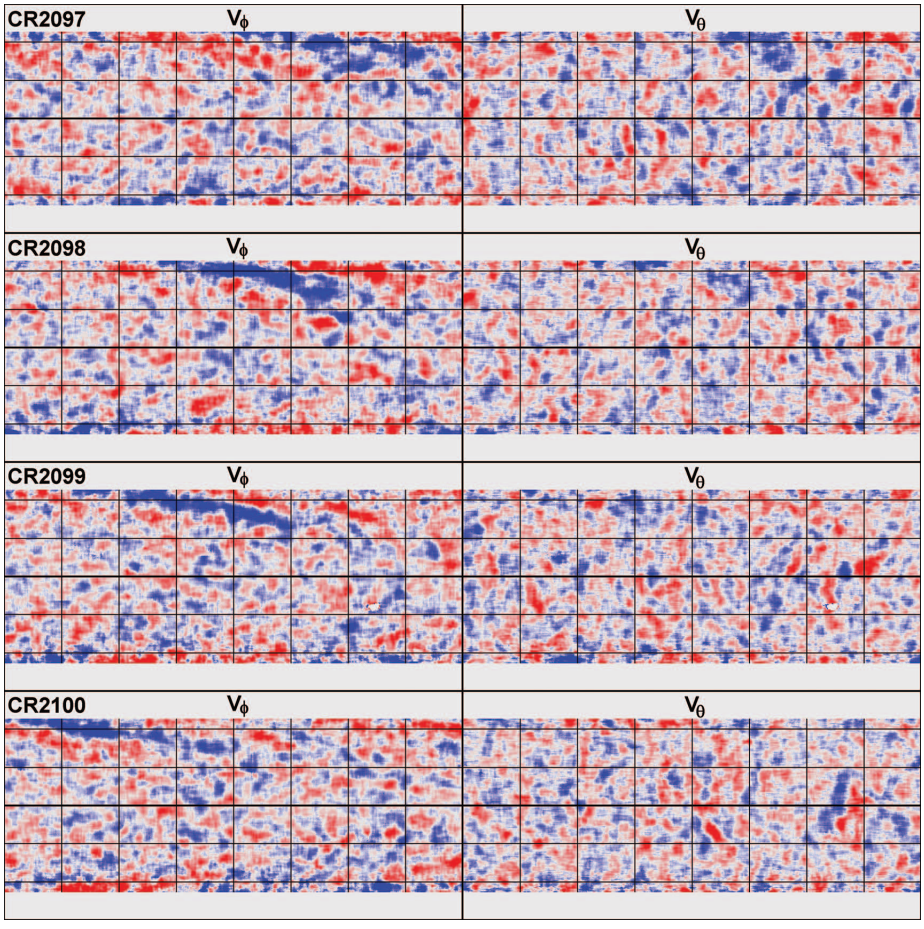

Fig. 2. Supergranule flow velocity maps. This sequence (top-to-bottom) of Mercator projection maps of the (**left**) longitudinal and (**right**) latitudinal velocity of the supergranules was obtained from four rotations of the Sun from May to August 2010 (prograde and southward velocities are red, and retrograde and northward velocities are blue, with a range of ±20 m s^{-1}). All maps cover the full 360° of longitude but are limited to ±70° latitude. The vertical lines are at 45° longitude intervals, whereas the horizontal lines are at 30° latitude intervals.

root-mean-square velocities are 16 m s^{-1} with 24-hour time lags but only 10 and 8 m s^{-1} at 16- and 8-hour time lags, respectively. The measured differential rotation and meridional flow also vary systematically with increasing time lag (rotation rate increases while the meridional flow velocity decreases). These variations are thought to be due to flow variations with depth (*15*, *16*). The correlations at longer time lags are dominated by larger supergranules that live longer, extend deeper into the Sun, and are transported by the flows at those greater depths (~50 Mm for the 24-hour time lag). This implies that the giant cell-flow velocities decrease in amplitude as they approach the surface, and it helps to explain the low upper limits on giant cell flow velocities given by previous searches (*17*, *18*). Measurements with even longer time lags are possible, but the correlations are much weaker and give noisier results.

The preferential visibility of east-west structures in the longitudinal flow and north-south structures in the latitudinal flow is one indication of the effects of the Sun's rotation on these large-scale flows. The Coriolis force due to the Sun's rotation turns the flow velocities to be more parallel to these elongated structures. In addition, we found that the kinetic helicity—the correlation between diverging flows and flow vorticity—is negative in the north and positive in the south (Fig. 3). A more meaningful indication of the effect of the Sun's rotation is seen in the Reynolds stress component $\langle V_\phi V_\theta \rangle$, the correlation between longitudinal and latitudinal flows (Fig. 4). This stress is necessary in the hydrodynamical models (*4*–*6*) in order to produce a rapidly rotating equator. The presence of these statistical correlations in the observed flows is further evidence that we have indeed found giant convection cells.

Although many of the large-scale magnetic structures initially attributed to giant cells (*6*) can be explained with magnetic flux transport by other well-characterized flows (*7*), the initial formation of active regions may nonetheless be associated with these giant cell flows. On one hand, active region formation may be favored in diverging flows in which upflows carry the magnetic field to the surface. On the other hand, active regions may form in converging flows in which magnetic fields become concentrated. Our initial search for correlations between converging/diverging flows and active regions formation has been inconclusive. However, it would be surprising if these large-scale, long-lived flows did not substantially influence the evolution and structure of the Sun's magnetic field.

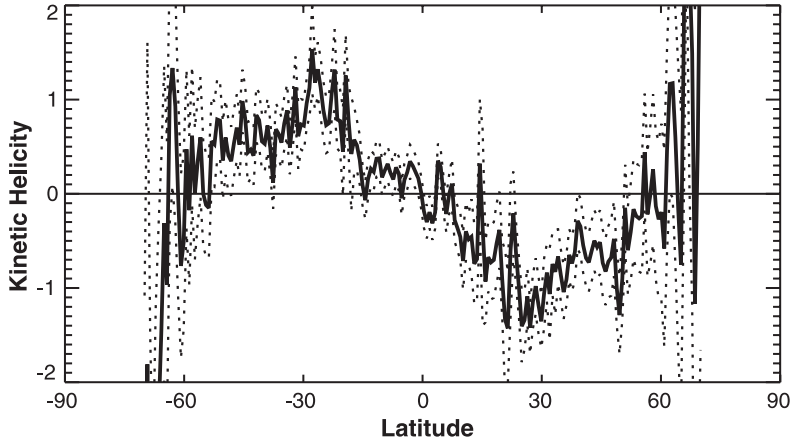

Fig. 3. The kinetic helicity produced by the giant cells as a function of latitude with 2σ error limits from the first 2 years of HMI. Kinetic helicity in arbitrary units; solid lines indicate the signal, and dotted lines indicate 2σ error limits. The correlation between diverging flows and vertical vorticity is negative in the northern hemisphere and positive in the southern hemisphere. This indicates clockwise circulation around high-pressure centers of divergence in the north and counterclockwise circulation around those in the south.

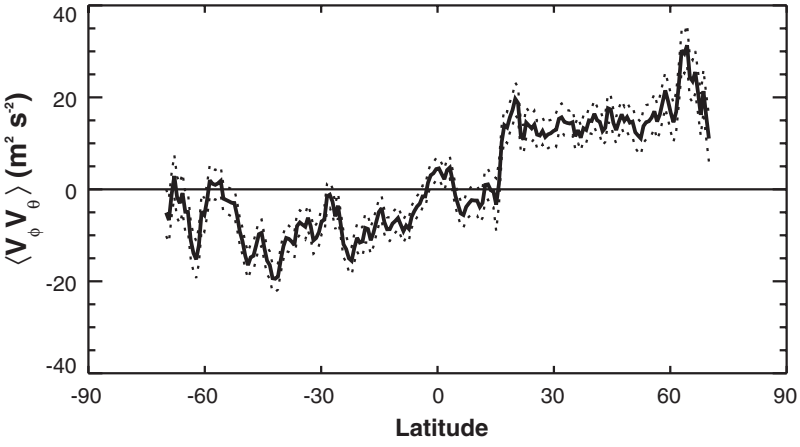

Fig. 4. The Reynolds stress $\langle V_\phi V_\theta \rangle$ produced by the giant cells as a function of latitude with 2σ error limits from the first 2 years of HMI. Solid lines indicate the Reynolds stress signal, and dotted lines indicate 2σ error limits. The correlation between prograde flow (positive V_ϕ) and southward flow (positive V_θ) is positive in the northern hemisphere and negative in the southern hemisphere. This indicates a transport of angular momentum equatorward, which is the required direction for maintaining the more rapid rotation of the Sun's equator.

References and Notes

1. A. B. Hart, *Mon. Not. R. Astron. Soc.* **116**, 38 (1956).
2. R. B. Leighton, R. W. Noyes, G. W. Simon, *Astrophys. J.* **135**, 474 (1962).
3. G. W. Simon, N. O. Weiss, *Z. Astrophys.* **69**, 435 (1968).
4. P. A. Gilman, *Astrophys. J.* **231**, 284 (1979).
5. J. R. Elliott, M. S. Miesch, J. Toomre, *Astrophys. J.* **533**, 546–556 (2000).
6. M. S. Miesch, A. S. Brun, M. L. DeRosa, J. Toomre, *Astrophys. J.* **673**, 557–575 (2008).
7. V. Bumba, *Sol. Phys.* **14**, 80 (1970).
8. A. A. van Ballegooijen, N. P. Cartledge, E. R. Priest, *Astrophys. J.* **501**, 866–881 (1998).
9. D. H. Hathaway *et al.*, *Science* **272**, 1306–1309 (1996).
10. J. G. Beck, T. L. Duvall Jr., P. H. Scherrer, *Nature* **394**, 653–655 (1998).
11. D. H. Hathaway *et al.*, *Sol. Phys.* **193**, 299–312 (2000).
12. P. H. Scherrer *et al.*, *Sol. Phys.* **275**, 207–227 (2012).
13. L. November *et al.*, in *Proc. 2nd Workshop on Theoretical Problems in High-Resolution Solar Physics*, NASA Conf. Pub. 2483, G. Athay, Ed. (NASA, Washington, DC, 1987), pp. 121–127.
14. J. P. Lisle, M. P. Rast, J. Toomre, *Astrophys. J.* **608**, 1167–1174 (2004).
15. D. H. Hathaway, *Astrophys. J.* **749**, L13 (2012).
16. D. H. Hathaway, *Astrophys. J.* **760**, 84 (2012).
17. H. B. Snodgrass, R. Howard, *Astrophys. J.* **284**, 848 (1984).
18. S. M. Hanasoge, T. L. Duvall Jr., M. L. DeRosa, *Astrophys. J.* **712**, L98–L102 (2010).

Acknowledgments: The SDO/HMI data described in this paper are archived at http://jsoc.stanford.edu. The SDO/HMI project is supported by NASA grant to Stanford University. D.H.H. was supported by a grant from the NASA Heliophysics Supporting Research and Technology (SR&T) Program to NASA/MSFC. L.U. was supported by a grant from the NASA Living With a Star (LWS) Program to NASA/MSFC. O.C. was supported as a Research Experience for Undergraduates (REU) summer student at the University of Alabama in Huntsville by funds from NSF grant AGS-1157027.

Supplementary Materials

www.sciencemag.org/content/342/6163/1217/suppl/DC1
Figs. S1 to S3

14 August 2013; accepted 1 November 2013
10.1126/science.1244682

Precision Spectroscopy of Polarized Molecules in an Ion Trap

H. Loh,[1]* K. C. Cossel,[1] M. C. Grau,[1] K.-K. Ni,[1]† E. R. Meyer,[2] J. L. Bohn,[1] J. Ye,[1]* E. A. Cornell[1]*

Polar molecules are desirable systems for quantum simulations and cold chemistry. Molecular ions are easily trapped, but a bias electric field applied to polarize them tends to accelerate them out of the trap. We present a general solution to this issue by rotating the bias field slowly enough for the molecular polarization axis to follow but rapidly enough for the ions to stay trapped. We demonstrate Ramsey spectroscopy between Stark-Zeeman sublevels in $^{180}Hf^{19}F^+$ with a coherence time of 100 milliseconds. Frequency shifts arising from well-controlled topological (Berry) phases are used to determine magnetic g factors. The rotating-bias-field technique may enable using trapped polar molecules for precision measurement and quantum information science, including the search for an electron electric dipole moment.

Quantum control of the rich internal structure of molecules may lead to advances in both fundamental and applied physics beyond those already gleaned from atoms (*1*). The same complex molecular structure makes it difficult to trap neutral molecules; in contrast, molecular ions can be easily trapped by time-dependent electric fields (*2*–*9*). However, the use of an ion trap has precluded taking advantage of the electric dipole moment of molecular ions, a vital ingredient of many experiments ranging from precision tests of fundamental physics (*2*, *6*, *10*) to quantum information (*11*).

The ability to polarize the molecules is, for example, a prerequisite for a search for the electron electric dipole moment (eEDM) with molecules (*12*): This search serves as a direct tabletop test of time-reversal violation (*13*) and as a probe of physics beyond the Standard Model (*14*). Trapped HfF^+ or ThF^+ molecular ions in the $^3\Delta_1$ state are excellent candidates for an eEDM search with several key advantages: small Ω-doublet splitting for a built-in rejection of many systematic errors (*15*–*17*), small magnetic moment for reduced magnetic field sensitivity (*18*), long coherence times for spectroscopy, and high internal electric fields for enhanced eEDM sensitivity (*2*, *18*–*20*). To access the high internal field, the molecules need to be polarized in the laboratory frame by an applied bias electric field; however, their position in the ion trap ensures that the time-averaged electric field is zero.

To address this issue, we apply a rotating bias electric field, realizing the proposal of (*2*). The frequency of rotation ω_{rot} is low enough for the molecular polarization axis to adiabatically follow the electric field but high enough for the ions to stay trapped.

At the heart of our experiment is a linear Paul trap with six radial confinement electrodes (Fig. 1, A and B). To form the rotating bias electric field $\boldsymbol{E}_{rot}$, we apply a set of sinusoidal voltages to the radial electrodes, such that the phases on successive electrodes are each advanced by 60°. $\boldsymbol{E}_{rot}$ causes the molecular ions to rotate in a circular micromotion (Fig. 1B). Compared to all other forms of ion motion, including radiofrequency micromotion, the circular micromotion occurs on the fastest time scale. The fast time scale, com-

[1]JILA, National Institute of Standards and Technology (NIST), and University of Colorado, and Department of Physics, University of Colorado, Boulder, CO 80309–0440, USA. [2]Department of Physics, Kansas State University, Manhattan, KS 66506–2601, USA.

*Corresponding author. E-mail: loh@jilau1.colorado.edu (H.L.); ye@jila.colorado.edu (J.Y.); cornell@jila.colorado.edu (E.A.C.)
†Present address: Department of Chemistry and Chemical Biology, Harvard University, Cambridge, MA 02138, USA.

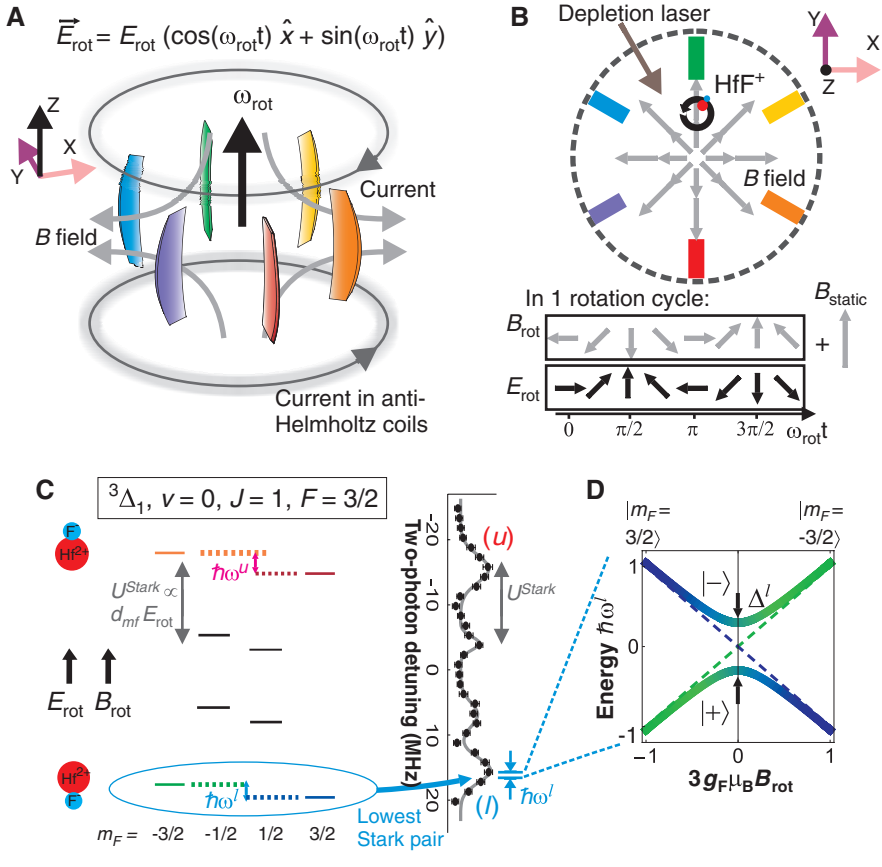

Fig. 1. Rotating-bias-field technique. (**A**) Three-dimensional view of a linear Paul trap (axial-confinement electrodes not shown). The colored radially confining electrodes carry an additional set of phase-shifted sinusoidal voltages to create a rotating bias field $\boldsymbol{E}_{rot}$. The pair of anti-Helmholtz coils creates a static magnetic-field gradient. (**B**) Top view of ion trap, with a depletion laser propagating between two radial electrodes. In one rotation cycle, the magnetic field (gray arrows) sampled by a molecular ion can be decomposed into a rotating component $\boldsymbol{B}_{rot}$ and a time-invariant component $\boldsymbol{B}_{static}$. (**C**) Rotating-frame HfF^+ energy level diagram for the $^3\Delta_1$ ($v = 0$, $J = 1$, $F = 3/2$) state in the presence of $\boldsymbol{E}_{rot}$ and $\boldsymbol{B}_{rot}$. $\boldsymbol{E}_{rot}$ splits the levels into four spectroscopically isolated Stark pairs. (**D**) Energies of sublevels within a single Stark pair. The rotation of the electric bias field couples the two sublevels, turning the linear Zeeman splitting (dashed lines) into an avoided crossing (solid lines) split by Δ at the point of zero B_{rot}. For a typical measurement, the Stark splitting, rotation rate, Zeeman splitting, and avoided-crossing mixing are given by 10 MHz, 250 kHz, 100 Hz, and 30 Hz, respectively.

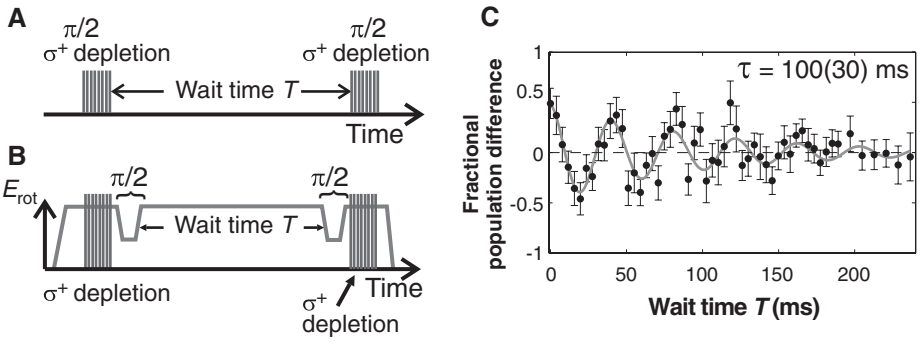

Fig. 2. Ramsey spectroscopy in rotating fields. Ramsey sequences (**A**) for $B_{rot} = 0$, where the σ^+-polarized depletion laser acts as both a polarizer and a $\pi/2$ pulse; (**B**) for high B_{rot}, where ramps in E_{rot} act as $\pi/2$ pulses. (**C**) Fractional difference of ions in $|m_F = 3/2\rangle$ versus that in $|m_F = -3/2\rangle$ as a function of the Ramsey wait time T, taken at $B_{rot} = 0$. The data are fit to a sinusoidal function with an exponential-decay time constant τ.

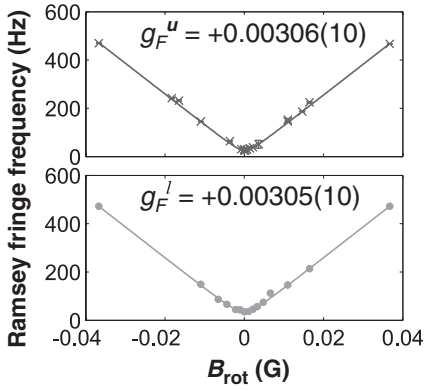

Fig. 3. Measurement of the avoided-crossing splitting. Avoided crossing for $E_{rot} = 11.6$ V/cm, experimentally mapped out using Ramsey spectroscopy for the upper (crosses) and lower (dots) Stark pairs. The upper and lower pair magnetic g factors g_F that have been obtained from the fits (solid lines) are nearly identical and quite small.

bined with the spatial uniformity and large amplitude of E_{rot}, ensures that all the ions synchronously undergo the same circular micromotion. In this paper, the quantization axis is given by the instantaneous electric field.

For a precision measurement of the eEDM, it is advantageous to apply a magnetic field aligned along or against the bias electric field because the Zeeman interaction between the electron magnetic dipole moment and the magnetic field shifts the eEDM signal away from possible low-frequency noise sources. In our experiment, such a magnetic field can be implemented by combining a static magnetic-field gradient with the ions' circular micromotion (Fig. 1B). The magnetic field experienced by an ion over a rotation cycle can be decomposed into a spatially dependent but roughly time-invariant component $\boldsymbol{B}_{static}(\boldsymbol{R})$ and a time-varying, almost spatially independent component $\boldsymbol{B}_{rot}(t) = \boldsymbol{r}_{rot}(t)\,\partial B_\rho/\partial\rho$, where $\boldsymbol{r}_{rot}(t)$ is the circular micromotion and B_ρ is the radial component of the magnetic field. $\boldsymbol{B}_{static}$ can be safely neglected because the rotating bias electric field results in sensitivity to only $\boldsymbol{B}_{rot}$ (*2*).

In the presence of a bias electric field and a coparallel magnetic field, the rotating-frame energy levels of the metastable $^3\Delta_1$ ($v = 0$, $J = 1$, $F = 3/2$) state of HfF^+ are split, where v is the vibrational quantum number, J is the rotational quantum number, and F is the hyperfine quantum number (Fig. 1C). The interaction between the molecules' electric dipole moment and the bias field gives rise to four pairs of Stark-split levels. The Stark spectrum in Fig. 1C is recorded by performing two-photon Raman transfer to populate ions in the desired $^3\Delta_1$ state from the ground $^1\Sigma^+$ state via an intermediate $^3\Pi_{0+}$ state. A particular Stark level-pair can thus be isolated by tuning the Raman transfer laser frequencies to the appropriate two-photon resonance.

For the eEDM measurement, we focus on either the uppermost (u) or lowermost (l) Stark pairs. In the absence of B_{rot}, the coupling from the electric field rotation results in an avoided crossing of the two eigenstates ($|+\rangle$ and $|-\rangle$) separated by the energy splitting Δ. The eigenstates are equal superpositions of the spin projections, i.e. $|\pm\rangle_{B_{rot}=0} = (|m_F = 3/2\rangle \pm |m_F = -3/2\rangle)/\sqrt{2}$, where m_F is the spin-projection quantum number. As the Zeeman energy increases relative to Δ, the eigenstates of the Hamiltonian evolve from different superpositions of $|m_F = \pm 3/2\rangle$ to pure spin states (Fig. 1D). For sufficiently large magnetic fields, the energy eigenstates at high B_{rot} are $|\pm\rangle = |m_F = \pm 3/2\rangle$ and their energies asymptote toward a linear Zeeman shift. In the presence of the avoided crossing, the rotating magnetic field is not merely an advantage for precision measurement; it is a necessity for experiments aiming to manipulate states of distinct m_F.

To probe the physics of the rotating-frame Hamiltonian within a single Stark pair, we perform Ramsey spectroscopy on the individual sublevels as a function of the rotating magnetic field. The Ramsey sequence always begins with populating ions in a single Stark pair and then optically pumping away ions in the $|m_F = -3/2\rangle$ state using a σ^+-polarized depletion laser. For small B_{rot} (i.e., small Zeeman splitting compared to Δ), the depletion process acts like a $\pi/2$ pulse, leaving the ions in a superposition of the eigenstates $|\pm\rangle$ (Fig. 2A). At high B_{rot}, the $\pi/2$ pulse is instead executed by fast ramps of the rotating electric field to and from a lower magnitude (*21*). The full Ramsey sequence (Fig. 2B) is the same as that used for an eEDM measurement.

The number of ions in either one of the two $|m_F\rangle$ states after the second $\pi/2$ pulse is determined by photodissociating the remaining ions in the $^3\Delta_1$, $J = 1$ state, and counting the dissociated ions via a mass-resolved ejection sequence. The fractional population difference between the two $|m_F\rangle$ states oscillates as a function of the wait time T between the two $\pi/2$ pulses at a frequency that is the avoided-crossing splitting (Fig. 2C). The decay time constant of the Ramsey fringe shows the ions maintaining coherence over a long period of 100(30) ms. The correspondingly high spectral resolution on the eEDM transition reduces vulnerability to potential systematic effects. The coherence time can potentially reach beyond 1 s, which is set by the $^3\Delta_1$ spontaneous-decay lifetime. The present limit most likely comes from ion-ion interactions.

Figure 3 shows the full avoided-crossing splittings for the upper and lower Stark pairs as a function of B_{rot} with a rotating bias field of 11.6 V/cm. A fit to the data yields the magnitude of the magnetic g factor, which is spectroscopically relevant for the eEDM experiment. We measured $g_F \equiv (g_F{}^u + g_F{}^l)/2 = +0.00306(10)$ and the difference in g factors to be $\delta g_F = g_F{}^u - g_F{}^l = 0.00001(2)$. As expected, $g_F << 1$ due to the cancellation of orbital and spin angular momenta in the $^3\Delta_1$ state (*2*). Further, the magnetic g factor is similar for both the upper and lower Stark manifolds, which is advantageous for suppressing systematic errors in an eEDM experiment. A nonzero electron EDM would lead to a horizontal offset of the upper and lower curves in Fig. 3 from each other. The data shown represent our first eEDM measurement and already constrain its magnitude to be less than 1.5×10^{-25} e·cm. A dedicated eEDM effort may lead to a statistical uncertainty of 1×10^{-28} e·cm in a day (*21*).

A Ramsey-spectroscopy measurement of the electron EDM will determine its sign relative to the sign of the molecule's magnetic g factor. Our

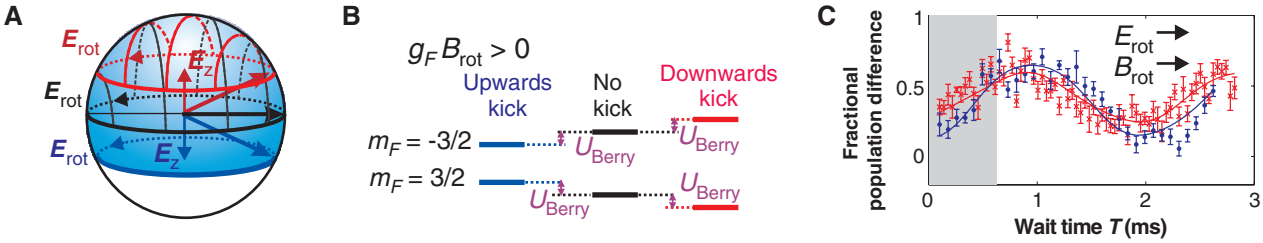

Fig. 4. Determination of the sign of the magnetic g factor using Berry phase. (**A**) Ions rotating in the $z = 0$ plane subtend a solid angle of 2π (black hatched hemisphere). As the ions are kicked above (below) the plane of rotation, they sample a force-restoring axial electric field E_z. The quantization axis thus tilts away from the plane of rotation, subtending a larger (smaller) solid angle indicated by the blue shaded (red hatched) region. (**B**) For $g_F B_{rot} > 0$, the additional Berry energy U_{Berry} from the axial kicks causes the $|m_F = \pm 3/2\rangle$ levels to move closer together or farther apart in energy. (**C**) Ramsey fringes recorded for $B_{rot} > 0$ (i.e., $\boldsymbol{B}_{rot}$ in phase with $\boldsymbol{E}_{rot}$), where the ions have been kicked above (blue dots) or below (red crosses) the plane of rotation. The relative phase shifts mean $g_F > 0$. The gray shaded region corresponds to half an axial trap oscillation, which is the time over which the ions are exclusively in either the $z > 0$ or $z < 0$ region. The solid lines are fits to the data, incorporating the frequency chirp expected as the ions oscillate axially.

tool for determining the sign of g_F is the Berry phase (*22*).

The Berry phase is a dynamical phase shift imprinted on a quantum mechanical state due to the Hamiltonian having explicit time dependence. Under the influence of a rotating bias field, the ions can accumulate a finite Berry phase if the quantization axis is tilted away from the plane of rotation (*23*). In our technique, the resultant Berry phase is much better controlled across the ion cloud compared with that for a trapped sample of neutrals (*24*, *25*).

To demonstrate this control, we explicitly incorporate its spectroscopic effect by giving the ions an impulse axial kick before performing the Ramsey sequence in a finite positive rotating magnetic field. The ions subsequently oscillate at the axial trap frequency. The Ramsey sequence is completed while the ions have only gone through half an axial oscillation, such that they are only present in either the $z > 0$ ($z < 0$) region for an upward (downward) kick. The downward-pointing (upward-pointing) trap field causes the quantization axis to tilt out of the plane of rotation, such that the solid angle Ω_{SA} subtended by the quantization axis is larger (smaller) than that without the kick (Fig. 4A). The resulting Berry phase ϕ_{Berry} manifests as a Berry energy $U_{Berry} = -\frac{\hbar\phi_{Berry}}{(2\pi)/\omega_{rot}} = \hbar m_F \frac{\omega_{rot}}{2\pi}\Omega_{SA}$ over one rotation cycle. For $g_F B_{rot} > 0$, the $m_F = 3/2$ level lies below the $m_F = -3/2$ level, so U_{Berry} causes the two m_F levels to move closer (split further apart) for an upward (downward) kick (see Fig. 4B). For a smaller (larger) energy splitting, the Ramsey fringe frequency is slower (faster), which looks like the Ramsey fringe has accumulated a positive (negative) initial phase shift. The two Ramsey fringes separately recorded with the ions kicked upward (dots) and downward (crosses) from the plane of rotation have a positive and negative phase shift, respectively (shaded region of Fig. 4C), which means that $g_F B_{rot} > 0$. Because $B_{rot} > 0$, we determine the magnetic g factor to be positive.

We have demonstrated coherent spectroscopy with molecular ions that are simultaneously polarized and trapped in a linear Paul trap with a rotating bias field. The rotating bias field and corotating magnetic field open up access to the manipulation of Stark-Zeeman sublevels within a hyperfine-rovibronic state. The long coherence time of a qubit encoded by Stark-Zeeman states, whose relative energies are much more stable (compared with rotational or even hyperfine levels) against Stark-shift–induced decoherence mechanisms, is useful for quantum information processing (*11*). For quantum simulation experiments, the direct ability to manipulate dipolar interactions with molecular ions potentially eliminates the need for using optical spin-dependent forces to achieve spin-spin couplings, as is the case for trapped atomic ions (*26*–*28*). Further, the 10-Hz–level high-resolution spectroscopy is directly relevant to precision tests of ab initio theory (*6*), time variations in fundamental constants (*29*), and symmetry violations (*30*).

Note added in proof: We recently became aware of a new eEDM result from the ACME collaboration by Baron *et al.* (*31*).

References and Notes

1. L. D. Carr, D. DeMille, R. V. Krems, J. Ye, *New J. Phys.* **11**, 055049 (2009).
2. A. E. Leanhardt *et al.*, *J. Mol. Spectrosc.* **270**, 1–25 (2011).
3. S. Willitsch, M. T. Bell, A. D. Gingell, T. P. Softley, *Phys. Chem. Chem. Phys.* **10**, 7200–7210 (2008).
4. P. F. Staanum, K. Hojbjerre, P. S. Skyt, A. K. Hansen, M. Drewsen, *Nat. Phys.* **6**, 271–274 (2010).
5. J. H. V. Nguyen *et al.*, *New J. Phys.* **13**, 063023 (2011).
6. U. Bressel *et al.*, *Phys. Rev. Lett.* **108**, 183003 (2012).
7. S. Ding, D. Matsukevich, *New J. Phys.* **14**, 023028 (2012).
8. J. E. Goeders *et al.*, *J. Phys. Chem. A* **117**, 9725–9731 (2013).
9. W. G. Rellergert *et al.*, *Nature* **495**, 490–494 (2013).
10. J. K. Thompson, S. Rainville, D. E. Pritchard, *Nature* **430**, 58–61 (2004).
11. D. I. Schuster, L. S. Bishop, I. L. Chuang, D. DeMille, R. J. Schoelkopf, *Phys. Rev. A* **83**, 012311 (2011).
12. J. J. Hudson *et al.*, *Nature* **473**, 493–496 (2011).
13. I. B. Khriplovich, S. K. Lamoreaux, *CP Violation Without Strangeness: Electric Dipole Moments of Particles, Atoms and Molecules* (Springer, Berlin, 1997).
14. E. D. Commins, in *Advances in Atomic, Molecular and Optical Physics*, vol. 40, B. Bederson, H. Walther, Eds. (Academic Press, 1999), pp. 1–55.
15. D. DeMille *et al.*, *Phys. Rev. A* **61**, 052507 (2000).
16. S. Eckel, P. Hamilton, E. Kirilov, H. W. Smith, D. DeMille, *Phys. Rev. A* **87**, 052130 (2013).
17. A. C. Vutha *et al.*, *J. Phys. B* **43**, 074007 (2010).
18. E. R. Meyer, J. L. Bohn, M. P. Deskevich, *Phys. Rev. A* **73**, 062108 (2006).
19. A. N. Petrov, N. S. Mosyagin, T. A. Isaev, A. V. Titov, *Phys. Rev. A* **76**, 030501 (2007).
20. E. R. Meyer, J. L. Bohn, *Phys. Rev. A* **78**, 010502 (2008).
21. Supplementary materials are available on *Science* Online.
22. M. V. Berry, *Proc. R. Soc. Lond. A Math. Phys. Sci.* **392**, 45–57 (1984).
23. E. R. Meyer, A. E. Leanhardt, E. A. Cornell, J. L. Bohn, *Phys. Rev. A* **80**, 062110 (2009).
24. J. M. Pendlebury *et al.*, *Phys. Rev. A* **70**, 032102 (2004).
25. M. Rupasinghe, N. E. Shafer-Ray, *Phys. Rev. A* **78**, 033427 (2008).
26. D. Porras, J. I. Cirac, *Phys. Rev. Lett.* **92**, 207901 (2004).
27. K. Kim *et al.*, *Phys. Rev. Lett.* **103**, 120502 (2009).
28. J. W. Britton *et al.*, *Nature* **484**, 489–492 (2012).
29. V. V. Flambaum, M. G. Kozlov, *Phys. Rev. Lett.* **99**, 150801 (2007).
30. H. Müller, S. Herrmann, A. Saenz, A. Peters, C. Lammerzahl, *Phys. Rev. D Part. Fields Gravit. Cosmol.* **70**, 076004 (2004).
31. J. Baron *et al.*, arXiv:1310.7534 (2013).

Acknowledgments: This work is supported by NIST, the Marsico Foundation, and NSF grant number 1125844. H. L. is partly funded by the Agency for Science, Technology and Research (Singapore). K.-K. N. acknowledges a NIST/NRC Postdoctoral Fellowship. We thank T. Fridey for his contributions and D. Gresh for discussions.

Supplementary Materials

www.sciencemag.org/content/342/6163/1220/suppl/DC1
Materials and Methods
Supplementary Text
Figs. S1 and S2
References (*32*–*36*)

24 July 2013; accepted 4 November 2013
10.1126/science.1243683

Phase Mismatch–Free Nonlinear Propagation in Optical Zero-Index Materials

Haim Suchowski,[1]* Kevin O'Brien,[1]* Zi Jing Wong,[1]* Alessandro Salandrino,[1] Xiaobo Yin,[1,2] Xiang Zhang[1,2]†

Phase matching is a critical requirement for coherent nonlinear optical processes such as frequency conversion and parametric amplification. Phase mismatch prevents microscopic nonlinear sources from combining constructively, resulting in destructive interference and thus very low efficiency. We report the experimental demonstration of phase mismatch–free nonlinear generation in a zero-index optical metamaterial. In contrast to phase mismatch compensation techniques required in conventional nonlinear media, the zero index eliminates the need for phase matching, allowing efficient nonlinear generation in both forward and backward directions. We demonstrate phase mismatch–free nonlinear generation using intrapulse four-wave mixing, where we observed a forward-to-backward nonlinear emission ratio close to unity. The removal of phase matching in nonlinear optical metamaterials may lead to applications such as multidirectional frequency conversion and entangled photon generation.

Nonlinear optics, the study of phenomena occurring when optical properties of a material are modified by the presence of light, plays a critical role in frequency conversion, nonlinear spectroscopy, and the generation of new light sources (*1*, *2*). A major problem in nonlinear optics is the inherent phase mismatch between the interacting waves propagating inside the nonlinear materials. This effect originates from material dispersion and causes a lack of optical momentum conservation between the photons involved in the nonlinear process. The phase mismatch prevents the constructive addition of the nonlinear fields, resulting in destructive interference and poor generation efficiency. To increase the amounts of nonlinear light, a compensation technique must be used. The most widely used methods (Fig. 1A) include birefringent phase matching, angle phase matching, and quasi–phase matching (*3*–*6*). Implementing each technique poses a number of challenges. The birefringent phase-matching technique uses the polarization-dependent indices to match the phase velocities of the interacting waves, but it is limited to birefringent materials (*1*, *2*). Angle phase matching uses geometrical alignments of the interacting waves to compensate the phases, but the noncollinear optical arrangement limits the interaction length (*1*, *2*). Quasi–phase matching cancels out the inherent phase mismatch using artificial momentum introduced by periodic and/or aperiodic poling of nonlinear crystals, which is restricted to certain nonlinear crystals and provides a limited range of mismatch that can be compensated. Moreover, all compensating schemes work only in a specific direction: either in the forward direction (*3*–*6*) or the backward direction (*7*, *8*), but not both. This restriction arises because the phase-matching process represents a balance between the momenta of the photons involved in the nonlinear interaction—a balance that is disturbed when the momentum of one photon changes sign because of a direction change.

We show that the requirement for phase matching can be eliminated using a metamaterial with a zero refractive index. In a zero-index material (*9*–*11*), the photons carry zero momentum and satisfy momentum conservation for any combination of photon directions, thereby allowing the nonlinearly generated waves to coherently build up in both forward and backward directions. We demonstrate the nonlinear dynamics through four-wave mixing (FWM) in a metamaterial with zero refractive index. Equal amounts of nonlinearly generated waves are observed in

[1]NSF Nanoscale Science and Engineering Center, University of California, Berkeley, CA 94720, USA. [2]Materials Sciences Division, Lawrence Berkeley National Laboratory, Berkeley, CA 94720, USA.

*These authors contributed equally to this work.
†Corresponding author. E-mail: xiang@berkeley.edu

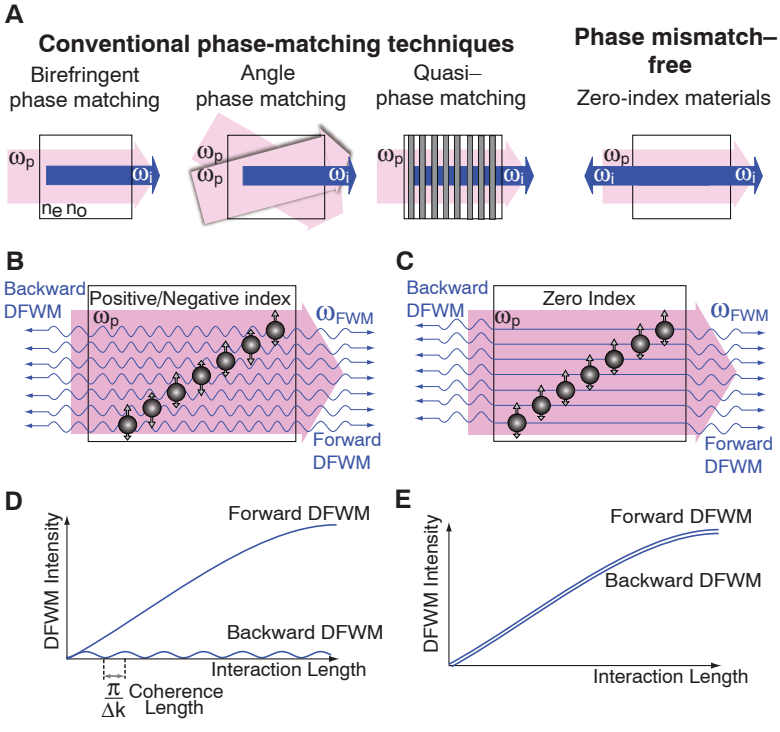

Fig. 1. The role of phase mismatch. Avoiding phase mismatch is critical for obtaining efficient nonlinear conversion. (**A**) The most widely used methods for phase matching—birefringence phase matching, angle phase matching, and quasi–phase matching—allow compensation either in the forward or backward directions, but not both. (**B** to **E**) In contrast, a zero-index metamaterial creates a phase mismatch–free environment for nonlinear propagation, eliminating the requirement for phase matching. In the microscopic picture of nonlinear generation, each source coherently emits equally in both directions, acquiring a phase that is proportional to the refractive index [(B) and (C)] as it propagates. All of these sources add up coherently to generate the net nonlinear emission. In a zero-index medium (C), the radiations from all nonlinear sources acquire no phase as they propagate, guaranteeing a constructive interference and an increase of the signal in both directions with propagation length (E). In contrast, in a finite-index medium (B), the emission acquires phase as it propagates, leading to destructive interference when the process is not phase-matched. For example, in a degenerate four-wave mixing (FWM) process in which $\omega_{signal} \approx \omega_{pump} \approx \omega_{idler}$, the sources destructively interfere in the backward direction (D), resulting in weaker backward emission.

both forward and backward propagation directions, matching well with the predictions from nonlinear scattering theory (*12*). In contrast, the forward and backward FWM generations are drastically different for metamaterials with a positive or a negative index, as expected from phase-matching considerations.

Metamaterials allow us to tailor the linear electromagnetic response and introduce new regimes of interaction between radiation and matter (*13*–*17*). The nonlinear properties of negative-index metamaterials have been explored both theoretically (*18*–*21*) and experimentally (*22*–*26*). The rich nonlinear dynamical behavior in metamaterials promises the realization of novel effects such as backward mirrorless parametric amplification (*18*, *19*), novel quantum switches (*20*), and cavity-free microscopic optical parametric oscillators (*21*).

To illustrate the phase mismatch–free nonlinear wave interactions in a zero-index material, we consider a degenerate FWM process in which the pump, signal, and idler photons have approximately the same wavelength ($\omega_{signal} \approx \omega_{pump} \approx \omega_{idler}$). In this process, the phase (momentum) mismatch in the forward and backward propagation directions can be expressed as $\Delta k_{\pm} = |2k_{pump} - k_{signal} \mp k_{idler}|$, where the plus and minus subscripts represent the forward and backward directions, respectively. In a conventional degenerate FWM system, when one of the propagation directions, say the forward direction, is perfectly phase-matched (i.e., $\Delta k_{+} \to 0$), the phase is then poorly matched in the backward propagation direction where $\Delta k_{-} \approx 2|k_{idler}|$. For a metamaterial with a zero refractive index at the idler frequency, however, the phase mismatch in both the forward and backward directions is zero. This important distinction between forward and backward nonlinear propagation allows us to explore nonlinear generation for negative-, positive-, and zero-index regimes. We expect that in the case of negative or positive index, because $\Delta k_{+} \to 0$ while $\Delta k_{-} \neq 0$, the generated forward light is accumulated in phase while the generated backward light is not, thus causing the degenerated FWM intensity to grow monotonically for the forward direction and to oscillate for the backward direction (Fig. 1, B and D). In contrast, in the zero-index regime, $\Delta k_{+} \to 0$ and also $\Delta k_{-} \to 0$, making both the generated forward light and backward light accumulate in phase, having the same yield in the forward and backward directions (Fig. 1, C and E). This is in stark contrast to nonlinear generation in negative-index materials, where the phase mismatch parameter has a finite value (*18*–*21*). A phase mismatch–free zero-index material allows the nonlinear process to be efficient regardless of directionality, and the need to carefully balance between the momenta of the waves involved in the nonlinear interaction is eliminated. In our experimental realization, the pump pulse has a positive Poynting vector in the material, so the direction of energy flux is the same as in free space. In contrast, the nonlinear emission has an energy flux in both directions, with the relative amounts influenced by the phase matching. The refractive index controls the direction of the phase velocity and canonical momentum relative to the direction of the energy flux (*13*, *27*), which influences the direction of energy propagation through the phase matching. In a zero-index medium, as seen, the energy flux in both directions is equal. Relative to the poorly phase-matched case, more energy will be extracted from the pump in a zero-index material.

Figure 2A shows the experimental apparatus for single-shot FWM, which allows intrapulse wave mixing between the different spectral components of ultrashort pump laser pulses (*28*). Before impinging on the samples, the transform-limited pump pulse is amplitude-shaped to remove the long-wavelength tail in the spectral domain. The generated intrapulse FWM is measured in both forward and backward directions within this filtered spectral regime. This method eliminates the need to overlap two laser pulse temporally and spatially, and maximizes the nonlinear yield (see fig. S3). An example measurement spectrum (Fig. 2B) shows both the generated FWM signal and the pump with their relative strengths. Note that the pump is far from depleted by the nonlinear process, as evident from the much weaker FWM signal than that of the pump. Operating in the weak-field regime (the generated intensity of the idler is on the order of 10^{-5} of the pump intensity) allows us to analyze the experimental observations with a perturbative approach. We verify the nonlinear origin of the emission by measuring the cubic scaling with pump power and quadratic spectral phase dependence (see supplementary materials).

We have chosen the fishnet metamaterial structure (*9*), a stack of metal-dielectric multilayers with perforated holes (Fig. 2). Fishnet metamaterials are widely used negative-index materials at optical frequencies because of their low loss, well-understood linear properties, and robust fabricability. Our fishnet metamaterial consists of 20 alternating 30-nm gold and 50-nm magnesium fluoride layers on a 50-nm-thick silicon nitride membrane. The magnetic moments (created by the antiparallel currents in neighboring conductive layers) and the electric responses of the perforated metallic thin films provide a positive, zero, or negative refractive index regime, depending on the wavelength. We measured the transmission and refractive index by spectrally and spatially resolved interferometry (*29*), which measures simultaneously the phase for an ultra-broadband optical range to an accuracy of greater than $\lambda/300$ (fig. S1). The zero crossing of the index is approximately 1325 to 1340 nm for the sample with period of 750 nm

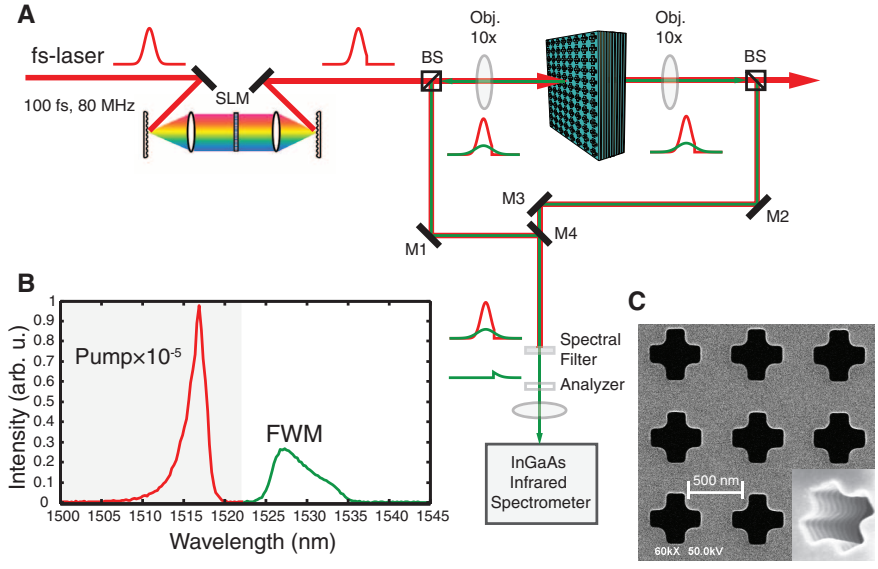

Fig. 2. Experimental apparatus for nonlinear measurements. (**A**) A transform-limited 100-fs laser pulse centered at 1315 nm or 1510 nm is amplitude-shaped through a spatial light modulator (SLM) to remove the long-wavelength tail of the pulse (red). The pulse is passed through a fishnet metamaterial, which generates a FWM nonlinear signal (green) in the backward and forward directions because of a third-order nonlinearity. The FWM signals are measured in an infrared spectrometer after filtering the pump pulse. The forward emission is measured without the flip mirror (M4). An analyzer is used before the spectrometer to control the detected polarization; a half-wave plate (not shown) controls the pump polarization. (**B**) An example measurement of the emission spectrum, showing both the generated FWM signal (green) and the filtered pump (red). The pump is undepleted by the nonlinear process, as evident by the much weaker FWM signal than that of the pump (the magnitude of the FWM is ~10^{-5} times the pump intensity), justifying the use of the perturbative approach in our analysis. (**C**) Scanning electron micrograph of the cross-fishnet structures. Inset shows an angled view. See supplementary materials for details of the single-shot FWM method.

and cross lateral holes of dimensions 475 nm × 175 nm (Fig. 2C). Using the measured refractive index values of the fishnet structures, the phase mismatch values can be calculated as a function of wavelength for forward and backward propagation (Fig. 3A). The forward phase mismatch is $\Delta k_+ \rightarrow 0$ for all wavelengths, whereas Δk_- has different values across the zero-index wavelength. However, in the wavelength regime of zero refractive index (~1330 nm), both the forward and backward directions are phase mismatch–free.

The intrapulse FWM signal in the zero-index regime (where the refractive index changes its sign) is shown for both the forward and the backward directions (Fig. 3B). The observed nonlinear yield is about the same in both directions. In contrast, in the negative-index regime, the intensities of the degenerate FWM signals in the opposite propagation directions are distinctly different (Fig. 3C). Because of the low transmission at 1530 nm, a different fishnet metamaterial with 800-nm period and perforated hole size of 560 nm by 250 nm was used. The zero crossing of the refractive index is at ~1460 nm and the refractive index is –0.5 at 1530 nm (fig. S1). The relative strength of the forward and backward FWM waves correlates with the predicted phase-matching difference for zero and negative indices, as illustrated in Fig. 1. In particular, at the zero refractive index, the observation of a forward/backward FWM ratio of unity indicates phase mismatch–free nonlinear interaction for both directions. Low transmission loss is critical for observing the effects of phase matching. High losses can also strongly affect the ratio of the forward and backward nonlinear emission for positive-, negative-, and zero-index regimes. Loss decreases the overall nonlinear emission and, because of the shorter propagation length of backward emission, increases the backward emission relative to the forward. The fabricated fishnet has a relatively low loss in the zero-index regime, allowing us to observe the effects of phase matching rather than absorption.

The phase mismatch–free nonlinear generation can be further demonstrated by measuring the nonlinear emission as a function of the polarization angle of the pump for the forward and backward FWM, shown in the insets of Fig. 3, B and C, for the zero-index and negative-index materials, respectively. The relative strength between the forward and backward nonlinear waves in the zero-index region is again about the same for all polar angles, whereas in the negative-index regime, the forward nonlinear waves remain stronger than the backward for all polarizations. The polarization-dependent FWM (with a horizontally polarized analyzer) matches well the analytical curve of $\cos^6 \theta$, a characteristic response of a third-order nonlinearity intensity signal. This angular dependence is particularly important, as it means that the nonlinearity originates from the light that is coupled into the metamaterial (see supplementary materials).

A numerical simulation of the dynamics as a function of thickness around the zero index predicts a ratio of unity for forward/backward nonlinear emission (fig. S2A), whereas in the negative-index regime, the forward generated nonlinear signal has a much higher yield than that of the backward signal (fig. S2B) for a thick fishnet of 20 layers. In contrast, for thin fishnets (fewer than five layers), the forward/backward ratio is unity regardless of the index of refraction, indicating that phase matching is not important in these structures (*23*–*26*). The nonlinear simulation is performed with nonlinear scattering theory (*12*), which calculates the nonlinear properties using the linear results from a full wave simulation of the metamaterial, taking into account the fabricated structure geometry and material losses. To further confirm that phase plays a dominant role in the dynamics with respect to loss or surface effects, we artificially removed the phase mismatch in the nonlinear simulation while keeping loss, thus forcing all waves to add up constructively. We found that the behavior in the zero-index region is unchanged, indicating that phase matching plays little role. In contrast, in the negative-index region, the forward and backward emissions became nearly equal, indicating that phase matching is critical in this region. Note that perfect phase matching using a zero refractive index is different from quasi–phase matching (*4*, *22*), in which the effective momentum supplied by a periodic structuring is used to compensate for a phase mismatch. In these experiments, the subwavelength spacing of the layers (80 nm) does not provide sufficient effective momentum to phase-match the backward nonlinear generation (see fig. S7).

The concept of phase mismatch–free nonlinear interaction in zero-index materials provides a new degree of freedom in controlling the nonlinear dynamics in a metamaterial and can be further explored in other nonlinear processes such as coherent Raman spectroscopy for remote sensing applications or spontaneous parametric down-conversions for entangled photon generation. The design of multivalued or broadband zero-index materials opens the opportunity to achieve phase mismatch–free dynamics for simultaneous nonlinear processes.

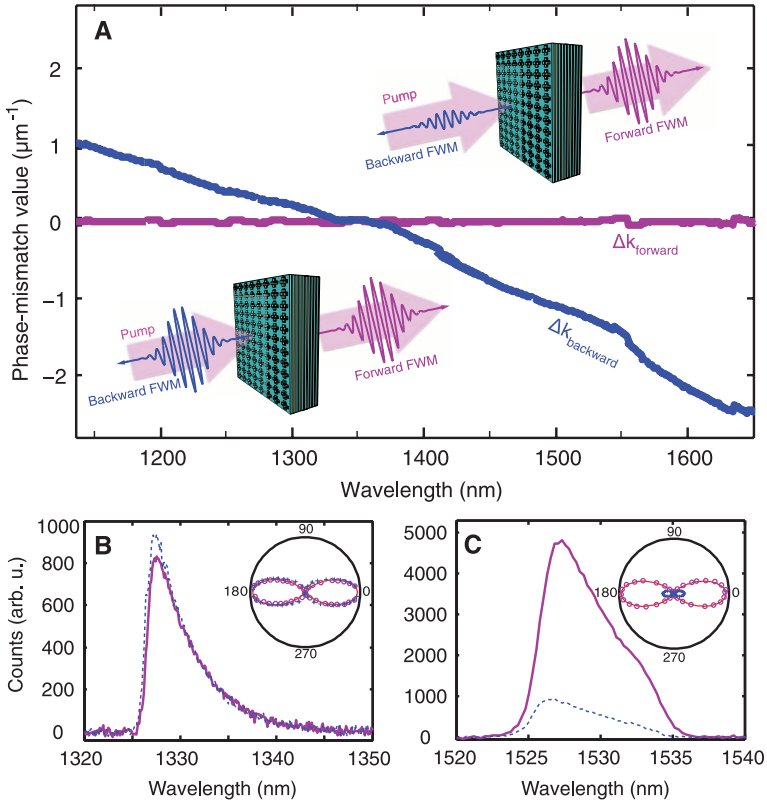

Fig. 3. Four-wave mixing in metamaterials with and without phase mismatch. (**A**) Phase mismatch of forward (purple) and backward (blue) FWM as a function of wavelength, based on experimentally measured refractive indices. The forward phase mismatch is near zero ($\Delta k_+ \rightarrow 0$) for all wavelengths; the backward has a large phase mismatch ($\Delta k_- \neq 0$) except when the index is near zero. (**B**) The measured FWM process in the zero-index regime has almost the same yield in both directions, illustrating the phase mismatch–free properties of zero-index materials. (**C**) In contrast, the forward-propagating FWM (solid purple) is much stronger than the backward (dashed blue) in the negative-index regime as a result of the phase mismatch. Insets in (B) and (C) show the dependence of the nonlinear emission (with a horizontally polarized analyzer) on pump polarization, which has the characteristic $\cos^6 \theta$ curve of $\chi^{(3)}$ dynamics. The nonlinear emission scales with the cube of the pump power and shows a spectral phase dependence demonstrating the nonlinear origin (fig. S6).

References and Notes

1. Y. R. Shen, *The Principles of Nonlinear Optics* (Wiley-Interscience, New York, 1984).
2. R. Boyd, *Nonlinear Optics* (Academic Press, New York, ed. 3, 2008).
3. J. A. Armstrong, N. Bloembergen, J. Ducuing, P. S. Pershan, *Phys. Rev.* **127**, 1918–1939 (1962).
4. D. S. Hum, M. M. Fejer, *C. R. Phys.* **8**, 180–198 (2007).
5. A. Arie, N. Voloch, *Laser Photonic Rev.* **4**, 355–373 (2010).
6. A. Rose, D. R. Smith, *Opt. Mater. Express* **1**, 1232–1243 (2011).
7. X. Gu, R. Y. Korotkov, Y. J. Ding, J. U. Kang, J. B. Khurgin, *J. Opt. Soc. Am. B* **15**, 1561–1566 (1998).
8. C. Canalias, V. Pasiskevicius, *Nat. Photonics* **1**, 459–462 (2007).
9. J. Valentine *et al.*, *Nature* **455**, 376–379 (2008).
10. C. Argyropoulos, P. Y. Chen, G. D'Aguanno, N. Engheta, A. Alù, *Phys. Rev. B* **85**, 045129 (2012).
11. E. J. R. Vesseur, T. Coenen, H. Caglayan, N. Engheta, A. Polman, *Phys. Rev. Lett.* **110**, 013902 (2013).
12. S. Roke, M. Bonn, A. V. Petukhov, *Phys. Rev. B* **70**, 115106 (2004).
13. V. G. Veselago, *Sov. Phys. Solid State* **8**, 2854–2856 (1967).
14. J. B. Pendry, *Phys. Rev. Lett.* **85**, 3966–3969 (2000).
15. R. A. Shelby, D. R. Smith, S. Schultz, *Science* **292**, 77–79 (2001).
16. V. M. Shalaev, *Nat. Photonics* **1**, 41–48 (2007).
17. N. Fang, H. Lee, C. Sun, X. Zhang, *Science* **308**, 534–537 (2005).
18. A. K. Popov, V. M. Shalaev, *Appl. Phys. B* **84**, 131–137 (2006).
19. A. K. Popov, V. M. Shalaev, *Opt. Lett.* **31**, 2169–2171 (2006).
20. A. K. Popov, S. A. Myslivets, V. M. Shalaev, *Opt. Lett.* **34**, 1165–1167 (2009).
21. M. Scalora *et al.*, *Opt. Express* **14**, 4746–4756 (2006).
22. A. Rose, D. Huang, D. R. Smith, *Phys. Rev. Lett.* **107**, 063902 (2011).
23. S. Tang *et al.*, *Opt. Express* **19**, 18283–18293 (2011).
24. K. M. Dani *et al.*, *Nano Lett.* **9**, 3565–3569 (2009).
25. A. Minovich *et al.*, *Appl. Phys. Lett.* **100**, 121113 (2012).
26. J. Reinhold *et al.*, *Phys. Rev. B* **86**, 115401 (2012).
27. S. M. Barnett, *Phys. Rev. Lett.* **104**, 070401 (2010).
28. N. Dudovich, D. Oron, Y. Silberberg, *Nature* **418**, 512–514 (2002).
29. K. O'Brien *et al.*, *Opt. Lett.* **37**, 4089–4091 (2012).

Acknowledgments: Supported by the U.S. Department of Energy, Office of Basic Energy Sciences, under contract no. DE-AC02-05CH11231 through the Materials Sciences Division of Lawrence Berkeley National Laboratory. H.S. and Z.J.W. acknowledge partial support by the Fulbright Foundation. We thank the Molecular Foundry, Lawrence Berkeley National Laboratory, for technical support in nanofabrication.

Supplementary Materials

www.sciencemag.org/content/342/6163/1223/suppl/DC1
Materials and Methods
Figs. S1 to S8
References (*30*–*33*)

6 August 2013; accepted 21 October 2013
10.1126/science.1244303

Interfollicular Epidermal Stem Cells Self-Renew via Autocrine Wnt Signaling

Xinhong Lim,[1]* Si Hui Tan,[2] Winston Lian Chye Koh,[3] Rosanna Man Wah Chau,[3] Kelley S. Yan,[4] Calvin J. Kuo,[4] Renée van Amerongen,[1]† Allon Moshe Klein,[5]‡ Roel Nusse[1]‡

The skin is a classical example of a tissue maintained by stem cells. However, the identity of the stem cells that maintain the interfollicular epidermis and the source of the signals that control their activity remain unclear. Using mouse lineage tracing and quantitative clonal analyses, we showed that the Wnt target gene *Axin2* marks interfollicular epidermal stem cells. These *Axin2*-expressing cells constitute the majority of the basal epidermal layer, compete neutrally, and require Wnt/β-catenin signaling to proliferate. The same cells contribute robustly to wound healing, with no requirement for a quiescent stem cell subpopulation. By means of double-labeling RNA in situ hybridization in mice, we showed that the *Axin2*-expressing cells themselves produce Wnt signals as well as long-range secreted Wnt inhibitors, suggesting an autocrine mechanism of stem cell self-renewal.

Stem cells residing in the adult interfollicular epidermis (IFE) regenerate the skin, but the nature of these cells and the molecular signals that regulate them remain incompletely understood. Because of their well-established importance in stem cell maintenance and hair growth, Wnts are candidate self-renewal factors for IFE stem cells. However, Wnt/β-catenin signaling is generally thought to control IFE differentiation rather than self-renewal (*1*, *2*). Reinforcing this view, interfollicular epidermal stem cells (IFESCs) have recently been suggested to originate from more primitive Wnt-independent ($Lgr6^+$) stem cells residing in the hair follicle (*3*). We sought to dissect the role of Wnt signaling in IFE homeostasis and regeneration. Because tissue stem cells are commonly influenced by signals secreted by nearby "niche" cells (*4*), we examined the presence of Wnts and Wnt inhibitors in the skin.

To determine whether Wnt-responding cells are present in the IFE, we looked in mouse skin for cells expressing *Axin2*, a well-known Wnt/β-catenin target gene. We focused on the mouse hindpaw (plantar) epidermis, a region devoid of hair follicles and sweat ducts (fig. S1A). We marked *Axin2*-expressing cells using Axin2-CreERT2 and found labeled cells in the basal layer (Fig. 1A and fig. S1E), consistent with Axin2 mRNA and reporter gene expression (fig. S1, B to D). These labeled cells generated clones in multiple IFE compartments that persisted for up to a year (Fig. 1A and fig. S1F), demonstrating that Axin2-CreERT2–labeled keratinocytes are self-renewing stem cells.

Recent studies examining epidermal stem cell fate provide little indication of the signaling pathways involved in cell fate choice. Using Axin2-CreERT2 as a combined lineage tracing and Wnt reporter tool, we studied the effect of Wnt signaling on cell fate, by analyzing labeled clones at high resolution in whole-mounted epidermis of Axin2-CreERT2/Rosa26-Rainbow (*5*) mice [Fig. 1B and supplementary theory (ST) section S-II]. We first asked whether long-lived Axin2-CreERT2–labeled clones might derive from slow-cycling stem cells that divide with invariant asymmetry to produce transit-amplifying cells (*6*, *7*), or equivalent "committed progenitors" and stem cells that divide with probabilistic fate (*8*–*10*). If Axin2-CreERT2 labeled only slow-cycling stem cells dividing with invariant asymmetry, we would expect to see labeled single cells that divide rarely and eventually give rise to stable, long-lived clones. In contrast, the probabilistic differentiation and self-renewal of stem cells and committed progenitors would lead to a rapid drop in the number of clones as a result of neutral clonal competition, with a concomitant increase in the average size of persisting clones to compensate for those that are lost (*11*). In addition, within a few cell divisions, the size distribution of the persisting clones would follow a simple exponential curve. Comparing the clonal data to these predictions, we found that the labeled Wnt-responding cells and their progeny exhibited all of the characteristics of probabilistic fate and neutral clonal competition (Fig. 1, C and D; fig. S2, A to C; and ST S-III and S-IV).

To determine whether active Wnt signaling, as indicated by *Axin2* expression, occurs in a functionally distinct subpopulation of IFESCs, we examined the number of Axin2-CreERT2–labeled cells in the basal layer over time. Between 3 days and 5 months after initial labeling, the total number of labeled cells in the basal layer of the epidermis remained constant (Pearson correlation coefficient $R = 0.08$ to time after labeling) (Fig. 1E and fig. S2H). This indicates that both Axin2-CreERT2–labeled and unlabeled cells have equal self-renewal capacity in homeostasis, suggesting that all IFESCs express *Axin2* (fig. S1, B to D), but only a subset is labeled when treated with

[1]Department of Developmental Biology, Howard Hughes Medical Institute (HHMI), Institute for Stem Cell Biology and Regenerative Medicine, School of Medicine, Stanford University, Stanford, CA, USA. [2]Program in Cancer Biology, School of Medicine, Stanford University, Stanford, CA, USA. [3]Department of Bio-engineering, Stanford University, Stanford, CA, USA. [4]Department of Medicine, School of Medicine, Stanford University, Stanford, CA, USA. [5]Department of Systems Biology, Harvard Medical School, Boston, MA, USA.

*Present address: Institute of Medical Biology, A*STAR, Singapore.
†Present address: Swammerdam Institute for Life Sciences, University of Amsterdam, Netherlands.
‡Corresponding author. E-mail: rnusse@stanford.edu (R.N.); allon_klein@hms.harvard.edu (A.M.K.)

Tamoxifen. Further supporting the notion that *Axin2*-expressing cells are representative of the general population of IFESCs, clonal outcomes showed the same probabilities of division and differentiation at early and late time points (fig. S2, D and E, and ST S-V). Thus, Axin2-CreERT2–labeled cells were not biased in their fate choice and were not enriched in a subpopulation of slow-cycling stem cells. If slow-cycling IFESCs are present, they too undergo neutral competition (ST S-VI). However, using a DNA label–retaining assay (*12*, *13*) (fig. S3A), we were unable to detect any label-retaining cells in or outside of persisting Axin2-CreERT2–labeled clones (Fig. 1, F and G; fig. S3, B to E; and ST S-VI).

To further test the regenerative potential of *Axin2*-expressing IFESCs, we induced full-thickness skin biopsy punch wounds in labeled Axin2-CreERT2/Rosa26-mTmG^{flox} mice (fig. S4A). We found large numbers of relatively even-sized clones radiating into the healed epidermis that persisted for up to 35 days (Fig. 2A and fig. S4B), showing that *Axin2*-expressing IFESCs robustly contribute to regeneration. However, the labeled cells constituted similar percentages of injured and uninjured skin (Fig. 2B and fig. S4C), indicating that labeled and unlabeled cells have equal abilities to regenerate. Consistent with data from our cell label–retention assays (Fig. 1, F and G; fig. S3; and ST S-VI), these results also indicate

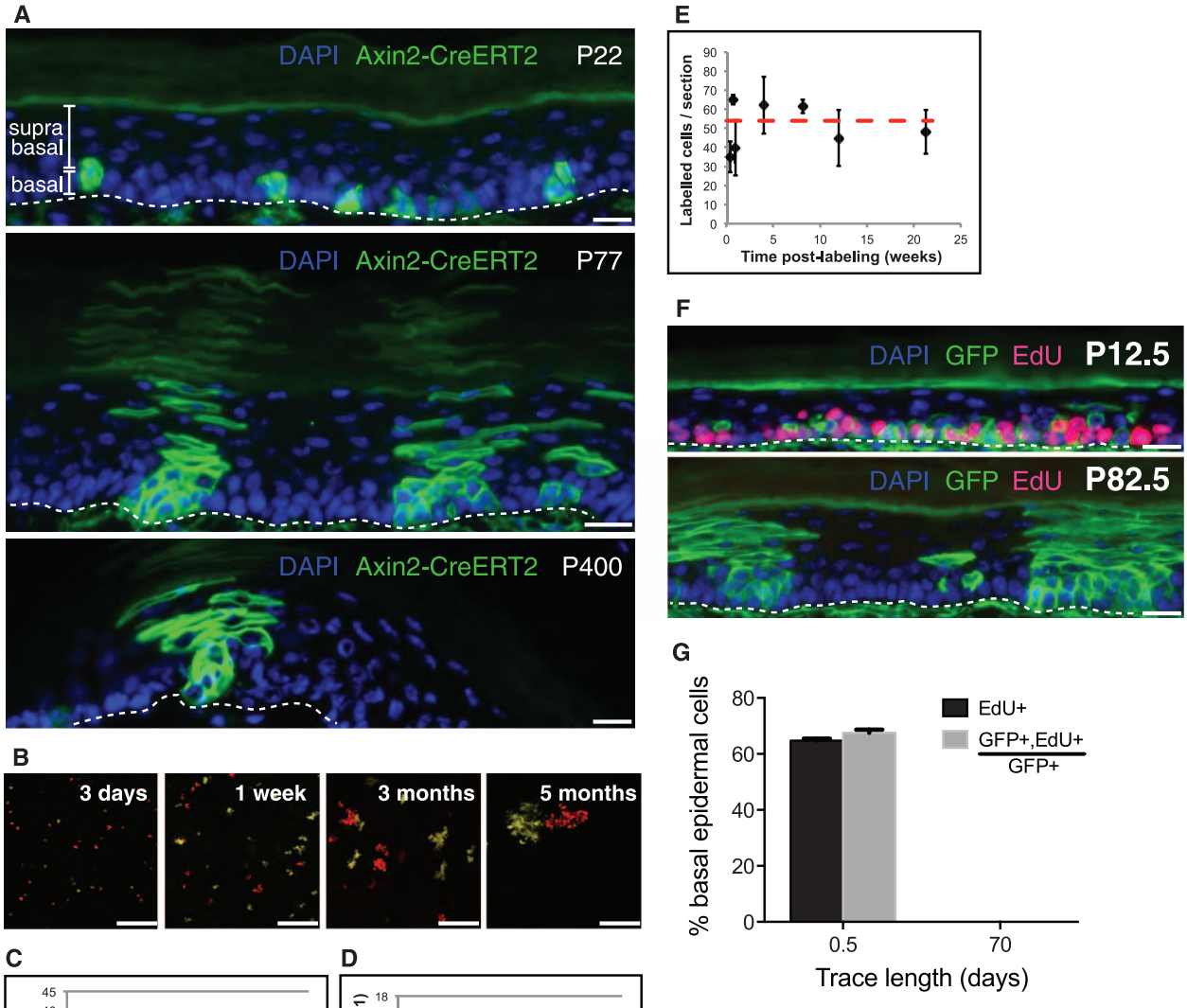

Fig. 1. *Axin2*-expressing basal interfollicular epidermal cells are stem cells that undergo neutral competition and exhibit probabilistic cell fate. (**A**) Histological sections of plantar epidermis from Axin2-CreERT2/Rosa26mTmG^{flox} mice chased for 1 day [postnatal day 22 (P22)], 2 months (P77), and more than 1 year (P400). Scale bars, 10 μm. Basal and suprabasal epidermal layers are indicated. The dashed line denotes the approximate location of the epidermis/dermis boundary. (**B**) Representative images of whole-mounted Axin2-CreERT2/Rosa26-Rainbow^{flox} plantar epidermis traced from 3 days to 5 months. Only mOrange and mCherry clones in the basal epidermal layer are shown and scored (ST S-II). Scale bars, 100 μm. (**C** and **D**) The number of clones per image section drops, whereas the average clone size (basal cells per clone) increases, consistent with a model of probabilistic stem cell fate and neutral competition (NC model, red curve) (error bars = SD, $n \geq 3$ mice). (**E**) The number of labeled basal cells per image section remains stable; the red dashed line shows the average over all time points. (**F**) Representative histological sections of Axin2-CreERT2/Rosa26mTmG^{flox} plantar epidermis chased for 0.5 days (P12.5) and 70.5 days (P82.5). The dashed line denotes the approximate location of the epidermis/dermis boundary. Scale bars, 10 μm. (**G**) Changes in the proportion of EdU$^+$ and GFP$^+$, EdU$^+$/GFP$^+$ basal cells (error bars indicate SEM). All counts were derived from $n \geq 2$ animals per time point and were subject to unpaired Student's *t* tests.

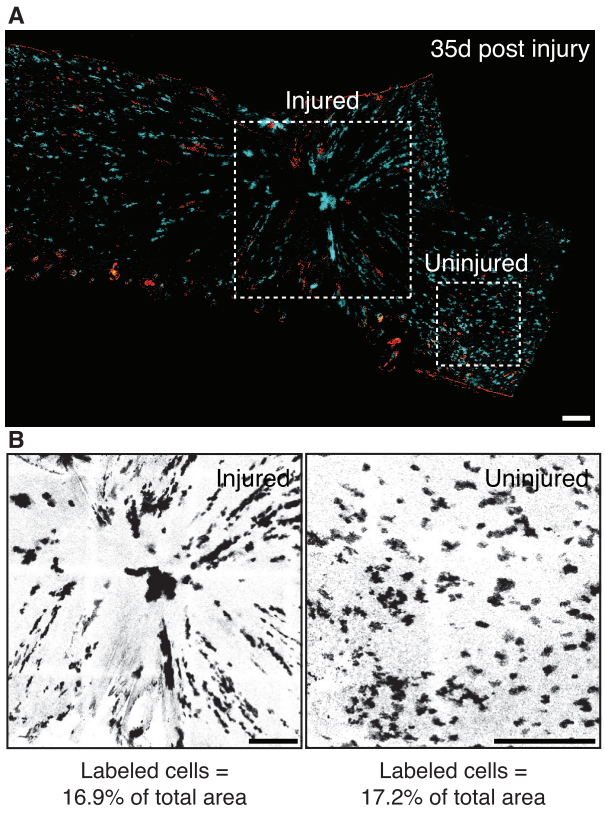

Fig. 2. *Axin2*-expressing interfollicular epidermal stem cells contribute robustly to wound repair. (**A**) Whole-mount views of healing Axin2-CreERT2/Rosa26-Rainbow^{flox} plantar epidermis at 35 days after wounding. Dashed squares denote approximate injured (left) and uninjured (right) areas. (**B**) Image masks of injured and uninjured areas. Scale bars, 300 μm.

that, if they are present, rare slow-cycling stem cells are not the primary contributors to epidermal wound repair as previously suggested (*10*).

We next tested whether *Axin2*-expressing IFESCs functionally require Wnt/β-catenin signaling, by conditionally inactivating the gene encoding β-catenin in *Axin2*-expressing cells. We found an average 30% reduction in the overall cellularity of mutant epidermises (Fig. 3, A and B). Consistent with this, 68 ± 3% of control basal cells expressed Ki67 (Fig. 3, C and D), a marker of proliferating cells, whereas only 35 ± 4% of mutant basal cells were Ki67-positive (Fig. 3, C and D), suggesting a proliferation defect. Similarly, the number of basal cells expressing phosphohistone-H3, another marker of dividing cells, was significantly decreased (fig. S5, A and B). To determine whether epidermal differentiation was also affected, we stained skins for Keratin-10 (K10), an early marker of keratinocyte differentiation. Only 18 ± 1% of control basal cells expressed K10, consistent with estimates obtained from clonal analysis (ST S-IV), whereas 36 ± 1% of mutant basal cells were K10-positive (Fig. 3, E and F). Although we cannot exclude systemic effects, our results suggest that IFESCs that are mutant for β-catenin stop proliferating and undergo differentiation. Taken together with our clonal analysis, this suggests that Wnt/β-catenin signal-

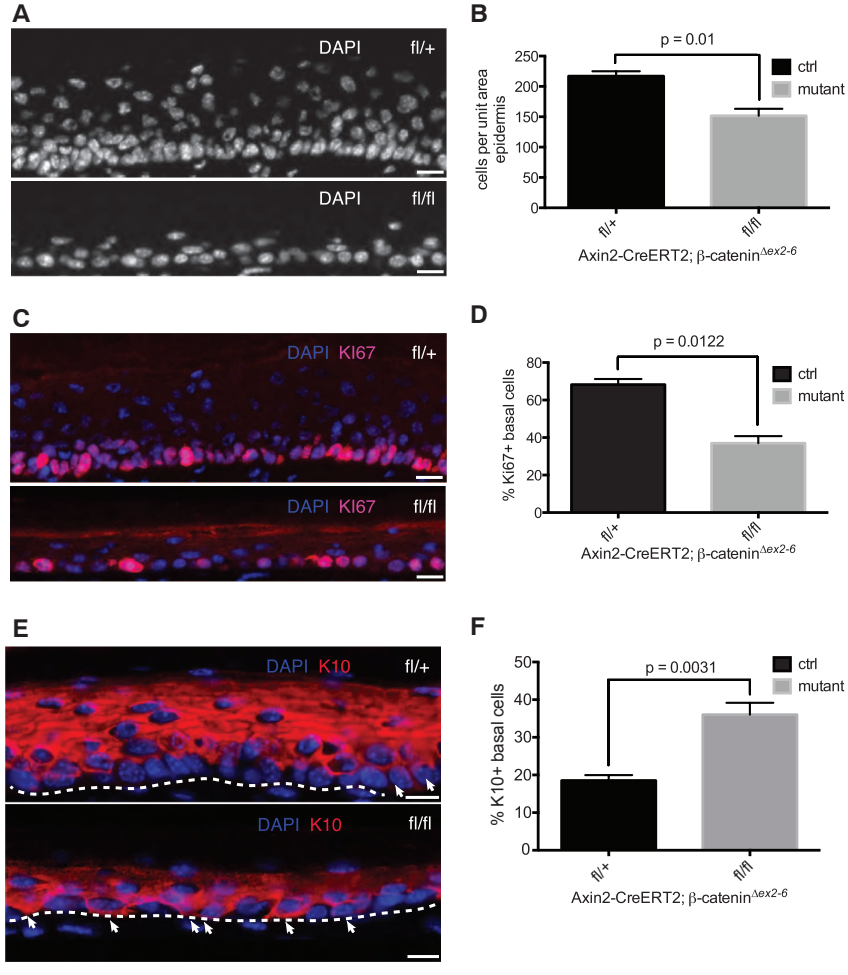

Fig. 3. *Axin2*-expressing interfollicular epidermal stem cells require β-catenin to proliferate and maintain normal epidermal homeostasis. (**A**, **C**, and **E**) Representative images of DAPI, Ki67, and K10 immunostaining of control Axin2-CreERT2/β-catenin$^{Δex2\text{-}6\text{-}fl/+ \text{ or } -del/+}$ and mutant Axin2-CreERT2/β-catenin$^{Δex2\text{-}6\text{-}fl/fl \text{ or } -fl/del}$ plantar epidermis. White arrows in (E) indicate basal epidermal cells staining positive for K10. Dashed lines denote the approximate location of the epidermis/dermis boundary. (**B**, **D**, and **F**) Changes in cellularity, proliferative index, and differentiation between control and mutant plantar epidermises as determined by counting and plotting (B) DAPI$^+$ nuclei, (D) Ki67$^+$ nuclei, and (F) K10$^+$ basal cells (error bars indicate SEM). All counts were derived from $n \geq 3$ independent experiments and were subject to pairwise Student's *t* tests. Scale bars, 10 μm.

ing maintains the IFE stem cell proliferative state but does not affect the likelihood of symmetric self-renewal or differentiation of individual cells.

So where do the Wnt signals come from, and how is the niche for IFESCs organized in a way that permits neutral competition? With the use of double-labeling RNA in situ hybridization, we found that *Axin2*-expressing basal cells in the postnatal epidermis are themselves the source of Wnt signals, expressing several Wnt genes, including *Wnt4* and *Wnt10a* (Fig. 4A and fig. S6B). This pattern of Wnt gene expression is consistent with previous reports regarding the embryonic basal epidermis (*14*, *15*). Further supporting this observation, primary basal epidermal cells isolated from human skin express *Wnt4*, whereas suprabasal epidermal cells do not (Fig. 4B) (*16*). Similarly, cultured primary adult human epidermal keratinocytes express various Wnt genes, as well as *Porcupine* (*Porcn*), which is required for Wnt secretion (fig. S7).

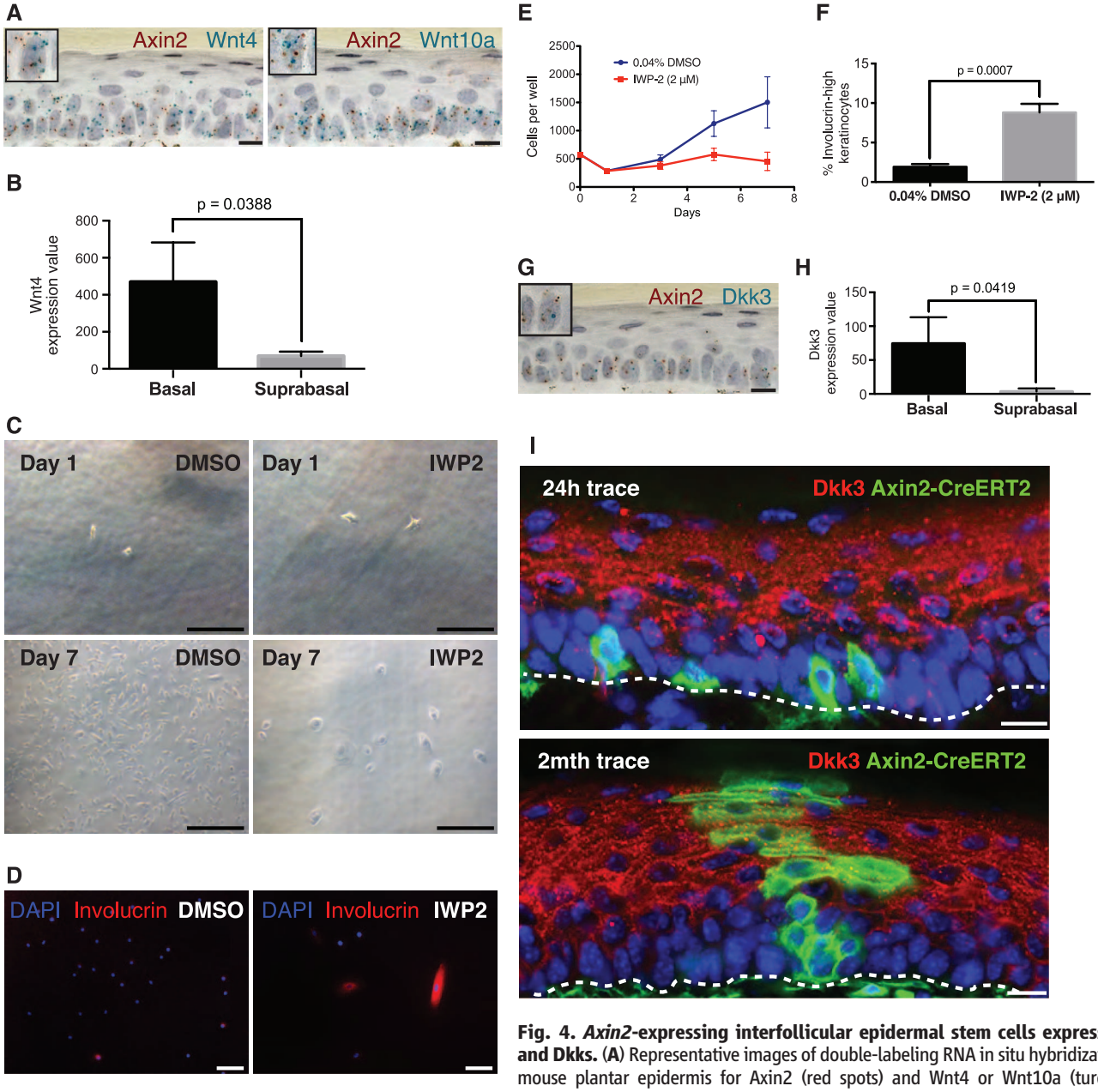

Fig. 4. *Axin2*-expressing interfollicular epidermal stem cells express Wnt and Dkks. (**A**) Representative images of double-labeling RNA in situ hybridization in mouse plantar epidermis for Axin2 (red spots) and Wnt4 or Wnt10a (turquoise spots). Inset boxes show a magnified view of individual basal cells expressing both Axin2 and Wnts. Scale bars, 10 μm. (**B**) Wnt4 expression in β4-integrin^{+} primary human basal epidermal keratinocytes versus β4-integrin-suprabasal epidermal keratinocytes (error bars indicate SD). Expression values are from the Gene Expression Omnibus (GEO) data set GSE26059. (**C** and **D**) Representative (C) bright-field or (D) immunofluorescence images of keratinocytes continuously cultured in defined medium with either 0.04% DMSO or 2 μM IWP-2, at the beginning (day 1) and the end (day 7) of the experiment, then stained for involucrin. Scale bars, 50 μm (bright-field image) or 100 μm (immunofluorescence image). (**E** and **F**) Changes in the (E) number of cells and (F) percentage of involucrin-high cells per well of keratinocytes treated with either 0.04% DMSO or 2 μM IWP-2 (error bars indicate SEM). Cell counts at all time points were derived from n = 3 replicate wells. (**G**) Representative image of double-labeling RNA in situ hybridization for Axin2 (red spots) and Dkk3 (turquoise spots). The inset box shows a magnified view of individual basal cells expressing both Axin2 and Dkk3. Scale bar, 10 μm. (**H**) Dkk3 expression in primary human β4-integrin$_{+}$ basal epidermal keratinocytes versus β4-integrin-suprabasal epidermal keratinocytes (error bars indicate SD). Expression values are from GEO data set GSE26059. (**I**) Representative images of Dkk3 immunostaining in plantar epidermises of Axin2-CreERT2/Rosa26mTmG^{flox} mice exposed to Tam at P21 and chased for 1 day (P22) and 2 months (P77). Scale bars, 10 μm.

To determine whether IFESCs functionally require the Wnt that they produce, we treated human epidermal keratinocytes with IWP-2, a validated small-molecule inhibitor of Wnt secretion, and cultured them at clonal density in a defined medium. IWP-2–treated keratinocytes were sparsely distributed and became large and flattened with arrested growth, unlike the densely packed, cuboidally shaped, control keratinocytes (Fig. 4, C and E). Many more IWP-2–treated keratinocytes also expressed high levels of involucrin, a marker of advanced keratinocyte differentiation (Fig. 4, D and F). These data are consistent with our in vivo observations that IFESCs undergo premature differentiation upon loss-of-function mutations in Wnt signaling (Fig. 3, E and F).

If IFESCs are both the source and the target of Wnt signals, how might they escape from this autocrine loop and enter a differentiation process? Several genes for secreted Wnt inhibitors, including *Dickkopf-1* (*Dkk1*), *Dkk3*, and *Wnt Inhibitory Factor-1* (*WIF1*) are expressed in the skin (*17*–*19*). With double-labeling RNA in situ hybridization, we saw overlapping expression of *Dkks* and *Axin2* expression in basal cells (Fig. 4G and fig. S6C). This is similar to the situation in human skin, in which primary human basal cells, either isolated from skin tissue or cultured in vitro, express *Dkks* (Fig. 4H and fig. S7). Although the Dkk (Fig. 4, G and H, and fig. S6C) and WIF1 (*19*) mRNAs are mostly located in basal cells, the secreted WIF1 and Dkk3 proteins accumulate at high levels in the suprabasal layers (*18*, *19*). By antibody staining for the Dkk3 protein, we confirmed that Dkk3 is localized to the suprabasal layers, directly adjacent to the *Axin2*-expressing basal progenitors (Fig. 4I and figs. S8, A and B, and S9) (*18*). We tested whether Dkk influences stem cells in the skin by adenoviral overexpression of Dkk, finding that this caused a thinned and hypoproliferative epidermis (fig. S10) resembling β-catenin mutant skin (Fig. 3A). These data suggest that the differential diffusion of Wnts and Dkk from the basal epidermal stem cells may restrict autocrine Wnt/β-catenin signaling to the basal layer of the epidermis (fig. S8C). IFESCs leaving the basal layer would encounter increased Wnt inhibitors and differentiate.

Functional redundancy between the various Wnt inhibitors and Wnts expressed in the skin (Fig. 4, A and G, and fig. S6, B and C) may explain the absence of overt phenotypes in mice mutant for these genes (*20*). However, there is genetic evidence supporting an essential role for Wnt signals in the epidermis. *Porcn*-knockout mice display a thinned epidermis, similar to that seen in human patients bearing *Porcn* mutations who develop focal dermal hypoplasia (*21*–*23*). Mutations in both Wnt effectors *Tcf3* and *Tcf4* result in a thinner epidermis (*24*), whereas deleting β-catenin using the basal epidermal specific driver Keratin-5-rtTA/tet-O-Cre also results in a thinner and hypoproliferative plantar epidermis (*25*).

Signals emerging from a distinct niche cell compartment are thought to be the main drivers of stem cell self-renewal. We find that epidermal stem cells themselves can be the source of their own self-renewing signals and differentiating signals for their progeny. We postulate that the multiplicity of Wnts and Wnt inhibitors produced by epidermal stem cells allows for fine-tuning of epidermal thickness and wound repair.

References and Notes

1. J. Huelsken, R. Vogel, B. Erdmann, G. Cotsarelis, W. Birchmeier, *Cell* **105**, 533–545 (2001).
2. S. Beronja *et al.*, *Nature* **501**, 185–190 (2013).
3. H. J. Snippert *et al.*, *Science* **327**, 1385–1389 (2010).
4. V. P. Losick, L. X. Morris, D. T. Fox, A. Spradling, *Dev. Cell* **21**, 159–171 (2011).
5. H. Ueno, I. L. Weissman, *Dev. Cell* **11**, 519–533 (2006).
6. I. C. Mackenzie, *Nature* **226**, 653–655 (1970).
7. C. S. Potten, *Cell Tissue Kinet.* **7**, 77–88 (1974).
8. E. Clayton *et al.*, *Nature* **446**, 185–189 (2007).
9. D. P. Doupé, A. M. Klein, B. D. Simons, P. H. Jones, *Dev. Cell* **18**, 317–323 (2010).
10. G. Mascre *et al.*, *Nature* **489**, 257–262 (2012).
11. A. M. Klein, B. D. Simons, *Development* **138**, 3103–3111 (2011).
12. J. R. Bickenbach, J. McCutecheon, I. C. Mackenzie, *Cell Prolif.* **19**, 325–333 (1986).
13. K. M. Braun *et al.*, *Development* **130**, 5241–5255 (2003).
14. S. Reddy *et al.*, *Mech. Dev.* **107**, 69–82 (2001).
15. F. Witte, J. Dokas, F. Neuendorf, S. Mundlos, S. Stricker, *Gene Expr. Patterns* **9**, 215–223 (2009).
16. N. Radoja, A. Gazel, T. Banno, S. Yano, M. Blumenberg, *Physiol. Genomics* **27**, 65–78 (2006).
17. Y. Yamaguchi *et al.*, *J. Cell Biol.* **165**, 275–285 (2004).
18. G. Du *et al.*, *Exp. Dermatol.* **20**, 273–277 (2011).
19. H. Schlüter, H.-J. Stark, D. Sinha, P. Boukamp, P. Kaur, *J. Invest. Dermatol.* **133**, 1669–1673 (2013).
20. I. del Barco Barrantes *et al.*, *Mol. Cell. Biol.* **26**, 2317–2326 (2006).
21. J. J. Barrott, G. M. Cash, A. P. Smith, J. R. Barrow, L. C. Murtaugh, *Proc. Natl. Acad. Sci. U.S.A.* **108**, 12752–12757 (2011).
22. W. Liu *et al.*, *PLOS ONE* **7**, e32331 (2012).
23. J. L. Bolognia, J. L. Jorizzo, J. V. Schaffer, in *Dermatology* (Mosby-Saunders, London, 2012), pp. 869–885.
24. H. Nguyen *et al.*, *Nat. Genet.* **41**, 1068–1075 (2009).
25. Y. S. Choi *et al.*, *Cell Stem Cell* 10.1016/j.stem.2013.10.00 (2013).

Acknowledgments: These studies were supported by the HHMI, California Institute of Regenerative Medicine grant TR1-01249, and NIH grants NIH 1U01DK085527, 1R01DK085720, and 5K08DK096048. We thank L. De Simone, A. E. Marcy, and P. H. Chia for cell quantification assistance; C. Logan, S. J. Habib, and A. Oro for manuscript comments; and J. Akech and L.-C. Wang at Advanced Cell Diagnostics for assistance with RNA in situ hybridization. X.L., S.H.T., W.L.C.K., and R.M.W.C. are supported by National Science Scholarships from A*STAR, Singapore. A.M.K. holds a Career Award at the Scientific Interface from the Burroughs Wellcome Fund. K.S.Y. has a Burroughs Wellcome Fund Career Award for Medical Scientists. R.v.A. was supported by a European Molecular Biology Organization long-term fellowship (ALTF 122-2007) and a Dutch Cancer Society fellowship.

Supplementary Materials

www.sciencemag.org/content/342/6163/1226/suppl/DC1
Materials and Methods
Supplementary Theory and Data Analysis
Figs. S1 to S10
References (*26*–*40*)

29 April 2013; accepted 28 October 2013
10.1126/science.1239730

Preferential Recognition of Avian-Like Receptors in Human Influenza A H7N9 Viruses

Rui Xu,[1] Robert P. de Vries,[2] Xueyong Zhu,[1] Corwin M. Nycholat,[2] Ryan McBride,[2] Wenli Yu,[1] James C. Paulson,[2]* Ian A. Wilson[1,3]*

The 2013 outbreak of avian-origin H7N9 influenza in eastern China has raised concerns about its ability to transmit in the human population. The hemagglutinin glycoprotein of most human H7N9 viruses carries Leu^{226}, a residue linked to adaptation of H2N2 and H3N2 pandemic viruses to human receptors. However, glycan array analysis of the H7 hemagglutinin reveals negligible binding to humanlike α2-6–linked receptors and strong preference for a subset of avian-like α2-3–linked glycans recognized by all avian H7 viruses. Crystal structures of H7N9 hemagglutinin and six hemagglutinin-glycan complexes have elucidated the structural basis for preferential recognition of avian-like receptors. These findings suggest that the current human H7N9 viruses are poorly adapted for efficient human-to-human transmission.

In the spring of 2013, an outbreak of human infections caused by avian-origin H7N9 subtype influenza A virus occurred in the eastern provinces of China (*1*). By the end of May 2013, 132 cases of laboratory-confirmed H7N9 influenza were reported, resulting in 37 deaths (*2*). These patients generally presented influenza-like illnesses that frequently progressed to acute respiratory distress syndrome and severe pneumonia (*3*, *4*). However, natural infection by H7N9 viruses in avian hosts are asymptomatic, which allows the virus to spread among birds and not be readily detected by surveillance (*2*).

The H7N9 outbreak has raised concerns about its potential for causing human pandemics or epidemics (*5*, *6*). Compared with H5N1 viruses, H7N9 appears to transmit from birds to humans more readily, with reports of a relatively large

number of recent human infections in a short period of time. Fortunately, avian influenza viruses such as H7N9 must overcome a species barrier that prevents efficient transmission from human to human and thereby attain wide circulation in an antigenically naïve human population. Early reports have suggested that exposure to poultry was responsible for over 75% of the documented human cases of H7N9 influenza, but limited human-to-human transmission cannot be ruled out, especially in a few small clusters of human infections (*4*). Sequence analysis of the H7N9 viral proteins revealed that the virus has acquired several amino acid changes associated with adaptation to human receptor binding and transmission in prior human pandemics (*7*–*9*). The PB2 protein of the H7N9 virus contains a Glu (E)–to–Lys (K) mutation at position 627 (E627K) that is important in other viruses for respiratory droplet transmission among humans (*10*). Furthermore, the hemagglutinins (HAs) from most H7N9 human isolates have Leu at position 226 (H3 numbering) instead of Gln, which is conserved in avian H7 HAs (*7*, *8*), as well as in other avian subtypes (*11*, *12*). The Gln-to-Leu mutation is one of the hallmarks of the switch to human receptor binding specificity that occurred in the 1957 H2N2 and 1968 H3N2 human influenza virus pandemics, representing an adaptation believed to be required for efficient human-to-human transmission (*11*–*13*). Recent studies suggested that the H7N9 virus could efficiently transmit among experimental ferrets via direct contact (*14*–*16*), but respiratory droplet transmission, the mode of transmission relevant to human pandemics, is less efficient, as demonstrated by results from five independent studies (*9*, *14*–*18*). Thus, it is of major interest for public health to understand the extent to which the current H7N9 viruses have evolved to acquire capabilities for human-to-human transmission.

Most avian H7 viruses, including those associated with previous human outbreaks, contain highly conserved avian-specific residues, including Gln^{226}, in their receptor binding sites that enable them to specifically recognize terminal sialic acids in an α2-3 linkage to galactose (*19*, *20*). In contrast, whereas the first human H7N9 virus isolated contained Gln^{226} (A/Shanghai/1/2013, abbreviated as Sh1), most other human H7N9 viruses analyzed so far carry Leu^{226} (e.g., A/Shanghai/2/2013, Sh2), with a few isolates containing Ile^{226} (e.g., A/Hangzhou/1/2013, Hz1) (*7*). The Gln-to-Leu mutation is associated with improved affinity for human receptors where sialic acid is α2-6–linked to galactose (*7*, *8*). In avian H2 and H3 HA, the Q226L (Q, Gln; L, Leu) mutation by itself greatly decreases HA affinity for α2-3–linked glycans while substantially improving binding to α2-6–linked glycans (*21*, *22*). Recent studies have showed that H7N9 viruses with Leu^{226} can bind to receptors on the human tracheal epithelium (*23*) and are able to replicate in the upper respiratory tract of ferrets (*14*, *15*). Unlike previous H7 viruses isolated in humans (such as H7N7), which exhibit contact transmission between ferrets but no respiratory droplet transmission (*24*), the human H7N9 viruses exhibit limited transmission by respiratory droplets (*9*, *14*–*16*, *18*), heightening concern that receptor binding changes might support more efficient transmission in humans (*24*).

We determined the crystal structure of Sh2 H7 HA at 2.7 Å resolution (Fig. 1A and table S1) and found that it is structurally similar to the HA from a highly pathogenic avian H7N7 virus that infected humans (A/Netherlands/219/2003, Neth219) [Protein Data Bank (PDB) entry 4DJ6] (*20*) [Cα root mean square deviation (RMSD) of 1.2 Å and only 0.4 Å for the receptor binding domain]. The main differences around the receptor binding site arise from the Q226L mutation and the absence of an *N*-linked glycosylation site at Asn^{133} in Sh2 because of a T135A (T, Thr; A, Ala) substitution (Fig. 1B).

Although studies evaluating receptor binding by using whole viruses (*14*–*16*, *25*, *26*) have reported that the Leu^{226} mutation increases binding of H7N9 viruses to human receptors, binding to avian- and human-type receptors is influenced by the neuraminidase, which preferentially cleaves avian-type receptors (*15*, *25*). To directly examine the intrinsic receptor specificity of the H7N9 HA, we analyzed HA binding to sialosides in plate-based assays and glycan arrays by using soluble recombinant trimeric HAs expressed in mammalian cells (Fig. 2). In the plate assay, Sh2 HA strongly prefers α2-3–sialylated di-*N*-acetyllactosamine (SLNLN), although weak binding to α2-6 SLNLN at high protein concentrations is also observed (Fig. 2A) (*27*). Substitution of Leu^{226} to Gln, as in Sh1, or Ile, as in Hz1 strains, slightly increases avidity for α2-3 SLNLN but completely abrogates binding to α2-6 SLNLN in this assay (Fig. 2A). The preferential binding of recombinant Sh2 HA to α2-3 sialosides in analogous plate assays or in biosensor-based assays has also been recently reported by other groups (*28*–*30*).

The H7N9 HA receptor binding properties were further investigated by using a custom influenza receptor glycan microarray comprised of diverse α2-3 sialosides [numbers (nos.) 3 to 35] and α2-6 sialosides (nos. 36 to 56) that correspond to *N*- and *O*-linked glycans and linear

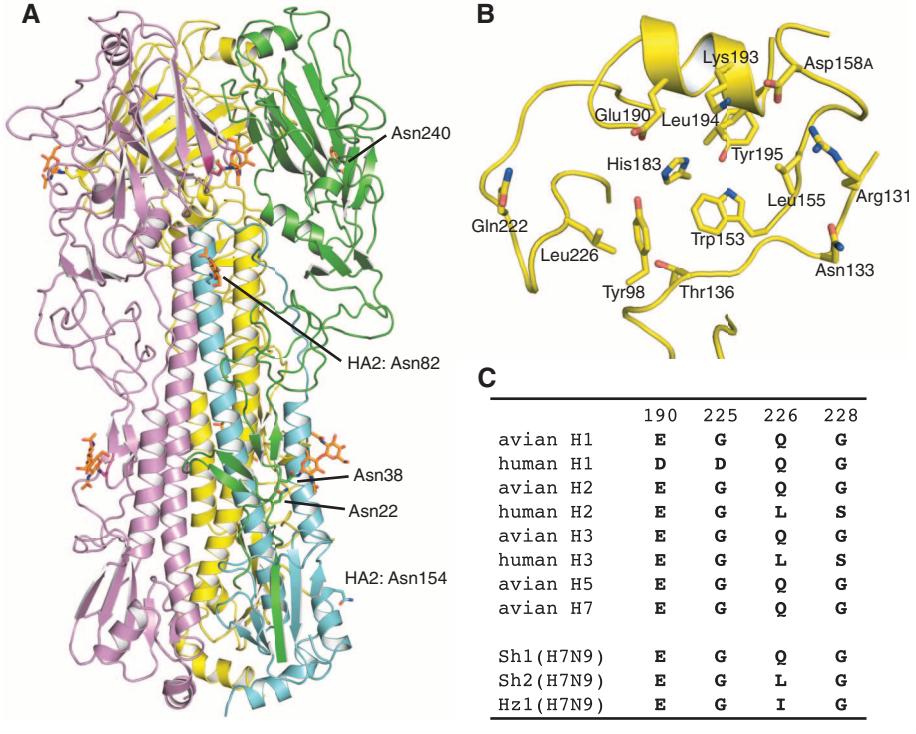

Fig. 1. Crystal structure of the HA from a human H7N9 virus (A/Shanghai/2/2013, Sh2). (**A**) HA trimer is shown in cartoon representation. For one of the protomers, HA1 is colored in green and HA2 in cyan. The other two protomers (B and C) of the trimer are in yellow and magenta, respectively. *N*-glycosylation sites and *N*-linked glycans are highlighted in sticks and numbered at the Asn attachment site. (**B**) Human H7 HA has Leu^{226} in its receptor binding site. (**C**) Variation at the four HA positions that are known to mediate the switch in receptor binding specificity for human H1, H2, and H3 pandemic viruses and the corresponding sequences in H1, H2, H3, H5, and H7 subtypes in avian viruses in comparison with human H7N9. G, Gly; S, Ser.

[1]Department of Integrative Structural and Computational Biology, The Scripps Research Institute, 10550 North Torrey Pines Road, La Jolla, CA 92037, USA. [2]Department of Cell and Molecular Biology and Department of Chemical Physiology, The Scripps Research Institute, 10550 North Torrey Pines Road, La Jolla, CA 92037, USA. [3]Skaggs Institute for Chemical Biology, The Scripps Research Institute, 10550 North Torrey Pines Road, La Jolla, CA 92037, USA

*Corresponding author. E-mail: wilson@scripps.edu (I.A.W.); jpaulson@scripps.edu (J.C.P.)

fragments of glycans on mammalian glycoproteins and glycolipids (see list in table S3). Sh2 with Leu^{226} shows highly restricted binding to a small number of α2-3–sialylated glycans, and no detectable binding to α2-6–sialylated glycans, consistent with the more stringent requirements for binding in this assay (*31*). This subset of α2-3–sialosides includes sulfated linear glycans (nos. 3, 4, and 7), linear and branched *O*-linked glycans (nos. 20, 21, 23, and 24), and biantennary *N*-linked glycans (nos. 25 to 27). Specificity for sulfated glycans nos. 3 {NeuAcα2-3Galβ1-4[6S]GlcNAc, where NeuAc is *N*-acetylneuraminic acid, Gal is galactose, and GlcNAc is *N*-acetylglucosamine} and 4 {NeuAcα2-3Galβ1-4(Fucα1-3) [6S]GlcNAc, where Fuc is fucose} are characteristic of H7 avian viruses, including those from poultry and aquatic birds (*19*, *24*, *32*). The L226I and L226Q (I, Ile) substitutions change the distribution of glycan receptors that Sh2 HA binds, but specificity for α2-3–sialylated glycans is maintained (Fig. 2B) (*33*). A similar strict specificity for α2-3–sialylated glycans was observed for recombinant H7 HAs expressed in a baculovirus expression system (figs. S1 and S2) (*34*). In summary, Sh2 HA with Leu^{226} still maintains strong avian-type receptor specificity, with only very weak binding to human-type α2-6 receptors.

Previous structural analyses of HA-receptor recognition and specificity have been limited to a small group of linear glycan receptor analogs, including short synthetic fragments of glycans on glycoproteins and glycolipids (3′-SLN, NeuAcα2-3Galβ1-4GlcNAc, and 6′-SLN, NeuAcα2-6Galβ1-4GlcNAc) and related oligosaccharides from human milk [LSTa, NeuAcα2-3Galβ1-3GlcNAcβ1-3Galβ1-4Glc; LSTc, NeuAcα2-6Galβ1-4GlcNAcβ1-3Galβ1-4Glc; and LSTb, Galβ1-4(NeuAcα2-6)GlcNAcβ1-3Galβ1-4Glc] (Fig. 3A) (*30*, *35*). Notwithstanding, these ligands have provided valuable information on how avian and human HAs differentially recognize α2-3– and α2-6–linked sialosides.

We determined crystal structures of Sh2 H7 HA with avian receptor analog LSTa at 2.6 to 2.7 Å resolution and found that only sialic acid 1 (Sia-1) and Gal-2 of LSTa were ordered (Fig. 3B and fig. S3). A comparison of human and avian H7 HA structures reveals several differences in receptor recognition. In avian H7 from Neth219 virus (PDB entry 4DJ7) (*20*), preferential binding to avian receptors is mediated by Gln^{226}, which hydrogen bonds with the Gal-2 O3 atom at the Sia-Gal linkage and the 4-hydroxyl group of Gal-2 (Fig. 3D). In addition, the Sia-1 carboxyl group is located within 3.5 Å of Gln^{226}. This mode of recognition is highly conserved in other avian HA subtypes (*35*). In Sh2, the hydrophobic Leu^{226} does not support such a hydrogen-bonding network, and Gal-2 moves away from Leu^{226}, which results in LSTa taking a slightly different trajectory exiting the binding pocket. No significant interactions were visualized with the glycan ligand beyond Sia-1, suggesting a weak interaction that was not improved by increased soaking time and concentration of LSTa (fig. S3 and table S1).

Similarly, in the crystal structure of Sh2 with human receptor analog LSTc at 2.9 Å resolution, only Sia-1 and Gal-2 could be modeled (Fig. 3C). Leu^{226} mediates hydrophobic interactions with the Gal-2 hydrophobic face through its C6 and C4 atoms. Although the specific interactions involving Gal-2 are similar in the human H2 HA complex with LSTc (PDB entry 2WR7) (Fig. 3E) (*36*), other structural features in H7N9 HA may prevent further stabilization of the glycan receptor analog beyond GlcNAc-3. Similar to avian H7 HA (*20*), the 150 loop of Sh2 H7 HA is closer to the receptor binding site than it is in H2 HA (Fig. 3, C and E).

These Sh2 HA structures with receptor analogs (LSTa and LSTc) then suggest that Leu^{226} modifies HA recognition of glycans with an α2-3 linkage but does not adapt the HA receptor binding site for binding of α2-6–linked glycans (Fig. 3, B and C). These structural findings are generally consistent with other recent structural studies on human H7 (*25*, *29*). The most notable difference is the cis configuration of α2-3 linkage in these structures, which may result from use of different receptor analogs (*37*).

To further explore the structural basis for retention of avian-type receptor specificity, we determined crystal structures of Sh2 H7 HA at 2.5 to 2.85 Å resolution with glycans 3, 21, and 23, which were identified as specific binders on the microarray (Fig. 4 and table S2). In each case, additional HA-glycan contacts are created distal

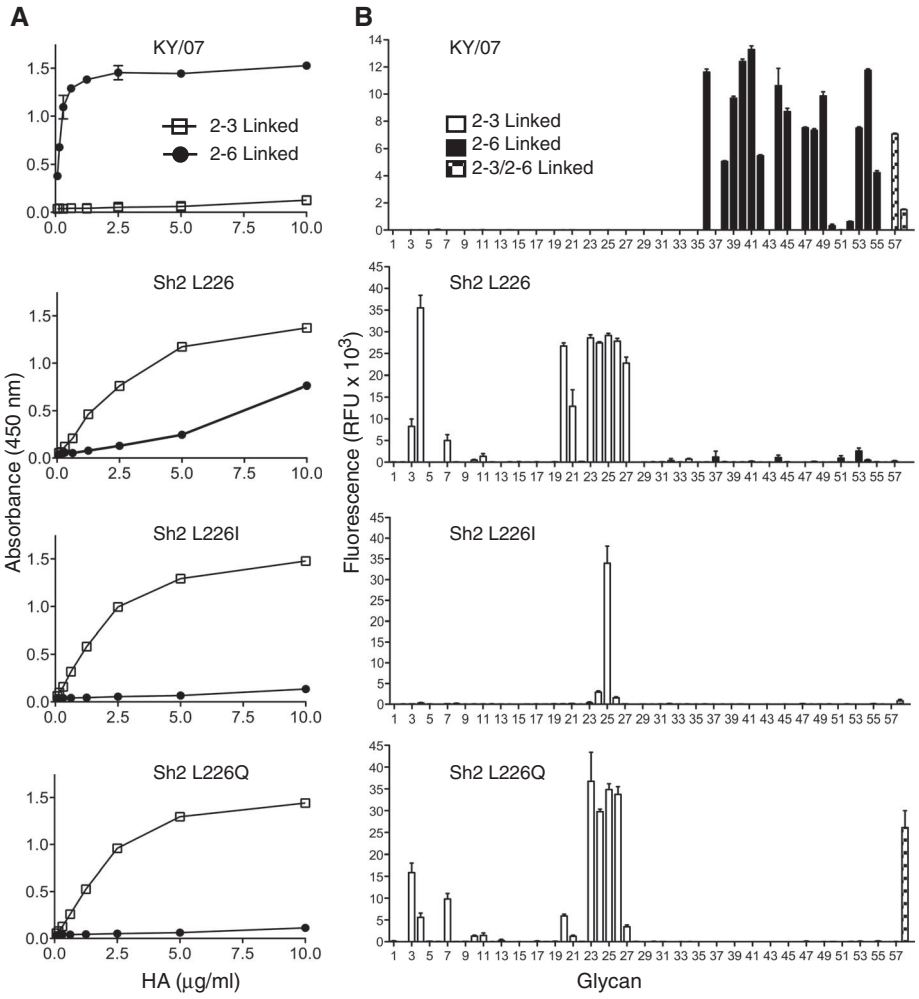

Fig. 2. Receptor binding specificity of H7N9 HAs determined by plate-based glycan binding and glycan microarray analyses. (A) Enzyme-linked immunosorbant assay (ELISA) plates coated with either α2-3– or α2-6–linked SLNLN-PAA were probed with recombinant HAs produced in human embryonic kidney (HEK293S GnTI^{-}) cells. The HAs were human H1N1 seasonal strain KY/07 or H7N9 Sh2 wild type containing Leu (L) at position 226 and mutants at this position harboring Ile (I) or Gln (Q). Shown are data representative of three independent experiments, each done in triplicate, with binding to α2-6–glycans in solid circles and α2-3–glycans in open squares. Error bars indicate standard errors. **(B)** The same recombinant HA proteins were used for assessment of receptor binding specificity on a glycan array. The mean signal and standard error were calculated from six independent replicates on the array. α2-3 sialosides are shown in white bars (glycans 3 to 35), α2-6 sialosides in black (glycans 36 to 56), and striped bars denoted mixed biantennary glycans containing both α2-3– and α2-6–linked sialylated glycans (glycans 57 and 58). Glycans imprinted on the array are listed in table S3.

to the Sia-Gal linkage, so that efficient binding to α2-3–linked glycans is achieved despite Leu^{226} (Fig. 5). Most relevant is glycan no. 3 (NeuAcα2-3Galβ1-4[6S]GlcNAc), which has been demonstrated to be a receptor analog recognized by all avian H7 viruses (*19*, *32*). Previous efforts to model sulfated glycans in the avian H7 structure positioned the sulfo group in the vicinity of Lys^{193} for favorable charge interactions (*19*, *32*) and were supported by the crystal structure of H5 HA with a sulfated sialoside (*38*). Perhaps unexpectedly, we found that the sulfo group is located near the 220 loop between Leu^{226} and Val^{186} (Figs. 4D and 5C) and hydrogen bonds to the Ser^{227} main-chain amide and Glu^{190}. The Sia-Gal linkage adopts a trans configuration, similar to linear avian receptor analogs in avian H7 and Sh2 H7 structures (Fig. 5A). The glycan exits the receptor binding site above the 220 loop and follows a trajectory similar to those of avian receptors in H7 and other avian HAs. The sulfated GlcNAc-3, however, rotates its linkage with Gal-2 by about 180° to bring the sulfated 6-hydroxyl group over to the side of the 190 helix rather than proximal to the 130 loop. Electron density for the sulfo group is substantially better defined than GlcNAc-3, suggesting that glycan no. 3 binding to HA is mainly anchored by Sia-1 and the sulfo group, with flexibility in the rest of the receptor.

The *O*-linked glycans (nos. 21 and 23) share a common terminal sequence analogous to 3′-SLN. For glycan no. 21 (NeuAcα2-3Galβ1-4GlcNAcβ1-3GalNAcα–Thr, where GalNAc indicates *N*-acetyl galactosamine) in complex with Sh2 HA, the Siaα2-3Gal linkage adopts a cis configuration (Fig. 4E). Gal-2 rotates about 180° (Fig. 5B), bringing its 6-hydroxyl group into hydrogen-bonding distance with the Gly^{225} carbonyl oxygen. The receptor analog exits over the 220 loop and turns away from the receptor binding site between GlcNAc-3 and GalNAc-4, where Gln^{222} mediates hydrogen bonds with O3 in the linkage as well as the acetamido carbonyls from GlcNAc-3 and GalNAc-4 (Figs. 4E and 5D). Glycan no. 23 is a biantennary structure with one arm identical to glycan no. 21 (Fig. 4, B and C). Only this arm is visualized in the electron density map and binds HA similarly to glycan no. 21 (Fig. 4, F and G). Sh2 HA also recognizes other α2-3–linked biantennary glycans (*N*-linked glycans 24 to 27), and their longer arms may allow the glycan to span HA trimers to improve avidity.

The HA complexes with these three avian-type receptor glycans reveal different binding modes that highlight the enormous diversity in HA-glycan recognition. Preferential binding for these glycans is mediated by HA-receptor interactions that were not predictable without these crystal structures. These interactions can compensate for unfavorable contacts between Leu^{226} and the α2-3 linkage, allowing human H7N9 HA to effectively maintain avian-type receptor specificity.

The combination of glycan microarrays and x-ray structural determination has enabled us to demonstrate that the HA from current human H7N9 viruses retains specificity for sulfated α2-3–linked sialylated glycans that are recognized by avian H7 viruses (*19*, *32*) and that H7N9 HA is not optimally evolved for recognition of human-like receptors. Because acquisition of human-type receptor specificity of HA is considered a risk factor for human-to-human transmission, reports of binding to human-type (α2-6) receptors (*14*–*16*, *23*, *25*, *26*) have raised concern for the potential for H7N9 to become a pandemic virus. However, we and others have found that the human H7 HA is predominantly specific for avian-type (α2-3) receptors with only weak binding to human receptors (*28*–*30*). Thus, additional mutations will be needed for the HA to achieve specificity for human-type receptors as observed in previous human pandemic viruses. We suggest that the intrinsic weak avidity to human receptors in receptor assays is exaggerated in studies with whole virus by preferential cleavage of the avian-type receptors by the neuraminidase (*15*, *25*) and the high valency of HA on the virus that can amplify binding to receptors of weaker affinity. This explanation is consistent with previous observations from analysis of a human H7N7 virus (A/NY/107/03); this recombinant H7 HA exhibited strong preference for avian-type receptors (*39*), but whole virus showed significant binding to human-type receptors and manifests contact transmission, but not respiratory droplet transmission, in ferrets (*24*, *39*). The situation for human H7N9 viruses is also analogous to H5N1 viruses, where other mutations, in addition to Q226L, are required to achieve human-type receptor specificity that enables respiratory droplet transmission in ferrets (*31*). Thus, the weak avidity for human-type receptors may contribute

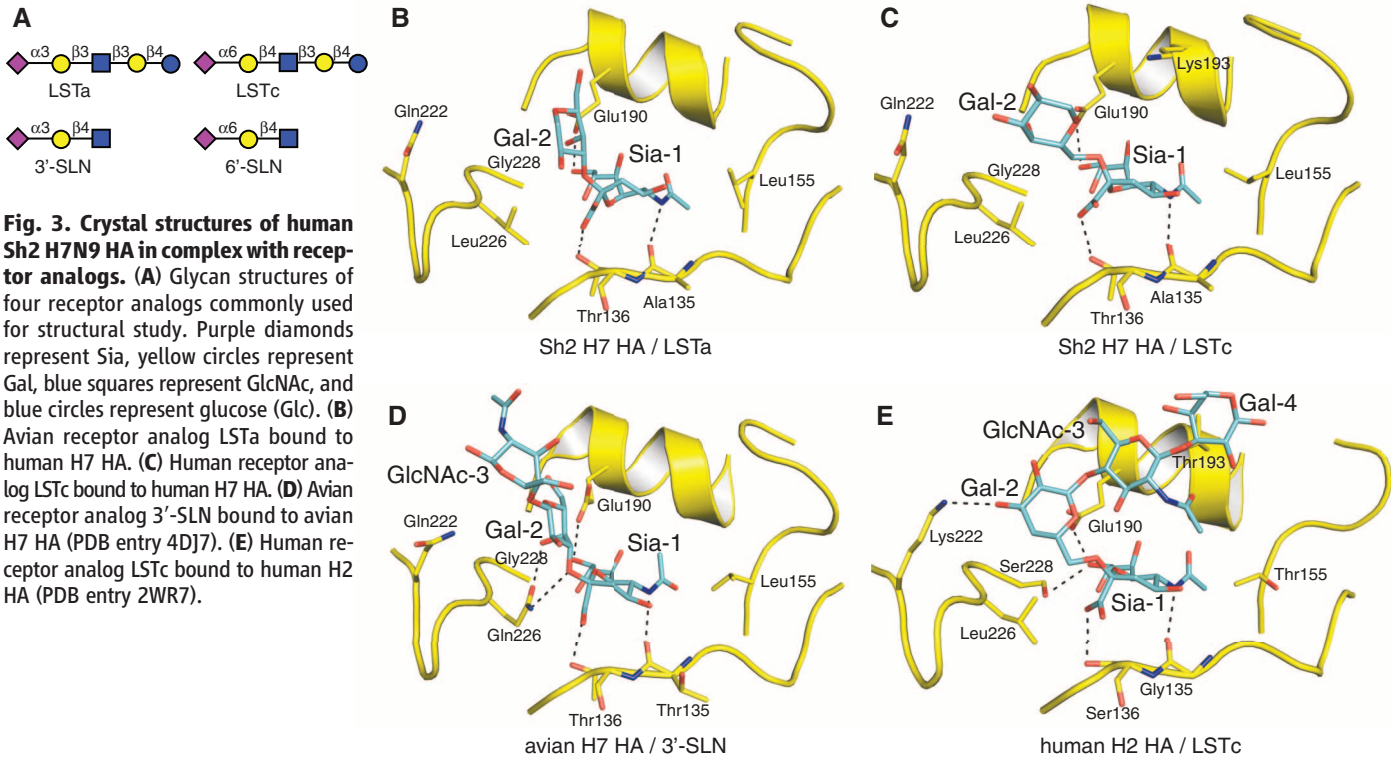

Fig. 3. Crystal structures of human Sh2 H7N9 HA in complex with receptor analogs. (**A**) Glycan structures of four receptor analogs commonly used for structural study. Purple diamonds represent Sia, yellow circles represent Gal, blue squares represent GlcNAc, and blue circles represent glucose (Glc). (**B**) Avian receptor analog LSTa bound to human H7 HA. (**C**) Human receptor analog LSTc bound to human H7 HA. (**D**) Avian receptor analog 3′-SLN bound to avian H7 HA (PDB entry 4DJ7). (**E**) Human receptor analog LSTc bound to human H2 HA (PDB entry 2WR7).

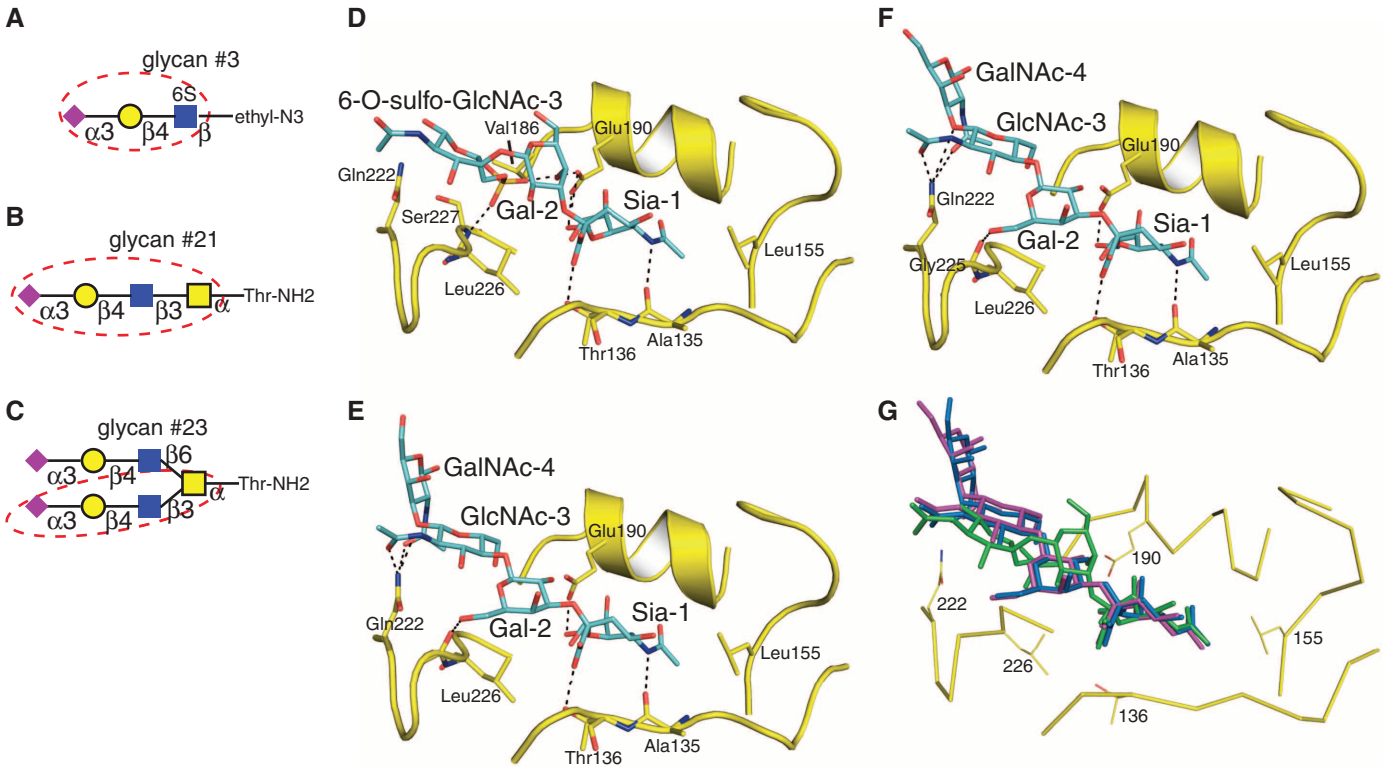

Fig. 4. Crystal structures of human Sh2 H7N9 HA in complex with three avian-type receptor glycans recognized in the glycan array. (**A** to **C**) Glycan compounds used for structural determination. The glycan portion that could be built in the final model is highlighted by a red dashed circle. Purple diamonds represent Sia, yellow circles represent Gal, and blue and yellow squares represent GlcNAc and GalNAc, respectively. (**D**) Sulfated glycan no. 3 bound to human H7N9 HA. (**E**) Glycan no. 21 bound to human H7N9 HA. (**F**) Biantennary glycan no. 23 bound to H7N9 HA using one of its two arms. (**G**) Superposition of glycan no. 23 (colored in purple), glycan no. 21 (in blue), and glycan no. 3 (in green) in the HA receptor binding site. Glycans 21 and 23 share a similar mode of ligand recognition.

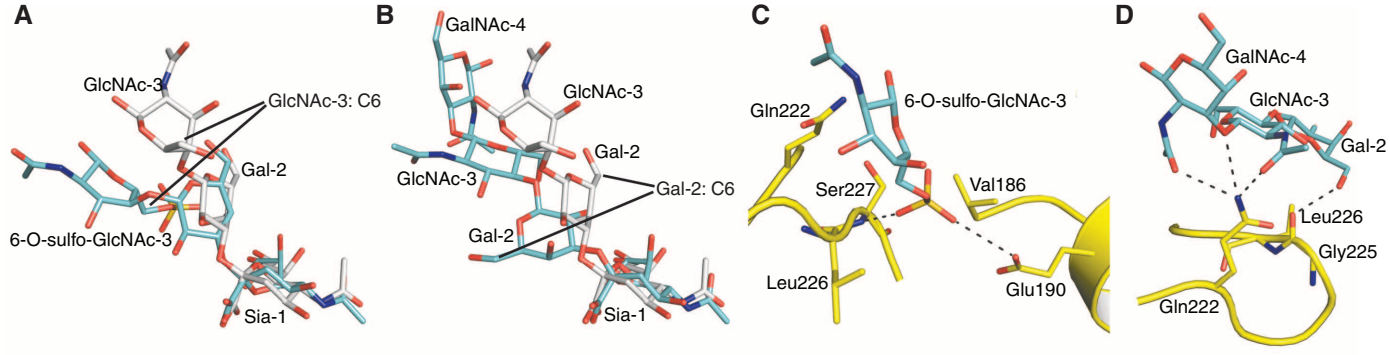

Fig. 5. Preferential binding of human Sh2 H7N9 HA to avian-type α2-3–linked glycans is achieved by flexible twisting of the glycan rings that create additional HA-glycan contacts away from Leu^{226}. (**A**) Superposition of glycan no. 3 (cyan) and 3′-SLN (gray, from PDB entry 4DJ7) in the HA receptor binding site. (**B**) Superposition of glycan no. 21 (cyan) and 3′-SLN (gray) in the HA receptor binding site. (**C**) The sulfo group of glycan 3 is located near the amide nitrogen of Ser^{227} and within hydrogen-bonding distance of Glu^{190}. (**D**) Preferential binding to glycan 21 is mediated by hydrophilic interactions between Gln^{222} and the glycosidic linkage between GlcNAc-3 and GalNAc-4.

to poor transmission by respiratory droplet in the ferret model (*14*–*16*, *18*) and the lack of sustained transmission in humans (*7*, *8*).

References and Notes

1. Centers for Disease Control and Prevention (CDC), *MMWR Morb. Mortal. Wkly. Rep.* **62**, 366–371 (2013).
2. World Health Organization, "Overview of the emergence and characteristics of the avian influenza A (H7N9) virus" (2013), www.who.int/influenza/human_animal_interface/influenza_h7n9/WHO_H7N9_review_31May13.pdf.
3. R. Gao *et al.*, *N. Engl. J. Med.* **368**, 1888–1897 (2013).
4. Q. Li *et al.*, *N. Engl. J. Med.*, published online 24 April 2013 (10.1056/NEJMoa1304617).
5. D. M. Morens, J. K. Taubenberger, A. S. Fauci, *N. Engl. J. Med.* **368**, 2345–2348 (2013).
6. R. E. Kahn, J. A. Richt, *Vector Borne Zoonotic Dis.* **13**, 347–348 (2013).
7. D. Liu *et al.*, *Lancet* **381**, 1926–1932 (2013).
8. T. Kageyama *et al.*, *Euro Surveill.* **18**, 20453 (2013).
9. D. A. Steinhauer, *Nature* **499**, 412–413 (2013).
10. E. K. Subbarao, W. London, B. R. Murphy, *J. Virol.* **67**, 1761–1764 (1993).
11. M. Imai, Y. Kawaoka, *Curr. Opin. Virol.* **2**, 160–167 (2012).
12. M. Matrosovich, J. Stech, H. D. Klenk, *Rev. Sci. Tech.* **28**, 203–217 (2009).
13. R. J. Connor, Y. Kawaoka, R. G. Webster, J. C. Paulson, *Virology* **205**, 17–23 (1994).
14. H. Zhu *et al.*, *Science* **341**, 183–186 (2013); 10.1126/science.1239844.
15. T. Watanabe *et al.*, *Nature* **501**, 551–555 (2013).
16. J. A. Belser *et al.*, *Nature* **501**, 556–559 (2013).
17. Q. Zhang *et al.*, *Science* **341**, 410–414 (2013); 10.1126/science.1240532.
18. M. Richard *et al.*, *Nature* **501**, 560–563 (2013).
19. A. S. Gambaryan *et al.*, *J. Virol.* **86**, 4370–4379 (2012).

20. H. Yang, P. J. Carney, R. O. Donis, J. Stevens, *J. Virol.* **86**, 8645–8652 (2012).
21. R. Xu, R. McBride, J. C. Paulson, C. F. Basler, I. A. Wilson, *J. Virol.* **84**, 1715–1721 (2010).
22. G. N. Rogers *et al.*, *J. Biol. Chem.* **260**, 7362–7367 (1985).
23. K. Tharakaraman *et al.*, *Cell* **153**, 1486–1493 (2013).
24. J. A. Belser *et al.*, *Proc. Natl. Acad. Sci. U.S.A.* **105**, 7558–7563 (2008).
25. X. Xiong *et al.*, *Nature* **499**, 496–499 (2013).
26. J. Zhou *et al.*, *Nature* **499**, 500–503 (2013).
27. As a control, the HA from a representative human seasonal H1N1 strain (A/Kentucky/UR06-0258/2007, KY/07) displays characteristic strong binding to α2-6 SLNLN and negligible binding to α2-3 SLNLN (Fig. 2A).
28. I. Ramos *et al.*, *J. Gen. Virol.* **94**, 2417–2423 (2013).
29. Y. Shi *et al.*, *Science* **342**, 243–247 (2013); 10.1126/science.1242917.
30. H. Yang, P. J. Carney, J. C. Chang, J. M. Villanueva, J. Stevens, *J. Virol.* **87**, 12433–12446 (2013).
31. J. C. Paulson, R. P. de Vries, *Virus Res.* **178**, 99–113 (2013).
32. A. S. Gambaryan *et al.*, *Virol. J.* **5**, 85 (2008).
33. As a control, human HA KY/07 binds broadly to α2-6-linked glycans on the array (Fig. 2B), and avian H7 HA recognizes a large number and variety of α2-3-sialylated glycans (fig. S2).
34. The L226Q mutant produced in insect cells showed robust binding to the array, revealing stronger avidity to most α2-3-glycans but still no binding to α2-6-sialosides.
35. R. Xu, I. A. Wilson, in *Structural Glycomics*, E. Yuriev, P. A. Ramsland, Eds. (CRC Press, Boca Raton, FL, 2012), pp. 235–257.
36. J. Liu *et al.*, *Proc. Natl. Acad. Sci. U.S.A.* **106**, 17175–17180 (2009).
37. Xiong *et al.* used 3′-SLN as an avian-like receptor analog. Shi *et al.* used α2-3-SLNLN. In our study, we used LSTa.
38. X. Xiong *et al.*, *Virus Res.* **178**, 12–14 (2013).
39. K. Srinivasan, R. Raman, A. Jayaraman, K. Viswanathan, R. Sasisekharan, *PLOS ONE* **8**, e49597 (2013).

Acknowledgments: This work was supported in part by NIH R56 AI099275 (I.A.W.) and the Skaggs Institute for Chemical Biology, the Scripps Microarray Core Facility, and a contract from the Centers for Disease Control (J.C.P.). R.P.d.V. is a recipient of a Rubicon grant from the Netherlands Organization for Scientific Research (NWO). Several glycans used for HA binding assays were provided by the Consortium for Functional Glycomics (www.functionalglycomics.org/) funded by National Institute of General Medical Sciences (NIGMS) grant GM62116 (J.C.P.). X-ray diffraction data were collected at the Advanced Photon Source beamline 23ID-B (GM/CA CAT) and the Stanford Synchrotron Radiation Lightsource (SSRL) beamline 12-2. GM/CA CAT is funded in whole or in part with federal funds from the National Cancer Institute (Y1-CO-1020) and the NIGMS (Y1-GM-1104). Use of the Advanced Photon Source was supported by the U.S. Department of Energy (DOE), Basic Energy Sciences, Office of Science, under contract no. DE-AC02-06CH11357. The SSRL is a Directorate of Stanford Linear Accelerator Center National Accelerator Laboratory and an Office of Science User Facility operated for the U.S. DOE Office of Science by Stanford University. The SSRL Structural Molecular Biology Program is supported by the DOE Office of Biological and Environmental Research and by the NIH, NIGMS (including P41GM103393) and the National Center for Research Resources (NCRR, P41RR001209). The contents of this publication are solely the responsibility of the authors and do not necessarily represent the official views of NIGMS, NCRR, or NIH. This is publication 24079 from the Scripps Research Institute. Coordinates and structure factors are deposited in the PDB (4N5J, 4N5K, 4N60, 4N61, 4N62, 4N63, and 4N64).

Supplementary Materials

www.sciencemag.org/content/342/6163/1230/suppl/DC1
Materials and Methods
Figs. S1 to S5
Tables S1 to S3
References (*40*–*47*)

25 July 2013; accepted 28 October 2013
10.1126/science.1243761

HCF-1 Is Cleaved in the Active Site of O-GlcNAc Transferase

Michael B. Lazarus,[1,4]*† Jiaoyang Jiang,[1]*‡ Vaibhav Kapuria,[2] Tanja Bhuiyan,[2] John Janetzko,[4] Wesley F. Zandberg,[3] David J. Vocadlo,[3,5] Winship Herr,[2]§ Suzanne Walker[1]§

Host cell factor–1 (HCF-1), a transcriptional co-regulator of human cell-cycle progression, undergoes proteolytic maturation in which any of six repeated sequences is cleaved by the nutrient-responsive glycosyltransferase, O-linked N-acetylglucosamine (O-GlcNAc) transferase (OGT). We report that the tetratricopeptide-repeat domain of O-GlcNAc transferase binds the carboxyl-terminal portion of an HCF-1 proteolytic repeat such that the cleavage region lies in the glycosyltransferase active site above uridine diphosphate–GlcNAc. The conformation is similar to that of a glycosylation-competent peptide substrate. Cleavage occurs between cysteine and glutamate residues and results in a pyroglutamate product. Conversion of the cleavage site glutamate into serine converts an HCF-1 proteolytic repeat into a glycosylation substrate. Thus, protein glycosylation and HCF-1 cleavage occur in the same active site.

O-linked *N*-acetylglucosamine (O-GlcNAc) transferase (OGT) is a Ser/Thr (S/T) glycosyltransferase that O-GlcNAcylates nuclear and cytoplasmic proteins, thus influencing their activity, localization, and overall function (*1*–*3*). Because OGT activity is sensitive to uridine diphosphate (UDP)–GlcNAc concentrations, OGT is proposed to regulate cellular responses to nutrient status (*4*–*6*). Human HCF-1 is a transcriptional coregulator involved in regulating cell-cycle progression (*7*, *8*). In an unusual proteolytic maturation process (*9*–*11*), any of six centrally located 20 to 26 amino acid sequence repeats called HCF-1_{PRO} repeats (Fig. 1A) are cleaved by OGT in the presence of UDP-GlcNAc (*12*), providing a link between cell-cycle progression and nutrient levels. The HCF-1_{PRO} repeats contain two essential regions for proteolysis: a threonine-rich region proposed to be an OGT-binding site and the cleavage site, which contains a conserved Cys-Glu-Thr (CET) sequence (*10*, *11*).

OGT can cleave a fragment of HCF-1, called HCF-1rep1, which contains the first HCF-1_{PRO} repeat plus N-terminal HCF-1 sequences containing several O-GlcNAc sites (*12*) (Fig. 1A). To elucidate the cleavage process, we first analyzed the effect of amino acid substitutions in OGT (Fig. 1B and fig. S1) and the HCF-1_{PRO} repeat (Fig. 1C) on cleavage and glycosylation. Three OGT active site residues implicated in S/T glycosylation were evaluated: K842, which is involved in binding and activation of UDP-GlcNAc for glycosyl-transfer; H498, which contacts the C2-N-acetyl group of UDP-GlcNAc; and H558, which contacts a backbone carbonyl of glycosylation substrates (*13*–*17*). Substitution of K842 with methionine prevented S/T glycosylation upstream of the proteolytic repeat as well as cleavage within the repeat region. Substitution of H498 or H558 with alanine decreased S/T glycosylation but had a negligible effect on the extent of cleavage after 16 hours. K842 is an essential residue for glycosylation (*14*, *15*), and its importance in cleavage suggests that UDP-GlcNAc is involved in the cleavage mechanism.

Next, we tested substitutions in the proteolytic repeat of HCF-1rep1. We previously showed that alanine substitution of glutamate E10 leads to loss of cleavage (*11*, *12*). To probe the role of E10 in more detail, we substituted it with glutamine (E10Q), aspartate (E10D), and serine (E10S). All three substitutions blocked cleavage (Fig. 1C), indicating that the chemical nature of the glutamate residue is critical for OGT-mediated HCF-1_{PRO}-repeat cleavage. In contrast, the C9 position can tolerate alanine and serine substitution (*12*) (fig. S2).

Because S/T glycosylation upstream of the cleavage site in HCF-1rep1 complicates study of the cleavage requirements, we identified a cleavage substrate consisting of the first three proteolytic repeats (HCF3R, Fig. 1A), which did not undergo substantial glycosylation. No cleavage products were observed when HCF3R was incubated with OGT alone or in the presence of UDP, but several products were observed in reactions containing both OGT and UDP-GlcNAc (Fig. 2A). These products did not form if HCF3R was incubated with a K842A OGT mutant incapable of

[1]Department of Microbiology and Immunobiology, Harvard Medical School, Boston, MA 02115, USA. [2]Center for Integrative Genomics, University of Lausanne, Génopode, 1015 Lausanne, Switzerland. [3]Department of Chemistry, Simon Fraser University, Burnaby, BC V5A 1S6, Canada. [4]Department of Chemistry and Chemical Biology, Harvard University, Cambridge, MA 02138, USA. [5]Department of Molecular Biology and Biochemistry, Simon Fraser University, Burnaby, British Columbia, Canada.

*These authors contributed equally to this work.
†Present address: Department of Cellular and Molecular Pharmacology, University of California, San Francisco, San Francisco, CA 94158, USA.
‡Present address: School of Pharmacy, University of Wisconsin–Madison, Madison, WI 53705, USA.
§Corresponding author. E-mail: Suzanne_Walker@hms.harvard.edu (S.W.); winship.herr@unil.ch (W.H.)

catalyzing glycosylation (*13*, *16*) or when wild-type OGT was pretreated with 1.5 equivalents of a previously described inhibitor that covalently inactivates the enzyme by cross-linking the active site (*18*). Cleavage was also inhibited if UDP was added to reactions containing OGT and UDP-GlcNAc (fig. S3A) but accelerated by adding alkaline phosphatase, which destroys UDP. Because intact UDP-GlcNAc, but not UDP, promoted HCF3R cleavage, we tested cleavage in the presence of UDP-5SGlcNAc, an isostere of UDP-GlcNAc that adopts the same conformation within the active site, yet is resistant to glycosylation and hydrolysis (*14*, *19*). Almost no peptide cleavage was observed (Fig. 2A and fig. S3B), implying that the UDP-GlcNAc does not simply fulfill a structural function but must react for HCF3R cleavage to occur. Consistent with this proposal, UDP-5SGlcNAc was found to inhibit cleavage of HCF-1rep1 when added to reactions containing UDP-GlcNAc (fig. S3C).

We next examined the cleavage products using liquid chromatography–mass spectrometry (LC-MS). Previous analysis of products isolated from cells concluded that cleavage occurs at the E-T peptide bond of the CET sequence (*10*, *11*), but none of the four products we observed had masses consistent with E-T cleavage (Fig. 2B and fig. S4). Instead, they were consistent with cleavage at the preceding C-E bond except that all the C-terminal fragments were 18 daltons lower in mass than expected. We hypothesized that the 18-dalton difference resulted from generation of an N-terminal pyroglutamate. Indeed, cleavage of a simplified HCF3R substrate possessing a single active HCF-1_{PRO} repeat (HCF3R-EAA) led to the production of one dehydrated C-terminal product (Fig. 2C and fig. S5). Pyroglutamate aminopeptidase (PGAP) treatment reduced the mass of this product by 111 daltons, corresponding to loss of pyroglutamate (Fig. 2C and fig. S6). The earlier proposed cleavage site was probably misidentified because N-terminal pyroglutamates are resistant to the Edman sequencing method used in those studies, and cellular PGAPs likely processed some cleavage products (*10*, *11*).

To gain additional insight into how OGT cleaves HCF-1, we solved crystal structures of OGT-HCF-1_{PRO}-repeat complexes (tables S1 and S2). We solved a 1.8 Å structure of OGT containing UDP and a 16 amino acid peptide comprising the threonine-rich region of the HCF-1_{PRO} repeat (Fig. 3, A and B). We also solved a 1.9 Å structure with UDP and a full HCF-1_{PRO} repeat containing an E10A mutation, but density was only observed for the threonine-rich portion of the repeat (Fig. 3C and fig. S7). These two structures show the threonine-rich peptide bound in an extended conformation along the channel formed by the tetratricopeptide-repeat (TPR) domain (*13*, *20*, *21*) of OGT (Fig. 3B and fig. S7). Five conserved asparagine residues within the TPR domain form a series of interactions, four being bidentate, with the amides of alternating residues along the peptide backbone (Fig. 3C). A lysine side chain also contacts the peptide backbone. Four aspartates of OGT form hydrogen bonds to the threonine side chains of the HCF-1 repeat. The binding mode in the crystal structures is consistent with mutational data demonstrating the importance of the OGT asparagines (Fig. 3D and fig. S8) and the conserved HCF-1_{PRO}-repeat threonines (*12*) (Figs. 3E and 1C) for both cleavage and binding.

Because intact UDP-GlcNAc is required for OGT-catalyzed cleavage of HCF-1_{PRO}-repeats, we thought the UDP-5SGlcNAc analog might stabilize density for a full repeat. Indeed, we obtained a structure of OGT with UDP-5SGlcNAc and a 26 amino acid peptide corresponding to HCF-1_{PRO} rep2, but with an E10Q substitution. In this structure, the C-terminal threonine-rich region binds to the TPR domain as described above, and the N-terminal cleavage region is now visible (Fig. 4A) and forms an extensive binding interface with UDP-5SGlcNAc (Fig. 4B). A structure containing UDP-GlcNAc and a wild-type repeat confirms the binding mode of the E10Q peptide (fig. S9). Remarkably, the cleavage region binds in a mode almost identical to that of a glycosylation-competent peptide substrate (*14*), and residue 10 aligns perfectly with the glycosyl acceptor amino acid (Fig. 4C). The structures suggested that an

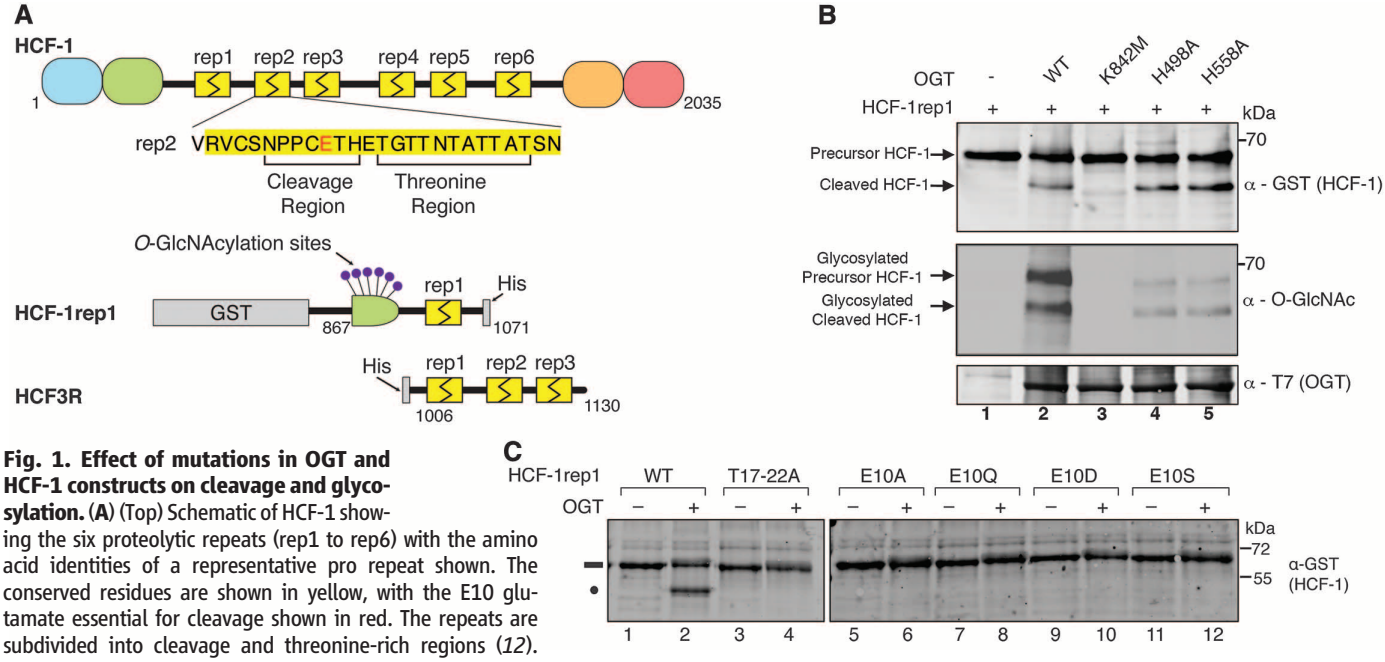

Fig. 1. Effect of mutations in OGT and HCF-1 constructs on cleavage and glycosylation. (**A**) (Top) Schematic of HCF-1 showing the six proteolytic repeats (rep1 to rep6) with the amino acid identities of a representative pro repeat shown. The conserved residues are shown in yellow, with the E10 glutamate essential for cleavage shown in red. The repeats are subdivided into cleavage and threonine-rich regions (*12*). Site-specific proteolysis by OGT leads to the formation of HCF-1_N and HCF-1_C subunits. (Bottom) Schematic of HCF-1 constructs used in this study. Glutathione *S*-transferase (GST)–HCF-1rep1 contains the first HCF-1_{PRO} repeat and surrounding sequences fused to GST. Several S/T glycosylation sites are found in the HCF-1rep1 construct as schematized. The HCF3R construct contains only the first three HCF-1_{PRO} repeats fused to an N-terminal His-tag. (**B**) Comparative cleavage and glycosylation activities of wild-type (WT) OGT and several catalytic domain mutants. GST–HCF-1rep1 was incubated in the absence (lane 1) or presence of WT OGT (lane 2) or the indicated mutants (lanes 3 to 5). HCF-1rep1 cleavage was detected by Western blot analysis with antibody to GST, and HCF-1rep1 glycosylation was detected with antibody to O-GlcNAc (RL2). (**C**) Cleavage activities of WT and mutant HCF-1rep1 constructs. WT GST–HCF1rep1 (lanes 1 and 2) or a threonine-rich region mutant (T17-22A; lanes 3 and 4) or the indicated E10 cleavage site mutants (E10A, E10Q, E10D, and E10S; lanes 5 to 12) were incubated in the absence (–) or presence (+) of WT OGT as described in the supplementary materials. Cleavage was detected as in (B).

E10S mutation, which prevents cleavage (Fig. 1D), would be glycosylated at residue 10. Indeed, unlike HCF3R-EAA, the E10S analog (HCF3R-SAA) was glycosylated effectively (Fig. 4D and fig. S10). Thus, the identity of the amino acid at position 10 of an HCF-1_{PRO} repeat—glutamate or serine—can dictate whether OGT cleaves or glycosylates the substrate.

Previous hypotheses suggested that OGT contains a dedicated protease active site or acts as a coprotease to template HCF-1 autocatalysis (*12*). Instead, OGT promotes cleavage of the HCF-1_{PRO} repeat using the same catalytic region as for glycosylation. The threonine-rich region of the HCF-1_{PRO} repeat binds in the channel formed by the TPR domain of OGT, stabilized by the contacts described above. The cleavage region threads into the active site and binds over UDP-GlcNAc in the same conformation that a glycosylation substrate would, with the glutamate side chain positioned near the anomeric carbon of the sugar. Because a pyroglutamate product is formed, and spontaneous cyclization of N-terminal glutamates is kinetically very slow (*22*), the glutamate side chain is likely activated by formation of an ester species as part of the cleavage mechanism. We speculate that the glutamate side chain traps a transient oxocarbenium ion formed within the active site, producing a glutamyl ester that can undergo intramolecular attack, leading ultimately to formation of the N-terminal pyroglutamate. We note that pyroglutamates are proposed species in other biological phenomena (*23*). Possible mechanisms for cleavage proceeding from a glutamyl ester are suggested (fig. S11). Although direct physical evidence for a glutamyl-sugar intermediate has yet to be obtained, glycosylation of the glutamate side chain before cleavage is consistent with the structural data, the strict requirement for glutamate at the cleavage site, the formation of a pyroglutamate product, and the observation that cleavage of HCF-1_{PRO} repeats requires UDP-GlcNAc and depends on an OGT residue, K842, which is essential for catalyzing glycosylation.

These studies provide insight into two important aspects of OGT function. First, they provide a view of a peptide bound to OGT's TPR domain, which is thought to play a central role in substrate selection (*20*, *21*, *24*, *25*). The structures reported suggest that some glycosylation substrates may bind in a manner similar to the HCF-1_{PRO} repeats, with the glycosylation site separated by several residues from a C-terminal recognition motif that binds in the channel formed by the TPR domain. Adaptor proteins that recruit glycosylation substrates to OGT might also contain threonine-rich recognition motifs. Second, they suggest an unprecedented mechanism of proteolysis in which OGT uses UDP-GlcNAc as a co-substrate in a cleavage reaction that takes place in the active site for glycosylation. Indeed, we show that two very different posttranslational protein modifications—proteolysis and addition of a sugar residue—can occur in the same active site, with the outcome determined by the identity of a single amino acid in the substrate.

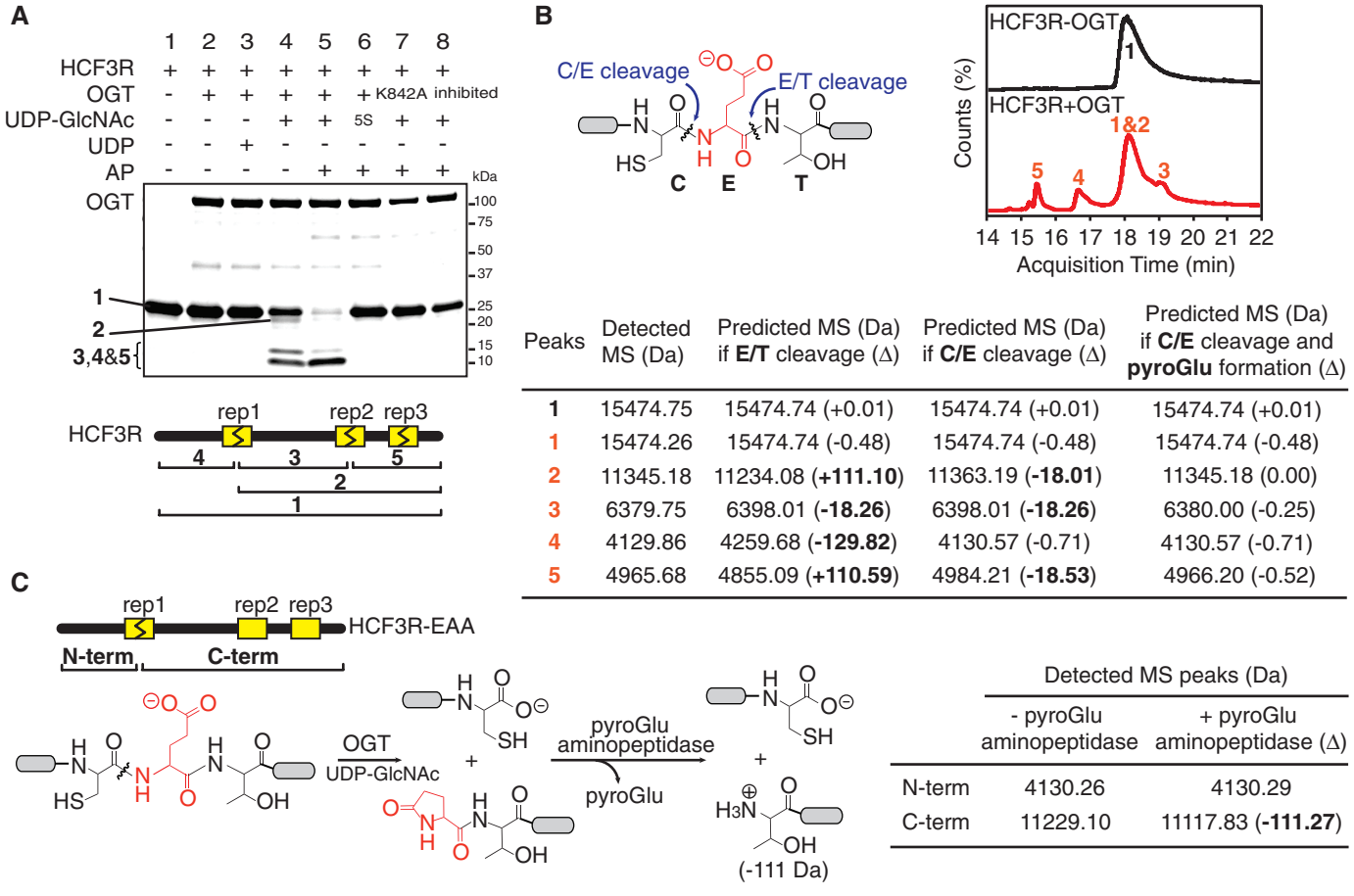

Peaks	Detected MS (Da)	Predicted MS (Da) if **E/T** cleavage (Δ)	Predicted MS (Da) if **C/E** cleavage (Δ)	Predicted MS (Da) if **C/E** cleavage and **pyroGlu** formation (Δ)
1	15474.75	15474.74 (+0.01)	15474.74 (+0.01)	15474.74 (+0.01)
1	15474.26	15474.74 (-0.48)	15474.74 (-0.48)	15474.74 (-0.48)
2	11345.18	11234.08 (**+111.10**)	11363.19 (**-18.01**)	11345.18 (0.00)
3	6379.75	6398.01 (**-18.26**)	6398.01 (**-18.26**)	6380.00 (-0.25)
4	4129.86	4259.68 (**-129.82**)	4130.57 (-0.71)	4130.57 (-0.71)
5	4965.68	4855.09 (**+110.59**)	4984.21 (**-18.53**)	4966.20 (-0.52)

	Detected MS peaks (Da)	
	- pyroGlu aminopeptidase	+ pyroGlu aminopeptidase (Δ)
N-term	4130.26	4130.29
C-term	11229.10	11117.83 (**-111.27**)

Fig. 2. HCF-1_{PRO}-repeat cleavage results in formation of a pyroglutamate product. (**A**) Cleavage of HCF3R requires UDP-GlcNAc. HCF3R was incubated with WT OGT (lanes 2 to 6), with K842A OGT (lane 7) or with OGT treated with a previously reported (*18*) covalent inhibitor BZX2 (lane 8), in the presence of UDP (lane 3), UDP-GlcNAc (lanes 4, 5, 7, and 8), or UDP-5SGlcNAc (5S) (lane 6). Alkaline phosphatase (AP) was added to some reactions, as indicated. Cleavage products were separated by SDS–polyacrylamide gel electrophoresis (SDS-PAGE) and stained with Coomassie Blue. (**B**) LC-MS analysis of untreated HCF3R (black) and HCF3R cleavage products (red) after incubation with OGT and UDP-GlcNAc shows unexpected mass peaks. Detected and predicted MS peaks for different cleavage products are tabulated. (**C**) Mutation of E10 to alanine in the cleavage region of the second and third HCF-1_{PRO} repeats produces a construct, HCF3R-EAA, containing only a single cleavable repeat. Pyroglutamate (pyroGlu) aminopeptidase removed a 111-dalton fragment from the HCF3R-EAA C-terminal cleavage product, confirming the formation of pyroglutamate in the cleavage reaction.

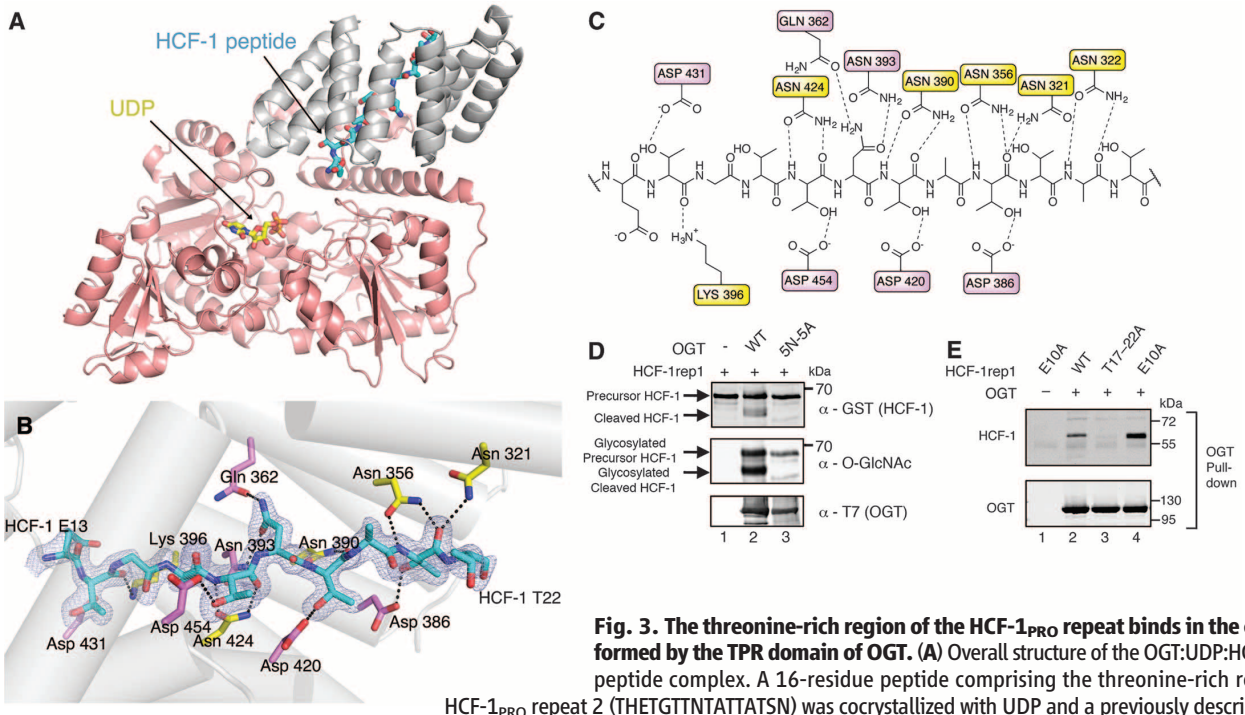

Fig. 3. The threonine-rich region of the HCF-1_{PRO} repeat binds in the channel formed by the TPR domain of OGT. (**A**) Overall structure of the OGT:UDP:HCF-1_{11-26} peptide complex. A 16-residue peptide comprising the threonine-rich region of HCF-1_{PRO} repeat 2 (THETGTTNTATTATSN) was cocrystallized with UDP and a previously described (*13*) N-terminally truncated OGT construct (hOGT$_{4.5}$) and refined to 1.8 Å. The OGT catalytic domain (red) and TPR domain (gray), along with the HCF-1_{11-26} peptide (cyan) and UDP (yellow), are shown. (**B**) Close-up view of OGT-peptide interactions. The electron density around the visible portion of HCF-1_{11-26} is shown as an F_O-F_C difference map contoured at 3σ. The peptide is shown in cyan. OGT side chains that contact the peptide backbone are shown in yellow, and OGT side chains that contact HCF-1 peptide side chains are shown in magenta. (**C**) Schematic of contacts between OGT side chains and the threonine-rich region of the HCF-1_{PRO} repeat 2 from the complex of OGT:UDP:HCF-1-E10A$_{1-26}$. OGT side chains are numbered and colored as in (B). (**D**) Mutations in the TPR domain of OGT (5N-5A) inhibit cleavage. Cleavage and glycosylation of GST–HCF-1rep1 were assayed, as in Fig. 1C, in the absence (lane 1) or presence (lane 2) of WT OGT or the 5N-5A TPR-domain mutant in which Asn residues 322, 356, 390, 424, and 458 are mutated to alanine (lane 3). (**E**) OGT does not bind effectively in vitro to an HCF-1_{PRO} repeat mutant containing mutations in the threonine-rich region (T17–22A). WT (lane 2) and mutant (lanes 1, 3, and 4) GST–HCF-1rep1 substrates were tested for OGT binding in the presence of UDP-GlcNAc using an OGT-directed pull-down assay. Antibodies to GST and T7 were used to detect GST–HCF-1rep1 (top) and OGT (bottom), respectively, by Western blotting. Single-letter abbreviations for the amino acid residues are as follows: A, Ala; C, Cys; D, Asp; E, Glu; F, Phe; G, Gly; H, His; I, Ile; K, Lys; L, Leu; M, Met; N, Asn; P, Pro; Q, Gln; R, Arg; S, Ser; T, Thr; V, Val; W, Trp; and Y, Tyr.

Fig. 4. HCF-1 cleavage takes place in the glycosyltransferase active site of OGT. (**A**) Overall structure of the OGT:UDP-5SGlcNAc:HCF-1-E10Q$_{1-26}$ complex. The HCF-1 peptide is shown as spheres in cyan, with the UDP-5SGlcNAc in yellow. (**B**) Close-up view of the two substrate analogs shown in yellow in the OGT active site. The entire cleavage region can be seen, and the C-E10Q-T residues are annotated. The anomeric carbon of UDP-5SGlcNAc is indicated (C1). (**C**) Overlay of the substrate analogs from the OGT:UDP-5SGlcNAc:HCF-1 peptide complex (yellow) and the previously reported (*14*) OGT:UDP-5SGlcNAc:CKIIA complex (cyan). CKII is a well-characterized OGT glycosylation substrate. The E10Q side chain of the HCF-1 peptide is shown as transparent just after the β carbon. (**D**) Mutating E10 to S in an HCF-1_{PRO} repeat converts a cleavage substrate (HCF3R-EAA) into a glycosylation substrate (HCF3R-SAA), which is defective in cleavage. (Left) Cleavage products of HCF3R-EAA and HCF3R-SAA were separated by SDS-PAGE and stained with Coomassie Blue. (Right) Glycosylation of WT and mutant HCF3R substrates was carried out with ^{14}C-UDP-GlcNAc and analyzed by PAGE. Full gels are shown in fig. S10.

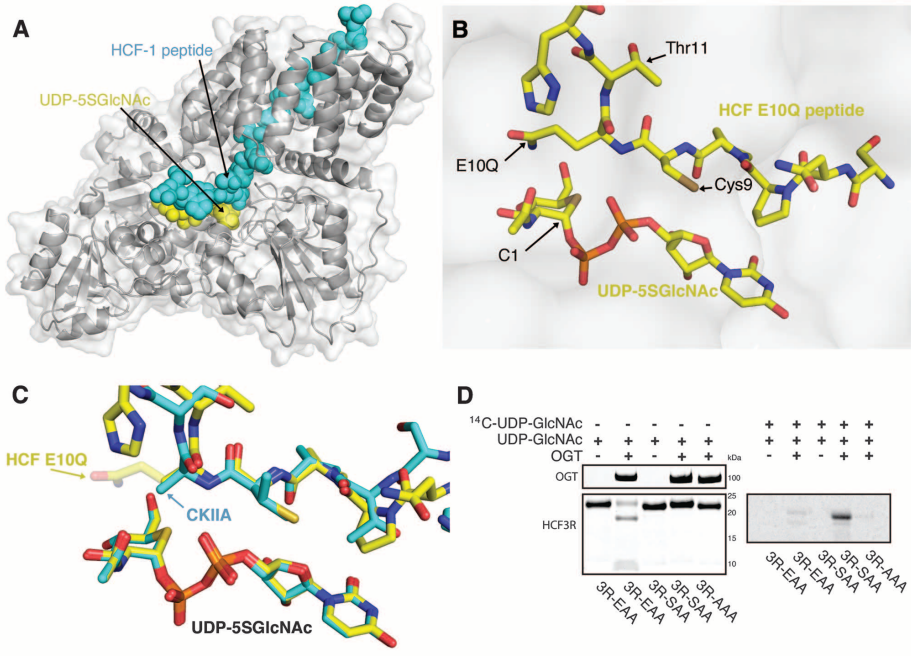

References and Notes

1. L. Wells, K. Vosseller, G. W. Hart, *Science* **291**, 2376–2378 (2001).
2. L. K. Kreppel, M. A. Blomberg, G. W. Hart, *J. Biol. Chem.* **272**, 9308–9315 (1997).
3. J. A. Hanover, M. W. Krause, D. C. Love, *Nat. Rev. Mol. Cell Biol.* **13**, 312–321 (2012).
4. G. W. Hart, M. P. Housley, C. Slawson, *Nature* **446**, 1017–1022 (2007).
5. W. Yi *et al.*, *Science* **337**, 975–980 (2012).
6. R. Dentin, S. Hedrick, J. Xie, J. Yates 3rd, M. Montminy, *Science* **319**, 1402–1405 (2008).
7. J. Wysocka, W. Herr, *Trends Biochem. Sci.* **28**, 294–304 (2003).
8. Z. Zargar, S. Tyagi, *Transcription* **3**, 187–192 (2012).
9. S. Daou *et al.*, *Proc. Natl. Acad. Sci. U.S.A.* **108**, 2747–2752 (2011).
10. T. M. Kristie, J. L. Pomerantz, T. C. Twomey, S. A. Parent, P. A. Sharp, *J. Biol. Chem.* **270**, 4387–4394 (1995).
11. A. C. Wilson, M. G. Peterson, W. Herr, *Genes Dev.* **9**, 2445–2458 (1995).
12. F. Capotosti *et al.*, *Cell* **144**, 376–388 (2011).
13. M. B. Lazarus, Y. Nam, J. Jiang, P. Sliz, S. Walker, *Nature* **469**, 564–567 (2011).
14. M. B. Lazarus *et al.*, *Nat. Chem. Biol.* **8**, 966–968 (2012).
15. M. Schimpl *et al.*, *Nat. Chem. Biol.* **8**, 969–974 (2012).
16. C. Martinez-Fleites *et al.*, *Nat. Struct. Mol. Biol.* **15**, 764–765 (2008).
17. A. J. Clarke *et al.*, *EMBO J.* **27**, 2780–2788 (2008).
18. J. Jiang, M. B. Lazarus, L. Pasquina, P. Sliz, S. Walker, *Nat. Chem. Biol.* **8**, 72–77 (2011).
19. T. M. Gloster *et al.*, *Nat. Chem. Biol.* **7**, 174–181 (2011).
20. M. Jínek *et al.*, *Nat. Struct. Mol. Biol.* **11**, 1001–1007 (2004).
21. W. A. Lubas, J. A. Hanover, *J. Biol. Chem.* **275**, 10983–10988 (2000).
22. D. R. Twardzik, A. Peterkofsky, *Proc. Natl. Acad. Sci. U.S.A.* **69**, 274–277 (1972).
23. S. A. Khan, B. W. Erickson, *J. Biol. Chem.* **257**, 11864–11867 (1982).
24. L. K. Kreppel, G. W. Hart, *J. Biol. Chem.* **274**, 32015–32022 (1999).
25. S. P. Iyer, G. W. Hart, *J. Biol. Chem.* **278**, 24608–24616 (2003).

Acknowledgments: This work was supported by National Institutes of Health (NIH) grant R01GM094263 to S.W., Swiss National Science Foundation (SNSF) grant 31003A_130829 and the University of Lausanne to W.H., and the Natural Sciences and Engineering Research Council of Canada (NSERC) and Simon Fraser University to D.J.V. M.B.L. is a Merck Fellow of the Helen Hay Whitney Foundation. V.K. is an European Molecular Biology Organization (EMBO) long-term fellowship recipient. J.J. is an NSERC PGS-M and D3 fellowship recipient. D.J.V. is a recipient of an E. W. R. Steacie Memorial Fellowship and holds a Canada Research Chair in Chemical Glycobiology. We thank A. Heroux (B.N.L.) for assistance with x-ray data collection. We thank V. Zoete for helpful discussions and M. Bogyo for reading the manuscript. Coordinates and structure factors have been deposited in the Protein Data Bank with accession nos. 4N39, 4N3A, 4N3B, and 4N3C.

Supplementary Materials

www.sciencemag.org/content/342/6163/1235/suppl/DC1
Materials and Methods
Figs. S1 to S11
Tables S1 and S2
References (*26*–*39*)

30 July 2013; accepted 28 October 2013
10.1126/science.1243990

Crosstalk Between Microtubule Attachment Complexes Ensures Accurate Chromosome Segregation

Dhanya K. Cheerambathur, Reto Gassmann,* Brian Cook, Karen Oegema, Arshad Desai†

The microtubule-based mitotic spindle segregates chromosomes during cell division. During chromosome segregation, the centromeric regions of chromosomes build kinetochores that establish end-coupled attachments to spindle microtubules. Here, we used the *Caenorhabditis elegans* embryo as a model system to examine the crosstalk between two kinetochore protein complexes implicated in temporally distinct stages of attachment formation. The kinetochore dynein module, which mediates initial lateral microtubule capture, inhibited microtubule binding by the Ndc80 complex, which ultimately forms the end-coupled attachments that segregate chromosomes. The kinetochore dynein module directly regulated Ndc80, independently of phosphorylation by Aurora B kinase, and this regulation was required for accurate segregation. Thus, the conversion from initial dynein-mediated, lateral attachments to correctly oriented, Ndc80-mediated end-coupled attachments is actively controlled.

The four-subunit Ndc80 complex, whose Ndc80 subunit harbors direct microtubule-binding activity, is the central component of the microtubule end-coupled attachments that segregate chromosomes on mitotic spindles (*1*, *2*). In metazoans, initial lateral capture of microtubules by dynein motors localized to kinetochores kinetically accelerates the formation of end-coupled attachments and ensures their correct orientation (*3*–*7*). How kinetochores transition from an initial laterally bound state to the final end-coupled state is unclear.

Ludwig Institute for Cancer Research, Department of Cellular and Molecular Medicine, University of California San Diego, La Jolla, CA 92093, USA.

*Present address: Instituto de Biologia Molecular e Celular, Universidade do Porto, Rua do Campo Alegre 823, 4150-180 Porto, Portugal.

†Corresponding author. E-mail: abdesai@ucsd.edu

The kinetochore dynein module is composed of the three-subunit RZZ (Rod-Zw10-Zwilch) complex, which recruits dynein to kinetochores via Spindly (Fig. 1A) (*7*–*9*). Formation of end-coupled microtubule attachments was assessed during the first division of the *Caenorhabditis elegans* embryo by visualizing chromosome dynamics (Fig. 1B) and by quantifying the kinetics of spindle pole separation (Fig. 1C) (*10*, *11*). Removal of Spindly (SPDL-1 in *C. elegans*) was nearly equivalent to removal of NDC-80 (Fig 1, B and C). As expected (*7*, *12*), the failure to establish end-coupled attachments resulting from SPDL-1 depletion was suppressed by codepletion of RZZ (Fig. 1B); the double inhibition exhibited only the mild delay in end-coupled attachment formation expected for loss of kinetochore dynein. Thus, RZZ inhibits the formation of NDC-80–mediated microtubule attachments, and relief of this inhibition requires SPDL-1.

Aurora B kinase inhibits microtubule binding of Ndc80 by phosphorylating its basic tail (*13*–*15*). To determine whether RZZ inhibits NDC-80 by promoting Aurora B–mediated phosphorylation of NDC-80, we created an RNA interference (RNAi)–resistant transgenic system (fig. S1, A and B) to replace endogenous NDC-80 with transgene-encoded NDC-80^{WT} or a phosphorylation-resistant NDC-80^{4A} mutant (fig. S1, C and D) (*13*). NDC-80^{WT} and NDC-80^{4A} mutants both rescued the severe chromosome segregation defect and embryonic lethality of NDC-80 depletion (Fig 1D and fig. S1, E and F). Furthermore, NDC-80^{WT} and NDC-80^{4A} were equally sensitive to inhibition by RZZ—after SPDL-1 depletion, both exhibited severe chromosome segregation (Fig. 1D) and pole separation (fig. S1G) defects indicative of a failure to form end-coupled attachments. Thus, Aurora B–mediated phosphorylation of the NDC-80 tail is not required for RZZ to inhibit NDC-80–mediated end-coupled attachments.

We next tested if the RZZ complex directly interacts with NDC-80 and inhibits its microtubule-binding activity. ROD-1 has an N-terminal β-propeller domain that binds to Zwilch^{ZWL-1} followed by an extended α solenoid that binds Zw10^{CZW-1} (Fig. 2A) (*16*). The N-terminal β-propeller domain of ROD-1 and the N-terminal microtubule-binding region of NDC-80 interacted in a yeast two-hybrid assay (Fig. 2B and fig. S2A). Deletion of the basic tail of NDC-80 abolished its interaction with ROD-1 without affecting binding to its Nuf2^{HIM-10} partner; by contrast, mimicking an Aurora B–phosphorylated NDC-80 tail by mutation of four target sites to aspartic acid (4D) did not affect the ROD-1 interaction (Fig. 2B). Binding assays with a partially reconstituted RZZ complex composed of the N terminus of ROD-1 and Zwilch^{ZWL-1} (termed R^{N}Z) confirmed a direct tail-dependent interaction between R^{N}Z and NDC-80 (Fig. 2B). To test if the ROD-1–NDC-80 interaction regulates NDC-80 microtubule binding, we used reconstituted *C. elegans* NDC-80 complex (fig. S2B)

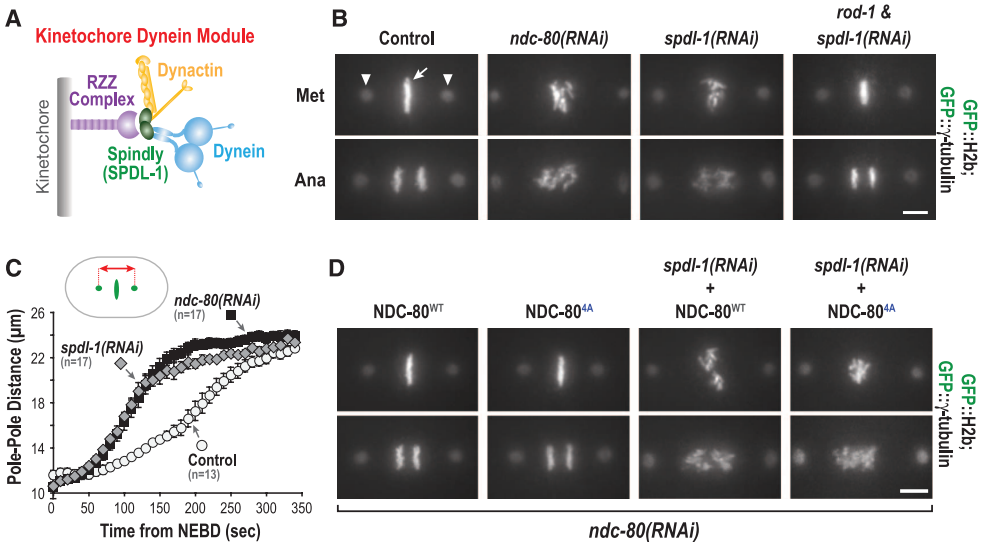

Fig. 1. RZZ inhibits microtubule attachment formation at kinetochores independently of Aurora B phosphorylation of NDC-80. (**A**) Cartoon depiction of the kinetochore dynein module. (**B**) Chromosome segregation phenotypes for the indicated conditions. Green fluorescent protein (GFP)::H2b (arrow) and GFP::γ-tubulin (arrowhead) signals are indicated. Bar, 5 μm. (**C**) Plot of spindle pole separation kinetics, which serves as a readout for kinetochore-microtubule attachment formation. Error bars are SEM with a 95% confidence interval. (**D**) Chromosome segregation phenotypes for the indicated conditions (see also fig. S1). Bar, 5 μm.

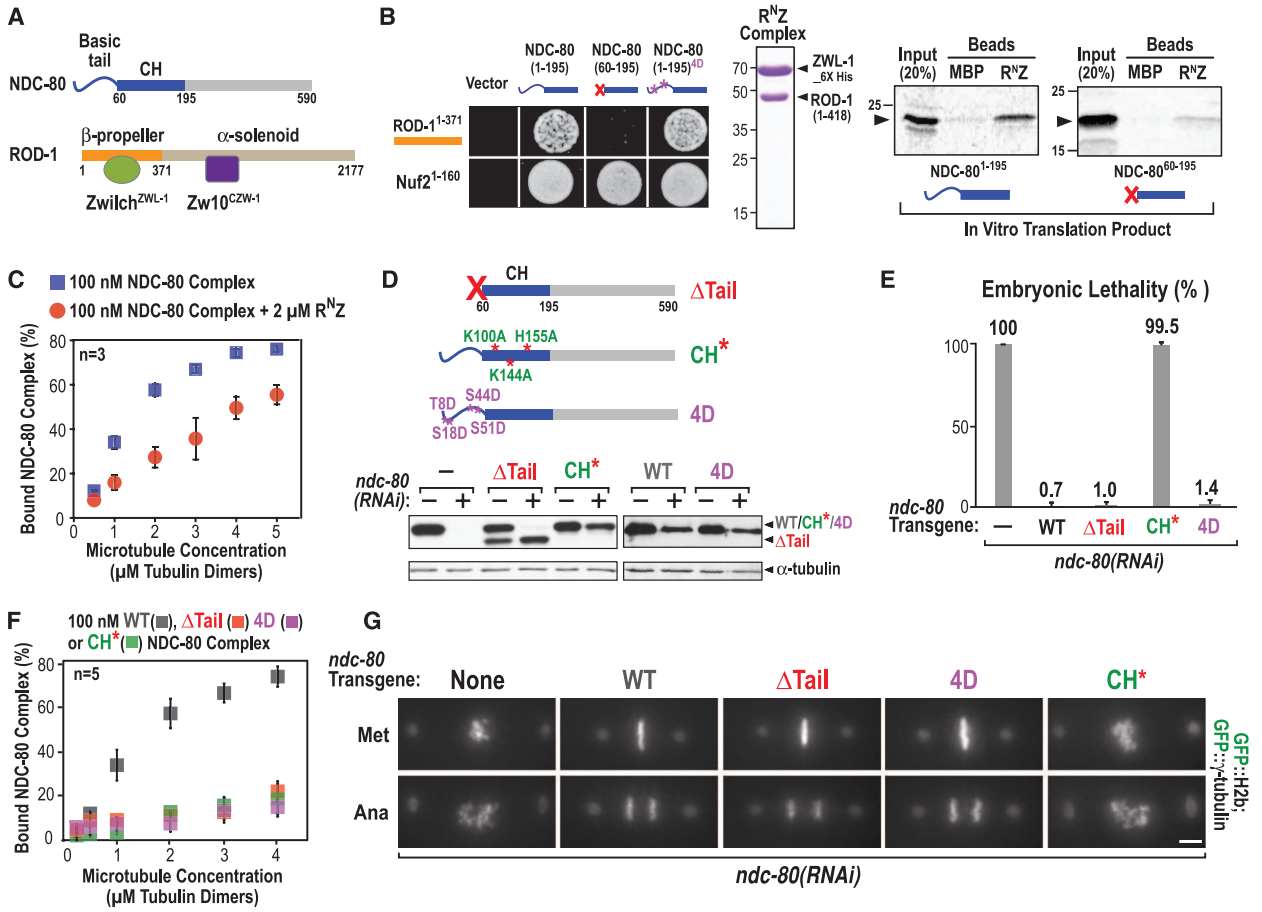

Fig. 2. RZZ interacts with and inhibits NDC-80. (**A**) Schematics of NDC-80 and the RZZ complex. (**B**) (Left) NDC-80 tail-dependent yeast two-hybrid interaction with ROD-1; $Nuf2^{HIM-10}$ served as a positive control (fig. S2). (Right) Recombinant R^NZ complex and autoradiogram of binding assay with R^NZ complex–coated beads and in vitro–translated S^{35}-labeled NDC-80 N terminus. Maltose binding protein (MBP)–coated beads are negative controls. (**C**) Microtubule cosedimentation with 100 nM NDC-80 complex, indicated concentration of Taxol-stabilized microtubules, 2 μM R^NZ complex, and 5 μM bovine serum albumin. Binding was quantified with anti–NDC-80 immunoblots of supernatant and pellet fractions (see also fig. S2). (**D**) (Top) Schematic of mutations engineered in NDC-80 (fig. S3). (Bottom) Anti–NDC-80 immunoblot showing replacement of endogenous NDC-80 by transgene-encoded NDC-80 WT (wild type) and variants (see also fig. S1). (**E**) Embryo viability analysis for the indicated conditions. Error bars are SD of embryo lethality per worm; >10 worms and >1000 embryos were scored per condition. (**F**) Microtubule cosedimentation, as in (C), with indicated NDC-80 complex variants (fig. S2). (**G**) Chromosome segregation phenotypes for the indicated conditions. Bar, 5 μm.

to perform microtubule cosedimentation assays in the presence or absence of purified R^NZ complex. R^NZ suppressed NDC-80 complex binding to microtubules (Fig. 2C and fig. S2C). R^NZ did not associate with microtubules on its own, excluding competition for lattice-binding sites as a mechanism underlying this suppression (fig. S2D).

ROD-1 binding to the NDC-80 basic tail may mask an electrostatic interaction required for the NDC-80 complex to bind to microtubules (*17*–*19*). To test this possibility, we analyzed three mutant forms of NDC-80 in vitro and in vivo: a tail deletion ($NDC\text{-}80^{\Delta Tail}$), an Aurora B phosphorylation-mimicking tail mutant ($NDC\text{-}80^{4D}$), and a calponin homology (CH) domain mutant ($NDC\text{-}80^{CH*}$) in which three basic residues were changed to alanine (Fig. 2D and fig. S3A) (*20*). $NDC\text{-}80^{CH*}$, $NDC\text{-}80^{\Delta Tail}$, and $NDC\text{-}80^{4D}$ mutations all inhibited reconstituted NDC-80 complex microtubule binding to the same extent in vitro (Fig. 2F and fig. S2B) (*15*, *21*–*23*). However, only the $NDC\text{-}80^{CH*}$ mutant resulted in embryonic lethality (Fig. 2E). Consistent with the lack of embryonic lethality, $NDC\text{-}80^{\Delta Tail}$ and $NDC\text{-}80^{4D}$ were able to segregate chromosomes, whereas $NDC\text{-}80^{CH*}$ was defective in chromosome segregation (Fig. 2G). In pole-tracking analysis, $NDC\text{-}80^{\Delta Tail}$ overlapped $NDC\text{-}80^{WT}$ (fig. S3B); in addition, removal of the microtubule-binding Ska complex (*24*) did not enhance the phenotype of $NDC\text{-}80^{\Delta Tail}$ (fig. S4). Thus, although the basic NDC-80 tail was required for microtubule binding in vitro, it was not required to form end-coupled kinetochore-microtubule attachments in the *C. elegans* embryo. Thus, RZZ cannot inhibit NDC-80 in vivo by masking an electrostatic interaction between the tail and the microtubule lattice.

To determine whether the ROD-1–NDC-80 tail interaction was required for RZZ inhibition, we analyzed the effect of depleting SPDL-1 (to trigger persistent RZZ-mediated inhibition) in embryos in which endogenous NDC-80 was replaced by $NDC\text{-}80^{WT}$, $NDC\text{-}80^{\Delta Tail}$, or $NDC\text{-}80^{4D}$. Consistent with the tail dependence of the ROD-1–NDC-80 interaction, the failure to form end-coupled attachments after SPDL-1 depletion was completely suppressed in embryos expressing $NDC\text{-}80^{\Delta Tail}$ (Fig. 3, A and B). By contrast, the $NDC\text{-}80^{4D}$ mutant that still interacted with ROD-1 (Fig. 2B) but failed to bind to microtubules in vitro (Fig. 2F) was as sensitive to SPDL-1 depletion as $NDC\text{-}80^{WT}$ (Fig. 3A and fig. S3C). Thus, the ability of NDC-80 to be regulated by RZZ correlates with its tail-dependent interaction with ROD-1 and not with in vitro microtubule binding.

In $NDC\text{-}80^{WT}$ embryos, SPDL-1 depletion prevented formation of end-coupled attachments, whereas RZZ depletion only delayed attachment formation owing to the absence of dynein-mediated acceleration of microtubule capture (Fig. 3, A and B) (*7*). If $NDC\text{-}80^{\Delta Tail}$ is resistant to RZZ inhibition, the marked difference in phenotypic severity between RZZ and SPDL-1 depletion observed with $NDC\text{-}80^{WT}$ should be lost

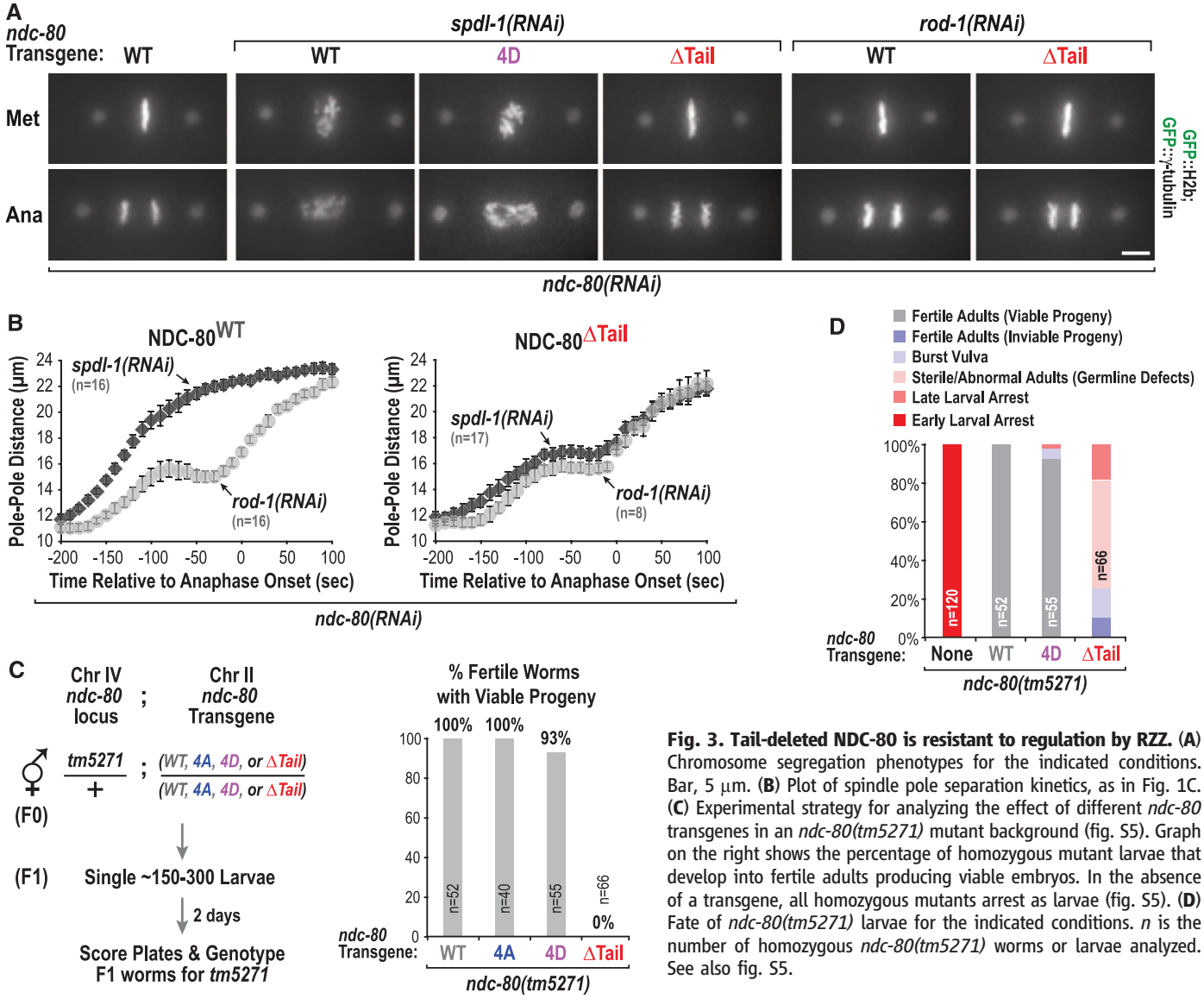

Fig. 3. Tail-deleted NDC-80 is resistant to regulation by RZZ. (**A**) Chromosome segregation phenotypes for the indicated conditions. Bar, 5 μm. (**B**) Plot of spindle pole separation kinetics, as in Fig. 1C. (**C**) Experimental strategy for analyzing the effect of different *ndc-80* transgenes in an *ndc-80(tm5271)* mutant background (fig. S5). Graph on the right shows the percentage of homozygous mutant larvae that develop into fertile adults producing viable embryos. In the absence of a transgene, all homozygous mutants arrest as larvae (fig. S5). (**D**) Fate of *ndc-80(tm5271)* larvae for the indicated conditions. *n* is the number of homozygous *ndc-80(tm5271)* worms or larvae analyzed. See also fig. S5.

in the presence of NDC-80$^{\Delta Tail}$. Both visualization of chromosome segregation and quantitative pole tracking confirmed this prediction (Fig. 3, A and B). Because the tail was not required for the formation of end-coupled attachments (Fig. 2G and fig. S3B), binding of RZZ to the NDC-80 tail probably prevents the adjacent functionally critical CH domain from interacting with microtubules.

We next used a genetic approach to analyze phenotypes observed after replacement of endogenous NDC-80 with transgene-encoded variants. We analyzed the fate of embryos homozygous for *ndc-80(tm5271)* (fig. S5A) derived from a heterozygous mother that also harbored homozygous *ndc-80* transgene insertions (Fig. 3C). Whereas the *ndc-80*^{WT}, *ndc-80*^{4D}, and the *ndc-80*^{4A} transgenes supported development of *ndc-80(tm2571)* larvae into fertile adults, the *ndc-80*$^{\Delta Tail}$ transgene did not (Fig. 3C). The phenotypes observed in the presence of NDC-80$^{\Delta Tail}$ included late larval arrest, bursting at the vulva, and absence of a germ line, leading to sterility (Fig. 3D and fig. S5B). Similar phenotypes are observed in *C. elegans* mutants that compromise the spindle checkpoint, a well-studied pathway ensuring accurate chromosome segregation (*25*). Because NDC-80$^{\Delta Tail}$ exhibited normal checkpoint signaling (fig. S6A) and synthetic embryonic lethality with checkpoint inhibition (fig. S6B), the observed phenotypes were not due to a defect in checkpoint signaling. Thus, NDC-80$^{\Delta Tail}$ exhibited a spectrum of defects associated with reduced accuracy of chromosome segregation in *C. elegans* and failed to rescue the lethality caused by the *ndc-80* mutation. Because similar-severity defects were not observed with NDC-80^{4D}, which inhibits NDC-80 complex microtubule binding activity in vitro, these defects are most likely due to loss of NDC-80 regulation by RZZ. A mutant in ROD-1 that selectively disrupts regulation of NDC-80 will be necessary to confirm this conclusion.

To understand how RZZ inhibition of NDC-80 was alleviated by SPDL-1, we focused on the conserved motif in Spindly family proteins required for dynein recruitment (Fig. 4A) (*26*). We replaced endogenous SPDL-1 with SPDL-1^{WT} or a single–amino acid mutant in the motif required for dynein binding (SPDL-1^{F199A}; Fig. 4A and fig. S7, A to D). Analogous to human cells, SPDL-1^{F199A} localized to kinetochores (fig. S7C) but abrogated dynein recruitment (Fig. 4B). SPDL-1^{F199A} exhibited a chromosome segregation defect of similar severity to that caused by removal of SPDL-1 (Fig. 4C and fig. S8). In addition, the severe chromosome segregation defect of SPDL-1^{F199A} was suppressed by codepletion of RZZ (Fig. 4C and fig. S7E). Thus, dynein recruitment by SPDL-1 turns off RZZ-mediated inhibition of end-coupled attachment formation (fig. S9).

Regulation of Ndc80 by RZZ represents an Aurora B–independent mechanism for the control of kinetochore-microtubule attachments. This regulation could prevent NDC-80–mediated attachments from occurring during an initial laterally attached state to minimize the potential for merotely, in which a single kinetochore becomes erroneously linked to both spindle poles and results in missegregation (*27*). Dynein activity could reduce the probability of merotely by coordinating chromosome orientation with activation of NDC-80, either by inducing a change in RZZ conformation or by dissociating RZZ from the kinetochore (fig. S9). Because both the kinetochore dynein module and the Ndc80 complex are conserved throughout metazoans, the mechanism we elucidate here is also likely to be conserved.

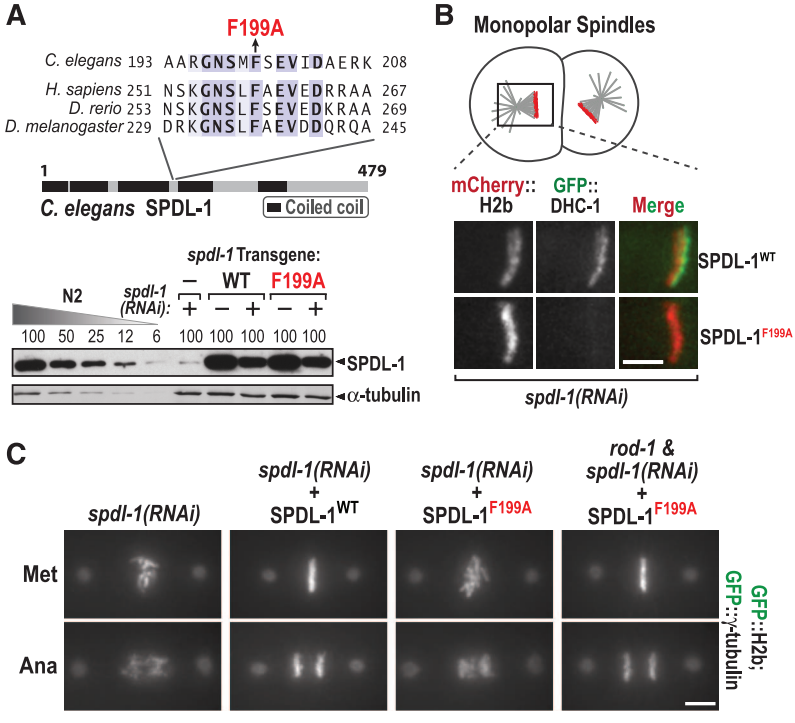

Fig. 4. Dynein recruitment by SPDL-1 is required to turn off RZZ-mediated inhibition of NDC-80. (**A**) (Top) The mutation (F199A) engineered in the Spindly motif. (Bottom) Anti–SPDL-1 immunoblot, as in fig. S1D. α-Tubulin is a loading control. (**B**) Analysis of dynein heavy chain (DHC-1) recruitment to unattached kinetochores of monopolar spindles generated by depleting the centriole duplication kinase ZYG-1 (fig. S7). Bar, 5 μm. (**C**) Chromosome segregation phenotypes for the indicated conditions. See also figs. S7 and S8. Bar, 5 μm.

References and Notes

1. I. M. Cheeseman, A. Desai, *Nat. Rev. Mol. Cell Biol.* **9**, 33–46 (2008).
2. S. Santaguida, A. Musacchio, *EMBO J.* **28**, 2511–2531 (2009).
3. C. L. Rieder, S. P. Alexander, *J. Cell Biol.* **110**, 81–95 (1990).
4. C. L. Rieder, E. D. Salmon, *Trends Cell Biol.* **8**, 310–318 (1998).
5. F. Scaërou *et al.*, *J. Cell Sci.* **112**, 3757–3768 (1999).
6. D. A. Starr, B. C. Williams, T. S. Hays, M. L. Goldberg, *J. Cell Biol.* **142**, 763–774 (1998).
7. R. Gassmann *et al.*, *Genes Dev.* **22**, 2385–2399 (2008).
8. R. Karess, *Trends Cell Biol.* **15**, 386–392 (2005).
9. E. R. Griffis, N. Stuurman, R. D. Vale, *J. Cell Biol.* **177**, 1005–1015 (2007).
10. K. Oegema, A. Desai, S. Rybina, M. Kirkham, A. A. Hyman, *J. Cell Biol.* **153**, 1209–1226 (2001).
11. A. Desai *et al.*, *Genes Dev.* **17**, 2421–2435 (2003).
12. M. Barisic *et al.*, *Mol. Biol. Cell* **21**, 1968–1981 (2010).
13. I. M. Cheeseman, J. S. Chappie, E. M. Wilson-Kubalek, A. Desai, *Cell* **127**, 983–997 (2006).
14. J. G. DeLuca *et al.*, *Cell* **127**, 969–982 (2006).
15. C. Ciferri *et al.*, *Cell* **133**, 427–439 (2008).
16. F. Çivril *et al.*, *Structure* **18**, 616–626 (2010).
17. G. J. Guimaraes, Y. Dong, B. F. McEwen, J. G. Deluca, *Curr. Biol.* **18**, 1778–1784 (2008).
18. S. A. Miller, M. L. Johnson, P. T. Stukenberg, *Curr. Biol.* **18**, 1785–1791 (2008).
19. N. T. Umbreit *et al.*, *Proc. Natl. Acad. Sci. U.S.A.* **109**, 16113–16118 (2012).
20. G. M. Alushin *et al.*, *Nature* **467**, 805–810 (2010).
21. R. R. Wei, J. Al-Bassam, S. C. Harrison, *Nat. Struct. Mol. Biol.* **14**, 54–59 (2007).
22. F. Lampert, C. Mieck, G. M. Alushin, E. Nogales, S. Westermann, *J. Cell Biol.* **200**, 21–30 (2013).
23. J. P. I. Welburn *et al.*, *Mol. Cell* **38**, 383–392 (2010).
24. J. C. Schmidt *et al.*, *Dev. Cell* **23**, 968–980 (2012).
25. K. K. Stein, E. S. Davis, T. Hays, A. Golden, *Genetics* **175**, 107–123 (2007).
26. R. Gassmann *et al.*, *Genes Dev.* **24**, 957–971 (2010).
27. D. Cimini *et al.*, *J. Cell Biol.* **153**, 517–528 (2001).

Acknowledgments: We thank the Japanese National BioResource Project for the *ndc-80* deletion strain, K. Corbett for helpful discussions, and B. Green for comments on the manuscript. The data described here are tabulated in the main paper and the supplementary materials. This work was supported by an NIH grant (GM074215) to A.D; A.D. and K.O. receive salary and other support from the Ludwig Institute for Cancer Research.

Supplementary Materials

www.sciencemag.org/content/342/6163/1239/suppl/DC1
Materials and Methods
Figs. S1 to S9
Tables S1 and S2
References (*28*–*36*)

20 September 2013; accepted 1 November 2013
Published online 14 November 2013;
10.1126/science.1246232

Nonredundant Function of Soluble LTα$_3$ Produced by Innate Lymphoid Cells in Intestinal Homeostasis

Andrey A. Kruglov,[1,2]* Sergei I. Grivennikov,[3] Dmitry V. Kuprash,[2,4] Caroline Winsauer,[1] Sandra Prepens,[1] Gitta Maria Seleznik,[5] Gerard Eberl,[6] Dan R. Littman,[7] Mathias Heikenwalder,[5,8] Alexei V. Tumanov,[9] Sergei A. Nedospasov[1,2,4]*

Immunoglobulin A (IgA) production at mucosal surfaces contributes to protection against pathogens and controls intestinal microbiota composition. However, mechanisms regulating IgA induction are not completely defined. We show that soluble lymphotoxin α (sLTα$_3$) produced by RORγt$^+$ innate lymphoid cells (ILCs) controls T cell–dependent IgA induction in the lamina propria via regulation of T cell homing to the gut. By contrast, membrane-bound lymphotoxin β (LTα$_1$β$_2$) produced by RORγt$^+$ ILCs is critical for T cell–independent IgA induction in the lamina propria via control of dendritic cell functions. Ablation of LTα in RORγt$^+$ cells abrogated IgA production in the gut and altered microbiota composition. Thus, soluble and membrane-bound lymphotoxins produced by ILCs distinctly organize adaptive immune responses in the gut and control commensal microbiota composition.

Production of immunoglobulin A (IgA) at mucosal surfaces contributes to host defense against intestinal pathogens and governs quantitative and qualitative control of commensal microbiota composition by the host (*1*, *2*). IgA can be induced by distinct T cell–dependent or T cell–independent pathways. T cell–dependent regulation of IgA production takes place mainly in Peyer's patches and requires the formation of germinal centers and the interaction of B cells with follicular helper T cells (*3*). T cell–independent mucosal IgA is produced both in isolated lymphoid follicles (ILFs) and in the lamina propria aided by exposure of B cells to various cytokines and growth factors, without the formation of germinal centers (*4*, *5*).

Lymphotoxin α (LTα) and lymphotoxin β (LTβ) are trimeric cytokines of the tumor necrosis factor (TNF) superfamily that are expressed in either soluble (sLTα$_3$) or membrane-bound (LTα$_1$β$_2$) forms by T and B cells, as well as by retinoic acid–related orphan receptor positive (RORγt$^+$) innate lymphoid cells (ILCs) (*6*). Soluble lymphotoxin is a TNF-like cytokine and its signaling is mediated via both TNFR1 and TNFR2, whereas membrane-bound lymphotoxin signals via LTβR (*6*). Ablation of the surface lymphotoxin–driven pathway via inactivation of the genes encoding LTα, LTβ, or LTβR results in block of lymphoid organ development and in diminished IgA plasma cell numbers in mucosal tissues (*7*, *8*), indicating that membrane-bound lymphotoxin is critical for intestinal IgA production. However, the possible contribution of soluble lymphotoxin to this process is not known.

ILCs were recently described as an important subset of innate immune cells that lack specific antigen receptors but are able to produce a range of effector cytokines (*9*). They are predominantly located in mucosal tissues and provide the first line of defense against various mucosal pathogens (*9*–*14*). In particular, RORγt$^+$ ILCs, via LT production, induce the development of gut-associated lymphoid tissues such as lymph nodes, Peyer's patches, and isolated lymphoid follicles (*8*, *15*, *16*) and are critical for protection against intestinal pathogens (*10*, *11*, *17*), for maintenance of the epithelial barrier, and for the prevention of systemic dissemination of commensal microbiota (*16*, *18*). However, the molecular mechanisms that mediate host control of commensals by RORγt$^+$ ILCs remain largely unknown.

We used mice lacking LTα or LTβ production by RORγt-expressing cells (LTα$^{\Delta ILC,T}$ and LTβ$^{\Delta ILC,T}$ mice, respectively) (*19*, *20*) (fig. S1). Because the transcription factor RORγt is expressed in double positive (CD4$^+$CD8$^+$) thymocytes, these mice also exhibit LT gene deletion in all αβ T cells (*21*) in addition to RORγt$^+$ ILCs. Therefore, to define the role of LT expressed specifically by RORγt$^+$ ILCs, we included mice with T cell ablation of LTα and LTβ, using CD4-Cre transgenic mice (LTα$^{\Delta T}$ and LTβ$^{\Delta T}$, respectively) as controls in all our analyses (fig. S1). Mice lacking expression of either the *LTα* or *LTβ* gene in T cells showed no developmental defects in their secondary lymphoid tissues (*20*), whereas LTβ$^{\Delta ILC,T}$ mice lacked Peyer's patches, isolated lymphoid follicles, and all peripheral lymph nodes except mesenteric (fig. S1), recapitulating the anatomical phenotype of complete LTβ ablation (*22*). LTα$^{\Delta ILC,T}$ mice lacked Peyer's patches, isolated lymphoid follicles, and all lymph nodes (fig. S1). Together, these data demonstrated the role of LT produced by RORγt$^+$ ILCs during embryogenesis for secondary lymphoid organ development (*15*).

Membrane-bound lymphotoxin produced by RORγt$^+$ ILCs is implicated as one of the critical cytokines required for generation of mucosal IgA through the formation of ILFs (*8*). However, LTβ$^{\Delta ILC,T}$ animals that lacked ILFs exhibited normal fecal IgA levels and only slightly diminished blood IgA levels relative to wild-type controls (Fig. 1, A and B). By contrast, concomitant inactivation of surface and soluble lymphotoxins via deletion of the *LTα* gene, in both RORγt$^+$ ILCs and αβ T cells (but not in αβ T cells alone), led to a striking decrease in both blood and fecal IgA levels and was essential for the presence of IgA$^+$ cells in the lamina propria (Fig. 1, A to C). By contrast, LTα expression by T cells was not required either for IgA production or for the recruitment of major immune cell subsets in the small intestine (Fig. 1, A to C, and fig. S2). To rule out a possible contribution from mesenteric lymph nodes that are present in LTβ$^{\Delta ILC,T}$ animals (but not in LTα$^{\Delta ILC,T}$ mice), we established bone marrow transfers into lethally irradiated LTα-deficient recipients that lacked gut-associated lymphoid tissue. In contrast to wild-type, LTα$^{\Delta T}$, and LTβ$^{\Delta ILC,T}$ bone marrow cells, transfer of LTα$^{\Delta ILC,T}$ bone marrow cells failed to induce IgA in recipient mice (Fig. 1D); this result implies a direct role of LTα produced by RORγt$^+$ ILCs in this process, irrespective of the presence of mesenteric lymph nodes and consistent with previous findings in LTα-deficient mice (*7*, *23*).

One of the known functions of IgA in mucosal tissues is to contain and control the composition of commensal microbiota (*24*). Deep sequencing analysis of ileal commensal microflora in wild-type and LTα$^{\Delta ILC,T}$ animals, and further real-time polymerase chain reaction (PCR) of selected intestinal commensals, revealed a marked expansion of segmented filamentous bacteria and a reduction in Bacteroidetes in mice lacking LTα expression by RORγt$^+$ cells (Fig. 1, E and F), implicating LT expression by RORγt$^+$ ILCs in the control of gut microbiota.

Although wild-type, LTα$^{\Delta T}$, LTβ$^{\Delta ILC,T}$, LTα$^{\Delta ILC,T}$, and LTα$^{-/-}$ animals showed similar ILC numbers in the lamina propria (figs. S3 and S4), c-Kit and CCR6 expression by the small intestinal lymphoid tissue inducer-like (LTi) (CD45$^+$Thy1.2$^+$ c-Kit^{high}IL-7Rα$^+$CCR6$^+$) cells was controlled by membrane-bound lymphotoxin produced by RORγt$^+$ ILCs (fig. S3). However, comparable phenotypic changes were found in adult LTi cells from LTβ$^{\Delta ILC,T}$, LTα$^{\Delta ILC,T}$, and LTα$^{-/-}$ mice (fig. S4); therefore, this cannot explain the lack

[1]German Rheumatism Research Center (DRFZ), a Leibniz Institute, Berlin 10117, Germany. [2]Belozersky Institute of Physico-Chemical Biology and Biological Faculty, Lomonosov Moscow State University, Moscow 119991, Russia. [3]Cancer Prevention and Control Program, Fox Chase Cancer Center, Philadelphia, PA 19111, USA. [4]Engelhardt Institute of Molecular Biology, Russian Academy of Sciences, Moscow 119991, Russia. [5]Department of Pathology, Institute of Clinical Pathology, University Hospital Zürich, CH 8091 Zürich, Switzerland. [6]Institut Pasteur and Centre National de la Recherche Scientifique, Unité de Recherche Associée 1961, 75724 Paris, France. [7]Howard Hughes Medical Institute and Molecular Pathogenesis Program, Kimmel Center for Biology and Medicine, Skirball Institute, New York University School of Medicine, New York, NY 10016, USA. [8]Institute of Virology, Helmholtz Zentrum München, Technische Universität München, D-81675 München, Germany. [9]Trudeau Institute, Saranac Lake, NY 12983, USA.

*Corresponding author. E-mail: andrey_krugloff@mail.ru (A.A.K.); sergei@nedos.net (S.A.N.)

of intestinal IgA observed in the two latter gene-deficient animals.

Signaling via both TNFR1 and TNFR2 contributed to intestinal IgA production, whereas complete genetic ablation of TNF did not affect fecal IgA levels (fig. S5), consistent with the role for soluble LT produced by RORγt$^+$ ILCs. Furthermore, both TNFR1 and TNFR2 expressed by non-hematopoietic cells contributed to IgA induction, as revealed by reciprocal bone marrow transfer experiments (fig. S5). Therefore, soluble lymphotoxin acts via TNFR1 and TNFR2 expressed by lamina propria stromal cells to promote IgA production.

In the context of intestinal immunity, LTβR signaling is important for B cell homing to the gut (*7*). We found significantly reduced expression of chemokine and adhesion molecules such as CXCL13, VCAM-1, and CCL20 in the small intestine upon ablation of LTα, but not of LTβ, from RORγt$^+$ cells, whereas MAdCAM-1 and CCL21 expression remained unaffected (fig. S5). Moreover, both soluble and membrane-bound lymphotoxins expressed by RORγt$^+$ ILCs facilitated the homing of lamina propria IgM$^+$ B cells (Fig. 2, A and B).

Because intestinal IgA plasma cells can develop from peritoneal IgM$^+$ B cells recruited to the gut (*25*), we assessed the influence of LTα and LTβ expression by RORγt$^+$ ILCs in the peritoneal B cell compartment. Indeed, peritoneal cavity exudate cells from both LTα$^{\Delta ILC,T}$ and LTβ$^{\Delta ILC,T}$ mice contained increased numbers of B1 and B2 B cells (fig. S6), whereas numbers of B cells in the spleen and bone marrow were normal (fig. S6). Additionally, B cells from LTα$^{\Delta ILC,T}$ mice were able to undergo class switching toward IgA in vitro, ruling out a B cell–intrinsic defect in class switch recombination (fig. S6).

Unexpectedly, when LTβ$^{\Delta ILC,T}$ mice were crossed onto a T cell receptor (TCR) αβ–deficient background, we found reduced IgA levels both in the feces and blood (Fig. 2, C and D), which correlated with the absence of IgA$^+$ plasma cells in the lamina propria (Fig. 2, E to G). T cell deficiency in LTβ$^{\Delta ILC,T}$ mice did not further affect homing of B cells to the lamina propria (Fig. 2F and fig. S7). B cell proliferation, activation, and expression of activation-induced cytidine deaminase (AID) are all required for class switch recombination in B cells (*26*), and, indeed, no AID mRNA was detected in freshly isolated lamina propria lymphocytes from LTβ$^{\Delta ILC,T}$ TCRαβ$^{-/-}$ mice, whereas lamina propria lymphocytes from LTβ$^{\Delta ILC,T}$ mice showed AID expression (fig. S7). Moreover, lamina propria B cells in LTβ$^{\Delta ILC,T}$ mice were actively proliferating as revealed by KI67 staining (fig. S7). Taken together, these findings indicate that in the absence of surface lymphotoxin expression by RORγt$^+$ ILCs, IgA class switching can occur in the lamina propria, and that αβ T cells are crucial for this process.

LT expression by RORγt$^+$ ILCs did not affect the development of various dendritic cell (DC) subsets

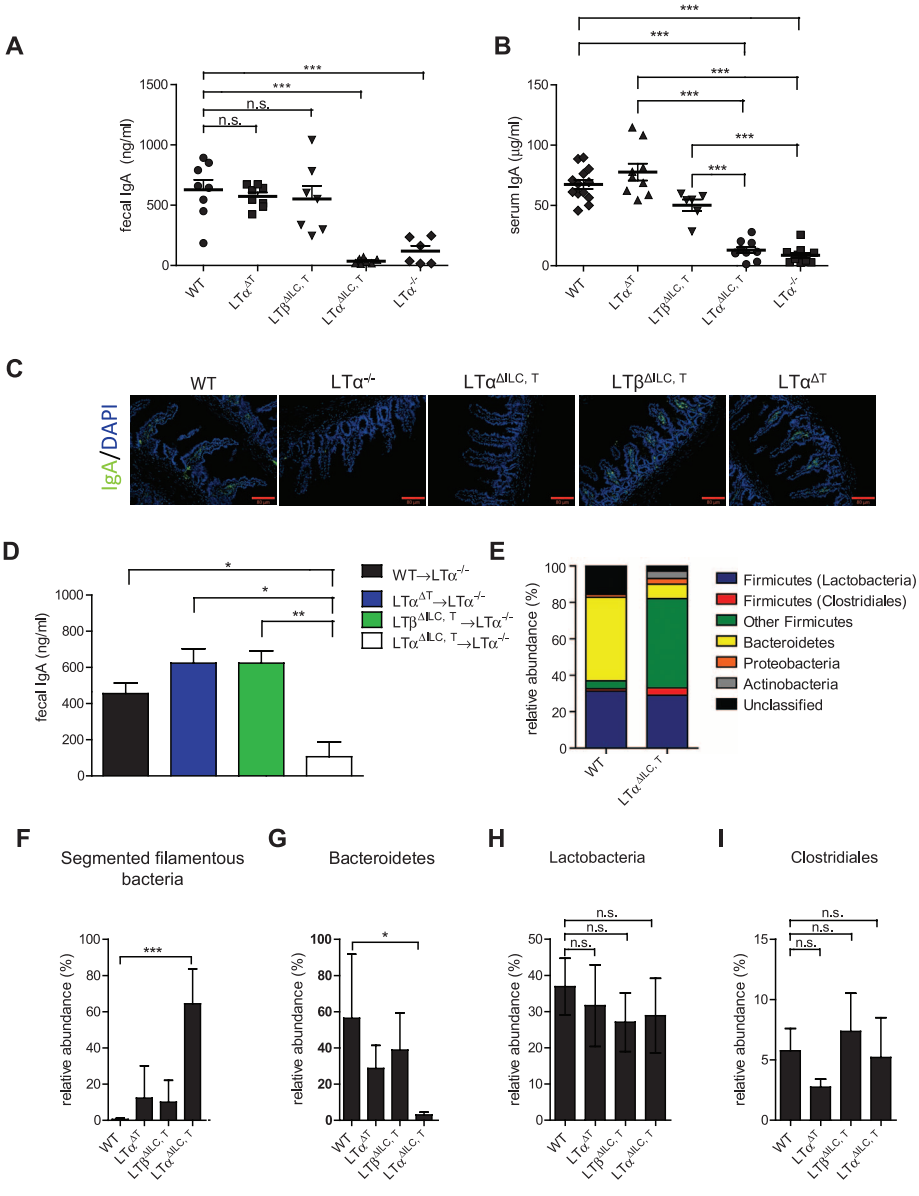

Fig. 1. Soluble LTα$_3$ produced by RORγt$^+$ ILCs regulates IgA production and microbiota composition in the gut. (**A**) Fecal IgA levels in naïve wild-type (WT), LTα$^{\Delta T}$, LTα$^{\Delta ILC,T}$, LTβ$^{\Delta ILC,T}$, and LTα$^{-/-}$ animals. (**B**) Serum IgA levels in naïve WT, LTα$^{\Delta T}$, LTα$^{\Delta ILC,T}$, LTβ$^{\Delta ILC,T}$, and LTα$^{-/-}$ animals. (**C**) Immunofluorescence analysis of IgA expression in the small intestine in naïve mice lacking LTα and LTβ expression by RORγt$^+$ cells. Scale bars, 80 μm. (**D**) Fecal IgA levels in LTα$^{-/-}$ recipients, reconstituted with WT, LTα$^{\Delta T}$, LTα$^{\Delta ILC,T}$, and LTβ$^{\Delta ILC,T}$ bone marrow. Feces were collected 2 months after bone marrow transfer; IgA fecal levels were measured as described (*30*). (**E**) Deep sequencing analysis of microbiota composition from terminal ileum of LTα$^{\Delta ILC,T}$ mice and littermate WT controls. Representative microbiota composition in WT and LTα$^{\Delta ILC,T}$ ileum is presented (n = 2 mice per group). (**F** to **I**) Real-time PCR analysis of microbiota composition in terminal ileum of naïve WT, LTα$^{\Delta T}$, LTα$^{\Delta ILC,T}$, and LTβ$^{\Delta ILC,T}$ animals. Error bars, SEM; *P < 0.05, **P < 0.01, ***P < 0.001 (Student's t test). All data, except deep sequencing analysis, are representative of two or more independent experiments with $n \geq 3$ mice.

in mesenteric lymph nodes and in the small intestine (fig. S8), but $LT\alpha_1\beta_2$ expression by $ROR\gamma t^+$ cells did control inducible nitric oxide synthase (iNOS) expression by mesenteric lymph node $CD11c^+$ DCs (Fig. 2H), which is known to be critical for IgA induction (*27*, *28*). Moreover, $CD11c^+$ DCs isolated from mesenteric lymph nodes of $LT\beta^{\Delta ILC,T}$ mice were less potent in inducing IgA in vitro (Fig. 2I). Together, these data indicated that $LT\alpha_1\beta_2$ may control T cell–independent IgA production via regulation of iNOS expression by DCs. Furthermore, our analysis revealed a reduction of CD40L mRNA levels in the small intestine of $LT\beta^{\Delta ILC,T}$ mice after T cell ablation (Fig. 3A). When the T cell compartment in $LT\beta^{\Delta ILC,T}$ $TCR\beta\delta^{-/-}$ animals was reconstituted with wild-type or $CD40L^{-/-}$ αβ T cells, we found that wild-type, but not $CD40L^{-/-}$, T cells could induce IgA production (Fig. 3, B and C). Interestingly, LTα, but not LTβ, expressed by $ROR\gamma t^+$ cells controlled T cell numbers in the lamina propria (Fig. 3, D and E). However, LTα produced by $ROR\gamma t^+$ cells did not affect the numbers of gut-homing T cells on the periphery (fig. S8).

Consistently, we found significant reduction of CD40L mRNA expression in $LT\alpha^{\Delta ILC,T}$ animals relative to littermate controls (Fig. 3F), which led us to hypothesize that soluble lymphotoxin may regulate IgA induction via control of T cell homing to the lamina propria. Indeed, forced activation of CD40 signaling by agonistic antibody in $LT\alpha^{\Delta ILC,T}$ mice resulted in IgA induction (Fig. 3, G and H) without affecting T and B cell homing to the small intestine (fig. S9), further implying that T cells may contribute to the regulation of IgA switching in the lamina propria via the CD40-CD40L pathway. Notably, the induction of unspecific intestinal inflammation, such as dextran sodium sulfate–induced colitis, failed to induce generation of IgA plasma cells (fig. S9). Collectively, these data indicated that $sLT\alpha_3$ derived from ILCs may control IgA induction via regulation of T cell homing to the lamina propria.

Induction of fully competent adaptive immune responses in the intestinal tract is a host defense mechanism directed against potential pathogens, which also allows control of commensal microbiota by the host. Here, we delineated distinct functions for membrane-bound and soluble lymphotoxins expressed by $ROR\gamma t^+$ ILCs in the induction of IgA in the lamina propria (fig. S10). We found that production of membrane-bound lymphotoxin by ILCs regulates T cell–independent IgA induction via iNOS production by $CD11c^+$ DCs. We further demonstrated that ILC-derived soluble LT regulates the

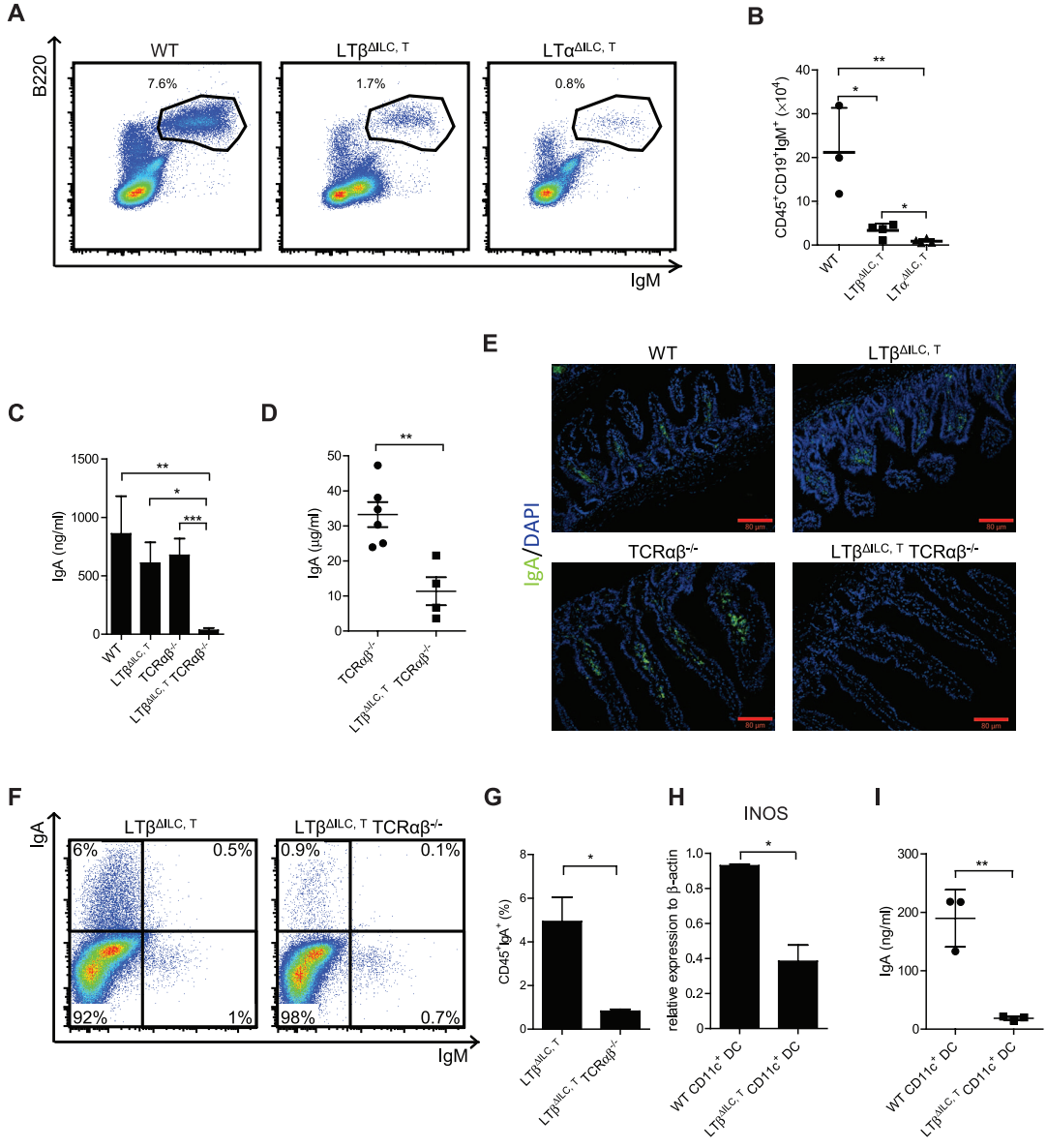

Fig. 2. Membrane-bound $LT\alpha_1\beta_2$ produced by $ROR\gamma t^+$ cells controls T cell–independent IgA induction in the lamina propria in the absence of organized gut-associated lymphoid tissue. (**A**) B cell frequencies in the lamina propria of WT, $LT\beta^{\Delta ILC,T}$, and $LT\alpha^{\Delta ILC,T}$ mice. (**B**) Numbers of $CD45^+CD19^+IgM^+$ cells in the lamina propria of WT, $LT\beta^{\Delta ILC,T}$, and $LT\alpha^{\Delta ILC,T}$ mice. (**C**) Fecal IgA levels in WT, $LT\beta^{\Delta ILC,T}$, $TCR\alpha\beta^{-/-}$, and $LT\beta^{\Delta ILC,T}$ $TCR\alpha\beta^{-/-}$ mice. (**D**) Serum IgA levels in $TCR\alpha\beta^{-/-}$ and $LT\beta^{\Delta ILC,T}$ $TCR\alpha\beta^{-/-}$ mice. (**E**) Immunofluorescence analysis of IgA expression in the small intestine in WT, $LT\beta^{\Delta ILC,T}$, $TCR\alpha\beta^{-/-}$, and $LT\beta^{\Delta ILC,T}$ $TCR\alpha\beta^{-/-}$ mice. Scale bar, 80 μm. (**F** and **G**) Representative fluorescence-activated cell sorter (FACS) dot plots (F) and frequencies (G) of $CD45^+IgA^+$ cells in lamina propria of $LT\beta^{\Delta ILC,T}$ and $LT\beta^{\Delta ILC,T}$ $TCR\alpha\beta^{-/-}$ mice. (**H**) iNOS mRNA expression levels in $CD11c^+$ cells sorted from mesenteric lymph nodes. (**I**) IgA levels in 5-day cultures of WT splenic IgM^+ B cells together with $CD11c^+$ DCs isolated from mesenteric lymph nodes of WT or $LT\beta^{\Delta ILC,T}$ mice. All data are representative of two or more independent experiments with $n \geq 3$ mice. Error bars, SEM; $^*P < 0.05$, $^{**}P < 0.01$, $^{***}P < 0.001$ (Student's *t* test).

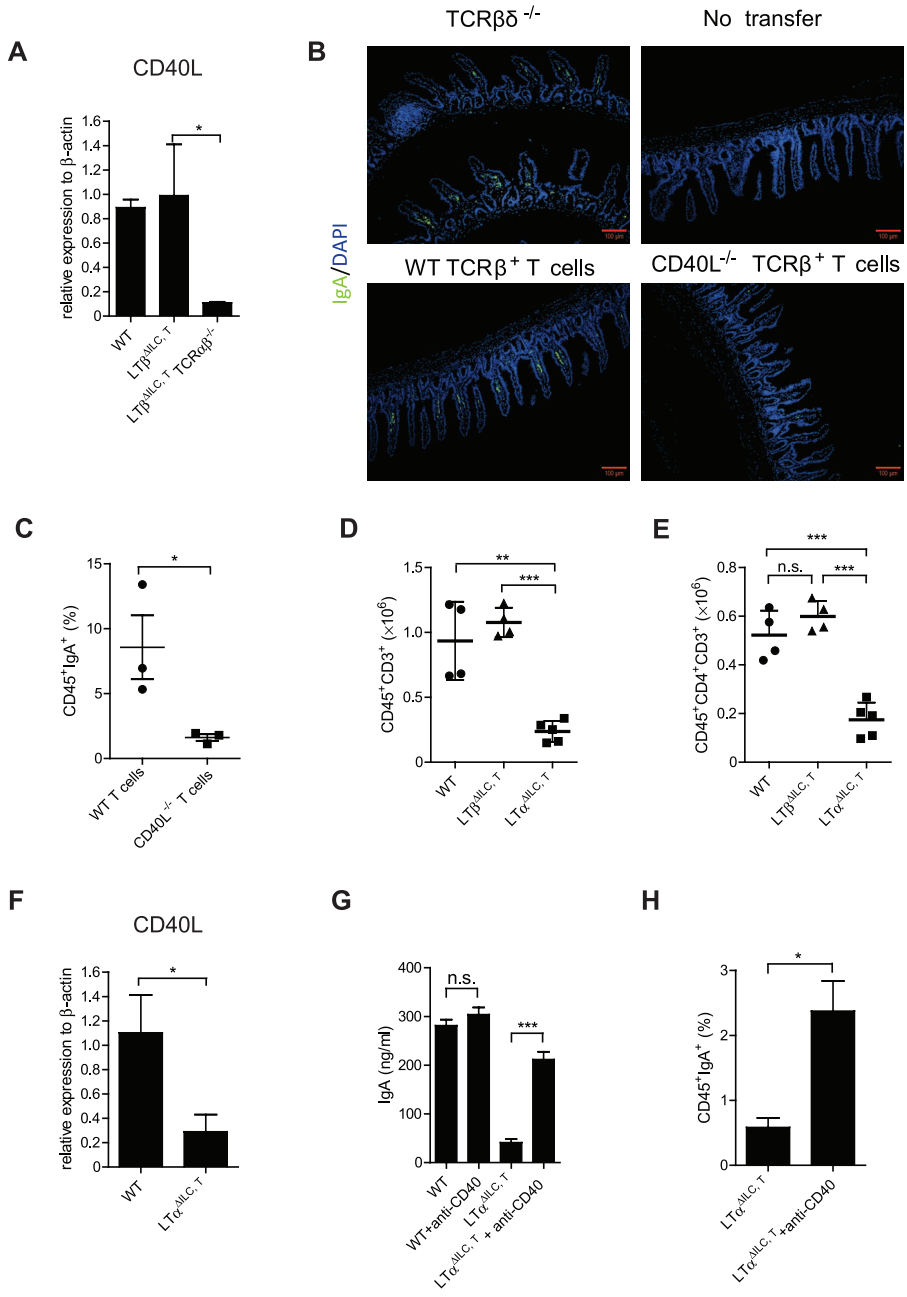

Fig. 3. Regulation of T cell–dependent IgA production by soluble LTα_3 produced by RORγt$^+$ ILCs. (**A**) CD40L mRNA levels in jejunum of naïve WT, LT$\beta^{\Delta ILC,T}$, and LT$\beta^{\Delta ILC,T}$ TCR$\alpha\beta^{-/-}$ mice. (**B**) Immunofluorescence analysis of IgA expression in the small intestine in naïve TCR$\beta\delta^{-/-}$, LT$\beta^{\Delta ILC,T}$ TCR$\beta\delta^{-/-}$ mice, as well as in LT$\beta^{\Delta ILC,T}$ TCR$\beta\delta^{-/-}$ mice, reconstituted with WT or CD40L$^{-/-}$ $\alpha\beta$ T cells. Scale bar, 100 μm. (**C**) Frequency of CD45$^+$IgA$^+$ cells in the lamina propria of LT$\beta^{\Delta ILC,T}$ TCR$\beta\delta^{-/-}$ mice 2 weeks after adoptive transfer of WT or CD40L$^{-/-}$ $\alpha\beta$ T cells. (**D** and **E**) Numbers of CD45$^+$CD3$^+$ cells (D) and CD45$^+$CD3$^+$CD4$^+$ cells (E) in the lamina propria of WT mice and mice with LTα or LTβ ablation in RORγt$^+$ cells. (**F**) CD40L mRNA levels in jejunum of WT and LT$\alpha^{\Delta ILC,T}$ animals. (**G**) In vivo induction of IgA in LT$\alpha^{\Delta ILC,T}$ mice by agonistic antibody to CD40. (**H**) CD45$^+$IgA$^+$ cells in the lamina propria of LT$\alpha^{\Delta ILC,T}$ mice after anti-CD40 treatment. All data are representative of two or more independent experiments with $n \geq 3$ mice. Error bars, SEM; *$P < 0.05$, **$P < 0.01$, ***$P < 0.001$ (Student's t test).

T cell–dependent pathway of IgA production via control of T cell homing to the gut. Through these processes, lymphotoxins produced by RORγt$^+$ ILCs control microbiota composition in the host and may influence various pathophysiological processes. Our findings highlight a rare nonredundant function of soluble lymphotoxin and may be relevant for anti-TNF therapy using etanercept, as this drug can block not only TNF but also soluble lymphotoxin (*29*), and thus the effects of such treatment may affect IgA levels and gut microbiota in patients.

References and Notes

1. K. Honda, D. R. Littman, *Annu. Rev. Immunol.* **30**, 759–795 (2012).
2. A. Cerutti, K. Chen, A. Chorny, *Annu. Rev. Immunol.* **29**, 273–293 (2011).
3. S. Fagarasan, S. Kawamoto, O. Kanagawa, K. Suzuki, *Annu. Rev. Immunol.* **28**, 243–273 (2010).
4. A. J. Macpherson *et al.*, *Science* **288**, 2222–2226 (2000).
5. J. R. Mora *et al.*, *Science* **314**, 1157–1160 (2006).
6. C. F. Ware, *Annu. Rev. Immunol.* **23**, 787–819 (2005).
7. H. S. Kang *et al.*, *Nat. Immunol.* **3**, 576–582 (2002).
8. M. Tsuji *et al.*, *Immunity* **29**, 261–271 (2008).
9. H. Spits, T. Cupedo, *Annu. Rev. Immunol.* **30**, 647–675 (2012).
10. G. F. Sonnenberg, L. A. Monticelli, M. M. Elloso, L. A. Fouser, D. Artis, *Immunity* **34**, 122–134 (2011).
11. Y. Wang *et al.*, *Immunity* **32**, 403–413 (2010).
12. L. A. Zenewicz *et al.*, *Immunity* **29**, 947–957 (2008).
13. N. Satoh-Takayama *et al.*, *Immunity* **29**, 958–970 (2008).
14. M. R. Hepworth *et al.*, *Nature* **498**, 113–117 (2013).
15. G. Eberl *et al.*, *Nat. Immunol.* **5**, 64–73 (2004).
16. D. Bouskra *et al.*, *Nature* **456**, 507–510 (2008).
17. A. V. Tumanov *et al.*, *Cell Host Microbe* **10**, 44–53 (2011).
18. G. F. Sonnenberg *et al.*, *Science* **336**, 1321–1325 (2012).
19. D. J. Liepinsh *et al.*, *Mol. Cell. Biol.* **26**, 4214–4225 (2006).
20. A. Tumanov *et al.*, *Immunity* **17**, 239–250 (2002).
21. G. Eberl, D. R. Littman, *Science* **305**, 248–251 (2004).
22. M. B. Alimzhanov *et al.*, *Proc. Natl. Acad. Sci. U.S.A.* **94**, 9302–9307 (1997).
23. R. D. Newberry, J. S. McDonough, K. G. McDonald, R. G. Lorenz, *J. Immunol.* **168**, 4988–4997 (2002).
24. K. Suzuki *et al.*, *Proc. Natl. Acad. Sci. U.S.A.* **101**, 1981–1986 (2004).
25. F. G. Kroese *et al.*, *Int. Immunol.* **1**, 75–84 (1989).
26. M. Muramatsu *et al.*, *Cell* **102**, 553–563 (2000).
27. H. Tezuka *et al.*, *Nature* **448**, 929–933 (2007).
28. J. H. Fritz *et al.*, *Nature* **481**, 199–203 (2012).
29. D. Tracey, L. Klareskog, E. H. Sasso, J. G. Salfeld, P. P. Tak, *Pharmacol. Ther.* **117**, 244–279 (2008).
30. See supplementary materials on *Science* Online.

Acknowledgments: We thank S. Fillatreau, J. Gommerman, A. Rudensky, and F. Melchers for useful discussions and critiques; K. Holden-Dye for editing of the manuscript; L. Drutskaya, K. Horn, M. Drutskaya, and D. Schlienz for expert technical support throughout the project; H. Schäfer, S. Gruczek, and M. Ohde for excellent animal husbandry; the members of the German Rheumatism Research Center Flow Cytometry Core Facility (T. Kaiser, J. Kirsch) for help with FACS analysis and cell sorting; H. Hecker-Kia, H. Schliemann, and T. Geske for antibody preparation; and J. Hirscher for help with figure preparation. Supported by Deutsche Forschungsgemeinschaft grants (SFB633 A13 and NE1466/2-1) and the MCB Program of the Russian Academy of Sciences (S.A.N. and D.V.K.), and the Crohn's and Colitis Foundation (A.V.T.). Bacterial 16*S* rRNA pyrosequencing reads have been deposited in the NCBI Short Read Archive database with accession numbers SRX362155, SRX362156, SRX362157, and SRX362158. Author contributions: A.A.K. and S.A.N. designed research; A.A.K., D.V.K., S.I.G., S.P., C.W., G.M.S., M.H., and A.V.T. performed experiments; D.R.L. and G.E. provided RORγt-Cre animals and discussed the data; and A.A.K. and S.A.N. wrote the manuscript.

Supplementary Materials

www.sciencemag.org/content/342/6163/1243/suppl/DC1
Materials and Methods
Figs. S1 to S10
Table S1
References (*31*–*38*)

17 July 2013; accepted 24 October 2013
10.1126/science.1243364

Hedgehog Signaling Controls T Cell Killing at the Immunological Synapse

Maike de la Roche,[1] Alex T. Ritter,[1,3] Karen L. Angus,[1] Colin Dinsmore,[2] Charles H. Earnshaw,[1] Jeremy F. Reiter,[2] Gillian M. Griffiths[1]*

The centrosome is essential for cytotoxic T lymphocyte (CTL) function, contacting the plasma membrane and directing cytotoxic granules for secretion at the immunological synapse. Centrosome docking at the plasma membrane also occurs during cilia formation. The primary cilium, formed in nonhematopoietic cells, is essential for vertebrate Hedgehog (Hh) signaling. Lymphocytes do not form primary cilia, but we found and describe here that Hh signaling played an important role in CTL killing. T cell receptor activation, which "prearms" CTLs with cytotoxic granules, also initiated Hh signaling. Hh pathway activation occurred intracellularly and triggered Rac1 synthesis. These events "prearmed" CTLs for action by promoting the actin remodeling required for centrosome polarization and granule release. Thus, Hh signaling plays a role in CTL function, and the immunological synapse may represent a modified cilium.

Cytotoxic T lymphocytes (CTLs) recognize tumor and virally infected cells via their T cell receptor (TCR). Recognition triggers a cascade of intracellular signaling that leads to the formation of the immunological synapse and polarization of the centrosome to contact the plasma membrane (*1*) at the central supramolecular activation complex (cSMAC) (*2*) where TCRs cluster within the synapse (*1*, *3*). Cytotoxic granules move toward the docked centrosome and deliver their contents precisely at the point of TCR-mediated recognition, which focuses secretion toward the target cell to be destroyed. Docking of the centrosome also occurs during cilia formation, when the mother centriole contacts the plasma membrane, forming the basal body from which the cilium extends. Although lymphocytes are one of very few cell types that do not form primary cilia (*4*), morphological and functional similarities can be drawn between the immunological synapse and cilia. Endocytosis and exocytosis are focused at the point of centrosome docking in both cases (*5*); ciliary intraflagellar transport (IFT) proteins are found in T cells (*6*), and both structures form important signaling platforms (*1*, *2*, *7*, *8*).

In Hedgehog (Hh) signaling, binding of exogenous Sonic, Indian, or Desert Hh (Shh, Ihh, or Dhh) to the transmembrane receptor Patched (Ptch) regulates translocation of Smoothened (Smo) to primary cilia (*9*, *10*). The ciliary localization of Smo is required to initiate transduction of *Gli*-mediated transcription of target genes, including *Gli1*, which serves as a reporter of Hh signaling (*7*, *8*). We asked whether proteins of the Hh pathway are expressed in T cells and whether TCR activation triggered Hh signaling. Naïve CD8 T cells and CTLs derived after 4 to 5 days of in vitro TCR activation were isolated from OT-I TCR transgenic mice. TCR cross-linking was triggered in both naïve CD8 T cell and CTL populations using plate-bound antibody against CD3 (Fig. 1A). In naïve CD8 T cells, *Gli1* mRNA was not detected, but expression was induced upon TCR cross-linking, peaking at 12 hours. Controls lacking antibody against CD3 showed no *Gli1* expression. CTLs had low *Gli1* mRNA levels that increased 180-fold after TCR ligation (Fig. 1A). In addition, the genes encoding Ptch1 and 2 receptors, the signal transducer Smo, and the ligand Ihh were all expressed in both naïve CD8 T cells and CTLs (fig. S1A), and protein expression of Ptch, Gli1, and Ihh increased after TCR activation of naïve CD8 cells (Fig. 1B) and CTLs (fig. S1B). Neither *Shh* nor *Dhh* were detected in CD8 T cells before or after 24-hour TCR activation or in EL4 and P815 target cell lines (fig. S1, C and D). When TCR signaling was severely impaired by deletion of the upstream tyrosine kinase Lck (*11*), induction of *Gli1* was also diminished in naïve CD8 T cells (Fig. 1, C and D). Thus, CD8 T cells express Hh pathway components and require TCR signaling to trigger Hh signaling.

Because only T cells were present in these assays, CD8 T cells must have both synthesized and responded to Hh proteins to activate this signaling pathway. This is unusual, as Hh signaling is usually paracrine, with one cell type producing Hh and another responding to this cue. We noted that Ihh was detected as a 45-kD protein, which indicated that it was not fully processed into the secreted form (*12*, *13*). This

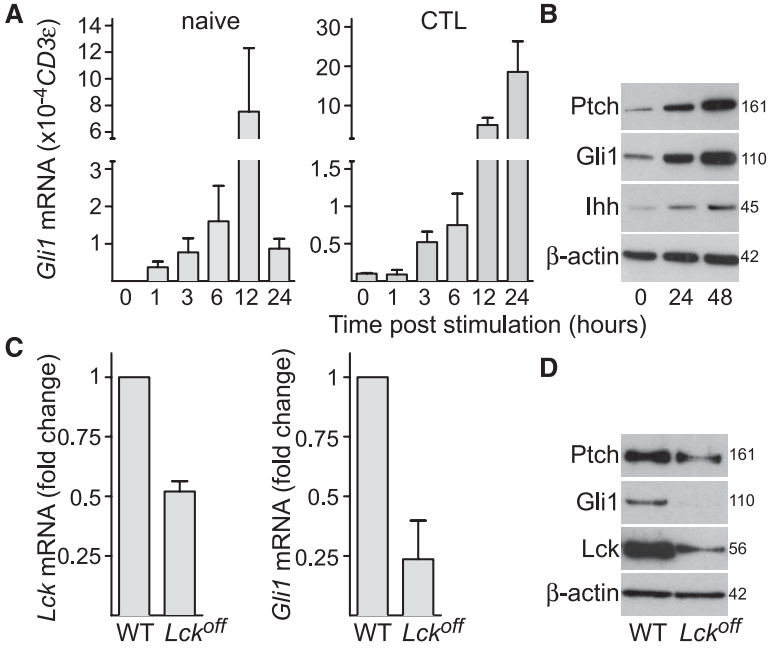

Fig. 1. TCR activation triggers Hh signaling and expression of Hh components in CD8 T cells. (**A**) Quantitative polymerase chain reaction (qPCR) showing mRNA levels of *Gli1* in naïve CD8 T cells (left) and CTLs (right) at times shown after TCR cross-linking with plate-bound antibody against CD3 relative to *CD3ε* as a reference gene; $n = 3$ (naïve) or 2 (CTLs); data are means ± SD. Similar results were obtained using the gene for TATA box–binding protein (Tbp) as a reference gene (not shown). Cells plated without antibody against CD3 showed no *Gli1* induction over 12 hours. (**B**) Immunoblot analysis of protein expression of Ptch, Gli1, Ihh, and actin at 0, 24, and 48 hours after TCR stimulation in naïve CD8 T cells; $n = 3$. Molecular masses are shown in kilodaltons. Similar results were also obtained from CD8 T cells derived from C57BL/6 and BALB/c mice (not shown). (**C** and **D**) Naïve CD8 T cells were purified from spleens of wild-type (WT) or Lck^{off} mice and stimulated for 12 hours with plate-bound antibody against CD3. (C) Graphs showing mRNA levels of *Lck* (left) and *Gli1* (right) in Lck^{off} CD8 T cells relative to WT control; $n = 2$, data are means ± SD. (D) Immunoblot analysis of Ptch, Gli1, Lck, and actin in Lck^{off} and WT control CD8 T cells after 12 hours of TCR stimulation; $n = 3$. Molecular masses are shown in kilodaltons.

[1]Cambridge Institute for Medical Research, University of Cambridge, Hills Road, Cambridge CB2 0XY, UK. [2]Department of Biochemistry and Biophysics, Cardiovascular Research Institute, University of California, San Francisco, CA 94158, USA. [3]National Institute of Child Health and Development, National Institutes of Health, Bethesda, MD 20892, USA.

*Corresponding author. E-mail: gg305@cam.ac.uk

raised the possibility that Ihh might bind Ptch intracellularly. We used recombinant Ihh protein to ask whether CTLs responded to exogenous Ihh. Although cross-linking of TCRs triggered *Gli1* expression, stimulating CTLs with extracellular Ihh alone did not. Furthermore, exogenous Ihh did not enhance *Gli1* expression in response to TCR activation (fig. S1E). Thus, Ihh encounters its receptor, Ptch, intracellularly in CTLs.

We next asked where Ptch, Ihh, and Smo localize in CTLs using antibodies to detect endogenous Ihh and endogenous Smo and Ptch1 fused with enhanced yellow fluorescent protein (Ptch1-EYFP) to localize the receptor (Fig. 2). In CTLs, Ptch1 was found on intracellular vesicles (Fig. 2A). Ihh colocalized with Ptch1 on a subset of these vesicles, which polarized toward the immunological synapse upon recognition of a target cell (Fig. 2, B and C). This is consistent with the idea that Ihh-mediated signaling via Ptch1 takes place intracellularly, and we confirmed the interaction between Ihh and Ptch1 on intracellular vesicles using a proximity ligation assay (fig. S2A). Ihh was also seen near sites of actin accumulation (fig. S2, B and C), which raised the possibility that Ihh may also influence actin, as shown for other Hh components (*14*, *15*). Endogenous Smo was also associated with intracellular vesicles in CTLs (Fig. 2D) that are predominantly Lamp1-positive (fig. S2D) and distinct from the Ihh-positive compartment (fig. S2E). Live imaging of Smo fused with enhanced green fluorescent protein (Smo-EGFP) expressed in CTLs showed that, upon recognition of a target cell via TCR, the intracellular pool of Smo polarized to the immunological synapse (Fig. 2E and movie S1), analogous to the Hh-triggered translocation of Smo into the cilium (*9*, *10*, *16*, *17*).

To determine whether TCR-triggered Hh signaling affects CTL-mediated killing, we made use of a genetic model in which *Smo* is conditionally deleted. Although Hh signaling is required for T cell development (*18*–*21*), T cells from mice in which exon 1 of *Smo* is inducibly deleted in adult hemopoietic cells under Mx1-Cre control devel-

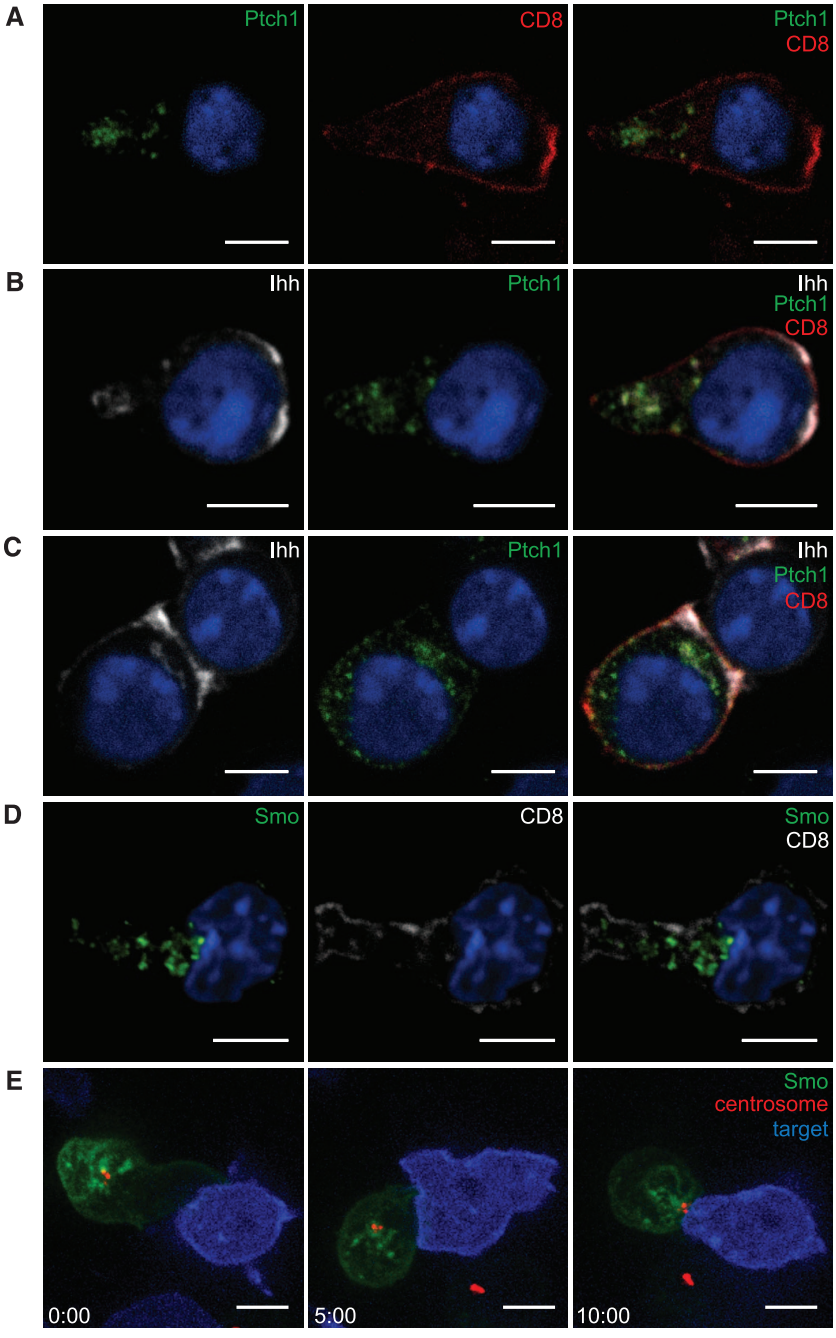

Fig. 2. Ihh, Ptch1, and Smo are localized on intracellular vesicles that polarize toward the immunological synapse. OT-I CTLs transduced with Ptch1-EYFP and labeled with antibodies to EYFP (green), CD8 (red), and Ihh (white). (**A** and **B**) show OT-1 CTLs alone and (**C**) conjugated with EL4 target cells. (**D**) Endogenous Smo (green) and CD8 (white) in OT-I CTLs. Single *x-y* confocal sections are shown. Nuclei are stained with Hoechst (blue). (A: $n > 75$;B and C: $n > 35$;D: $n > 85$; two to four independent experiments each). (**E**) Individual frames of a movie (movie S1) showing OT-I CTLs nucleofected with Smo-EGFP and PACT-RFP (centrosome marker, red), forming a synapse with EL4 target cells (blue). Time after initial contact is shown in minutes ($n = 33$). Scale bars: 5 μm.

op normally (*22*, *23*). CTLs generated from *Smo*-deleted mice showed greatly reduced (1.5%) levels of *Smo* mRNA relative to controls and greatly reduced Smo protein levels (Fig. 3, A and B). *Gli1* mRNA up-regulation in response to TCR ligation was also reduced: CTLs from control mice showed a threefold increase in levels of *Gli1* mRNA, whereas CTLs from *Smo*-deleted mice gave only a 1.5-fold increase (Fig. 3A). TCR signaling was not altered in *Smo*-deleted CTLs (Fig. 3C and fig. S3). However, when we assessed *Smo*-deleted CTLs for their cytotoxic effector function, we found reduced levels of target cell killing compared with control CTLs (Fig. 3D), which suggested that Hh signaling contributes to CTL killing. Because centrosome polarization to the plasma membrane is a key step in CTL-mediated killing, we asked whether Hh signaling affected centrosome docking at the cSMAC during conjugate formation between CTLs and target cells. *Smo*-deleted CTLs showed a ~50% reduction in centrosomal docking at the cSMAC (Fig. 3E), which was consistent with the reduction in Smo protein levels and CTL killing.

We also confirmed that Hh signaling is important for centrosome polarization and CTL-mediated killing using three separate inhibitors: cyclopamine and vismodegib (GDC-0449), both of which inhibit Smo (*24*, *25*), and GANT61, which targets Gli transcription factors (*26*). The inhibitors reduced levels of Gli1 and Ptch protein, both targets of the Hh signaling pathway, but did not affect levels of TCR-associated kinases Lck and extracellular signal–regulated kinase (ERK) or granzyme A and perforin, two CTL proteins required for target cell lysis (Fig. 3F and fig. S4A). TCR signaling was also unaffected by these inhibitors (Fig. 3G and fig. S4B). All three inhibitors diminished CTL-mediated killing in a dose-dependent manner (Fig. 3H and fig. S4C), without impairing conjugate formation with target cells or clustering of Lck at the cSMAC in response to TCR signaling (fig. S4, E and F). Centrosome docking at the cSMAC was also reduced in conjugates formed by CTLs treated with inhibitor (Fig. 3I).

Centrosome polarization has been correlated with actin remodelling at the immunological synapse (*1*, *3*). Carrier-treated CTLs reorganized actin into a distal ring at the immunological synapse and polarized the centrosome within 5 min of encountering the target (fig. S5A and movie S2). By contrast, in cyclopamine-treated CTLs, actin accumulated across the immunological synapse [at time (t) = 0], but failed to reorganize into the distal actin ring (fig. S5B). Centrosome polarization to the plasma membrane was also disrupted (movie S3): 92% of conjugates polarized the centrosome to the synapse in control

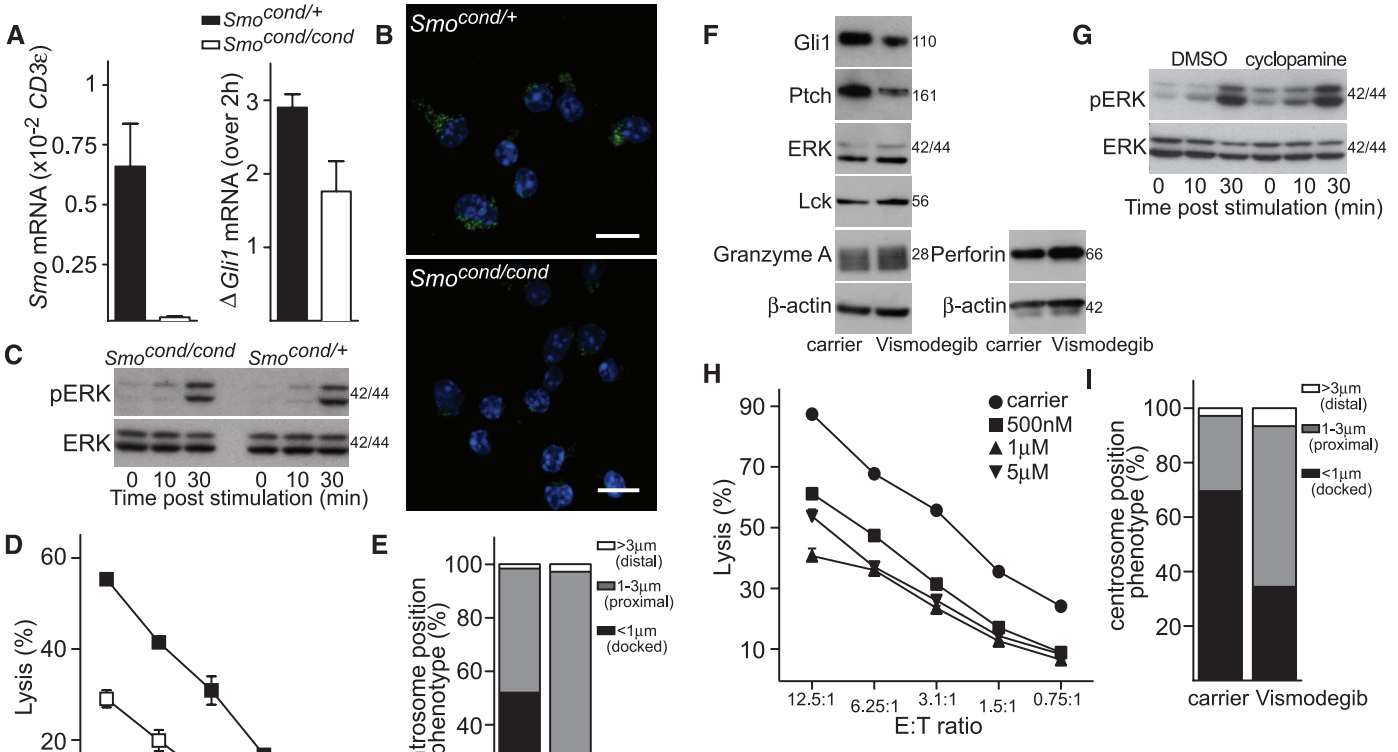

Fig. 3. Hh signaling is required for CTL killing and centrosome polarization to the immunological synapse. (**A**) qPCR analysis of *Smo* mRNA expression in *Mx1-Cre Smo*$^{cond/cond}$ and control *Mx1-Cre Smo*$^{cond/+}$ CTLs relative to *CD3*ε as a reference gene (left) (n = 4, data are means ± SD); or *Gli1* mRNA levels 2 hours after TCR activation with plate-bound antibody against CD3 for *Mx1-Cre Smo*$^{cond/+}$ and *Mx1-Cre Smo*$^{cond/cond}$ CTLs relative to unstimulated (right); n = 3, data are means ± SD. (**B**) Representative staining of endogenous Smo (green) expression in *Mx1-Cre Smo*$^{cond/+}$ and *Mx1-Cre Smo*$^{cond/cond}$ CTLs. Nuclei stained with Hoechst (blue); n > 100. Scale bars: 5 μm. (**C**) *Mx1-Cre Smo*$^{cond/+}$ and *Mx1-Cre Smo*$^{cond/cond}$ CTLs were stimulated with plate-bound CD3-specific antibody for times indicated and blotted for protein expression of phosphorylated ERK (pERK) and ERK; n = 2. Molecular masses are shown in kilodaltons. (**D**) Percentage lysis of P815 target cells by *Mx1-Cre Smo*$^{cond/+}$ and *Mx1-Cre Smo*$^{cond/cond}$ CTLs at effector:target (E:T) ratios shown (n = 6). (**E**) Centrosome position relative to clustered Lck was classified as <1 μm (docked), 1 to 3 μm (proximal) or >3 μm (distal) as percentage of conjugates of *Mx1-Cre Smo*$^{cond/+}$ (n = 129) and *Mx1-Cre Smo*$^{cond/cond}$ (n = 121) with P815 targets as depicted in fig. S4 (n = 3), data are means ± SD. (**F**) Immunoblots of cell lysates from OT-I CTLs treated with 5 μM vismodegib for 36 hours, probed with antibodies against Gli1, Ptch, ERK, Lck, granzyme A, perforin, and β-actin; n = 2. (**G**) OT-I CTLs treated with 10 μM cyclopamine for 24 hours, stimulated with plate-bound CD3-specific antibody for times indicated and blotted for protein expression of pERK and ERK; n = 2. Molecular masses are shown in kilodaltons. (**H**) Percentage lysis of EL4 target cells by OT-I CTLs treated with vismodegib at concentrations stated; n = 5. The x axis shows varying CTL effector:target (E:T) ratios. (**I**) OT-I CTLs treated with vismodegib (5 μM) were labeled with antibodies against Lck, γ-tubulin, and CD8. Quantification of centrosome polarization after treatment is shown (n > 60).

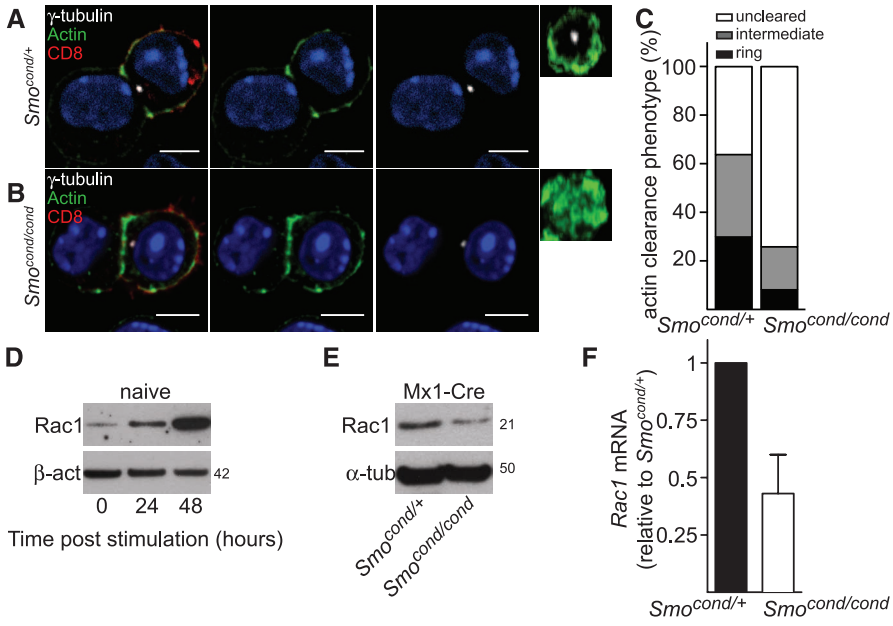

Fig. 4. Hh signaling in CTLs controls Rac1 expression and actin reorganization at the immunological synapse. (**A** to **C**) *Mx1-Cre Smo*$^{cond/+}$ (A) and *Mx1-Cre Smo*$^{cond/cond}$ CTLs (B) were conjugated to P815 target cells for 15 min, then fixed and stained by using antibodies against CD8, γ-tubulin, and actin. Single *x-y* confocal sections and en face (*y-z*) constructions through the synapse are shown, which demonstrate that the actin ring does not form properly in *Mx1-Cre Smo*$^{cond/cond}$ CTLs. Nuclei stained with Hoechst (blue). Scale bars: 5 μm. (**C**) Quantification of actin clearance at the immunological synapse, depicting the percentage of CTLs in which actin remains distributed throughout the synapse (not cleared), show an intermediate phenotype, or are cleared to form an actin ring (*Smo*$^{cond/+}$ $n = 47$; *Mx1-Cre Smo*$^{cond/cond}$ $n = 62$). Immunoblot analyses of protein expression of Rac1, actin, and calnexin (**D**) at 0, 24, and 48 hours after TCR stimulation in naïve CD8 T cells ($n = 3$) and (**E**) *Mx1-Cre Smo*$^{cond/+}$ and *Mx1-Cre Smo*$^{cond/cond}$ CTLs ($n = 2$). Molecular masses are shown in kilodaltons. (**F**) qPCR showing mRNA levels of *Rac1* in *Mx1-Cre Smo*$^{cond/cond}$ CTLs relative to *Mx1-Cre Smo*$^{cond/+}$ control CTLs $n = 3$, data are means ± SD.

carrier–treated CTLs compared with 59% of conjugates in cyclopamine-treated CTL. Actin clearance from the immunological synapse was also greatly reduced in CTLs from *Smo*-deleted mice (Fig. 4, A to C), and *Smo*-deleted CTLs showed a 60% reduction in actin clearance from the synapse compared with control CTLs. Thus, Hh signaling might also be required to promote actin reorganization at the immunological synapse.

Centrosome polarization in T cells is driven by a process of microtubule end-on capture-shrinkage, in which microtubules emanating from the centrosome are captured at the cortex and then undergo shrinkage (*27*). Both this process and actin remodeling are mediated by Rac1 (*28*–*30*). Furthermore, the Hh pathway has been implicated in Rac1-mediated actin remodelling in neurons and fibroblasts (*14*, *15*). Therefore, we examined Rac1 expression during induction of CTLs from naïve T cells. Rac1 protein levels increased after TCR stimulation of naïve T cells (Fig. 4D). By contrast, both protein and mRNA levels of Rac1 were diminished in *Smo*-deleted CTLs (Fig. 4, E and F), which suggested that Rac1 levels were regulated by Hh signaling via a transcriptional effect.

These findings support a model for the regulation of CTL-mediated killing by Hh signaling (fig. S5C). Naïve T cells are small, round cells lacking both the cytotoxic granules and the highly developed cytoskeleton required for target cell killing. Upon TCR activation, these cells develop over 4 to 5 days into mature CTLs prearmed with cytotoxic granules. We now show that TCR activation also triggers Hh signaling during this time, which increases levels of Rac1 and thereby promotes centrosome polarization, actin remodeling, granule release, and target cell killing. In this way, Hh signaling prearms CTLs with the ability to rapidly polarize the cytoskeleton and deliver the cytotoxic granules within minutes when CTLs encounter targets. Our results reveal molecular parallels between primary cilia and the immunological synapse, which highlight the possible origin of the immunological synapse as a modified cilium.

References and Notes

1. J. C. Stinchcombe, E. Majorovits, G. Bossi, S. Fuller, G. M. Griffiths, *Nature* **443**, 462–465 (2006).
2. C. R. Monks, B. A. Freiberg, H. Kupfer, N. Sciaky, A. Kupfer, *Nature* **395**, 82–86 (1998).
3. J. C. Stinchcombe, G. M. Griffiths, *Annu. Rev. Cell Dev. Biol.* **23**, 495–517 (2007).
4. D. N. Wheatley, *Pathobiology* **63**, 222–238 (1995).
5. G. M. Griffiths, A. Tsun, J. C. Stinchcombe, *J. Cell Biol.* **189**, 399–406 (2010).
6. F. Finetti *et al.*, *Nat. Cell Biol.* **11**, 1332–1339 (2009).
7. V. Singla, J. F. Reiter, *Science* **313**, 629–633 (2006).
8. S. C. Goetz, K. V. Anderson, *Nat. Rev. Genet.* **11**, 331–344 (2010).
9. K. C. Corbit *et al.*, *Nature* **437**, 1018–1021 (2005).
10. R. Rohatgi, L. Milenkovic, M. P. Scott, *Science* **317**, 372–376 (2007).
11. R. J. Salmond, A. Filby, I. Qureshi, S. Caserta, R. Zamoyska, *Immunol. Rev.* **228**, 9–22 (2009).
12. R. P. Valentini *et al.*, *J. Biol. Chem.* **272**, 8466–8473 (1997).
13. T. B. Kornberg, *Sci. Signal.* **4**, pe44 (2011).
14. N. Sasaki, J. Kurisu, M. Kengaku, *Mol. Cell. Neurosci.* **45**, 335–344 (2010).
15. A. H. Polizio *et al.*, *J. Biol. Chem.* **286**, 19589–19596 (2011).
16. Y. Wang, Z. Zhou, C. T. Walsh, A. P. McMahon, *Proc. Natl. Acad. Sci. U.S.A.* **106**, 2623–2628 (2009).
17. L. Milenkovic, M. P. Scott, R. Rohatgi, *J. Cell Biol.* **187**, 365–374 (2009).
18. A. El Andaloussi *et al.*, *Nat. Immunol.* **7**, 418–426 (2006).
19. S. V. Outram *et al.*, *Blood* **113**, 2217–2228 (2009).
20. A. Uhmann *et al.*, *Blood* **110**, 1814–1823 (2007).
21. T. Crompton, S. V. Outram, A. L. Hager-Theodorides, *Nat. Rev. Immunol.* **7**, 726–735 (2007).
22. I. Hofmann *et al.*, *Cell Stem Cell* **4**, 559–567 (2009).
23. J. Gao *et al.*, *Cell Stem Cell* **4**, 548–558 (2009).
24. J. K. Chen, J. Taipale, M. K. Cooper, P. A. Beachy, *Genes Dev.* **16**, 2743–2748 (2002).
25. J. A. Low, F. J. de Sauvage, *J. Clin. Oncol.* **28**, 5321–5326 (2010).
26. M. Lauth, A. Bergström, T. Shimokawa, R. Toftgård, *Proc. Natl. Acad. Sci. U.S.A.* **104**, 8455–8460 (2007).
27. J. Yi *et al.*, *J. Cell Biol.* **202**, 779–792 (2013).
28. T. Wittmann, G. M. Bokoch, C. M. Waterman-Storer, *J. Biol. Chem.* **279**, 6196–6203 (2004).
29. E. L. Filbert, M. Le Borgne, J. Lin, J. E. Heuser, A. S. Shaw, *J. Immunol.* **188**, 5421–5427 (2012).
30. Y. Nishimura, K. Applegate, M. W. Davidson, G. Danuser, C. M. Waterman, *PLOS ONE* **7**, e41413 (2012).

Acknowledgments: We thank R. Rohatgi for the MSCV-Ptch1-EYFP construct and the Smo antibodies; S. Munro (Cambridge) for PACT (pericentrin)-RFP; M. Davidson (University of Florida) for Farnesyl-5-TagBFP2; R. Zamoyska for Lck-depleted spleens; D. Fearon, T. Crompton, J. Kaufman, M. A. de la Roche, and A. Schuldt for helpful discussions and critical reading of the manuscript; and R. Rohatgi and J. Stinchcombe for helpful discussions. We also thank the flow cytometry core facility at the Cambridge Institute for Medical Research (CIMR) for cell sorting and assistance with the calcium assay. This work was supported by a Wellcome Trust Principal Research Fellowship to G.M.G. (075880), a Wellcome Trust Strategic Award for core facilities at the CIMR (100140), NIH (R01AR05439 and R01GM095941), the Burroughs Wellcome Fund, the David and Lucile F. Packard Foundation, and the Sandler Family Supporting Foundation to J.R. The data presented in this paper are provided in the main paper and supplementary materials.

Supplementary Materials

www.sciencemag.org/content/342/6163/1247/suppl/DC1
Materials and Methods
Figs. S1 to S6
Movies S1 to S3
References (*31*–*38*)

14 August 2013; accepted 18 October 2013
10.1126/science.1244689

Intact But Less Accessible Phonetic Representations in Adults with Dyslexia

Bart Boets,[1,2]* Hans P. Op de Beeck,[3] Maaike Vandermosten,[2] Sophie K. Scott,[4] Céline R. Gillebert,[5] Dante Mantini,[5,6] Jessica Bulthé,[3] Stefan Sunaert,[7] Jan Wouters,[8] Pol Ghesquière[2]

Dyslexia is a severe and persistent reading and spelling disorder caused by impairment in the ability to manipulate speech sounds. We combined functional magnetic resonance brain imaging with multivoxel pattern analysis and functional and structural connectivity analysis in an effort to disentangle whether dyslexics' phonological deficits are caused by poor quality of the phonetic representations or by difficulties in accessing intact phonetic representations. We found that phonetic representations are hosted bilaterally in primary and secondary auditory cortices and that their neural quality (in terms of robustness and distinctness) is intact in adults with dyslexia. However, the functional and structural connectivity between the bilateral auditory cortices and the left inferior frontal gyrus (a region involved in higher-level phonological processing) is significantly hampered in dyslexics, suggesting deficient access to otherwise intact phonetic representations.

Speech perception involves the mapping of spectrally complex and rapidly changing acoustic signals onto discrete and abstract phonetic sound categories or phonemes (*1*). Developmental dyslexia is a hereditary neurological disorder characterized by severe and persistent reading and/or spelling impairments (*2*). Individuals with dyslexia perform poorly on tasks that require phonological awareness, verbal short-term memory, and lexical access. Performance on these phonological tasks predicts reading acquisition in both normal and dyslexic readers (*3*). One view is that success on these tasks reflects the quality of underlying phonological (phonetic) representations (*4*) and that these representations of speech sounds are distorted or less well specified in individuals with dyslexia (*5*). An alternative view holds that in people with dyslexia, representations are intact but access to the representations is problematic (*6*, *7*). Here, we combined functional magnetic resonance imaging (fMRI) with multivoxel pattern analysis (MVPA) (*8*–*10*) and functional and structural connectivity analysis to disentangle whether dyslexia is caused by poor quality of the phonetic representation or by difficulty in accessing an intact representation.

We collected whole-brain functional images in 23 adults with a diagnosis of dyslexia and 22 matched normal readers (table S1) (*11*–*13*) while they listened to different versions of four sublexical speech sounds (fig. S1) and performed an easy phoneme discrimination task. The selection of stimuli allowed us to investigate both vowel and stop-consonant discrimination, which rely on spectral and spectrotemporal acoustic feature processing, respectively. If dyslexia is related to a deficit in the quality of phonetic representations, then we expect that the neural representations would be less robust and distinct in individuals with dyslexia than in normal readers. Given dyslexics' particular problems processing temporal cues, such as those involved in consonant discrimination (*11*), we expected the most prominent group differences for neural patterns distinguishing between consonants.

We analyzed the pattern of multivoxel activity within six left-hemisphere and six right-hemisphere regions involved in speech processing and within one non–speech control region (primary visual cortex V1) (table S2) (*8*, *14*). For each of these regions, we correlated the activity pattern in response to each stimulus in one-half of the data with the activity pattern in response to each stimulus in the remaining data (fig. S2). Figure 1 displays averaged correlations as a function of the phonetic similarity of the pairs: phonetically identical, differing in consonant, differing in vowel, and differing in both consonant and vowel. Comparison of these correlations indicates to what extent various acoustic realizations of the same phoneme elicit a similar activation pattern while different phonemes elicit a distinct activation pattern. We found significant differences between the four phonetic comparisons in bilateral primary auditory cortex (PAC), superior temporal gyrus (STG), middle temporal gyrus (MTG), and supramarginal gyrus (SMG) (Ps < 0.0003), and unilaterally in right angular gyrus (AG) and right inferior frontal gyrus (IFG) (Ps < 0.03) [repeated-measures analyses of variance (ANOVAs) with group as between-subject factor and phonetic comparison as within-subject factor]. We found no differences between phonetic comparisons for left AG and left IFG and for area V1 (F < 1). Activity patterns were equally reliable in both groups, except for right SMG, where the neural representations of the dyslexic readers were significantly more distinct than those of the normal readers (group × comparison interaction: P = 0.024). Focusing on the most crucial comparison entailing temporal cues, we observed that speech sounds differing in consonant could be differentiated in left PAC, STG, MTG, and SMG (Ps < 0.02; for all other regions, Ps > 0.16). Activity patterns differentiating between consonants were equally reliable in both groups (all group × comparison interactions: P > 0.28), except for right STG, where differentiation between consonants was feasible for dyslexic (P = 0.037) but not for normal readers (P = 0.977). Across all regions and for both reading groups, left-hemisphere regions were significantly more sensitive than right-hemisphere regions to differences in consonants (P = 0.017) [consistent with the left-hemisphere bias for temporal cues as described in the literature (*10*, *15*)]. We found no lateralization for vowel decoding in either normal or dyslexic readers (F < 1).

To ensure that we did not overlook any brain region hosting superior representations in normal as compared to dyslexic readers, we performed a whole-brain searchlight MVPA (*16*). A spherical "searchlight" was moved across the entire brain, and for every local region we calculated how well the response patterns differentiated between speech sounds. This analysis confirmed that phonetic representations are primarily hosted bilaterally in primary and secondary auditory cortices and that both normal and dyslexic readers shared similar quality of these representations (fig. S4).

Thus, we have no indication of poorer quality of phonetic representations in dyslexic readers. The MVPA results show that phonetic representations of dyslexic readers were at least as robust and distinct as those of normal readers. It may be that dyslexic readers achieve normal neural representations through greater than normal effort. Indeed, on the phoneme discrimination task administered during scanning, dyslexic readers achieved normal accuracy (as such, we avoided the issue that findings pertaining to brain activity may be confounded by differences in accuracy), but at slower speed (table S1). Attention may modulate brain activity and alter brain activity profiles (*17*). To investigate phonetic representations under conditions that elicit less compensational processing, we recalculated the previous analyses using only the activity pattern in response to speech sounds that were less relevant for the task at hand (the third speech sound in a stimulus block of four). As these stimuli were processed less intentionally, they yielded less brain activity (table S3). Nonetheless, even under this more stringent condition, speech sounds could be differentiated in left and right PAC, STG, MTG, and SMG (Ps < 0.05). And again, although dyslexic readers overall presented less activation

[1]Child and Adolescent Psychiatry, KU Leuven, 3000 Leuven, Belgium. [2]Parenting and Special Education Research Unit, KU Leuven, 3000 Leuven, Belgium. [3]Laboratory of Biological Psychology, KU Leuven, 3000 Leuven, Belgium. [4]Institute of Cognitive Neuroscience, University College London, London WC1N 3AR, UK. [5]Department of Experimental Psychology, University of Oxford, Oxford OX1 3UD, UK. [6]Department of Health Sciences and Technology, ETH Zürich, 8092 Zürich, Switzerland. [7]Department of Radiology, KU Leuven, 3000 Leuven, Belgium. [8]ExpORL, Department of Neurosciences, KU Leuven, 3000 Leuven, Belgium.

*Corresponding author. E-mail: bart.boets@ppw.kuleuven.be

(table S3), the quality of the phonetic representations was equal in both groups (all group × comparison interactions: $P > 0.25$) (fig. S5).

Thus, we found no difference in the neural quality of phonetic representations between dyslexic and normal readers. Although we cannot rule out that dyslexics' neural representations may have been less well specified at a younger age or would follow a different temporal trajectory detectable through techniques such as electroencephalography (*18*), our results indicate that the phonetic representations can be intact in adult dyslexics despite persisting reading difficulties (*6*, *7*). Therefore, we sought to investigate the alternative hypothesis of impaired access to phonetic representations.

Several studies have shown that Broca's area, particularly the left IFG pars opercularis, is involved in sensory-motor integration and effortful phonological processing (*19*, *20*). Hence, this area, which itself does not host phonetic representations, must access the representations in primary and secondary auditory cortices to compute the required phonological manipulations. We investigated the efficiency of access or the quality of interregional brain communication by assessing intrinsic functional connectivity between each possible pairing of the 13 anatomical regions shown in Fig. 1 (*21*). In each region we selected the most active cluster during task performance, and we calculated the correlations between the residualized signal intensity time series of each pair of these 13 predefined seed regions (Fig. 2) (*22*). Both groups showed equally strong connectivity among bilateral temporal areas (primary and secondary auditory cortices) across both hemispheres. Bilateral temporal areas were functionally connected with left IFG, but this connection was smaller in the dyslexic group, in particular for left STG and right PAC (Ps < 0.005, corrected for multiple comparisons). Without multiple testing correction, the group difference in functional connectivity between left IFG and right STG (P = 0.067) and between left IFG and right MTG (near to superior temporal sulcus) (P = 0.051) also approached significance. Individual differences in the strength of functional connectivity between left STG and left IFG correlated with behavioral indices of word reading (r = 0.40), nonword reading (r = 0.48), spelling (r = 0.53), phonological awareness (r = 0.46), verbal short-term memory (r = 0.44), and lexical access (r = 0.46), as well as with reaction time on the phoneme discrimination task performed in the scanner (r = –0.51) (all Ps < 0.01).

At a neuroanatomical level, adequate communication between left IFG and left STG is effected by the left arcuate fasciculus, the major language tract that ensures an efficient signal transmission between Wernicke's and Broca's areas. We recently collected diffusion tensor imaging data in a subsample (N = 32) of our participants and delineated the left arcuate fasciculus and its three constituent segments (direct, anterior, and posterior) on the basis of whole-brain

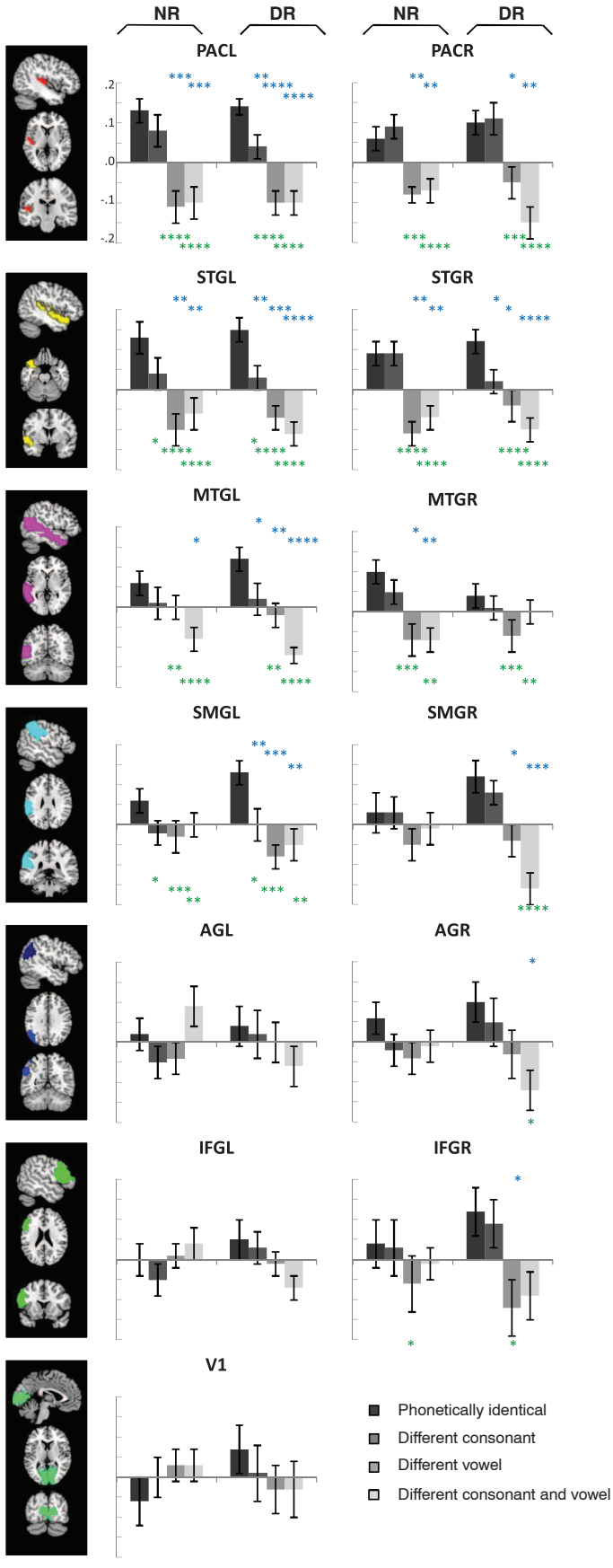

Fig. 1. Quality of phonetic representations as derived from multivoxel pattern analysis. Average correlations between the (normalized) activity patterns elicited by phonetically identical syllables, syllables differing in consonant, syllables differing in vowel, and syllables differing in both consonant and vowel for dyslexic (DR) and normal readers (NR) in each of the anatomical regions; error bars represent SE. The larger the overall quality of the phonetic representations, the larger the differences between the baseline correlation (between phonetically identical syllables) and the other correlations. Correlations differing from this baseline correlation are indicated with blue asterisks (paired *t* tests) and green asterisks (repeated-measures ANOVA, Tukey-corrected post hoc *t* tests) (*P < 0.05, **P < 0.01, ***P < 0.001, ****P < 0.0001). Images at left are representations of the left hemisphere anatomical regions.

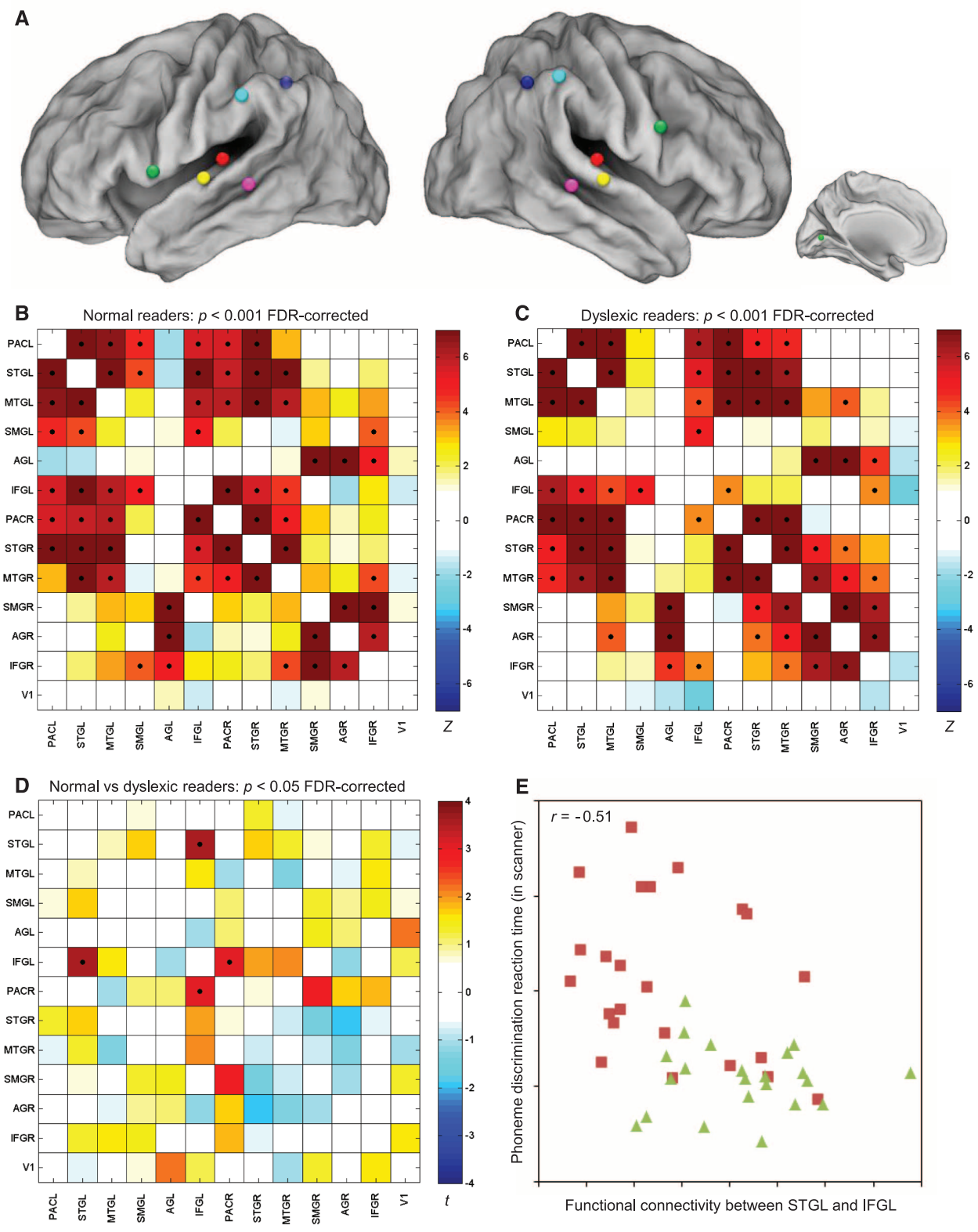

Fig. 2. Functional connectivity analysis. (**A**) Schematic representation of the predefined seed regions. The color coding corresponds with that used in Fig. 1. (**B** and **C**) Color-coded matrices represent functional connectivity (expressed as *Z* scores) among the 13 seed regions in normal and dyslexic readers. Significant correlations ($P < 0.001$, false discovery rate–corrected) are indicated by a black dot. (**D**) Statistical comparison of the functional connectivity between the groups. Significant group differences in functional connectivity are indicated by a black dot (independent *t* test, $P < 0.05$, false discovery rate–corrected). (**E**) Scatterplot of the association between reaction time on the phoneme discrimination task in the scanner (*y* axis) and intrinsic functional connectivity between left STG and left IFG (*x* axis). Dyslexic readers are depicted by red squares, normal readers by green triangles.

tractography (*12*). For the present report, we complemented these data and analyses to comprise the full sample ($N = 45$). Group comparisons (table S1) revealed significantly reduced white matter integrity of the left arcuate fasciculus in dyslexics ($P = 0.019$), in particular in the segment that directly connects posterior temporal and frontal areas ($P = 0.038$); this result provides neuroanatomical evidence that corroborates the deficiency in functional connectivity between left IFG and left STG. The functional and structural connectivity measures were not mutually related ($r = 0.06$, $P = 0.70$). This is in line with recent evidence highlighting the differences between the two types of connectivity measures (*21*, *23*) and suggests that both measures are complementary, each capturing a different aspect of the communication between left frontal and temporal language areas. Together, the functional and structural connectivity measures accounted for 35% of the variance in reading and spelling ability, and they predicted reading status (dyslexic versus normal reader) with an accuracy of 73%. This finding adds to the growing recognition of dyslexia as a disconnection syndrome (*24*, *25*).

Our results indicate that deficient phonetic representations are not the core problem in dyslexia. Does this imply that it is time to abandon the influential phonological deficit hypothesis? No, certainly not. The behavioral data of our dyslexic participants reveal that they do show severe deficits in the traditional phonological domains, including phonological awareness, verbal short-term memory, and lexical access (table S1) (*11*, *13*). Yet our neuroimaging findings suggest that it is not a deficit in underlying representations that characterizes dyslexia. Instead, our results suggest that a dysfunctional connection between frontal and temporal language areas impedes efficient access to otherwise intact representations of speech sounds, thus hampering a person's ability to manipulate them fluently.

References and Notes

1. E. F. Chang *et al.*, *Nat. Neurosci.* **13**, 1428–1432 (2010).
2. F. R. Vellutino, J. M. Fletcher, M. J. Snowling, D. M. Scanlon, *J. Child Psychol. Psychiatry* **45**, 2–40 (2004).
3. B. Boets *et al.*, *Br. J. Dev. Psychol.* **28**, 5–31 (2010).
4. R. K. Wagner, J. K. Torgesen, *Psychol. Bull.* **101**, 192–212 (1987).
5. U. Goswami, *Dyslexia* **6**, 133–151 (2000).
6. F. Ramus, G. Szenkovits, *Q. J. Exp. Psychol.* **61**, 129–141 (2008).
7. F. Ramus, M. Ahissar, *Cogn. Neuropsychol.* **29**, 104–122 (2012).
8. K. A. Norman, S. M. Polyn, G. J. Detre, J. V. Haxby, *Trends Cogn. Sci.* **10**, 424–430 (2006).
9. E. Formisano, F. De Martino, M. Bonte, R. Goebel, *Science* **322**, 970–973 (2008).
10. J. Obleser, A. M. Leaver, J. Vanmeter, J. P. Rauschecker, *Front. Psychol.* **1**, 232 (2010).
11. M. Vandermosten *et al.*, *Proc. Natl. Acad. Sci. U.S.A.* **107**, 10389–10394 (2010).
12. M. Vandermosten *et al.*, *Brain* **135**, 935–948 (2012).
13. B. De Smedt, B. Boets, *Neuropsychologia* **48**, 3973–3981 (2010).
14. H. P. Op de Beeck, K. Torfs, J. Wagemans, *J. Neurosci.* **28**, 10111–10123 (2008).
15. R. J. Zatorre, J. T. Gandour, *Philos. Trans. R. Soc. London Ser. B* **363**, 1087–1104 (2008).
16. N. Kriegeskorte, R. Goebel, P. Bandettini, *Proc. Natl. Acad. Sci. U.S.A.* **103**, 3863–3868 (2006).
17. J. F. Jehee, D. K. Brady, F. Tong, *J. Neurosci.* **31**, 8210–8219 (2011).
18. J. Hornickel, N. Kraus, *J. Neurosci.* **33**, 3500–3504 (2013).
19. S. Bookheimer, *Annu. Rev. Neurosci.* **25**, 151–188 (2002).
20. S. K. Scott, I. S. Johnsrude, *Trends Neurosci.* **26**, 100–107 (2003).
21. C. R. Gillebert, D. Mantini, *Neuroscientist* **19**, 509–522 (2013).
22. D. A. Fair *et al.*, *Neuroimage* **35**, 396–405 (2007).
23. J. M. Tyszka, D. P. Kennedy, R. Adolphs, L. K. Paul, *J. Neurosci.* **31**, 15154–15162 (2011).
24. M. Vandermosten, B. Boets, J. Wouters, P. Ghesquière, *Neurosci. Biobehav. Rev.* **36**, 1532–1552 (2012).
25. S. van der Mark *et al.*, *Neuroimage* **54**, 2426–2436 (2011).

Acknowledgments: Supported by KU Leuven (OT/07/034, IDO/10/003), Research Foundation Flanders (G0331.08, postdoctoral fellowship of B.B. and M.V.), European Research Council (grant ERC-2011-Stg-284101), Federal Research Action (IUAP/PAI P7/11), Queen Fabiola Foundation, Wellcome Trust [Sir Henry Wellcome fellowship of C.R.G. (098771/Z/12/Z), Sir Henry Dale fellowship of D.M. (101253/Z/13/Z), and grant WT090961MA of S.K.S.], and the Royal Society (D.M.: 101253/Z/13/Z). Matlab scripts are available in the supplementary materials. We thank R. Peeters and H. Poelmans for assistance. B.B., H.P.O.d.B., M.V., S.K.S., S.S., J.W., and P.G. designed the study; B.B. and M.V. collected the data; B.B. analyzed the data and wrote the manuscript; H.P.O.d.B. and J.B. contributed to MVPA analyses; M.V. and S.S. contributed to DTI analyses; C.R.G. and D.M. contributed to functional connectivity analyses; and all authors discussed the results and commented on the manuscript.

Supplementary Materials

www.sciencemag.org/content/342/6163/1251/suppl/DC1
Materials and Methods
Supplementary Text
Figs. S1 to S5
Tables S1 to S4
References (*26*–*30*)
Matlab Scripts

6 August 2013; accepted 21 October 2013
10.1126/science.1244333

MicroRNA-128 Governs Neuronal Excitability and Motor Behavior in Mice

Chan Lek Tan,[1]* Joshua L. Plotkin,[2] Morten T. Venø,[3] Melanie von Schimmelmann,[1,4] Philip Feinberg,[1,4] Silas Mann,[1,4] Annie Handler,[1] Jørgen Kjems,[3] D. James Surmeier,[2] Dónal O'Carroll,[5,6] Paul Greengard,[1] Anne Schaefer[1,4]†

The control of motor behavior in animals and humans requires constant adaptation of neuronal networks to signals of various types and strengths. We found that microRNA-128 (miR-128), which is expressed in adult neurons, regulates motor behavior by modulating neuronal signaling networks and excitability. miR-128 governs motor activity by suppressing the expression of various ion channels and signaling components of the extracellular signal–regulated kinase ERK2 network that regulate neuronal excitability. In mice, a reduction of miR-128 expression in postnatal neurons causes increased motor activity and fatal epilepsy. Overexpression of miR-128 attenuates neuronal responsiveness, suppresses motor activity, and alleviates motor abnormalities associated with Parkinson's–like disease and seizures in mice. These data suggest a therapeutic potential for miR-128 in the treatment of epilepsy and movement disorders.

MicroRNA-128 (miR-128) is one of the most abundant and highest enriched miRNAs in the adult mouse and human brain (fig. S1A) (*1*, *2*). The expression of miR-128 in the mouse brain increases gradually during postnatal development and peaks in adulthood (fig. S1B) (*3*, *4*). miR-128's expression in diverse brain regions (fig. S1C) suggests an important role for this miRNA in processes that are common to many neuronal cell types.

The indication of a potent regulatory role for miR-128 in brain function came from our observation of early-onset fatal epilepsy in mice deficient in miR-128 (Fig. 1A). miR-128 is encoded by two separate genes, *miR-128-1* and *miR-128-2*, on mouse chromosomes 1 and 9 (fig. S2, A and B) or human chromosomes 2 and 3, respectively. In mice, germline *miR-128-2* deficiency results in an 80% reduction of miR-128 expression in the forebrain, whereas ablation of the *miR-128-1* gene eliminates only 20% of miR-128 (fig. S2, A and

[1]Laboratory of Molecular and Cellular Neuroscience, The Rockefeller University, New York, NY 10065, USA. [2]Department of Physiology, Feinberg School of Medicine, Northwestern University, Chicago, IL 60611, USA. [3]Interdisciplinary Nanoscience Center (iNANO) and Department of Molecular Biology and Genetics, Faculty of Science, Aarhus University, DK-8000 Aarhus, Denmark. [4]Fishberg Department of Neuroscience, Department of Psychiatry, The Friedman Brain Institute, Icahn School of Medicine at Mount Sinai, New York, NY 10029, USA. [5]European Molecular Biology Laboratory, Mouse Biology Unit, Via Ramarini 32, Monterotondo Scalo 00015, Italy. [6]Laboratory of Immune Cell Epigenetics and Signaling, The Rockefeller University, New York, NY 10065, USA.

*Present address: Department of Physiology, University of California, San Francisco, CA 94143, USA.
†Corresponding author. E-mail: anne.schaefer@mssm.edu

B). The profound decline in miR-128 expression levels in *miR-128-2*$^{-/-}$ but not *miR-128-1*$^{-/-}$ mice is associated with the development of hyperactivity and increased exploration at 4 weeks of age (Fig. 1A and fig. S2, C and D). The juvenile hyperactivity in *miR-128-2*$^{-/-}$ mice progresses quickly to severe seizures and death at 2 to 3 months of age (Fig. 1, A and B, and movie S1). The lethal impact of miR-128 deficiency in mice can be prevented by treatment with the anticonvulsant drug valproic acid (Fig. 1C), thus demonstrating the causal role of seizures in the animals' death.

The hyperactivity and fatal epilepsy in *miR-128-2*–deficient mice reflects the ability of miR-128 to control the excitability of postnatal neurons. Selective inactivation of the *miR-128-2* gene in forebrain neurons (*Camk2a-cre; miR-128-2*$^{fl/fl}$) leads to a reduction of miR-128 expression, followed by early onset hyperactivity, seizures, and death, as observed in *miR-128-2*$^{-/-}$ mice (Fig. 1, B and D, and fig. S3A). Moreover, correction of miR-128 deficiency by ectopic *miR-128-2* expression in neurons normalizes motor activity and prevents the seizure-induced death (Fig. 1E and fig. S4, A and C).

To gain an understanding of the mechanism that mediates miR-128–dependent control of motor activity, and to avoid interference between phenotypes caused by the loss of miR-128 in diverse neuronal cell types, we restricted the *miR-128-2* deficiency to dopamine-responsive neurons that regulate motor behavior in mice and humans. There are two major dopamine-responsive Camk2a-expressing neuron types in the mouse forebrain, which have distinct contributions to motor activity (*5*). Although activation of the dopamine 1 receptor–expressing neurons (D1-neurons) increases locomotion, activation of dopamine 2 receptor–expressing neurons (D2-neurons) reduces locomotion in mice (*6*). We found that miR-128 deficiency in D1-neurons (*Drd1a-cre;miR-128-2*$^{fl/fl}$), but not in D2-neurons (*A2a-cre;miR-128-2*$^{fl/fl}$), leads to juvenile hyperactivity, followed by lethal seizures at ~5 months of age (Fig. 1F and fig. S3, B and C).

To identify miR-128 targets that are responsible for the abnormal motor activity, we analyzed mRNAs associated with the RNA-induced silencing complex (RISC) in adult neurons in vivo. The RISC-bound mRNAs represent the pool of cellular mRNAs that become a subject of miRNA-mediated suppression (*7*). We used mice that express the epitope-tagged RISC component Argonaute 2 (Ago2) (*8*) in Camk2a-neurons (fig. S5A). Immunoprecipitation of Ago2 [high-throughput sequencing of RNA isolated by crosslinking immunoprecipitation (HITS-CLIP) (*9*)] from the forebrain of these mice yielded the neuron-specific RISC-associated mRNAs (fig. S5, A and B). The perfect base pairing of at least six nucleotides between the miRNA seed sequence and the 3′ untranslated region (3′UTR) of the RISC-associated mRNAs (*10*) was considered to be the minimal requirement for any potential miRNA-mediated mRNA suppression (fig. S5, B and C). Using these criteria, we found that the miR-128 seed target sequence (ACUGUG) is the most represented hexamer among all RISC-associated mRNAs (fig. S5C and table S1) and identified a total of 1061 potential miR-128 target mRNAs in adult neurons (table S2).

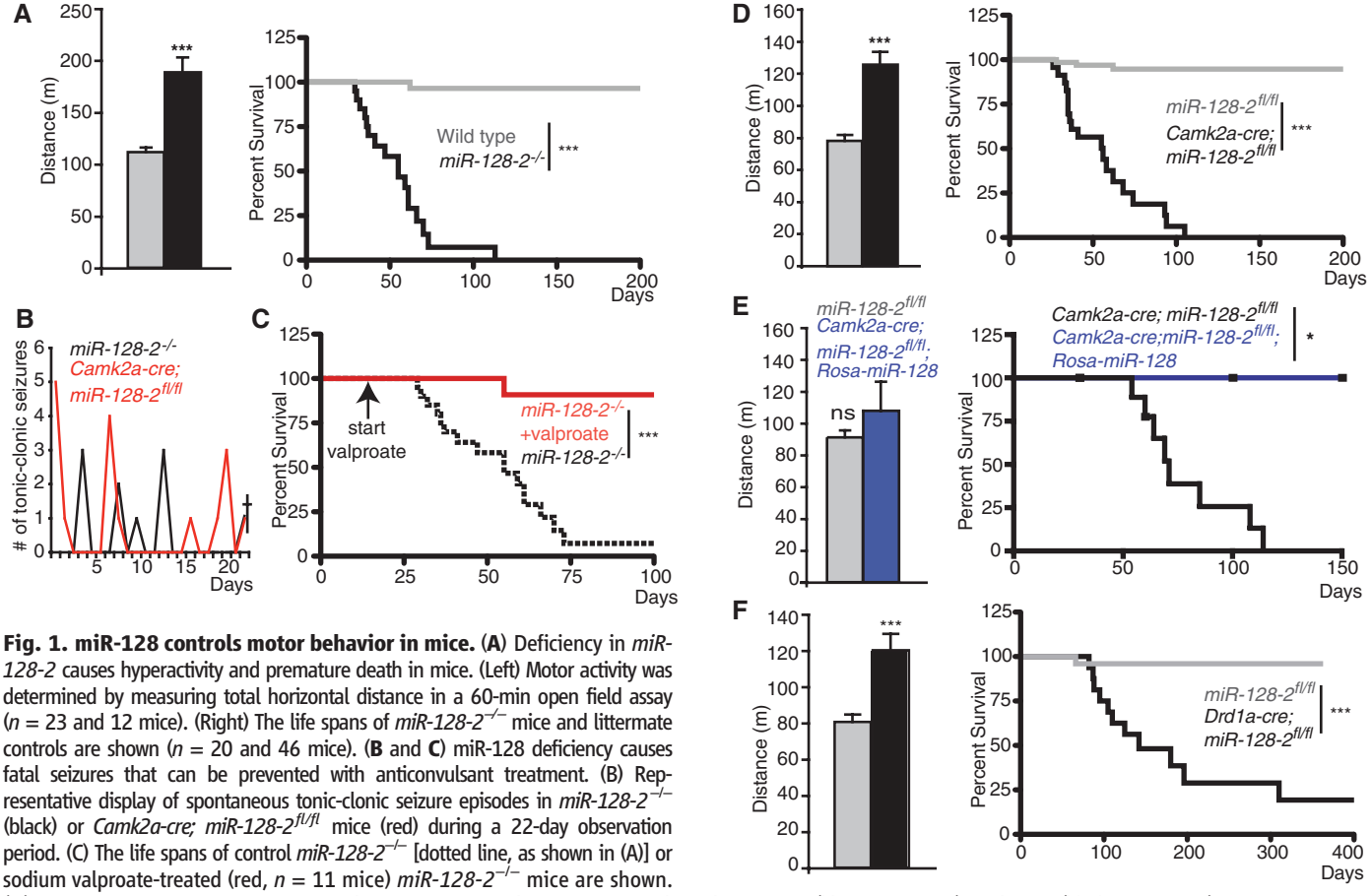

Fig. 1. miR-128 controls motor behavior in mice. (**A**) Deficiency in *miR-128-2* causes hyperactivity and premature death in mice. (Left) Motor activity was determined by measuring total horizontal distance in a 60-min open field assay (n = 23 and 12 mice). (Right) The life spans of *miR-128-2*$^{-/-}$ mice and littermate controls are shown (n = 20 and 46 mice). (**B** and **C**) miR-128 deficiency causes fatal seizures that can be prevented with anticonvulsant treatment. (B) Representative display of spontaneous tonic-clonic seizure episodes in *miR-128-2*$^{-/-}$ (black) or *Camk2a-cre; miR-128-2*$^{fl/fl}$ mice (red) during a 22-day observation period. (C) The life spans of control *miR-128-2*$^{-/-}$ [dotted line, as shown in (A)] or sodium valproate-treated (red, n = 11 mice) *miR-128-2*$^{-/-}$ mice are shown. (**D**) Deficiency in miR-128 in postnatal neurons causes hyperactivity and fatal epilepsy. Motor activity and survival rates of *Camk2a-cre; miR-128-2*$^{fl/fl}$ mice (n = 21 and 25 mice) and littermates (n = 8 and 47 mice) are shown. (**E**) Ectopic expression of miR-128 normalizes hyperlocomotion and prevents death of *Camk2a-cre; miR-128-2*$^{fl/fl}$ mice. Motor activity in *Camk2a-cre; miR-128-2*$^{fl/fl}$; *Rosa-miR-128* (blue, n = 4 mice) and control mice (gray, n = 10 mice) are shown. The life spans of *Camk2a-cre; miR-128-2*$^{fl/fl}$ mice in the presence (blue, n = 4 mice) or absence (black, n = 9 mice) of ectopic miR-128 expression are shown. (**F**) miR-128 deficiency in D1-neurons causes hyperactivity and fatal epilepsy. Motor activity (n = 26 and 42 mice) and life spans (n = 16 and 28 mice) of mice with a D1-neuron–specific miR-128 deficiency or control mice are shown. Error bars show SEM, Welch's t test, nonsignificant (ns), *$P \leq 0.05$, **$P \leq 0.01$, ***$P \leq 0.001$. Kaplan-Meier graph shows survival curves of mutant and littermate control mice; *$P \leq 0.05$, ***$P \leq 0.001$, log rank tests.

We investigated these miR-128 target genes by analyzing their expression in neurons deficient for miR-128. We expected that mRNA transcripts that are targeted directly by miR-128 in neurons would show an increase in mRNA expression and subsequent ribosome association in the miR-128–deficient cells. We reasoned that the relative homogeneity of the D1-neuron population might provide the most accurate assessment of miR-128–dependent target genes that are responsible for controlling motor activity. The impact of miR-128 deficiency on mRNA expression was evaluated by D1 cell-type–specific translating ribosome affinity purification (TRAP) in mice (*11*). The TRAP approach allows a direct comparison between ribosome-associated mRNAs from wild-type and miR-128–deficient D1-neurons in vivo (fig. S6A). Using Sylamer analysis (*12*), we confirmed the expected enrichment of potential miR-128 binding sites among the most up-regulated genes in miR-128–deficient D1-neurons (fig. S6B).

We found that the deficiency of miR-128 in D1-neurons results in a significant up-regulation of 154 of the predicted RISC-associated miR-128 target genes (Fig. 2A and table S3). The fact that only ~15% of the potential RISC-associated miR-128 targets display increased expression is likely to reflect the known redundancy among miRNAs. Many mRNAs are regulated by more than one miRNA (*13*, *14*), thus limiting the actual impact of individual miRNA deficiency on the expression of miRNA targets in vivo.

Bioinformatic network and pathway analyses of the miR-128 target genes indicate the ability of miR-128 to affect molecular processes that are intrinsically linked to the regulation of neuronal excitability and motor behavior in mice and humans (Fig. 2B). In particular, miR-128 regulates the expression of numerous ion channels and transporters, as well as genes that contribute to neurotransmitter-driven neuronal excitability and motor activity (Fig. 2B and tables S3 and S4). Several of these genes are linked to epilepsy in humans, some of which—including the neurotransmitter γ-aminobutyric acid transporter *Slc6a1*, the high-affinity glutamate receptor *Slc1a1*, the voltage-gated sodium channels *Scn2b* and *Scn4b*, the voltage-dependent calcium channels *Cacna2d3* and *Cagn2*, as well as the carbonic anhydrase *Car7*—are potential targets of clinically approved anti-seizure drugs (tables S3 and S4) (*15*). The high abundance of extracellular signal–regulated kinase (ERK1/2) signaling network components among the miR-128 targets underscores the potential of this miRNA to control signaling processes associated with neuronal excitability (Fig. 2B). Moreover, many of the neuronal signaling proteins and channels that we identified as direct miR-128 target genes are involved in the regulation of upstream signaling events, which can affect ERK activity (tables S3 and S4). Although ERK1 and ERK2 are not directly targeted by miR-128, the ERK network appears to be at

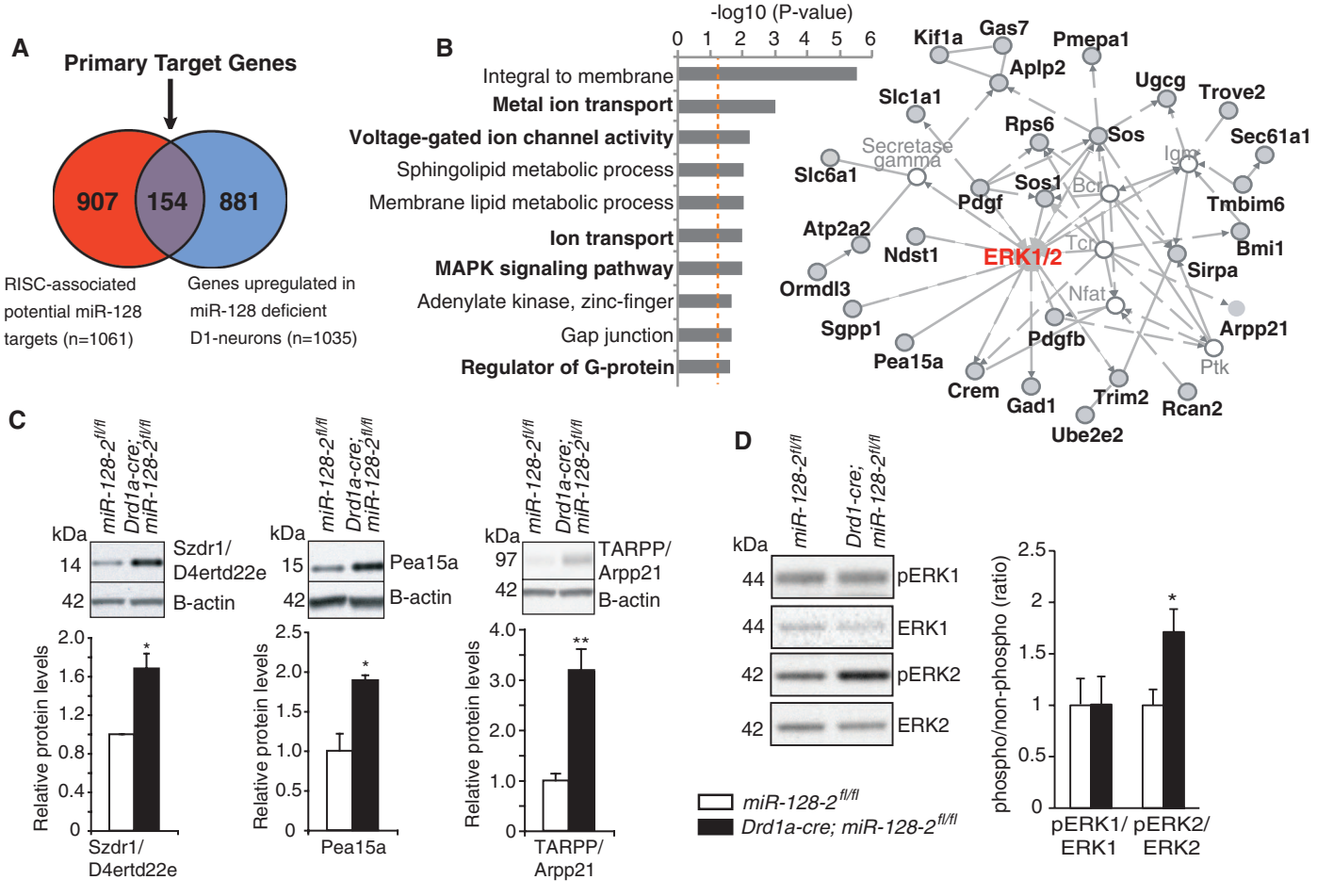

Fig. 2. miR-128 controls signaling protein expression and activation of the ERK signaling network in neurons. (**A**) Venn diagram shows the RISC-associated mRNA targets of miR-128 (red) and mRNAs that are up-regulated in miR-128–deficient D1-neurons (blue). The overlapping 154 mRNAs are considered as direct miR-128 targets. (**B**) (Left) Gene ontology annotations of the 154 miR-128 target genes are shown with pathway enrichment presented as –log10 (*P* value). The dotted orange line indicates $P = 0.05$. (Right) The components of the ERK1/2 network ($P = 10^{-46}$, right-tailed Fisher's exact test) that are directly targeted by miR-128 are indicated in solid gray. (**C**) Expression levels of miR-128–targeted ERK regulators in the striatum of *Drd1a-cre; miR-128-2$^{fl/fl}$* and littermate controls were analyzed by means of Western blotting ($n = 4$ mice each). (**D**) Increased ERK2 phosphorylation in the striatum of mice with D1-neuron–specific miR-128 deficiency. Representative Western blot analysis of ERK1/2 phosphorylation in the striatum of control and *Drd1a-cre; miR-128-2$^{fl/fl}$* mice is shown; bar graphs display phospho-ERK/ERK protein ratios ($n = 4$ mice). Error bars show SEM, Welch's *t* test, $^{*}P \leq 0.05$, $^{**}P \leq 0.01$.

the center of the miR-128–controlled signaling circuit in neurons. The protein expression levels of potent ERK network regulators, which are directly targeted by miR-128—such as Pea15a (*16*), D4Ertd22e/Szrd1 (*17*), and the TARPP protein that is encoded by the long splice variant of the *miR-128-2* host gene *Arpp21* (*18*, *19*)—are increased in the striatum of mice with a D1-neuron–specific deficiency in miR-128 (Fig. 2C and fig. S7). Furthermore, mice with a D1-neuron–specific deficiency of *miR-128-2* display an increase in ERK2 activation as compared with that of their littermate controls (Fig. 2D). Only ERK2, but not ERK1, displays increased phosphorylation (Fig. 2D). Deficiency of miR-128 in D1-neurons appears to specifically activate ERK2 phosphorylation, without affecting the activation of other MAP kinase pathways components, such as the stress-activated protein kinase/Jun-amino-terminal kinase (SAPK/JNK) or protein kinase B (AKT) (fig. S8).

Electrophysiological studies in striatal slices from *Drd1a-cre; miR-128-2*$^{fl/fl}$ mice revealed an increase in D1-neuron excitability. The miR-128–deficient D1-neurons show normal membrane excitability at the soma (fig. S9A) but display enhanced dendritic excitability (Fig. 3A) as well as a ~20% increase of functional dendritic spines (Fig. 3B and fig. S9B). These findings are consistent with a critical role of the ERK2 network in neuronal excitability and synaptic plasticity (*20*, *21*).

Enhanced ERK2 activation is linked to increased motor activity and seizures in mice (*22*–*24*). The hyperactivation of ERK2 and concomitant increase in D1-neuron sensitivity to dopamine occurs also during Parkinson's-like disease in mice caused by chemically induced depletion of dopamine in the mouse striatum (*25*–*27*). The reduced levels of dopamine and concurrent increase of D1-neuron sensitivity result in hyperresponsiveness to the motor activity–inducing effects of dopamine (*26*–*28*). In humans, the D1-neuron hyperresponsiveness is one of the major causes of dyskinesia, a side effect of L-DOPA treatment in Parkinson's disease (*25*–*27*).

We found that miR-128 deficiency in striatal D1-neurons mimics the hypersensitivity of D1-neurons in mice suffering from Parkinson's-like syndrome. The deficiency of miR-128 in D1-neurons enhances motor activity in response to Drd1-specific agonist treatment in mice (Fig. 3C). The D1-neuron hyperresponsiveness to the Drd1 agonist is also associated with an increase in ERK2 phosphorylation in the striatum of *Drd1a*-cre; *miR-128-2*$^{fl/fl}$ mice (Fig. 3D). The increase in dopamine sensitivity and enhanced ERK2 activation in mice with Parkinson's-like disease are accompanied by increased expression of dopamine-induced immediate early genes (IEGs) in D1-neurons (*25*–*27*). Similarly, Drd1 agonist treatment enhances IEG expression in miR-128–deficient D1-neurons as compared with the D1-neurons of control mice (Fig. 3E). The increased locomotor activity characteristic of *Drd1a*-cre; *miR128-2*$^{fl/fl}$ mice was normalized by means of pharmacological inhibition of the mitogen-activated protein kinase kinase MEK1, a major activator of ERK2 in neurons. In vivo–administered MEK1-specific inhibitor SL327 does not affect motor activity in wild-type mice (*22*) but does normalize ERK2 phosphorylation and motor activity in the mutant mice (Fig. 4A). In turn, overexpression of miR-128 in Camk2a-neurons is associated

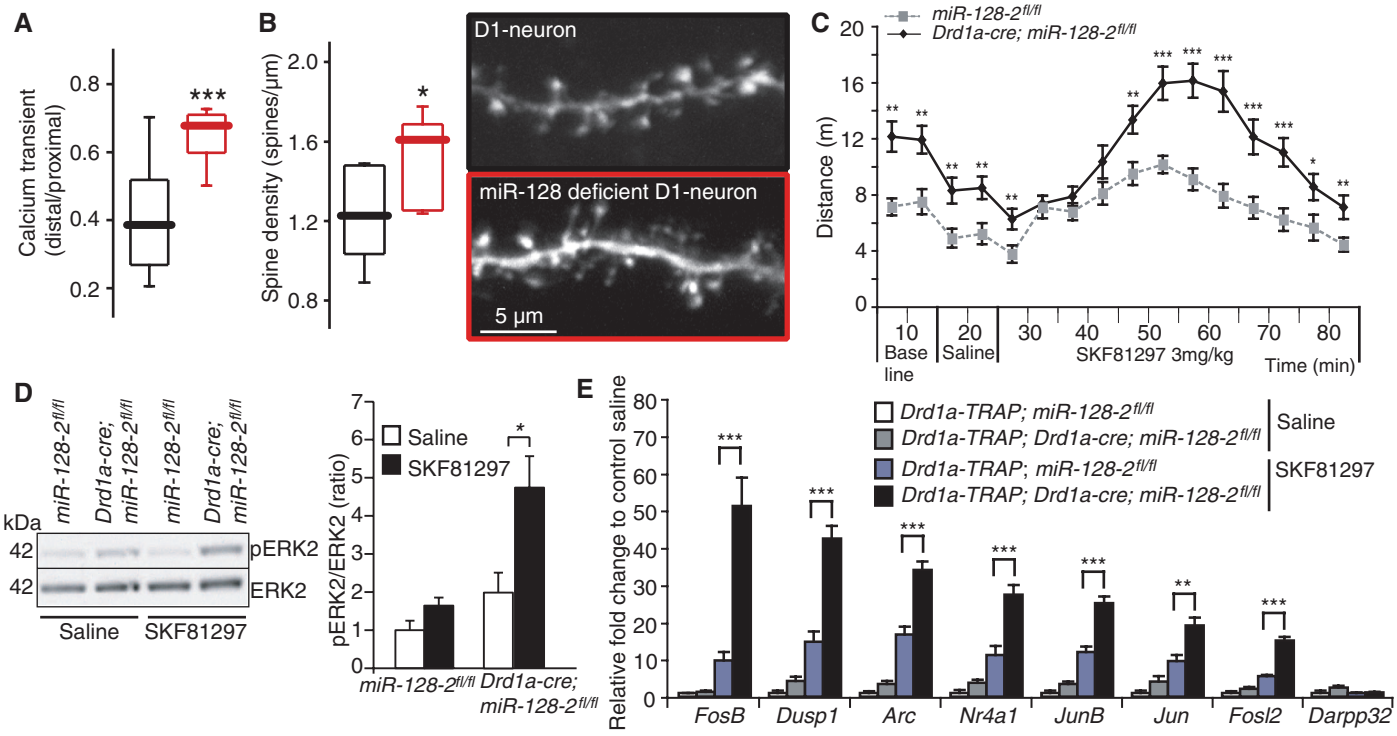

Fig. 3. miR-128 controls D1-neuron excitability and responsiveness to dopamine. (**A** and **B**) miR-128 regulates D1-neuron dendritic excitability and number of spines. (A) Single action potentials were generated in the soma, and action potential invasion was calculated by dividing the distal calcium signal by the maximum proximal calcium signal per cell (n = 4 cells, 11 to 21 shafts per group). Mann-Whitney nonparametric test, ***$P \leq 0.001$. (B) Representative maximum intensity projection images of distal dendrites in control and mutant D1-neurons are shown. Boxplots display population spine densities (n = 10 to 11 cells per group). Mann-Whitney nonparametric test, error bars show 90th percentile interval, *$P \leq 0.05$. (**C** to **E**) miR-128 regulates motor response, ERK2 phosphorylation, and immediate early gene (IEG) induction upon dopamine D1 receptor (Drd1) activation in D1-neurons. (C) Motor activity of *Drd1a-cre; miR-128-2*$^{fl/fl}$ and control mice (n = 25 and 30 mice) was evaluated in an open-field chamber. Saline and 3 mg/kg Drd1 agonist SKF81297 were injected intraperitoneally at 10 and 20 min, respectively. (D) ERK2 phosphorylation was quantified by means of Western blotting of striatal lysates derived from *Drd1a-cre; miR-128-2*$^{fl/fl}$ and control mice that received saline or D1-agonist SKF81297 injection (n = 5 mice each). Bar graph displays the ratio of phospho-ERK2 to total ERK2 expression. (E) IEG and D1-neuron–expressed *Darpp32* gene expression levels were measured by means of quantitative reverse transcription polymerase chain reaction of D1-neuron–specific polyribosome-associated mRNAs purified from saline or SKF81297-treated *Drd1a-TRAP; Drd1a-cre; miR-128-2*$^{fl/fl}$ and control mice (n = 5 mice each). Error bars display SEM, Welch's t test, *$P \leq 0.05$, **$P \leq 0.01$, ***$P \leq 0.001$.

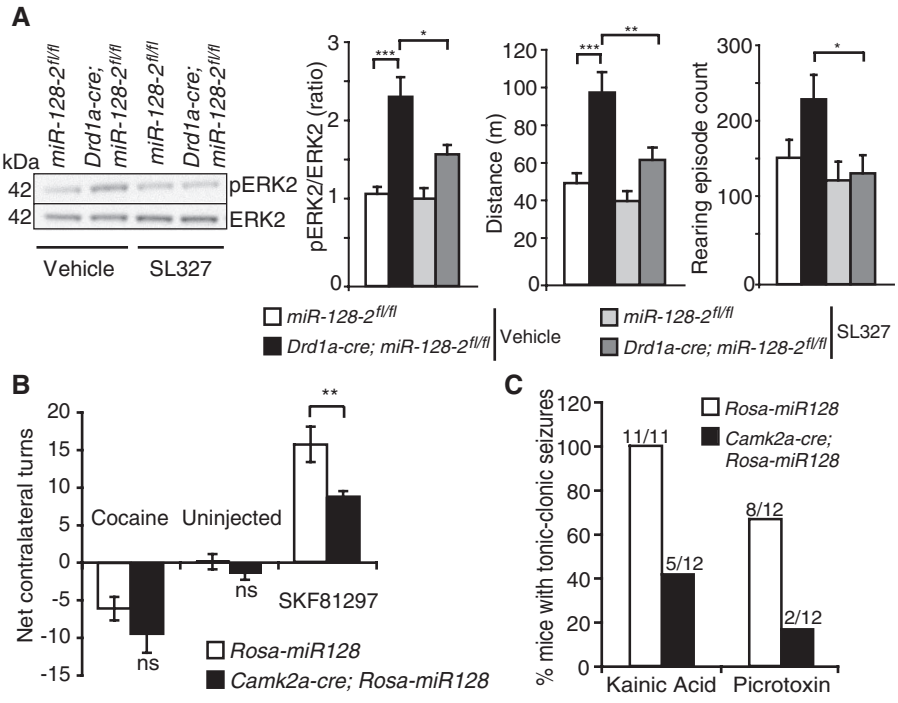

Fig. 4. Abnormal motor activity caused by miR-128 deficiency is corrected by pharmacological ERK inhibition or ectopic miR-128 expression. (**A**) *Drd1a-cre; miR-128-2$^{fl/fl}$* and littermate control mice were injected intraperitoneally with either vehicle or 12 mg/kg of the MEK1 inhibitor SL327 (n = 5 mice per group). Western blot analysis of ERK2 phosphorylation at 30 min after drug injection (left) and motor activity after vehicle or SL327 injection (right) are shown. Two-way analysis of variance followed by Bonferroni post-test. Error bars show SEM, $^{*}P \leq 0.05$, $^{**}P \leq 0.01$, $^{***}P \leq 0.001$. (**B**) Overexpression of miR-128 suppresses D1-neuron hyperresponsiveness in the dopamine-depleted striatum. The number of contralateral rotations at baseline and in response to cocaine (10 mg/kg) or D1-agonist SKF81297 (5 mg/kg) in unilateral 6-hydroxydopamine–lesioned *Camk2a-cre; Rosa-miR-128* or control mice (n = 11 mice per group) are shown. Error bars show SEM,Welch's t test, $^{**}P \leq 0.01$. (**C**) miR-128 reduces the susceptibility to chemically induced seizures in mice. The numbers of *Camk2a-cre; Rosa-miR-128* or littermate control mice (n = 12 mice per group) that exhibit tonic-clonic seizures 60 min after intraperitoneal injection of proconvulsive drugs kainic acid (30 mg/kg, P = 0.005) or picrotoxin (3 mg/kg, P = 0.04) are shown. P values were calculated by means of Fisher's exact test.

with reduced ERK2 activation (fig. S10A) and decreased motor activity (fig. S4B) in mice. The effect of increased miR-128 expression in adult neurons protects mice against abnormal motor activities associated with chemically induced Parkinson's disease (Fig. 4B and fig. S10B) and seizures (Fig. 4C).

We have identified miR-128 as a modulator of signaling pathways that control neuronal excitability and motor activity in mice. The human *miR-128-2* gene on chromosome 3p lies within a region that has been linked to idiopathic generalized epilepsy (*29*, *30*). It is tempting to speculate that changes in miR-128 or miR-128 target gene expression could be a potential cause of increased neuronal excitability and epilepsy in humans. Our understanding of miR-128's role in neuronal signaling could prove advantageous in the design of novel therapeutics for epilepsy and motor disorders.

References and Notes

1. M. He *et al.*, *Neuron* **73**, 35–48 (2012).
2. N. Y. Shao *et al.*, *BMC Genomics* **11**, 409 (2010).
3. E. A. Miska *et al.*, *Genome Biol.* **5**, R68 (2004).
4. A. M. Krichevsky, K. S. King, C. P. Donahue, K. Khrapko, K. S. Kosik, *RNA* **9**, 1274–1281 (2003).
5. C. R. Gerfen, *Annu. Rev. Neurosci.* **15**, 285–320 (1992).
6. A. V. Kravitz *et al.*, *Nature* **466**, 622–626 (2010).
7. M. R. Fabian, N. Sonenberg, W. Filipowicz, *Annu. Rev. Biochem.* **79**, 351–379 (2010).
8. A. Schaefer *et al.*, *J. Exp. Med.* **207**, 1843–1851 (2010).
9. S. W. Chi, J. B. Zang, A. Mele, R. B. Darnell, *Nature* **460**, 479–486 (2009).
10. D. P. Bartel, *Cell* **136**, 215–233 (2009).
11. M. Heiman *et al.*, *Cell* **135**, 738–748 (2008).
12. S. van Dongen, C. Abreu-Goodger, A. J. Enright, *Nat. Methods* **5**, 1023–1025 (2008).
13. A. Grimson *et al.*, *Mol. Cell* **27**, 91–105 (2007).
14. J. G. Doench, P. A. Sharp, *Genes Dev.* **18**, 504–511 (2004).
15. M. J. Brodie, *Seizure* **19**, 650–655 (2010).
16. J. W. Ramos *et al.*, *Mol. Biol. Cell* **11**, 2863–2872 (2000).
17. A. Matsuda *et al.*, *Oncogene* **22**, 3307–3318 (2003).
18. S. V. Rakhilin *et al.*, *Science* **306**, 698–701 (2004).
19. M. Megraw *et al.*, *Theor. Chem. Acc.* **125**, 593–598 (2010).
20. J. D. Sweatt, *Curr. Opin. Neurobiol.* **14**, 311–317 (2004).
21. G. M. Thomas, R. L. Huganir, *Nat. Rev. Neurosci.* **5**, 173–183 (2004).
22. E. Valjent, J. C. Corvol, J. M. Trzaskos, J. A. Girault, D. Hervé, *BMC Neurosci.* **7**, 20 (2006).
23. A. S. Nateri *et al.*, *EMBO J.* **26**, 4891–4901 (2007).
24. C. Mazzucchelli *et al.*, *Neuron* **34**, 807–820 (2002).
25. C. R. Gerfen, S. Miyachi, R. Paletzki, P. Brown, *J. Neurosci.* **22**, 5042–5054 (2002).
26. M. Feyder, A. Bonito-Oliva, G. Fisone, *Front. Behav. Neurosci.* **5**, 71 (2011).
27. M. A. Cenci, C. Konradi, *Prog. Brain Res.* **183**, 209–233 (2010).
28. D. S. Kim, M. S. Szczypka, R. D. Palmiter, *J. Neurosci.* **20**, 4405–4413 (2000).
29. M. A. Blair, B. Abou-Khalil, A. Crunk, J. L. Haines, P. Hedera, *Epilepsia* **52**, 993–999 (2011).
30. B. A. Chioza *et al.*, *Epilepsy Res.* **87**, 247–255 (2009).

Acknowledgments: We thank K. Rajewsky, G. Schuetz, and N. Heintz for mice and reagents. We thank C. Bargman and A. Tarakhovsky for valuable comments and P. Zamore for advice and critical reading of the manuscript. This work was supported by the NIH 1DP2MH100012-01 and DA025962 (A.S.), P50MH090963 (P.G., A.S., and D.J.S.), DA10044 (P.G.), NS34696 (D.J.S.), the Seaver Autism Foundation (A.S.), the USAMRAA W81XWH-090100402 and JPB Foundation (P.G.), the Lundbeck Foundation and Center for Integrative Sequencing at Aarhus University (M.T.V. and J.K), and the CHDI Foundation (D.J.S.). The authors declare no competing financial interests. The microarray data reported in this paper are archived at the Gene Expression Omnibus (GEO) Repository (www.ncbi.nlm.nih.gov/geo, accession no. GSE48813). Correspondence and requests for materials should be addressed to A.S. via anne.schaefer@mssm.edu. Mount Sinai and The Rockefeller University filed a United State provisional patent application (61/896,463 and 61/898,952) that covers the treatment of epilepsy using miR-128.

Supplementary Materials

www.sciencemag.org/content/342/6163/1254/suppl/DC1
Materials and Methods
Figs. S1 to S10
Tables S1 to S4
References (*31*–*39*)
Movie S1

5 August 2013; accepted 25 October 2013
10.1126/science.1244193

abcam®
discover more

What can RabMAb® do for you?

Our Rabbit monoclonal antibody (RabMAb) range offers multiple advantages to bring you the highest quality antibody possible.

Learn more at abcam.com/RabMAb

Better results — on any sequencing platform

Get the most from your NGS

Discover new and innovative solutions, dedicated for use with any NGS workflow

Streamline your next-generation sequencing (NGS) workflow and achieve high-quality results you can rely on.

- **Highly specific and selective nucleic acid purification and target enrichment**
- **Unbiased whole genome amplification from a single cell**
- **High DNA library yields using optimized workflows that allow ~50% time-savings**
- **Outstanding results on any sequencing platform**
- **Intuitive, knowledge-based data interpretation for deeper insight into NGS results**

Visit www.qiagen.com/goto/NGS to learn more!

QIAGEN®

Sample & Assay Technologies

NEW ENGLAND BioLabs® Inc.
enabling technologies in the life sciences

Make ends meet.

Gibson Assembly® Cloning Kit

New England Biolabs has revolutionized your laboratory's standard cloning methodology. The Gibson Assembly Cloning Kit combines the power of the Gibson Assembly Master Mix with NEB 5-alpha Competent *E. coli*, enabling fragment assembly and transformation in just under two hours. Save time, without sacrificing efficiency.

Making ends meet is now quicker and easier than ever before, with the Gibson Assembly Cloning Kit from NEB.

NEBuilder™ for Gibson Assembly

Visit **NEBGibson.com** to view the latest tutorials and to try our primer design tool.

Gibson Assembly Cloning Kit provides robust transformation efficiencies

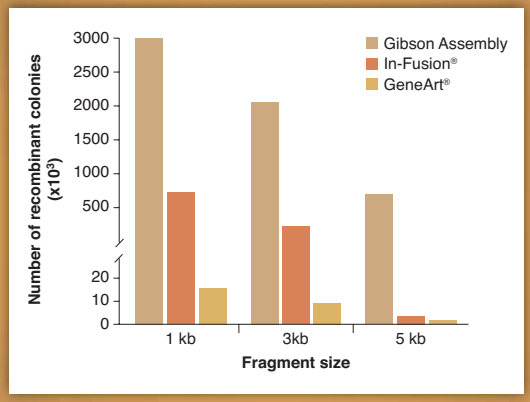

Assembly reactions containing 25 ng of linear pUC19 vector and 0.04 pmol of each fragment were performed following individual suppliers' recommended protocols and using the competent cells provided with the kit. The total number of recombinant colonies was calculated per 25 ng of linear pUC19 vector added to the assembly reaction.

SGI DNA

Reliable. Trusted. Proven.

Matt, Director of Products, has been at CST for over 11 years and is one of the original Phospho-Akt product scientists.

The reliability of CST™ Phospho-Akt antibodies is proven by peer-reviewed publications, and supported by 13 years of Akt expertise.

Learn more about Akt signaling with our updated PI3 Kinase/Akt Signaling Pathway Poster and Akt Substrates Guide. To request your copy of each, please visit our website.

www.cellsignal.com/aktguide

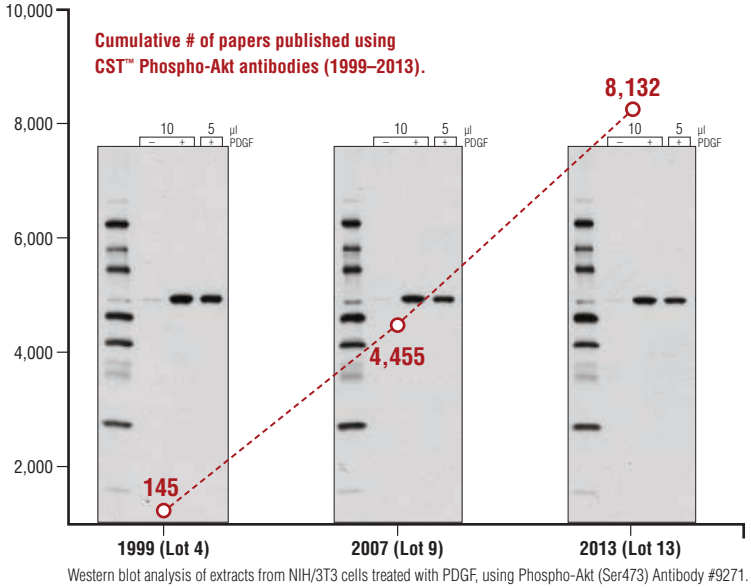

Western blot analysis of extracts from NIH/3T3 cells treated with PDGF, using Phospho-Akt (Ser473) Antibody #9271.

Cell Signaling TECHNOLOGY®

BD Accuri™ C6 Systems

Perfectly suited to support demanding educational environments.

BD

Helping all people live healthy lives

Learn. Teach. Master.

The BD Accuri C6 is a perfect fit for personal research, student mastery, and core lab use. It's easy to learn and operate, powerful enough for the majority of routine flow applications, and small enough for easy transport, making it perfect for the demands of the educational environment. Affordably priced, it may just be one of the best valued instrument in your lab.

The 4-color BD Accuri C6 allows for teaching and learning in a guided way, through templates, and factory pre-sets. The system also collects and stores 7.2 decades of data to empower novice users to make corrections if errors are made.

Those new to flow cytometry will appreciate the simplicity of the BD Accuri C6, while experts will appreciate the extensive capabilities and workflow advantages. Core lab managers will be able to better allocate resources, offloading routine applications and reserving higher-end systems for more complex, multi-parameter duties. Researchers will find it empowering for personal research and affordable.

Find out how your teaching institution and lab could benefit from owning BD Accuri C6 systems by visiting **bdbiosciences.com/go/learn.**

BD Biosciences
2350 Qume Drive
San Jose, CA 95131
bdbiosciences.com

American Association for Cancer Research

SCIENTIFIC CONFERENCES 2014:

Presenting the most significant research on cancer etiology, prevention, diagnosis, and treatment

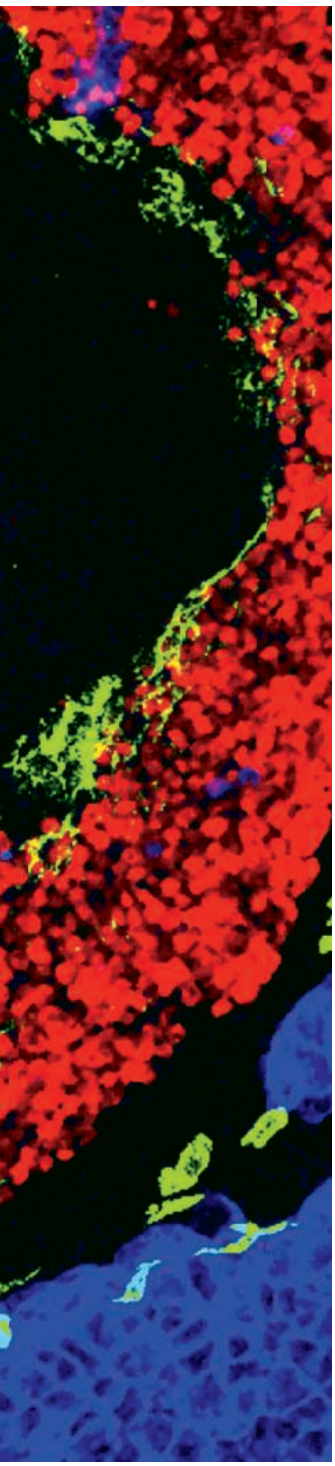

AACR-IASLC Joint Conference on Molecular Origins of Lung Cancer
Co-Chairpersons: Roy Herbst, Elisabeth Brambilla, Pasi Jänne, and William Pao
January 6-9, 2014
San Diego, CA

AACR-Prostate Cancer Foundation Conference on Advances in Prostate Cancer Research
Co-Chairpersons: Arul M. Chinnaiyan, William G. Nelson, June M. Chan, and Jonathan W. Simons
January 18-21, 2014 • San Diego, CA
Advance registration deadline:
Monday, December 9

Cancer Susceptibility and Cancer Susceptibility Syndromes
Co-Chairpersons: Alan D. D'Andrea, Phillip A. Dennis, and Pier Paolo Pandolfi
January 29-February 1, 2014 • San Diego, CA
Advance registration deadline:
Monday, December 9

RAS Oncogenes: From Biology to Therapy
Co-Chairpersons: Frank McCormick, Dafna Bar-Sagi, and Channing J. Der
February 24-27, 2014 • Lake Buena Vista, FL
Abstract submission and award application deadline:
Friday, December 6
Advance registration deadline:
Monday, January 13

Cellular Heterogeneity in the Tumor Microenvironment
Co-Chairpersons: Mary Helen Barcellos-Hoff, Michele De Palma, and M. Celeste Simon
February 26-March 1, 2014 • San Diego, CA
Abstract submission and award application deadline: **Monday, December 16**
Advance registration deadline:
Monday, January 13

AACR Annual Meeting 2014
Chairperson: Scott W. Lowe
April 5-9, 2014
San Diego, CA

Pancreatic Cancer
Co-Chairpersons: Dafna Bar-Sagi, David A. Tuveson, Christine Iacobuzio-Donahue, Alec Kimmelman, and Andrew M. Lowy
May 18-21, 2014
New Orleans, LA

Targeting PI3K/mTOR Networks in Cancer
Co-Chairpersons: Lewis C. Cantley, Jose Baselga, Joan S. Brugge, Brendan J. Manning, and Malte Peters
September 14-17, 2014
Philadelphia, PA

Melanoma
Co-Chairpersons: Levi A. Garraway, Keith T. Flaherty, and Suzanne L. Topalian
September 20–23, 2014
Philadelphia, PA

13th Annual International Conference on Frontiers in Cancer Prevention Research
Program Committee Chairperson: Phillip A. Dennis
September 28-October 1, 2014
New Orleans, LA

Tumor Immunology
Co-Chairpersons: Robert H. Vonderheide, Nina Bhardwaj, Stanley Riddell, and Cynthia L. Sears
December 1-4, 2014
Orlando, FL

Call for 2013 Cozzarelli Prize Nominations

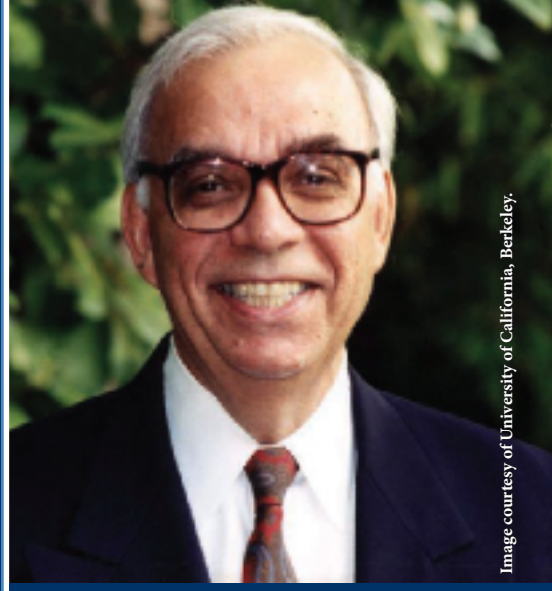

Nicholas R. Cozzarelli, former PNAS Editor-in-Chief

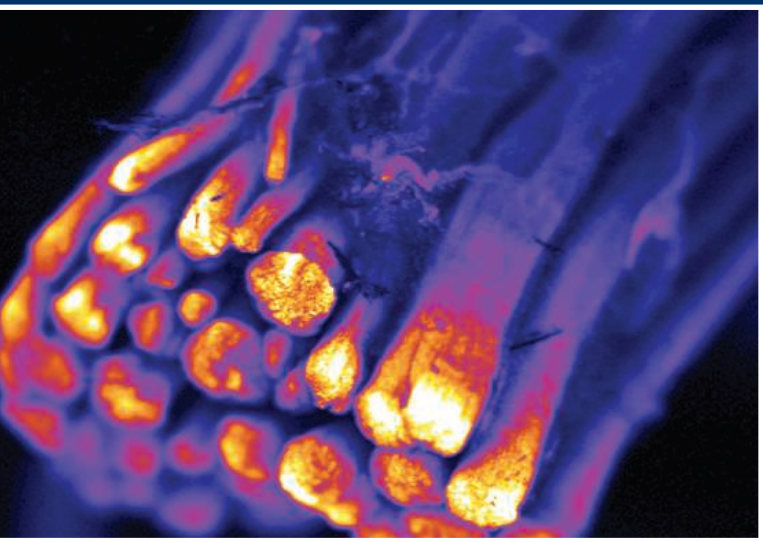

The PNAS Editorial Board is now accepting nominations through January 10, 2014 for the 2013 Cozzarelli Prize. This award recognizes scientific excellence and will be given to six papers published in PNAS during 2013.

Nominations should be sent to pnas@nas.edu and should include a citation and brief explanation of the merits of the work. The award recipients will be recognized during the PNAS Editorial Board Meeting and the NAS Annual Meeting Awards Ceremony on April 27, 2014 in Washington, DC.

PNAS
www.pnas.org

For more information and a list of previous winners visit www.pnas.org/cozzarelliprize.

Gordon Research Conferences

frontiers of science

Gordon Research Conferences (Hong Kong) Limited

戈登研究會議(香港)有限公司

A registered charitable organization in Hong Kong

The GRC expansion in Hong Kong aims to improve scientific collaborations around the world, increase networking opportunities and facilitate advancements in new scientific fields.

The following meetings are scheduled to take place in Hong Kong in 2014:

***NEW!* Advanced Materials for Sustainable Infrastructure Development**
Advanced Materials for Sustainable Energy Efficient Buildings
August 3-8, 2014
The Hong Kong University of Science and Technology
Chair: Zongjin Li

***NEW!* Complex Adaptive Matter**
Towards a Unifying Perspective of Emergent Complexity
July 13-18, 2014
The Chinese University of Hong Kong
Chair: Robert H. Austin

***NEW!* Genomic Instability**
Mechanisms that Cause DNA Damage and Related Diseases
July 6-11, 2014
The Hong Kong University of Science and Technology
Chairs: Bik K. Tye & Marco Foiani

Green Chemistry
Industrial Successes and Challenges
July 27 - August 1, 2014
The Chinese University of Hong Kong
Chairs: Kenneth Seddon & Mark A. Harmer

Green Chemistry (GRS) *
Applications for a Sustainable Future
July 26-27, 2014
The Chinese University of Hong Kong
Chair: Magdalena B. Foreiter

***NEW!* Hybrid Electronic & Photonic Materials and Phenomena**
June 22-27, 2014
The Hong Kong University of Science and Technology
Chairs: Michael Graetzel & Ben Zhong Tang

Molecular & Cellular Neurobiology
Mechanisms of Neural Development, Circuit Assembly, Synaptic Plasticity and Neuropsychiatric Disorders
June 29 - July 4, 2014
The Hong Kong University of Science and Technology
Chair: Eric J. Huang

Molecular & Cellular Neurobiology (GRS) *
Exploring the Frontiers of Foundational and Translational Neuroscience
June 28-29, 2014
The Hong Kong University of Science and Technology
Chair: Sarah X. Luo

***NEW!* Structural Nanomaterials**
Recent Advances in Understanding the Structures and Properties of Nanomaterials
July 20-25, 2014
The Chinese University of Hong Kong
Chairs: Chain T. Liu & T.G. Nieh

** Gordon Research Seminars (GRS) are 2-day meetings for graduate students and post-docs that precede an associated GRC.*

GRC provides an atmosphere and format that fosters informal discussion and networking among scientists. Our high quality, cost-effective meetings are widely recognized as the world's premier scientific conferences. Visit us at ***www.grc.org****.*

Living Large:
Scaling Up Cell Culture

Whether for structural biology, regenerative medicine, or translational research, basic scientists often find themselves needing larger quantities of cellular products than typical lab-scale techniques can produce. New technologies such as disposable bioreactors and multilayered culture flasks can help address some of the challenges of scaling up. **By Alan Dove**

"You can try different types of shaker flasks, different types of spinner flasks that can handle enough volume for initial work, and if you need a little bit more volume you can go into small bioreactors."

Bioreactor

CREDIT: (FROM TOP) IMAGE COURTESY THERMO FISHER SCIENTIFIC; ISTOPHOTO.COM/BASTAR

Traditional laboratory biology is a small-scale operation; tissue culture dishes are seldom much larger than the experimenter's hand, volume measurements are in milliliters, and a protein purification that yields a few micrograms is a success. With burgeoning interest in translational research, structural biology, and regenerative medicine, many scientists are starting to think bigger. Whether trying to purify grams of protein for crystallography or testing the feasibility of turning a novel gene product into a new drug, these researchers soon find themselves pondering the complications of larger-scale cell culture.

Thanks to the success of the biotechnology industry, cell culture scale up has become a well-paved path. "The field has exploded, because a lot of products are being made, drugs are being made in mammalian cells in large quantities in very big bioreactors," says Joseph Shiloach, head of the Biotechnology Core Lab at the **National Institute of Diabetes and Digestive and Kidney Diseases** in Bethesda, Maryland. He adds that depending on the cell type, the necessary equipment and reagents are often available off the shelf.

CHECK THE SUSPENSION

For many scientists, the most obvious choice for growing larger batches of cells is a technique they already understand: suspension culture. Numerous cell lines are already adapted to grow in small spinner bottles, so initial scale up can be as simple as buying a larger spinner. Suspension cultures also give researchers multiple options for expanding further.

Cultures in shaker flasks are particularly flexible, allowing researchers to step up through multiple sizes on a single platform—literally. "You can get a small size platform [shaker] that you can put right into your incubator, and … start with tubes that contain just a few milliliters of culture, all the way up to multiple liters of culture in large flasks," says Henry Chiou, senior product manager for cell biology at **Life Technologies** in Carlsbad, California.

Suspension cultures adapted to either shakers or spinner bottles are usually easy to expand to even larger sizes if necessary. "You can try different types of shaker flasks, different types of spinner flasks that can handle enough volume for initial work, and if you need a little bit more volume you can go into small bioreactors," says Shiloach.

The biopharmaceutical industry routinely uses suspension cell cultures in bioreactors to manufacture clinically approved products, so vendors produce such systems in sizes that range from benchtop models all the way up to industrial units. Many of these bioreactors now use disposable growth chambers to eliminate the difficulties of sterilization. "The whole bioreactor is disposable, so you can get it already equipped with everything you need, you just have to put in the media," says continued>

Upcoming Features

RNA Technologies—January 17
Proteomics—February 21
Toxicology—March 14

Whatever types of cell cultures researchers need to expand, the recent technological advances by equipment makers have smoothed the path considerably.

Shiloach. He adds that "the smaller fermenters you can handle in the beginning very similarly to a shaker flask, you can take it into the hood, you can inoculate it … and then you can put it in place and hook it to the system."

While the initial move from smaller to larger spinner or shaker cultures and even small bioreactors often seems simple, new problems can crop up as the scale increases. Larger bioreactors often need more complex support hardware and more careful and frequent testing to maintain pH and nutrient levels, so researchers may need additional training to use them. "Once you start scaling up and you need a certain yield, the yield is really quite dependent on the health of the cells," says Chiou, adding that "really monitoring your cultures very carefully becomes … more critical."

Several vendors offer slightly different spinners, suspension flasks, and bioreactors, often with novel twists to address specific problems. **Pall Life Sciences** in Port Washington, New York, for example, now sells a benchtop-size bioreactor that agitates a disposable plastic bag full of cells and media. The bag rests atop a special shaker table that rocks through two separate axes. The combination of low shear forces and a disposable growth chamber might help maintain consistency from one cell batch to the next. **GE Healthcare Life Sciences** in Piscataway, New Jersey takes a similar approach with its WAVE bioreactors, which also feature disposable bag-like growth chambers on rocking platforms, in sizes ranging from 100 mL to 500 L.

Given the variety of options, scientists should spend some time figuring out which is likely to work best for them. Shiloach suggests asking about the support equipment and testing each system requires, particularly for maintaining parameters such as dissolved oxygen and pH. If a system seems suitable, "I think the best thing is to get one and try it," Shiloach says.

RATHER SWITCH THAN FIGHT

Researchers whose chosen cells don't grow in suspension need to find another approach to scale up—or not. In many cases, the most sensible choice is to switch to suspension culture. "If you have a product that you want to test and you need a few milligrams just to find out if the biological activity is what you want, you can start doing it in adherent [cells], but if the product seems to be promising, I think it would be better to try and adapt the cells or maybe try another cell line … and then go into suspension," says Shiloach.

If the goal is a clinical therapy, switching cell lines could also help speed regulatory approval. Established suspension culture systems such as Chinese hamster ovary (CHO) and human embryonic kidney 293 (HEK-293) cells form the backbone of current biopharmaceutical production, so regulators are already comfortable with them.

Switching to a suspension-adapted line is an especially good strategy for scaling up protein production. "When we've gone out and talked to lots of folks, there [are] not that many instances where they need to actually be in a specific cell line for protein expression. The standard ones that are typically out there, 293s and CHOs, seem to fit the vast majority of needs," says Chiou.

To cater to those needs, several companies offer strains of 293 and CHO cells especially adapted for large-scale suspension growth and protein production. For example, Life Technologies' Expi293 system uses a special strain of 293 cells and a proprietary medium to achieve high levels of transient protein expression. The company claims Expi293 can produce three- to fivefold more protein per liter than conventional culture systems. Higher production means less need for larger-scale cultures. "In the past if somebody felt like they needed to scale up to a 5 L reaction in order to get enough protein, they can now stick with a 1 L or 2 L reaction," says Chiou, adding that "that really helps to lower the impact of scaling that they need to do."

Even increasing the required culture size a little bit can often entail major increases in cost and complexity, as scaling problems tend to be nonlinear. Moving from 1 L of culture to 2 L might only entail using a bigger shaker flask, but moving from 5 L to 6 L could mean buying a benchtop bioreactor and learning how to use it. "The inflection points tend to happen as you change the type of vessel you're using," says Chiou.

When standard protein expression lines such as CHO and 293 won't work—perhaps because of a need for specific glycosylation patterns that these cells can't perform—some researchers turn to microcarriers. These tiny plastic beads provide a surface for adherent cells to bind. Once seeded, the microcarriers and their attached cells can be suspended in shaker or spinner flasks. This decades-old technique provides many of the benefits of suspension culture for cells that can't adapt to it otherwise. Microcarriers are best suited for protein or virus production, as recovering viable cells from the beads can be tricky. Several equipment suppliers offer microcarriers, including GE and **Sigma-Aldrich** as well as **Labtech** of Uckfield, United Kingdom.

MORE IS MORE

For some cell types and projects, none of the existing suspension culture

systems will work. Stem cells are particularly reluctant to grow in suspension, and Vero cells, a common line for vaccine production, also need to attach firmly to plates. Fortunately, scientists trying to grow larger batches of such adamantly adherent cells can choose from several well-developed techniques.

The simplest strategy is to increase the available surface area in each culture flask, by using special flasks with multiple layers of plates inside. This parallel plate approach is somewhat more cumbersome than suspension cultures, but equipment manufacturers have worked hard to optimize it. "We were the first company that came up with this design decades ago with the Cell Factory, and we have a variety of choices in that particular product line," says Cindy Neeley, field applications specialist for cell culture at **Thermo Fisher** in Waltham, Massachusetts. Other companies also offer layered bioreactors for adherent cells, often optimized for specific uses. For example, the CELLine bioreactors from Sigma-Aldrich in St. Louis, Missouri are specifically designed for scaling up protein expression systems and monoclonal antibody production.

Moving cells from small single-layer culture flasks into parallel plate vessels brings its own set of challenges. Neeley points out that even though all of the plates in a multilayer flask are right next to each other, conditions can vary from one layer to another. "Anything more than 10 layers, you're going to encounter issues with distribution of nutrients as well as gas conditions between layers, and that is obviously a challenge for us," says Neeley. As a result, large parallel plate systems often come with special support equipment.

When shopping for such a system, researchers should also consider what surface their cells currently prefer. Cells adapted to adhere to one type of coated flask may grow poorly when moved to a multilayer flask with a different coating. For established cell lines, the solution is often as easy as buying a parallel plate system from the same vendor that provided the smaller flasks, to ensure the coatings are the same.

That won't work for researchers at the cutting edge of regenerative medicine, though. Stem cells are often too finicky to grow on any of the generic surfaces available off the shelf, instead requiring special coating reagents such as **BD Biosciences**' Matrigel. Coating a large parallel plate flask with such reagents would be cumbersome and costly. That puts parallel plate systems out of reach for stem cell work, at least for now. "We're not there yet, but companies in our position need to think in that direction, to come up with … vessels that would allow these stem cells to attach and grow," says Neeley.

For cells that can grow in parallel plate flasks, though, subsequent increases in scale—all the way up to industrial sizes—are relatively straightforward. Indeed, the largest version of Thermo's Cell Factory is already a common sight in vaccine production facilities, where the flasks are so huge that simply moving them around is one of the biggest challenges.

The difficulty of manipulating multiple large parallel plate flasks has led other equipment developers to create more compact systems. The xPansion multilayer bioreactor from **ATMI** in Brussels, Belgium uses thinner plates and puts them closer together than the Thermo Cell Factory. That allows the xPansion to pack 20 Cell Factories' worth of cells into a single container. Besides saving space, the more compact system reduces the number of flasks that have to be manipulated each time technicians need to change media or harvest cells.

Like other flask makers, ATMI is also trying to coat its plates with surfaces suitable for more exotic cell types. "Today we have only one coating, but we are actually working on specific coatings [for stem cells]," says Jose Castillo, director of cell culture technologies at ATMI.

GOING WITH THE FLOW

Researchers who are using adherent cells as expression systems for secreted proteins should also consider another strategy for scaling up: fixed-bed bioreactors. In this approach, cells adhere to small beads or fibers that are packed into a large container. Medium circulates through the matrix continuously, bringing fresh nutrients and oxygen into the bed and pulling cellular waste and secreted proteins out. It's difficult or impossible to recover the cells from the fixed bed once they've adhered, but for secreted protein production that isn't usually a problem.

Fixed-bed systems can fit a large number of adherent cells into a relatively small volume. The iCells 500, for example, holds 500 m^2 of adherent cell culture surface—roughly two tennis courts' worth—in a volume of only 25 L. The high surface-to-volume ratio can make fixed-bed systems even better than suspension cultures for protein expression and viral vaccine production. "You will be able to optimize your perfusion process in such a way that the [product] is actually harvested into a smaller volume when compared to the reference process of a stirred tank bioreactor," says Castillo. This makes the iCells 500 appropriate for laboratory as well as industry applications.

Whatever types of cell cultures researchers need to expand, the recent technological advances by equipment makers have smoothed the path considerably. Shiloach explains that just in the past few years, "the media are much better, the cell lines are better, also they have better ways of doing all the molecular biology. It seems to me that it's much more difficult to identify the right product than to produce it."

Alan Dove is a science writer and editor based in Massachusetts.

DOI: 10.1126/science.opms.p1300080

Featured Participants

ATMI
www.atmi.com

BD Biosciences
www.bdbiosciences.com

GE Healthcare Life Sciences
www.gelifesciences.com

Labtech
www.labtech.co.uk

Life Technologies
www.lifetechnologies.com

National Institute of Diabetes and Digestive and Kidney Diseases
www2.niddk.nih.gov

Pall Life Sciences
www.pall.com

Sigma-Aldrich
www.sigmaaldrich.com

Thermo Fisher
www.thermofisher.com

AUTOMATED CELL CULTURE SYSTEM

The new Cellmate Mk9 automated cell culture system is designed for safe, high throughput production of adherent cell-based vaccines in a GMP environment. Cellmate Mk 9 is an evolution of the well-established Cellmate technology that automates the manufacturing processes associated with production of vaccines using adherent cell-based methods in roller bottles and T-flasks within a Class 100 laminar airflow cabinet. The latest Cellmate system can be UL certified and includes an inline particle counter that can be used to monitor non-viable particle loading in the processing area. The inline particle monitoring helps address increasing demands from regulators for assurance about the environmental quality used in manufacturing processes. Cellmate Mk9 supports the OPC interoperability standard for industrial automation allowing users remote access to process information. The Cellmate software retains 21 CFR Part 11 compliance and TAP provides full support for IQ and OQ, which makes implementing Cellmate into GMP vaccine production facilities a straightforward task.

TAP Biosystems

For info: +44-(0)-1763-227200 | www.tapbiosystems.com

HUMAN ES/IPS MEDIUM

The new PluriSTEM Human ES/iPS Medium is designed for the routine expansion of human embryonic and induced pluripotent stem cells in feeder- and serum-free conditions with less frequent feeding and cell culture time. It is the first human ES/iPS media to combine small molecule inhibitors with pluripotent specific growth factors and supplements to enable a less rigorous cell culture regiment. The medium consists of fourteen components and is fully defined. The proprietary formulation includes Activin-A, TGFβ1, and b-FGF to promote stem cell self-renewal and potent small molecule combinations to inhibit unwanted spontaneous differentiation as well as human serum albumin (HSA) to aid in overall colony morphology. The culture of human ES/iPS cells has traditionally required feeding every day, including weekends, as well as significant technical expertise. This new medium addresses these challenges by providing an efficient and robust culture method that allows for feeding every other day, excluding weekends.

EMD Millipore

For info: 800-645-5476 | www.emdmillipore.com/pluristem

SECONDARY ANTIBODIES

New Alexa Fluor 405/568/750 conjugated secondary antibodies have been added to the existing Alexa Fluor 488/555/594/647 conjugates. The Alexa Fluor range guarantees bright staining and low background. The different color variants were selected to provide an increased selection for multicolor staining. The Alexa Fluor portfolio comprises antibodies raised against mouse/rabbit/rat/chicken/goat/sheep/guinea-pig IgG and against mouse/rabbit IgM. It also includes a large selection of pre-adsorbed/cross-adsorbed and F(ab')2 fragment secondaries to ensure low species cross-reactivity. A dilution range of 1/200 -1/1000 in IF/ICC allows for at least 250 stainings per product to improve cost efficiency. The Alexa range expansion adds a blue emitting fluorophore, Alexa Fluor 405, and a near IR dye, Alexa Fluor 750. The addition of Alexa Fluor 568 is ideal for confocal laser-scanning, as most of these microscopes have a 561 nm laser, which optimally excites the Alexa Fluor 568 dye. Alexa Fluor secondaries are ideal for multicolor staining.

Abcam

For info: 888-772-2226 | www.abcam.com/alexa

PRIMARY NEURON SERUM-FREE MEDIA

Developed as an alternative to B27, GS21 is a next generation serum-free neural media supplement, based on the formulation of NS21 Supplement, designed to improve the overall growth and performance of primary neurons. GS21 has been specifically optimized for the maturation and long-term viability of primary rat and mouse neurons in culture, without the need for co-culture with astrocyte feeder cells. In experimental tests, GS21 has been shown to significantly improve long-term viability of rat and mouse primary neurons in vitro as well as enhance neurite outgrowth of primary neurons in culture. Beneficially, GS21 also supports growth and maintenance of primary neurons at low or high cell density plating.

AMS Biotechnology

For info: +44-(0)-1235-828200 | www.amsbio.com/B-27.aspx

CELL THERAPY MANUFACTURING

Xuri is a new technology family designed specifically to support and advance the field of cell therapy. Cell therapy and regenerative medicine, the use of cells to replace damaged tissue or to treat disease, shows great promise for treating many life-threatening and life-limiting illnesses. The widespread adoption of these therapies will require the development of robust, scalable manufacturing tools and workflows to generate sufficient, high-quality cells for infusion into patients. With an estimated 2,500 on-going cell therapy and regenerative medicine clinical trials worldwide, many research groups are now looking at how to move from small-scale expansion of cells to a cost-effective, industrialized process. GE Healthcare's new Xuri Cell Expansion System W25 is a functionally closed, automated system, specifically designed to be suitable for the requirements of scaling-out cell therapies in a clinical setting. The system is equipped with dedicated software applications to make it suitable for a regulated manufacturing environment and has been validated for T-cell growth. The Xuri W25 builds on the GE Healthcare's WAVE Bioreactor technology which is widely used in the development and manufacture of biopharmaceuticals globally.

GE Healthcare

For info: 800-526-3593 | www.gehealthcare.com

Electronically submit your new product description or product literature information! Go to **www.sciencemag.org/products/newproducts.dtl** for more information.

Newly offered instrumentation, apparatus, and laboratory materials of interest to researchers in all disciplines in academic, industrial, and governmental organizations are featured in this space. Emphasis is given to purpose, chief characteristics, and availability of products and materials. Endorsement by *Science* or AAAS of any products or materials mentioned is not implied. Additional information may be obtained from the manufacturer or supplier.

Join Keystone Symposia for Two Unique Events

HIV/AIDS: Strategies for an Endgame

December 13, 2013 | 1:00–2:30 PM EST

Our first FREE, LIVE webcast.

This 90-minute event will aim to determine the optimal strategy to end the AIDS epidemic, with a particular focus on discussing the merits of pre-exposure prophylaxis versus vaccines.

Moderator: Bruce Walker
Panelists: Myron (Mike) Cohen, Betsy Herold, Julie McElrath and Gary Nabel

Visit **www.keystonesymposia.org/KSHIV** to register and to submit a question/topic that you would like addressed during the discussion.

Big Data in Biology

March 23–25, 2014 | San Francisco, California, USA

Our first SHORT, TWO-DAY symposium.

This conference will address the challenges of sharing, archiving, integrating and analyzing the vast amounts of biological data now being generated. The event will bring together various research specialties that rarely interact, including plant scientists, medical geneticists, genomicists, microscopists and neurobiologists, as well as computer scientists, computational biologists, mathematicians and technologists. Event sessions start at 8 AM on March 24.

Scientific Organizers: Lincoln D. Stein, Doreen Ware and Michael Schatz

Session Topics:

- **Databases and Clouds**
- **Panel on Big Data Challenges and Solutions: Control Access to Individual Genomes**
- **Personal Genomes**
- **Imaging/Pharmacogenomics**

Discounted Abstract Deadline: ***November 19, 2013***
Student/Postdoc Scholarship Application Deadline: ***November 19, 2013***
Abstract Deadline: ***December 18, 2013***
Discounted Registration Deadline: ***January 21, 2014***

For more information and to view the full program, visit **www.keystonesymposia.org/14F2**

CONFIRMED SPEAKERS
(as of November 4, 2013):

Laura Clarke, European Bioinformatics Institute
Mark Gerstein, Yale University
David Haussler*, UC Santa Cruz
Jill P. Mesirov, Broad Institute
John Overington, European Molecular Biology Laboratory
Ajay Royyuru, IBM T.J. Watson Research Center
Michael Schatz, Cold Spring Harbor Laboratory
Dan Stanzione, University of Texas at Austin
Lincoln D. Stein, Ontario Institute for Cancer Research
Susan Sunkin, Allen Institute for Brain Science
Jason Swedlow, University of Dundee
Matt Wood, Amazon Web Services, Inc.

**Keynote Speaker*

KEYSTONE SYMPOSIA™
on Molecular and Cellular Biology
Accelerating Life Science Discovery

www.keystonesymposia.org | 970.262.1230 | 800.253.0685

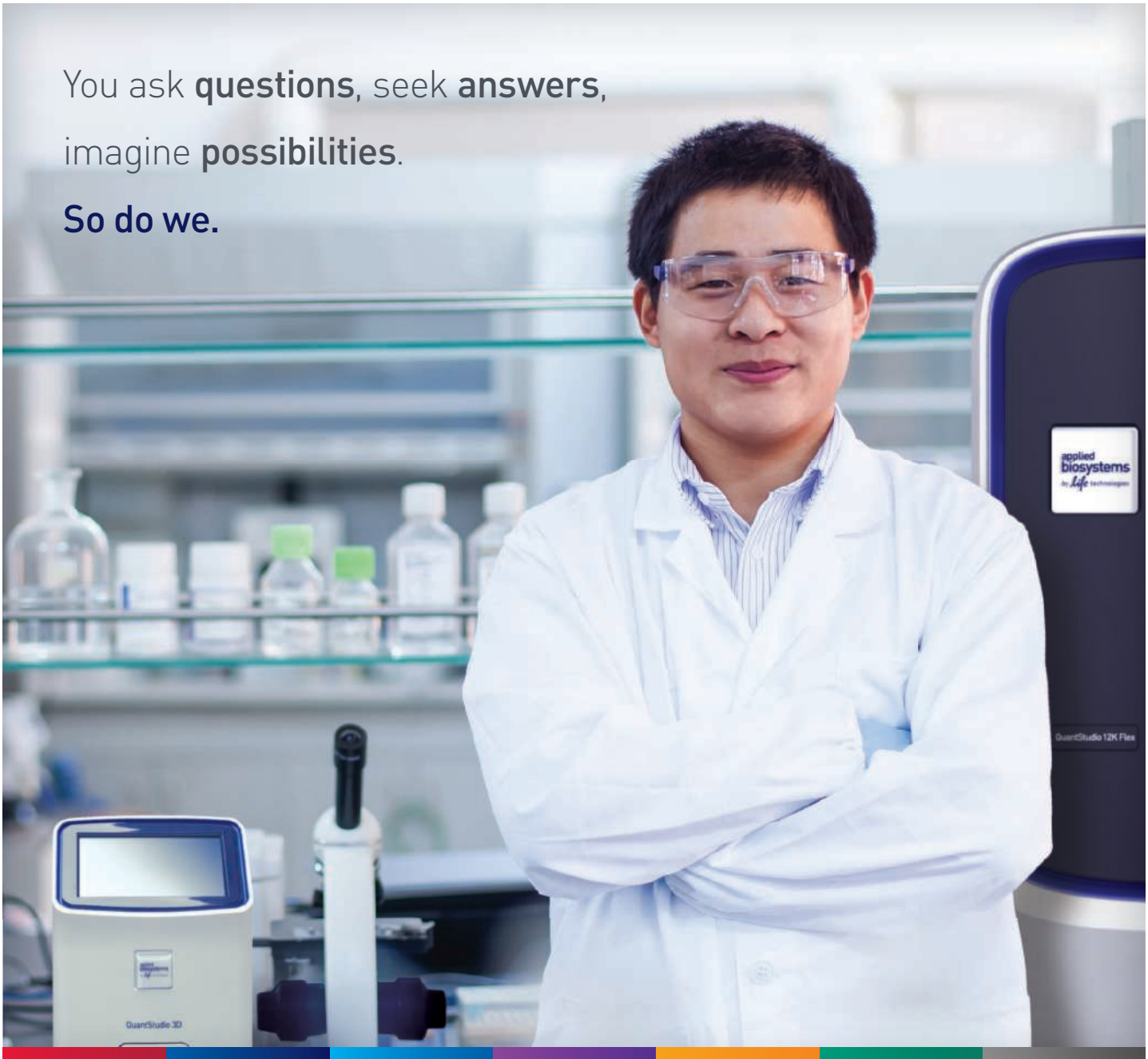

Your passion drives our **innovation**

Designing around your needs, we innovate new solutions to help you advance your research, faster and with more confidence.

Tour our latest innovations in molecular biology at
lifetechnologies.com/labtour

life technologies™

College of Basic Medical Sciences
Transforming the Future of Education and Research

As an important research- and teaching-oriented center of the Third Military Medical University and a National Key University in China, the College of Basic Medical Sciences (CBMS) is dedicated to pursuing research in the basic medical and life sciences, to developing new innovations in medical education, and to attracting and cultivating talent from around the world. After more than two decades of progress, CBMS is now among the top basic medical science colleges in China.

Yuzhang Wu
Director, CBMS

Editors: Tianna Hicklin, Ph.D., Sean Sanders, Ph.D.
Guest Editor: Xiaoyun Sun, Ph.D.
Writer: Wayne Peng, Ph.D.
Proofreader/Copyeditor: Yuse Lajiminmuhip
Designer: Amy Hardcastle

Contents

Sponsored by

崇德崇實 求精求新

The College of Basic Medical Sciences, Third Military Medical University. For more information
e-mail: wuyuzhang@tmmu.edu.cn

International Collaboration and *Science* Custom Publishing
Global Director: Bill Moran +1-202-326-6438 | bmoran@aaas.org

Associate Director for China, Singapore, Korea, Thailand, and Vietnam:
Ruolei Wu +86-1367-101-5294 | rwu@aaas.org

This feature was produced by the *Science*/AAAS Custom Publishing Office and supported by CBMS. Materials that appear in this feature were commissioned, edited, and published by the *Science*/AAAS Custom Publishing Office and were not reviewed or assessed by *Science*'s Editorial staff.

Introducing CBMS: Leading Medical Research and Education for 20 Years

Chongqing, one of the four municipalities directly under the central government, is famous for three millennia of rich culture and history in the fertile valley in southwestern China and has a population of more than 30 million people. It is also home to the highly regarded Third Military Medical University (TMMU) and the College of Basic Medical Sciences (CBMS).

Over the past 20 years, CBMS has become known for its groundbreaking basic research and innovative medical education. Founded in 1992, CBMS has morphed from a simple teaching unit into a powerhouse of medical research and scientific training. In 2011, when Yuzhang Wu became the director of CBMS, the institution began another transformation, through which "research-based education" would become a cornerstone of the institution's mission.

Growing Basic Research

Shortly after its foundation, CBMS received one of the first research grants awarded by the National Natural Science Foundation of China (NSFC). Since then, its researchers have secured more and more competitive research grants year after year. This year alone, CBMS has received nearly 40 million yuan (US$6.5 million) in funding from the central and local governments.

A significant portion of the funding growth is specific to immunology research, Wu's area of expertise. CBMS' Institute of Immunology is a designated State Key Discipline (SKD) and receives direct support from the central government. The institute also serves as the immunology command center for the People's Liberation Army of China (PLA), providing strategic support and advice.

Other areas of research showing significant expansion include the Department of Anatomy and the Department of Histology and Embryology, which are both part of the Ministry of Education's Cultivating State Key Discipline Program, aiming to develop more SKDs in top research centers throughout the country. Researchers in these departments study cutting-edge topics in developmental biology, such as brain cell development, vascular biology, and stem cells.

One aspect these departments all have in common is teamwork. "Chinese culture stresses working in union toward a common goal," explains Wu, who is leveraging this unique strength of Chinese researchers to stimulate networking, collaboration, and project coordination.

Already the institution's collaborative efforts, combined with ample funding, have resulted in high-quality publications. "During 2012 alone, CBMS researchers published more than 100 papers in international journals and 15 papers in journals with an impact factor of five or higher," explains Wu. "This is a gigantic leap in research output compared with 15 years ago, when CBMS researchers only published one immunology paper the entire year." Patent applications have also risen rapidly since CBMS was granted its first patent in 2000, with nearly 20 applications under consideration in the first half of 2013.

Going forward, CBMS plans to develop a world-class faculty by recruiting young talent and by building interdisciplinary research projects with Chinese scientists and international partners. "Our goal in the future is to increase our research competitiveness—both within China and on the global stage," says Jijian Zhang, associate director of research at CBMS.

Revolutionizing Education

A pivotal force of research competitiveness is the graduate students, and Wu has tasked the institution with providing a "research-based education." Wu has implemented a number of programs to boost students' research skills and critical thinking ability, including journal clubs and interdisciplinary co-mentorships.

CBMS is also introducing innovative teaching strategies into the rigid medical education system. "In addition to the textbook knowledge required for board exams, we encourage critical thinking from our undergraduate students," says Wengang Xiao, associate director of education at CBMS. Wu and Xiao have introduced materials from scientific journals, rigorous debates and discussions, and presentation practices into the classroom. "We ask students to challenge authority, both teachers and textbooks, when it comes to science," says Wu.

Also bringing in new ideas are the many young professors joining the faculty who have received their training overseas. "Ninety percent of the current faculty have either acquired their Ph.D. or done their postdoctoral research abroad," says Wu. Moreover, there are currently 28 adjunct professors located internationally who regularly visit CBMS to teach and to advise on research directions.

Over the last 20 years, CBMS has developed into a respected, global medical research institution. With its state-of-the-art research facilities, internationally minded faculty, and revamped educational system, CBMS is poised to solve critical problems in medicine and become one of the top basic medicine and biomedicine research centers in China.

Insights from the Director: Making Grand Visions a Reality

The director of CBMS has grand visions for the institute. As a trained immunologist and a pioneer of epitope-based rational vaccine design, Yuzhang Wu has had a successful research career. He is a winner of the National Outstanding Youth Science Fund and a designated Changjiang Scholar Distinguished Professor for the Chinese Ministry of Education, one of the most prestigious distinctions for Chinese scholars. When he became the director of CBMS in 2011, he immediately saw opportunities to make an impact in three areas: creating an internationally trained faculty, boosting translational research, and revamping pedagogical strategies.

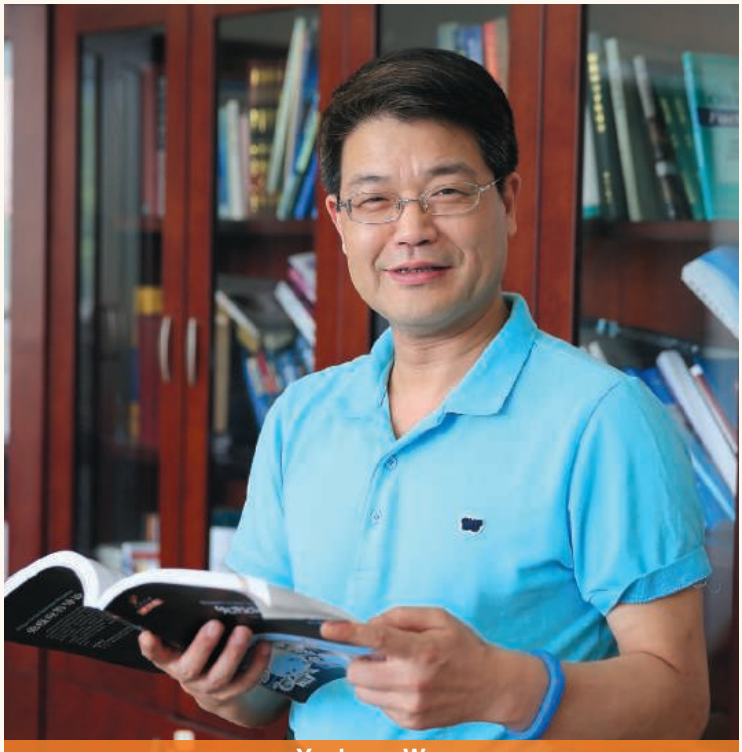

Yuzhang Wu

Faculty Training

Previous to Wu's leadership, CBMS faculty did not follow an international model for research and education. Therefore, Wu began recruiting young researchers from overseas who were "highly motivated and eager to embark on new research directions." Wu explains that they "have recruited several junior investigators who have a strong work ethic as well as extensive international connections, which has been raising the level of education and research significantly."

Because these new generations of faculty are still early in their careers, Wu has begun to coach them on how to think strategically and focus more broadly in their field. "Many of these talented young investigators have spent years studying a small part of a larger problem," he explains. "They're still learning how to navigate the big picture and how to strategically compete with others." These skills are even more critical in China where research competition is fierce and pressure for fast success is high.

Interdisciplinary Collaboration and Translational Research

One advantage of CBMS being located in Chongqing is that the culture is known for friendliness and cooperation, which makes it easier for researchers to form collaborations and interdisciplinary projects. To further facilitate this, Wu has taken full advantage of the three large hospitals affiliated with CBMS and implemented a co-mentorship program and a "clinical-basic research salon." He hopes these programs will facilitate strong translational-research collaborations between the faculty and the hospital's clinical staff.

Eventually, Wu dreams of incorporating industry into these collaborations. "Integrating with industry will help us commercialize our research findings," he says. "Although this has been more difficult than forming academic collaborations, we are getting there." His goal is to reduce the reliance on central government funding and to build a clinically oriented biotechnology base in China.

Innovative Education Strategies

Ultimately, education is the key to producing top-notch researchers, clinicians, and biotechnology leaders, which is why Wu so strongly values education reform. Traditional medical education in China has failed to deliver translationally focused scientists and clinicians. Wu's reform begins at the undergraduate level, with the goal of changing the focus of education from simple memorization toward critical thinking and understanding. Wu has already implemented a number of classroom strategies to help achieve this goal (see Innovation in Education, page 1268).

In his view, the gap between graduate training in China and in the West is even wider than that of undergraduate education. Many graduate students in China have simply become technicians who run repetitive experiments, rather than scientists in training. His graduate education reform aims to change this by implementing new strategies. Within the new paradigm, graduate students will be expected to independently identify important questions in their field of interest and then address these questions using logical reasoning and up-to-date information from the scientific literature rather than from textbooks.

Wu believes that a shortage of research-focused educators contributes to the lack of this type of education, highlighting the need for better teacher training to raise the standard of education. He encourages CBMS faculty to not only focus on writing scientific research papers but also to develop teaching strategies and publish their experiences in education-oriented journals.

In his first two years, Wu has made great strides in steering CBMS toward becoming an international center with a talented faculty, robust research output, and world-class scientific training. Already, CBMS has moved into a stronger position and is producing quality clinical research. Wu believes the institution's future is bright, but that fully realizing his dreams will only be made possible by the diligent work of everyone at CBMS.

State Key Discipline: At the Front Line of Immunology


The Institute of Immunology

The Institute of Immunology at CBMS leads basic and applied immunology research for the armed forces of China; more importantly, it is designated a State Key Discipline (SKD) and is therefore eligible to receive direct government funding. Scientists at the institute focus on advancing cutting-edge topics—from understanding the mechanisms underlying early immune responses to developing new vaccines.

Understanding and Harnessing Immune System Responses


Zhiren Zhang


Ying Wan

The body's immune response is a complex process. The Institute of Immunology has brought together scientists with a broad range of backgrounds to investigate mechanistic questions about the immune system and to find ways of harnessing the body's immune responses for clinical benefit.

After years spearheading the T cell vaccine development efforts at CBMS, Ying Wan, a principle investigator at the institute, has shifted his attention to dendritic cells and the role microRNAs play in immune response initiation. "We collaborate with research teams at Duke University and the University of California at Berkeley on these interesting topics, providing state-of-the-art research equipment," says Wan.

Zhiren Zhang, associate head of the institute, began studying inflammation at the Universität Tübingen in Germany. He moved his lab to the Institute of Immunology in 2011 because the "funding situation is better right now at CBMS than in Germany," explains Zhang. At the institute, his group investigates molecular targets for suppressing excess inflammation.


Guohong Deng

To fully understand how the immune system fights microbial infection, Wei Liu, principle investigator, uses X-ray crystallography to obtain detailed structural information of the key protein players in an effort to dissect the molecular mechanisms of innate immunity. Prior to joining the institute in 2011, Liu, who has a background in biochemistry, spent nearly a decade at the Karolinska Institute in Sweden studying structural biology.

Combating Disease


Guilian Xu

One of the most serious chronic infections in China is hepatitis B. "It is estimated that a third of the world's chronic hepatitis B cases are in China," says Guohong Deng, principle investigator, whose lab investigates how a patient's genetic background affects the T cell response to the hepatitis B virus (HBV). Meanwhile, Guilian Xu, a principle investigator also studying virus-host genome interactions, works toward revising the conventional theory that the complement system only acts on innate immunity. Based on genetic evidence, she argues


Bing Ni


Xinyuan Zhou


Yongwen Chen

that the system also participates in adaptive immune responses, especially when certain viral infections, such as HBV, are present.

Epigenetic mechanisms also play a role in the immune response to HBV infection, and are the focus of Associate Head Bing Ni's research. After Ni graduated from the Third Military Medical University, he attended the University of Toronto for his postdoctoral training; however, he decided to come back to CBMS because there are abundant resources for studying "the three most clinically important immunology problems: infection, cancer, and autoimmunity," Ni explains. His research focuses on epigenetic changes, such as histone modifications, in regulatory T cells.

Understanding immune responses to other pathogens is important to many CBMS researchers. Principle Investigator Xinyuan Zhou, for example, investigates the mechanism of T cell memory using established infection models—lymphocytic choriomeningitis and *Listeria* infections. "We are looking at ways to enhance T cell memory for treating chronic infection," says Zhou. Complementing Zhou's work, another principle investigator, Yongwen Chen, who did his postdoctoral research at Sweden's Karolinska Institute, is looking at the role of natural killer cells and macrophages in resolving chronic HBV infection.

Advancing Vaccine Development


Li Wang


Wei Liu

Yuzhang Wu, director of CBMS and head of the Institute of Immunology, is a pioneer in epitope-based rational vaccine design—stimulating the desired immune response using synthesized peptides that present the "optimal" antigenicity. Under his leadership, the institute has attracted some of the best minds to research and has developed prophylactic and therapeutic vaccines for critical diseases in China.

One such researcher is Li Wang, associate head of the institute. She is looking for ways to modulate specific T cell responses to treat diseases and is "developing therapeutic vaccines for various cancers," she explains. Wang is trying to attenuate autoreactive T cells in type 1 diabetes in the hopes of slowing down the destruction of insulin-producing cells in the pancreas.

Successful vaccine development also involves understanding how existing vaccines work. Lilin Ye, principle investigator and an expert on immunological responses to vaccines and viral infection, designs new and improved versions of old vaccines. His group's latest work is focused on developing "mucosal vaccines and therapeutic antibodies against important diseases, such as hepatitis B and avian influenza," Ye says.

As a well-funded SKD, the Institute of Immunology has enlisted an interdisciplinary team of talented scientists to begin unraveling how the immune system works and to develop ways to design the most effective therapeutics. Given the progress the institute has made thus far, many more avenues for developing vaccines and combating chronic diseases will surely emerge in the future.

Cultivating New State Key Disciplines: Modernizing Basic Medical Sciences


Dajun Ying


Chuhong Zhu


Wenqing Cai


Lan Xiao


Xiaotang Fan

At TMMU, the faculty of CBMS is responsible for the university's basic medical education, which begins with anatomy and histology lessons. However, CBMS educators go beyond textbook lessons and incorporate their own research into classroom learning. Some of the noteworthy projects being used for medical education at CBMS include the world's second virtual human project, blood vessel engineering, and nervous system development research. As a result of this high-quality research, the Department of Anatomy and the Department of Histology and Embryology are poised to become the next State Key Disciplines at CBMS.

Chinese Virtual Human Project

CBMS is a leader in the creation of digital human atlases. In the late 1990s, Shaoxiang Zhang, vice president of TMMU and former director of CBMS, led the team of surgeons and computer scientists who developed the Chinese Virtual Human Project (CVHP).


Shaoxiang Zhang

"CVHP is the largest virtual human dataset in the world," Zhang says. Although released a few years after the U.S. Virtual Human Project (VHP), CVHP has a number of notable advantages. CVHP was made using 0.1 mm slices, compared with the 1 mm slices used for VHP, Zhang explains, "making the CVHP data of much higher resolution." Additionally, the imaging resolution of each slice is also higher than that of VHP.

"Right now, the utilization rate of CVHP is on par with that of VHP," says Zhang. Virtual human databases are very useful for medical education, and CVHP is now being licensed by many medical schools in China and abroad. Moreover, the CVHP data is extremely valuable for education and applications in Asia, since there are a number of notable anatomical differences between the Chinese/Asian CVHP body and the Caucasian body used in VHP.

For future applications of CVHP, Zhang explains, they are looking at using the dataset in conjunction "with 3-D printing technology to create artificial human organs for transplantation."

Blood Vessel Engineering

Anatomical and histological research at CBMS has also brought about innovative discoveries in blood vessel engineering. Dajun Ying, professor emeritus, has been studying blood vessels in the human head since the 1980s. His early work, as a graduate student at TMMU, focused on mapping the capillaries that feed the brain, head, and facial tissues. After moving into the field of biomechanics, he began working on the role of hemodynamics in endothelial cell biology and capillary physiology. Ying then began using molecular biology to understand the signal transduction pathways underlying the action of hemodynamic forces. Currently, he is involved in application-oriented projects such as stem cell-based tissue engineering.

Ying's innovative attitude has inspired the next generation of scientists, including Chuhong Zhu, head of the Department of Anatomy. Continuing his work from a stint in the University of Minnesota, Zhu engineers artificial cardiovascular tissue using new biomaterials and stem cells. He is constructing tissue-engineered small-diameter blood vessels from captured endothelial progenitor cells in vivo, which enables endothelization of tissue-engineered blood vessels. Zhu is committed to producing these blood vessels for clinical applications. He also investigates neural regulation of blood vessel physiology and development.

Neural Development

Developmental biology is also a strong focus at CBMS. Professor Emeritus Wenqing Cai was one of the pioneers who introduced immunohistochemistry methods to China in the 1980s. She has trained many scientists at CBMS who are now leaders in developmental biology.

One such person is Lan Xiao, head of the Department of Histology and Embryology, who studied development neurobiology and neuropsychiatry as a postdoctoral fellow at the University of Saskatchewan, Canada. "We are especially interested in the development of oligodendrocytes, the myelin forming cells in the central nervous system," says Xiao, "because we have found from animal models that oligodendroglia dysfunction or demyelination may be involved in the pathogenesis of psychiatric disorders like schizophrenia."

Other researchers in the department are looking for therapeutic agents to correct neurodevelopmental defects. Xiaotang Fan, a principle investigator in the same department, is particularly interested in nuclear receptors as therapeutic targets. "The key to successfully applying developmental biology for therapeutic application in neurology is to pinpoint tissue and temporal specificities of potential therapeutic targets," explains Fan, "because the time window for therapeutic intervention is quite narrow for neurodevelopment defects."

Taken together, these research projects have not only advanced the medical education at CBMS, but are also supporting the Department of Anatomy and the Department of Histology and Embryology in their quest to become State Key Disciplines.

Innovation in Education: Training Physician-Scientists

Graduate Students Discussing an Experiment in the Lab

Summer School for Undergraduates

A key objective of Director Yuzhang Wu's vision for CBMS is to reform all levels of the educational system, including physician-scientist training. "Our goal is to train our brightest students to become physician-scientists who can identify important questions and critically investigate the answers," says Wu. Below is a look at some of the current physician-scientist students' experiences and accomplishments, which demonstrate how Wu's plan is being implemented and is improving medical education.

Dali Zhang and Kaiyuan Zhang are both starting their senior year at TMMU. In an immunology course taught by Professor Li Wang last year, Dali Zhang was asked to design his own scientific experiments. He became so interested in the intellectual exercise that he asked if he could carry out the experiments in Wang's lab over the summer break. Wang agreed to mentor the student's project because "teaching and learning are mutually beneficial," explains Wang. "I also gain new insights by discussing different papers' experimental design and results with my students." After finishing his summer project, Zhang is now considering either a basic research career or a clinically focused career after he graduates. "I am glad to have had the chance to learn both clinical and basic research skills here," says Zhang. "In China, we have a unique opportunity to conduct translational research because we have access to a huge patient pool."

His classmate Kaiyuan Zhang has been working in the lab for much longer, since his freshman year to be exact. Kaiyuan Zhang, who studies molecular neurophysiology with Jun Zhang, principle investigator in the Department of Physiology, cannot hide his passion and excitement when talking about his work on sleep biology and the neurotransmitter orexin. "I am inclined to pursue basic research after graduation because of the happiness it brings me," says Zhang. "I enjoy using deductive logic and applying the latest techniques to solve important questions." He is just one of many success stories in Wu's undergraduate education reform.

Xiaoyun Shang just received his Ph.D. from CBMS this summer. He worked in Director Yuzhang Wu's lab studying vaccine design. "The most important lesson I have learned here is critical thinking," says Shang. "There is so much knowledge beyond the textbooks we used in college. I've learned the importance of identifying key questions and applying up-to-date technical know-how to answer these questions," he says. He has accepted a postdoctoral fellowship in the United States, where he hopes to gain additional skills to advance his career in therapeutic cancer vaccine development.

Kaijun Liu is a second-year Ph.D. student in the lab of Shaoxiang Zhang, vice president of TMMU and the project leader for the Chinese Virtual Human Project (CVHP) (see page 1267). Liu also did his undergraduate work at TMMU and has worked in Zhang's lab since 2005. "Back then, we did not have the innovative education platform put together recently by Director Wu, so there has been some trial and error in the process [of learning to be a critical-thinking scientist]," says Liu, who equates the transition from undergraduate research to studying for a Ph.D. to climbing a mountain. "You see the field more broadly and clearly as you climb," says Liu, explaining that as he advanced toward completing the degree, he began to see the bigger picture questions in his field. In Zhang's lab, Liu learned about computer reconstruction and image processing, but has recently become interested in immunology, and now wants to combine these different fields to create new ideas, such as creating a model of the lymph system using the CVHP dataset.

Overall, "the ultimate goal [of this education reform] is to break old habits, the inertia, and the short-sightedness of the traditional medical education," says Professor Zhongxiang Yao, who has over 25 years of teaching experience. Fundamental changes in guidelines and evaluation systems are necessary to ensure that undergraduate and graduate students can develop a productive career, and CBMS is dedicated to hastening the reform and inspiring the next generation of scientists.

International Talents: Fostering a Global Reach

In recent years, many Chinese universities have significantly stepped up their efforts to bring their science to the international stage. CBMS is one such institution that has been implementing strategies to become more competitive in the global arena. In the last two to three years alone, CBMS has seen an uptick in bidirectional global connections, but staying competitive means being able to recruit a top-notch faculty both locally and abroad.

Helping achieve this talent recruitment goal is China's "Go West" strategy, which has been encouraging economical, educational, scientific, and technological developments in the country's western region and providing policy and funding support over the last decade. Given this increased focus on the West, Chongqing—the largest city in China—is poised to become a new center of international outreach.

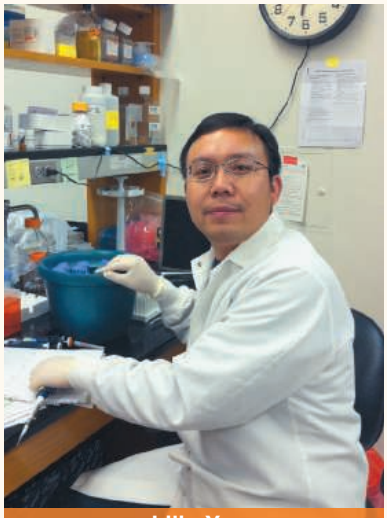
Lilin Ye

Professor Xiaowei Chen, who graduated from CBMS several years ago and recently returned from his postdoctoral training at the Technische Universität München in Germany to be the head of the Brain Research Center, says the livability of Chongqing compared with that in major coastal cities allows him to "concentrate on doing science without worrying about money and housing." This is important for Chen since he feels a strong emotional attachment to the institute and plans to build China's first marmoset center for large-animal experiments right in Chongqing. Another example is Lilin Ye, a principle investigator who brought his research developing novel therapeutic vaccines to CBMS in 2012 from Emory University in Atlanta in the United States, explains that some other benefits of being in Chongqing are that the "kindergarten and school education is better than that provided by other institutions in Beijing or Shanghai."

CBMS also strives to stay competitive with universities located on either side of the Atlantic Ocean by providing top-notch research facilities as well as generous starter packages. "There are also fewer restrictions here as to how starter funds can be used," says Yi Zhou, professor of neuroscience, who joined CBMS at the same time as Chen. He moved from the University of Southern California to open his own lab studying how complex information is processed in the brain. Zhou is particularly impressed by the leadership at CBMS and TMMU. "The director of the college works harder than us!" he says. "We can bring bureaucratic issues, such as difficulties navigating complicated procedures, directly to him," and he provides strong support to young investigators at TMMU, says Zhou. "Once he replied by e-mail after midnight, and my problem was resolved before the next day started," he explains.

CBMS has also set specific recruitment goals to help strengthen its faculty. "We want [to recruit] junior-level talent who are not afraid of challenging the existing paradigms and exploring new theories," explains Yuzhang Wu, director of CBMS, "rather than transplanting established research groups from overseas." Wu hopes these free-thinking scientists will bring the scientific cultures from the countries where they were trained to China. Evidence of this can be found in many of the innovative teaching methods and evaluation systems CBMS has implemented in recent years, which have their roots in the places where CBMS researchers have been educated, such as Europe or the United States.

Scientists returning home to China don't leave their professional lives behind. Maintaining connections and collaborations with scientists outside China is very important to CBMS researchers. "There are no real differences between being located in Chongqing and being in Beijing or Shanghai," says Chen, "especially in the era of the Internet and frequent air travel." He still communicates regularly with former colleagues in Munich about collaborative projects.

Another strategy for CBMS in acquiring top talent is recruiting domestically. Jun Zhang, a principle investigator in the Department of Physiology, who specializes in sensory-motor integration, moved from Nanjing University (800 miles east of Chongqing) to CBMS in 2011. Zhang says that "Chongqing, and the surrounding Sichuan region, has always been a resource-rich area in China, and this is also true in terms of scientific research support thanks to ample funding and talent from all over the world."

More than 1,300 years ago, poets wrote about how quickly one could travel from Chongqing (the "White Emperor Castle") to Nanjing via the Three Gorges and Yangtze River, in only one day. With today's technology, the distance between Chongqing and other cities has become virtually nonexistent, making Chongqing a great location to conduct world-class research as well as stay connected to the global community.

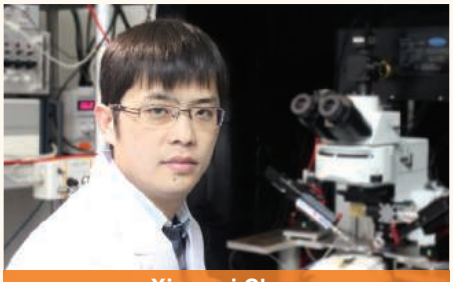
Xiaowei Chen


Yi Zhou


Jun Zhang

Department of Science and Technology
Ministry of Science & Technology
Government of India
Technology Bhavan, New Mehrauli Road, New Delhi- 110016.

Jawaharlal Nehru Science Fellowships

CALL FOR NOMINATIONS

The Department of Science and Technology has instituted Jawaharlal Nehru Science Fellowship, in order to promote cutting-edge scientific research in centres of excellence in India. Eminent scientist of any nationality desirous of carrying out research in Indian Institutions for a period of 12 months in a three year duration would be enabled by this Fellowship Scheme. Nominations of eminent scientists for the Award of Jawaharlal Nehru Science Fellowships are invited from Heads of Academic/Research Institutions, Presidents/Fellows of Science Academies and global leaders in science.

SCOPE

Areas in Natural and

Physical Sciences including Mathematics.

ELIGIBILITY

- The Fellowship is open to overseas scientists with high academic distinction and achievements.
- High academic distinctions accompanied by election to the fellowships like Royal Society, US and French Academies and their equivalent.
- The nominated scientists should continue to be active in Research, as evidenced from R&D Outputs over the past five years.

DURATION

The Fellowship would be availed for a duration of 12 months during a period of three years, from the date of offer of the Fellowship Award.

NATURE OF SUPPORT

- Value of the Fellowship is US$ 100,000 for a 12 months period.
- In addition, each Fellow will receive aggregated research grant of Rs. 5.5 million part of which may be utilised to engage project staff (2 Research Fellows or 1 Post-doctoral Research Fellow), international / local travel and other contingent expenses to carry out research.
- The selected scientists could choose :
  - Their place of research anywhere in India.
  - Duration (total of 12 months spread over a period of up to three years).
  - Research theme for pursuing their research.
  - Research collaboration in India, if any.

25 Fellowships for the period 2014-17.

HOST INSTITUTION

The Host Institutions for the Jawaharlal Nehru Science Fellows would need to provide the necessary infrastructure, furnished housing and administrative support to the Fellow. The Department of Science and Technology (DST), Government of India, would provide Rs 1 million to the host institute to cover the expenses of such support.

METHODOLOGY FOR SELECTION

- Nominations for the Fellowship are solicited through an open call.
- A Search Committee will select and recommend suitable nominations to the Government of India.

HOW TO APPLY

The nominations for the Fellowship may be sent to **Secretary, Department of Science and Technology, Technology Bhawan, New Mehrauli Road, New Delhi – 110016 through dstsec@nic.in (please mention "Attention SS Kohli, Director, DST" in the subject of the email).** There is no prescribed format for nomination. The nomination letters should be accompanied by a recent and detailed CV of the nominee and expressed willingness to accept the Fellowship, if offered.

Since the Government of India wishes to initiate the Fellowship scheme by January, 2014, early nomination by December, 2013 are solicited.
To see further details log on to www.dst.gov.in.

TEXAS A&M
HEALTH SCIENCE CENTER
COLLEGE OF MEDICINE

Institute for Regenerative Medicine
at Scott and White, Temple TX
Positions for Post-Doctoral Fellows and Other Lab Personnel

The Texas A & M Institute for Regenerative Medicine is seeking Ph.D. level post-doctoral fellows and other lab personnel for research on adult stem/progenitor cells referred to as mesenchymal stem cells or multipotent mesenchymal cells (MSCs). The Institute is dedicated to research both on the basic biology of MSCs and the therapeutic products they produce. Current research includes development of new therapies for diseases of the eye, myocardial infarction, cancer, diabetes, stroke, epilepsy and traumatic brain injury. The Institute occupies newly renovated laboratories and a series of core laboratories equipped with state-of-the-art instrumentation. It also includes a newly renovated vivarium for small animal experiments. Post-doctoral appointments are contingent on funding and will be for one year with the opportunity to renew for a second and third year. Post-doctoral candidates should have excellent communication skills both verbally and written and a Ph.D. or M.D. degree from a well recognized university. Other lab personnel should have some laboratory experience, preferably with tissue culture of mammalian cells. Salaries and benefits are competitive. Log onto our website at **http://medicine.tamhsc.edu/irm/** to read more about our facility.

For requirements and duties of positions listed above as well as completing the application, please visit **https://jobs.tamhsc.edu/**. The posting number for Postdoctoral Research Associate NOV 14079, Research Assistant NOV 14080, Technician II NOV 14075 and Technician NOV 14081.

The Texas A&M Health Science Center is an AA/EO Employer.

Jefferson Science Fellowship

The National Academies is pleased to announce a call for nominations and applications for the 2014 Jefferson Science Fellows program. Initiated by the Secretary of State in 2003, this fellowship program engages the American academic science, technology, engineering and medical communities in the design and implementation of U.S. foreign policy.

Jefferson Science Fellows (JSF) spend one year at the U.S. Department of State or the U.S. Agency for International Development (USAID) for an on-site assignment in Washington, D.C. that may also involve extended stays at U.S. foreign embassies and/or missions.

The fellowship is open to tenured, or similarly ranked, academic scientists, engineers and physicians from U.S. institutions of higher learning. Nominees/applicants must hold U.S. citizenship and will be required to obtain a security clearance.

The deadline for 2014-2015 program year applications/nominations is **January 13, 2014.** To learn more about the Jefferson Science Fellowship and to apply, visit the website at:

www.nas.edu/jsf

THE NATIONAL ACADEMIES
Advisers to the Nation on Science, Engineering, and Medicine

UNIVERSITY OF CALIFORNIA
UCRIVERSIDE

Tenure Track Assistant Professor of Neuroscience

The Department of Psychology, University of California, Riverside, invites applications for a tenure-track Assistant Professor position in the systems neuroscience area, beginning July 1, 2014. The Ph.D. degree is required and post-doctoral experience is preferred. Applicants should have demonstrated compelling promise of research and publication using modern molecular, cellular, systems or behavioral approaches to address fundamental problems of mammalian brain function, and be interested in interacting with a broad-based psychology department. Individuals with research focused on mechanisms of cortical development, plasticity or function are especially encouraged to apply, as are those whose research emphasizes linkages between animal and human models. Applicants should also be committed to excellence in undergraduate and graduate education. Salary will be commensurate with education and experience.

Review of completed applications begins **January 17, 2014** and continues until the position is filled. Interested candidates should send a cover letter describing research and teaching interests, their curriculum vitae, reprints and preprints if available, and arrange to have three letter of recommendation provided, all using the following link: **https://aprecruit.ucr.edu/JPF00035**. Questions about the position should be directed to Professor Peter Hickmott, Chair, Systems Neuroscience Area Search Committee, at **peter.hickmott@ucr.edu**.

The Riverside campus of the University of California is growing rapidly and has an excellent psychology department with a strong record of success in research, teaching and extramural funding. For information on the Department of Psychology, see our web site at: www.psych.ucr.edu. For collaborative opportunities via the Neuroscience Graduate Program, see http://neurograd.ucr.edu. The campus is centrally located in Southern California, about 50 miles east of Los Angeles and less than an hour's drive from the area's mountains, deserts and beaches.

The University of California, Riverside is an Equal Opportunity/Affirmative Action Employer.

PURDUE
UNIVERSITY

Two Faculty Positions in the Department of Botany and Plant Pathology

The Department of Botany and Plant Pathology is seeking applicants for two Assistant Professor tenure track faculty positions in Plant Biology. Both positions are academic year appointments. Successful candidates will be expected to develop internationally-recognized extramurally-funded research programs, interact with diverse faculty, staff and students across campus, demonstrate excellence in their teaching of graduate and/or undergraduate courses, and function as an active member of the department and university faculty.

1. Root/Rhizosphere Biology – closing date 12/15/2013 or until a suitable candidate is identified

Applicants for the Root/Rhizosphere Biology position will have a Ph.D. in the biological or computational sciences and postdoctoral research experience. A complete position description is available at **https://ag.purdue.edu/btny/Pages/JobListings.aspx**

2. Plant Growth Regulator/Hormone Biology – closing date 1/20/2014 or until a suitable candidate is identified

Applicants for the Plant Growth Regulator/Hormone Biology position will have a Ph.D. in biology, biochemistry, computational biology or a related field and at least two years of postdoctoral research experience and expertise in plant biology. A complete position description is available at **https://ag.purdue.edu/btny/Pages/JobListings.aspx**.

Applicants should submit a letter of application outlining their research interests and describing their philosophical and conceptual approach to a research/teaching position at a land-grant university. Applicants should also include a complete resume and the contact information for three references. These materials should be sent electronically to **mowp@purdue.edu**. A background check will be required for employment in these positions.

Purdue University is an Equal Opportunity/Equal Access/Affirmative Action Employer fully committed to achieving a diverse workforce.

PEDIATRIC Infectious Diseases

Open Rank, Open Tenure. The Division of Infectious Diseases in the Department of Pediatrics is seeking applications from highly qualified M.D., M.D./Ph.D. or Ph.D., for faculty positions. The Division of Infectious Diseases has a long history of NIH supported laboratory and clinical research. The selected individuals will work collaboratively to expand current research programs as well as establish new areas of research in respiratory viruses and bacterial infections. These positions will be provided generous start-up packages as well as secondary appointment in basic science department and Centers of Excellence at UAB to further the capacity of research in infectious diseases at UAB.

QUALIFICATIONS

The successful candidates for these positions must have a successful record in research with current NIH funding. In addition, the ideal candidates should possess:

- Experience in the academic medical center setting
- A proven track record of research initiation
- Demonstrated research collaboration skills
- Strong communication skills and the highest of ethical standards

Interested applicants should contact:
William Britt, M.D.
Professor, Division of Ped Infectious Diseases
1600 7th Avenue South, CHB #107
Birmingham, AL 35233
Email: wbritt@peds.uab.edu

UAB is an Equal Opportunity/Affirmative Action Employer committed to fostering a diverse, equitable and family-friendly environment in which all faculty and staff can excel and achieve work/life balance irrespective of ethnicity, gender, faith, gender identity and expression as well as sexual orientation. A pre-employment background investigation is performed on candidates selected for employment. In addition, UAB Medicine maintains a drug-free and tobacco-free work environment. Physicians and other clinical faculty candidates, who will be employed by the University of Alabama Health Services Foundation (UAHSF) or other UAB Medicine entities, must successfully complete a pre-employment drug and nicotine screen to be hired. UAB also encourages applications from individuals with disabilities and veterans.

Princeton Environmental Institute (PEI) and the Department of Civil and Environmental Engineering (CEE) at Princeton University seek outstanding applications for a new faculty position in water science. The position is a tenure-track position at the rank of Assistant Professor, with a preferred start date of September 1, 2014. The successful candidate will have a PhD in an appropriate field and a proven record of innovation and creativity in conducting quantitative research addressing important and emerging topics within the broad scope of hydrological sciences. Areas of interest include: (1) water and climate, (2) water and energy, (3) water and environmental quality, (4) water and ecosystem integrity, and (5) water and food security.

In all cases, it is expected that the candidate would be able to immediately make meaningful contributions to the diverse, interdisciplinary environmental research and teaching mission of PEI and CEE's Environmental Engineering and Water Resources Program (EEWR). PEI is the interdisciplinary center of environmental research, education, and outreach at Princeton University. PEI's mission is to advance knowledge and to develop the next generation of leadership by providing outstanding academic programs and opportunities for advanced scholarship, research, and civic engagement. The goal of CEE's EEWR program is to train outstanding engineers and scientists and to conduct advanced research in areas that are vital to national and international needs in the areas of environmental engineering and water resources. A successful candidate will be expected to complement existing strengths in the program, which include environmental problems in areas such as ecohydrology, land surface - atmosphere interactions including energy and moisture fluxes and their relationship to large-scale climate modeling, remote sensing of environmental variables such as soil moisture and rainfall intensity, carbon mitigation and climate change, subsurface flows & reactive transport, atmospheric dynamics and atmospheric chemistry, the urban environment, and biogeochemistry of contaminated waters.

Applicants should apply online at **https://jobs.princeton.edu**, requisition number **1300834**; and should submit their CV, contact information for five references, and separate statements of research and teaching vision. The statements of research and teaching vision should include the candidate's sense of the field and his or her vision for advancing in the context of such a position. Evaluation of applicants will begin on **January 15, 2014** and continue until the position is filled. Inquiries regarding this position should be addressed to **Prof. Kelly Caylor (kcaylor@princeton.edu)**.

Princeton is an Equal Opportunity Employer and complies with applicable equal opportunity and affirmative action regulations. We strongly encourage applications from underrepresented minorities, women, veterans, and those with disabilities.

Recruit and Promote Your Brand All Year Long

Science Careers will publish a 2014 Career Directory that will be promoted and distributed all year long.

A combination of career development content alonside your branding ads makes this the pefect place to promote your organization's mission and the areas where you typically recruit. With bonus distributions to meetings and career fairs throughout the year and push marketing including banner ads and e-mail blasts to potential candidates, your company receives ongoing exposure to scientists eager to know about career opportunities.

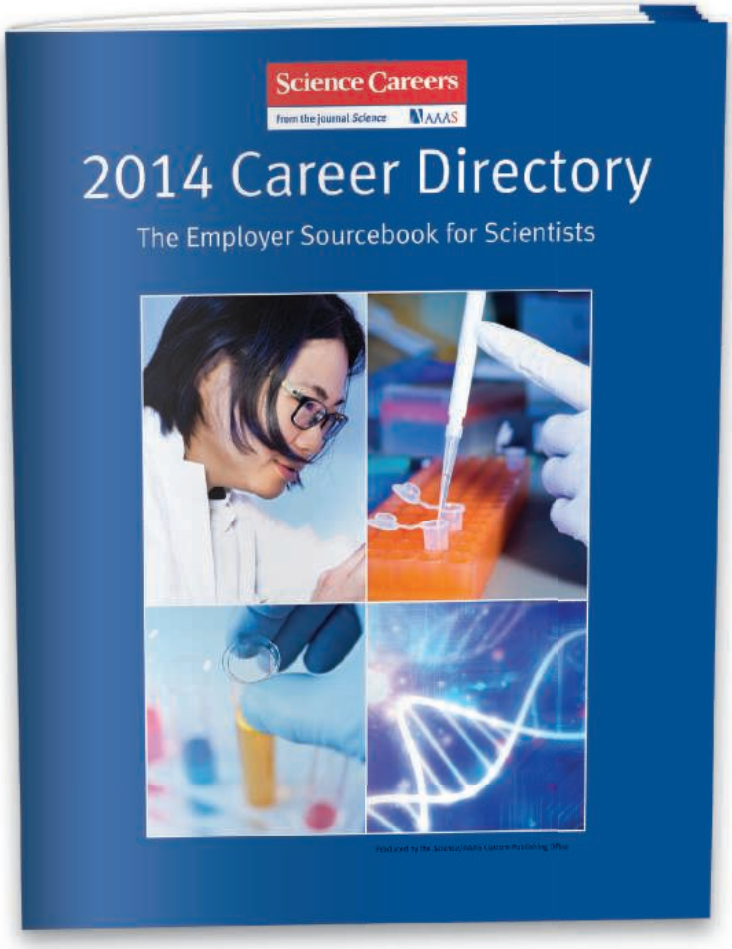

Benefits to your company

- Opportunity to brand your organization to scientists beyond your normal reach.
- Print bonus distribution of 3,500 copies to career fairs and meetings around the globe.
- Digital copy e-mailed to 100,000 scientists including all *Science* Careers registrants.
- Your logo included in two Career Path newsletters.
- A PDF of the booklet will also be posted on *Science* Careers for one year with marketing to drive readers to the booklet. Marketing includes banners, e-mail blasts, and promotion across AAAS/*Science* newsletters.

To book your ad or for more information:
E-mail: advertise@sciencecareers.org

Or telephone us:
US/Canada/South America:
202-326-6582

Europe/India/Australia/New Zealand/Rest of World: +44 (0) 1223 326500

Japan: +81-(0)90-9110-1719

China/Korea/Singapore/Taiwan/Thailand: +86-1367-1015-294

Reserve space by December 20, 2013
Ad materials due January 10, 2014
Rate: US$2,995

For recruitment in science, there's only one Science

Produced by the *Science*/AAAS Custom Publishing Office

Science Careers
From the journal *Science* AAAS

ScienceCareers.org

ASSISTANT PROFESSOR

Freshwater Ecologist

The Department of Biological Sciences at the University of Alabama invites applicants for a full-time (9-month) tenure-track faculty position at the Assistant Professor level. The successful applicant will establish an extramurally funded and internationally recognized research program in freshwater ecology. Preference will be given to applicants with a background in state-of-the-art, quantitative methods serving studies of freshwater ecosystems such as those related to, but not restricted to, food-webs, ecosystem energy and nutrient fluxes, metabolic theory, climate change, ecohydrology and macrosystems ecology. We define ecosystem studies broadly and encourage applications from individuals with a demonstrated record of integrating population- and community-level research with ecosystem perspectives.

The University of Alabama (UA) is near the geographic center of the Mobile River drainage, a true hot-spot for global freshwater biodiversity. Successful candidates will be encouraged to leverage this unique resource to support an innovative research program, and to forge collaborations with the new NOAA National Water Center, which will open on the UA campus in 2014, and the diverse faculty at UA and Dauphin Island Sea Lab with interests in freshwater ecology. Aquatic mesocosm facilities are available near the UA campus at the Tanglewood Biological Station. Teaching responsibilities will include basic undergraduate courses in biology, as well as specialized undergraduate and graduate courses in the successful candidate's area of expertise.

Applicants must have a Ph.D., postdoctoral training, and demonstrated research productivity. Queries regarding additional details should be addressed to the chair of the search committee: Dr. Alexander D. Huryn at **huryn@bama.ua.edu**.

To apply, go to **https://facultyjobs.ua.edu**, complete the online application (Job # 0808674), and upload (1) an application letter with a list of three to five references (including contact information); (2) CV; (3) statement of research interests and goals; and (4) statement of teaching interests and philosophy. Consideration of applications will begin January 15, 2014, and will continue until the position is filled. Prior to hiring, the final candidate will be required to pass a pre-employment background investigation. The anticipated start date is August 16, 2014.

Additional information about the Department of Biological Sciences and this available position can be found on our website at **http://bsc.ua.edu**.

The University of Alabama is an Equal Opportunity/Equal Access Employer and actively seeks diversity among its employees.

touching lives
THE UNIVERSITY OF ALABAMA

深圳大学

2013 Shenzhen University Oversea Recruitment

Shenzhen University (SZU) was founded as a public university in 1983 with the accreditation of the State Council of the People's Republic of China.
There are many famous scholars in SZU. Currently, there are 1,500 teachers on campus and about 60% of them have gotten Phd. Now, SZU has 2 Academicians of Chinese Academy of Sciences, 3 Academicians of Chinese Academy of Engineering, 2 members of "1000-Talents Scheme", 6 scholars who have won awards from the National Science Foundation for Distinguished Young Scholars, 4 scholars who have won awards from the "Chang Jiang Scholars Program", 3 members of New Century Millions of Talents Project at national level and 3 chief scientists in the National 973 Academic Program.

SZU, thirsty for talents, warmly welcomes numerous outstanding elites to join us as distinguished professors, associated professors or lecturers.

A. Distinguished professor
1) Eligibility: Candidates of the national "1000-Talents Scheme", "1000-Young-Talents Scheme", "Outstanding Youth", "Chang Jiang Scholars Program" and "100-Talents Scheme" of the CAS, professors or associated professors from overseas famous universities and outstanding scholars having fundamental academic influence.
2) Remuneration: It is yearly payroll for a distinguished professor, about RMB500,000-1,200,000. SZU will provide support in scientific research expenses and laboratory construction fee for a distinguished professor as well as in constructing his academic research team. Especially, Shenzhen local government will give scientific research expenses of RMB2,000,000 – 5,000,000 to a candidate who study such subjects as science, engineering and medicine and are eligible for the Peacock Program or Shenzhen High-Level Talent Program.

B. Professor, associated professor, lecturer and Liyuan Scholar Plan
(1) Professor, associated professor and lecturer
SZU warmly welcome oversea scholars who have achieved a Phd degree or have experiences of post-doctoral research and are competent for our positions of professor, associated professor and lecturer. Excellent candidates will be engaged as professors or associated professors directly by SZU according to their academic achievements.

Remuneration: the minimum annual salary is RMB310,000 for a professor, RMB250,000 for an associated professor and RMB180,000 for a lecturer.
Any professor, associated professor and lecturer could apply for Liyuan Scholar Plan, Peacock Program or Shenzhen High-Level Talents Program. If any person achieved any of the above plans, he could apply to Shenzhen Government for different subsidies by relevant plan.

(2) Liyuan Scholar Plan
Any teacher could apply for this plan. There are three levels for this plan, such as "Liyuan Leading Scholar", "Liyuan Outstanding Scholar" and "Liyuan Excellent Youth" respectively.
1) Three-level scholars: Liyuan leading scholar will be awarded to full-time teachers as a top-leader in his academic area. Liyuan outstanding scholar will be awarded to full-time teachers, aged under 45 and having 3 years' working experiences. Liyuan excellent youth will be awarded to young scholars aged under 35 who had gotten Phd and had one year's academic research experience in relevant research institutions.
2) Award standards: SZU will provide a living allowance for Liyuan leading scholars in 5 years, including two levels, RMB500,000 per year At the first level and RMB150,000 per year at the second. SZU will give a living allowance to Liyuan outstanding scholars in 3 years, RMB100,000 per year. SZU will give a living allowance to Liyuan excellent youth in 9 years at the most, RMB100,000 per year.

C. Shenzhen Oversea High Level Talents Policy
1) Candidates: oversea experts or oversea scholars. There are three levels for this plan, Level A , B and C respectively
2) Remuneration: candidates will receive an award of RMB500,000-1,500,000. Candidates whose research program is in such subjects as science, engineering and medicine respectively could enjoy scientific research expenses from RMB200,000 to 5,000,000. Talents at Level A could apply for scientific research expenses of more than RMB5,000,000.

Contact Us
For more information, please visit **http://www.szu.edu.cn**. If you're interested, please send your CV and relevant materials to any of the following email addresses:
Miss Liyun liyun@szu.edu.cn, 0086-755-26536111
Miss Gaoying gaoying@szu.edu.cn, 0086-755-26535295
Mr. Renqiang szursc@sina.cn , 0086-755-26535295

POSITIONS OPEN

UCSD Jacobs | Department of Bioengineering

FACULTY POSITIONS
University of California, San Diego
Department of Bioengineering

The Department of Bioengineering in the Jacobs School of Engineering at the University of California, San Diego is inviting applications for one or more Tenure-Track or Tenured Faculty Positions at the **ASSISTANT PROFESSOR, ASSOCIATE PROFESSOR,** or **FULL PROFESSOR** levels. To obtain more information or submit your application materials, go to **website: https://apol-recruit.ucsd.edu/apply** and apply to **position number 10-650.**

TENURE-TRACK FACULTY POSITIONS in Genomics and Evolutionary Biology

The Department of Biology at Saint Louis University, a Catholic, Jesuit institution dedicated to student learning, research, health, and service, is seeking applicants for two tenure-track faculty positions: One in Genomics and one in Evolutionary Biology. Competitive applicants will have a Ph.D., postdoctoral experience, a record of research productivity, and a commitment to undergraduate and graduate student training (M.S. and Ph.D. Students). The successful candidates will be expected to establish independent, extramurally funded research programs and participate in graduate training.

For the Genomics position, we seek candidates whose research addresses biological questions using the analysis of large data sets; the specific area of research is open. Both wet laboratory and high-performance computing facilities are available and will be matched to the candidate's needs. The successful candidate will teach a genomics course at the graduate level and contribute to an undergraduate course for biology majors.

For the Evolutionary Biology position, possible areas of research inquiry include, but are not limited to, development, ecology, physiology, functional morphology and biomechanics, behavior, and host/pathogen interactions. Both wet laboratory and high performance computing facilities are available and will be matched to the candidate's needs. The successful candidate will teach an evolution course at the graduate level and contribute to an undergraduate course for biology majors.

Excellent facilities and competitive startup packages are provided, and abundant opportunities exist to develop collaborative projects with Saint Louis University researchers and with scientists and educators at the nearby Missouri Botanical Garden, Danforth Plant Science Center, St. Louis Zoo, St. Louis Science Center, and local universities.

All applications must be made online at **website: http://jobs.slu.edu** (**Req ID 20130884**) and include a cover letter, curriculum vitae, three representative publications, a research statement, and a statement of teaching experience and philosophy. In addition, please have three letters of reference sent to: **Dr. Robert Wood, Department of Biology, Saint Louis University, 3507 Laclede Avenue, St. Louis, MO, 63103.** Review of applications will begin December 16, 2013 and continue until the position is filled. Additional information on the Department of Biology can be found at **website: http://www.slu.edu/x14762.xml.**

Saint Louis University is an Affirmative Action/Equal Opportunity Employer (AA/EOE), and encourages nominations of and applications from women and minorities.

POSITIONS OPEN

BIOMOLECULAR NMR SPECTROSCOPY
Position at the University of Minnesota

The Department of Biochemistry, Molecular Biology & Biophysics at the University of Minnesota invites applicants with a Ph.D. or M.D. degree in Biochemistry, Chemistry, or related fields to apply for a tenure-track/tenured position at the **ASSISTANT, ASSOCIATE,** or **FULL PROFESSOR** level. The successful candidate is expected to develop a creative and vibrant research program in Structural Biology and Biophysics in association with the Minnesota NMR Center (**website: http://www1.umn.edu/nmr/**). The Center consists of several high-field spectrometers including a 900, 850, two 700, and two 600 MHz spectrometers equipped with cryogenic probes. In addition, two solid-state NMR spectrometers are equipped with MAS and static NMR probes.

Preference will be given to scientists focusing on structural analysis of biomacromolecules relevant to any area of cellular biophysics and applications are encouraged from investigators studying human physiology or pathology, signaling systems or membrane proteins. Candidates must be able to teach undergraduate and graduate level Biophysical Chemistry and Biochemistry courses.

Applicants must apply online at **website: employment.umn.edu.** Click on Search Postings, and enter **187414** into the **requisition number** field. Applicants should attach a cover letter, curriculum vitae, and a detailed description of the proposed research. Review of complete applications will begin immediately and continue until the position is filled. More information concerning the Department and this position can be website: found at **website: http://www.cbs.umn.edu/bmbb.**

The University of Minnesota provides equal access to and opportunity in its programs, facilities, and employment without regard to race, color, creed, religion, national origin, gender, age, marital status, disability, public assistance status, veteran status, sexual orientation, gender identity, or gender expression. The University supports the work-life balance of its faculty and especially encourages applications from women and members of underrepresented groups.

The Illinois Natural History Survey (INHS) is soliciting applications for a two-year **POSTDOCTORAL RESEARCH ASSOCIATE.** Scientists whose research interests fit within those of the Illinois Natural History Survey are encouraged to apply. A salary of $42,000 per year with benefits is provided, as well as a $5,000/year research stipend. Applicants should submit curriculum vitae and Research Proposal. The Research Proposal is limited to three pages, not including references, and should address the research plan proposed for the two-year postdoctoral position. In advance of the application deadline, applicants must identify and contact a research sponsor at the INHS (**website: http://wwx.inhs.illinois.edu/opportunities/postdoc-sponsors/list/**) who is willing to host the Postdoctoral Associate. Preference will be given to applicants who can develop a strong research plan that merits additional and continued external funding. Research plans that build on existing INHS research strengths by adding new directions or new analytical techniques are encouraged.

Applicants should have completed a Ph.D. by the start date of the position (expected before December 31, 2014) and within the last five years. In addition to the Research Proposal and curriculum vitae, applicants should arrange for two letters of recommendation to be sent. Applications must be sent electronically to **e-mail: hroffice@inhs.illinois.edu** by January 31, 2014.

BIOENGINEER TENURE-TRACK PROFESSOR

The School of Engineering invites applications from distinguished scholars for a position at the either the **ASSISTANT** (tenure-track) or **ASSOCIATE/FULL** (tenured) level in Bioengineering at the newest University of California campus in Merced, California. The research emphasis for this position is a rather broad including: biological modeling, biosensors, tissue engineering, and preclinical biomedical imaging. To apply or for more information, please visit our **website: http://jobs.ucmerced.edu/n/academic/position.jsf?positionId=4996.**

POSITIONS OPEN

GENOMICS/FORENSIC MOLECULAR BIOLOGIST

As part of a strong faculty research emphasis in molecular biology and a developing program in forensic biology, the Department of Biological Sciences at Bowling Green State University (BGSU) seeks a tenure-track **ASSISTANT PROFESSOR** with demonstrated experience in genomics or bioinformatics approaches with potential forensic applications. Postdoctoral experience required. Successful candidates are expected to develop highly productive, externally funded research, and contribute to the graduate (Ph.D./M.S., n>90) and undergraduate programs. To apply, submit electronically a single PDF containing cover letter, curriculum vitae, statements of research plans and teaching perspective, representative publications, and, separately, three reference letters to **e-mail: dmclean@bgsu.edu** by January 6, 2014. *A background check is required for employment.* Contact **George Bullerjahn** at **e-mail: bullerj@bgsu.edu** with questions. Further information about our department can be found at **website: http://www.bgsu.edu/departments/biology.** *BGSU is an Affirmative Action/Equal Opportunity Employer/Educator and encourages applications from women, minorities, veterans, and persons with disabilities.*

abcam®
discover more

What can RabMAb® do for you?

Our Rabbit monoclonal antibody (RabMAb) range offers multiple advantages to bring you the highest quality antibody possible.

Learn more at abcam.com/RabMAb

Better results — on any sequencing platform

Get the most from your NGS

Discover new and innovative solutions, dedicated for use with any NGS workflow

Streamline your next-generation sequencing (NGS) workflow and achieve high-quality results you can rely on.

- **Highly specific and selective nucleic acid purification and target enrichment**
- **Unbiased whole genome amplification from a single cell**
- **High DNA library yields using optimized workflows that allow ~50% time-savings**
- **Outstanding results on any sequencing platform**
- **Intuitive, knowledge-based data interpretation for deeper insight into NGS results**

Visit www.qiagen.com/goto/NGS to learn more!

QIAGEN®

Sample & Assay Technologies

NEW ENGLAND BioLabs® Inc.
enabling technologies in the life sciences

Make ends meet.

Gibson Assembly® Cloning Kit

New England Biolabs has revolutionized your laboratory's standard cloning methodology. The Gibson Assembly Cloning Kit combines the power of the Gibson Assembly Master Mix with NEB 5-alpha Competent *E. coli*, enabling fragment assembly and transformation in just under two hours. Save time, without sacrificing efficiency.

Making ends meet is now quicker and easier than ever before, with the Gibson Assembly Cloning Kit from NEB.

NEBuilder™ for Gibson Assembly

Visit **NEBGibson.com** to view the latest tutorials and to try our primer design tool.

Gibson Assembly Cloning Kit provides robust transformation efficiencies

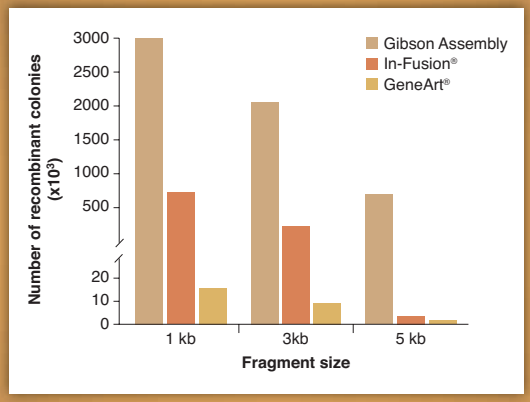

Assembly reactions containing 25 ng of linear pUC19 vector and 0.04 pmol of each fragment were performed following individual suppliers' recommended protocols and using the competent cells provided with the kit. The total number of recombinant colonies was calculated per 25 ng of linear pUC19 vector added to the assembly reaction.

SGI DNA

Reliable. Trusted. Proven.

Matt, Director of Products, has been at CST for over 11 years and is one of the original Phospho-Akt product scientists.

The reliability of CST™ Phospho-Akt antibodies is proven by peer-reviewed publications, and supported by 13 years of Akt expertise.

Learn more about Akt signaling with our updated PI3 Kinase/Akt Signaling Pathway Poster and Akt Substrates Guide. To request your copy of each, please visit our website.

www.cellsignal.com/aktguide

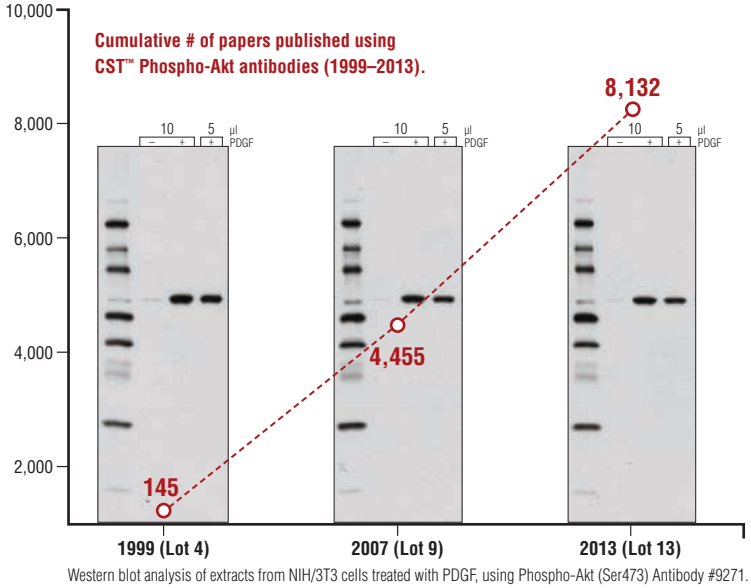

Western blot analysis of extracts from NIH/3T3 cells treated with PDGF, using Phospho-Akt (Ser473) Antibody #9271.

Cell Signaling TECHNOLOGY®

BD Accuri™ C6 Systems

Perfectly suited to support demanding educational environments.

BD

Helping all people live healthy lives

Learn. Teach. Master.

The BD Accuri C6 is a perfect fit for personal research, student mastery, and core lab use. It's easy to learn and operate, powerful enough for the majority of routine flow applications, and small enough for easy transport, making it perfect for the demands of the educational environment. Affordably priced, it may just be one of the best valued instrument in your lab.

The 4-color BD Accuri C6 allows for teaching and learning in a guided way, through templates, and factory pre-sets. The system also collects and stores 7.2 decades of data to empower novice users to make corrections if errors are made.

Those new to flow cytometry will appreciate the simplicity of the BD Accuri C6, while experts will appreciate the extensive capabilities and workflow advantages. Core lab managers will be able to better allocate resources, offloading routine applications and reserving higher-end systems for more complex, multi-parameter duties. Researchers will find it empowering for personal research and affordable.

Find out how your teaching institution and lab could benefit from owning BD Accuri C6 systems by visiting **bdbiosciences.com/go/learn.**

BD Biosciences
2350 Qume Drive
San Jose, CA 95131
bdbiosciences.com

American Association for Cancer Research

SCIENTIFIC CONFERENCES 2014:

Presenting the most significant research on cancer etiology, prevention, diagnosis, and treatment

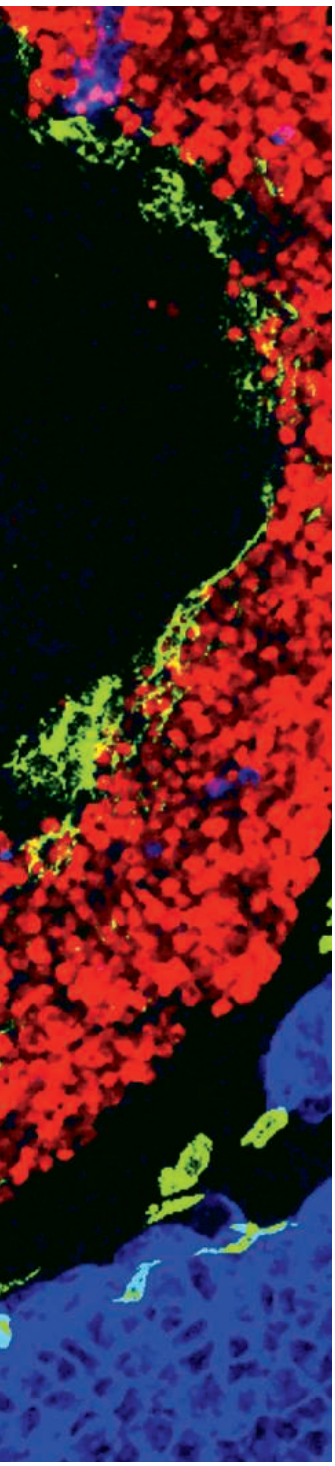

AACR-IASLC Joint Conference on Molecular Origins of Lung Cancer
Co-Chairpersons: Roy Herbst, Elisabeth Brambilla, Pasi Jänne, and William Pao
January 6-9, 2014
San Diego, CA

AACR-Prostate Cancer Foundation Conference on Advances in Prostate Cancer Research
Co-Chairpersons: Arul M. Chinnaiyan, William G. Nelson, June M. Chan, and Jonathan W. Simons
January 18-21, 2014 • San Diego, CA
Advance registration deadline:
Monday, December 9

Cancer Susceptibility and Cancer Susceptibility Syndromes
Co-Chairpersons: Alan D. D'Andrea, Phillip A. Dennis, and Pier Paolo Pandolfi
January 29-February 1, 2014 • San Diego, CA
Advance registration deadline:
Monday, December 9

RAS Oncogenes: From Biology to Therapy
Co-Chairpersons: Frank McCormick, Dafna Bar-Sagi, and Channing J. Der
February 24-27, 2014 • Lake Buena Vista, FL
Abstract submission and award application deadline:
Friday, December 6
Advance registration deadline:
Monday, January 13

Cellular Heterogeneity in the Tumor Microenvironment
Co-Chairpersons: Mary Helen Barcellos-Hoff, Michele De Palma, and M. Celeste Simon
February 26-March 1, 2014 • San Diego, CA
Abstract submission and award application deadline: **Monday, December 16**
Advance registration deadline:
Monday, January 13

AACR Annual Meeting 2014
Chairperson: Scott W. Lowe
April 5-9, 2014
San Diego, CA

Pancreatic Cancer
Co-Chairpersons: Dafna Bar-Sagi, David A. Tuveson, Christine Iacobuzio-Donahue, Alec Kimmelman, and Andrew M. Lowy
May 18-21, 2014
New Orleans, LA

Targeting PI3K/mTOR Networks in Cancer
Co-Chairpersons: Lewis C. Cantley, Jose Baselga, Joan S. Brugge, Brendan J. Manning, and Malte Peters
September 14-17, 2014
Philadelphia, PA

Melanoma
Co-Chairpersons: Levi A. Garraway, Keith T. Flaherty, and Suzanne L. Topalian
September 20–23, 2014
Philadelphia, PA

13th Annual International Conference on Frontiers in Cancer Prevention Research
Program Committee Chairperson: Phillip A. Dennis
September 28-October 1, 2014
New Orleans, LA

Tumor Immunology
Co-Chairpersons: Robert H. Vonderheide, Nina Bhardwaj, Stanley Riddell, and Cynthia L. Sears
December 1-4, 2014
Orlando, FL

Call for 2013 Cozzarelli Prize Nominations

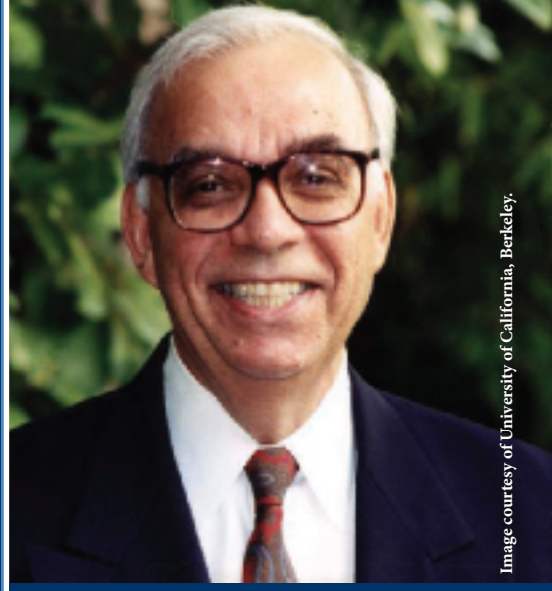

Nicholas R. Cozzarelli, former PNAS Editor-in-Chief

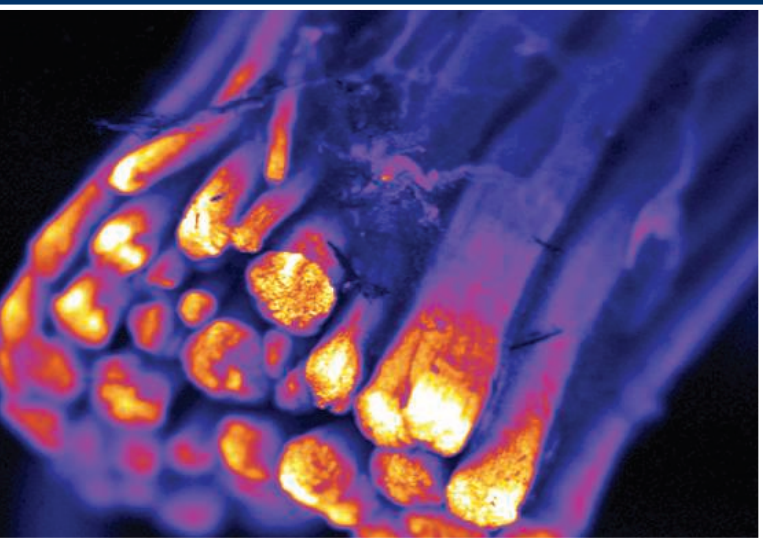

The PNAS Editorial Board is now accepting nominations through January 10, 2014 for the 2013 Cozzarelli Prize. This award recognizes scientific excellence and will be given to six papers published in PNAS during 2013.

Nominations should be sent to pnas@nas.edu and should include a citation and brief explanation of the merits of the work. The award recipients will be recognized during the PNAS Editorial Board Meeting and the NAS Annual Meeting Awards Ceremony on April 27, 2014 in Washington, DC.

PNAS
www.pnas.org

For more information and a list of previous winners visit www.pnas.org/cozzarelliprize.

Gordon Research Conferences

frontiers of science

Gordon Research Conferences (Hong Kong) Limited

戈登研究會議(香港)有限公司

A registered charitable organization in Hong Kong

The GRC expansion in Hong Kong aims to improve scientific collaborations around the world, increase networking opportunities and facilitate advancements in new scientific fields.

The following meetings are scheduled to take place in Hong Kong in 2014:

***NEW!* Advanced Materials for Sustainable Infrastructure Development**
Advanced Materials for Sustainable Energy Efficient Buildings
August 3-8, 2014
The Hong Kong University of Science and Technology
Chair: Zongjin Li

***NEW!* Complex Adaptive Matter**
Towards a Unifying Perspective of Emergent Complexity
July 13-18, 2014
The Chinese University of Hong Kong
Chair: Robert H. Austin

***NEW!* Genomic Instability**
Mechanisms that Cause DNA Damage and Related Diseases
July 6-11, 2014
The Hong Kong University of Science and Technology
Chairs: Bik K. Tye & Marco Foiani

Green Chemistry
Industrial Successes and Challenges
July 27 - August 1, 2014
The Chinese University of Hong Kong
Chairs: Kenneth Seddon & Mark A. Harmer

Green Chemistry (GRS) *
Applications for a Sustainable Future
July 26-27, 2014
The Chinese University of Hong Kong
Chair: Magdalena B. Foreiter

***NEW!* Hybrid Electronic & Photonic Materials and Phenomena**
June 22-27, 2014
The Hong Kong University of Science and Technology
Chairs: Michael Graetzel & Ben Zhong Tang

Molecular & Cellular Neurobiology
Mechanisms of Neural Development, Circuit Assembly, Synaptic Plasticity and Neuropsychiatric Disorders
June 29 - July 4, 2014
The Hong Kong University of Science and Technology
Chair: Eric J. Huang

Molecular & Cellular Neurobiology (GRS) *
Exploring the Frontiers of Foundational and Translational Neuroscience
June 28-29, 2014
The Hong Kong University of Science and Technology
Chair: Sarah X. Luo

***NEW!* Structural Nanomaterials**
Recent Advances in Understanding the Structures and Properties of Nanomaterials
July 20-25, 2014
The Chinese University of Hong Kong
Chairs: Chain T. Liu & T.G. Nieh

** Gordon Research Seminars (GRS) are 2-day meetings for graduate students and post-docs that precede an associated GRC.*

GRC provides an atmosphere and format that fosters informal discussion and networking among scientists. Our high quality, cost-effective meetings are widely recognized as the world's premier scientific conferences. Visit us at ***www.grc.org****.*

Living Large:
Scaling Up Cell Culture

Whether for structural biology, regenerative medicine, or translational research, basic scientists often find themselves needing larger quantities of cellular products than typical lab-scale techniques can produce. New technologies such as disposable bioreactors and multilayered culture flasks can help address some of the challenges of scaling up. **By Alan Dove**

"You can try different types of shaker flasks, different types of spinner flasks that can handle enough volume for initial work, and if you need a little bit more volume you can go into small bioreactors."

Bioreactor

CREDIT: (FROM TOP) IMAGE COURTESY THERMO FISHER SCIENTIFIC; ISTOPHOTO.COM/BASTAR

Traditional laboratory biology is a small-scale operation; tissue culture dishes are seldom much larger than the experimenter's hand, volume measurements are in milliliters, and a protein purification that yields a few micrograms is a success. With burgeoning interest in translational research, structural biology, and regenerative medicine, many scientists are starting to think bigger. Whether trying to purify grams of protein for crystallography or testing the feasibility of turning a novel gene product into a new drug, these researchers soon find themselves pondering the complications of larger-scale cell culture.

Thanks to the success of the biotechnology industry, cell culture scale up has become a well-paved path. "The field has exploded, because a lot of products are being made, drugs are being made in mammalian cells in large quantities in very big bioreactors," says Joseph Shiloach, head of the Biotechnology Core Lab at the **National Institute of Diabetes and Digestive and Kidney Diseases** in Bethesda, Maryland. He adds that depending on the cell type, the necessary equipment and reagents are often available off the shelf.

CHECK THE SUSPENSION

For many scientists, the most obvious choice for growing larger batches of cells is a technique they already understand: suspension culture. Numerous cell lines are already adapted to grow in small spinner bottles, so initial scale up can be as simple as buying a larger spinner. Suspension cultures also give researchers multiple options for expanding further.

Cultures in shaker flasks are particularly flexible, allowing researchers to step up through multiple sizes on a single platform—literally. "You can get a small size platform [shaker] that you can put right into your incubator, and … start with tubes that contain just a few milliliters of culture, all the way up to multiple liters of culture in large flasks," says Henry Chiou, senior product manager for cell biology at **Life Technologies** in Carlsbad, California.

Suspension cultures adapted to either shakers or spinner bottles are usually easy to expand to even larger sizes if necessary. "You can try different types of shaker flasks, different types of spinner flasks that can handle enough volume for initial work, and if you need a little bit more volume you can go into small bioreactors," says Shiloach.

The biopharmaceutical industry routinely uses suspension cell cultures in bioreactors to manufacture clinically approved products, so vendors produce such systems in sizes that range from benchtop models all the way up to industrial units. Many of these bioreactors now use disposable growth chambers to eliminate the difficulties of sterilization. "The whole bioreactor is disposable, so you can get it already equipped with everything you need, you just have to put in the media," says continued>

Upcoming Features

RNA Technologies—January 17
Proteomics—February 21
Toxicology—March 14

Whatever types of cell cultures researchers need to expand, the recent technological advances by equipment makers have smoothed the path considerably.

Shiloach. He adds that "the smaller fermenters you can handle in the beginning very similarly to a shaker flask, you can take it into the hood, you can inoculate it … and then you can put it in place and hook it to the system."

While the initial move from smaller to larger spinner or shaker cultures and even small bioreactors often seems simple, new problems can crop up as the scale increases. Larger bioreactors often need more complex support hardware and more careful and frequent testing to maintain pH and nutrient levels, so researchers may need additional training to use them. "Once you start scaling up and you need a certain yield, the yield is really quite dependent on the health of the cells," says Chiou, adding that "really monitoring your cultures very carefully becomes … more critical."

Several vendors offer slightly different spinners, suspension flasks, and bioreactors, often with novel twists to address specific problems. **Pall Life Sciences** in Port Washington, New York, for example, now sells a benchtop-size bioreactor that agitates a disposable plastic bag full of cells and media. The bag rests atop a special shaker table that rocks through two separate axes. The combination of low shear forces and a disposable growth chamber might help maintain consistency from one cell batch to the next. **GE Healthcare Life Sciences** in Piscataway, New Jersey takes a similar approach with its WAVE bioreactors, which also feature disposable bag-like growth chambers on rocking platforms, in sizes ranging from 100 mL to 500 L.

Given the variety of options, scientists should spend some time figuring out which is likely to work best for them. Shiloach suggests asking about the support equipment and testing each system requires, particularly for maintaining parameters such as dissolved oxygen and pH. If a system seems suitable, "I think the best thing is to get one and try it," Shiloach says.

RATHER SWITCH THAN FIGHT

Researchers whose chosen cells don't grow in suspension need to find another approach to scale up—or not. In many cases, the most sensible choice is to switch to suspension culture. "If you have a product that you want to test and you need a few milligrams just to find out if the biological activity is what you want, you can start doing it in adherent [cells], but if the product seems to be promising, I think it would be better to try and adapt the cells or maybe try another cell line … and then go into suspension," says Shiloach.

If the goal is a clinical therapy, switching cell lines could also help speed regulatory approval. Established suspension culture systems such as Chinese hamster ovary (CHO) and human embryonic kidney 293 (HEK-293) cells form the backbone of current biopharmaceutical production, so regulators are already comfortable with them.

Switching to a suspension-adapted line is an especially good strategy for scaling up protein production. "When we've gone out and talked to lots of folks, there [are] not that many instances where they need to actually be in a specific cell line for protein expression. The standard ones that are typically out there, 293s and CHOs, seem to fit the vast majority of needs," says Chiou.

To cater to those needs, several companies offer strains of 293 and CHO cells especially adapted for large-scale suspension growth and protein production. For example, Life Technologies' Expi293 system uses a special strain of 293 cells and a proprietary medium to achieve high levels of transient protein expression. The company claims Expi293 can produce three- to fivefold more protein per liter than conventional culture systems. Higher production means less need for larger-scale cultures. "In the past if somebody felt like they needed to scale up to a 5 L reaction in order to get enough protein, they can now stick with a 1 L or 2 L reaction," says Chiou, adding that "that really helps to lower the impact of scaling that they need to do."

Even increasing the required culture size a little bit can often entail major increases in cost and complexity, as scaling problems tend to be nonlinear. Moving from 1 L of culture to 2 L might only entail using a bigger shaker flask, but moving from 5 L to 6 L could mean buying a benchtop bioreactor and learning how to use it. "The inflection points tend to happen as you change the type of vessel you're using," says Chiou.

When standard protein expression lines such as CHO and 293 won't work—perhaps because of a need for specific glycosylation patterns that these cells can't perform—some researchers turn to microcarriers. These tiny plastic beads provide a surface for adherent cells to bind. Once seeded, the microcarriers and their attached cells can be suspended in shaker or spinner flasks. This decades-old technique provides many of the benefits of suspension culture for cells that can't adapt to it otherwise. Microcarriers are best suited for protein or virus production, as recovering viable cells from the beads can be tricky. Several equipment suppliers offer microcarriers, including GE and **Sigma-Aldrich** as well as **Labtech** of Uckfield, United Kingdom.

MORE IS MORE

For some cell types and projects, none of the existing suspension culture

systems will work. Stem cells are particularly reluctant to grow in suspension, and Vero cells, a common line for vaccine production, also need to attach firmly to plates. Fortunately, scientists trying to grow larger batches of such adamantly adherent cells can choose from several well-developed techniques.

The simplest strategy is to increase the available surface area in each culture flask, by using special flasks with multiple layers of plates inside. This parallel plate approach is somewhat more cumbersome than suspension cultures, but equipment manufacturers have worked hard to optimize it. "We were the first company that came up with this design decades ago with the Cell Factory, and we have a variety of choices in that particular product line," says Cindy Neeley, field applications specialist for cell culture at **Thermo Fisher** in Waltham, Massachusetts. Other companies also offer layered bioreactors for adherent cells, often optimized for specific uses. For example, the CELLine bioreactors from Sigma-Aldrich in St. Louis, Missouri are specifically designed for scaling up protein expression systems and monoclonal antibody production.

Moving cells from small single-layer culture flasks into parallel plate vessels brings its own set of challenges. Neeley points out that even though all of the plates in a multilayer flask are right next to each other, conditions can vary from one layer to another. "Anything more than 10 layers, you're going to encounter issues with distribution of nutrients as well as gas conditions between layers, and that is obviously a challenge for us," says Neeley. As a result, large parallel plate systems often come with special support equipment.

When shopping for such a system, researchers should also consider what surface their cells currently prefer. Cells adapted to adhere to one type of coated flask may grow poorly when moved to a multilayer flask with a different coating. For established cell lines, the solution is often as easy as buying a parallel plate system from the same vendor that provided the smaller flasks, to ensure the coatings are the same.

That won't work for researchers at the cutting edge of regenerative medicine, though. Stem cells are often too finicky to grow on any of the generic surfaces available off the shelf, instead requiring special coating reagents such as **BD Biosciences**' Matrigel. Coating a large parallel plate flask with such reagents would be cumbersome and costly. That puts parallel plate systems out of reach for stem cell work, at least for now. "We're not there yet, but companies in our position need to think in that direction, to come up with … vessels that would allow these stem cells to attach and grow," says Neeley.

For cells that can grow in parallel plate flasks, though, subsequent increases in scale—all the way up to industrial sizes—are relatively straightforward. Indeed, the largest version of Thermo's Cell Factory is already a common sight in vaccine production facilities, where the flasks are so huge that simply moving them around is one of the biggest challenges.

The difficulty of manipulating multiple large parallel plate flasks has led other equipment developers to create more compact systems. The xPansion multilayer bioreactor from **ATMI** in Brussels, Belgium uses thinner plates and puts them closer together than the Thermo Cell Factory. That allows the xPansion to pack 20 Cell Factories' worth of cells into a single container. Besides saving space, the more compact system reduces the number of flasks that have to be manipulated each time technicians need to change media or harvest cells.

Like other flask makers, ATMI is also trying to coat its plates with surfaces suitable for more exotic cell types. "Today we have only one coating, but we are actually working on specific coatings [for stem cells]," says Jose Castillo, director of cell culture technologies at ATMI.

GOING WITH THE FLOW

Researchers who are using adherent cells as expression systems for secreted proteins should also consider another strategy for scaling up: fixed-bed bioreactors. In this approach, cells adhere to small beads or fibers that are packed into a large container. Medium circulates through the matrix continuously, bringing fresh nutrients and oxygen into the bed and pulling cellular waste and secreted proteins out. It's difficult or impossible to recover the cells from the fixed bed once they've adhered, but for secreted protein production that isn't usually a problem.

Fixed-bed systems can fit a large number of adherent cells into a relatively small volume. The iCells 500, for example, holds 500 m^2 of adherent cell culture surface—roughly two tennis courts' worth—in a volume of only 25 L. The high surface-to-volume ratio can make fixed-bed systems even better than suspension cultures for protein expression and viral vaccine production. "You will be able to optimize your perfusion process in such a way that the [product] is actually harvested into a smaller volume when compared to the reference process of a stirred tank bioreactor," says Castillo. This makes the iCells 500 appropriate for laboratory as well as industry applications.

Whatever types of cell cultures researchers need to expand, the recent technological advances by equipment makers have smoothed the path considerably. Shiloach explains that just in the past few years, "the media are much better, the cell lines are better, also they have better ways of doing all the molecular biology. It seems to me that it's much more difficult to identify the right product than to produce it."

Alan Dove is a science writer and editor based in Massachusetts.

DOI: 10.1126/science.opms.p1300080

Featured Participants

ATMI
www.atmi.com

BD Biosciences
www.bdbiosciences.com

GE Healthcare Life Sciences
www.gelifesciences.com

Labtech
www.labtech.co.uk

Life Technologies
www.lifetechnologies.com

National Institute of Diabetes and Digestive and Kidney Diseases
www2.niddk.nih.gov

Pall Life Sciences
www.pall.com

Sigma-Aldrich
www.sigmaaldrich.com

Thermo Fisher
www.thermofisher.com

AUTOMATED CELL CULTURE SYSTEM

The new Cellmate Mk9 automated cell culture system is designed for safe, high throughput production of adherent cell-based vaccines in a GMP environment. Cellmate Mk 9 is an evolution of the well-established Cellmate technology that automates the manufacturing processes associated with production of vaccines using adherent cell-based methods in roller bottles and T-flasks within a Class 100 laminar airflow cabinet. The latest Cellmate system can be UL certified and includes an inline particle counter that can be used to monitor non-viable particle loading in the processing area. The inline particle monitoring helps address increasing demands from regulators for assurance about the environmental quality used in manufacturing processes. Cellmate Mk9 supports the OPC interoperability standard for industrial automation allowing users remote access to process information. The Cellmate software retains 21 CFR Part 11 compliance and TAP provides full support for IQ and OQ, which makes implementing Cellmate into GMP vaccine production facilities a straightforward task.

TAP Biosystems

For info: +44-(0)-1763-227200 | www.tapbiosystems.com

HUMAN ES/IPS MEDIUM

The new PluriSTEM Human ES/iPS Medium is designed for the routine expansion of human embryonic and induced pluripotent stem cells in feeder- and serum-free conditions with less frequent feeding and cell culture time. It is the first human ES/iPS media to combine small molecule inhibitors with pluripotent specific growth factors and supplements to enable a less rigorous cell culture regiment. The medium consists of fourteen components and is fully defined. The proprietary formulation includes Activin-A, TGFβ1, and b-FGF to promote stem cell self-renewal and potent small molecule combinations to inhibit unwanted spontaneous differentiation as well as human serum albumin (HSA) to aid in overall colony morphology. The culture of human ES/iPS cells has traditionally required feeding every day, including weekends, as well as significant technical expertise. This new medium addresses these challenges by providing an efficient and robust culture method that allows for feeding every other day, excluding weekends.

EMD Millipore

For info: 800-645-5476 | www.emdmillipore.com/pluristem

SECONDARY ANTIBODIES

New Alexa Fluor 405/568/750 conjugated secondary antibodies have been added to the existing Alexa Fluor 488/555/594/647 conjugates. The Alexa Fluor range guarantees bright staining and low background. The different color variants were selected to provide an increased selection for multicolor staining. The Alexa Fluor portfolio comprises antibodies raised against mouse/rabbit/rat/chicken/goat/sheep/guinea-pig IgG and against mouse/rabbit IgM. It also includes a large selection of pre-adsorbed/cross-adsorbed and F(ab')2 fragment secondaries to ensure low species cross-reactivity. A dilution range of 1/200 -1/1000 in IF/ICC allows for at least 250 stainings per product to improve cost efficiency. The Alexa range expansion adds a blue emitting fluorophore, Alexa Fluor 405, and a near IR dye, Alexa Fluor 750. The addition of Alexa Fluor 568 is ideal for confocal laser-scanning, as most of these microscopes have a 561 nm laser, which optimally excites the Alexa Fluor 568 dye. Alexa Fluor secondaries are ideal for multicolor staining.

Abcam

For info: 888-772-2226 | www.abcam.com/alexa

PRIMARY NEURON SERUM-FREE MEDIA

Developed as an alternative to B27, GS21 is a next generation serum-free neural media supplement, based on the formulation of NS21 Supplement, designed to improve the overall growth and performance of primary neurons. GS21 has been specifically optimized for the maturation and long-term viability of primary rat and mouse neurons in culture, without the need for co-culture with astrocyte feeder cells. In experimental tests, GS21 has been shown to significantly improve long-term viability of rat and mouse primary neurons in vitro as well as enhance neurite outgrowth of primary neurons in culture. Beneficially, GS21 also supports growth and maintenance of primary neurons at low or high cell density plating.

AMS Biotechnology

For info: +44-(0)-1235-828200 | www.amsbio.com/B-27.aspx

CELL THERAPY MANUFACTURING

Xuri is a new technology family designed specifically to support and advance the field of cell therapy. Cell therapy and regenerative medicine, the use of cells to replace damaged tissue or to treat disease, shows great promise for treating many life-threatening and life-limiting illnesses. The widespread adoption of these therapies will require the development of robust, scalable manufacturing tools and workflows to generate sufficient, high-quality cells for infusion into patients. With an estimated 2,500 on-going cell therapy and regenerative medicine clinical trials worldwide, many research groups are now looking at how to move from small-scale expansion of cells to a cost-effective, industrialized process. GE Healthcare's new Xuri Cell Expansion System W25 is a functionally closed, automated system, specifically designed to be suitable for the requirements of scaling-out cell therapies in a clinical setting. The system is equipped with dedicated software applications to make it suitable for a regulated manufacturing environment and has been validated for T-cell growth. The Xuri W25 builds on the GE Healthcare's WAVE Bioreactor technology which is widely used in the development and manufacture of biopharmaceuticals globally.

GE Healthcare

For info: 800-526-3593 | www.gehealthcare.com

Electronically submit your new product description or product literature information! Go to **www.sciencemag.org/products/newproducts.dtl** for more information.

Newly offered instrumentation, apparatus, and laboratory materials of interest to researchers in all disciplines in academic, industrial, and governmental organizations are featured in this space. Emphasis is given to purpose, chief characteristics, and availability of products and materials. Endorsement by *Science* or AAAS of any products or materials mentioned is not implied. Additional information may be obtained from the manufacturer or supplier.

Join Keystone Symposia for Two Unique Events

HIV/AIDS: Strategies for an Endgame

December 13, 2013 | 1:00–2:30 PM EST

Our first FREE, LIVE webcast.

This 90-minute event will aim to determine the optimal strategy to end the AIDS epidemic, with a particular focus on discussing the merits of pre-exposure prophylaxis versus vaccines.

Moderator: Bruce Walker
Panelists: Myron (Mike) Cohen, Betsy Herold, Julie McElrath and Gary Nabel

Visit **www.keystonesymposia.org/KSHIV** to register and to submit a question/topic that you would like addressed during the discussion.

Big Data in Biology

March 23–25, 2014 | San Francisco, California, USA

Our first SHORT, TWO-DAY symposium.

This conference will address the challenges of sharing, archiving, integrating and analyzing the vast amounts of biological data now being generated. The event will bring together various research specialties that rarely interact, including plant scientists, medical geneticists, genomicists, microscopists and neurobiologists, as well as computer scientists, computational biologists, mathematicians and technologists. Event sessions start at 8 AM on March 24.

Scientific Organizers: Lincoln D. Stein, Doreen Ware and Michael Schatz

Session Topics:

- **Databases and Clouds**
- **Panel on Big Data Challenges and Solutions: Control Access to Individual Genomes**
- **Personal Genomes**
- **Imaging/Pharmacogenomics**

Discounted Abstract Deadline: ***November 19, 2013***
Student/Postdoc Scholarship Application Deadline: ***November 19, 2013***
Abstract Deadline: ***December 18, 2013***
Discounted Registration Deadline: ***January 21, 2014***

For more information and to view the full program, visit **www.keystonesymposia.org/14F2**

CONFIRMED SPEAKERS
(as of November 4, 2013):

Laura Clarke, European Bioinformatics Institute
Mark Gerstein, Yale University
David Haussler*, UC Santa Cruz
Jill P. Mesirov, Broad Institute
John Overington, European Molecular Biology Laboratory
Ajay Royyuru, IBM T.J. Watson Research Center
Michael Schatz, Cold Spring Harbor Laboratory
Dan Stanzione, University of Texas at Austin
Lincoln D. Stein, Ontario Institute for Cancer Research
Susan Sunkin, Allen Institute for Brain Science
Jason Swedlow, University of Dundee
Matt Wood, Amazon Web Services, Inc.

**Keynote Speaker*

KEYSTONE SYMPOSIA™
on Molecular and Cellular Biology
Accelerating Life Science Discovery

www.keystonesymposia.org | 970.262.1230 | 800.253.0685

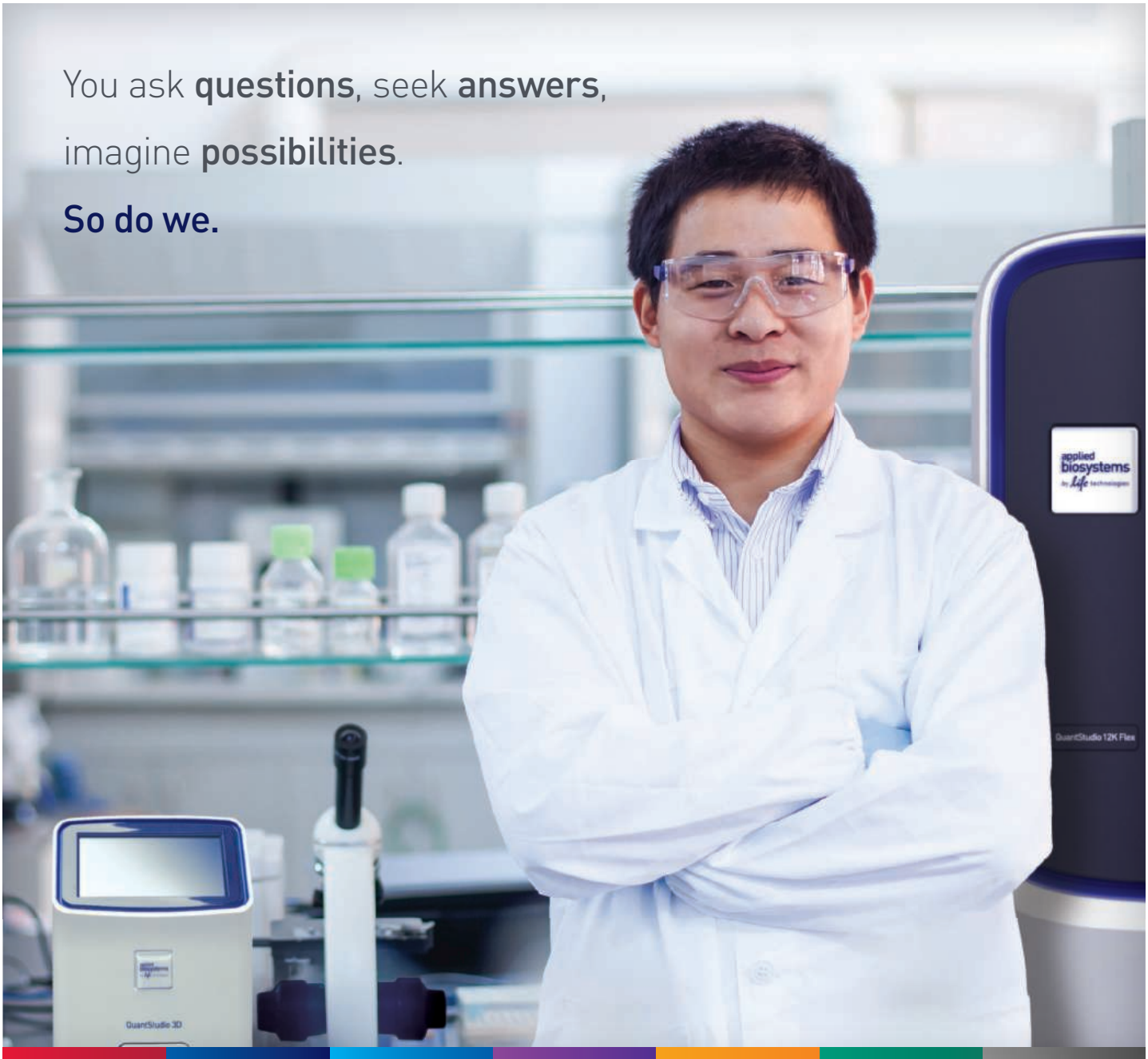

Your passion drives our **innovation**

Designing around your needs, we innovate new solutions to help you advance your research, faster and with more confidence.

Tour our latest innovations in molecular biology at
lifetechnologies.com/labtour

life technologies™

College of Basic Medical Sciences
Transforming the Future of Education and Research

As an important research- and teaching-oriented center of the Third Military Medical University and a National Key University in China, the College of Basic Medical Sciences (CBMS) is dedicated to pursuing research in the basic medical and life sciences, to developing new innovations in medical education, and to attracting and cultivating talent from around the world. After more than two decades of progress, CBMS is now among the top basic medical science colleges in China.

Yuzhang Wu
Director, CBMS

Editors: Tianna Hicklin, Ph.D., Sean Sanders, Ph.D.
Guest Editor: Xiaoyun Sun, Ph.D.
Writer: Wayne Peng, Ph.D.
Proofreader/Copyeditor: Yuse Lajiminmuhip
Designer: Amy Hardcastle

Contents

Sponsored by

崇德崇實 求精求新

The College of Basic Medical Sciences, Third Military Medical University. For more information
e-mail: wuyuzhang@tmmu.edu.cn

International Collaboration and *Science* Custom Publishing
Global Director: Bill Moran +1-202-326-6438 | bmoran@aaas.org

Associate Director for China, Singapore, Korea, Thailand, and Vietnam:
Ruolei Wu +86-1367-101-5294 | rwu@aaas.org

This feature was produced by the *Science*/AAAS Custom Publishing Office and supported by CBMS. Materials that appear in this feature were commissioned, edited, and published by the *Science*/AAAS Custom Publishing Office and were not reviewed or assessed by *Science*'s Editorial staff.

Introducing CBMS: Leading Medical Research and Education for 20 Years

Chongqing, one of the four municipalities directly under the central government, is famous for three millennia of rich culture and history in the fertile valley in southwestern China and has a population of more than 30 million people. It is also home to the highly regarded Third Military Medical University (TMMU) and the College of Basic Medical Sciences (CBMS).

Over the past 20 years, CBMS has become known for its groundbreaking basic research and innovative medical education. Founded in 1992, CBMS has morphed from a simple teaching unit into a powerhouse of medical research and scientific training. In 2011, when Yuzhang Wu became the director of CBMS, the institution began another transformation, through which "research-based education" would become a cornerstone of the institution's mission.

Growing Basic Research

Shortly after its foundation, CBMS received one of the first research grants awarded by the National Natural Science Foundation of China (NSFC). Since then, its researchers have secured more and more competitive research grants year after year. This year alone, CBMS has received nearly 40 million yuan (US$6.5 million) in funding from the central and local governments.

A significant portion of the funding growth is specific to immunology research, Wu's area of expertise. CBMS' Institute of Immunology is a designated State Key Discipline (SKD) and receives direct support from the central government. The institute also serves as the immunology command center for the People's Liberation Army of China (PLA), providing strategic support and advice.

Other areas of research showing significant expansion include the Department of Anatomy and the Department of Histology and Embryology, which are both part of the Ministry of Education's Cultivating State Key Discipline Program, aiming to develop more SKDs in top research centers throughout the country. Researchers in these departments study cutting-edge topics in developmental biology, such as brain cell development, vascular biology, and stem cells.

One aspect these departments all have in common is teamwork. "Chinese culture stresses working in union toward a common goal," explains Wu, who is leveraging this unique strength of Chinese researchers to stimulate networking, collaboration, and project coordination.

Already the institution's collaborative efforts, combined with ample funding, have resulted in high-quality publications. "During 2012 alone, CBMS researchers published more than 100 papers in international journals and 15 papers in journals with an impact factor of five or higher," explains Wu. "This is a gigantic leap in research output compared with 15 years ago, when CBMS researchers only published one immunology paper the entire year." Patent applications have also risen rapidly since CBMS was granted its first patent in 2000, with nearly 20 applications under consideration in the first half of 2013.

Going forward, CBMS plans to develop a world-class faculty by recruiting young talent and by building interdisciplinary research projects with Chinese scientists and international partners. "Our goal in the future is to increase our research competitiveness—both within China and on the global stage," says Jijian Zhang, associate director of research at CBMS.

Revolutionizing Education

A pivotal force of research competitiveness is the graduate students, and Wu has tasked the institution with providing a "research-based education." Wu has implemented a number of programs to boost students' research skills and critical thinking ability, including journal clubs and interdisciplinary co-mentorships.

CBMS is also introducing innovative teaching strategies into the rigid medical education system. "In addition to the textbook knowledge required for board exams, we encourage critical thinking from our undergraduate students," says Wengang Xiao, associate director of education at CBMS. Wu and Xiao have introduced materials from scientific journals, rigorous debates and discussions, and presentation practices into the classroom. "We ask students to challenge authority, both teachers and textbooks, when it comes to science," says Wu.

Also bringing in new ideas are the many young professors joining the faculty who have received their training overseas. "Ninety percent of the current faculty have either acquired their Ph.D. or done their postdoctoral research abroad," says Wu. Moreover, there are currently 28 adjunct professors located internationally who regularly visit CBMS to teach and to advise on research directions.

Over the last 20 years, CBMS has developed into a respected, global medical research institution. With its state-of-the-art research facilities, internationally minded faculty, and revamped educational system, CBMS is poised to solve critical problems in medicine and become one of the top basic medicine and biomedicine research centers in China.

Insights from the Director: Making Grand Visions a Reality

The director of CBMS has grand visions for the institute. As a trained immunologist and a pioneer of epitope-based rational vaccine design, Yuzhang Wu has had a successful research career. He is a winner of the National Outstanding Youth Science Fund and a designated Changjiang Scholar Distinguished Professor for the Chinese Ministry of Education, one of the most prestigious distinctions for Chinese scholars. When he became the director of CBMS in 2011, he immediately saw opportunities to make an impact in three areas: creating an internationally trained faculty, boosting translational research, and revamping pedagogical strategies.

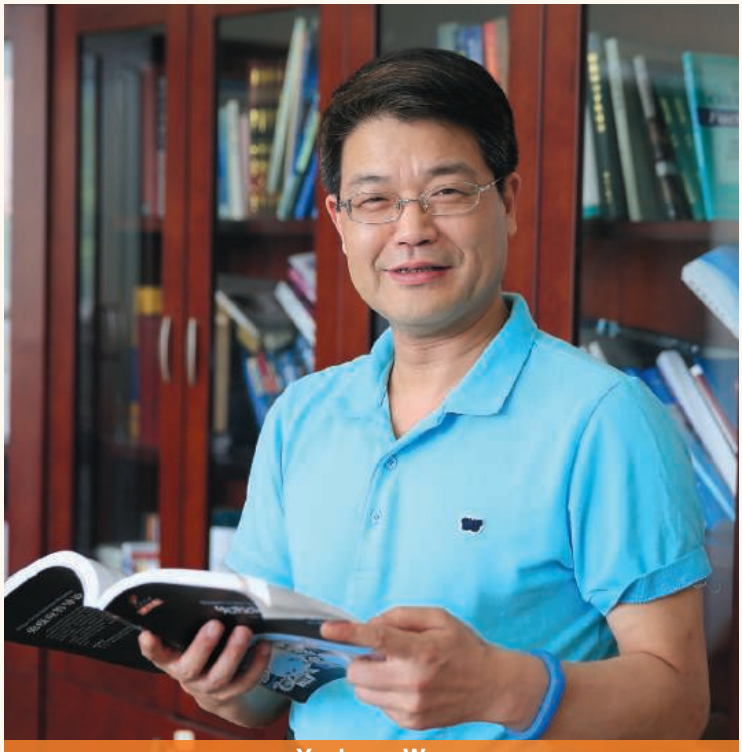

Yuzhang Wu

Faculty Training

Previous to Wu's leadership, CBMS faculty did not follow an international model for research and education. Therefore, Wu began recruiting young researchers from overseas who were "highly motivated and eager to embark on new research directions." Wu explains that they "have recruited several junior investigators who have a strong work ethic as well as extensive international connections, which has been raising the level of education and research significantly."

Because these new generations of faculty are still early in their careers, Wu has begun to coach them on how to think strategically and focus more broadly in their field. "Many of these talented young investigators have spent years studying a small part of a larger problem," he explains. "They're still learning how to navigate the big picture and how to strategically compete with others." These skills are even more critical in China where research competition is fierce and pressure for fast success is high.

Interdisciplinary Collaboration and Translational Research

One advantage of CBMS being located in Chongqing is that the culture is known for friendliness and cooperation, which makes it easier for researchers to form collaborations and interdisciplinary projects. To further facilitate this, Wu has taken full advantage of the three large hospitals affiliated with CBMS and implemented a co-mentorship program and a "clinical-basic research salon." He hopes these programs will facilitate strong translational-research collaborations between the faculty and the hospital's clinical staff.

Eventually, Wu dreams of incorporating industry into these collaborations. "Integrating with industry will help us commercialize our research findings," he says. "Although this has been more difficult than forming academic collaborations, we are getting there." His goal is to reduce the reliance on central government funding and to build a clinically oriented biotechnology base in China.

Innovative Education Strategies

Ultimately, education is the key to producing top-notch researchers, clinicians, and biotechnology leaders, which is why Wu so strongly values education reform. Traditional medical education in China has failed to deliver translationally focused scientists and clinicians. Wu's reform begins at the undergraduate level, with the goal of changing the focus of education from simple memorization toward critical thinking and understanding. Wu has already implemented a number of classroom strategies to help achieve this goal (see Innovation in Education, page 1268).

In his view, the gap between graduate training in China and in the West is even wider than that of undergraduate education. Many graduate students in China have simply become technicians who run repetitive experiments, rather than scientists in training. His graduate education reform aims to change this by implementing new strategies. Within the new paradigm, graduate students will be expected to independently identify important questions in their field of interest and then address these questions using logical reasoning and up-to-date information from the scientific literature rather than from textbooks.

Wu believes that a shortage of research-focused educators contributes to the lack of this type of education, highlighting the need for better teacher training to raise the standard of education. He encourages CBMS faculty to not only focus on writing scientific research papers but also to develop teaching strategies and publish their experiences in education-oriented journals.

In his first two years, Wu has made great strides in steering CBMS toward becoming an international center with a talented faculty, robust research output, and world-class scientific training. Already, CBMS has moved into a stronger position and is producing quality clinical research. Wu believes the institution's future is bright, but that fully realizing his dreams will only be made possible by the diligent work of everyone at CBMS.

State Key Discipline: At the Front Line of Immunology


The Institute of Immunology

The Institute of Immunology at CBMS leads basic and applied immunology research for the armed forces of China; more importantly, it is designated a State Key Discipline (SKD) and is therefore eligible to receive direct government funding. Scientists at the institute focus on advancing cutting-edge topics—from understanding the mechanisms underlying early immune responses to developing new vaccines.

Understanding and Harnessing Immune System Responses


Zhiren Zhang


Ying Wan

The body's immune response is a complex process. The Institute of Immunology has brought together scientists with a broad range of backgrounds to investigate mechanistic questions about the immune system and to find ways of harnessing the body's immune responses for clinical benefit.

After years spearheading the T cell vaccine development efforts at CBMS, Ying Wan, a principle investigator at the institute, has shifted his attention to dendritic cells and the role microRNAs play in immune response initiation. "We collaborate with research teams at Duke University and the University of California at Berkeley on these interesting topics, providing state-of-the-art research equipment," says Wan.

Zhiren Zhang, associate head of the institute, began studying inflammation at the Universität Tübingen in Germany. He moved his lab to the Institute of Immunology in 2011 because the "funding situation is better right now at CBMS than in Germany," explains Zhang. At the institute, his group investigates molecular targets for suppressing excess inflammation.


Guohong Deng

To fully understand how the immune system fights microbial infection, Wei Liu, principle investigator, uses X-ray crystallography to obtain detailed structural information of the key protein players in an effort to dissect the molecular mechanisms of innate immunity. Prior to joining the institute in 2011, Liu, who has a background in biochemistry, spent nearly a decade at the Karolinska Institute in Sweden studying structural biology.

Combating Disease


Guilian Xu

One of the most serious chronic infections in China is hepatitis B. "It is estimated that a third of the world's chronic hepatitis B cases are in China," says Guohong Deng, principle investigator, whose lab investigates how a patient's genetic background affects the T cell response to the hepatitis B virus (HBV). Meanwhile, Guilian Xu, a principle investigator also studying virus-host genome interactions, works toward revising the conventional theory that the complement system only acts on innate immunity. Based on genetic evidence, she argues


Bing Ni


Xinyuan Zhou


Yongwen Chen

that the system also participates in adaptive immune responses, especially when certain viral infections, such as HBV, are present.

Epigenetic mechanisms also play a role in the immune response to HBV infection, and are the focus of Associate Head Bing Ni's research. After Ni graduated from the Third Military Medical University, he attended the University of Toronto for his postdoctoral training; however, he decided to come back to CBMS because there are abundant resources for studying "the three most clinically important immunology problems: infection, cancer, and autoimmunity," Ni explains. His research focuses on epigenetic changes, such as histone modifications, in regulatory T cells.

Understanding immune responses to other pathogens is important to many CBMS researchers. Principle Investigator Xinyuan Zhou, for example, investigates the mechanism of T cell memory using established infection models—lymphocytic choriomeningitis and *Listeria* infections. "We are looking at ways to enhance T cell memory for treating chronic infection," says Zhou. Complementing Zhou's work, another principle investigator, Yongwen Chen, who did his postdoctoral research at Sweden's Karolinska Institute, is looking at the role of natural killer cells and macrophages in resolving chronic HBV infection.

Advancing Vaccine Development


Li Wang


Wei Liu

Yuzhang Wu, director of CBMS and head of the Institute of Immunology, is a pioneer in epitope-based rational vaccine design—stimulating the desired immune response using synthesized peptides that present the "optimal" antigenicity. Under his leadership, the institute has attracted some of the best minds to research and has developed prophylactic and therapeutic vaccines for critical diseases in China.

One such researcher is Li Wang, associate head of the institute. She is looking for ways to modulate specific T cell responses to treat diseases and is "developing therapeutic vaccines for various cancers," she explains. Wang is trying to attenuate autoreactive T cells in type 1 diabetes in the hopes of slowing down the destruction of insulin-producing cells in the pancreas.

Successful vaccine development also involves understanding how existing vaccines work. Lilin Ye, principle investigator and an expert on immunological responses to vaccines and viral infection, designs new and improved versions of old vaccines. His group's latest work is focused on developing "mucosal vaccines and therapeutic antibodies against important diseases, such as hepatitis B and avian influenza," Ye says.

As a well-funded SKD, the Institute of Immunology has enlisted an interdisciplinary team of talented scientists to begin unraveling how the immune system works and to develop ways to design the most effective therapeutics. Given the progress the institute has made thus far, many more avenues for developing vaccines and combating chronic diseases will surely emerge in the future.

Cultivating New State Key Disciplines: Modernizing Basic Medical Sciences


Dajun Ying


Chuhong Zhu


Wenqing Cai


Lan Xiao


Xiaotang Fan

At TMMU, the faculty of CBMS is responsible for the university's basic medical education, which begins with anatomy and histology lessons. However, CBMS educators go beyond textbook lessons and incorporate their own research into classroom learning. Some of the noteworthy projects being used for medical education at CBMS include the world's second virtual human project, blood vessel engineering, and nervous system development research. As a result of this high-quality research, the Department of Anatomy and the Department of Histology and Embryology are poised to become the next State Key Disciplines at CBMS.

Chinese Virtual Human Project

CBMS is a leader in the creation of digital human atlases. In the late 1990s, Shaoxiang Zhang, vice president of TMMU and former director of CBMS, led the team of surgeons and computer scientists who developed the Chinese Virtual Human Project (CVHP).


Shaoxiang Zhang

"CVHP is the largest virtual human dataset in the world," Zhang says. Although released a few years after the U.S. Virtual Human Project (VHP), CVHP has a number of notable advantages. CVHP was made using 0.1 mm slices, compared with the 1 mm slices used for VHP, Zhang explains, "making the CVHP data of much higher resolution." Additionally, the imaging resolution of each slice is also higher than that of VHP.

"Right now, the utilization rate of CVHP is on par with that of VHP," says Zhang. Virtual human databases are very useful for medical education, and CVHP is now being licensed by many medical schools in China and abroad. Moreover, the CVHP data is extremely valuable for education and applications in Asia, since there are a number of notable anatomical differences between the Chinese/Asian CVHP body and the Caucasian body used in VHP.

For future applications of CVHP, Zhang explains, they are looking at using the dataset in conjunction "with 3-D printing technology to create artificial human organs for transplantation."

Blood Vessel Engineering

Anatomical and histological research at CBMS has also brought about innovative discoveries in blood vessel engineering. Dajun Ying, professor emeritus, has been studying blood vessels in the human head since the 1980s. His early work, as a graduate student at TMMU, focused on mapping the capillaries that feed the brain, head, and facial tissues. After moving into the field of biomechanics, he began working on the role of hemodynamics in endothelial cell biology and capillary physiology. Ying then began using molecular biology to understand the signal transduction pathways underlying the action of hemodynamic forces. Currently, he is involved in application-oriented projects such as stem cell-based tissue engineering.

Ying's innovative attitude has inspired the next generation of scientists, including Chuhong Zhu, head of the Department of Anatomy. Continuing his work from a stint in the University of Minnesota, Zhu engineers artificial cardiovascular tissue using new biomaterials and stem cells. He is constructing tissue-engineered small-diameter blood vessels from captured endothelial progenitor cells in vivo, which enables endothelization of tissue-engineered blood vessels. Zhu is committed to producing these blood vessels for clinical applications. He also investigates neural regulation of blood vessel physiology and development.

Neural Development

Developmental biology is also a strong focus at CBMS. Professor Emeritus Wenqing Cai was one of the pioneers who introduced immunohistochemistry methods to China in the 1980s. She has trained many scientists at CBMS who are now leaders in developmental biology.

One such person is Lan Xiao, head of the Department of Histology and Embryology, who studied development neurobiology and neuropsychiatry as a postdoctoral fellow at the University of Saskatchewan, Canada. "We are especially interested in the development of oligodendrocytes, the myelin forming cells in the central nervous system," says Xiao, "because we have found from animal models that oligodendroglia dysfunction or demyelination may be involved in the pathogenesis of psychiatric disorders like schizophrenia."

Other researchers in the department are looking for therapeutic agents to correct neurodevelopmental defects. Xiaotang Fan, a principle investigator in the same department, is particularly interested in nuclear receptors as therapeutic targets. "The key to successfully applying developmental biology for therapeutic application in neurology is to pinpoint tissue and temporal specificities of potential therapeutic targets," explains Fan, "because the time window for therapeutic intervention is quite narrow for neurodevelopment defects."

Taken together, these research projects have not only advanced the medical education at CBMS, but are also supporting the Department of Anatomy and the Department of Histology and Embryology in their quest to become State Key Disciplines.

Innovation in Education: Training Physician-Scientists

Graduate Students Discussing an Experiment in the Lab

Summer School for Undergraduates

A key objective of Director Yuzhang Wu's vision for CBMS is to reform all levels of the educational system, including physician-scientist training. "Our goal is to train our brightest students to become physician-scientists who can identify important questions and critically investigate the answers," says Wu. Below is a look at some of the current physician-scientist students' experiences and accomplishments, which demonstrate how Wu's plan is being implemented and is improving medical education.

Dali Zhang and Kaiyuan Zhang are both starting their senior year at TMMU. In an immunology course taught by Professor Li Wang last year, Dali Zhang was asked to design his own scientific experiments. He became so interested in the intellectual exercise that he asked if he could carry out the experiments in Wang's lab over the summer break. Wang agreed to mentor the student's project because "teaching and learning are mutually beneficial," explains Wang. "I also gain new insights by discussing different papers' experimental design and results with my students." After finishing his summer project, Zhang is now considering either a basic research career or a clinically focused career after he graduates. "I am glad to have had the chance to learn both clinical and basic research skills here," says Zhang. "In China, we have a unique opportunity to conduct translational research because we have access to a huge patient pool."

His classmate Kaiyuan Zhang has been working in the lab for much longer, since his freshman year to be exact. Kaiyuan Zhang, who studies molecular neurophysiology with Jun Zhang, principle investigator in the Department of Physiology, cannot hide his passion and excitement when talking about his work on sleep biology and the neurotransmitter orexin. "I am inclined to pursue basic research after graduation because of the happiness it brings me," says Zhang. "I enjoy using deductive logic and applying the latest techniques to solve important questions." He is just one of many success stories in Wu's undergraduate education reform.

Xiaoyun Shang just received his Ph.D. from CBMS this summer. He worked in Director Yuzhang Wu's lab studying vaccine design. "The most important lesson I have learned here is critical thinking," says Shang. "There is so much knowledge beyond the textbooks we used in college. I've learned the importance of identifying key questions and applying up-to-date technical know-how to answer these questions," he says. He has accepted a postdoctoral fellowship in the United States, where he hopes to gain additional skills to advance his career in therapeutic cancer vaccine development.

Kaijun Liu is a second-year Ph.D. student in the lab of Shaoxiang Zhang, vice president of TMMU and the project leader for the Chinese Virtual Human Project (CVHP) (see page 1267). Liu also did his undergraduate work at TMMU and has worked in Zhang's lab since 2005. "Back then, we did not have the innovative education platform put together recently by Director Wu, so there has been some trial and error in the process [of learning to be a critical-thinking scientist]," says Liu, who equates the transition from undergraduate research to studying for a Ph.D. to climbing a mountain. "You see the field more broadly and clearly as you climb," says Liu, explaining that as he advanced toward completing the degree, he began to see the bigger picture questions in his field. In Zhang's lab, Liu learned about computer reconstruction and image processing, but has recently become interested in immunology, and now wants to combine these different fields to create new ideas, such as creating a model of the lymph system using the CVHP dataset.

Overall, "the ultimate goal [of this education reform] is to break old habits, the inertia, and the short-sightedness of the traditional medical education," says Professor Zhongxiang Yao, who has over 25 years of teaching experience. Fundamental changes in guidelines and evaluation systems are necessary to ensure that undergraduate and graduate students can develop a productive career, and CBMS is dedicated to hastening the reform and inspiring the next generation of scientists.

International Talents: Fostering a Global Reach

In recent years, many Chinese universities have significantly stepped up their efforts to bring their science to the international stage. CBMS is one such institution that has been implementing strategies to become more competitive in the global arena. In the last two to three years alone, CBMS has seen an uptick in bidirectional global connections, but staying competitive means being able to recruit a top-notch faculty both locally and abroad.

Helping achieve this talent recruitment goal is China's "Go West" strategy, which has been encouraging economical, educational, scientific, and technological developments in the country's western region and providing policy and funding support over the last decade. Given this increased focus on the West, Chongqing—the largest city in China—is poised to become a new center of international outreach.

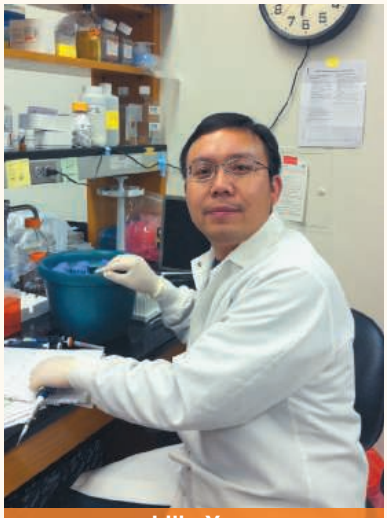
Lilin Ye

Professor Xiaowei Chen, who graduated from CBMS several years ago and recently returned from his postdoctoral training at the Technische Universität München in Germany to be the head of the Brain Research Center, says the livability of Chongqing compared with that in major coastal cities allows him to "concentrate on doing science without worrying about money and housing." This is important for Chen since he feels a strong emotional attachment to the institute and plans to build China's first marmoset center for large-animal experiments right in Chongqing. Another example is Lilin Ye, a principle investigator who brought his research developing novel therapeutic vaccines to CBMS in 2012 from Emory University in Atlanta in the United States, explains that some other benefits of being in Chongqing are that the "kindergarten and school education is better than that provided by other institutions in Beijing or Shanghai."

CBMS also strives to stay competitive with universities located on either side of the Atlantic Ocean by providing top-notch research facilities as well as generous starter packages. "There are also fewer restrictions here as to how starter funds can be used," says Yi Zhou, professor of neuroscience, who joined CBMS at the same time as Chen. He moved from the University of Southern California to open his own lab studying how complex information is processed in the brain. Zhou is particularly impressed by the leadership at CBMS and TMMU. "The director of the college works harder than us!" he says. "We can bring bureaucratic issues, such as difficulties navigating complicated procedures, directly to him," and he provides strong support to young investigators at TMMU, says Zhou. "Once he replied by e-mail after midnight, and my problem was resolved before the next day started," he explains.

CBMS has also set specific recruitment goals to help strengthen its faculty. "We want [to recruit] junior-level talent who are not afraid of challenging the existing paradigms and exploring new theories," explains Yuzhang Wu, director of CBMS, "rather than transplanting established research groups from overseas." Wu hopes these free-thinking scientists will bring the scientific cultures from the countries where they were trained to China. Evidence of this can be found in many of the innovative teaching methods and evaluation systems CBMS has implemented in recent years, which have their roots in the places where CBMS researchers have been educated, such as Europe or the United States.

Scientists returning home to China don't leave their professional lives behind. Maintaining connections and collaborations with scientists outside China is very important to CBMS researchers. "There are no real differences between being located in Chongqing and being in Beijing or Shanghai," says Chen, "especially in the era of the Internet and frequent air travel." He still communicates regularly with former colleagues in Munich about collaborative projects.

Another strategy for CBMS in acquiring top talent is recruiting domestically. Jun Zhang, a principle investigator in the Department of Physiology, who specializes in sensory-motor integration, moved from Nanjing University (800 miles east of Chongqing) to CBMS in 2011. Zhang says that "Chongqing, and the surrounding Sichuan region, has always been a resource-rich area in China, and this is also true in terms of scientific research support thanks to ample funding and talent from all over the world."

More than 1,300 years ago, poets wrote about how quickly one could travel from Chongqing (the "White Emperor Castle") to Nanjing via the Three Gorges and Yangtze River, in only one day. With today's technology, the distance between Chongqing and other cities has become virtually nonexistent, making Chongqing a great location to conduct world-class research as well as stay connected to the global community.

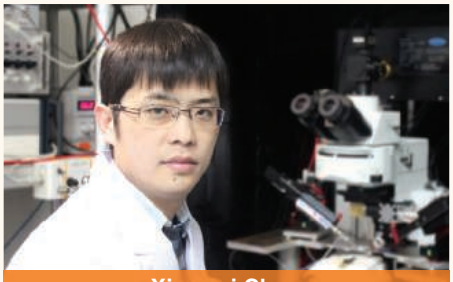
Xiaowei Chen


Yi Zhou


Jun Zhang

Department of Science and Technology
Ministry of Science & Technology
Government of India
Technology Bhavan, New Mehrauli Road, New Delhi- 110016.

Jawaharlal Nehru Science Fellowships

CALL FOR NOMINATIONS

The Department of Science and Technology has instituted Jawaharlal Nehru Science Fellowship, in order to promote cutting-edge scientific research in centres of excellence in India. Eminent scientist of any nationality desirous of carrying out research in Indian Institutions for a period of 12 months in a three year duration would be enabled by this Fellowship Scheme. Nominations of eminent scientists for the Award of Jawaharlal Nehru Science Fellowships are invited from Heads of Academic/Research Institutions, Presidents/Fellows of Science Academies and global leaders in science.

SCOPE

Areas in Natural and

Physical Sciences including Mathematics.

ELIGIBILITY

- The Fellowship is open to overseas scientists with high academic distinction and achievements.
- High academic distinctions accompanied by election to the fellowships like Royal Society, US and French Academies and their equivalent.
- The nominated scientists should continue to be active in Research, as evidenced from R&D Outputs over the past five years.

DURATION

The Fellowship would be availed for a duration of 12 months during a period of three years, from the date of offer of the Fellowship Award.

NATURE OF SUPPORT

- Value of the Fellowship is US$ 100,000 for a 12 months period.
- In addition, each Fellow will receive aggregated research grant of Rs. 5.5 million part of which may be utilised to engage project staff (2 Research Fellows or 1 Post-doctoral Research Fellow), international / local travel and other contingent expenses to carry out research.
- The selected scientists could choose :
  - Their place of research anywhere in India.
  - Duration (total of 12 months spread over a period of up to three years).
  - Research theme for pursuing their research.
  - Research collaboration in India, if any.

25 Fellowships for the period 2014-17.

HOST INSTITUTION

The Host Institutions for the Jawaharlal Nehru Science Fellows would need to provide the necessary infrastructure, furnished housing and administrative support to the Fellow. The Department of Science and Technology (DST), Government of India, would provide Rs 1 million to the host institute to cover the expenses of such support.

METHODOLOGY FOR SELECTION

- Nominations for the Fellowship are solicited through an open call.
- A Search Committee will select and recommend suitable nominations to the Government of India.

HOW TO APPLY

The nominations for the Fellowship may be sent to **Secretary, Department of Science and Technology, Technology Bhawan, New Mehrauli Road, New Delhi – 110016 through dstsec@nic.in (please mention "Attention SS Kohli, Director, DST" in the subject of the email).** There is no prescribed format for nomination. The nomination letters should be accompanied by a recent and detailed CV of the nominee and expressed willingness to accept the Fellowship, if offered.

Since the Government of India wishes to initiate the Fellowship scheme by January, 2014, early nomination by December, 2013 are solicited.
To see further details log on to www.dst.gov.in.

TEXAS A&M
HEALTH SCIENCE CENTER
COLLEGE OF MEDICINE

Institute for Regenerative Medicine
at Scott and White, Temple TX
Positions for Post-Doctoral Fellows and Other Lab Personnel

The Texas A & M Institute for Regenerative Medicine is seeking Ph.D. level post-doctoral fellows and other lab personnel for research on adult stem/progenitor cells referred to as mesenchymal stem cells or multipotent mesenchymal cells (MSCs). The Institute is dedicated to research both on the basic biology of MSCs and the therapeutic products they produce. Current research includes development of new therapies for diseases of the eye, myocardial infarction, cancer, diabetes, stroke, epilepsy and traumatic brain injury. The Institute occupies newly renovated laboratories and a series of core laboratories equipped with state-of-the-art instrumentation. It also includes a newly renovated vivarium for small animal experiments. Post-doctoral appointments are contingent on funding and will be for one year with the opportunity to renew for a second and third year. Post-doctoral candidates should have excellent communication skills both verbally and written and a Ph.D. or M.D. degree from a well recognized university. Other lab personnel should have some laboratory experience, preferably with tissue culture of mammalian cells. Salaries and benefits are competitive. Log onto our website at **http://medicine.tamhsc.edu/irm/** to read more about our facility.

For requirements and duties of positions listed above as well as completing the application, please visit **https://jobs.tamhsc.edu/**. The posting number for Postdoctoral Research Associate NOV 14079, Research Assistant NOV 14080, Technician II NOV 14075 and Technician NOV 14081.

The Texas A&M Health Science Center is an AA/EO Employer.

Jefferson Science Fellowship

The National Academies is pleased to announce a call for nominations and applications for the 2014 Jefferson Science Fellows program. Initiated by the Secretary of State in 2003, this fellowship program engages the American academic science, technology, engineering and medical communities in the design and implementation of U.S. foreign policy.

Jefferson Science Fellows (JSF) spend one year at the U.S. Department of State or the U.S. Agency for International Development (USAID) for an on-site assignment in Washington, D.C. that may also involve extended stays at U.S. foreign embassies and/or missions.

The fellowship is open to tenured, or similarly ranked, academic scientists, engineers and physicians from U.S. institutions of higher learning. Nominees/applicants must hold U.S. citizenship and will be required to obtain a security clearance.

The deadline for 2014-2015 program year applications/nominations is **January 13, 2014.** To learn more about the Jefferson Science Fellowship and to apply, visit the website at:

www.nas.edu/jsf

THE NATIONAL ACADEMIES
Advisers to the Nation on Science, Engineering, and Medicine

UNIVERSITY OF CALIFORNIA
UCRIVERSIDE

Tenure Track Assistant Professor of Neuroscience

The Department of Psychology, University of California, Riverside, invites applications for a tenure-track Assistant Professor position in the systems neuroscience area, beginning July 1, 2014. The Ph.D. degree is required and post-doctoral experience is preferred. Applicants should have demonstrated compelling promise of research and publication using modern molecular, cellular, systems or behavioral approaches to address fundamental problems of mammalian brain function, and be interested in interacting with a broad-based psychology department. Individuals with research focused on mechanisms of cortical development, plasticity or function are especially encouraged to apply, as are those whose research emphasizes linkages between animal and human models. Applicants should also be committed to excellence in undergraduate and graduate education. Salary will be commensurate with education and experience.

Review of completed applications begins **January 17, 2014** and continues until the position is filled. Interested candidates should send a cover letter describing research and teaching interests, their curriculum vitae, reprints and preprints if available, and arrange to have three letter of recommendation provided, all using the following link: **https://aprecruit.ucr.edu/JPF00035**. Questions about the position should be directed to Professor Peter Hickmott, Chair, Systems Neuroscience Area Search Committee, at **peter.hickmott@ucr.edu**.

The Riverside campus of the University of California is growing rapidly and has an excellent psychology department with a strong record of success in research, teaching and extramural funding. For information on the Department of Psychology, see our web site at: www.psych.ucr.edu. For collaborative opportunities via the Neuroscience Graduate Program, see http://neurograd.ucr.edu. The campus is centrally located in Southern California, about 50 miles east of Los Angeles and less than an hour's drive from the area's mountains, deserts and beaches.

The University of California, Riverside is an Equal Opportunity/Affirmative Action Employer.

PURDUE
UNIVERSITY

Two Faculty Positions in the Department of Botany and Plant Pathology

The Department of Botany and Plant Pathology is seeking applicants for two Assistant Professor tenure track faculty positions in Plant Biology. Both positions are academic year appointments. Successful candidates will be expected to develop internationally-recognized extramurally-funded research programs, interact with diverse faculty, staff and students across campus, demonstrate excellence in their teaching of graduate and/or undergraduate courses, and function as an active member of the department and university faculty.

1. Root/Rhizosphere Biology – closing date 12/15/2013 or until a suitable candidate is identified

Applicants for the Root/Rhizosphere Biology position will have a Ph.D. in the biological or computational sciences and postdoctoral research experience. A complete position description is available at **https://ag.purdue.edu/btny/Pages/JobListings.aspx**

2. Plant Growth Regulator/Hormone Biology – closing date 1/20/2014 or until a suitable candidate is identified

Applicants for the Plant Growth Regulator/Hormone Biology position will have a Ph.D. in biology, biochemistry, computational biology or a related field and at least two years of postdoctoral research experience and expertise in plant biology. A complete position description is available at **https://ag.purdue.edu/btny/Pages/JobListings.aspx**.

Applicants should submit a letter of application outlining their research interests and describing their philosophical and conceptual approach to a research/teaching position at a land-grant university. Applicants should also include a complete resume and the contact information for three references. These materials should be sent electronically to **mowp@purdue.edu**. A background check will be required for employment in these positions.

Purdue University is an Equal Opportunity/Equal Access/Affirmative Action Employer fully committed to achieving a diverse workforce.

PEDIATRIC Infectious Diseases

Open Rank, Open Tenure. The Division of Infectious Diseases in the Department of Pediatrics is seeking applications from highly qualified M.D., M.D./Ph.D. or Ph.D., for faculty positions. The Division of Infectious Diseases has a long history of NIH supported laboratory and clinical research. The selected individuals will work collaboratively to expand current research programs as well as establish new areas of research in respiratory viruses and bacterial infections. These positions will be provided generous start-up packages as well as secondary appointment in basic science department and Centers of Excellence at UAB to further the capacity of research in infectious diseases at UAB.

QUALIFICATIONS

The successful candidates for these positions must have a successful record in research with current NIH funding. In addition, the ideal candidates should possess:

- Experience in the academic medical center setting
- A proven track record of research initiation
- Demonstrated research collaboration skills
- Strong communication skills and the highest of ethical standards

Interested applicants should contact:
William Britt, M.D.
Professor, Division of Ped Infectious Diseases
1600 7th Avenue South, CHB #107
Birmingham, AL 35233
Email: wbritt@peds.uab.edu

UAB is an Equal Opportunity/Affirmative Action Employer committed to fostering a diverse, equitable and family-friendly environment in which all faculty and staff can excel and achieve work/life balance irrespective of ethnicity, gender, faith, gender identity and expression as well as sexual orientation. A pre-employment background investigation is performed on candidates selected for employment. In addition, UAB Medicine maintains a drug-free and tobacco-free work environment. Physicians and other clinical faculty candidates, who will be employed by the University of Alabama Health Services Foundation (UAHSF) or other UAB Medicine entities, must successfully complete a pre-employment drug and nicotine screen to be hired. UAB also encourages applications from individuals with disabilities and veterans.

Princeton Environmental Institute (PEI) and the Department of Civil and Environmental Engineering (CEE) at Princeton University seek outstanding applications for a new faculty position in water science. The position is a tenure-track position at the rank of Assistant Professor, with a preferred start date of September 1, 2014. The successful candidate will have a PhD in an appropriate field and a proven record of innovation and creativity in conducting quantitative research addressing important and emerging topics within the broad scope of hydrological sciences. Areas of interest include: (1) water and climate, (2) water and energy, (3) water and environmental quality, (4) water and ecosystem integrity, and (5) water and food security.

In all cases, it is expected that the candidate would be able to immediately make meaningful contributions to the diverse, interdisciplinary environmental research and teaching mission of PEI and CEE's Environmental Engineering and Water Resources Program (EEWR). PEI is the interdisciplinary center of environmental research, education, and outreach at Princeton University. PEI's mission is to advance knowledge and to develop the next generation of leadership by providing outstanding academic programs and opportunities for advanced scholarship, research, and civic engagement. The goal of CEE's EEWR program is to train outstanding engineers and scientists and to conduct advanced research in areas that are vital to national and international needs in the areas of environmental engineering and water resources. A successful candidate will be expected to complement existing strengths in the program, which include environmental problems in areas such as ecohydrology, land surface - atmosphere interactions including energy and moisture fluxes and their relationship to large-scale climate modeling, remote sensing of environmental variables such as soil moisture and rainfall intensity, carbon mitigation and climate change, subsurface flows & reactive transport, atmospheric dynamics and atmospheric chemistry, the urban environment, and biogeochemistry of contaminated waters.

Applicants should apply online at **https://jobs.princeton.edu**, requisition number **1300834**; and should submit their CV, contact information for five references, and separate statements of research and teaching vision. The statements of research and teaching vision should include the candidate's sense of the field and his or her vision for advancing in the context of such a position. Evaluation of applicants will begin on **January 15, 2014** and continue until the position is filled. Inquiries regarding this position should be addressed to **Prof. Kelly Caylor (kcaylor@princeton.edu)**.

Princeton is an Equal Opportunity Employer and complies with applicable equal opportunity and affirmative action regulations. We strongly encourage applications from underrepresented minorities, women, veterans, and those with disabilities.

Recruit and Promote Your Brand All Year Long

Science Careers will publish a 2014 Career Directory that will be promoted and distributed all year long.

A combination of career development content alonside your branding ads makes this the pefect place to promote your organization's mission and the areas where you typically recruit. With bonus distributions to meetings and career fairs throughout the year and push marketing including banner ads and e-mail blasts to potential candidates, your company receives ongoing exposure to scientists eager to know about career opportunities.

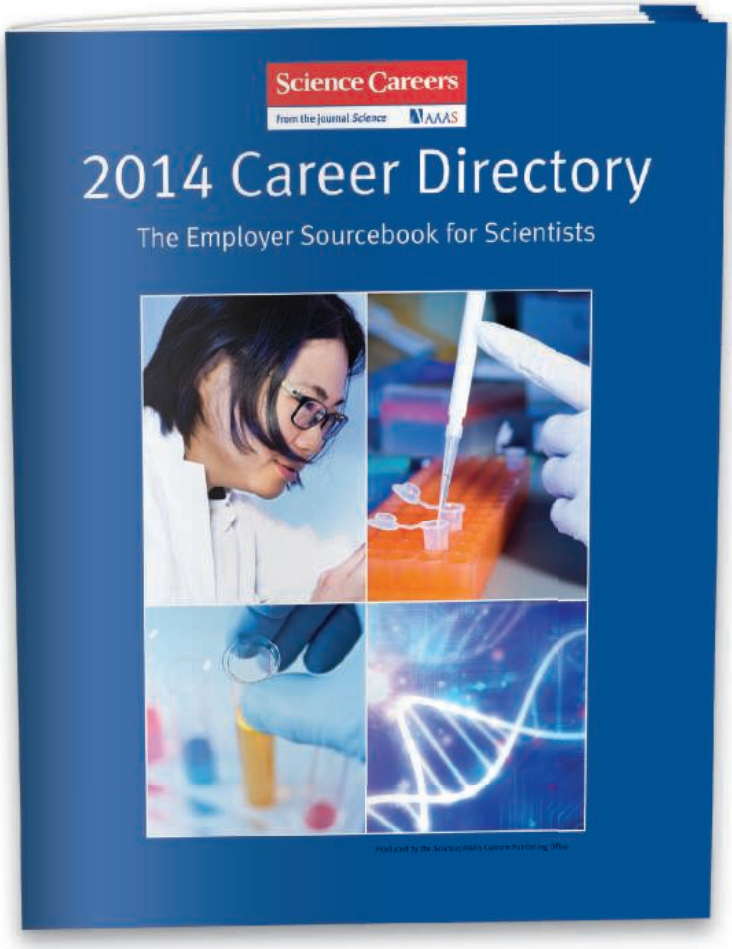

Benefits to your company

- Opportunity to brand your organization to scientists beyond your normal reach.
- Print bonus distribution of 3,500 copies to career fairs and meetings around the globe.
- Digital copy e-mailed to 100,000 scientists including all *Science* Careers registrants.
- Your logo included in two Career Path newsletters.
- A PDF of the booklet will also be posted on *Science* Careers for one year with marketing to drive readers to the booklet. Marketing includes banners, e-mail blasts, and promotion across AAAS/*Science* newsletters.

To book your ad or for more information:
E-mail: advertise@sciencecareers.org

Or telephone us:
US/Canada/South America:
202-326-6582

Europe/India/Australia/New Zealand/Rest of World: +44 (0) 1223 326500

Japan: +81-(0)90-9110-1719

China/Korea/Singapore/Taiwan/Thailand: +86-1367-1015-294

Reserve space by December 20, 2013
Ad materials due January 10, 2014
Rate: US$2,995

For recruitment in science, there's only one Science

Produced by the *Science*/AAAS Custom Publishing Office

Science Careers
From the journal *Science* AAAS

ScienceCareers.org

ASSISTANT PROFESSOR

Freshwater Ecologist

The Department of Biological Sciences at the University of Alabama invites applicants for a full-time (9-month) tenure-track faculty position at the Assistant Professor level. The successful applicant will establish an extramurally funded and internationally recognized research program in freshwater ecology. Preference will be given to applicants with a background in state-of-the-art, quantitative methods serving studies of freshwater ecosystems such as those related to, but not restricted to, food-webs, ecosystem energy and nutrient fluxes, metabolic theory, climate change, ecohydrology and macrosystems ecology. We define ecosystem studies broadly and encourage applications from individuals with a demonstrated record of integrating population- and community-level research with ecosystem perspectives.

The University of Alabama (UA) is near the geographic center of the Mobile River drainage, a true hot-spot for global freshwater biodiversity. Successful candidates will be encouraged to leverage this unique resource to support an innovative research program, and to forge collaborations with the new NOAA National Water Center, which will open on the UA campus in 2014, and the diverse faculty at UA and Dauphin Island Sea Lab with interests in freshwater ecology. Aquatic mesocosm facilities are available near the UA campus at the Tanglewood Biological Station. Teaching responsibilities will include basic undergraduate courses in biology, as well as specialized undergraduate and graduate courses in the successful candidate's area of expertise.

Applicants must have a Ph.D., postdoctoral training, and demonstrated research productivity. Queries regarding additional details should be addressed to the chair of the search committee: Dr. Alexander D. Huryn at **huryn@bama.ua.edu**.

To apply, go to **https://facultyjobs.ua.edu**, complete the online application (Job # 0808674), and upload (1) an application letter with a list of three to five references (including contact information); (2) CV; (3) statement of research interests and goals; and (4) statement of teaching interests and philosophy. Consideration of applications will begin January 15, 2014, and will continue until the position is filled. Prior to hiring, the final candidate will be required to pass a pre-employment background investigation. The anticipated start date is August 16, 2014.

Additional information about the Department of Biological Sciences and this available position can be found on our website at **http://bsc.ua.edu**.

The University of Alabama is an Equal Opportunity/Equal Access Employer and actively seeks diversity among its employees.

touching lives
THE UNIVERSITY OF ALABAMA

深圳大学

2013 Shenzhen University Oversea Recruitment

Shenzhen University (SZU) was founded as a public university in 1983 with the accreditation of the State Council of the People's Republic of China.
There are many famous scholars in SZU. Currently, there are 1,500 teachers on campus and about 60% of them have gotten Phd. Now, SZU has 2 Academicians of Chinese Academy of Sciences, 3 Academicians of Chinese Academy of Engineering, 2 members of "1000-Talents Scheme", 6 scholars who have won awards from the National Science Foundation for Distinguished Young Scholars, 4 scholars who have won awards from the "Chang Jiang Scholars Program", 3 members of New Century Millions of Talents Project at national level and 3 chief scientists in the National 973 Academic Program.

SZU, thirsty for talents, warmly welcomes numerous outstanding elites to join us as distinguished professors, associated professors or lecturers.

A. Distinguished professor
1) Eligibility: Candidates of the national "1000-Talents Scheme", "1000-Young-Talents Scheme", "Outstanding Youth", "Chang Jiang Scholars Program" and "100-Talents Scheme" of the CAS, professors or associated professors from overseas famous universities and outstanding scholars having fundamental academic influence.
2) Remuneration: It is yearly payroll for a distinguished professor, about RMB500,000-1,200,000. SZU will provide support in scientific research expenses and laboratory construction fee for a distinguished professor as well as in constructing his academic research team. Especially, Shenzhen local government will give scientific research expenses of RMB2,000,000 – 5,000,000 to a candidate who study such subjects as science, engineering and medicine and are eligible for the Peacock Program or Shenzhen High-Level Talent Program.

B. Professor, associated professor, lecturer and Liyuan Scholar Plan
(1) Professor, associated professor and lecturer
SZU warmly welcome oversea scholars who have achieved a Phd degree or have experiences of post-doctoral research and are competent for our positions of professor, associated professor and lecturer. Excellent candidates will be engaged as professors or associated professors directly by SZU according to their academic achievements.

Remuneration: the minimum annual salary is RMB310,000 for a professor, RMB250,000 for an associated professor and RMB180,000 for a lecturer.
Any professor, associated professor and lecturer could apply for Liyuan Scholar Plan, Peacock Program or Shenzhen High-Level Talents Program. If any person achieved any of the above plans, he could apply to Shenzhen Government for different subsidies by relevant plan.

(2) Liyuan Scholar Plan
Any teacher could apply for this plan. There are three levels for this plan, such as "Liyuan Leading Scholar", "Liyuan Outstanding Scholar" and "Liyuan Excellent Youth" respectively.
1) Three-level scholars: Liyuan leading scholar will be awarded to full-time teachers as a top-leader in his academic area. Liyuan outstanding scholar will be awarded to full-time teachers, aged under 45 and having 3 years' working experiences. Liyuan excellent youth will be awarded to young scholars aged under 35 who had gotten Phd and had one year's academic research experience in relevant research institutions.
2) Award standards: SZU will provide a living allowance for Liyuan leading scholars in 5 years, including two levels, RMB500,000 per year At the first level and RMB150,000 per year at the second. SZU will give a living allowance to Liyuan outstanding scholars in 3 years, RMB100,000 per year. SZU will give a living allowance to Liyuan excellent youth in 9 years at the most, RMB100,000 per year.

C. Shenzhen Oversea High Level Talents Policy
1) Candidates: oversea experts or oversea scholars. There are three levels for this plan, Level A , B and C respectively
2) Remuneration: candidates will receive an award of RMB500,000-1,500,000. Candidates whose research program is in such subjects as science, engineering and medicine respectively could enjoy scientific research expenses from RMB200,000 to 5,000,000. Talents at Level A could apply for scientific research expenses of more than RMB5,000,000.

Contact Us
For more information, please visit **http://www.szu.edu.cn**. If you're interested, please send your CV and relevant materials to any of the following email addresses:
Miss Liyun liyun@szu.edu.cn, 0086-755-26536111
Miss Gaoying gaoying@szu.edu.cn, 0086-755-26535295
Mr. Renqiang szursc@sina.cn , 0086-755-26535295

POSITIONS OPEN

UCSD Jacobs | Department of Bioengineering

FACULTY POSITIONS
University of California, San Diego
Department of Bioengineering

The Department of Bioengineering in the Jacobs School of Engineering at the University of California, San Diego is inviting applications for one or more Tenure-Track or Tenured Faculty Positions at the **ASSISTANT PROFESSOR, ASSOCIATE PROFESSOR,** or **FULL PROFESSOR** levels. To obtain more information or submit your application materials, go to **website: https://apol-recruit.ucsd.edu/apply** and apply to **position number 10-650.**

TENURE-TRACK FACULTY POSITIONS in Genomics and Evolutionary Biology

The Department of Biology at Saint Louis University, a Catholic, Jesuit institution dedicated to student learning, research, health, and service, is seeking applicants for two tenure-track faculty positions: One in Genomics and one in Evolutionary Biology. Competitive applicants will have a Ph.D., postdoctoral experience, a record of research productivity, and a commitment to undergraduate and graduate student training (M.S. and Ph.D. Students). The successful candidates will be expected to establish independent, extramurally funded research programs and participate in graduate training.

For the Genomics position, we seek candidates whose research addresses biological questions using the analysis of large data sets; the specific area of research is open. Both wet laboratory and high-performance computing facilities are available and will be matched to the candidate's needs. The successful candidate will teach a genomics course at the graduate level and contribute to an undergraduate course for biology majors.

For the Evolutionary Biology position, possible areas of research inquiry include, but are not limited to, development, ecology, physiology, functional morphology and biomechanics, behavior, and host/pathogen interactions. Both wet laboratory and high performance computing facilities are available and will be matched to the candidate's needs. The successful candidate will teach an evolution course at the graduate level and contribute to an undergraduate course for biology majors.

Excellent facilities and competitive startup packages are provided, and abundant opportunities exist to develop collaborative projects with Saint Louis University researchers and with scientists and educators at the nearby Missouri Botanical Garden, Danforth Plant Science Center, St. Louis Zoo, St. Louis Science Center, and local universities.

All applications must be made online at **website: http://jobs.slu.edu** (**Req ID 20130884**) and include a cover letter, curriculum vitae, three representative publications, a research statement, and a statement of teaching experience and philosophy. In addition, please have three letters of reference sent to: **Dr. Robert Wood, Department of Biology, Saint Louis University, 3507 Laclede Avenue, St. Louis, MO, 63103.** Review of applications will begin December 16, 2013 and continue until the position is filled. Additional information on the Department of Biology can be found at **website: http://www.slu.edu/x14762.xml.**

Saint Louis University is an Affirmative Action/Equal Opportunity Employer (AA/EOE), and encourages nominations of and applications from women and minorities.

POSITIONS OPEN

BIOMOLECULAR NMR SPECTROSCOPY
Position at the University of Minnesota

The Department of Biochemistry, Molecular Biology & Biophysics at the University of Minnesota invites applicants with a Ph.D. or M.D. degree in Biochemistry, Chemistry, or related fields to apply for a tenure-track/tenured position at the **ASSISTANT, ASSOCIATE,** or **FULL PROFESSOR** level. The successful candidate is expected to develop a creative and vibrant research program in Structural Biology and Biophysics in association with the Minnesota NMR Center (**website: http://www1.umn.edu/nmr/**). The Center consists of several high-field spectrometers including a 900, 850, two 700, and two 600 MHz spectrometers equipped with cryogenic probes. In addition, two solid-state NMR spectrometers are equipped with MAS and static NMR probes.

Preference will be given to scientists focusing on structural analysis of biomacromolecules relevant to any area of cellular biophysics and applications are encouraged from investigators studying human physiology or pathology, signaling systems or membrane proteins. Candidates must be able to teach undergraduate and graduate level Biophysical Chemistry and Biochemistry courses.

Applicants must apply online at **website: employment.umn.edu.** Click on Search Postings, and enter **187414** into the **requisition number** field. Applicants should attach a cover letter, curriculum vitae, and a detailed description of the proposed research. Review of complete applications will begin immediately and continue until the position is filled. More information concerning the Department and this position can be website: found at **website: http://www.cbs.umn.edu/bmbb.**

The University of Minnesota provides equal access to and opportunity in its programs, facilities, and employment without regard to race, color, creed, religion, national origin, gender, age, marital status, disability, public assistance status, veteran status, sexual orientation, gender identity, or gender expression. The University supports the work-life balance of its faculty and especially encourages applications from women and members of underrepresented groups.

The Illinois Natural History Survey (INHS) is soliciting applications for a two-year **POSTDOCTORAL RESEARCH ASSOCIATE.** Scientists whose research interests fit within those of the Illinois Natural History Survey are encouraged to apply. A salary of $42,000 per year with benefits is provided, as well as a $5,000/year research stipend. Applicants should submit curriculum vitae and Research Proposal. The Research Proposal is limited to three pages, not including references, and should address the research plan proposed for the two-year postdoctoral position. In advance of the application deadline, applicants must identify and contact a research sponsor at the INHS (**website: http://wwx.inhs.illinois.edu/opportunities/postdoc-sponsors/list/**) who is willing to host the Postdoctoral Associate. Preference will be given to applicants who can develop a strong research plan that merits additional and continued external funding. Research plans that build on existing INHS research strengths by adding new directions or new analytical techniques are encouraged.

Applicants should have completed a Ph.D. by the start date of the position (expected before December 31, 2014) and within the last five years. In addition to the Research Proposal and curriculum vitae, applicants should arrange for two letters of recommendation to be sent. Applications must be sent electronically to **e-mail: hroffice@inhs.illinois.edu** by January 31, 2014.

BIOENGINEER TENURE-TRACK PROFESSOR

The School of Engineering invites applications from distinguished scholars for a position at the either the **ASSISTANT** (tenure-track) or **ASSOCIATE/FULL** (tenured) level in Bioengineering at the newest University of California campus in Merced, California. The research emphasis for this position is a rather broad including: biological modeling, biosensors, tissue engineering, and preclinical biomedical imaging. To apply or for more information, please visit our **website: http://jobs.ucmerced.edu/n/academic/position.jsf?positionId=4996.**

POSITIONS OPEN

GENOMICS/FORENSIC MOLECULAR BIOLOGIST

As part of a strong faculty research emphasis in molecular biology and a developing program in forensic biology, the Department of Biological Sciences at Bowling Green State University (BGSU) seeks a tenure-track **ASSISTANT PROFESSOR** with demonstrated experience in genomics or bioinformatics approaches with potential forensic applications. Postdoctoral experience required. Successful candidates are expected to develop highly productive, externally funded research, and contribute to the graduate (Ph.D./M.S., n>90) and undergraduate programs. To apply, submit electronically a single PDF containing cover letter, curriculum vitae, statements of research plans and teaching perspective, representative publications, and, separately, three reference letters to **e-mail: dmclean@bgsu.edu** by January 6, 2014. *A background check is required for employment.* Contact **George Bullerjahn** at **e-mail: bullerj@bgsu.edu** with questions. Further information about our department can be found at **website: http://www.bgsu.edu/departments/biology.** *BGSU is an Affirmative Action/Equal Opportunity Employer/Educator and encourages applications from women, minorities, veterans, and persons with disabilities.*